Application of Acoustic Emission Sensing for the Non-Destructive Evaluation of Advanced Composite Materials

A thesis presented to Brunel University
for the Degree of Doctor of Philosophy
in the Faculty of Technology

by

Paul W.R. Baillie

Brunel Centre of Manufacturing Metrology,
Brunel University, Cleveland Road, Uxbridge, Middlesex

August 12th, 1999

Abstract

To evaluate the state of health of the composite, a real-time, in-situ acoustic emission (AE) damage detection system has been developed, where the monitoring of AE activity emitted from within a carbon/epoxy composite material (CFRP) is achieved using an all-fibre Mach-Zehnder interferometric sensor. The basic Mach-Zehnder configuration was modified to achieve the sensitivity needed to detect the low amplitude signals associated with AE. An active homodyne feedback loop was employed to maintain quadrature, whereas polarisation controllers ensured that the state of polarisation of the guided beams were equal. Two additional components were included in the AE detection system; fibre collimators and a demountable composite test section. The fibre collimators adjusted the optical path length in one of the arms of the interferometer to help maintain system sensitivity from test to test. The demountable test section ensured ease of testing, without the need for continual fusion splicing.

The characterisation of the fibre optic sensor was achieved by an analysis of its response to known acoustic disturbances. The fibre optic sensors response to continuous and transient acoustic excitation sources demonstrated the feasibility of using an embedded fibre optic Mach-Zehnder interferometric sensor for the evaluation of composite materials. The sensor's potential for non-destructive evaluation (NDE) was investigated by placing CFRP specimens with the embedded sensors under sufficient tension to cause damage. Signal analysis was performed on the detected AE data, using the time domain parameters and the cumulative event count. The change in the slope of the cumulative count curve coincided with the point where the accumulated damage seriously compromised the structural integrity of the sample. As a damage detection system the fibre optic sensor was adequate, however, the correlation of the time domain parameters with specific damage mechanisms proved inconclusive. Specially designed samples were manufactured to help the fibre optic sensor differentiate between mechanisms. Fibre optic sensor component failure resulted in the testing and analysis using the piezoelectric transducer only.

Amplitude and frequency distribution analysis of the piezoelectrically detected signals from these specially designed composite samples was attempted. From the results, it was evident that a correlation could be made between some of the damage mechanisms and the detected AE signals. However, it was apparent that a mixing of distribution occurred in some of the tests. Despite this, the results obtained using the piezoelectric transducer highlighted the benefits of attempting these specially designed tests in future fibre optic sensor work.

Papers Published

P.W.R. Baillie, K.F. Hale, G.F.Fernando, and B.E. Jones, *Optical fibre sensing of acoustic emission in fibre reinforced composites*, Proc. Conf. Sensors and their Applications VII, Dublin, September 1995, pp125-130 (IoP: ed. A.T. Augousti)

P.W.R. Baillie, K.F. Hale, B.E. Jones, and G.F.Fernando, *A study of the acoustic emission behaviour from carbon fibre reinforced plastic composites using an optical fibre sensor*, Proc. M&ES Doctoral Research Conference, Brunel University, June 1996, pp3/1-8

Contents

page no.

Appendices

References

List of Figures and Tables

page no.

FIGURES

Chapter 4

Chapter 5

Chapter 7

Chapter 8

TABLES

Acknowledgements

I am indebted to Dr. Ken F. Hale and Prof. Barry E. Jones, as my supervisors, for their support throughout this research work. I am also grateful to Dr. Gerard Fernando, Dr. Jo Au and Dr. Dave Andrews for their continuous interest and contributions to this research.

I would like to express my gratitude to The Engineering and Physical Science Research Council (EPSRC) for their financial support through three years of this Ph.D.

I would like to thank the lads from MB4 (past and present) and the members of the 'Sensors for Materials' group for their help within peer group meetings and for their personal advice throughout the years. A special thanks goes to Rob Campbell for his encouragement through the good times and bad. I would also like to thank the technical staff in the Dept. of Materials, especially John and George, for their support.

I am eternally indebted to my fiancée, Fiona, for her encouragement, love and understanding, without which I would never have been able to sanely complete this Ph.D. Finally, my greatest debt is to my mother and stepfather, Ann and Terry, for their love and the sacrifices they have made over the years.

Declaration

I declare that, to the best of my knowledge, no portion of the work referred to in this thesis has been submitted in support of an application for another degree or qualification of this or any other university, or other institute of learning.

The candidate also received distinct help from the following:
(i) Heriot-Watt University (Edinburgh), for the designing and construction of the active homodyne detection system and polarisation controllers.
(ii) Ciba-Geigy Composites for their donation of carbon/epoxy pre-impregnated tape.

Paul W.R. Baillie

CHAPTER 1

INTRODUCTION

1. Introduction

1.1 The Evaluation Of The Structural Integrity Of Composite Structures Using Acoustic Emission

In recent years there has been a rapid growth in the use of fibre reinforced plastic composite materials offering enormous potential for use in a wide number of engineering applications, ranging from sports goods to advanced aircraft structures. These materials offer high specific strength and stiffness properties, excellent fatigue and corrosion resistance and can be used to manufacture intricate components with lower weight at reduced cost (Harris, 1986). However, the manufacturing process may introduce unwanted materials and defects such as voids, inclusions and resin-rich areas into the composite, which may be difficult to detect (Cantwell and Morton, 1992). The structural integrity of the composite material may deteriorate due to these defects, in some cases leading to failure.

The in-service operation of composite materials can also result in damage and material degradation. Typical causes of damage include continuous cyclic loading, rapid deviations in environmental conditions, and impact loading. Once started, the region of damage can develop over a period of months or years and is not often evident from visual inspection. Once the damage reaches a critical level, the resulting failure of the material could be disastrous. At the onset of micro-damage, there is a sudden release of energy within the material. Some of this energy is dissipated in the form of elastic waves, known as Acoustic Emission (AE) (Cole, 1988). Generally, these structural alterations are the result of internally generated or externally applied mechanical or thermal stresses. Numerous mechanisms have been proposed and confirmed as sources of AE. Therefore, the goal of an AE measuring system is to detect the acoustic event and provide suitable signal processing to characterise it and determine its significance. The most critical component of any AE measurement system is the transducer (Hamstad and Sendeckyj, 1993). The conventional non-destructive evaluation (NDE) technique for monitoring material degradation through AE is based on piezoelectric (PZ) transducers.

These transducers are sensitive, relatively easy to apply to external surfaces, and an established technology in ultrasonics as well as AE (Scruby, 1987). This external sensing is beset with attenuation problems as the wave propagation in the material is affected by interactions with the material microstructure and inhomogenities. This difficulty in monitoring in-depth defects in composite components has led to the concept of incorporating internally embedded optical fibres to measure AE and provide the possibility of giving early warning of potential structural failure.

1.2 Synthesis Of Fibre-Reinforced Composite Structures

The demands of modern construction, such as lower cost, better aesthetics, higher performance and longer life, have led the industry to develop more "advanced" structural materials that satisfy todays needs. Traditionally, structural materials, such as wood, steel, and concrete, have been combined to form structural members of higher performance. A structural member constructed by a combination of different materials is considered a *composite material* member. The overall performance of a composite material is generally superior than that of the performance of each constituent material. Reinforced concrete is a conventional composite material that has been successfully used in a variety of structures. Other combinations such as steel-concrete and wood-steel are also routinely used in modern structures.

Using composite material technology, materials that satisfy most construction needs can be created. Material properties can be tailored according to specific needs, redundant use of material can be avoided and hence material performance can be maximised without a high increase in construction costs. All this effort leads to lighter and usually thinner structures.

Structural parts made of composite materials can be categorised as *fibrous* (which consist of fibres in a matrix), *laminated* (which are layers of various materials) and *particulate* (which are composed of particles in a matrix) composites. In fibrous composites the laminae are fabricated by combining two or more materials called matrix and fibres. The matrix is a weaker material with lower values of elastic

properties compared to the fibres. The matrix holds together the fibres transfers and distributes the external loads and protects them from external damage. Matrices are usually characterised by relatively low physical properties and provide cohesion with the other constituent materials. The fibres are usually stronger and are characterised by high values of elastic properties, thus playing the role of reinforcement. The final product of such a fibre-matrix combination is a solid body that to some extent retains the properties of the constituent materials.

Fibres can be made of glass, carbon, polymers or metals. E-glass is especially designed high-strength glass fibres that are extensively used in composite industry. Carbon and graphite fibres also have high modulus and strength and became economical over the last decades as a result of production capacity and demands. Polymer fibres, such as aramid fibres, can also be used in composites. A matrix can be made of polymers, metals or ceramics. The materials that are most widely used as matrix in modern composites are polymers such as epoxy, polyester, vinylester and several others, generally called plastics.

Fibres can be orientated in the matrix in several different manners. When all fibres are continuous and have the same direction, the composite is called unidirectional. If the fibres are randomly oriented in the matrix, the composite is called random. Fibres can also be non-continuous. An example of a unidirectional composites are schematically shown in Figure 1.1.

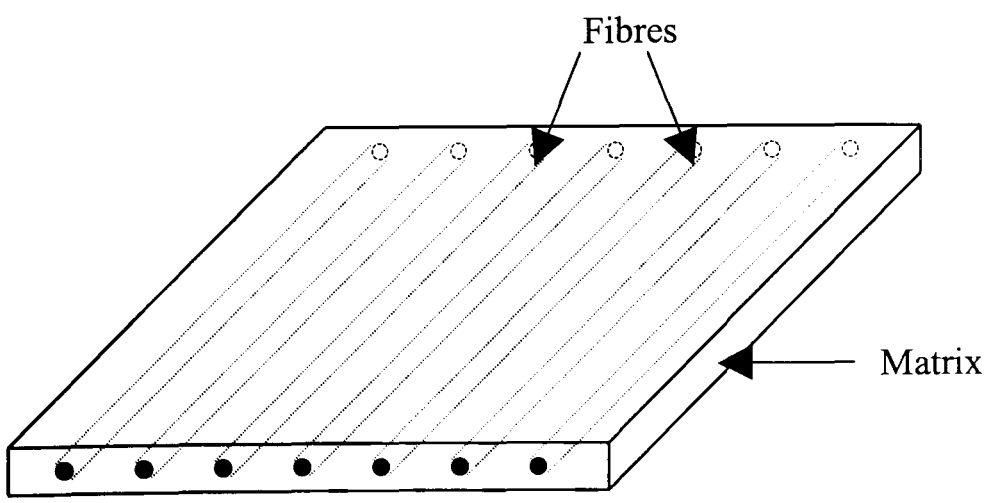

Figure 1.1 Unidirectional fibre reinforced composite

The composite structures that have been used in this thesis were fabricated from pre-impregnated unidirectional carbon fibre tape. However, in addition to unidirectional composites, a cross-ply composite structure was manufactured. For these types of structures, some layers of pre-impregnated tape were laid in a pre-determined fashion to ensure that the reinforcing fibres were orthogonal to each other. These samples were manufactured with embedded optical fibres to provide the overall structure with a built-in sensing system, which monitors the overall health of the material.

1.3 The Potential Benefits For Advanced Composite Materials That Could Arise From The Development Of Smart Structure Technology

The development of a built-in damage detection and evaluation system based on optical fibres embedded within the composite structure at the time of manufacture represents a new method of non-destructive evaluation (NDE). This represents the initial step towards 'smart structures' which would continuously monitor their internal strain and deformation, vibration, temperature, as well as structural integrity. This built-in sensing system might also be capable of monitoring the degree of cure during fabrication. This clearly has both safety and economic advantages and therefore could lead to a greater confidence in the use of advanced composite materials. In addition, the weight savings through the avoidance of over design should be of particular interest to the aerospace industry because of the substantial multiplier effect of such savings in aircraft and space structures. Figure 1.2 indicates the potential benefits for composite materials that could stem from smart structure technology.

Fibre optic sensors (FOS) offer a number of advantages over conventional sensors which have been considerably exploited with different types of sensors being developed over the last decade that can monitor virtually all physical parameters. Fibre optic sensors are still rapidly developing and significant advances in their use have been seen in the medical, engineering and scientific fields (Fuhr, 1993 and Melle, 1994).

These unique properties which have helped fuel the upsurgence of optical fibre systems in military and commercial applications are listed below.

- Increased sensitivity
- High bandwidth
- High linearity
- Geometric versatility
- Immunity from the effects of electromagnetic interference (EMI)
- High electrical isolation
- Performs sensing functions in hostile environments such as explosive or high temperature-prone areas.
- corrosion and fatigue resistant
- Practically incapable of initiating fires or explosions
- composite compatibility
- lightweight
- small and easily embeddable within the composite

These characteristics make optical fibres suitable for embedding within advanced composite materials, where they can both serve as sensors and as sensory signal carriers. This dual-purpose of fibres could be integrated into the 'fly-by-light' concept currently being considered for the next generation of aircraft. However, the realisation of such a concept could be set in motion by the advent of a smart component.

The realisation of a smart component can only be achieved if the component can recognise when it has been 'hurt' and assess the damage. This is analogous to a biosystem where the nervous system does this. Therefore embedded optical fibres have the potential to serve as an optical equivalent of such nerves. However, structures with a built-in sensing system only sense the environment but do not have the capability to determine the appropriate response to an environmental stimulus could be labelled 'sensory' structures. The term smart structure could then be utilised to describe structures that not only sense their state but have the ability to rectify it through structurally integrated actuator systems. Further development could lead to

the birth of 'intelligent' structures where the integration of neural network systems gives the structure the capability of adaptive learning. In short, the structure would **observe-analyse-decide-act**. If this was possible there would be an enormous potential in the following fields of application: Automotive, Aerospace, Defence, Civil Engineering, Advanced Manufacturing, and Biomedical. At present there are no truly intelligent systems, however, there are two routes that could be taken:

a) The construction of smart systems from existing technologies.

b) The development of smart systems from first principles, that is, new technologies.

At present, smart structures are being developed by bringing together existing technologies although 'clever' new materials such as electro-rheological fluids and shape memory alloys could provide the scope for development in the near future. However, the realisation of smart structures must commence with the development of a structural integrated fibre optic sensor. The four main important types of sensing relevant to smart materials and structures are (Measures, 1991):

- Strain measurements.
- Structural integrity measurements.
- Composite cure evaluation.
- Temperature mapping.

The damage detection of composite structures with embedded fibre optic sensors is one of the primary tasks for the development of smart materials and structures (Measures, 1989).

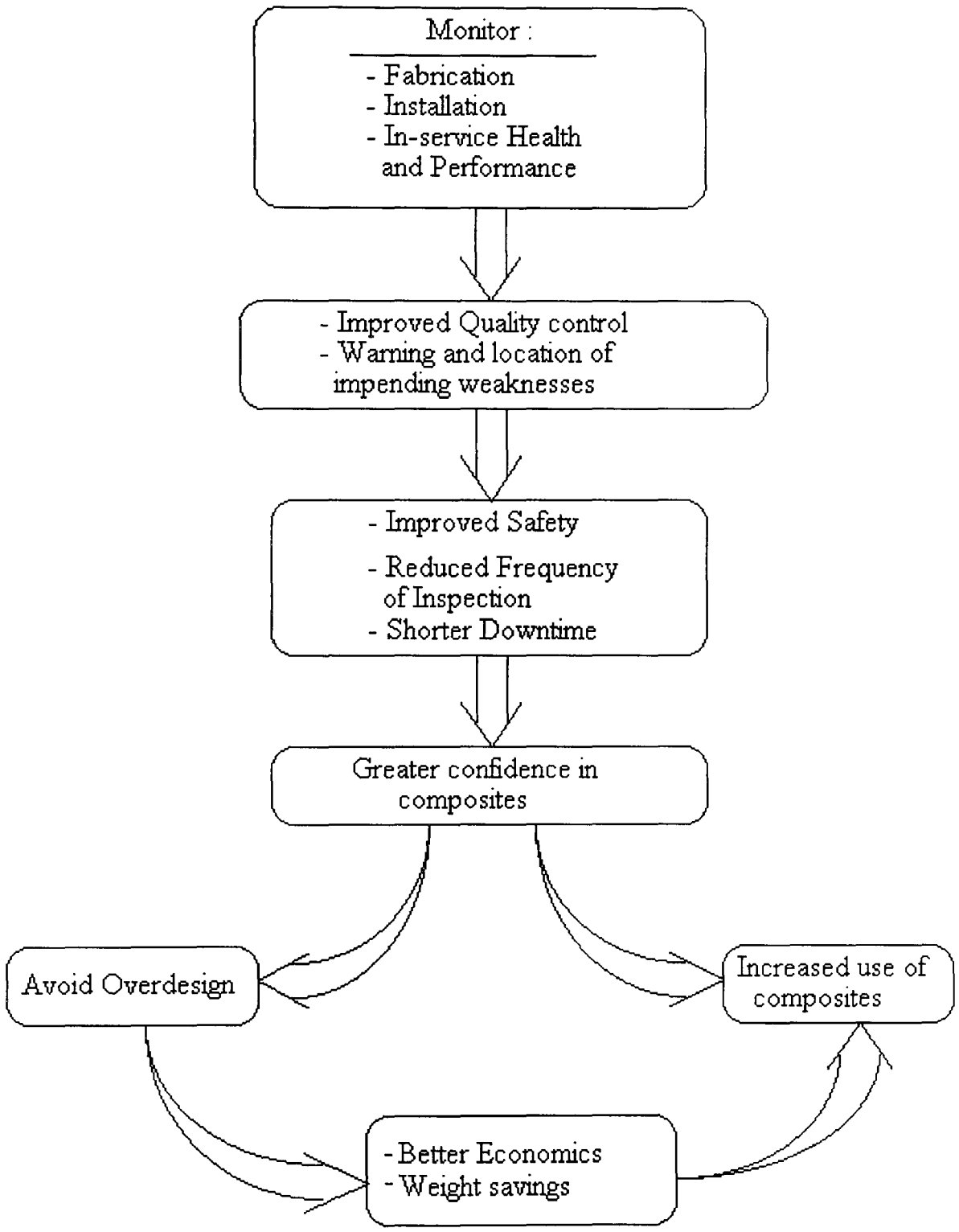

Figure 1.2 The potential benefits for composites from smart structure technology

1.4 Aims And Objectives Of This Thesis

This thesis aims to evaluate the state of health of a carbon fibre reinforced plastic (CFRP) composite component using both the all-fibre Mach-Zehnder interferometer and the PZ transducer. The primary aim of the reported research has been to demonstrate the feasibility of using this embedded fibre optic sensor to monitor the damage which had occurred under load in composites through the detection of the associated AE. The secondary aim was the interpretation of the collected AE information from both sensors. There were two categories of interpretation which were investigated: (1) the correlation of the AE data to the source of emission, that is, the specific damage mechanism, and (2) the determination of the point where the accumulated damage has become severe enough that the overall structural integrity of the component under consideration has been compromised in terms of safety and reliability.

The achieve these aims the following objectives have been satisfied :

1. Establish details of the application (Chapter 1)

2. Survey the possible structural evaluation techniques as it applies to composites and give the argument why AE is better than these other NDE techniques (Chapter 2).

3. Review the sources of AE in composites and how this AE is detected, processed and analysed (Chapter 3).

4. Review the technology which could be used to internally monitor its surrounding environment and the integrity of the composite component itself (Chapter 4).

5. Modify existing fibre optic sensor technology for the purpose of in-situ damage detection (Chapter 5).

6. Characterise the AE from composite samples under tensile loading using both the optical fibre sensor and PZ transducer (Chapters 6, 7, and 8).

7. Assess the prospects of this new approach in industry (Chapter 9).

1.5 Summary

The use of advanced composite materials, such as carbon fibre reinforced plastics, to form part or all of major structural components has become more common. Therefore, it is important to monitor the overall health of the component in-service. Many techniques have been developed in recent years to deal with effective non-destructive evaluation of composites. The detection and interpretation of acoustic emission events has been gaining a great deal of attention of the last twenty years and has emerged as a valuable NDE technique. Damage-induced acoustic emission can be detected easily using piezoelectric transducers, however, these transducers are contacted externally to the material surface. The development of a built-in damage detection and evaluation system based on optical fibres embedded within the composite structure at the time of manufacture represents a new method of non-destructive evaluation (NDE). The remainder of this thesis presents the development, evaluation and implementation of an embedded Mach-Zehnder interferometer fibre optic acoustic emission sensor, intended to monitor the damage sustained under load in carbon fibre reinforced plastics.

CHAPTER 2

SURVEY OF POSSIBLE NON-DESTRUCTIVE EVALUATION TECHNIQUES AS IT APPLIES TO COMPOSITES

2. Survey Of Possible Non-Destructive Evaluation Techniques As It Applies To Composites

2.1 Introduction To Non-Destructive Evaluation

In the time since the end of World War II, fibre reinforced plastics (FRP) have developed from a laboratory curiosity to a multi-million pound industry. The use of advanced composite materials to form part or all of major structural components is becoming all the more common and this marks a trend which is expected to continue into the next century. Currently, composite materials are employed in a variety of diverse items, such as aircraft, boats, Formula 1 cars, bullet proof jackets, and high performance sports equipment.

Clearly, if advanced composite materials are to be used in primary structural components, methods for characterising and monitoring internal flaws are required. The physical and chemical aspects of materials have been allied with the rapid advances in electronics and computing to produce the discipline of non-destructive testing (NDT) or non-destructive evaluation (NDE). In NDT, in flaw applications, the end product is taken to be the description of the flaws which have been detected, that is, their nature, size, and location. This information can be used in conjunction with either a standard for acceptable/rejectable flaws, or knowledge of the physics and chemistry of materials to come to a decision about the overall health of the tested item. This decision is either made by the designer or inspector. In NDE, it is assumed that this acceptance/rejection of flaws is part of the non-destructive testing process.

Composite materials must be regarded as very different media from metals when considering which NDT methods are appropriate. Generally, fibre reinforced plastics have low thermal conductivity, poor electrical conductivity, high acoustic attenuation and most importantly anisotropy of the mechanical and physical properties. The life of a metal component is determined by the nucleation and growth of cracks or damage in the material. The size of sub-critical flaws can be identified on the development of linear elastic fracture mechanics. However, a fibre reinforced composite is a

heterogeneous medium which can contain multiple defect geometries. Therefore, no single failure model can adequately describe the level of damage which is critical.

The ideal damage detection technique should be simple to use and be capable of identifying all of the failure mechanisms observed in composite materials. Flaws can be inadvertently introduced into composite laminates during processing and fabrication. These include contaminants, porosity and voids, fibre-matrix debonding, resin-rich areas, ply waviness, fibre and matrix fracture, inclusions and delaminations. These defects can also be induced or enlarged in service with age, loading and environmental conditions. These include matrix degradation, moisture absorption, surface cracks and scratches, damage zones around initial stress concentrations, impact damage and delaminations. The failure to detect defects associated with one of these factors can lead to the premature failure of the composite structure at some later date while still in-service.

Non-destructive evaluation has three major functions for research development and application in composite materials. These are:-

1) Initial inspection of test specimens and confirmation of the structural integrity of new components

2) Monitoring sample tests in progress, or components subjected to service loads.

3) Analysing test results after failure, or proof loading of components during service life.

The NDE of composite materials uses methods of damage detection and characterisation after fabrication and in-service to monitor damage growth under loading and environmental variations. This discipline also assesses the effects of these defects and establishes whether the structural integrity of the composite 'safe' or not.

At present, there are a number of NDT techniques available, however no technique is universal in its ability to identify all types of damage. The NDT technologies applicable to fibre reinforced plastics can be divided into three broad categories: electromagnetic, spectroscopic and mechanical. Figure 2.1 below indicates the techniques available under the above headings, sequenced from high to low frequency. In the following section a brief summary of a few techniques under the electromagnetic and mechanical categories will be given. The NDT techniques applied to fibre reinforced materials have been comprehensively reviewed in many publications (e.g. Summerscales, 1987, Summerscales, 1990, and Halmshaw, 1991).

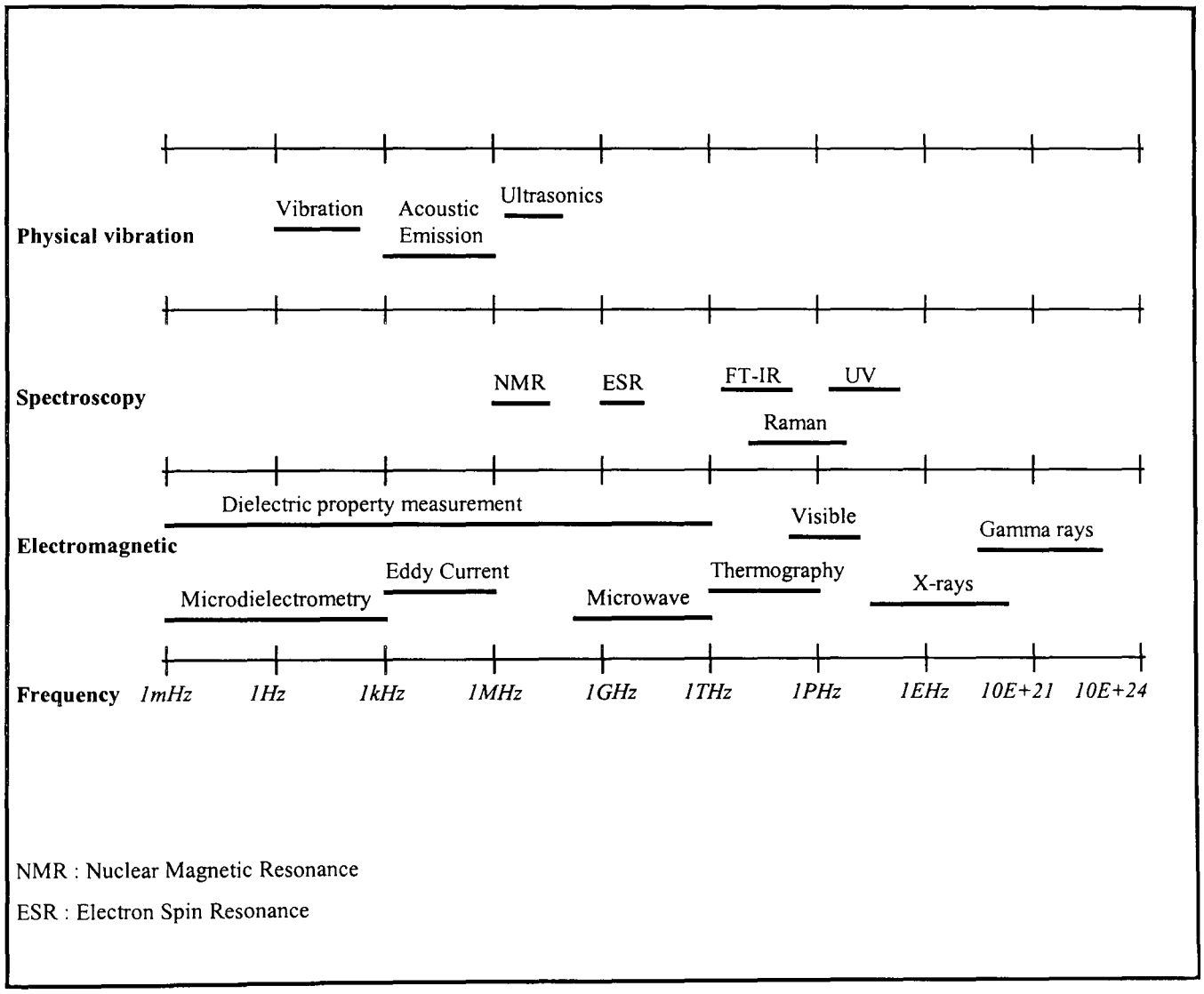

Figure 2.1 The frequency spectrum of non-destructive testing

2.2 Electromagnetic NDE Techniques

2.2.1 Radiography

The term radiography encompasses several methods of using high energy radiation for the examination of opaque objects. The beam energy can be generated electrically (for example, X-rays with a broad spread of wavelengths), by radioactive isotopes (e.g. gamma rays with discrete wavelengths), and by nuclear reactors. The output is typically recorded as a shadow-graph on photographic film. The molecules in FRP composites are usually of low atomic weight nuclei, and hence absorption of X- and gamma-rays is low and contrast is poor especially for thin laminates. Sufficient contrast may be developed with 'soft' low voltage X-rays. The use of penetrant (sulphur, tetrabromethane, silver iodide) enhancement produces improved images of surface breaking cracks. However, care must be taken to avoid penetrant systems which degrade the performance of the composite.

2.2.2 Visible Light

Visual testing can be one of the simplest of the NDT techniques for defects in transparent and translucent materials and surface defects in opaque materials. Various aids, such as magnifying glasses, microscopes, and high level illumination, can enhance visual tests.

In liquid penetrant techniques, the process relies on capillary action causing the liquid to enter surface breaking openings. This technique involves brushing, spraying or dipping of a pre-cleaned surface in the liquid. The surface is rinsed, dried, and a developer applied to draw the penetrant to the surface from the openings. However, the interpretation and analysis of the results often requires considerable experience in this type of technique. Brittle lacquer techniques have a similar capability to follow cracking as the specimen is loaded.

Another visible NDT technique is edge replication. Here, the edge of the sample is fine polished such that it is possible to view the fibres and matrix of the composite through a microscope. Acetate sheets can then be softened by acetone and pressed onto the edge of the sample to give a perfect replication of the damage at a specific point in the test. Liu et al (1987) extended the use of the edge replication from identification of matrix cracks in damaged composites to the study of delamination. Results from CFRP plates were in good agreement with other NDT techniques.

Other visible light NDT techniques include Moire pattern analysis, photoelasticity and optical caustics.

2.2.3 Coherent Light

The coherent light techniques are equally as applicable to conventional materials as to composites, as they monitor surface deformations. Surface finishes (smoothness and reflectivity) may affect the usefulness of these techniques, and the anisotropy may affect subsequent analysis. The three main techniques using coherent light are interferometry, speckle interferometry, and holography.

In interferometry, the interaction of beams of coherent light produce fringes which may be used for the measurement of surface deformation, and by subsequent analysis can produce strain plots.

Holography detects flaws by cancellations and interferences between two laser beams. Inhomogeneities or discontinuities affect the way the material deforms and causes a differential interference pattern to that in an undamaged composite. The technique is very sensitive and hence only minimal stresses, typically one or two degrees Celsius or a few millibars pressure change, are necessary to indicate defects. Detectable flaws include cracks, impact damage and delaminations.

In speckle interferometry, any diffusely reflecting surface, when illuminated by coherent light, appears to be covered by multiple bright and dark points. This speckle

field is recorded in coherent addition with either a reference beam or a further speckle field. This speckle interferometric technique is very sensitive (nanometre to micrometre movements) but suited only to small changes.

2.2.4 Thermography

Defects in composites exposed to either Externally Applied Thermal Fields (EATF) or Stress Generated Thermal Fields (SGTF) can be imaged by colour change coatings or by infrared cameras. The defect acts as a barrier to thermal conduction through the material or the stress concentration generates heat under stress, and therefore the thermal field differs from that of a good material.

2.2.5 Microwaves

Microwaves are a band of frequencies from 225 MHz to 100 GHz and are capable of penetrating most non-metallic materials, reflecting and scattering from internal boundaries and interacting with the molecules. Three factors (shape/dimensions, dielectric constant, and loss tangent) influence the penetration of materials by microwaves. The sensitivity to the dielectric properties of the material makes microwave testing particularly effective for internal structure (orientation), homogeneity (resin-rich or resin-poor areas), state of cure, moisture content, ageing, and porosity. Microwave systems are also capable of detecting internal flaws (such as delaminations, voids, and inclusions) as well as precise measurement of distance, thickness and surface waviness.

2.2.6 Electric

The electrical resistivity of commercial FRP varies in value by fifteen decades from the high resistivities of aramid/epoxy to the conducting carbon fibre materials. These properties have been used non-destructively to monitor laminate thickness, fibre orientation, moisture content and crack growth. The current-voltage characteristics

have been used to monitor the curing reaction of the thermosetting resin and to follow thermal degradation.

2.3 Mechanical Vibration NDE Techniques

Another broad NDT area of interest is that of mechanical testing. This category is sub-divided into three areas: vibration, acoustic emission and ultrasonics. Mechanical vibration can be propagated in solids, liquids and gases. The actual particles of matter vibrate, and if the mechanical movements of the particles have a regular motion, the vibrations can be assigned a frequency. There are many techniques which use mechanical vibration to help determine the structural integrity of composite structures. Figure 2.2 shows the spectrum of vibration and sound used for inspection and testing.

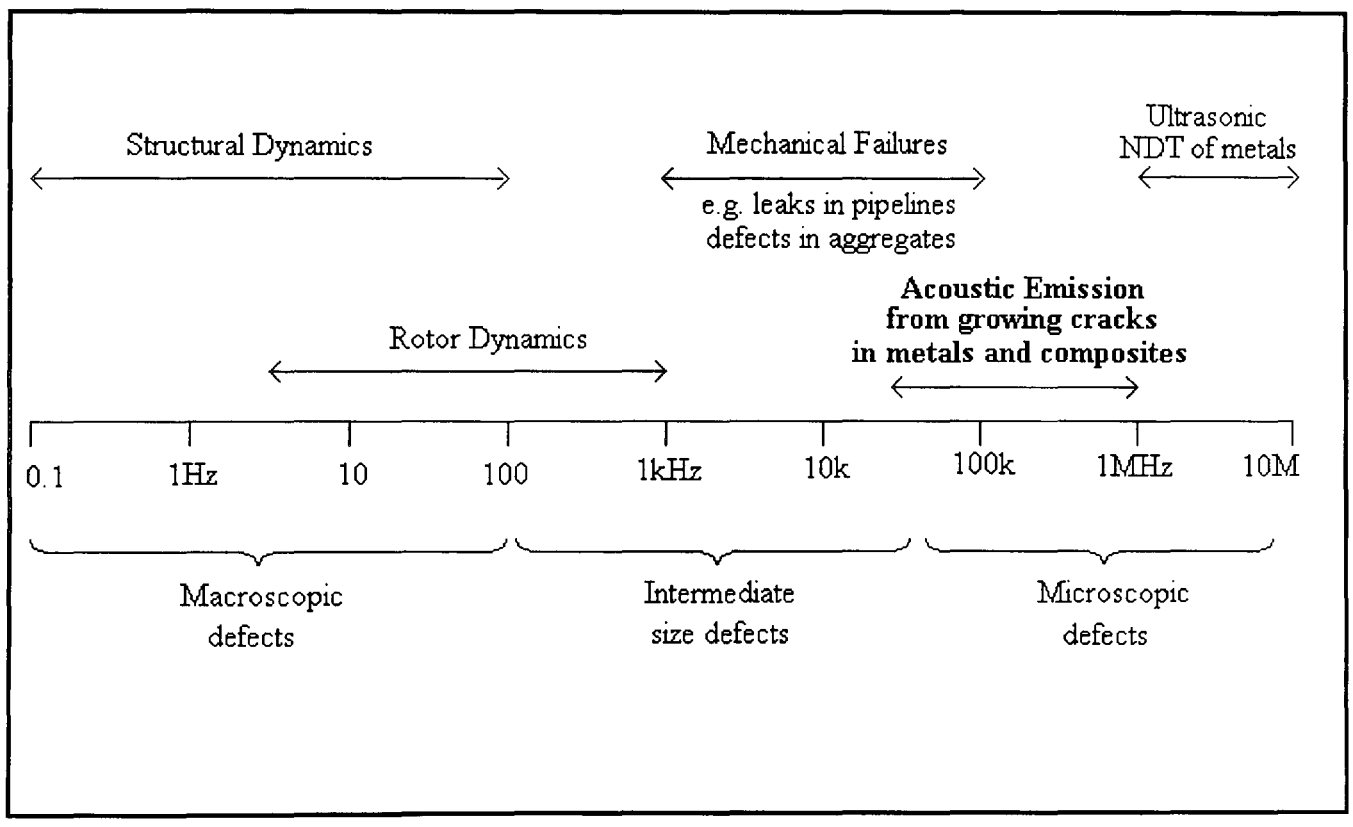

Figure 2.2 Spectrum of vibration and sound used for inspection and testing

2.3.1 Ultrasonics

There are a few ultrasonic methods which can monitor the health of a composite structure; through-thickness, in-plane and Lamb wave. The simplest method of

ultrasonic testing is to transmit a short pulse of high-frequency (typically 550k-10MHz) energy through the specimen and to measure the transit time or attenuation of the signal. The measurement may be either through-thickness (separate transmit and receive transducers on opposed faces of the sample) or pulse echo (reflecting the signal from a flaw or from the back face of the specimen and using a single transmit-receive transducer). The attenuation is a function of the state of cure/viscoelasticity of the matrix resin, and the condition of the fibre/resin interface with dispersion due to the fibres, voids, delaminations and foreign inclusions.

There are several display options used for ultrasonic testing with the most commonly used modes being A-scan, which presents only data at a single position, and C-scan which presents a plan view of the attenuation as a grey-level or colour-coded image. The A-scan contains all the data required to establish the position and severity of individual flaws, while the C-scan presents an integration of that data through the depth of the component.

The wave-velocity and attenuation of ultrasonic waves travelling in the plane of the plate (rather than through the thickness) can also be used in ultrasonic NDT. These parameters are orientation dependent. The wave-velocity in the material is a function of the elastic modulus (appropriate to the mode of propagation) which is affected by the presence of flaws. When the wavelength is large relative to the flaws the sound velocity reflects the changed stiffness and signal attenuation is increased by scattering with a strong dependence on the volume fraction of the inclusions. A critical frequency (attributed to the excitation of fundamental resonances of fibres and voids) exists where both wave-velocity and attenuation are highly sensitive functions of frequency. As damage increases, the ultrasonic pulses are broadened (dispersive effects) and measurements of acoustic parameters become increasingly difficult.

Composite materials are usually employed as thin-shelled structures, and as such the introduction of ultrasonic energy can result in plate waves in the component, rather than the body waves used for traditional ultrasonic NDT. The propagation of plate (Lamb) waves is more complex than that of body waves. Several modes of

propagation exist, being either symmetric (longitudinal) or asymmetric (flexural) with respect to the midplane of the plate. Lamb waves are dispersive (velocity depends on wave number and hence on frequency) and a cut-off frequency exists below which the Lamb wave cannot propagate.

2.3.2 Acousto-Ultrasonics

In the acousto-ultrasonic technique, a broadband pulser delivers a repeating series of 'low-frequency' ultrasonic pulses into the structure. The modified stress wave received by an acoustic emission transducer contains a 'fingerprint' of the structure which is a characteristic of the defective material between the two transducers. As the stress wave travels through an impacted area there is a loss of high frequency energy and a slowing of the wave propagation velocity. Examination or the amplitude-frequency-time parameters provides qualitative information on the integrity of the structure. Such information is often quantified as Stress Wave Factors (SWF).

2.3.3 Fracto-Emission

Fracto-emission is the release of particles (electrons, positive ions and ground-state or excited neutral particles) and photons (light and radiowaves) before, during and after the propagation of a crack in a stressed material. These various types of fracto-emission, together with acoustic emission, share some common features indicating that they are all produced by a common mechanism. Photon emission is more frequently referred to as chemiluminescence, mechanoluminescence or triboluminescence.

2.3.4 Vibration

When a complete object is caused to vibrate at its natural frequency, it will ring in a characteristic way if good but sound dull if cracked or defective. The use of a single tap to excite the vibration of the complete structure is known as 'wheel-tapping'. The logical progression from wheel-tapping is the use of modal analysis in which a

structure is continuously excited by a slow-ramp changing frequency and the damping of the structure is monitored. This method has been used for inspecting filament wound tubes in a production environment.

The quality of a composite material can also be assessed by tapping a succession of locations with a coin or tapping-hammer. the sound of good and bad areas is qualitatively different to the human ear, with a clear ring at good positions and a dull sound in poor areas. The technique has been automated by an instrument known as the Tapometer.

2.4 Acoustic Emission And Its Advantages Over Other NDE Techniques

Previous sections have indicated that major NDT techniques use either electromagnetic waves (from high frequency gamma- and X-rays through visible light to low frequency eddy current methods) or high frequency sound waves (ultrasonics in its various forms). One method that falls into the second category is **Acoustic Emission** (AE). The term acoustic emission, sometimes referred to as stress wave emission, is a collective term for the generation, propagation and detection of stress waves resulting from rapid changes in the local internal stress state of a structure.

The phenomena of AE was discovered nearly 60 years ago, however, it has been claimed (Drouillard, 1988) that the first documented observation of AE may have been made by Jabir ibn Hayyan in the 8th century. Initial documentation reported the phenomena emanating from metals, rocks and pit props (Scott, 1991). The resulting clicks from the formation of martensite in high nickel steel are taken to be the first authentic documentation on acoustic emission. A report published for the U.S. Bureau of Mines commented on the 'use of sub-audible noise for prediction of rock bursts'. This report noted that the noise rate increased as the structure became more highly loaded. Historically, a few high energy AE processes have been observed from twinning in tin (or 'tin cry' as it is commonly known).

The first major systematic approach to acoustic emission from materials under stress is generally accepted to be the thesis by Josef Kaiser at the technical high school in Munich in 1950. This breakthrough, in terms of involving the detection, processing and analysis of the AE activity, involved single and repeated load tests on metals. Kaiser concluded that the number of emissions increased with the applied stress and that after unloading there was no acoustic emission upon reloading until the previous maximum load was exceeded (Henning, 1988). This latter effect is known as the Kaiser Effect and is observed in both metals and composites. However, the Kaiser Effect does not always occur. Fowler (1982) presented the case where emissions did occur upon reloading at the specific fraction of the previous load. This is known as the Felicity Ratio.

Over the past 40 years, AE has developed rapidly from a laboratory technique to an industrial NDT method. Early work concentrated on the use of AE to monitor the structural integrity of various metals, although more recent work has been much wider, with demonstrated capabilities for monitoring structural integrity, detecting leaks and incipient failures in mechanical equipment, and for characterising materials behaviour (Ono, 1995).

AE offers a number of advantages which give this technique some unique capabilities and are the reason behind the upsurgence in this technique (Miller, 1987). Among these are:

1. *High sensitivity*

   AE can be sensitive to minute increments in crack length (approximately 1 micron).

2. *Real-time capability*

   AE testing can take place while the structure is still in-service. Ultrasonic C-scan techniques requires that the component to be tested must be taken out of service for immersion in an ultrasonic scanning tank. Ultrasonic techniques

usually require computer operation and control and expensive automated systems (offshore-divers, adverse weather conditions).

3. Passive technique

Energy that is detected is released from within the test material rather than being supplied by the non-destructive method. Ultrasound and radiography (X-rays) transmit energy through the material on a path that will properly intersect the area of interest to assess the damage.

4. Essentially non-localised

It is not necessary for the receiving transducer to be particularly near the source of the emissions or the area under inspection. AE examination is non-directional. Most AE sources appear to function as point source emitters that radiate energy in spherical wavefronts. A sensor located anywhere in the vicinity of an AE source can detect the resulting AE. This is in contrast to other methods of NDT which depend on prior knowledge of the probable location and orientation of a discontinuity in order to direct a beam of energy through the structure on a path that will properly intersect the area of interest.

5. Ability to monitor larger volumes of material

AE can detect and evaluate the significance of discontinuities throughout an entire structure during a single test. In offshore applications the structural integrity of a critical section can be monitored using a dozen AE transducers whereas ultrasonic methods would need approximately a thousand sensors.

6. Only limited access to material under inspection is required

Discontinuities can be detected in parts of the structure which are inaccessible to other NDT techniques.

7. Capable of detecting dynamic processes associated with the degradation of structural integrity

AE is a dynamic inspection method, in that it provides a response to discontinuity growth under an imposed structural stress. Static discontinuities will not generate acoustic emission.

The advances in signal detection, processing and analysis techniques have also increased the interest in the structural evaluation of composites. Recent trends indicate an abundance of faster digital instruments including computers and user friendly AE instrumentation.

2.5 Summary

In recent years there has been an increased use of advanced composite materials in a variety of applications, for example, aircraft structures, sports equipment and automotive components. These materials offer high specific strength and stiffness properties, excellent fatigue and corrosion resistance and can be used to manufacture complex component shapes. However, the structural integrity of the component may deteriorate under service conditions and environmental effects. Once initiated, damage can develop and is not readily by evident visual inspection or other NDT techniques. The phenomena of AE lends itself well to the NDE of composites because it arises from a flaw under load or a damage event in a material, and the generated elastic waves propagate outwards from the source site. Secondly, AE examination is non-directional. Often, a sensor located anywhere in the vicinity of an AE source can detect the resulting AE, which is in contrast to other methods of NDE. These advantages have lead to the increasing use of AE as a measurement tool to provide advance warning of potential structural failure.

CHAPTER 3

ACOUSTIC EMISSION IN COMPOSITE MATERIALS

3. Acoustic Emission In Composite Materials

The development of an optical fibre sensor for acoustic emission detection in composite materials requires an understanding of several distinct fields of study. To understand the performance of the sensor and to appreciate the difficulties associated with the system, consideration must be given to the nature and sources of acoustic emission in a solid material, the properties of acoustic waves propagating in a composite material, and the acoustic emission signal detection processing and analysis. This chapter considers each of the above mentioned topics in turn, with the aim of providing the necessary background for the subsequent components of this thesis.

3.1 Understanding The Phenomena of Acoustic Emission

An understanding of the phenomena of acoustic emission is fundamental to the development of the FOS system designed for its detection. Therefore, it is useful to consider the basic definition of AE, its mathematical description, and the sources of AE in composite materials. Acoustic emission is generally defined as a rapid release of internally stored energy from localised sources within a material; the energy appears in the form of transient elastic waves.

It is evident from section 2.4 that the phenomena of AE lends itself readily to non-destructive evaluation due its various advantages over other techniques. This technique significantly differs in two respects. Firstly, the energy that is detected arises from a damage event in a material, and the generated elastic waves propagate outward from the source site. Secondly, dynamic processes associated with the degradation of the health of the composite can be detected through AE. Over the past few decades the advantages of AE over other techniques has resulted in a sharp increase in activity among those interested in exploiting this technique as a diagnostic tool for materials and structures. The flaw type, damage severity and location can be ascertained from the analysis and interpretation of the signal characteristics.

3.1.1 Mathematical Description Of Acoustic Emission Signals

Acoustic emission, as defined in section 3.1, is the term given to an elastic wave generated by the redistribution of stress in a material. It is important to distinguish between an AE wave and an AE signal; the latter refers to the electrical response of the sensor employed for the detection of the propagating wave. The characteristics of the signal are not necessarily those of the source due to distortions introduced by the material properties, the geometry of the specimen, and the sensor itself.

Acoustic emission signals have been observed to have amplitudes much higher than the background level and relatively short durations (a few μsec to a few msec). Although the signals are rarely simple waveforms, they usually reach maximum amplitude early in the signal, and decay exponentially to the level of background noise. Based on these observations, it seems appropriate to adopt a simple model for the emission waveform that takes the form of an exponentially decaying sinusoid (Miller and McIntyre, 1987),

$$V(t) = V_o\exp(-Bt)\sin(\omega t) \qquad \text{(eq. 3.1)}$$

where V(t) is the output voltage of the sensor, V_o is the initial signal amplitude, B is the decay constant, ω is the signal frequency, and t represents time. The graph of (eq. 3.1) is represented in figure 3.1.

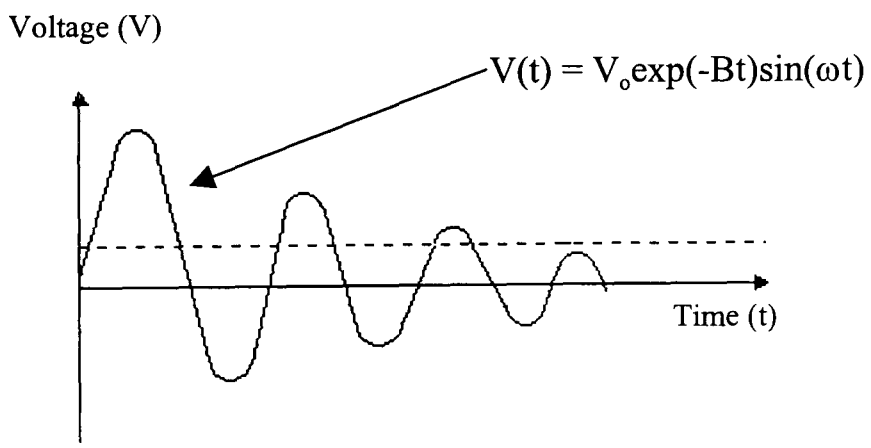

Figure 3.1 Schematic diagram of an acoustic emission signal based on a simple mathematical model.

Signals are often broadly classified as either burst-type or continuous emissions. The differences found between these two types are the amplitude levels, durations, and time between signals. Some authors maintain that continuous emission is actually a superposition of many burst-type events, spaced so closely in time that the instrumentation cannot resolve the individual events (Raj and Jha, 1994). The amplitude of continuous emission is typically lower than that of burst emission. The amplitude of an acoustic emission process generally has some correlation with the volume of the region producing it. Since continuous emission is a superposition of many bursts, the volume of each region producing a burst is necessarily small. Therefore, the amplitude of each burst is small and thus the continuous emission is low (typically slightly above background levels). However, burst emissions are characterised by signal amplitudes appreciably larger than background levels, short duration, and a large separation time between signals.

3.1.2 Damage Mechanisms In Composite Materials

The development of damage in a composite material is a complicated process and can involve several fracture mechanisms. The primary sources of acoustic emission from a composite specimen undergoing damage are:

(i) *Fibre fracture*

Since the fibres represent the principal load-bearing constituent of a fibre reinforced composite, fibre fracture can have a severe effect upon both the stiffness and strength of a multi-directional composite. Fibre fractures are likely to be the most detrimental to the tensile strength of a composite specimen. In fibre fracture, the energy released depends on the fibre-matrix interaction, and increases when fibre-matrix adhesion decreases. A fibre break involves a redistribution of stresses in adjacent fibres and can originate multiple fibre fractures. In the same way, a fibre break can involve processes of interlaminar failure or matrix cracking parallel to the fibre in the neighbouring crossed layers.

(ii) *Matrix fracture*

Matrix cracking can occur in three different modes: transverse cracking normal to the fibres, longitudinal cracking parallel to the fibres, and interlaminar cracking, according to the composite microstructure and loading conditions. In unidirectional composites loaded at 0° with fibre direction, matrix cracking occurs essentially transversely to the fibres. The cracks, initiated either in the matrix or at the fibre/matrix interface, propagate in the matrix by jumps from one fibre to another.

(iii) *Fibre/matrix debonding*

When the stress in the fibre-matrix interface exceeds the local strength, debonding occurs and a crack forms.

(iv) *Fibre/matrix rubbing*

Once the fibre has debonded, further loading results in a differential displacement between the fibre and the matrix, and a frictional force occurs between the two constituents.

(iv) *Fibre pullout*

In a region of high stress concentration, such as at a tip of an advancing crack, fibres often fail and fracture. As the crack front continues to advance, these fibres are pulled out of the surrounding matrix.

In terms of macroscopic sources, AE will arise from:

(v) *The propagation of intralaminar and interlaminar cracks*

During these failure processes, relatively large fracture surfaces are created. Therefore, sometimes it is suggested that high amplitudes are associated with these rupture processes in the case of carbon composites. However, if a signal corresponds to a unique event a high value of surface created will be associated with a large event duration.

(vi) *Debonding between lamina (delamination)*

Delamination is one of the most frequently discussed modes of failure. In multi-directional composites, delamination propagates at the ply interfaces. Liu (1988) has shown that under low velocity impact loading conditions delamination is most severe at interfaces at which the difference in relative angle between the upper and lower plies is greatest.

Amongst the failure modes presented above, delamination-type damage gives the greatest cause for concern since large areas of this form of interlaminar fracture can be generated under low impact conditions. Other forms of damage, such as fibre fracture and matrix cracking, are also detrimental to the residual performance of composite materials. Although the extent and severity of damage incurred may be less severe than delamination, they can reduce the short and long-term strength of the material significantly.

There exists, therefore, a clear need to identify and characterise damage in composite materials at the earliest possible opportunity. The ideal damage detection technique should be simple to use and be capable of identifying all of the failure modes observed in composite materials.

The amplitude and spectral content of AE signals generated in composites are dependent upon applied load, existing material damage, and type of material under examination. Applied load determines the amount of energy stored in the material, and the material properties determine the amount of dispersion and attenuation a propagating acoustic wave will experience.

Attempts have been made to obtain an 'acoustic signature' for the specific damage mechanism responsible for a given acoustic signal, but only limited success has been achieved. Results reported in literature have utilised a variety of measured parameters and some authors claim to have established links between measured quantities and actual damage mechanisms.

Sato et al (1986) attempted to characterise the AE from CFRP using amplitude distribution analysis. They reported that a close correspondence between the acoustic signal and the crack formation that was obtained. They stated that the acoustic signal at lower amplitude which occurred over the whole load range, corresponded to fibre breakage and matrix cracking. Whilst higher amplitudes, occurring just before failure, corresponded to partial delamination. Mittleman and Roman (1991) used the event count rate and the skewness of the peak amplitude distribution to correlate the mechanical and damage mechanisms in unidirectional Kevlar/epoxy composites loaded in tension. They found that towards failure the skewness of the peak amplitude distribution increased due to macroscopic failure modes.

Barre and Benzeggagh (1994) performed tensile and crack propagation tests on short glass-fibre-reinforced thermoplastics to identify damage mechanisms by their AE amplitudes. Using scanning electron microscopy to confirm the mechanisms present they were able to establish that matrix cracking exhibited the lowest amplitude distribution with fibre fracture having the highest. They also found that interface fracture and fibre pull-out had amplitude distributions in the intermediate range with the former exhibiting amplitudes lower than the latter. Ceysson et al (1996) also claimed success in identifying matrix cracking and delamination in carbon fibre/epoxy; they analysed the peak amplitudes of the collected AE signals to associate the matrix cracking and delamination to two distributions (centred at 50dB and 62dB respectively). Ono (1988) reported on the acoustic emission behaviour from specially designed CFRP composite samples. The discrimination between fibre fracture, delamination, debonding and friction could be made on the basis of peak amplitude and event durations of the observed AE signals.

Kawamoto and Ono (1986) used the pattern recognition analysis method to analyse the AE signals from CFRP samples under tension. They were able to classify signals corresponding to delamination in lap-joint samples. Degroot et al (1995) monitored the AE frequencies characteristics generated by different failure mechanisms. Using specially designed samples they were able to determine that low and high frequency distributions were due to matrix cracking and fibre fracture respectively. Berthelot and

Rhazi (1990) claimed success in correlating certain damage mechanisms to acoustic activity in CFRP samples. The test specimens used were subjected to flexural loading so as to separate fracture initiation and propagation. Using amplitude analysis and event duration, the authors were able to discriminate between fibre fracture, matrix cracking, delamination and fractured surface frictions.

Zimcik et al (1988) use waveform analysis for carbon/epoxy composites taken during mechanical (impact) testing to identify mode and location of impending failure. They detected the presence of a predominant high frequency component at the onset of internal damage. As the load increased, they reported that additional frequency components appeared. Near the mid-range of the load, a medium range frequency component also appeared followed by the addition of a low frequency component near the failure load. They attributed the low and high frequency components to matrix cracking and fibre fracture respectively. They suggested that the mid-frequency range was linked to other possible damage mechanisms.

Hamstad and Moore (1986) attempted to characterise the acoustic emission from Kevlar filament fracture by loading Kevlar fibre, in the form of single filaments and fibre bundles, to failure. They reported that a statistical study of peak amplitude, number of counts, and event duration showed considerable variation for the single-source mechanism of filament fracture.

Qi et al (1997) have used wavelet-transform-based decomposition of the AE signals to help distinguish between the damage mechanisms occurring in unidirectional and cross-ply carbon fibre reinforced composite specimens under static loading. The authors resolved the AE signals into the time and frequency domains and then decomposed into various wavelet levels. Each level was examined for its specific frequency range, energy change rate, and percentage of total energy. They found that energy in the AE signals was concentrated in three levels representing the frequency ranges of 50-150kHz, 150-250kHz, and 250-310kHz. They concluded that matrix cracking, fibre/matrix debonding, and fibre fracture were responsible for these respective frequency ranges.

Wevers (1997) monitored the AE signals from a quasi-isotropic CFRP as it was step-wise loaded in tension up to 70% of its ultimate tensile strength. From this data, cluster analysis was carried out for each step of the monotonic tensile test. Pattern recognition analysis was also carried out on all of the data detected. The use of penetrant enhanced radiography helped the author correlate the clusters to certain damage mechanisms. The author concluded that the initiation and growth of matrix cracks exhibited amplitudes which varied from low to medium (40-60dB). Delamination exhibited amplitudes which varied from medium to high (>60dB), while friction caused AE signals with medium amplitude values. The author also concluded that certain damage mechanisms could only be proven by using other complementary non-destructive techniques such as edge replication and radiography.

Pappas et al (1998) presented an innovative methodology for the analysis of AE activity monitored during the quasi-static tensile loading of centre hole ceramic matrix composites. The authors developed an analysis algorithm which contained descriptor selection procedures, validation techniques, filtering and statistical analysis of AE data. They also used the knowledge of the damage mechanisms appearing in these types of composites through microscopical fractographic examination. From this, the authors were able to make a correlation between clusters and different failure mechanisms such as friction, multi-fibre failure, fibre/matrix debonding and fibre pull-out.

Philippidis et al (1998) stated that previous work on CFRP specimens involved amplitude distribution analysis of the AE signals. They mention that matrix cracks give rise to AE signals with amplitudes lower than 45dB, fibre/matrix debonding between 45-70dB, while fibre breaks give signals with amplitudes higher than 75dB. However, they state that these results do not have any universal validity for FRP composites. To correlate the AE signals to the failure mechanisms occurring in Carbon/Carbon woven laminates, the authors used the unsupervised pattern recognition technique detailed in Pappas et al (1998). Through a modified Learning Vector Quantisation (LVQ) technique, the authors were able to identify various failure mechanisms that occur in woven composites from clusters of AE signals.

Takahashi and Choi (1998) analysed the AE signals that emanated from short-fibre reinforced plastic composites under tension. They concluded that AE with higher amplitude was due to fibre breakage, whilst fibre/matrix debonding and matrix cracking emitted lower amplitude waves.

Krietsch & Bohse (1998) introduced a new selection method which works for transient acoustic emissions from composite specimens. The method simplified the parameters of waveform recording and reduced noise parts of AE data files. The authors suggest that their selection method could help save storage by directly recording emissions instead of using fixed record times and threshold parameters. They also suggest that the classification of selected damage mechanisms could be made by averaging the power spectra in combination with amplitude filters. The results obtained by the authors showed that matrix cracks exhibit low frequencies, whereas fibre breaks exhibit high frequencies.

3.2 The Propagation of Acoustic Waves In Solid Materials

The description of sound waves propagating in a solid material is one of considerable complexity. It is instructive to first examine the basic features of acoustic wave motion which can be accomplished by considering wave propagation in an infinite elastic and isotropic medium. Once the fundamental characteristics are established a more complete description of acoustic wave propagation in a material can be constructed by replacing each simplifying assumption with a more realistic one. In the case of a composite material, this involves consideration of inhomogeneity, anisotropy and the material boundaries.

3.2.1 Bulk Waves In Isotropic Solids

The simplest case of wave propagation is that in an infinite unbounded solid medium, that is, a medium which has no boundaries. Two and only two distinct types of bulk waves can exist in an infinite isotropic elastic media (Miller and McIntyre, 1987).

Longitudinal or primary waves (P-waves) are associated with volume changes in the material and are characterised by coincident particle displacement and propagation directions (figure 3.2a).

This schematic shows the motion of particles in a medium in which a plane longitudinal wave is propagating. In this diagram, the circles represent the adjacent particles in the medium and the direction of wave propagation is from left to right. As the wave propagates through the material, the particles move closer together and then move apart. This occurs along the axis parallel to the direction of wave propagation. However, the particles retain their original spacing when the wave passes.

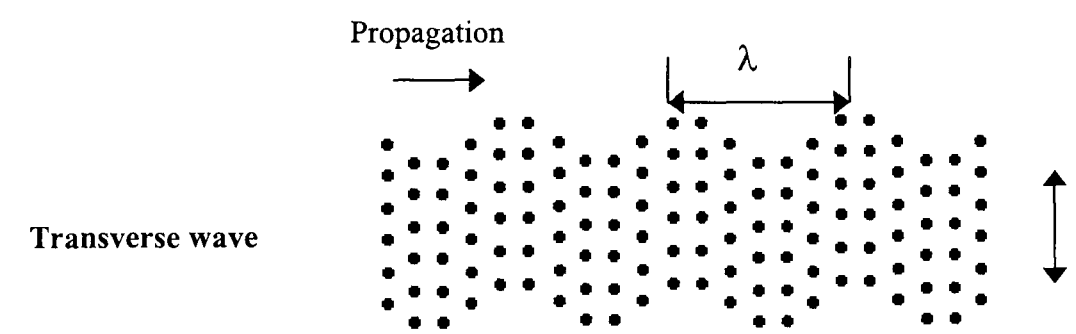

Figure 3.2 (a) Longitudinal and (b) transverse (shear) waves in solids [adapted from Miller and McIntyre (1987)]

The second type of bulk waves is the transverse or secondary waves (S-waves), these are associated with shear motions, such that the particle displacement and direction of propagation are mutually normal (figure 3.2b). Here, the particles move in a vertical direction as the wave propagates from left to right. Since transverse waves involve shear deformations in the solid, they are referred to as Shear waves. There is no coupling between the two modes, so longitudinal and transverse waves represent independent motions.

The propagation velocities of these waves are determined by the mechanical properties of the solid. In terms of these properties, S-wave velocity (c_β) is determined solely by the shear modulus of the medium, whereas the P-wave velocity (c_α) is influenced by both the shear and bulk moduli. The velocities can be expressed in terms of the elastic properties of the medium under consideration:

$$c_\alpha = \sqrt{(\lambda+2\mu)/\rho} \qquad \text{(eq. 3.2)}$$

and

$$c_\beta = \sqrt{\mu/\rho} \qquad \text{(eq. 3.3)}$$

In the above equations, ρ is the density of the material, and λ and μ represent the bulk and shear moduli, respectively. Another important acoustic parameter when considering the propagation of sound waves in a material is characteristic impedance. This can be expressed as:

$$Z_i = \rho V_i \qquad \text{(eq. 3.4)}$$

where ρ is density (as above) and V_i is the speed of the particular wave under consideration. When considering an interface between materials, the difference in characteristic impedance between the two determines the relative amount of reflected and transmitted acoustic energy.

3.2.2 Boundary Effects

When boundary conditions are imposed by the introduction of free surfaces, the picture becomes considerably more complex. Near a surface, the longitudinal and transverse waves that propagate through the bulk of the material combine to form a type of surface wave known as a Rayleigh wave.

Rayleigh waves exhibit a particle motion that is neither purely longitudinal nor purely transverse. These type of waves occur because compression displacements near a surface generate corresponding transverse displacements in accordance with the Poisson's ratio of the material. Another class of surface waves (Love waves) exist; a distinction is made between Rayleigh and Love waves because the former identify particle motion perpendicular to the boundary (surface), whereas the latter identify particle motion parallel to the boundary. Most surface mounted acoustic emission sensors respond to motion perpendicular to the surface, and are therefore detecting Rayleigh, as opposed to Love waves.

Rayleigh waves are associated with characteristic velocities, which can be calculated from the physical constant of the material. In particular, the Poisson's ratio of the material figures prominently in determining the Rayleigh wave speed. Generally speaking, the Rayleigh wave velocity will be lower than that of either bulk wave. That is:

$$c_R < c_\beta < c_\alpha$$

In a medium bounded by two surfaces (that is, a plate), the waveforms couple at the surfaces to produce Lamb waves of two basic modes: symmetric and asymmetric. The two modes are distinguished by the particle displacement at the plate centre line; symmetric modes show longitudinal displacement and asymmetric modes show transverse displacement (figure 3.3). When the acoustic wavelengths approach the dimensions of the plate thickness, higher order modes of each type are possible, each mode with a characteristic group velocity dependent on the plate thickness. At these wavelengths, dispersion will be evident for a given plate thickness regardless of material considerations.

3.2.3 The Effects Of A Non Ideal Material On The Wave Propagation

Other important factors that influence the propagation of acoustic wave in a solid material are inhomogeneity and anisotropy. Composite materials, because they are

made up of two or more physically distinct constituents, are inhomogeneous by definition. For the purpose of describing the effects of inhomogeneities on acoustic waves, the material fibres of the composite can be viewed as obstacles that will be encountered by an acoustic disturbance propagating through the host medium.

(c) Rayleigh wave

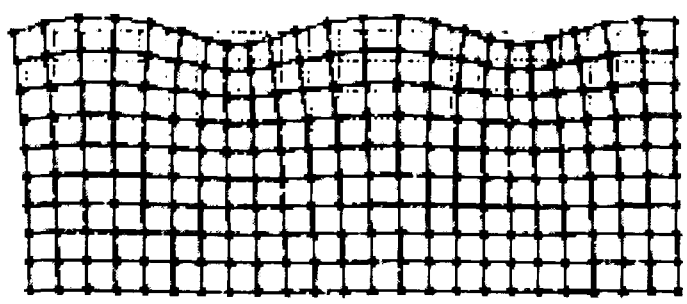

(b) Plate wave - first symmetric mode

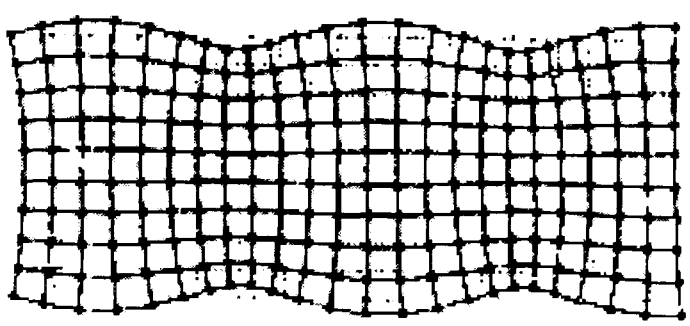

(c) Plate wave - first asymmetric mode

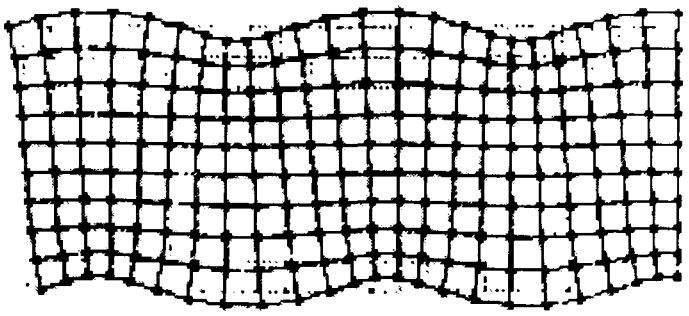

Figure 3.3 Particle displacements for acoustic waves

There are several phenomena of interest when considering wave-obstacle interactions. Diffraction of the original disturbance occurs, which essentially means that the wave has deviated from its original path. As well, the obstacle itself comes a source of radiation after being excited by the original disturbance, and give rise to scattered waves in a surrounding medium and refracted waves within the obstacle. Composite laminates, in addition to being inhomogeneous, are anisotropic materials. The effect of this anisotropy is to create different wave velocities in different directions. The net result of the various factors mentioned above is to considerably alter the nature of the

wave originally emitted as it travels from source to detector, making the source characteristics difficult to recover.

3.3 Failure Mode Depends on Loading

Examination of a failed fibre-reinforced plastic (FRP) composite generally provides clues as to the type of load that caused failure. The illustration below (figure 3.4) show the principle failure modes in a uni-directional composite caused by tensile, compressive, and shear loads.

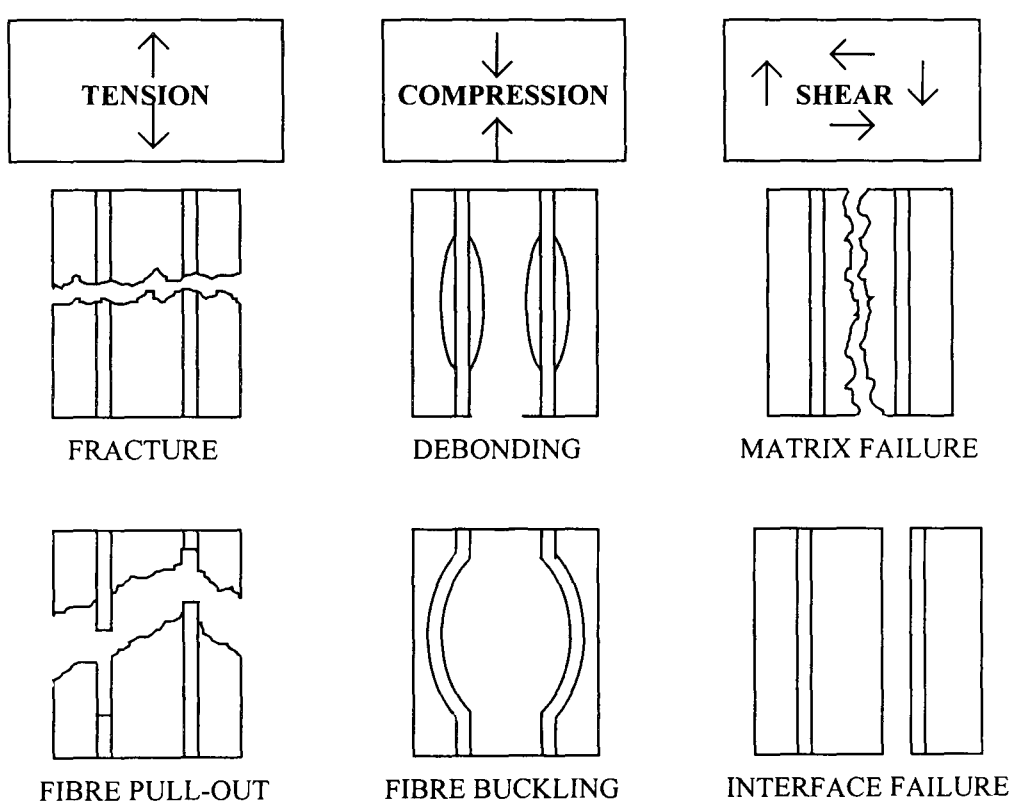

Figure 3.4 Principal failure modes in unidirectional composites

The loading mode and direction have a strong influence on the failure of a FRP composite. This is due to the directional characteristics of this type of composite. Tensile failure in fibre dominated composites is usually controlled by fibre failure or by the fibre pulling out of the matrix. Tensile loading in any other direction other than that of the fibre, however, usually results in the failure of the matrix or of the fibre/matrix interface. Compressive failure in the fibre direction can be fibre-dominated in some cases, with the fibres actually failing in compression. More

commonly, however, the matrix or the interface dominates in a compressive-load failure. The same is true in a shear failure, regardless of the type and orientation of fibre reinforcement. Good design, using a composite material to its full potential, requires that the fibres carry the loads and that high matrix stresses be avoided.

3.4 The significance of manufacturing defects

Composites are complex materials exhibiting distinct anisotropic properties. Fundamentally, a composite can be considered as being composed of three constituents: the fibre, the matrix, and an interface region of finite thickness responsible for assuring adhesion between the fibre and matrix. During the manufacture of composite components, thin plies or layers of pre-impregnated fibres, typically 125μm in thickness, are stacked in a desired order and the whole laminate is then processed to give a structurally sound component exhibiting the desired physical properties. Unfortunately, the manufacturing process may result in the presence or introduction of unwanted material and defects such as voids, resin-rich areas, and inclusions. Although many of these so-called defects may be difficult to detect, their effects on the overall structural integrity of the component may be serious, if not disastrous.

Apart from the manufacture of components, material degradation and damage can also occur during the in-service operation of composite components. The most likely causes of such damage are impact and cyclic loading, and rapid deviations in the local temperature. Such external influences can result in the failure of the composite component. The nature and extent of such damage depends on various parameters including the precise loading conditions, the fibre stacking sequence, the properties of the parts forming the composite, as well as the prevailing environmental conditions.

In most cases, the damage occurring in composites due to these external influences often develops over a long period of time (months or even years). Even so, this damage is not immediately visible to the trained eye. However, once the size of the defect or stress-raiser reaches a critical value, failure can be catastrophic and the

consequences severe. Therefore, there is a strong desire to identify as well as characterise the various types of damage in composite materials during manufacture and operational service.

To get an understanding of the various damage and failure mechanisms that occur in composites during the manufacturing process as well as operational service, it is important to investigate these mechanisms.

Resin-rich areas are often observed in composite materials even though the processing of the composite has followed the manufacturer's instruction. Figure 3.5 shows a micro-graph of a section of carbon fibre epoxy, where a location some distance from the area shown has been subjected to impact test. By examining the micro-graph, it can be seen that cracking occurs in the upper part of the resin-rich zone adjacent to the fibres. This localised failure is the first form of damage detected in this instance which suggests that such resin-rich imperfections may be responsible for reducing the mechanical performance of composite materials. If cracks initiate within these resin-rich areas, it is likely that delaminations would form under subsequent long term fatigue loading. When optical fibres are embedded into a composite othogonally to the material fibres the resin-rich area extends deeper into the composite thus possibly affecting the mechanical performance of the advanced material (Valis et al, 1991).

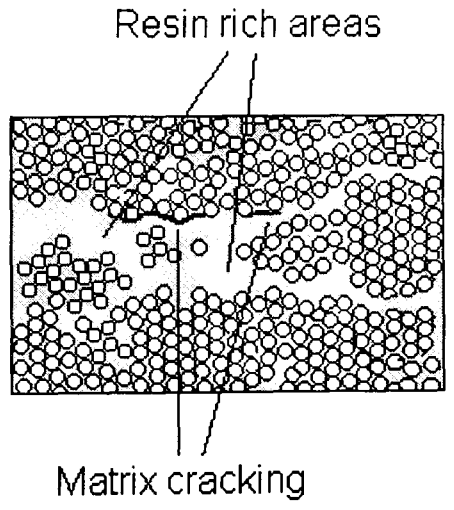

Figure 3.5 Damage initiation at a resin-rich area in a carbon fibre epoxy subjected to an impact energy

Voiding is a problem that is common to many composite parts. The level of porosity in a composite depends on the number of parameters including the water content, applied pressure during the cure cycle (Tang et al, 1987), and dwell time during cure (Thompson et al, 1973). Also, voiding is usually more common at angles or corners of composite parts. Voiding gives, perhaps, the greatest cause for concern since it is common to many components and has a serious effect on certain fundamental mechanical properties.

The processing stage can often result in the formation of *fibre kinks* or *ply waviness*. Such distortion of the principal load-bearing constituent (i.e. the fibre) may occur for a number of reasons:

1) Difference in the coefficients of thermal expansion of the fibres and matrix. This leads to a build up of residual stresses on cooling.
2) The process of crystallisation in a semi-crystalline material results in a volume contraction. This reduction in the matrix volume may generate a compressive stress field around the fibre and lead to fibre kinking.
3) Rapid cooling of the composite induces residual stresses due to the reduced time for material relaxation.

The *fibres* in a composite material are responsible for carrying the majority of the applied load. If these fibres are damaged or fractured, either in the handling or processing stage, the strength of the component may be greatly reduced.

Residual stresses resulting from cure or processing cycle can be also responsible for localised matrix cracking in multi-directional laminates, either in the matrix, or fibre-matrix interface region. Such cracks are frequently large, sometimes transversing a whole ply. The effect of such damage on the mechanical properties of the laminate can be significant. The inadvertent inclusion of a piece of pre-preg backing paper may well have serious consequences on the mechanical properties. The compressive strength can reduce by 25% in a catastrophic gross delamination-type mode.

3.5 Acoustic emission signal parameters and their analysis

In this section the various time domain parameters of the acoustic emission signal are explained with the aid of figure 3.6 .

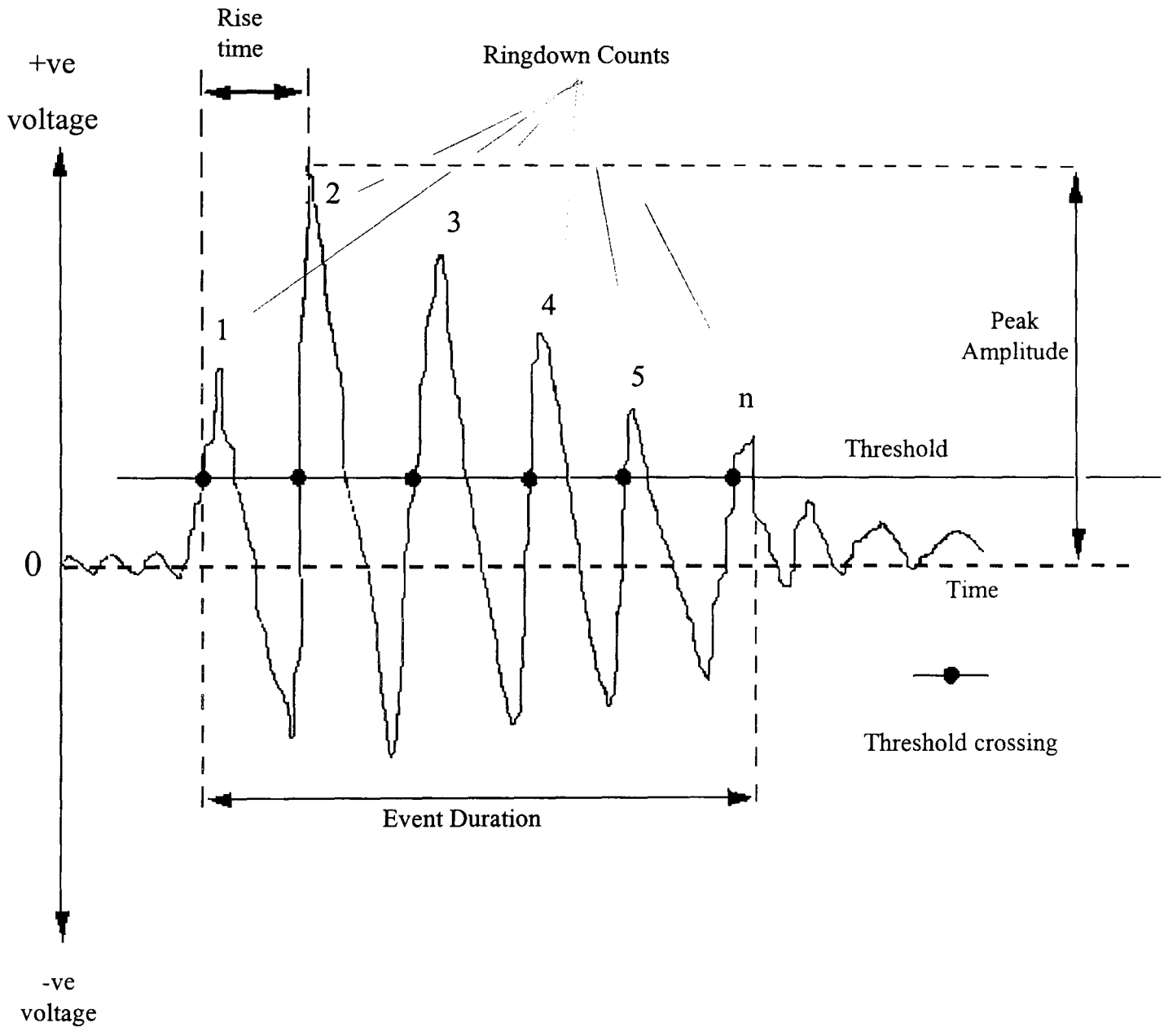

Figure 3.6 A typical acoustic emission signal

Event Counting

This is the simplest method of signal analysis, scoring out count per event. Electronically this is often achieved digitally, the chain of threshold crossing pulses is inspected for a time gap greater than a specified length. This is then used to indicate the end of the event. The time may be chosen so that fine structure and reverberations are allocated to the same source event.

Event duration

This is the time that the envelope remains above the threshold. It is closely related to ringdown counts, being approximately the number of ringdown counts multiplied by the time period of one oscillation of the sensor.

Rise time

This is the time that it takes the signal to rise from the threshold level to its peak value.

Ring Down Counting (RDC) Analysis

This type of analysis is one of the easiest and reliable method for analysing AE signal. The principle of RDC is to count the number of times a threshold voltage is crossed by an oscillating transducer output caused by acoustic emission. Advantages claimed by RDC are that the count obtained for a given event increases with signal amplitude and there is some weight in favour of events of larger energy. Secondly, RDC automatically improves noise rejection. However, results obtained by this analysis are strongly influenced by the geometry of the specimen, the properties of the transducer and its coupling to the specimen, the precise detection threshold and the performance of the amplifiers and filters. Therefore, there are difficulties in the use of this approach for fundamental studies.

Amplitude analysis

This is a more sophisticated analysis method. Amplitude distribution analysis is very useful in characterising the AE generated from a material. In this case the peak amplitude of each event as a distribution: either as a density, or as a cumulative plot. This is a powerful method of differentiating between different mechanisms.

Energy analysis

The energy is often measured after amplification of 80-100dB. The commonly measured root mean squared voltage (RMS) is closely related to the energy rate, that is, Energy=RMS x event duration. It has been shown that energy analysis has an advantage in signifying high amplitude events for which the RDC may fail to register the proper relative magnitudes. However, the absolute measurement of the AE source energy demands the consideration of the acoustic impedance of the transducer and specimen, the transducer efficiency, the geometry, attenuation and elastic properties of the sample and the amplifier gain along with the frequency response.

Frequency Analysis

The most common method of the determination of the frequency content of AE signals is to measure their power spectrum. Both frequency spectral analysis and auto-correlation analysis have been employed. Since the pre-dominant frequency present in the power spectrum is inversely proportional to the duration of the dynamic event, these measurements can provide information on the time scale of an AE process. This in turn may be used to characterise the evolution of the dynamic source event. In practice it can be considered that spectral analysis does provide some guidelines in selecting instrumentation components, optimising AE detectability, isolating background noise or extraneous AE and providing some qualitative insight to the AE source mechanism.

3.6 Systematic study of signal detection, processing and analysis

An evaluation of composite materials can be made by monitoring the acoustic emission (AE) emanating from the sample under investigation. The atomic rearrangements which occur within a material during deformation and cracking produce elastic waves which propagate through the material. The AE sources appear to function as point source emitters that radiate energy in spherical wavefronts (refer to figure 3.7).

When the AE wavefront impinges on the surface of the test object, very minute movements of the surface molecules occur. A sensor's function is to detect this mechanical movement (small surface displacements in the order of pico-metres) and convert it into an usable electrical signal. The transducer usually picks up a series of pulses of elastic energy rather than a continuous wave. The energy and the frequency spectra of the elastic wave packets coming from the defect depend on the material, the nature of the deformation process, the local stresses at the defect, and on the environment in which the material is placed.

The goal of an AE measuring system is to detect the acoustic event and provide suitable signal processing to characterise it and determine its significance. The most critical component of any AE measurement system is the transducer.

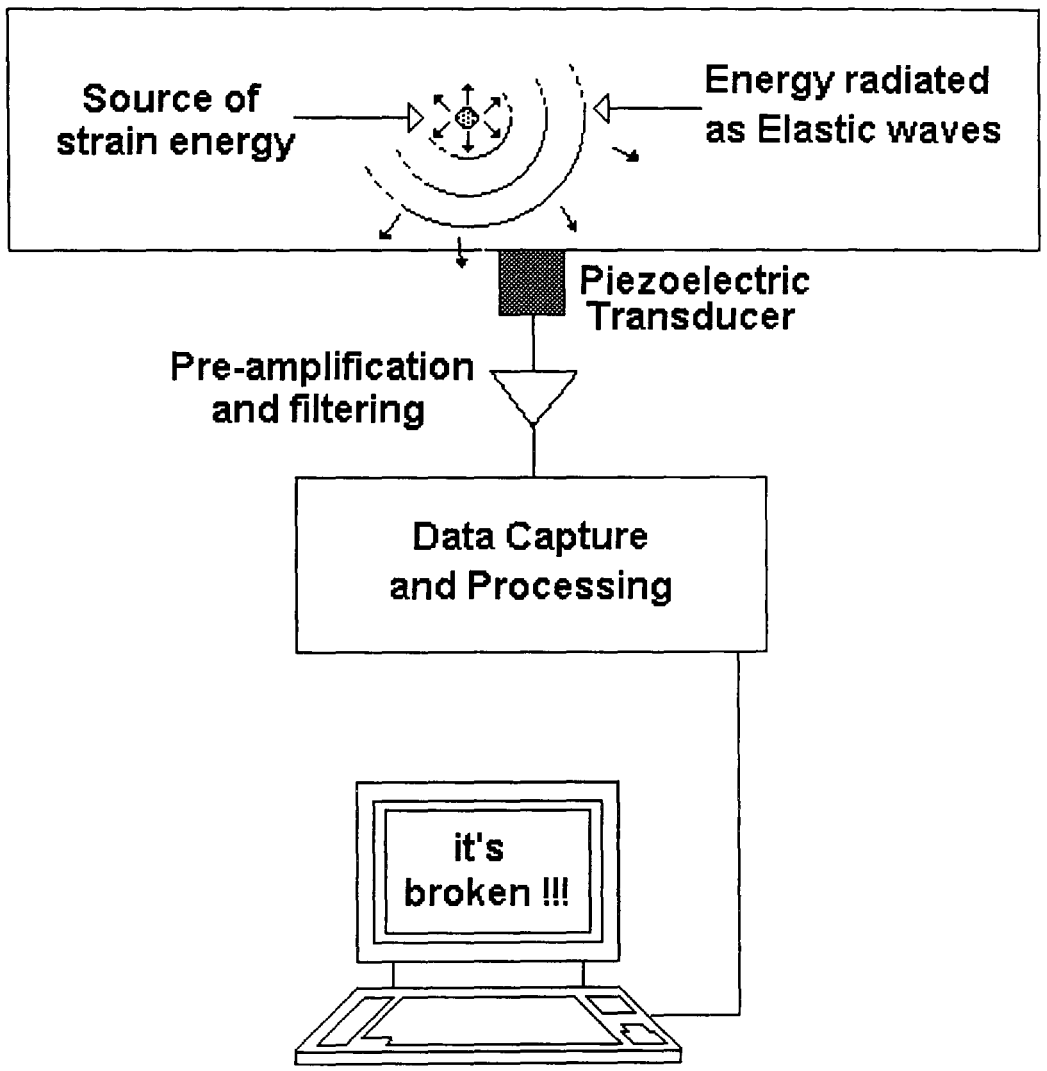

Figure 3.7 A typical AE set-up for the monitoring of damage in composite materials

3.6.1 Signal Detection

When an elastic wave propagates through the material to the surface it must be detected if any use is to made of its information content. The conventional non-destructive evaluation (NDE) technique for monitoring material degradation through AE is based on the piezoelectric effect. Piezoelectricity was discovered by the Curie brothers in 1880 and refers to the production of electric charges on the surface of crystals that have been deformed by the application of mechanical pressure. The most widely used transducers for AE detection are specially designed piezoelectrics (PZ), with lead titanate zirconium being the common choice for the active element. Piezoelectric transducers are sensitive, easy to apply, cheap and an established technology in ultrasonics as well as AE. Acoustic coupling of the AE sensor to the sample involves the use of a viscous couplant (e.g. vacuum grease or some other non-attenuating fluid) or an adhesive to reduce the air gaps present where the two surfaces are in contact. Too much or too little couplant could adversely affect the AE signal detection. Using force to attempt to increase the actual contact area is a considerably less efficient approach. The sensor can be clamped to the material using a constant force clamp or even using elastic bands.

However, these type of transducers are contacted externally to the material. This external sensing is beset with attenuation problems as the wave propagation in the material is affected by interactions with the material microstructure and inhomogenities for example.

Resonant AE sensors are the most common type of transducer used in commercial applications. This type of sensor has a piezoelectric ceramic element enclosed in a metal case for electrical shielding and protection of the ceramic element. The sensor includes a thin wear plate (usually plastic) for electrical isolation between the face of the ceramic element and the composite sample to be monitored (figure 3.8). This wear plate also protects the ceramic element face from damage (hence the name 'wear'). These piezoelectric ceramics take the form of a cylinder whose dimensions depend on the resonant frequency. Although the principal (or resonant) frequency of the sensor is

determined by the thickness of the element, there are radial resonances at lower frequencies. If the piezoelectric element is unbacked or undamped in any way, it acts as a resonator for incident and elastic waves so that the output voltage is a decaying sinusoid wave.

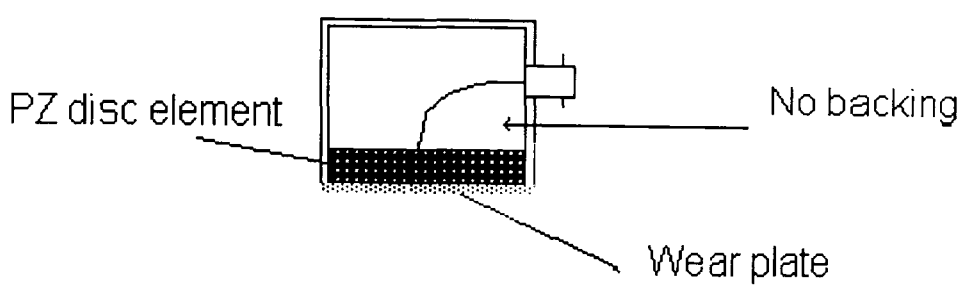

Figure 3.8 A typical resonant transducer.

Backing the element with an attenuating element (figure 3.9) produces a heavily damped transducer with a more *broad-band* response.

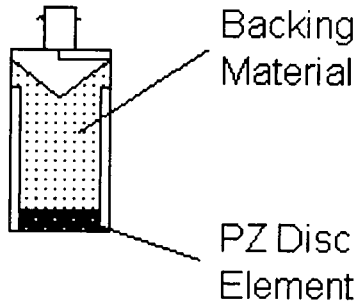

Figure 3.9 A typical broadband transducer

Most resonant AE transducers have frequencies which lie in the range 100 kHz to 1MHz. Therefore, it is clearly advantageous to optimise sensitivity by matching the resonant frequency of the transducer to the frequencies of the emissions. This is difficult to implement in the case of tensile testing of a composite as there is a wide range of frequencies in the output. Thus, a broad-band sensor could be more useful. Since AE emission responses are typically 100kHz to 2MHz, a PZ element with a resonant frequency between 2 and 4 MHz might be selected. This is common practice since damping such a resonator produces a flat response (below the natural frequency

of the element) in the pass-band of interest. Broad-band transducers are chosen when waveform analysis is desired.

There are many factors to be considered when developing a system to characterise emissions from a composite sample. In relation to the transducer selection, it is important to realise the fact that the propagated wave does not always strike the sensor face perpendicularly. Destructive interference distorts and reduces the bandwidth at other orientations. Thus broad-band response is not maintained. A possible solution is to replace the cylindrical disc by a cone (with a contact diameter of approximately 1mm) with a backing of brass (fig. 3.10). This transducer maintains its bandwidth at all orientations (i.e. behaves like a point receiver) but with a lower sensitivity.

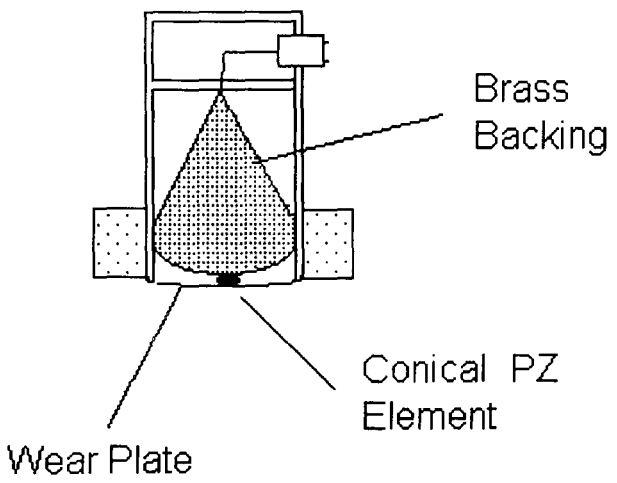

Figure 3.10 Point contact transducer (Pinducer)

Another consideration is the background noise present in the system, whether it is electrical or acoustic. AE events appear as random signals above a background noise level. Therefore, the success of any design would partly depend on the ability to minimise the effect of background noise. If the bandwidth of the signal is much less than the bandwidth of the noise then there is a large gain. But if the AE signal and the background noise are both broad-band then there may be little gain. The exception would be if the natural frequency of the sensor is carefully matched to the source emissions. Ideally, PZ materials with high intrinsic sensitivity should be used together

with low noise amplification. It is imperative that the system is isolated from as much acoustic noise and electromagnetic interference as possible

3.6.2 Signal Processing

The next stage in the development of a system to sense and analyse the acoustic emissions from composite materials is the *pre-amplifier* stage. This provides gain and bandpass filtering where its desired characteristics should include low electrical noise and a frequency response bandwidth as close as possible to the transducer response. Typical pre-amplifiers have flat amplitude response, but unknown phase response with frequency. For sensitive AE operation, the signal-to-noise (S/N) ratio is established by the pre-amplifiers. This is due to the fact that the band-pass filtering provided by the pre-amplifier reduces the bandwidth which normally improves the S/N ratio (only if responses of the pre-amp and transducer are closely matched). High frequency rejection reduces electronic noise while low frequency rejection ensures that acoustic vibrations, which usually have large amplitudes in test rigs, do not influence the results. The passive filters built into the pre-amplifiers are usually inadequate to eradicate these extraneous signals. An additional fast cut-off active filter is extremely helpful to ensure that the system passband is optimised to receive the AE signals and subdue the extraneous signals that could be associated with them. Since the pre-amplifier is driven by an external source it is possible that the system could be affected by electromagnetic interference. To counteract this, shielded cable can be used to provide the d.c. power for the pre-amplifier.

Another possibility is to use a transducer design which incorporates the pre-amplifier in the metal sensor case. Consequently, such pre-amplifier sensors eliminate the need for pre-amplifier cables and provide increased electrical shielding (against electromagnetic interference) of the signal. From the pre-amplifier, the AE signal is transmitted to the signal processing stage using the shielded cable.

In summary the signal processing stage carries out two tasks:

(1) to provide some gain to boost the signal to a less vulnerable level typically 40-60dB (100-1000 times)

(2) to provide filtration to reject noise from outside the sensors operating range

3.6.3 The AET 5500 data acquisition and processing system

The AET 5500 is a general purpose device that can monitor the type of acoustic emission events described to determine information on material/structured strength and integrity or to locate an acoustic emission source.

The AET 5500 (figure 3.11) can be configured with two to eight channels for monitoring and processing acoustic emission data. Sensors connected to these channels detect and acquire acoustic emissions for the processing unit. To monitor acoustic emissions, a sensor is mounted to the material or structure that is under investigation. The system allows the use of a single sensor and channel for some test situations and multiple sensors and channels for other more complex testing situations (for example, locating the source of an emission).

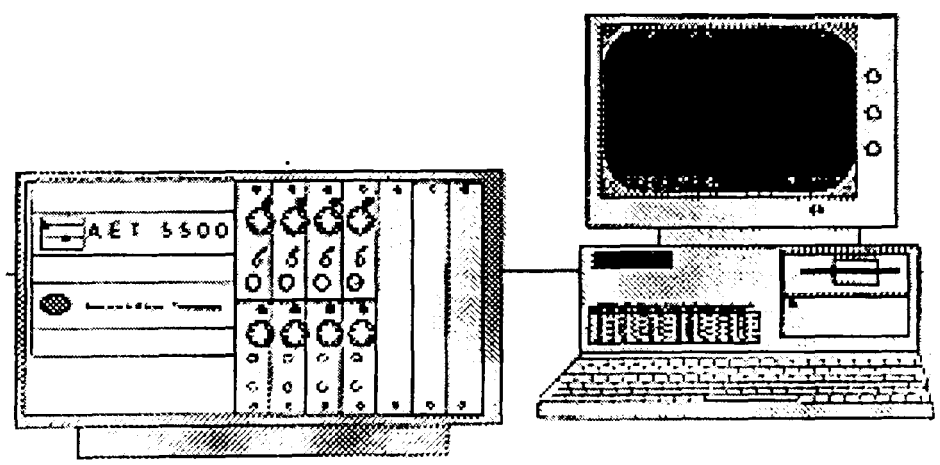

Figure 3.11 The AET5500 data acquisition and analysis unit

When an acoustic emission caused by an induced stress occurs in a test specimen, the sensors convert this acoustic wave into a voltage that is sent to the AET mainframe for processing. All signal processing occurs at the AET mainframes 16-bit processor. Before sending this signal (which is often very weak) to the mainframe, a preamplifer connected to the sensor increases the signal's strength by providing gain.

When the amplified and buffered signals reaches the mainframe, the mainframe may again amplify the signal (post amplification) before processing, depending on the signal characteristics that need to be monitored and the signals strength. When the mainframe does process the signal, it does so in accord with specific signal parameters that need to be set up by the user prior to the test using the systems versatile software.

The signal processing unit (figure 3.12) sends the signal to the systems digital modules when the signal crosses the desired threshold value, indicating an event of interest. An LED on the front of the processor flashes to indicate the threshold crossing. The AET system software allows the user to adjust the threshold level at a fixed or automated (floating) crossing.

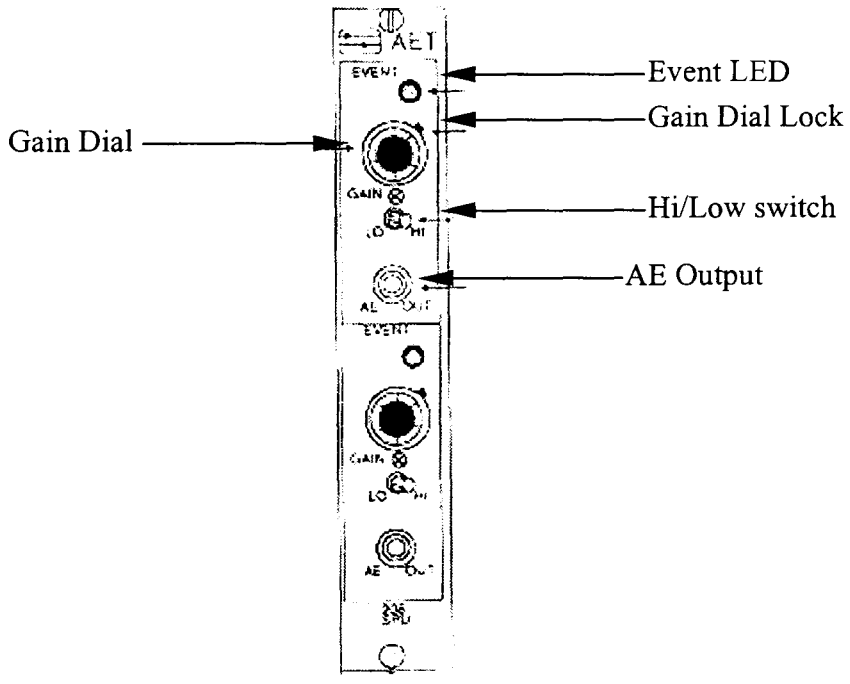

Figure 3.12 AET5500 signal processing unit

The automatic threshold lets the threshold level increase and decrease in response to changing levels of background noise to insure the recording of significant acoustic emission events only. The module also provides time duration information on the

event that produces the threshold crossing. The clock that determines the time duration is a unit that counts the pulses of a time base signal that is user configurable. After the signal is processed it is sent to the intelligent graphics terminal (IGT) where you can view a graphical representation or statistical table of the desired acoustic emission data.

With acoustic emissions processed and the desired display format set up, it is possible to key in a simple command for the sensor (or location test) whose data you want to observe. The data appears on the IGT screen where it is possible to view relationships between the desired acoustic emission characteristic and time or specified analogue parameter in a rate, distribution, or mean display.

The screen can show the following types of acoustic emission data in varying formats :

- Ringdown counts
- Events
- Event duration
- Peak amplitude
- Rise time
- Slope
- Voltage level (RMS)
- Energy
- Analogue parameters (such as load and strain)

If analysis of the real time data is not required, the user can specify that the data can be saved to file that you can view at another time. It is also possible to print the results of the test at a line printer.

The AET 5500 also has a powerful location test mode that lets the user monitor multi channel arrays (groups of channels that operate simultaneously yet independently from other sensors or arrays) to locate a linear or planar source of acoustic emission.

Using more than one channel for a test lets the user manipulate the AET 5500 to determine the location of the stress-relaxation mechanisms causing the emissions. Also, pre-sensor data can be obtained from any sensor(s) assigned to a running test. In a location test mode, it is possible to set up four different tests simultaneously using any combination of two sensors and two system channels. The user can initiate or terminate any array or single channel without affecting other channels or arrays.

3.7 Calibration Methods

The *calibration* of a sensor is the "measurement of its voltage output into an established load for a given mechanical load". Calibration results may be expressed either as a frequency response or as an impulse response (Miller and McIntyre, 1987).

3.7.1 Typical Calibration Method

The most common method of simulating acoustic emission signals in a material involves the fracture of graphite pencil lead (Hsa-Nielson source) while the lead is in contact with the surface of the material. The variation in lead diameters and types, orientation of the pencil, and applied force produce differing results. Therefore, there was a need to standardise this technique so researchers have developed a jig to hold the lead at a particular angle. The pencil-break tests (figure 3.13) are performed using a Teflon jig which maintained a constant angle between the pencil lead and the material surface (Halmshaw, 1987).

This pencil-break technique is used to evaluate the response of the piezoelectric transducer and the fibre optic system prior to collecting damage-induced acoustic emission data from materials. A mechanical pencil (Pentel) with 0.5mm diameter 2H graphite lead is held with its tip in contact with the graphite/epoxy composite specimen at 30 mm from the PZ transducer. The pencil is then pivoted until fracture occurs. The results yielded a reproducible high frequency acoustic pulse, which took the form of an exponentially decaying sinusoidal oscillation (Baillie et al, 1995) (figure 3.14). The threshold of the AET5500 is set above the noise level of this signal.

Alternatively, the PZ transducer response can be monitored by performing A pencil lead break 0.254m away from the sensor on a large, 3.1 mm thick aluminium plate (Halmstad, 1995).

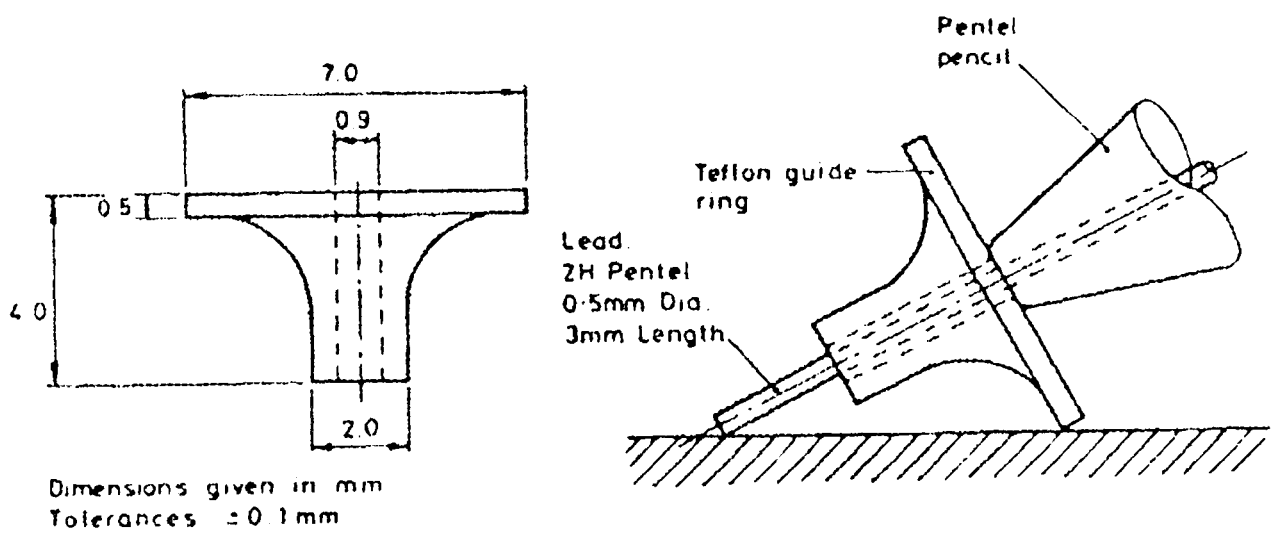

Figure 3.13. The Hsu-Neilson source

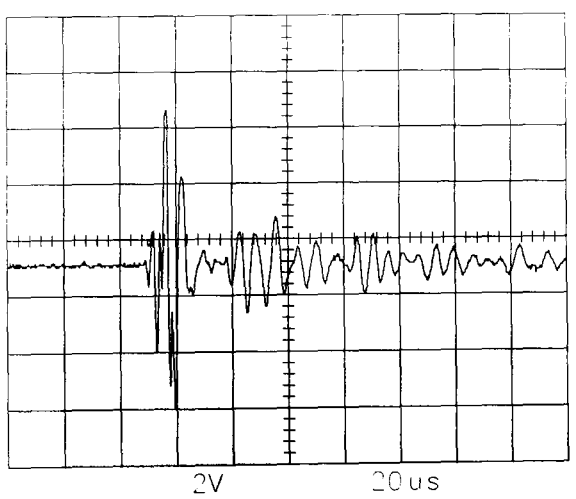

Fig 3.14 High frequency pulse from a pencil break

3.7.2 Instrument Calibration for Fibre Reinforced Plastic Tanks/Vessels

The performance and threshold definitions vary for different types of acoustic emission equipment. This section defines procedures prepared by the Committee on Acoustic Emission from Reinforced Plastics (CARP, 1982) and recommended by the American Society of Mechanical Engineers (ASME, 1983) for determining the threshold of acoustic emission detectability, reference amplitude threshold, and count criterion N_c from fibre reinforced plastic vessels.

(a) Threshold of Detectability

Threshold of acoustic emission should be determined using 1.22m by 1.83m by 13mm of 99% pure lead. The sheet should be suspended clear of the floor. The threshold of detectability is defined as the measured amplitude of an event generated by a 0.3mm Pentel pencil (2H) lead break at a distance of 1.3m from the sensor. The break should be done at a 30° angle to the test surface with a 2.5mm lead extension. The sensor should be mounted 152mm from the 1.22m side and mid-distance between 1.83m sides.

(b) Reference Amplitude Threshold

For large amplitude events, the reference amplitude threshold should be determined using a 3m by 51mm by 19mm clean, mild steel bar. The bar should be supported at each end on elastomeric, or similar, isolating pads. The reference amplitude threshold is defined as the measured amplitude of an event generated by a 0.3mm Pentel pencil (2H) lead break at a distance of 2.13m from the sensor. The break would be done at a 30° angle to the test surface with a 2.5mm lead extension. The sensor would be mounted 305mm from the end of the bar on the 51mm wide surface.

(c) Count Criterion N

The count criterion N shall be determined using an FRP sheet of such size that a 0.3mm Pentel pencil (2H) lead broken at different distances from the sensor will generate measured amplitudes equal to the threshold of detectability and the reference amplitude threshold. A calibration point on the 5-13mm thickness FRP sheet shall be selected so as to provide an amplitude decibel level midway between the threshold of detectability and the reference amplitude threshold.

3.8 Summary

There are many things to take into consideration when using AE to evaluate the integrity of composite materials. (i) choice of equipment, (ii) how wave propagation influences the AE signals, (iii) extraneous AE-noise sources, and (iv) the proper analysis of signals to ensure that the damage mechanisms can be characterised.

Acoustic emission is often a contest between signal and noise. In order to characterise the damage in materials it is necessary to enhance the signal whilst reducing the effect of noise at each stage in the acquisition and analysis of data. The techniques used to ensure this are: choice of sensor frequency and bandwidth, use of preamplifiers, the use of a filtering stage, the use of a floating threshold, and the use of acceptance windows.

Various features of the waveform can be used to give an indication of the damage in materials. Time and frequency domain analysis as well as pattern recognition schemes are used to enable the researcher to interpret the data. However one must be knowledgeable in the manipulation of data and therefore eradicating the possibility of guess work.

It is necessary to point out that it is important and maybe essential to identify the key source of friction-based AE that is present in all structures. The ability to distinguish friction or fretting from all other sources is the key because friction can occur at

essentially the same location where damage can occur (e.g., crack growth emanating from a fastener hole in a composite structure). Thus, if a friction source cannot be distinguished, friction may be mistaken for damage leading to false information that repairs are needed. Hence, it would be desirable to sort out friction based AE sources using other characteristics of the AE signal. Also, friction-based AE can provide key information about the type of damage which is present, for example, AE generated during unloading can be used to distinguish delaminations in composites (Awerbuch et al, 1983)

The question of determination of the AE source based on certain characteristics of the observed signal is probably the most debated and controversial issue in the AE field. Published literature can be found that seems to show that it is very easy to do source identification, for example, one only needs to measure the peak amplitude or another standard parameter (Rotem, 1984). There is also literature pointing out that source identification is more difficult and many factors must be taken into account (Kawamoto and Ono, 1989; Hamstad, 1992). To provide some background on this question, there are certain facts that are useful to review.

First the AE stress wave is greatly altered as the acoustic waves propagate from the source of origin to the various receiving sensor positions. For example, the frequency content instead of being dominated by the source becomes dominated by the structure in which the waves are propagating. Also, dispersion, material and geometric attenuation, reflections, mode conversion, etc. all distort the acoustic wave. The extent of these effects must be documented and accounted for prior to interpretation of AE data. Effects of wave propagation in composites also cause significant inaccuracy's in the data generated by the data acquisition and signal processing unit. Second, the typical AE sensor used further distorts the signal by such effects as significant aperture size, non flat frequency response, and velocity coupled with displacement sensitivity. The net result of all these distortion factors is that observed voltage-vs.-time waveform is not even close to that which would be obtained by a buried flat-response sensor located very close to the source.

CHAPTER 4

OPTICAL FIBRE SENSING OF ACOUSTIC EMISSION

4. Optical Fibre Sensing Of Acoustic Emission

An optical fibre sensor (Figure 4.1) can be defined as a device in which an optical signal is changed in some reproducible way by an external stimulus, such as temperature or strain. This definition covers a wide range of devices since an optical beam can be characterised by a number of variables such as intensity, wavelength, phase and state of polarisation.

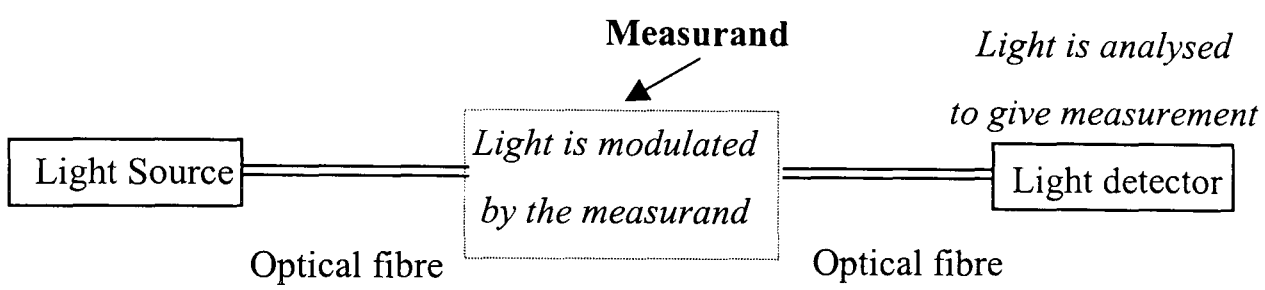

Figure 4.1 A basic optical fibre sensor

When the transduction mechanism is the modulation of optical phase, it is measured by interferometry (interferometric sensors). Interferometry is a well established classical optical technique which has been used for making very high resolution measurements. However, classical interferometry uses precision bulk optical components which need to be mounted with great stability. Due to this disadvantage, these bulk optic components are generally impractical for applications outside the laboratory.

The recent introduction of all-monomode fibre optic equivalents of many of the classical interferometers has resulted in a new range of sensors where the basic mechanism exploited is the measurand induced change in optical path length and/or the refractive index properties of the fibre. This type of sensor is labelled as intrinsic since the parameter to be measured interacts directly with the optical fibre.

When two or more beams of light interfere, the visibility of the interference fringes which are produced is controlled by the coherence of the light. Multimode optical

fibres do not maintain the spatial coherence of the guided beam, whereas monomode fibres do. It is for this reason that monomode fibres and associated components are preferred in the fabrication of interferometers.

4.1 Why Optical Fibres?

An advanced composite structure requires sensor technology to monitor the surrounding environment and integrity of the system itself. The conventional piezoelectric transducer technology, however, has a number of difficulties associated with its utilisation for this purpose. Fibre optic sensors have shown great potential to overcome these difficulties associated with conventional sensors. They offer a number of advantages over conventional sensors which have been considerably exploited with different types of sensors being developed over the last decade which can monitor virtually all physical parameters. Fibre optic sensors are still rapidly developing and significant advances in their use have been seen in the medical, engineering and scientific fields. The following unique properties have helped fuel the upsurgence of optical fibre systems (Measures and Liu, 1990, Jackson, 1985).

1. *Increased sensitivity.*

2. *High bandwidth*

   This is a feature which has already been exploited in the communications industry.

3. *High linearity*

4. *Geometrical versatility*

   Optical fibre can be configured into almost any shape thus enabling sensing in awkward areas, where irregular surfaces prevent proper acoustic coupling of piezoelectric transducers.

5. *Immunity to electromagnetic interference*

The long cables required for the use of piezoelectric transducers can act as large antennae and therefore they may pick up all kinds of noise. Since an optical fibre is dielectric, the sensor will be immune from the effects of electromagnetic interference. Therefore the validity of the data is guaranteed.

6. *High electrical isolation*

The sensor is immune from lightning strikes. High voltage and medical applications are areas which exploit this characteristic.

7. *Performs sensing functions in hostile environments*

Many structural systems are usually exposed to harsh environments, such as high or low temperature, corrosive surroundings, and external loads causing severe shock and vibration. Therefore, any sensor in such hostile environments needs to be rugged and durable. Optical fibre sensors are reliable under various adverse environmental conditions including high temperature. The sensor can be operated at higher temperatures than are allowed for electrical sensors. Optical fibre sensors are also capable of withstanding extremely high levels of vibration and shock. Electric short due to moisture does not happen to optical fibre cables, and hence they do not need to be heavily waterproofed.

8. *Practically incapable of initiating fires or explosions*

Optical fibre systems are generally considered to be intrinsically safe due to the small power levels of the light in the fibre. Therefore the application of such a system in a potentially explosive atmosphere would cause no problems as no electronics or power is required at the remote sensing point.

9. *Distributed property*

An advanced composite structure should have a self health monitoring function which examines, for example, the existence and severity of fatigue crack and other damage, ideally throughout the three-dimensional body of the structure for the ultimate purpose of ensuring structural safety and integrity. For this reason, a

sensor system with a distributed sensing capability is required. Optical fibre sensors in certain configurations can sense quantities distributed over a linear distance and in principle even in two- and three-dimensional arrays.

10. Lightweight

Optical fibre sensors and cables are lightweight, therefore increasing the weight budget for other instrumentation.

11. Composite compatibility

Optical fibres are significantly larger (125μm) in diameter than the reinforcing fibres (typically 5-10μm) in composite structures. Therefore, when optical fibres are embedded in composite laminates there will be an inevitable disruption of the reinforcing fibres in the vicinity of the optical fibre. However, research has shown that the introduction of an embedded optical fibre does not significantly reduce the strength or stiffness of the composite (section 4.9). Also, the embedding of optical fibres at the manufacturing stage is relatively simple.

12. Potential low costs

Another problem is that the conventional piezoelectric transducers and attendant cables may be too expensive to install over a large structure. Due to the large commercial telecommunication market, the costs of key optical fibres and components have been falling steadily. Once commercialised, an optical fibre sensing system could be significantly cheaper than its conventional counterpart.

These characteristics make optical fibres suitable for embedding within composite materials and meet exactly the requirements demanded for advanced composite structures, such as gas pressure vessels and aerospace structures, where they can both serve as sensors and as sensory signal carriers. This dual-purpose of fibres could be integrated into the 'fly-by-light' concept currently being considered for the next generation of aircraft. However, the realisation of such a concept could be set in motion by the advent of a smart component.

4.2 Optical Fibre Design

An optical fibre (figure 4.2) consists of a centre dielectric region of thickness d and refractive index n_1 surrounded by a dielectric region with a refractive index n_2, where $n_1 > n_2$. The central region guides the light and is called the core whilst the surrounding regions are termed the cladding. As the cladding has a lower refractive index than that of the core, the light propagating through the optical fibre is guided by the core. The outer layer of the optical fibre, termed the buffer, is a plastic material that is applied to the fibre to offer mechanical and environmental protection. The optical fibre used for the acoustic emission sensor had a core diameter of 3.8μm and a cladding diameter of 125μm.

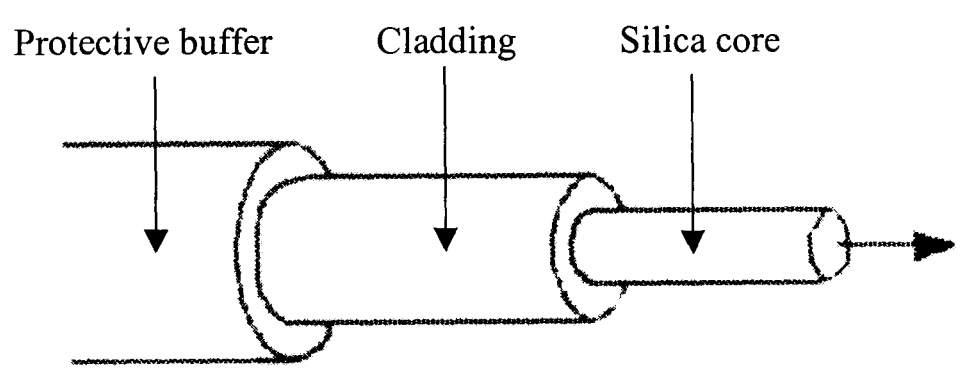

Figure 4.2 Optical fibre construction

4.3 Classification Of Optical Fibre Sensors

There are many ways to classify optical fibre sensors and a simple classification scheme is illustrated in figure 4.3. A optical fibre sensor is based on the principle that the light constrained within the fibre contributes in some way to the process of measuring some environmental parameter. The light is modulated by an external stimulus in some way between the light source and detector. There are two distinct forms of optical sensors: *intrinsic* and *extrinsic*.

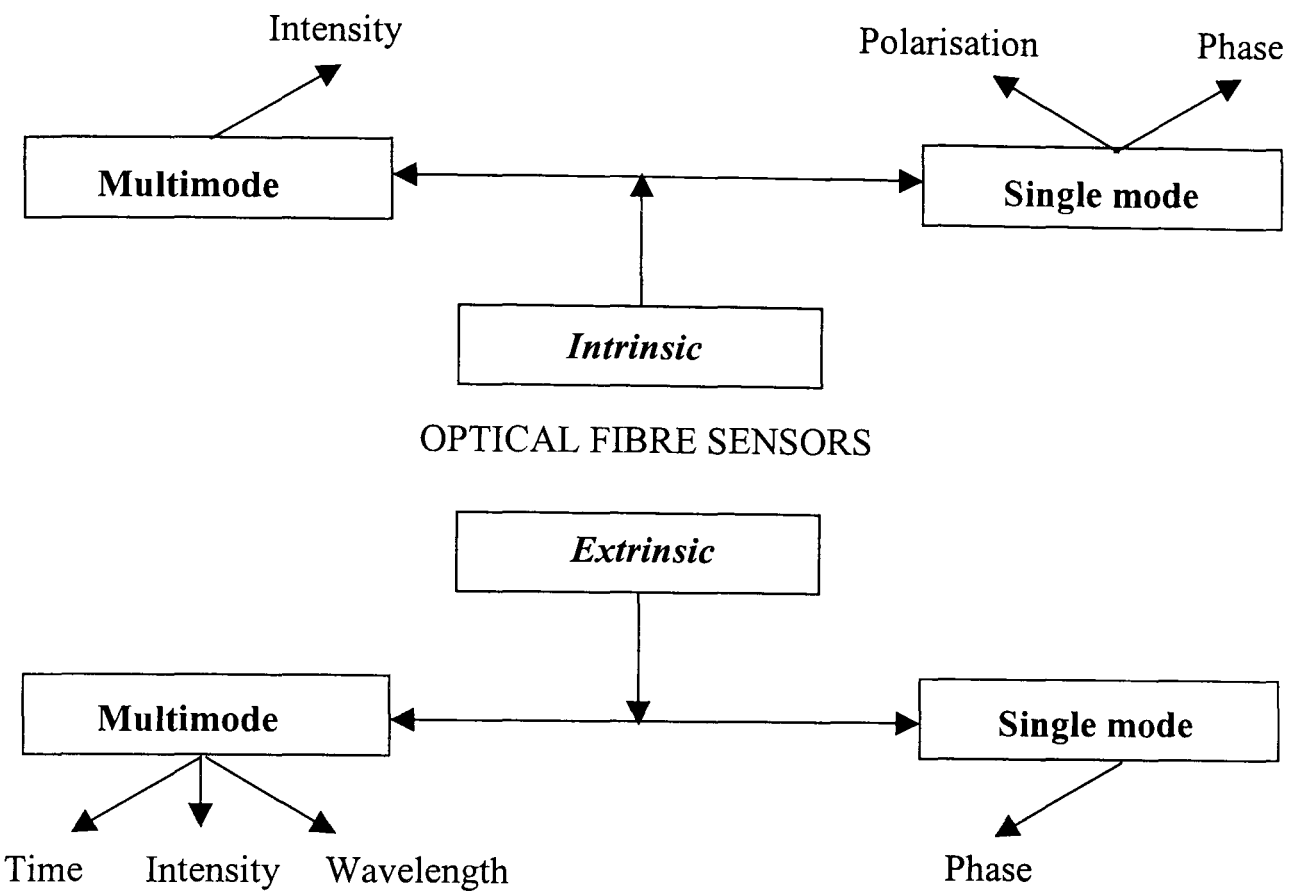

Figure 4.3 Classification of optical fibre sensors

In the first group of devices the optical fibre itself is the sensing element and the environmental influence directly modulates the characteristics of the light propagating through the fibre. In these type of sensors the propagating light does not leave the fibre between generation and detection. This style of device is termed an intrinsic optical fibre sensor. In some devices the optical fibre is not directly involved in the measurement but only acts as a light guide to convey information to and from a modulator. This type of device are known as extrinsic optical fibre sensors. These type of sensors can also use mechanical moving parts or electronics to modulate the light. Extrinsic and intrinsic fibre sensors have many advantages and disadvantages and these are listed in Table 4.1.

SENSOR TYPE	Advantages	Disadvantages	Comments
INTRINSIC	High sensitivity Inherently safe Simplicity No electronic parts	Intensity based Down-lead sensitive Requires referencing	Usually based on measurement of measurand using either stressing or straining of fibre.
EXTRINSIC **Electrically Passive**	High sensitivity No electronic parts	Mechanical moving parts modulate light. Poor stability Requires referencing Not absolute	The laser light is released from fibre and then recollected after modulation by measurand.
EXTRINSIC **Electrically Active**	Digital High sensitivity	Utilise electronics Requires EMI shielding Possible explosion hazard around fuel	Hybrid system in which transducers are interfaced to optically powered, low consumption, electronics..

Table 4.1 Advantages and disadvantages of intrinsic and extrinsic sensors

In the 1980's much of the work in the field of structural evaluation of composite materials using optical fibre sensors was concentrated in crack detection monitoring (Hale et al, 1980). Here, a system of optical fibres, either integrated into the composite structure during its manufacturing process or bonded to the structure's surface, could be used as a reliable monitoring device for structural damage. Fractures, cracks, or delaminations in a structure area can damage the optical fibre positioned there, and thus attenuate or interrupt the light flow. These were the first simple intrinsic fibre sensors for structural monitoring. In the intrinsic case, there are three characteristics of the light propagating in the optical fibre that can be interrogated: intensity, phase, and polarisation modulation.

INTENSITY is the parameter to which all optical detectors **finally** respond. Intensity modulation is simple, reliable and is low cost. However for good accuracy and stability it needs some form of referencing to avoid errors arising from source intensity variations, variable losses in fibres and connectors and sensitivity changes in detectors. Precise repeatable measurement of optical intensity over a wide dynamic range is quite difficult.

OPTICAL PHASE modulation, which is detected interferometrically, is one of the most sensitive ways of measuring physical changes with small changes of a micro-radian being detected. Optical phase in fibres is affected by temperature, pressure, strain, and rotation. As phase detection systems implicitly rely upon knowing the value of the optical intensity, variations in this or in the response function of the detector can manifest themselves as spurious fluctuations in scale factor.

POLARISATION modulation is in practice very similar to interferometry. Light is launched along the two principle axis of a delay medium, (i.e. two fibres) with equal intensities in each axis and is detected using a polarisation analyser which is usually located to receive equal intensities from each principle axis in the neutral state. The signal obtained through this analyser will behave exactly as the signal in an interferometer.

As stated above, with intrinsic sensors it is possible to modulate either the amplitude, the phase or the state of polarisation of the radiation in the fibre. In multimode fibres, however, mode coupling and the usually random relationships between the phases and polarisation states of the propagating modes generally rule out the use of phase or polarisation modulation. Therefore, intrinsic multimode fibre sensors almost invariably involve amplitude modulation. In single mode propagation the beam behaviour is much more well defined than in the multimode case. It is substantially more difficult to keep track of the optical phase in multimode propagation than in the single mode case. This is because the difference in velocity of the individual modes contribute to the total electromagnetic field with a phase and amplitude that are highly

unpredictable, dependent on the details of both propagation path and excitation conditions at the fibre entrance.

4.4 Phase Modulated Sensors

The first single-mode fibre intrinsic sensors were true interferometers (that is, they measured optical path difference), in which light from the source was divided to follow two (or more) fibre guided paths. The beams were then recombined to mix coherently together. From the intensity observed at the output from the interferometer, the phase difference between the optical paths, ϕ, may be determined. Most fibre interferometers are two beam devices in which one fibre is exposed to the measurand (the sensing fibre) and the other is isolated from it (the reference fibre). The phase sensitivity of a fibre interferometer to physical measurands such as temperature, pressure, and strain is very great. Based on single-mode optical fibres the three most widely studied interferometric configurations are: Mach-Zehnder, Michelson and Fabry-Perot as shown in figure 4.4. The advantages and disadvantages of these configurations can be shown in table 4.2.

The interferometric sensor for acoustic emission measurement is classified as an intrinsic phase modulated sensor as the parameter to be measured (acoustic disturbance) interacts directly with the optical fibre and modulates the phase of the light propagating down the fibre. The detection of this phase change can be made by comparing the phase of the beam propagating through the sensing fibre is compared to that of an isolated reference fibre.

In the all-fibre Mach-Zehnder interferometer the light is coupled from a coherent source (Helium-Neon laser or laser diode) into a single-mode optical fibre. The light propagating in the fibre is amplitude divided into two paths by means of a directional coupler. A directional coupler is the fibre optic analogue of the conventional beamsplitter. One arm is the sensing fibre, which interacts directly with the acoustic disturbance, while the other arm is the reference fibre, which is shielded from the effect and made insensitive to the parameter. The light from the two fibres are

recombined at a second directional coupler and mix coherently to produce interference that can be detected, giving two optical outputs at the detectors. The two resulting beams are then allowed to fall onto suitable photo-detectors. However, for optimum performance the states of polarisation of the recombining beams must be equivalent.

(a) Michelson

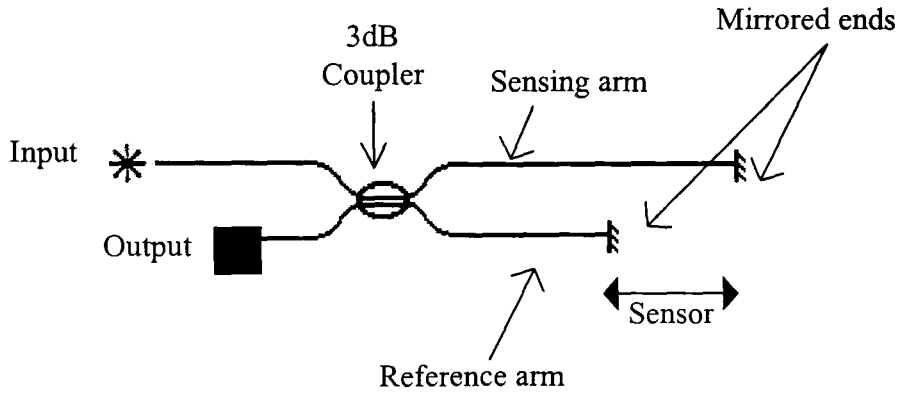

(b) Fabry-Perot

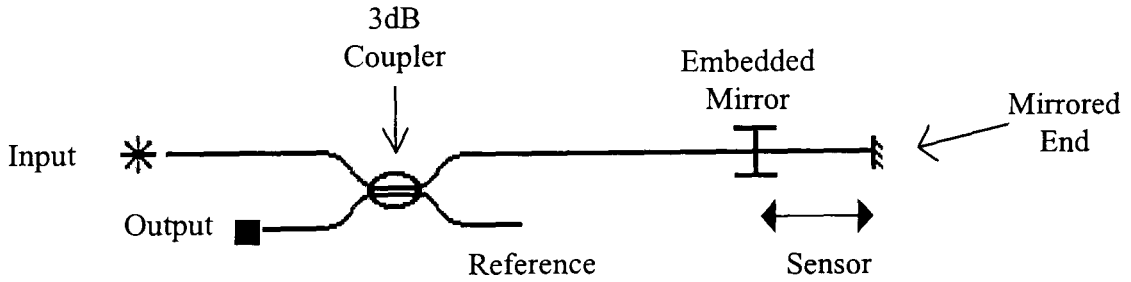

(c) Mach-Zehnder

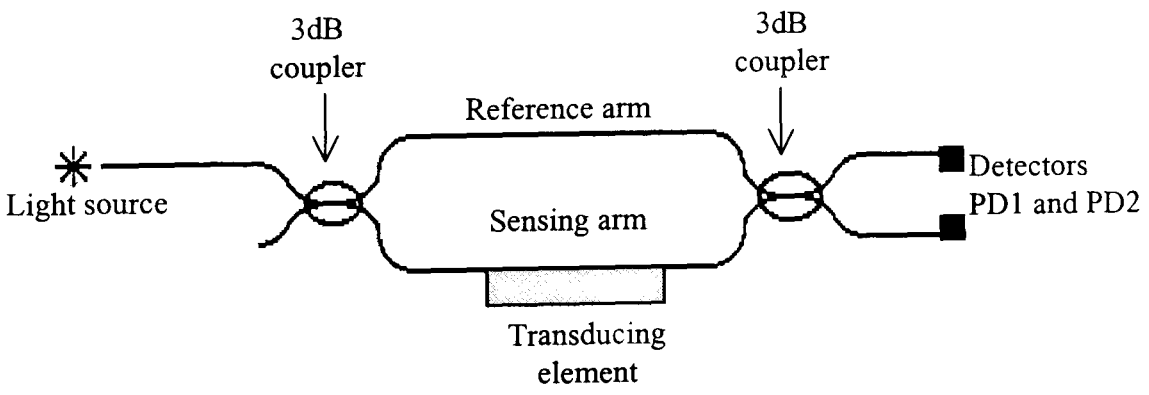

Figure 4.4 Basic optical configurations of single mode interferometric sensors

Configuration	Advantages	Disadvantages
Michelson	• High sensitivity • Ease of manufacture • Good localisation • Sensor length can be readily adjusted to millimetre range • Inexpensive	• Two fibre configuration (implies larger physical size, the need for two connectors, and greater noise sensitivity) • Connector problems • Non-common pathlengths in the leads causes additional phase noise • Needs sputtered mirrored ends
Mach-Zehnder	• Ease of manufacture • Inexpensive • Active and passive modulation can control the phase in the reference arm	• Non-identical path lengths of the two 'arm' can cause additional phase noise • Poor localisation • Two fibre configuration • Connector problems
Fabry-Perot	• High sensitivity • Single fibre • Single ended • Easier connectorisation • Varying sensor lengths may be manufactured	• High development costs (Sensors needs embedded and end mirrors) • Weak reflective fusion splice

Table 4.2 The merits and demerits of the Michelson, Mach-Zehnder, and Fabry-Perot interferometric configurations

It is necessary to examine the principles involved in the detection of acoustic energy. Firstly, it is instructive to consider the outputs expected from the interferometric sensor and secondly, investigate the transductions mechanisms involved in these types of sensors. Although phase demodulation of the optical carrier is achieved by interferometry, it is necessary to investigate the electronic processes which produce the useful outputs.

4.5 Mach-Zehnder Interferometry - A Mathematical Analysis

For reasons of simplicity, it is assumed that the state of polarisation (SOP) of the guided beam remains unchanged throughout. The Electric fields observed at detectors PD1 and PD2 (figure 4.4c) can be shown as

$$E_1 = k_{2R}\exp(i\phi_{ref})k_{1R}E_0(\tau_{ref}) + k_{2S}\exp(i\phi_{sig})k_{1S}E_0(\tau_{sig}) \qquad \text{(eq. 4.1)}$$

and

$$E_2 = k_{2S}\exp(i\phi_{ref})k_{1S}E_0(\tau_{ref}) + k_{2R}\exp(i\phi_{sig})k_{1R}E_0(\tau_{sig}) \qquad \text{(eq. 4.2)}$$

where

- subscripts sig and ref refer to the signal and reference arms respectively.

- k_{ij} are the amplitude coefficients for the *i*th directional coupler, where subscript S denotes the direct (transmitted) beam (for example, source to signal fibre) and R the indirect (coupled) (source to reference fibre) beam.

- ϕ_{sig} and ϕ_{ref} are the phase retardance of the signal and reference arms.

- E_0 is the electric field amplitude of the source and is time dependent, where τ_{sig} and τ_{ref} are the propagation times from the source to the detectors via the signal and reference arms respectively.

Due to the fact that polarisation effects are ignored, the electric field and the coupling coefficients are scalars. However, the coupling coefficients are complex, to allow for phase changes that take place on coupling. For an ideal 2X2 directional coupler, the coupled beam experiences an additional phase retardance of $\pi/2$ radians (90°). Therefore, the k_{iS} may be defined as real, so that the k_{iR} are imaginary, so that

$$k_{1R} = ik'_{1R} \qquad \text{where } k'_{1R} \text{ is real.} \tag{eq. 4.3}$$

However, photo-detectors are square law devices and therefore only detect intensity. We can now calculate the intensity I at the detectors using the relationship

$$I \propto \langle E.E^* \rangle \tag{eq. 4.4}$$

where the brackets denote time averages, and the asterisk the complex conjugate. Therefore, from (eq. 4.1) and (eq. 4.3) it can be seen that

$$\begin{aligned} I_1 = {} & k'^2_{1R} k'^2_{2R} \langle E_0^2(\tau_{ref}) + k^2_{1S} k^2_{2S} \langle E_0^2(\tau_{sig}) + \\ & 2\,\mathrm{Re}\left[-k'_{1R} k'_{2R} k_{1S} k_{2S} e^{i(\phi_{sig} - \phi_{ref})} \langle E_0(\tau_{sig}) \bullet E^*_0(\tau_{ref}) \rangle \right] \end{aligned} \tag{eq. 4.5}$$

This result may be simplified by noting that $\langle E^2_0(\tau_{sig}) \rangle$ and $\langle E^2_0(\tau_{ref}) \rangle$ are simply the source irradiance coupled into the fibre, I_0. It is possible to define the degree of coherence of the source by

$$\gamma(\tau_{sig} - \tau_{ref}) = \frac{\langle E_0(\tau_{sig}) \bullet E^*_0(\tau_{ref}) \rangle}{I_0} \tag{eq. 4.6}$$

so that

$$I_1 = I_0 \left[k'^2_{1R} k'^2_{2R} + k^2_{1S} k^2_{2S} - 2k'_{1R} k'_{2R} k_{1S} k_{2S} \gamma \cos(\phi_{sig} - \phi_{ref}) \right] \tag{eq. 4.7}$$

and following the same analysis by using (eq. 4.2) the following is obtained

$$I_2 = I_0\left[k'^2_{1R}k'^2_{2R} + k^2_{1S}k^2_{2S} + 2k'_{1R}k'_{2R}k_{1S}k_{2S}\gamma\cos(\phi_{sig} - \phi_{ref})\right] \quad \text{(eq. 4.8)}$$

It can be seen that the two signals vary in antiphase, which can be exploited to compensate for the effects of source intensity noise. The two signals can be simplified by defining the VISIBILITY of the interference by

$$V = \frac{(I_{max} - I_{min})}{(I_{max} + I_{min})} \quad \text{(eq. 4.9)}$$

where I_{max} and I_{min} are the maximum and minimum values that the irradiance can take as

ϕ_{sig} is varied.

It can be shown that

$$I_1 = I_0\,[1 - V\cos(\phi_{sig} - \phi_{ref})] \quad \text{(eq. 4.10)}$$

and

$$I_2 = I_0\,[1 + V\cos(\phi_{sig} - \phi_{ref})] \quad \text{(eq. 4.11)}$$

where

$$V = \frac{2k_{1R}k_{2R}k_{1S}k_{2S}}{k^2_{1R}k^2_{2R} + k^2_{1S}k^2_{2S}}\gamma \quad \text{(eq. 4.12)}$$

From (eq. 4.12) it can be seen that the visibility depends on the relative magnitudes of the optical powers propagating in the two arms of the interferometer. Also, the visibility is directly proportional to the degree of source coherence. From (eq. 4.6) it may be seen that

$$|\gamma(\tau)| = \lim_{T\to\alpha} \frac{1}{T} \int_0^T \exp i[\phi(t+\tau) - \phi(t)]dt \qquad \text{(eq. 4.13)}$$

The value of τ lies between unity, for a source with perfect temporal coherence, and zero, for completely incoherent source. Fibre interferometers usually use laser sources, which typically have a long coherence time, τ_c.Therefore, provided that

$$\tau_c >> \tau_{sig} - \tau_{ref} \qquad \text{(eq. 4.14)}$$

which is usually the case, then it can be assumed that $\gamma \approx 1$.

To obtain maximum Visibility, it is necessary for the powers of the guided beams in the signal and reference arms to be equal, which requires

$$k'_{iR} = k_{iS} = 1/\sqrt{2} \qquad \text{(eq. 4.15)}$$

Therefore, provided that $\gamma \approx 1$, then $V \approx 1$.

This, however, is the ideal situation. To summarise, the visibility will be less than unity for one or a combination of the following reasons:

1. The coherence length of the source is not large enough in comparison with the optical path imbalance between the interferometer arms;

2. The components of signal and reference beams reaching a specific detector are unequal in intensity;

3. The states of polarisation of the signal and reference beams are unequal.

In practice, single longitudinal mode diode lasers are often used as sources and have a coherence length of several metres, which is generally much greater than the path imbalance of the interferometer. In the experimental set-up shown the coherence

length of the HeNe laser is only 30cm. Therefore, an optical path difference of around 2mm may cause a decrease in visibility.

As stated earlier, equality of signal and reference beam intensities can be ensured by selecting directional couplers with suitable power splitting ratios. Both optical couplers used in the experimentation are not an equal split (48/52), therefore signal fading occurs. By substituting these values into (eq. 4.12), the visibility becomes 0.987. In a practical system there are many losses which are summarised below :-

(i) Losses in fibre (1.5dB/km)
(ii) Directional couplers (0.8dB excess loss)
(iii) fibre splices (approximately 0.1dB per splice)

In the above mathematical analysis, the polarisation effects have not been considered. Perfect visibility fringes may only be achieved when the states of polarisation of the recombining beams are equal. If the recombining states are orthogonal, then no interference is observed. It is difficult to ensure that the signal and reference beams have equal states of polarisation. This is because normal circular core optical fibre is slightly birefringent, with much of this birefringence arising from extrinsic sources, such as bends and twists in the fibre. The resulting output polarisation is therefore variable and unpredictable. The directional couplers may also introduce some birefringence. One solution is to construct the entire interferometer using highly birefringent fibre, and to illuminate only one polarisation eigenmode. Because the eigenmodes do not couple, the state of polarisation of the guided beam is preserved. However, this approach also demands that polarisation preserving couplers are used. A more straightforward solution is therefore to use normal circular core fibre, and to incorporate polarisation controllers, described later, into the interferometer. It is then possible to adjust the states of polarisation in the two beams until they are equal, indicated by maximum observed visibility. Such polarisation controllers may operate by introducing an adjustable amount of bending or twisting into the fibre.

4.6 Transduction Mechanisms

It is necessary to consider the effects which various quantities to be measured have on the phase of the radiation in a single mode fibre. For simplicity it is assumed that the mode behaves like a ray travelling down the centre of the fibre with velocity c/n . Thus the phase (in radians) associated with a length L of fibre may be expressed as

$$\phi = \frac{2\pi nL}{\lambda} = \beta L \qquad \text{(eq. 4.16)}$$

The total phase of the light path along an optical fibre depends on three properties of the fibre waveguide :

(1) Total physical length

(2) Refractive index and the Index profile

(3) Geometrical transverse dimensions of the guide.

It is assumed that the index profile remains constant with environmental variations, so that all the following analysis concentrates on evaluating the depth of phase modulation for variations in length, refractive index and guide dimensions alone. These variations may then themselves be evaluated for a given perturbation applied to the fibre, and therefore the phase sensitivity of the fibre to this perturbation can be estimated.

The total physical length of an optical fibre may be modulated by :

- Application of a longitudinal strain.
- Thermal expansion.
- Application of a hydrostatic pressure causing expansion via Poisson's ratio.

The refractive index varies with :

- Temperature.
- Pressure and longitudinal strain via the Photoelastic effect.

The guide dimensions vary with :

- Radial strain in the pressure field.
- Longitudinal strain through Poisson's ratio.
- Thermal expansion.

The design of an optical fibre phase modulated transducer is a two-stage process : the first stage involves the optics and the interferometer and the second the mechanical interactions between the measurand and the modulation of phase in the fibre.

The effect of a pressure wave on an optical fibre can be analysed in terms of the strain field that it gives rise to. The strain field can be represented by the following vector:

$$\varepsilon = \begin{bmatrix} \varepsilon_x \\ \varepsilon_y \\ \varepsilon_z \end{bmatrix} = \begin{bmatrix} -P(1-2\mu)/E \\ -P(1-2\mu)/E \\ -P(1-2\mu)/E \end{bmatrix} \qquad \text{(eq. 4.17)}$$

In this co-ordinate system, the z-axis coincides with the longitudinal axis of the fibre. The strain placed on the fibre causes the phase at the output to change by:

$$\Delta\phi = \beta\Delta L + L\Delta\beta \qquad \text{(eq. 4.18)}$$

The first term represents the effect of the physical dimensional change due to the strain. For the stress considered,

$$\beta\Delta L = \beta\varepsilon_z L = \frac{-\beta(1-2\mu)LP}{E} \qquad \text{(eq. 4.19)}$$

The second term in (eq. 4.18) is indicative of the response to a change in the propagation constant β. There are two effects that can cause a change in β : the strain-

optic effect and the wave guide dispersion effect. This can be shown mathematically as follows:

$$L\Delta\beta = L\frac{d\beta}{dn}\Delta n + L\frac{d\beta}{dD}\Delta D \qquad \text{(eq. 4.20)}$$

The strain-optic effect describes the phenomena whereby the strain field results in a change of the refractive index of the fibre. The strain-optic effect appears as change in the optical indicatrix:

$$\Delta\left(\frac{1}{n^2}\right)_i = \sum_{j=1}^{6} p_{ij}\varepsilon_{ij} \qquad \text{(eq. 4.21)}$$

where

ε_{ij} represents the components of the strain field,

p_{ij} represents the components of the strain-optic tensor.

The second term in (eq. 4.20) represents the change in the waveguide propagation constant due to a change in fibre diameter (D). Using the normalised parameters describing the waveguide mode and evaluating the $d\beta/dD$ term, Hocker (1979) has shown that the effects due to diameter change are negligible compared to the effect that length and refractive index changes have on the magnitude of the phase change. By neglecting the waveguide dispersion effect, the optical phase per unit length of optical fibre per unit of pressure P can be expressed as:

$$\frac{\Delta\phi}{PL} = \frac{\beta(1-2\mu)}{E} + \frac{\beta n^2}{2E}(1-2\mu)(2p_{12}+p_{11}) \qquad \text{(eq. 4.22)}$$

A more detailed description of the steps leading to equation 4.22 can be found in work by Hocker (1979). There have been a few assumptions made in order to achieve (eq. 4.22). The first of these is the assumption that the optical fibre is homogeneous and isotropic. Therefore, certain elements of the strain-optic tensor need only be considered. Secondly, the assumption that there are no shear stress components.

Therefore, the stress can be written as a component vector. The end result of these assumptions is that they allow the expressions for the strain and strain-optic tensors to be greatly simplified. These two assumptions hold true for cases where the wavelength of the of the acoustic wave is much larger than the fibre diameter.

4.7 Interferometric Response To Acoustic Energy

In the work undertaken the optical fibre is embedded into a composite structure, where acoustic energy or pressure in the material interacts with the fibre to produce dimensional changes in the fibre. This results in the modulation of the phase of the light travelling through the sensing fibre core. At the output of the interferometer, the light from the sensing fibre is combined with the light in the reference arm. If the irradiance output of the interferometer is monitored by a detector then the photo-current can be expressed as (eq. 4.23), that is

$$I_D = I_0(1+V\cos\phi(t)) \qquad \text{(eq. 4.23)}$$

where $\phi(t)$ is the time dependent phase difference between the arms of the interferometer. Therefore, any change in the phase of the light in the sensing beam will be recognised at the output of the interferometer as a change in the magnitude of the photo-current. The transfer function of the interferometer, shown as a function of phase ϕ is illustrated in figure 4.5. This response illustrates the basic problem with any interferometric sensor in that its response is periodic in the phase difference. From figure 4.5 it can also apparent that that the greatest sensitivity in signal is obtained when the interferometric system is operated at points midway between the maximum and minimum values of the relative output. These points of the slope are termed the *quadrature* points. Therefore, maximum sensitivity can be obtained when one arm of the interferometer is set to an odd multiple of $\pi/2$.

If the system drifts towards the maximum and minimum values of the relative output, the sensitivity tends towards zero. This is generally the case when the reference fibre is subjected to changes in ambient conditions. As detailed earlier, temperature and pressure variations may cause the fibre to elongate, hence leading to a path length imbalance between the interferometer arms. Therefore, the associated phase shift may drift with time and vary in-and-out of the quadrature point. This drift is detected as an output loss of the interferometer. Hence, it is necessary to implement a 'phase tracking' scheme into the interferometric system to produce a useful output.

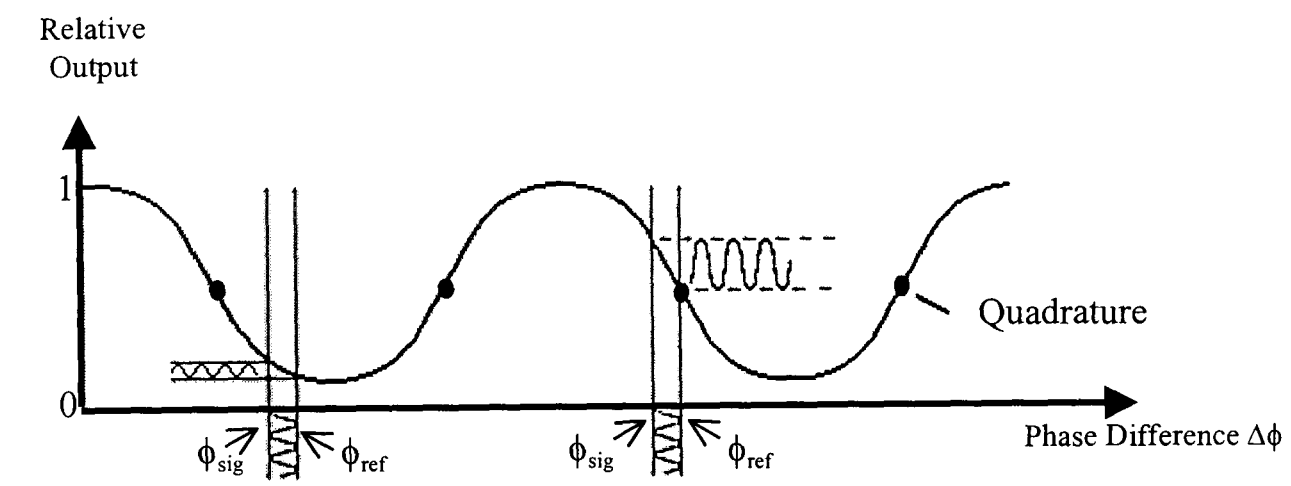

Figure 4.5 Relative output of a Mach-Zehnder interferometer as a function of phase difference between the two arms.

4.8 The Elimination Of Phase Drift In A Single-Mode Optical Fibre Interferometer Using A Piezoelectrically Stretched Coiled Fibre

In section 4.7 it has been shown that the sensitivity of an interferometer to an induced optical phase change is not constant, due to the periodic nature of the transfer function. This variable sensitivity is not acceptable as it causes signal fading, and interferometric sensors are usually operated such that the output is linearly related to the induced optical phase change.

There are three approaches which provide the signal processing to linearise the all-fibre interferometric sensor's transfer function: homodyne, heterodyne, and pseudo-heterodyne detection. The most straight-forward technique is known as the 'Active phase tracking homodyne scheme' as shown in figure 4.6. This set-up ensures the control of the phase of the reference arm. The simplest way to do this is to wrap the fibre around a cylinder of a piezoelectric material. When a voltage is applied to the cylinder it expands radially, thus stretching the fibre and hence inducing a phase change.

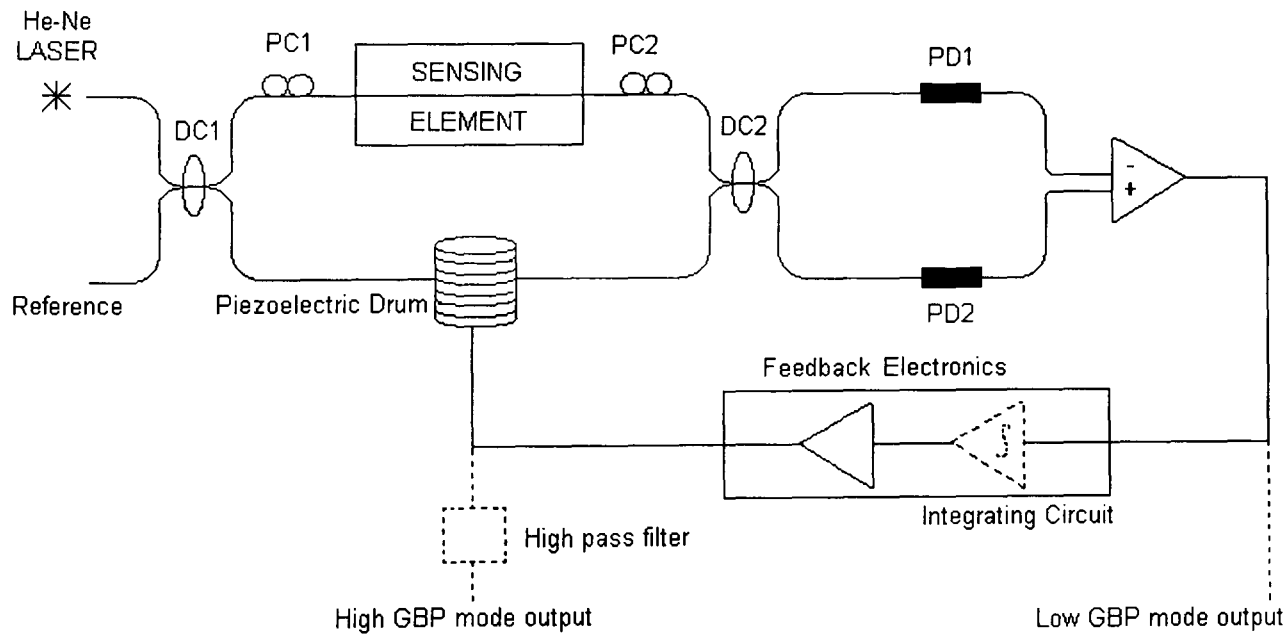

Figure 4.6 Active phase tracking homodyne system

If this induced phase change is written as $\Delta\phi_m$, then the system can be held at the quadrature point by requiring that

$$\Delta\phi_m + \Delta\phi_d = \frac{(2m+1)\pi}{2} \qquad \text{(eq. 4.24)}$$

where $\Delta\phi_d$ is the differential phase term and m is an integer.

(Note that $\Delta\phi$ represents the phase difference between the sensor and reference outputs and is made up of a differential phase term $\Delta\phi_d$ and a signal term ϕ_s, where $\Delta\phi = \Delta\phi_d + \phi_s$)

In the absence of any modulation of the sensing arm, this may be achieved by making the differential signal part of the feedback loop connected to the reference arm modulator, and then ensuring that the differential signal remains close to zero.

In the presence of a signal, the differential signal cannot be used directly in the feedback loop or else the signal information will be cancelled out. However, it is likely that any ambient modulation of the reference arm will take place at a lower frequency than that of the signal. Therefore the differential signal integrated over a long time compared to the signal modulation (and short compared to the ambient modulation) can often provide a suitable feedback signal.

The signal obtained before the feedback electronics will now be the same as in a 'perfect' system operating at the quadrature point and with no reference arm phase drift. Such a mode of operation is known as a low gain-bandwidth-product (GBP) mode. One problem with this mode of operation is that the output is only linear in $\Delta\phi$ when $\Delta\phi \langle\langle \pi$. In addition, phase excursions greater than 2π can lead to ambiguities because of the periodicity of the output. One way to avoid these difficulties is to operate the above system in a high GBP mode. That is, we remove the integrating circuit and operate the feedback circuit at frequencies high enough to include the signal frequency. At first sight, this would seem to obliterate the signal entirely;

however, it is still present in the signal applied to the phase modulator in the reference arm. Thus for operation at the quadrature point

$$\Delta\phi_d + \phi_s + \Delta\phi_m = \frac{(2m+1)}{2} \qquad \text{(eq. 4.25)}$$

or

$$\Delta\phi_m = \frac{(2m+1)}{2} - \Delta\phi_d - \phi_s \qquad \text{(eq. 4.26)}$$

Assuming therefore that $\Delta\phi_m$ is proportional to the feedback voltage applied to the modulator, the feedback signal is linear to $(\Delta\phi_d + \phi_s)$. This linearity will extend over many 2π phase changes, the only limitation being the phase range that can be covered by the modulator itself. The required phase ϕ_s may be separated out using electrical filters since ϕ_s usually oscillates at a higher frequency than $\Delta\phi_d$.

This active phase tracking homodyne scheme is easy to implement and is usually extremely linear in operation. However, there are many disadvantages with this system. This scheme uses an electrically active element which requires several hundred volts (typically 125V) for the piezoelectric element. This could reduce the sensor's role in an industrial environment as it is no longer an electrically 'safe' device. Furthermore, although the phase range is much in excess of 2π it is still limited, and large phase excursions may require the resetting of the system therefore resulting in the loss of some information.

4.9 Influence Of Embedded Optical Fibres On Composites

It is extremely important to establish the general rules for embedding optical fibres within complex composite lay-ups. Measures et al (1992a) have undertaken an extensive series of experiments to gain an insight into this and the principal mechanism responsible for the fracturing of embedded optical fibres. It has been determined that if the optical fibres are used as strain/temperature sensors they should be mounted between two co-linear plies and be aligned with the reinforcing fibres. However, if the optical fibres are acting as damage sensors through their fracture above certain critical loads, then the optimum sensitivity arises when the optical fibres are embedded as close to the surface of maximum tensile strain as possible and sandwiched orthogonally between a pair of co-linear plies (Measures et al, 1989) . If optical fibres are to be embedded within practical composite material structures they must not (Meaasure et al, 1992b)

(i) compromise the tensile or compressive strength
(ii) increase the damage vulnerability of the material
(iii) reduce the fatigue life of the material.

Glossop et al (1990) have shown that neither the tensile nor compressive strength of Kevlar/epoxy appears to be diminished by the presence of embedded optical fibres. It has also been demonstrated by Blagojevic et al (1990) that the interlaminar fracture toughness of the composite material is not reduced by the existence of embedded optical fibres. They have shown that the presence of optical fibres marginally improve the damage resistance of the material. Careful consideration must be given to the diameter of optical fibres and their type of coating if they are to be embedded within composite structures and function correctly for the useful life of the structure. The presence of optical fibres within laminated composite structures could increase the complexity of fabrication, design and analysis.

Fractographic studies reveal that optical fibres embedded at an angle to the adjacent ply directions of the composite material can create resin cavities (termed 'resin-eyes'

because of their shape). This is due to the rigidity of the reinforcing fibres causing them to bridge over the circular optical fibre cross-section. Dasgupta et al (1990) showed that the span of this lens shaped resin-rich area decreases with the angle between the optical fibre and the adjacent plies. Therefore, the aspect ratio of the of such an eye is larger the greater the angle and is a maximum when the optical fibre is embedded orthogonal to the adjacent plies. Optical fibres embedded at small angles should have less effect on the tensile strength, due to the higher fibre compaction. Therefore, in this case, optical fibres embedded parallel to reinforcing fibres should not create resin-eyes and therefore perturb the material minimally. However, figure 4.7 shows that a resin rich area can occur if the fibre is embedded between 0° and 90° plies.

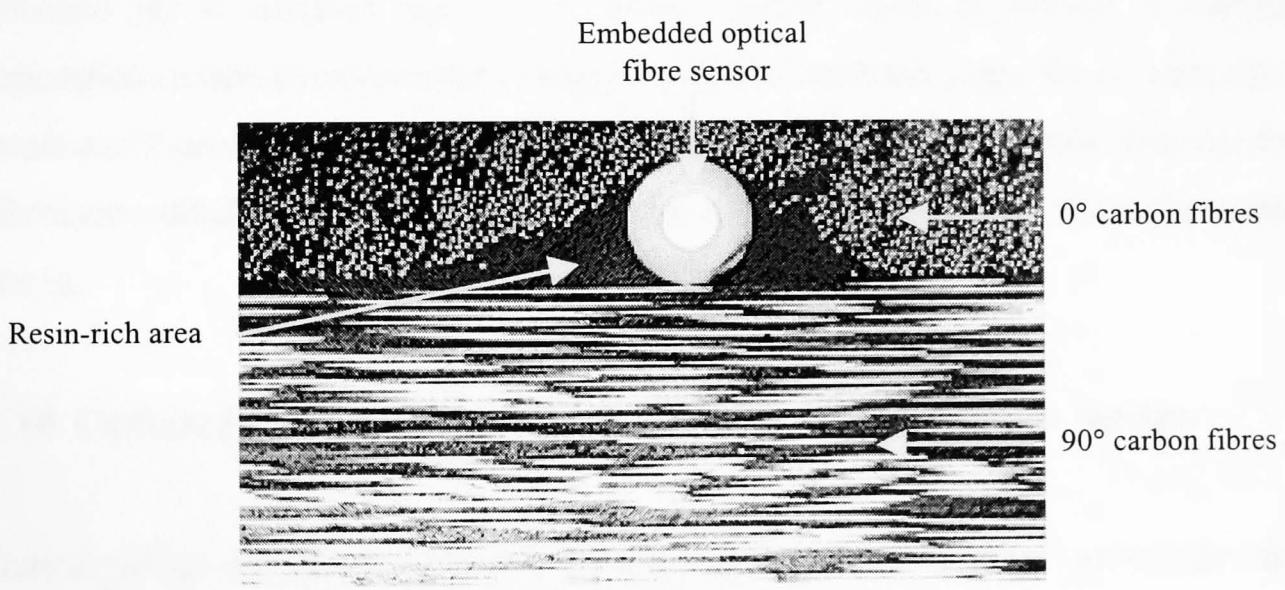

Figure 4.7 The optical fibre embedded in a cross-ply composite specimen

Typical optical fibre diameters are 12 to 100 times larger than most reinforcing fibre diameters, and two to three times the thickness of a single layer of an advanced composite material. The large size and reduced mechanical properties of optical fibres in comparison to the reinforcing fibres indicate that embedded optical fibres may act as physical intrusions, which cause a degree of structural degradation. A study by Glossop et al (1990) included a series of experiments to investigate the influence of

embedded optical fibres on the tensile strength of Kevlar/epoxy laminates. From the results obtained there was an indication of an increase in the average tensile strength of the laminates due to the embedded optical fibres. However, the variations in manufacturing the specimens reportedly gave a 10% spread in the data. In general, variations in cure cycle parameters such as cure cycle duration, applied temperature or pressure, may induce extraneous changes in the tensile failure strength.

In a related study Jensen et al (1992) compared experimental tensile strength and tensile data from seven configurations, fabricated with varying quantities of optical fibres embedded parallel to the loading direction. Significant strength and stiffness reductions (10-20%) were encountered. This study quantifies the effects of the orientation and location of embedded optical fibres on the uni-axial tensile behaviour of Graphite/Bismaleimide laminates. Experimental strength and stiffness data were obtained for 8 different test configurations. Optical fibres embedded in various orientations modestly reduce the tensile strength and stiffness properties of composite laminates (less than 10%). The largest reductions occur in composites with optical fibres embedded perpendicular to both the loading direction and the adjacent graphite fibres.

4.10 Optical Fibre Sensing Of Acoustic Emission - Literature Review

Optical fibres as intrinsic sensing elements have recently been studied for the detection of acoustical strain waves. Claus and Cantrell (1980) reported an experiment to detect the ultrasonic waves in solids using a Mach-Zehnder interferometric fibre sensor . In their system, laser light was split into two beams and launched into two separate fibres. The sensing arm of the interferometer was embedded in a plastic resin under test. The two beams were brought back together forming an interference pattern, which was spatially filtered and detected by a photodiode detector. The ultrasonic waves striking the material under test induced an optical phase delay in the optical fibre. The subsequent interference fringe shift was detected by the photodiode and converted into an electrical signal that could be analysed.

A Mach-Zehnder interferometer, with one of the single mode fibre arms attached to the graphite/epoxy composite, was used by Wade et al (1981). The detected signals correlated well with piezoelectrically detected acoustic emission events.

Two other methods which were used for the detection of acoustic emission were based on polarisation and intensity modulation. Both a polarimetric fibre optic sensor and a mode-coupling fibre optic intensity sensor for ultrasonic sensing were reported by Cielo and Lapierre (1982). The fibre was pressed against the surface of the material to be tested. Ultrasonic waves will then modulate the transverse stress in the fibre. In the first case, birefringence produced by the transverse stress in a single mode fibre generates a change of the state of polarisation, which was detected through a polarisation analyser and converted into an intensity modulation. The second approach uses a multimode fibre whose cladding has a higher compressibility than the core, such as plastic clad silica (PCS) fibre. Under compression, the refractive index of the cladding increases at a higher rate than the core. The numerical aperture of the fibre reduces as a consequence of this, resulting in a subsequent reduction in optical transmission. Both methods have been used to detect 1MHz ultrasound stress waves in materials.

Experiments have also been carried out using a few-mode optical fibre and mode-mode interference. Bennett and Claus (1986) reported a fibre optic modal domain interferometric sensor which used an optical fibre below its single-mode cut-off wavelength so that two transverse modes were generated. In these experiments, a He-Ne 633nm source and optical fibre with a cut-off frequency of 850nm had been used. If the fibre has been perturbed by acoustical pressure, the individual mode contributions to the far-field intensity function change due to the different phase delay in the two modes. The interference (or speckle) pattern shifts, and the detected signal varies. The detection was made by a spatial filter. This system has the advantage of being simple and inexpensive. It has been shown that the sensitivity and frequency response of this method allow discrimination between acoustic events generated by graphite fibre breakage and internal matrix cracking, by analysis of rise time and duration of the detected event.

However, in 1989 researchers at the University of Toronto Institute for Aerospace Studies (UTIAS) made a breakthrough in the development of a localised embedded acoustic emission detection system for composite damage monitoring based on fibre Michelson interferometry (Liu, 1989, and Liu, 1990a). At this time, little had been done to develop a fibre optic sensor for acoustic detection that could sense damage in real time. Their research included the development and testing of a system employing an active homodyne detection scheme (used to maintain linearity and maximum sensitivity). The Michelson fibre optic sensor (MFOS) system operates on the same principles as a bulk optic system (Jackson, 1985). A narrow band laser beam of long coherence length is launched into the core of a single mode fibre. A monomode (2X2) fibre directional coupler is then used to excite both the reference and signal fibre. The arms are mechanically coupled from the (2X2) coupler to the sensing region to provide common mode rejection. The signal arm is longer than the reference arm. The differential length determines the gauge length of the sensor. The ends of the two optical fibres are cleaved and mirrored and the two reflected beams recombine coherently at the coupler. The output is related to the relative optical phase difference between the arms of the interferometer corresponding to the strain experienced in the sensing region (Valis et al, 1990). The output of the MFOS represents a fringe pattern with a 2π period which corresponds to an effective change in the sensor gauge length of $\lambda/2$. The system provided single-ended sensing with real time monitoring capabilities and a certain degree of localisation. The optical fibre acoustic emission sensors were embedded into Kevlar/epoxy composite specimens. The specimens were subject to tensile loading and out of plane loading. The resulting acoustic emission signals were detected and found to have a broad-band response of 100kHz to 1MHz. Slightly later they installed a Faraday Isolator between the sensor and the laser diode to reduce the laser phase noise. The result is greater sensitivity. This added sensitivity allowed the Michelson fibre optic sensor to detect acoustic signals associated with the formation of threshold regions of delaminations (Measures et al, 1990).

In 1990 the UTIAS group described a Michelson fibre optic sensor which was capable of in-situ strain and vibration monitoring as well as acoustic emission detection in

composite structures (Liu et al, 1990b). The MFOS described above incorporates a (2X2) which has a sinusoidal response to a linear increase in strain. this relationship leads to a problem of signal fading and ambiguity in the direction of phase change (that is, due to increasing or decreasing load). This problem can be solved by operating the sensor in it's linear sensitivity range, known as the quadrature condition. A passive homodyne demodulation technique using (3X3) directional couplers were used because it allowed the integration of acoustic emission detection into the strain monitoring system, initially developed by Valis et al (1991). The sensor in this (3X3) MFOS system comprised of two unbuffered optical fibres with mirrored ends. Liu et al (1990b) performed the acoustic emission experiments using the same (3X3) coupler system. The specimens were embedded in graphite/epoxy and then subjected to three point (flexural) loading for acoustic emission detection. The acoustic emission signals were recovered, high pass filtered, and then processed with use of a PC.

Tapanes (1991) also used the same (3X3) MFOS system to monitor the strain and acoustic emission in a vibrating composite beam. The sensors were embedded at varying depths in different composites. The cantilever load frame allowed a one inch wide beam to be loaded in both tension and compression. The dynamic strain and its FFT spectral output were obtained for each sensor and were compared to a co-located electric strain gauge (ESG). A comparison showed that optical fibre sensor response compared favourably with the ESG response, irrespective of ply orientation or depth of optical sensor.

The incorporation of a strain sensor and an acoustic emission detector into one sensor offers clear advantages as damage sensitivity and structural integrity monitoring can be optimised and the required number of sensing elements in the structure will be reduced. The obvious advantages are lower costs and complexity of the structure (Tapanes, 1991).

Gunther et al (1993) described an impact detection and location system which used a fibre optic extrinsic Fizeau interferometric embedded in a graphite/epoxy laminate. In this paper, the AE generated by the impact events were detected by four fibre optic

sensors. They also developed a mathematical method and computer program which allowed the calculation of impact location from the sensor data. The authors were able to determine the impact location with a 0.5mm resolution and an accuracy typically less than 5mm. A subsequent paper by the authors (Murphy et al, 1994) described the development of an extrinsic Fabry-Perot interferometric acoustic emission sensor. This sensor could determine the location of AE in thin aluminium panels and graphite/epoxy composite laminates. This system could compute the coordinate of an AE source using the differential arrival times of the signals generated by the source. They stated that this sensor exhibited the same resolution and accuracy as their Fizeau interferometric sensor. The same group of authors (Greene et al, 1995) managed to improve the sensitivity of their AE location system by introducing high finesse Fabry-Perot cavities, which modified the output transfer function curve of the sensor.

A more recent paper by Carolan et al (1997) described the design of a non-contact fibre optic sensor for the detection of AE for structural integrity monitoring in high temperature power plant applications. This sensor was based on a Sagnac interferometer and produced an output proportional to the target velocity, without the need for active phase stabilisation. It was also inherently insensitive to low frequency perturbations of the instrument or the target. The sensor also provided anti-phase signals that are necessary for compensation of intensity noise from both the source and the target. This fibre optic sensor also incorporated an environmentally insensite downlead of arbitary length. The authors have shown that the sensor was capable of meeting the specifications for structural integrity monitoring of power plant components based on acoustic emission detection.

The use of optical fibre sensors is not limited to structural integrity monitoring. The acoustic emission from cutting processes and machine tool wear can be measured optically. The techniques used in this type of application possibly could be adapted for damage assessment. Research undertaken by Heriot Watt University, and latterly jointly with Brunel University show the possibility of adapting Michelson and Mach-Zehnder interferometers. Acoustic emission originates in the plastic deformation processes which are associated with chip formation in the tool as it wears.

AE is monitored using piezoelectric transducers(PZ), however, these cannot be installed directly on to tool. Indirect AE detection is therefore degraded by noise sources in the machine. Also the frequency range detectable is limited by the mechanical resonance of the PZ transducer. For these reasons, non-contacting measurements are attractive. Vibrations normal to the surface produced by AE are monitored remotely. The vibrations typically have amplitudes on the 0.1nm scale, in the frequency range 0.1-1MHz. It has shown by Palmer and Green (1977) that interferometry can be used to detect such vibrations. However, they proved this was possible using bulk optic components, which suffer from alignment and stability problems, and therefore such a system could only be used in the laboratory.

McBride et al from Heriot-Watt University have developed a Michelson interferometer for the remote detection of low amplitude, high frequency vibrations (McBride et al, 1990). Their initial tests on the interferometer were made in the laboratory by probing the surface of a commercial AE transducer which was driven to vibrate between 100-600kHz. The machine tests were carried out by probing the AE from a steel block being milled. The Michelson sensor offers high bandwidth, flat to > 1MHz. PZ transducers on the other hand have restricted bandwidths.

Zheng et al (1991a, 1991b) developed a novel optical fibre sensor for detection of acoustic emission. The sensor was intended for use in monitoring machine tool wear. The sensing element, a monomode optical fibre, was held in contact with the surface to be probed. The interferometer used was a Mach-Zehnder type. Light from a Helium Neon laser was launched via a microscope objective in to one arm of the directional coupler. In the signal arm, there is one polarisation before the sensing element for polarisation eigenmode selection, while another after the sensor for control of interferometer visibility. In the reference arm, phase modulation was achieved using several turns on a PZT tube. The probed surface was initially excited using a separate PZT transducer, at various frequencies in the range 190-990kHz .The response compared favourably with commercial PZT sensors in the range 0.2-1MHz. The Michelson interferometric sensor developed by Heriot-Watt was adapted to detect AE produced by metal cutting processes (McBride et al, 1991; and McBride et al, 1992).

The conclusions made by the group were that the interferometer operated successfully in a workshop environment. They also found that the results correlated very well with those from conventional transducers.

A recent paper by the group at Heriot-Watt University (Carolan et al, 1997b) investigated the relationship between tool wear and the AE energy produced during various face milling finishing operations. In these tests a non-contact fibre optic Michelson interferometer was employed for the AE detection from the workpiece. This interferometric system incorporates the active homodyne system, which helps maintain the interferometer at quadrature. This processing technique enabled the authors to monitor the low frequency vibrations, as well as the desired high frequency AE signal. The interferometric system was also able to produce the real-time displacement information over unlimited timescales. They also found that this fibre optic sensor had no resonances in the response (unlike conventional PZ transducers), and could achieve MHz bandwidths through conventional photodetector circuits. A subsequent publication by the author group (Carolan et al, 1997c) showed that the same Michelson interferometric sensor could monitor the frequency content of the AE signals produced during finish milling operations.

The papers highlighted in this section clearly indicate the possibility of using an optical fibre sensor to monitor damage that occurs in composite materials. There are many other papers using optical fibre sensors for detecting acoustic emission in other applications. Concrete structure monitoring, leak detection, surface acoustic wave monitoring, aerospace structure integrity monitoring and cure monitoring have been investigated.

For example, there are many publications which highlight the need for fibre optic sensors to detect leaks from fluid and gas-filled pipes. One such paper (Kurmer et al, 1993) presents a distributed fibre optic sensor capable of leak detection. This sensor, based on the Sagnac interferometer, was placed on the inside of the pipe. This sensor could locate leaks to within a few metres by monitoring the AE produced by fluid or gas as it escaped from the pipe.

It has been stated earlier that future advanced aerospaces vehicles will incorporate fibre optic smart sensor networks to monitor the structural integrity and manage overall structural health. Schoess and Zook (1993) and Schoess et al (1994) describe an AE micromachined sensor capable of monitoring the in-flight structural integrity of an aerospace structure. This unique sensor approach combines silicon sensor machining, optical fibres and connectors to measure acoustic emission event data relating to structural failure.

Robertson and Luddon (1997) have proposed a condition monitoring system for long synthetic ropes based on AE detection of yarn breakage using an array of fibre gratings distributed along the rope length. Optical time domain reflectometry was used to locate yarn breakage and provide positional information on the strain/temperature distribution. The authors also stated that this quasi-distributed fibre optic sensor would be suitable for monitoring other structures such as buildings, industrial process plants and bridges.

The use of fibre optic sensors for the detection of AE in industrial situations has increased over the last ten years. These publications highlight the fact that there are many applications in industry, where the detection of acoustic emission is of supreme importance.

4.11 Summary

Optical fibres have unique properties which have fuelled the rise in the use of optical fibre sensors in industrial, medical, and scientific fields. For structural integrity monitoring, it has been shown that the introduction of an embedded optical fibre into a composite structure does not significantly reduce the strength or stiffness of the composite. In these type of sensors, the characteristics of the light are modulated by an external stimulus, such as acoustic emission. The total phase of the light propagating along an optical fibre can be modulated due to the changes in the

properties of the fibre waveguide. The acoustic emission emanating from a source interacts directly with the fibre and hence modulates the phase. The detection of this phase change can made using interferometry. A review of the literature reveals that much work has been done in the area of optical fibre sensing of acoustic emission. However, most of the research studied involved the Michelson and Fabry-Perot interferometers, with little interest being shown in the Mach-Zehnder configuration. The Mach-Zehnder interferometer has the advantage that it does not require sputtered embedded or end mirrors. However, the simple Mach-Zehnder configuration needs to be modified if it is to be used as an acoustic emission sensor.

CHAPTER 5

DEVELOPMENT OF THE FIBRE OPTIC ACOUSTIC EMISSION DETECTION SYSTEM

5. Development Of The Fibre Optic Acoustic Emission Detection System

5.1 System Overview

The design of an optical fibre phase modulated transducer is a two-stage process. The first stage involves the sensing element, where the mechanical interactions between the measurand and the optical fibre produce a phase shift in light transmitted. In the second stage the interferometer detects these phase shifts by modulating the output intensity. The development of an optical fibre sensor to monitor acoustic emission (AE, the measurand) in advanced composite materials commenced with the selection of the Mach-Zehnder interferometer (figure 5.1) as the sensor.

A Mach-Zehnder interferometer was modelled on the tool wear monitoring sensor developed by Zheng et al (1992). However, many modifications were necessary to adapt this sensor to detect the damage mechanisms in composites, which can ultimately lead to the catastrophic failure of the material. To increase the sensitivity of the optical fibre sensor, the following changes were included: the sensor was embedded in the material, the reduction of optical feedback, better filtering electronics, a demountable test section, and the introduction of fibre collimators. The schematic illustrated in figure 5.2 shows the all-fibre Mach-Zehnder interferometer capable of sensing acoustic emission.

In the all-fibre Mach-Zehnder interferometer the light is coupled from a coherent source (for example, a polarised He-Ne laser or a laser diode) into a monomode optical fibre, and its amplitude is divided into two paths by means of a directional coupler (DC1). A directional coupler is the fibre optic analogue of the conventional beamsplitter. In a sensor, one of the arms is termed the sensing or signal arm, and the other the reference arm. In the signal arm, a polarisation controller precedes the sensing element for the selection of the polarisation eigenmode, while another succeeds the sensing region to control the interferometer visibility. This enables the

recombining beams to be mutually coherent and have identical polarisation states. One parameter, on which the sensitivity of the sensor is dependent, is the visibility. This parameter is in turn dependent on the optical path difference between the two arms of the interferometer. The introduction of the graded index lenses (that is, the fibre collimators) gives the opportunity to vary the optical path length of one of the arms manually. The fibre collimators help reduce the optical path difference to zero, thus increasing the sensitivity of the sensor. A piezoceramic phase modulator in the reference arm accomplishes the desired phase modulation. In short, this is achieved by wrapping several turns of fibre around a PZT tube driven by a high voltage feedback from the suitably filtered interferometer signal.

In the sensing element, a length of single mode optical fibre was embedded in a 16-ply carbon fibre reinforced polymer (CFRP) composite using single specimen moulds. A section of the sensing arm, equal to the embedded and pigtail lengths of the test piece, was cut out and replaced with a demountable composite test sample.

The signal and reference beams are recombined at a second directional coupler (DC2), giving two optical outputs at the detectors (PD1 and PD2). The signal beam is phase modulated by the external stimulus (that is, the measurand), whereas the phase of the reference beam remains constant. The resulting interference signal needs to be in quadrature. This is achieved by implementing an active homodyne feedback technique, which locks out any environmental phase perturbations. After passing through a high-pass filter (100kHz cut-off frequency) the output signal becomes the optical phase change induced by ultrasonic waves. The outputs from the fibre optic AE detection system will be monitored using a spectrum analyser and an Acoustic Emission signal analyser (AET5500). The AET5500 collects the output and determines in real-time a series of acoustic emission parameters which will help distinguish the level of damage.

More detailed descriptions of the components and techniques used to construct the all-fibre interferometric acoustic emission sensor can be found in the remaining sections of this chapter.

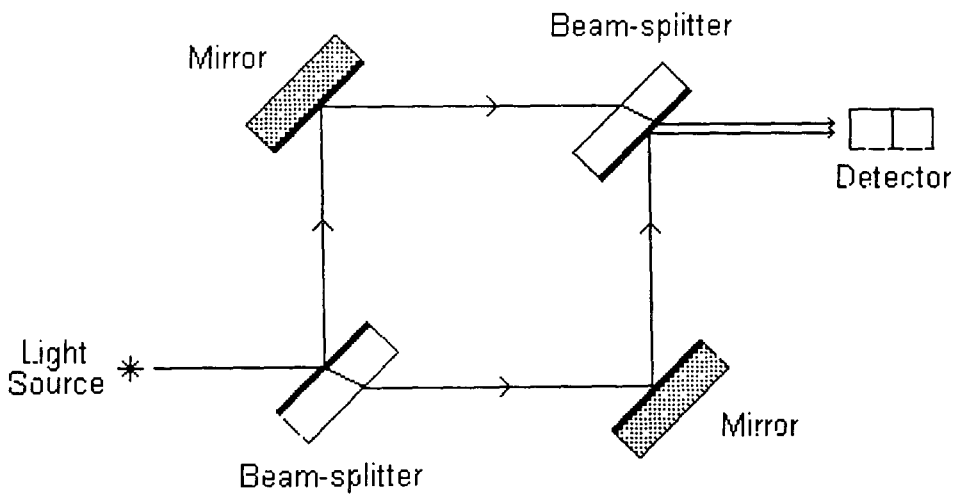

Figure 5.1 The Mach-Zehnder interferometer configurations. The top diagram shows the classical bulk optic version whilst the bottom illustrates the fibre optic equivalent.

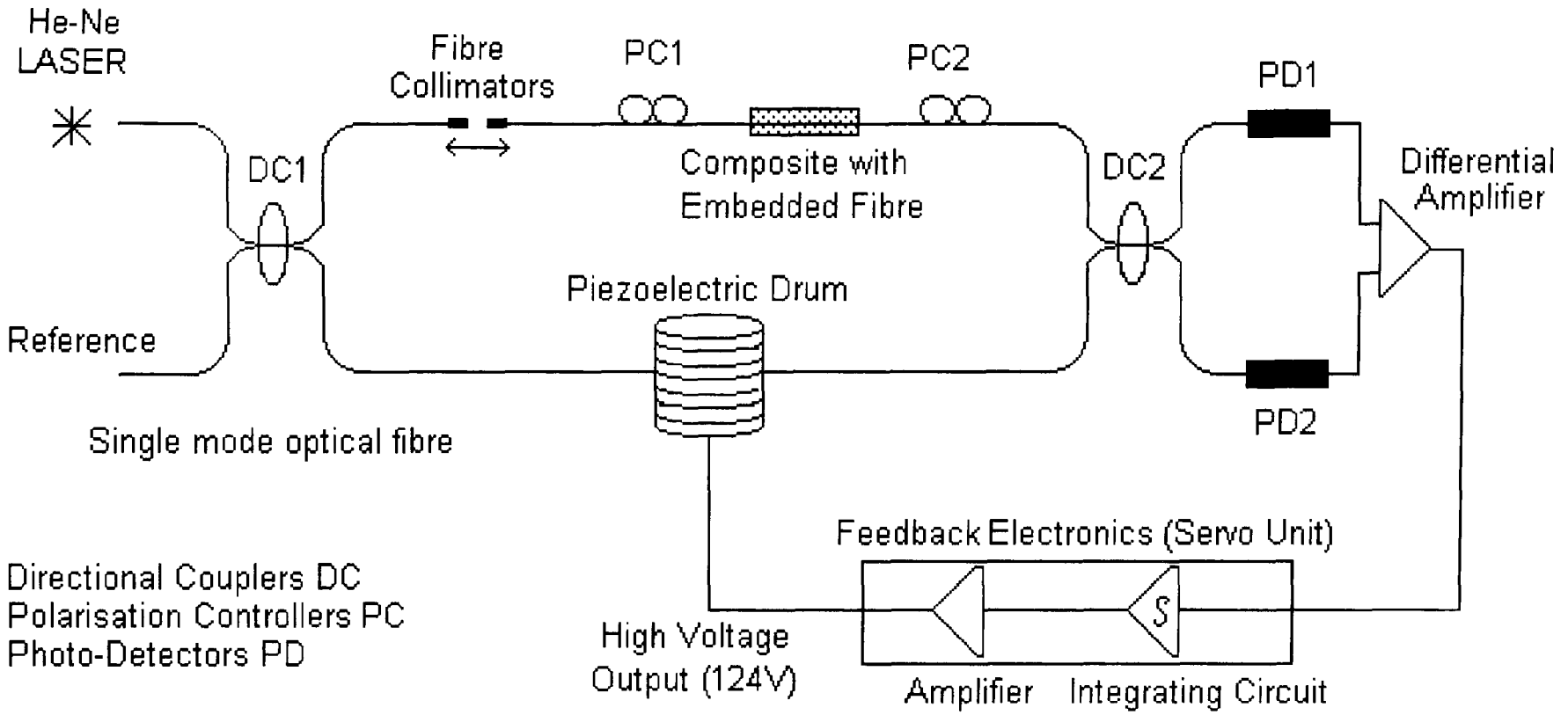

- Directional Couplers DC
- Polarisation Controllers PC
- Photo-Detectors PD

Figure 5.2 The Mach-Zehnder interferometric fibre optic sensor.

5.2 Components and Techniques

5.2.1 Laser

A Helium-Neon (HeNe) gas laser was used to provide coherent radiation for the interferometric acoustic emission detection system. In the system a 7mW, 632.8nm Uniphase (model 1125P) HeNe laser was used, which has a coherence length of approximately 200mm (figure 5.3). For interference to occur, the optical path difference between the to arms of the interferometer must be within the coherence length of the source. This means that the light will be coherent over the sensing length, and therefore the photons at a given position and time should be of the same phase and polarisation. The optical path difference between the two arms of the interferometer was of the order of a few millimetres throughout the experimentation, and therefore the laser coherence length was sufficient.

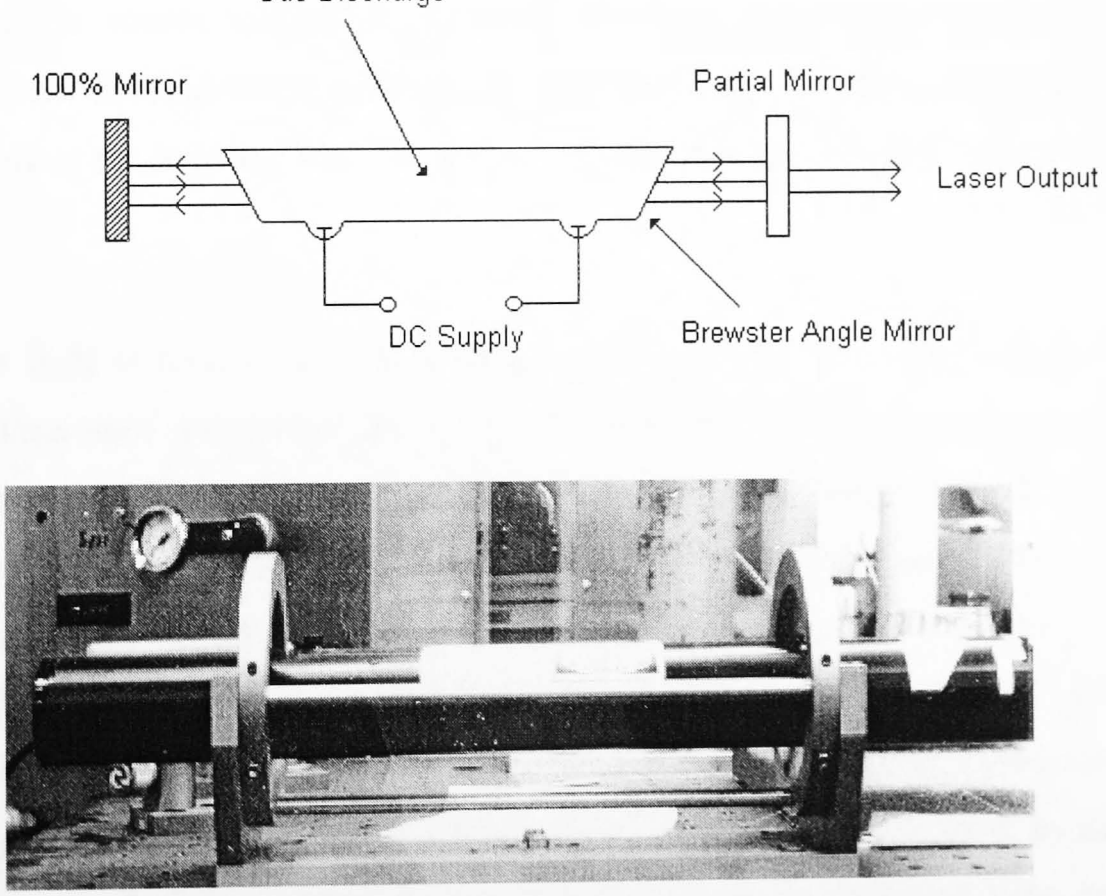

Figure 5.3 A basic schematic and photograph of the Helium-Neon laser used in the detection system.

The appearance of an optical path difference in an interferometer results in additional noise in the system. The larger the path difference, the greater the noise. Therefore, if a very low coherence source (in the order μm) was used in the system, the occurrence of interference would mean that the optical path difference would be close to zero. A low coherence LED source, with a coherence length of approximately 20μm, would have been preferred, however, financial restrictions prevented the use of such a source. A technique using fibre collimators has been used to reduce/maintain the optical path difference (explained in section 5.2.2).

5.2.2 Optical Path

(A) Launching Laser Into The Optical Fibre

The laser light is launched into the single mode optical fibre, with the help of a X20 microscope objective lens mounted onto a fixed point on a *Photon Control* optical module. The focusing lens reflects a sizeable amount of light back into the laser cavity, which causes instability and leads to phase noise at the output of the interferometer. To reduce the feedback into the laser cavity, the laser is positioned at a slight angle to the focusing lens. This, however, has its disadvantages (refer to Figure 5.4).

The laser light is focused at a slight angle to the cleaved fibre face, and since the focused laser spot dimensions are far greater than the fibre core, it is difficult to launch as much light as possible into the system. The fibre, which is held in the V-groove by small rubber-backed magnets, is adjusted to move closer to the focused spot of laser light by adjusting the XYZ positional controllers. Since the laser spot is greater than the fibre core, some light is launched into the cladding. Some of this light escapes the cladding and can be viewed by the naked eye. This can give a visual indication whether maximum light is being launched into the fibre, that is, by way of monitoring the 'bleeding light'. Experimentally, maximum launched light can be obtained by tracking the output using an oscilloscope.

The light is actually launched into one input port of a single mode Sifam 2X2 directional coupler, where it is split into two beams of equal intensity. The light travels down each arm of the interferometer to the two input ports of the second (or exit) 2X2 directional coupler. The two output ports of the directional couplers are connected to photodiodes. Sifam supplied the lengths of single mode fibre fused between the two directional couplers. This optical fibre had a core diameter of 4μm, and an outer cladding diameter of 125μm.

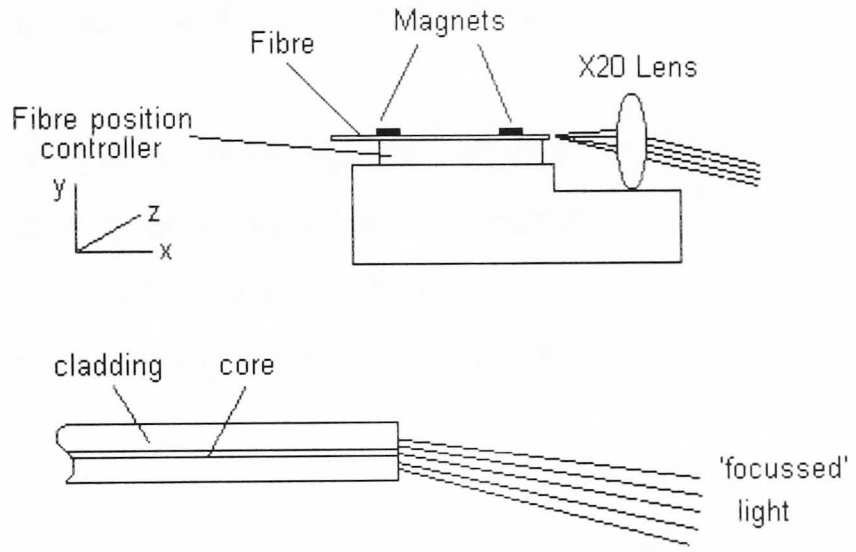

(a)

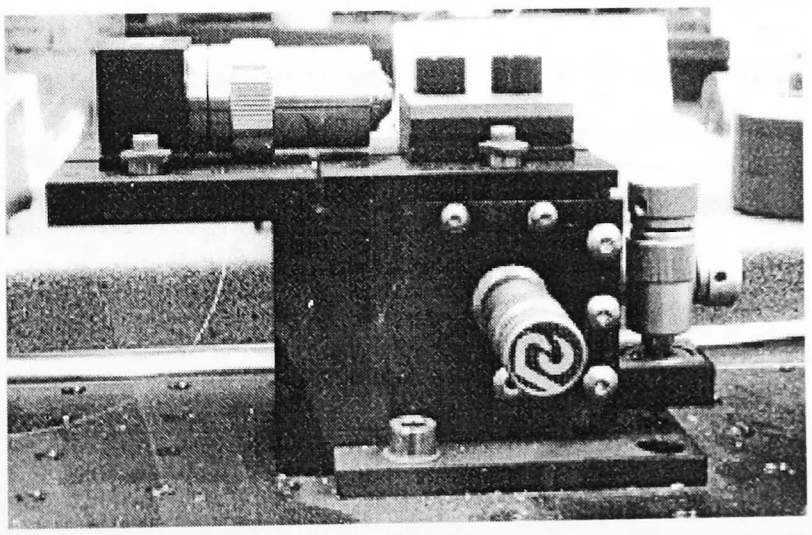

(b)

Figure 5.4 (a) Schematic of launching of laser light into the single mode fibre and (b) a photograph of the launching optics and module.

(B) The Sensing Region And Test Section

The entire sensing region of the fibre optic Mach-Zehnder interferometer is formed between the two 2X2 directional couplers. However, the actual sensing region is constrained by the length of the composite sample. The sensing length embedded optical fibre is 200 millimetres. The length of optical fibre was unbuffered; the acrylate buffer layer was physically removed from the silica fibre after firstly being softened with Nitromors® paint stripper. The bare fibre was then cleaned with alcohol/acetone to remove all dirt, dust etc. from the surface.

During the cure cycle of the composite, the bonding between the embedded silica fibre and the buffer layer becomes poor. The stripping of this plastic layer would give the best possible bonding between the composite material and the embedded silica fibre, therefore maximising the amount of acoustic energy coupled into the core of the optical fibre.

A convenient method of changing test samples in the sensing arm is needed. The composite samples have optical fibre pigtails (that is, fibres coming out from the ends of the composite) with a standard length of 1.61 metres. A demountable section (exactly 1.61 metres) of the interferometer is used as the test section. Since many samples are tested, reusable optical connectors are needed between the test section and the sensing arm. Mechanical splices were used because of their reliability and robustness (refer to 'Optical Connectors' section).

(C) Fibre Optic 2 X 2 Directional Coupler

When the laser light is launched into the input optical fibre a device is needed to direct the light into each arm of the Mach-Zehnder interferometer. In a conventional, bulk optic interferometer this task is executed by a beamsplitter. However, due to alignment problems and possible in-service vibrations, this type of device is typically used in the laboratory only. In an industrial environment, an all-fibre alternative is

preferred. A single mode fibre directional coupler serves the same purpose in a fibre optic interferometer as a beam splitter in a conventional interferometer. These bi-directional couplers take light and split into multiple paths or combine multiple paths together to give a coupler with N inputs and M output ports (refer to Figure 5.5).

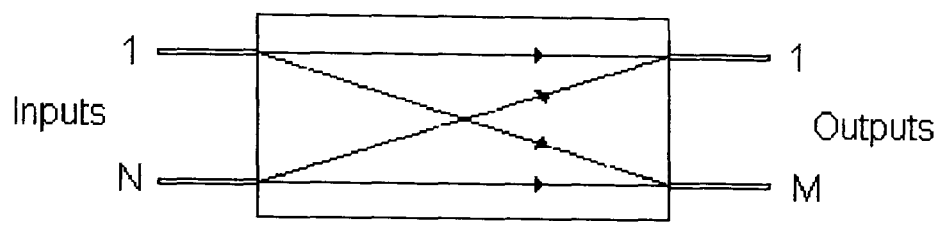

Figure 5.5 Schematic representation of a 2X2 (N=M=2) fibre coupler. Power flowing in either input fibre will be distributed in some predetermined ratio in the output fibres.

Since two paths, the reference and sensing paths, are present in a Mach-Zehnder interferometer, then 2X2 (N X M) couplers are needed. Sifam supplied the directional couplers used in the fabrication of the interferometric system. These particular couplers each had beam-splitting ratios of 50% +/- 5%, with an insertion loss of 0.8dB (17%) for wavelengths of 633nm. Sometimes these couplers are expressed with respect to decibel loss, that is, a 50% loss (or 1:1 splitting ratio) is equivalent to 3dB, and therefore are referred to as 3dB couplers.

(D) Optical Connectors

In this all fibre interferometric system there is a need for optical connectors. The reference and sensing arms of the system need to be connected between the 2X2 directional couplers. Also, the embedded optical fibre pigtails from the composite need to be connected to the test section of the sensing arm of the interferometer. The illustration below indicates these connection points.

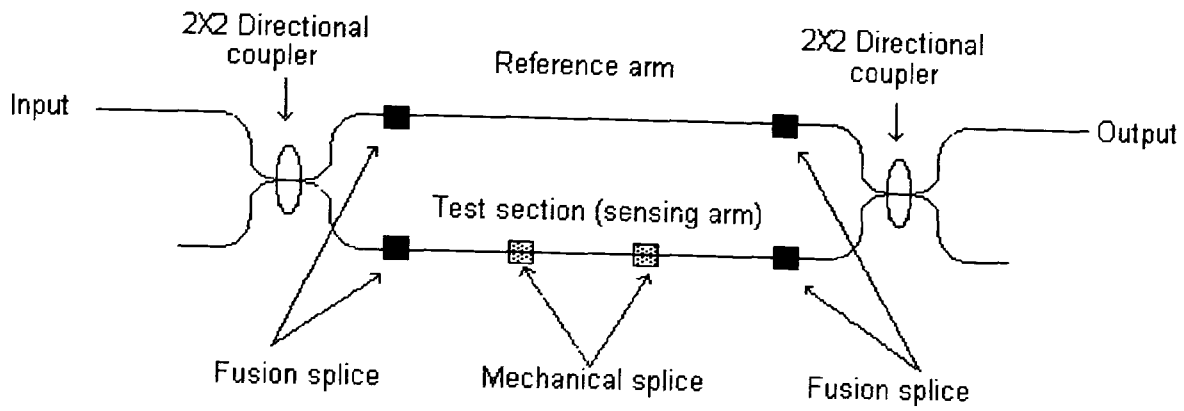

Figure 5.6 The optical connections in an all-fibre Mach-Zehnder interferometer

There were three points to be taken into consideration when constructing the all fibre Mach-Zehnder interferometer: (i) robustness of the splice, (ii) minimal loss of radiation, and (iii) a convenient method of changing the test specimens. There are many sources of radiation loss in a fibre-to-fibre connection, which are illustrated below.

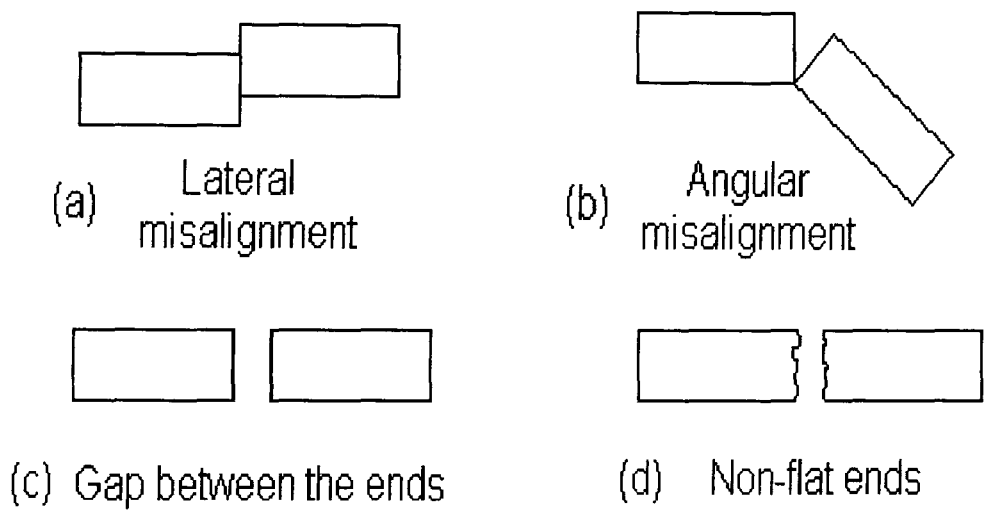

Figure 5.7 The radiation losses in a fibre-to-fibre connection.

There are two different methods of optical connection in an all fibre system: fusion splicing and mechanical splicing. A fusion splice consists of two carefully cleaned and cleaved optical fibres that are aligned and fused together with a high voltage electrical arc. The bare fusion splices need to be protected using a heat-shrinkable

plastic tube reinforced by metallic strength members. This splice protection increases the splice tensile strength and seals the bare splice from the external environment (OH ions) to ensure long term reliability. This type of connection was made between the directional couplers and the reference and sensing arms because this permanent fusion splice is more robust and reliable.

The fusion splicing can be achieved by using the BICC AFS 3100 fusion splicer. This arc-splicing machine also minimises the radiation losses in fibre-to-fibre connection. The machine can automatically align the fibres along three axes and perform a reliable and effective fusion of single mode fibres (eradicating losses caused by (a)-(c) shown in Figure 5.7). The quality of the cleave can be checked using the microscope of the fusion splicer (thus minimising the effect of problem (d) in Figure 5.7). When looking through the objective lens it is possible to check the cleave in both the horizontal and vertical direction.

Another method of joining optical fibres, although in a less permanent fashion, is via the mechanical splice. Lightbridge mechanical splices and an installation tool make this option possible. The splice is constructed of four moulded parts which include: the outer body structure, a fibre clamp with a 60° V-groove, and two identical jacket buffer adapters (which accommodate fibres with different jackets). These moulded parts are held together by a spring. Optical connection is achieved by placing the splice in the Lightbridge installation tool and then rotating the operating lever forward which opens the V-groove clamp. The mechanical splice is now ready to accept the stripped and cleaned fibres. Once the fibres are butted together they can be held in place by rotating the operating lever back. Coupling of the fibres is aided by the presence of index matching gel. Since these mechanical splices could be re-opened repeatedly, they were used in the test section to ensure that a reliable, consistent, and convenient method of optical connection was made between the sample and the interferometer. Before a new sample was inserted in the test section, the optical spice was cleaned out using a pin-like cleaning tool. Inserting new 3M index matching gel using a dispensing tip for splices made optical coupling.

(E) Fibre Collimators

In a Mach-Zehnder interferometer, the output can be maximised by equalising the optical path lengths of the reference and sensing arms. The method involves the use of Graded Index (GRIN) lenses. The GRIN lens or fibre collimator produces a collimated beam from a fibres output, receives an already collimated beam and focuses it into a fibre. Initially, two single mode 48/52 couplers were fused together such that the lengths of their arms were approximately the same lengths. The two GRIN lenses were mounted in one arm (the sensing arm) of the interferometer so that the difference in the two interferometer arms can be adjusted with great precision.

The first step is to properly align the two lenses. A possible set up is to use 'photon Control' XYZ positional controllers to ensure maximum alignment. The two collimators are placed in a housing (syringe tubing) to prevent accidental misalignment. One of the lens is held in position while the other only moves in the horizontal axis only.

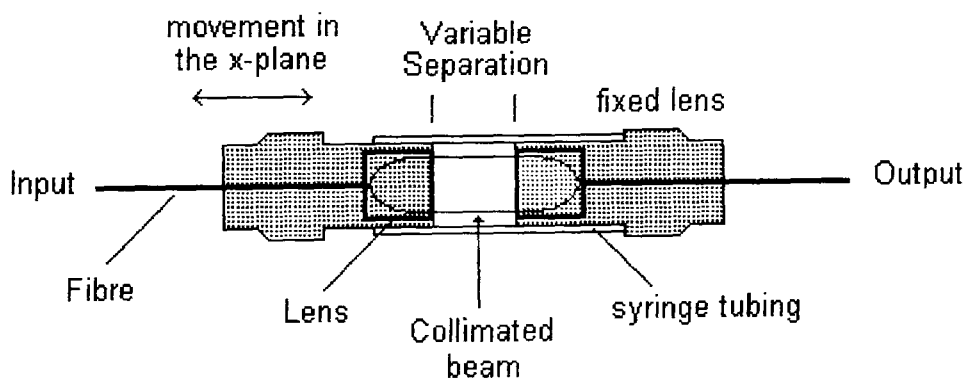

Figure 5.8 Equalising the optical pathlengths of the two arms of the interferometer using graded index lenses.

If the difference in the lengths of the two arms is greater than the coherence length of the light source, then there will be no fringes. The distance between the two GRIN lenses is varied until a fringe pattern begins to appear. Once this achieved, the GRIN lenses are finely adjusted to obtain maximum fringe contrast. It was mentioned earlier

that the fibre collimators were used to match the optical path lengths of the two arms. The length of each embedded fibre and its pigtails inserted into the test section may not be cut to the required length. Therefore, if the fibre is cut too small the distance between the collimators will be increased. Since it is possible that the fibre length could be too large, it was decided that the X-plane scale would be altered to plus/minus scale (with the collimator set at zero) to ensure that the collimator could move the same amount in each direction. Since the collimator can move a total of 8mm, the fibre to be embedded must be within the 4mm of the required standard length. A 'Selfoc' Fibre Collimator was used and comprises an optical fibre aligned to a 0.25 pitch Selfoc Lens, all inside a convenient housing.

5.2.3 Polarisation Controllers

The sensitivity of interferometric sensors can be limited by the fact that the HE_{11} mode can be decomposed into two non-degenerate polarisation modes for real fibres. As a result, long optical paths in doped silica produce a modification of the state of polarisation as a function of thermal and mechanical stresses in the circular shape of the core. So the introduction of a device that uses the birefringence created by bending will affect the overall sensitivity of the system. The device, which is the equivalent of the fractional wave plates of classical optics, is illustrated in figure 5.9. Leferve (1980) and Ulrich (1979) have both theoretically shown that the modification of the effective indices of both degenerated polarisation modes is due directly to the radius of the fibre and the radius of curvature of the fibre.

In optical fibre sensors using non-polarisation-maintaining (non-PM) fibres, the state of polarisation (SOP) at the receiving end fluctuates due thermal and mechanical perturbations of the fibre. When polarisation-sensitive elements are present, these fluctuations result in undesirable intensity noise and signal fading. The development of single polarisation (SP) and polarisation maintaining (PM) fibres have reduced these problems. These fibres, however, are very costly and therefore the need for fibre polarisation controllers still exists.

Polarisation controllers are devices which transform any given input SOP into an arbitrary output SOP. Since an SOP has two degrees of freedom, this function requires at least two control elements. As polarisation variations usually have a thermal origin, slow active control is generally sufficient. In applications requiring a precise (linear) polarisation at a given location along the fibre, the controller can be followed by a polariser. The general function of a controller is therefore usually limited to bringing the SOP to approximately the desired value.

In fibre polarisation controllers, birefringence is induced through either squeezing (Johnson, 1979), bending (Lefevre, 1980), or the Faraday effect (Okoshi, 1985) to form the fibre equivalent of fractional wave plates or rotators. They generally exhibit a limited tuning range, so that active control requires occasional resetting and momentary loss of signal (Ulrich, 1979). Endless polarisation control is a condition which avoids this difficulty and provides continuous control of the SOP.

A simple, passive device is made of a fibre which is coiled to induce asymmetric radial strains and birefringence. The two eigen-polarisations are parallel and perpendicular to the plane of the coil. The coil radius of curvature R is selected so that the phase retardation between the eigen-polarisations is either 90° ($\lambda/4$) or 180° ($\lambda/2$). The output SOP is adjusted by simply modifying the angular orientation of the coil about the AB axis (refer to figure 5.10 below).

This adjustment rotates the birefringent axis with respect to the incident SOP. A series of two $\lambda/4$ coils forms the most general controller. The insertion loss is primarily due to the bending loss in the fibre and can be made arbitrarily small by selecting a sufficiently large bend radius and correspondingly increasing the number of loops in the coil (Matsumato and Kano, 1986) . Endless control is possible with a few simple mechanical fixtures which allow the possibility of rotating each coil in the same direction indefinitely without twisting the fibre.

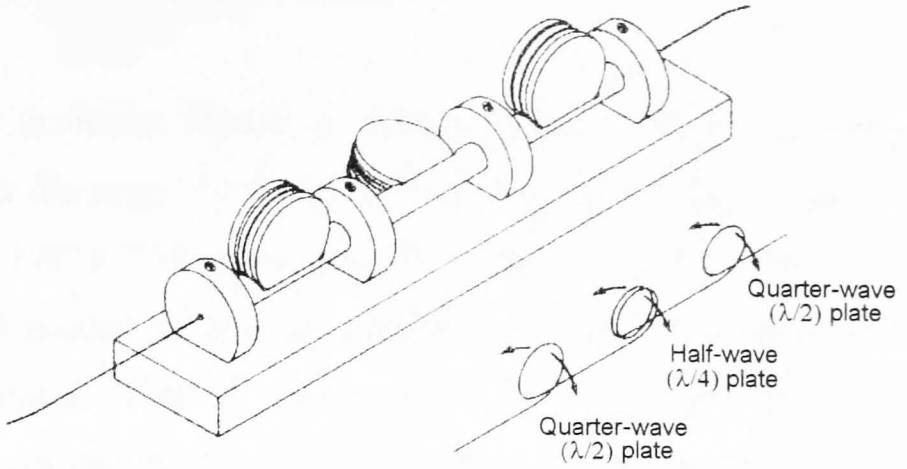

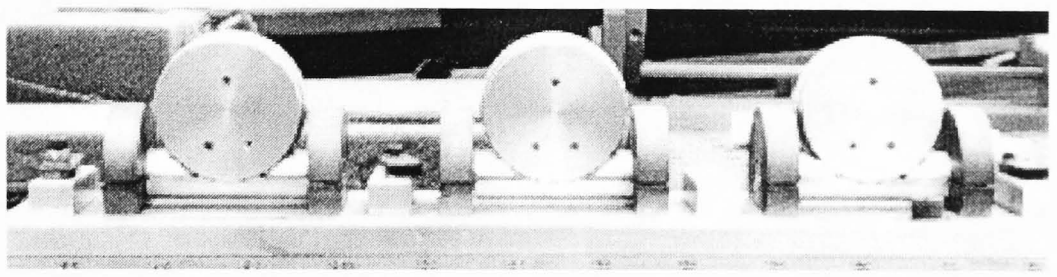

(C)

Figure 5.9 Polarisation control in single mode fibre. (A) Sketch of the device, (B) configuration of the fibre, indicating the freedom of rotation of plane of each individual coil, and (C) a photograph of the controller used in the system.

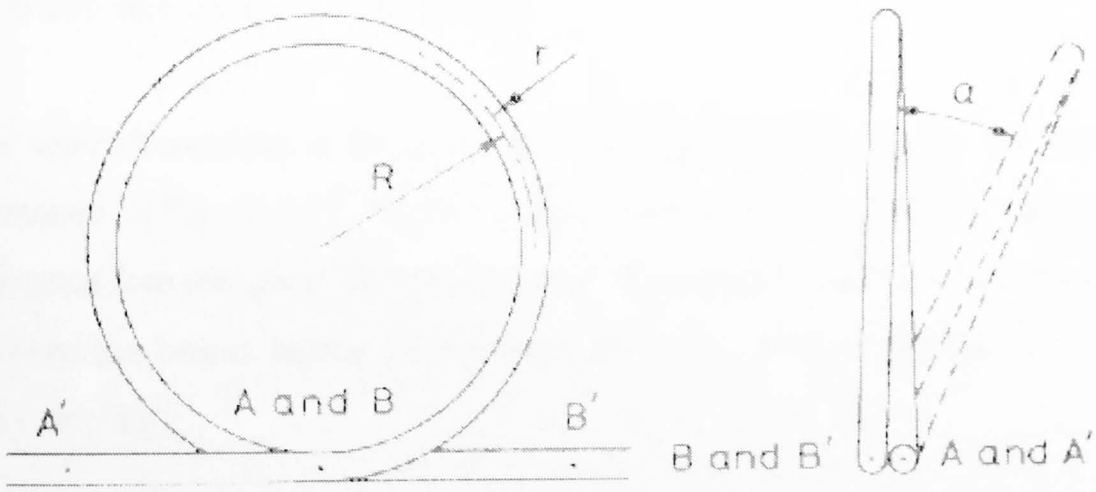

Figure 5.10 Lateral view, and axial view with rotation of the coil plane, in the particular case of a λ/m device with a single loop.

5.2.4 The Active Homodyne System

The acoustic emission signals of interest were found to generate displacement amplitudes in the range 10^{-12} to 10^{-9} m over the frequency range 100kHz-1Mhz (Zheng et al, 1992). To be able to detect small order phase shifts (< 0.1 rads), signal processing is needed to provide automatic linearised and real-time output of the measurand signal. This is accomplished by maintaining the interferometer at quadrature, such that the phase difference between the interfering light beams is $\pi/2$ radians. Environmental phase perturbations (low frequency vibrations and temperature changes) can cause the interferometer to drift away from its quadrature point, which can lead to loss of sensitivity and loss of signal.

There are two approaches to signal processing the data produced by the single mode fibre interferometer : homodyne and heterodyne detection. The most straight-forward technique is known as the 'Active phase tracking homodyne scheme'. This set-up employs a quadrature phase feedback technique, which controls the phase of the reference arm. This system compares the output signal from the interferometer with a reference level, which is maintained at its maximum sensitivity point (that is, its quadrature point). The difference between the two signals (the error signal) is amplified to drive a linear phase actuator within the interferometer to maintain the interferometer at this quadrature point.

The active homodyne scheme can be visualised with the aid of the block diagram illustrated in Figure 5.11 The two optical outputs from the directional couplers were converted into electrical signals by a pair of photodiodes. There is a phase difference between the beams falling on the detectors of π. The two signals, A and B, can be represented by

$$I_A = I_O[1 + V\cos(\phi_{sig} - \phi_{ref})]$$
$$I_B = I_O[1 - V\cos(\phi_{sig} - \phi_{ref})]$$

where V is the fringe visibility and I_O is the input laser intensity.

The two signals were combined in a difference amplifier to produce a signal proportional to the cosine of the phase difference between the reference and sensing arms. Since the quadrature condition is $\phi = (\phi_{sig} - \phi_{ref}) = \pi/2$, the output from the difference amplifier can be used as a suitable error signal.

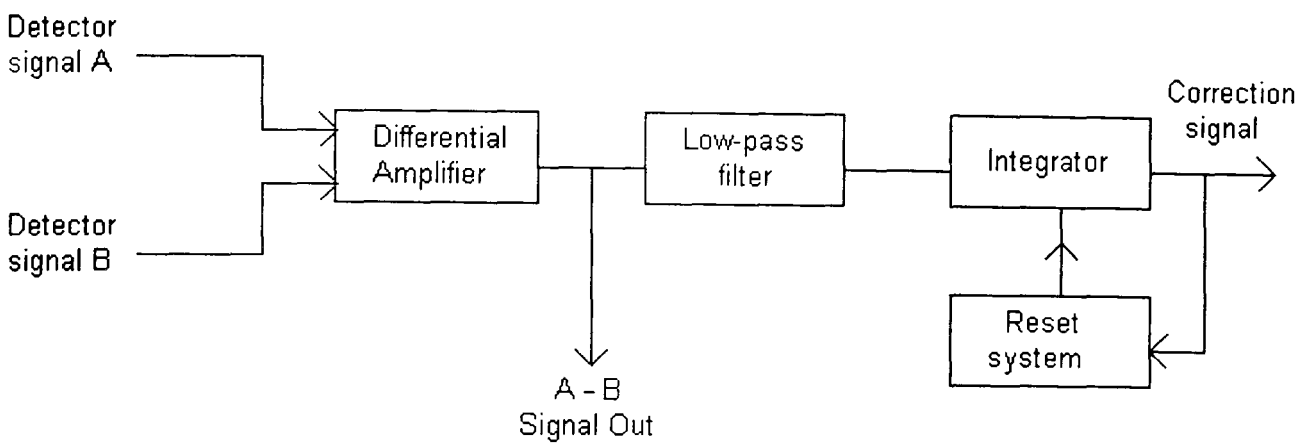

Figure 5.11 The block diagram of the Active Homodyne system.

Therefore, in the absence of any modulation of the sensing arm, the system may be held at quadrature by making the differential amplifier signal part of the feedback loop connected to the reference arm modulator, and then ensuring that the differential amplifier signal remains close to zero. In the presence of a signal, the differential signal cannot be used directly in the feedback loop because the signal information will also be cancelled out. However, it is likely that any ambient modulation of the reference arm will take place at a lower frequency (e.g. low frequency mechanical vibrations) than that of the signal. Thus the difference signal integrated over a long time compared to the signal (high frequency) modulation but short compared to the ambient modulation can often provide a suitable feedback signal. The output of the integrator was then applied to the reference arm modulator to continuously compensate the sensor to create a 'perfect' system operating at the quadrature point and with no reference arm phase drift. The output range of the integrator was limited to +/- 15 Volts. This corresponded to a phase compensation range of +/- $\pi/2$ radians. If the relative phase drift exceeded this value a reset electronic system was used. This

system caused the output of the integrator to be reset to 0 volts upon reaching either the -15V of +15V limit.

The simplest way of providing linear phase actuation is to use a piezoelectric (PZT) cylinder as a fibre stretcher. A substantial portion of the reference arm (approximately 9 metres) is wrapped around the cylindrical PZT. When the voltage, which is derived from the error signal, is applied across the walls of the cylinder, the circumference of the cylinder changes due to strain induced in its wall thickness, height and circumference, thus stretching the fibre and hence inducing a phase change.

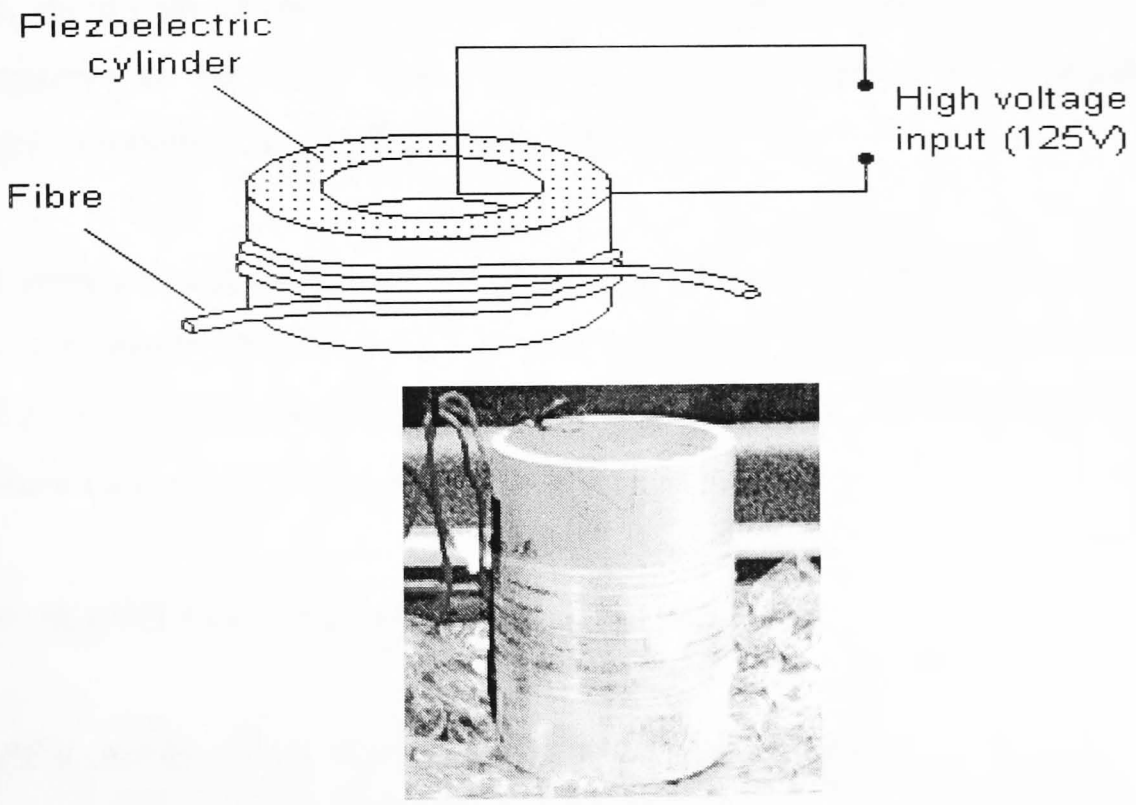

Figure 5.12 Schematic and photograph of the piezoelectric cylinder phase modulator.

The active phase tracking homodyne scheme is easy to implement and is usually extremely linear in operation. However, there are many disadvantages with this system. This scheme uses an electrically active element which requires a high voltage (typically 125V) for the piezoelectric element. This could reduce the sensor's role in an industrial environment as it is no longer an electrically 'safe' device. Furthermore,

although the phase range is much in excess of 2π it is still limited, and large phase deviations may require the resetting of the system, therefore resulting in the loss of some information. This particular problem does not apply in the case of acoustic emission monitoring as the induced optical phase change can be quite small ($\phi < 0.1$ rad).

5.2.5 The Custom-Built Active Homodyne Detection Unit

The system acquired to maintain the interferometer at quadrature was a custom built unit manufactured by Mirage. A schematic of the unit is shown in Figure 5.13. The two-tiered unit consists of sum and difference amplifiers, servo unit, power supply unit, and a high voltage amplifier. The *sum and difference amplifier* allows variable attenuation of the inputs with subsequent signal summation and subtraction. The subtraction output has switchable gains of 1, 10 and 100.

The *servo unit* allows variable coarse and fine offsets to be added to the input signal. This then passes through a loop filter, and then added to the optional modulation input and is outputted via BNC connections on the front panel. The modulation input has variable gain and can be switched in and out.

The ' SERVO TYPE ' control allows choice of loop filter :-

TYPE 0 : No loop filter - servo output is modulation signal .

TYPE 1 : Loop filter is an integrator with variable unity gain frequency.
X1, X10 and X100 settings give centre frequencies of 15Hz, 150Hz and 1.5kHz, adjustable to +/-1 decade by potentiometer gain control .

TYPE 2 : Loop filter is an integrator as above followed by a second integrator with stop. Integration unity gain frequency is 1.5kHz adjustable to +/-1 decade via front panel control ' F2 ' .

When the *reset* input is pulled negative, both integrators are reset. When this occurs, an LED flashes on for one second and, if enabled, a buzzer sounds. The *power supply* consists of a +/- 15V power supply with 3 pin DIN output sockets on the rear panel to supply all other units in the system .

The *high voltage (H.V.) power supply* is adjustable up to +250V d.c., connected internally to a high voltage amplifier. It has short circuit protection and an audible overload alarm. This unit also incorporates an interlock system : in order to enable the H.V. supply, +/-15V must be connected to the servo unit and the interlock used to return the signal to the H.V. unit. The meters on the lower unit refer to the current and voltage supplied to the H.V. amplifier, not the H.V. amplifier output.

The *high voltage amplifier* drives a piezo load via an output BNC connector. This device has a gain of 50 and has an internal offset giving an output of half the H.V. supply voltage with zero volts at input. A ÷50 buffered output is provided for monitoring output voltage. A reset output is provided which goes low (-15V) when the output voltage goes close to the supply rails. The 'clipping' LED's on the front panel give an indication of this. The complete system consists of two units : the upper unit includes the sum and difference amplifier, servo unit and modulation unit whereas the lower unit incorporates the high voltage supply and high voltage amplifiers (refer to figure 5.14).

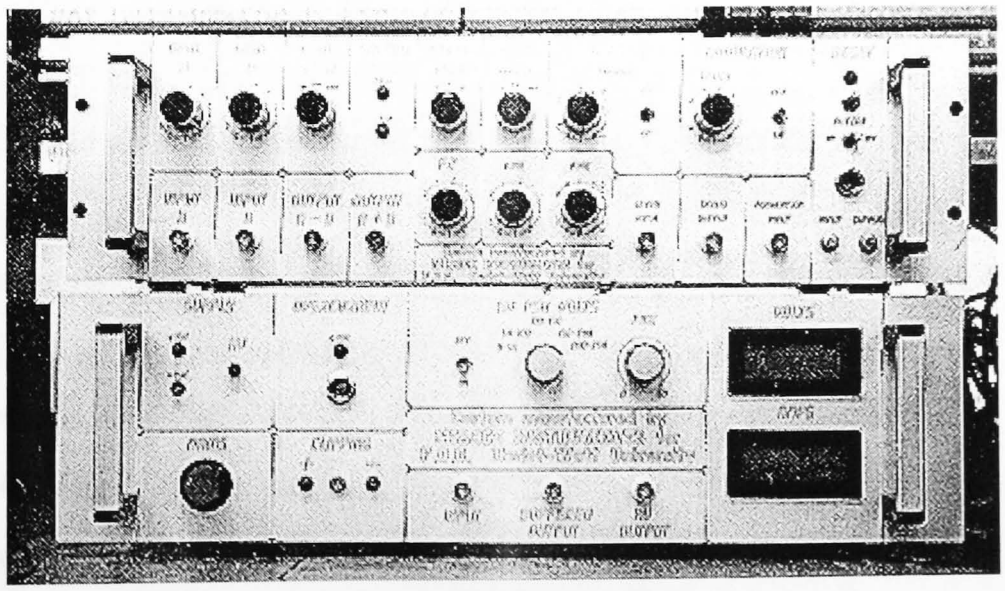

Figure 5.13 Photograph of the custom built active homodyne detection unit.

5.2.6 Reducing The Optical Phase Noise

As mentioned previously, the reflection of light from the launching lens back into the laser cavity can cause instability and therefore lead to phase noise at the output of the interferometer. Two techniques were used to reduce the feedback into the laser cavity. The first technique involved the simple tilting of the laser source so that the reflected light failed to enter the laser cavity (refer to figure 5.14). The reflected light can be seen as a bright spot on the laser casing, just above the cavity.

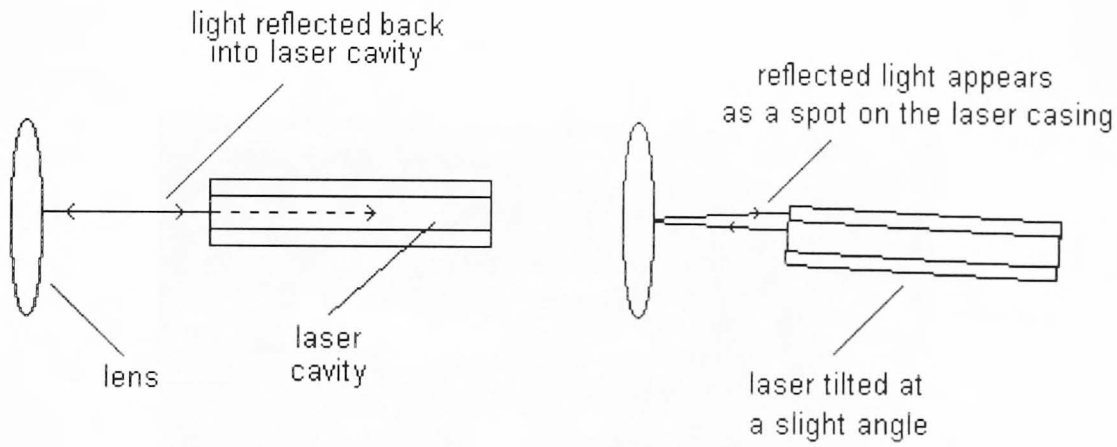

Figure 5.14 A technique for minimising the phase noise in an interferometeric system.

The second, and most difficult technique for minimising the phase noise present in an interferometric system is to match the optical path lengths of the reference and sensing arms as closely as possible. In practice, this technique was painstakingly accomplished by careful measurement of the directional coupler pigtails and single mode fibre, and careful cleaving. This technique, however, caused many problems, and only through patience and perseverance was a suitable method was devised which could match the optical path lengths to within a few millimetres.

5.2.7 Signal Conditioning Electronics

The detection of acoustic emission is possible using a fibre optic Mach-Zehnder interferometric sensor since acoustic pressure modulates the sensing region of the fibre. This modulation results in a detectable phase shift in the optical output. However, the purpose of any measurement system is to present the observer with a numerical value corresponding to the variable being measured. The information present at the output is in a form which is not suitable for further processing. The optical output is only of use when it is converted into an electrical signal. The conversion of optical to electrical energy is usually done by a photodetector. In this system, the conversion was accomplished by a wide band photodiode detector (figure 5.15).

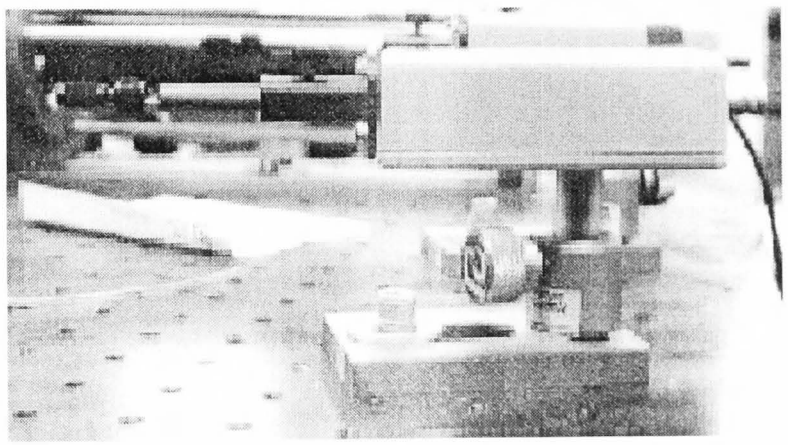

Figure 5.15 Photograph of the wide-band photodiode detector used in the fibre optic AE detection system.

The damage induced acoustic emission signals were expected to be of low amplitude and high frequency. The electrical signals obtained at the output using the photodetectors were typically in the order of microvolts for an average acoustic emission event, with frequencies ranging from a few kHz up to 1MHz. However, these signals were 'lost' in the higher voltage, lower frequency erroneous, unwanted noise. To recover the signals of interest from background noise and low frequency perturbations, an electronic filtering and amplification system was required. A 'Kemo' adjustable filter unit with a range of cut-off frequencies from 1Hz to 100kHz was

employed. The unit was adjusted to give a cut-off frequency of 100kHz and unity gain.

5.3 Summary

The components and techniques used to construct the interferometric acoustic emission detection system have been presented. Many modifications have been made to the basic Mach-Zehnder interferometer to ensure that it can detect acoustic emission signals. The first modification made to the basic configuration is the introduction of an active homodyne detection system. This system eliminates phase drift in the reference arm of the interferometer and maintains the phase at the quadrature point, and hence the interferometric system operates at its maximum sensitivity. The second modification is the use of polarisation controllers. These devices ensure that the recombining beams are mutually coherent and have identical polarisation states, therefore reducing signal fading. Since many tests are performed on the embedded optical fibre sensor with the composite samples being tensile tested to failure, it is impractical to keep fusion splicing the samples into the 'signal' arm. The introduction of a composite test section eradicates continual fibre splicing of the embedded optical fibre sensor into the 'signal' arm. The final modification made to the basic configuration was the use of fibre collimators to adjust the optical path difference of the system. Theoretically, it is possible to reduce the optical path difference to be approximately zero. However, since the length of the fibre in the test samples could not be cut to exactly the same length, the fibre collimators were used to maintain the optical path difference from test to test. This helped to maintain the fringe visibility of the two anti-phase signals. Once built, several tests were performed using the interferometric acoustic emission detection system to establish its feasibility as a potential NDE tool.

CHAPTER 6

EXPERIMENTS USING THE FIBRE OPTIC ACOUSTIC EMISSION SENSOR

6. Experiments Using The Fibre Optic Acoustic Emission Sensor

The primary aim of the experimentation was to demonstrate the feasibility of using an embedded fibre optic Mach-Zehnder interferometer to monitor the damage which occurs under load in carbon fibre reinforced plastic (CFRP) composites through the detection of the associated acoustic emission (AE). Initially, a series of tests were performed to characterise the fibre optic AE detection system. Once the system's ability to detect AE signals was confirmed, further experimentation was undertaken to investigate the system's potential as a diagnostic NDE tool. To examine the possibility of using this sensor in industry it was necessary to compare it with the established sensor technology. Therefore, the damage-induced AE from composite samples under load were monitored both by the fibre optic sensor and piezoelectric (PZ) transducer.

The secondary aim was the interpretation of the collected AE information from both sensors. Two categories of interpretation were investigated: (1) determine the point where the accumulated damage had become severe enough that the overall structural integrity of the component under consideration has been compromised in terms of safety and reliability and (2) to correlate the AE data to the source of emission, that is, the specific damage mechanism.

This chapter describes the tests performed using both the fibre optic AE sensor and the PZ transducer to help satisfy these aims. The characterisation of the fibre optic AE detection system is described, as well as the tests performed on CFRP specimens containing embedded fibre optic AE sensors and surface mounted PZ transducers.

6.1 Materials

6.1.1 Carbon/epoxy

The material used for the composite samples was Ciba Geigy T300/920 (denotes fibre type/resin type] pre-impregnated unidirectional carbon fibre sheets. The carbon fibre

sheets was specified to have a resin content of 42 % with a post cure ply thickness of 0.15 mm. The additional relevant specifications (Ciba Geigy, 1991) are shown in Table 6.1.

The carbon/epoxy material was chosen for the acoustic emission experimental program for two reasons. Firstly, the availability of the material, due to the financial constraints of the project it was impossible to purchase a roll of pre-impregnated sheet, however, Ciba Geigy donated a sufficient quantity of material to manufacture the necessary number of composite samples. Secondly, the members of the Sensors for Materials group in the Department of Materials Science have some experience in embedding optical fibres in carbon/epoxy material and therefore were able to assist in the preparation of the desired samples.

Fibredux 920CX-TS-133-42	
Tensile Modulus (GN/m^2)	120
Tensile Strength (MN/m^2)	1650
Flexural Modulus (GN/m^2)	110
Flexural Strength (MN/m^2)	1800
Interlaminar Shear (MN/m^2)	80
Fibre Density (g/m^3)	1.74

Table 6.1 Typical performance characteristics of the carbon/epoxy material used in the experiments.

6.2 The Preparation And Manufacture Of Composite Samples

This section describes the procedure for manufacturing composite samples for testing under tension. Three types of samples were used: two forms of plain samples (unidirectional and cross-ply) and cross-ply samples with embedded fibre optic

sensors. The term 'plain' is used to describe composite samples with no embedded optical fibre. The techniques involved in the manufacturing of these types of samples were different. The steps involved in the manufacture of plain composite samples from the pre-impregnated tape stage to cured, end-tabbed, polished specimens for piezoelectric tests is described in the following section. The procedure involved for the fabrication of the embedded fibre optic sensor specimens is outlined in the section 6.2.2.

6.2.1 Manufacturing Plain Composite Samples

The composite test specimens were manufactured from pre-impregnated carbon fibre/epoxy sheets described in section 6.1. The fabrication process required the cutting of squares of pre-preg, stacking these plies in the desired lay-up sequence, and then curing these samples under the guidelines stipulated by the manufacturer (Ciba Geigy, 1991).

The uncured panels measured 280mm square and consisted of 16 plies. The nature of the lay-up sequence was dictated by the type of damage being studied. The cross-ply lay-up was required to study delamination damage, which was known to occur between plies of differing orientation. The actual cross-ply lay-up sequence had the following orientations: $[0, 90, 90, 0, 0, 90, 0, 90]_S$. The suffix S indicates symmetry in the lay-up sequence. This lay-up sequence can be explained with the aid of figure 6.1.

The first ply in the sequence was laid on a template with the direction of the reinforcing fibres being parallel with the x-axis of the template. The second ply was then laid with its reinforcing fibres being orthogonal to the previous ply fibre orientation, that is, parallel to the y-axis of the template. The third ply was laid in the same manner as ply 2. This was continued until all 16 plies were laid-up.

To monitor other damage mechanisms some uncured plain unidirectional panels were also manufactured. However, some of these uncured panels were cut into individual samples. The orientation of the strengthening carbon fibres was varied in relation to

the direction of loading. These samples would then fail under well defined modes, such as matrix cracking, debonding between fibre and matrix, fibre pull-out and fibre failure.

These individual samples were then cured in single-specimen moulds under the same curing conditions used to manufacture embedded optical fibre composite samples (this technique will be explained in section 6.2.2).

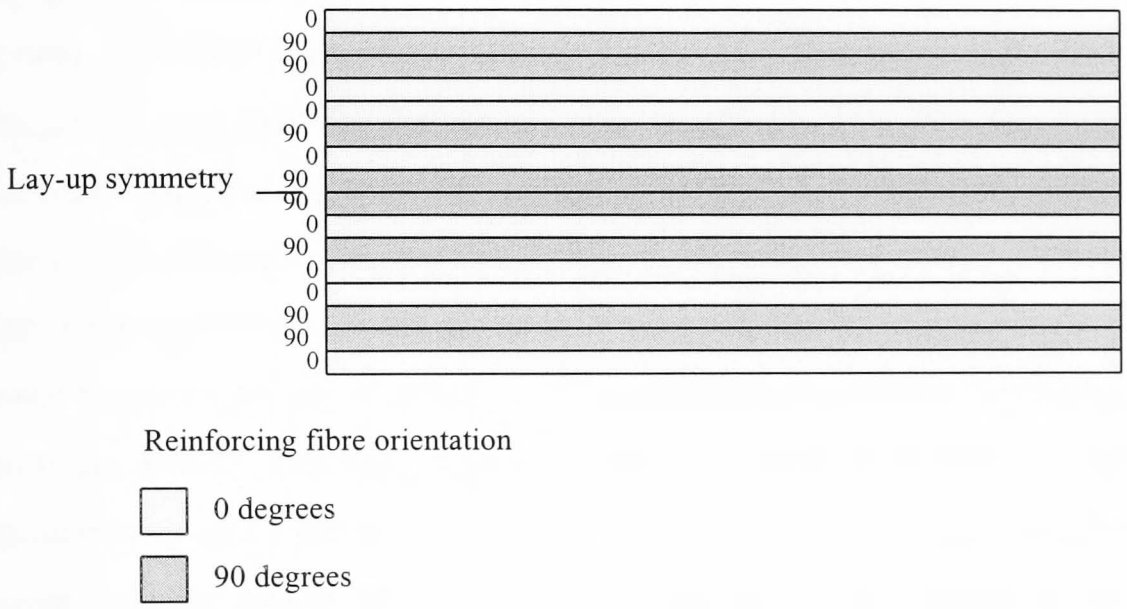

Figure 6.1 Lay-up sequence for plain cross-ply composites for piezoelectric tests

The composite panels were hand laid-up in the desired stacking sequence aided by a perspex template designed and built by the Materials Department. The template has many holes which enables the reduced air pressure to hold the pre-preg on the template. This ensured that the orientation of the strengthening fibres was correct from ply to ply. After each ply was laid the air was pressed out between the layers to avoid the introduction of artificial stress concentrators. It was also important to guard against the possibility of extraneous substances (such as hair, dust etc.) dropping onto the carbon fibres sheets. Once the desired number of plies were laid up, the panel was ready to be cured.

The cross-ply and unidirectional panels were placed in the 280mm square composite mould. The mould was placed in the hot-press and cured at a temperature and applied pressure of 125°C and 6 tonnes respectively for 1 hour. During the cure cycle it was important that the temperature of the top and bottom press were exactly the same. If the composite sample was cured in the hot-press with differing top and bottom plate temperatures, the result would be a bevelled composite panel.

The composite panel was removed from the mould and cut to the desired dimensions using a diamond saw. The CRAG standard for composite testing states the specimens should have the dimensions 20mm width and 200mm length. The composite specimens were then abraded with silicon carbide paper to provide a rougher surface for improved bonding with the end-tabs. The end-tabs were made from shot-blasted aluminium and had the dimensions 20mm width and 50mm length. The end-tabs were applied to the composite using two-part adhesive and placed in a press with the two metal sheets on the top and bottom. These sheets prevented the mould sticking to the press due to resin bleeding. A small pressure was applied (around 1.5 tonnes) and the temperatures of the top and bottom plates were set at 60°C. The specimens were left under these conditions for 3 hours. The end-tabs prevent slipping of the composite sample in the grips, and help prevent grip damage. The gauge length of the specimen was the distance between the two end-tabs, that is, 100mm.

The edges of the composite samples were polished so that it was possible to see the damage to the fibres and matrix using a microscope. The edge surfaces of the sample were polished with silicon carbide paper using a Struers Knuth rotor (which rotates at 300rpm). Polishing papers with various grades of roughness were used to ensure a smooth, flat surface. The lower grade papers removed the ragged edges and major scratches whereas finer polishing paper eliminated any minor scratches from the samples edge surfaces of the samples. To ensure that the fibres and matrix could be viewed separately it was necessary to use even finer polishing papers.

After the complete polishing process it was important that all edge surfaces were flat to ensure focused viewing through the microscope. To help achieve this the samples

were end-tabbed before the polishing stage. This prevented the samples 'wobbling' during polishing and the edges showed little or no bevelling.

6.2.2 Manufacturing Composite Samples With Embedded Optical Fibres

The single specimens were prepared in a specially designed mould with the following dimensions: 20mm width and 200mm length. Like the plain samples, the embedded fibre samples had 16 plies and the same orientation: $[0, 90, 90, 0, 0, 90, 0, 90]_S$. The technique of hand-laying is the same as is described in section 6.2.1.

However, sixteen plies were not stacked together. To be able to embed the optical fibre sensor and the dummy fibre, three composite panels were laid-up; two panels of [0,90,90,0] and one panel of $[0, 90, 90, 0]_S$. This lay-up sequence is shown in figure 6.2. The three composite panels were cut into 19.5mm X 199.5mm strips using a Stanley knife.

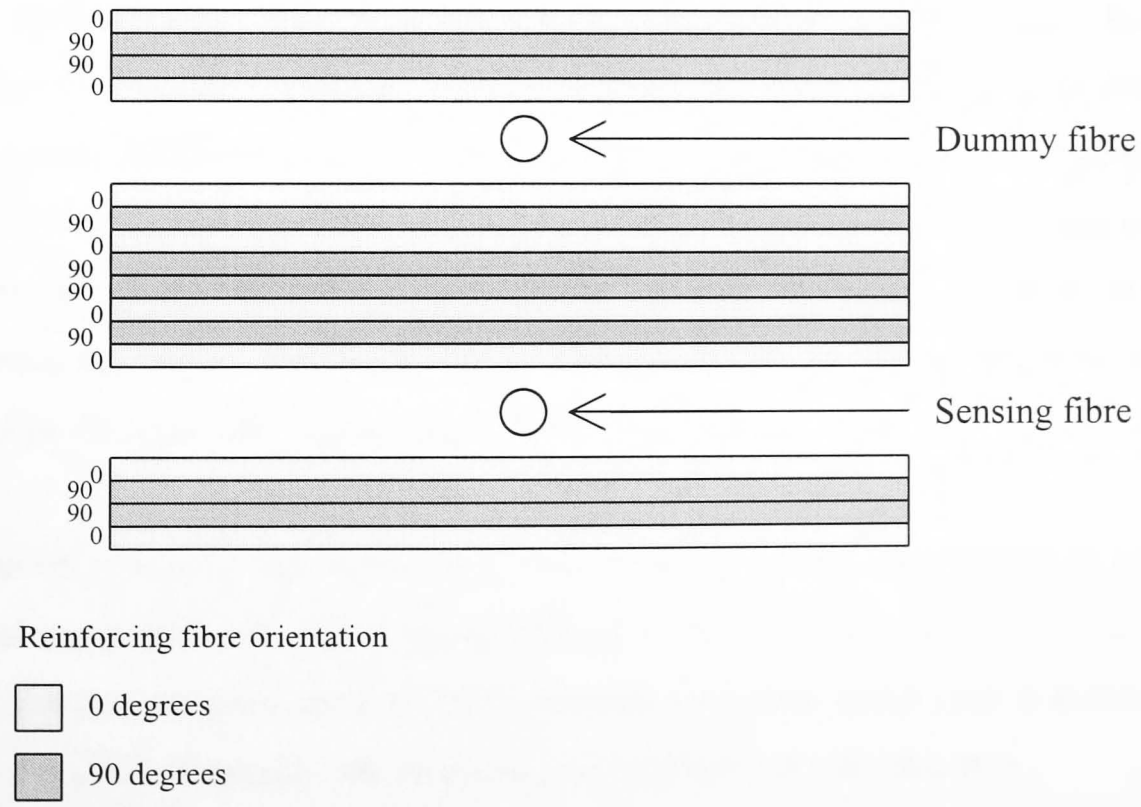

Figure 6.2 Lay-up sequence for cross-ply composites with embedded optical fibres

Two optical fibres were embedded into the sample. These fibres (single mode 4/125μm) were stripped of their acrylate buffer by using Nitromors paint remover and wiped

clean with acetone. The first fibre (a dummy fibre) was placed between the 4th and 5th ply to ensure that the sample maintained symmetry. The optical fibre sensor was sandwiched between the 12th and 13th ply. The ends of the fibres protruding from the specimen moulds were protected by PTFE tubing as resin bleeding at this interface can cause the fibre to become brittle. The single specimens were cured by hot pressing the moulds at pressure (0.5 tons for three moulds) and temperature (125°C) for one hour, after which they were allowed to cool down at room temperature. Once fully cured the ends of the composites were roughened with silicon carbide paper, degreased with acetone and then finished with aluminium end tabs bonded on with high shear strength epoxy. It was impossible to polish the edges of these samples as the fibre pigtails were very delicate and prone to breakage. Therefore, visual verification of damage during the test could not be obtained.

6.3 Tensile Testing Of The Composite Sample

The CFRP samples were damaged simply by applying a sufficient tensile load. In composite materials there are several different mechanisms of minor damage. The accumulation of this minor damage can compromise the structural integrity of the sample and even result in failure. However this type of minor damage, e.g. matrix cracking and fibre failure, can occur long before sufficient damage has accumulated to significantly reduce the strength of the composite sample. The crosshead speed has therefore been set low so that the stages of minor damage and the acceleration of damage can be detected before specimen failure.

The mechanical testing of the carbon fibre reinforced materials was performed on an Instron machine (model 1195). The spring assisted wedge grips were used for tensile tests. A diagram of the grips and how the specimens are placed in the grips is shown in Figure 6.3 and 6.4. Typically, the crosshead speed is set to 0.5 or 1mm/min.

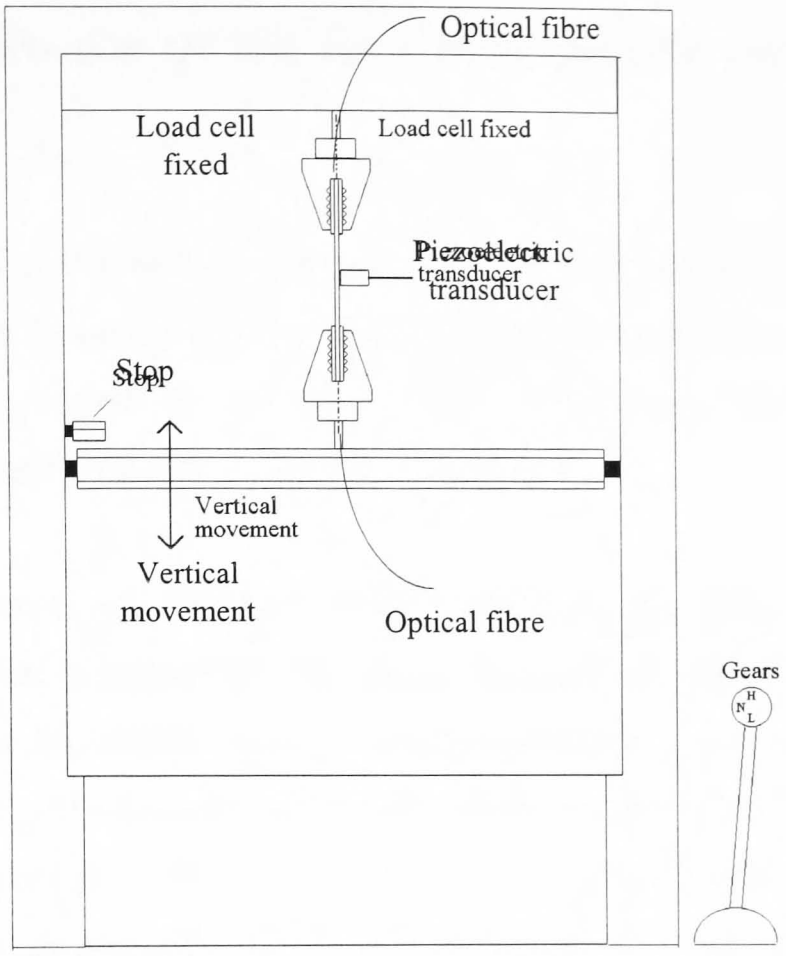

Figure 6.3 The Instron 1195 used to tensile test specimens to failure.

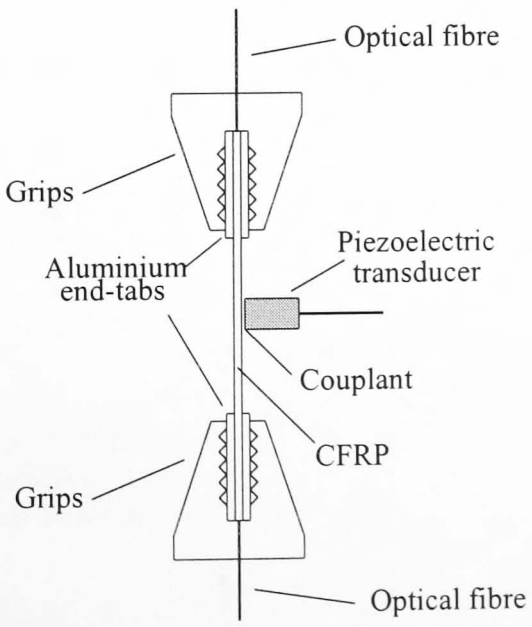

Figure 6.4 Diagram of the CFRP in the test grips.

6.4 Characterisation Of The Fibre Optic Acoustic Emission Detection System

It is essential to characterise the acoustic emission detection system before it can be used to measure damage induced acoustic signals. Several tests were carried out to characterise the system to known acoustic disturbances. These tests included simulated AE events and active acoustic stimulation.

The interferometric AE detection system set-up for the characterisation tests is illustrated in figure 6.5. The Mach-Zehnder interferometer is maintained in quadrature using the active homodyne system, therefore ensuring maximum sensitivity. The necessary connections between the Mach-Zehnder interferometer and the homodyne system are given in Appendix A. Before the characterisation tests could be undertaken, it was necessary to ensure that anti-phase signals could be obtained (figure 6.6). These signals were obtained by ensuring that the servo was out of lock. This was done by setting the servo unit switch in the homodyne system to position '0'. A 500Hz, 5V sinusoidal signal was then applied to the modulation unit input. The servo unit modulation was set to approximately '1' to produce the two signals in anti-phase. Too little or too much modulation causes a loss of the required signals. Finally the polarisation controllers were adjusted to give the maximum fringe visibility.

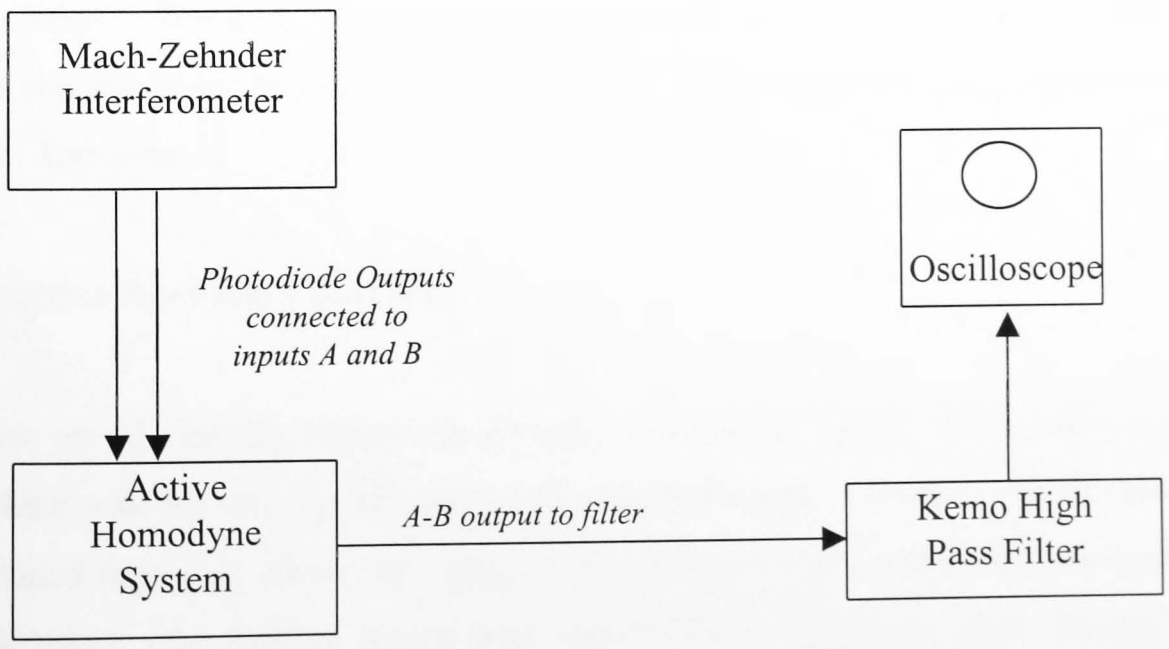

Figure 6.5 Experimental set-up for the characterisation tests.

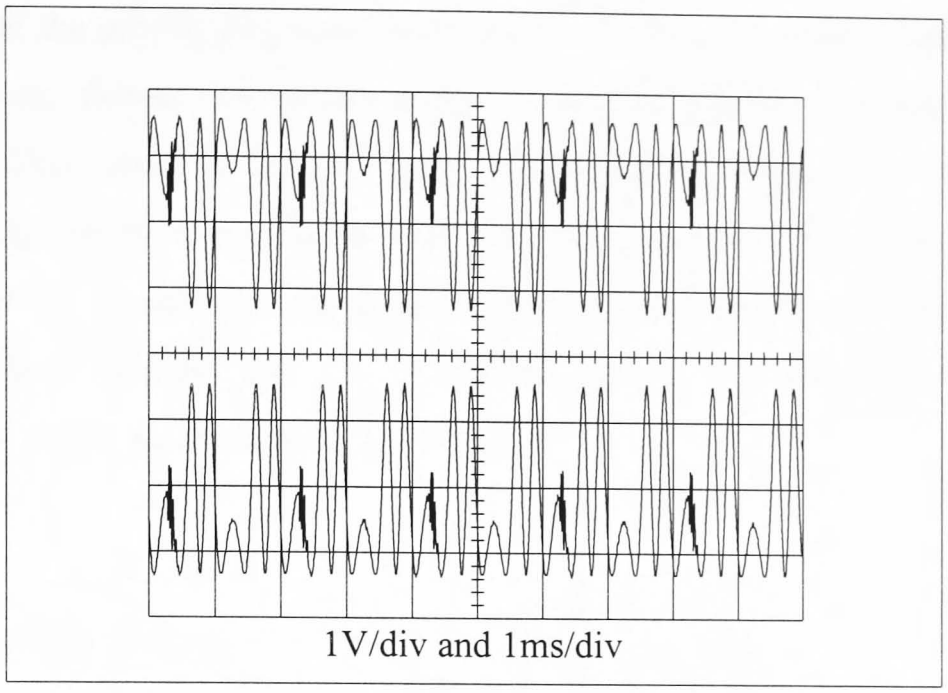

Figure 6.6 The anti-phase signals detected from the interferometer.

Once maximum fringe visibility was achieved it was now possible to lock the interferometric signal to quadrature. Initially, the frequency generator was switched off thus removing any form of modulation, alternatively, the servo unit modulation was switched off. The homodyne unit 'Servo Type' was switched to position '1' thus maintaining the interferometric signal at quadrature. The homodyne unit 'A-B' output (with gain A-B set at x10) was fed into the Kemo high pass filter (3dB point of 100kHz and unity gain). The output from the filter was monitored using a digital oscilloscope. At this point it was possible to implement the characterisation tests. A step by step guide to the experimental procedure and the signal processing details is given in Appendix A.

6.4.1 Active Acoustic Excitation

The first set of characterisation experiments involved an optical fibre, placed on a glass block with the sensing length dependent on the length in contact with the block. An elevated region of glass was etched on the surface to provide a platform for the sensing length (the sensing length was approximately 5mm). A glass 'bridge' is placed across the fibre to provide the necessary pressure on the fibre (figure 6.7). An

isotropic material was chosen as the test block to reduce the effects of material dispersion on the propagating acoustic waves. A surface-mounted piezoelectric (PZ) acoustic source, driven sinusoidally at approximately 160kHz, supplied the acoustic excitation. This acoustic source and a piezoelectric transducer were placed approximately 30mm from the glass platform. The response of the optical sensor was compared to the response of the piezoelectric transducer. The resulting fibre optic sensor response showed that the sinusoidal acoustic disturbance was detected, however, the signal was distorted (figure 6.8a).

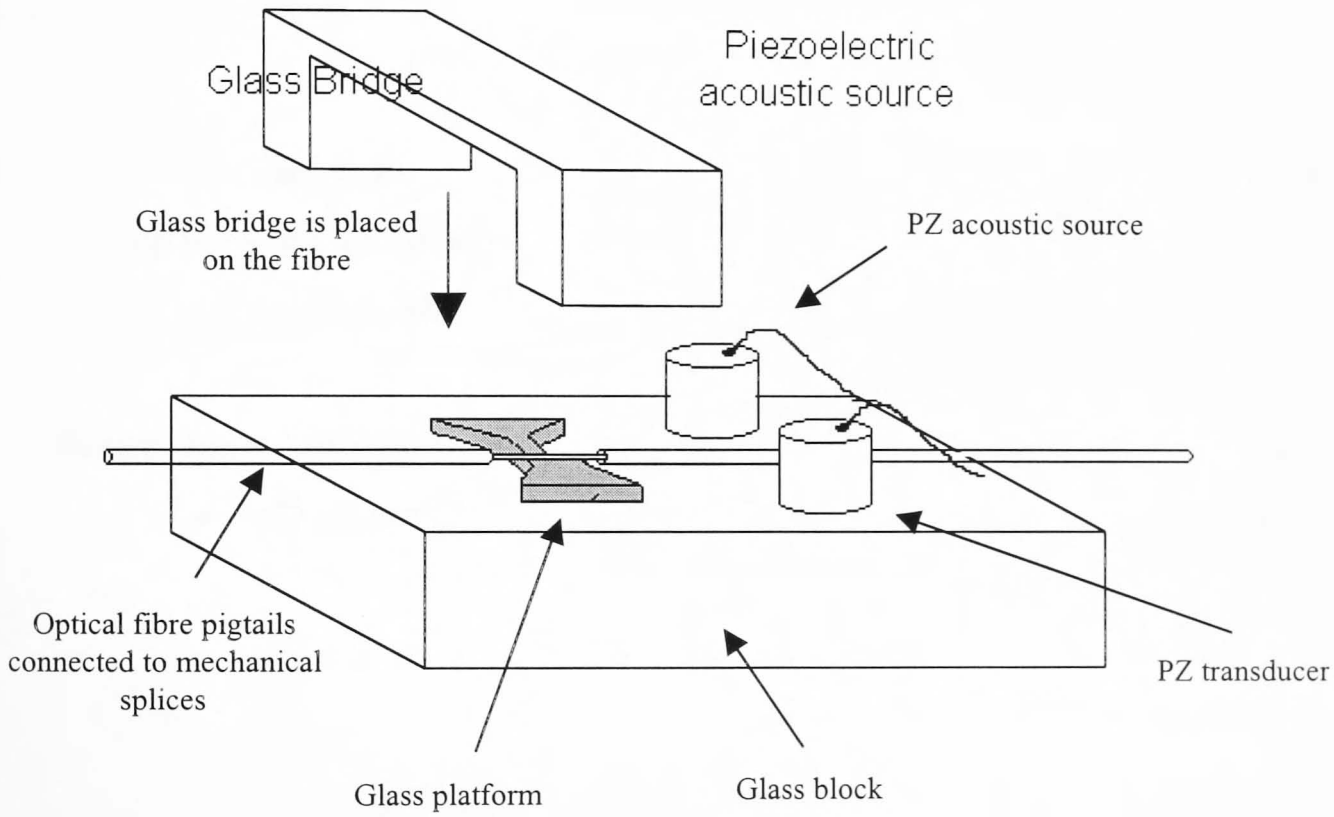

Figure 6.7 Coupling the acoustic disturbance to the optical fibre using a glass 'rig'.

Various weights were placed on the glass bridge to determine whether the coupling between the glass platform and the optical fibre increased due to increased weight. It was evident that an increase of weight on the fibre produced a vastly greater signal with less distortion. The increased weight compresses the buffer to produce a less elastic sensing region. The obvious step was therefore to strip away this elastic acrylate buffer. The test was repeated with the cladding exposed. A perfect sinusoidal response was achieved, that is, there was no distortion in the signal.

Graph (a)

Top trace- PZ Transducer

(10.1 Volts pk-to-pk)

Bottom trace- Fibre optic sensor

(1.1 Volts pk-to-pk)

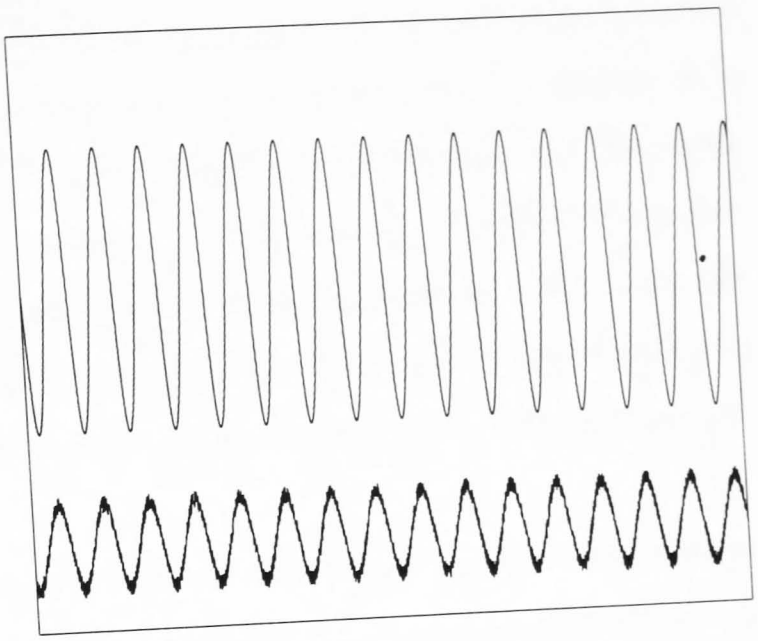

Graph (b)

Top trace- PZ Transducer

(11 Volts pk-to-pk)

Bottom trace- Fibre optic sensor

(1.4 Volts pk-to-pk)

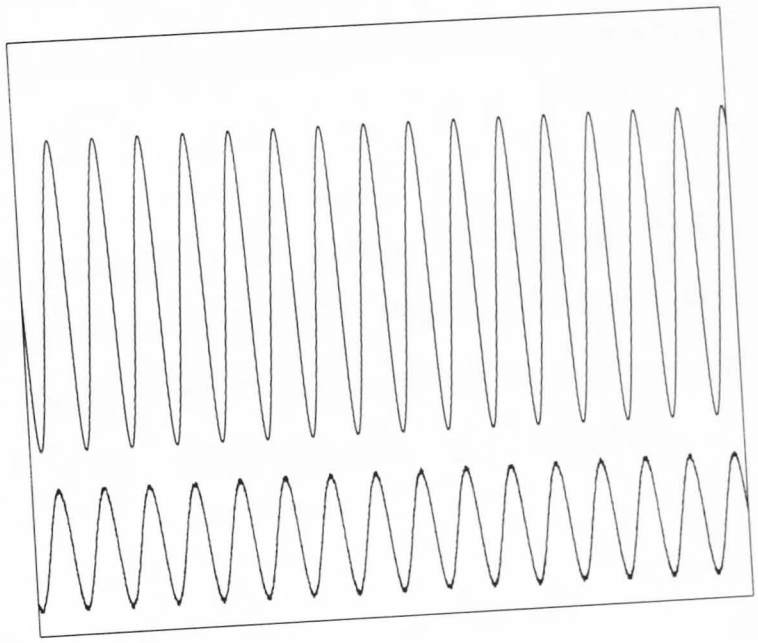

Graph (c)

Top trace- PZ Transducer

(9.2 Volts pk-to-pk)

Bottom trace- Fibre optic sensor

(2 Volts pk-to-pk)

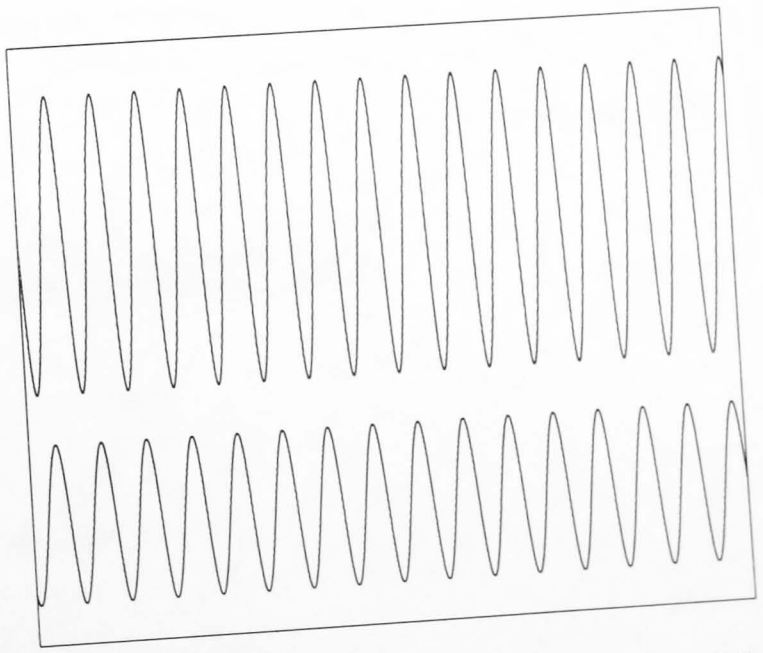

Figure 6.8 Results from the glass bridge tests on the fibre optic sensor: (a) no weight added to the glass bridge, (b) 50g added to the glass bridge, and (c) glass bridge on bufferless optical fibre.

Since composites by definition are inhomogeneous and anisotropic materials, the nature of the wave originally emitted from the source is considerably altered as it propagates to the detector. Therefore, a series of tests were performed on a fibre optic sensor mounted on the surface of a composite specimen. The acrylate buffer was removed from the fibre and the exposed sensing region was bonded to the composite (figure 6.9). The piezoelectric (PZ) acoustic source, again driven sinusoidally at approximately 160kHz, was mounted on the opposite surface to the fibre optic sensor.

The object of these tests was (a) to establish whether the acoustic disturbance could be coupled to the optical fibre through the bond, and (b) to determine whether the detected signal would be distorted due to the interaction of the acoustic disturbance with the material.

The fibre optic AE sensor response varied from test to test. This was due to the inconsistency in the bond between the optical fibre and the composite surface. Despite the variation in the response there was no distortion in the signal (figure 6.10a-c). The PZ transducer output varies slightly due to the variation in the acoustic coupling.

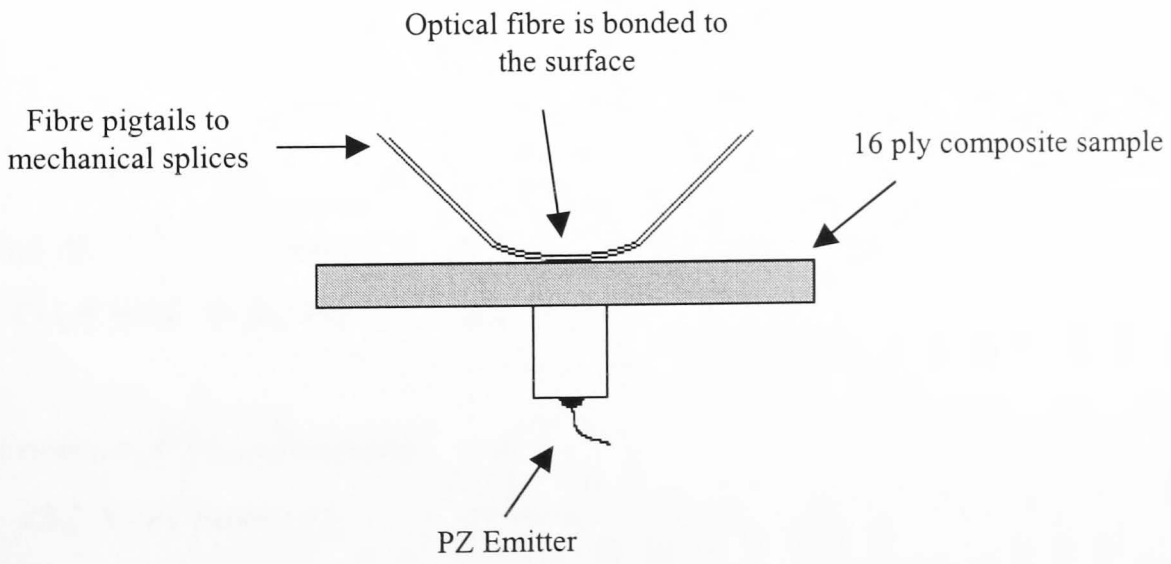

Figure 6.9 Surface mounted optical fibre sensor

Graph (a)

Top trace- PZ Transducer

(12.3 Volts pk-to-pk)

Bottom trace- Fibre optic sensor

(4.2 Volts pk-to-pk)

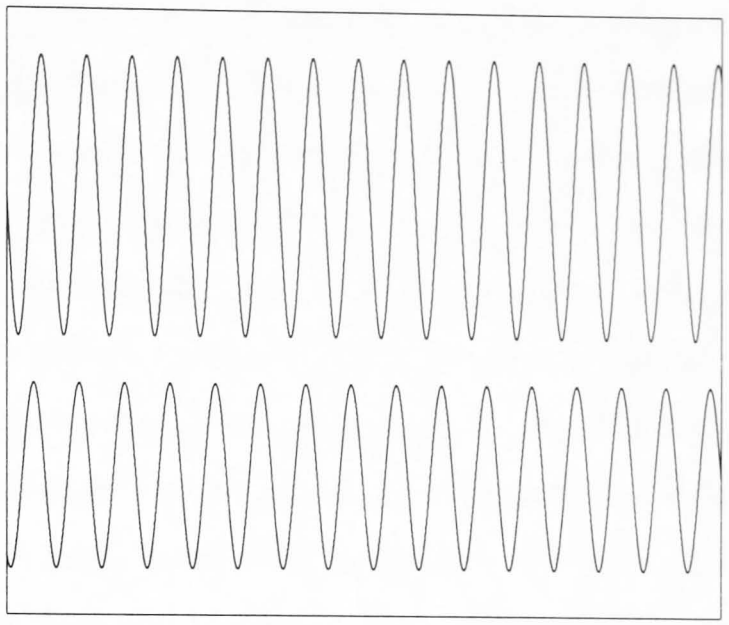

Graph (b)

Top trace- PZ Transducer

(10.9 Volts pk-to-pk)

Bottom trace- Fibre optic sensor

(2.1 Volts pk-to-pk)

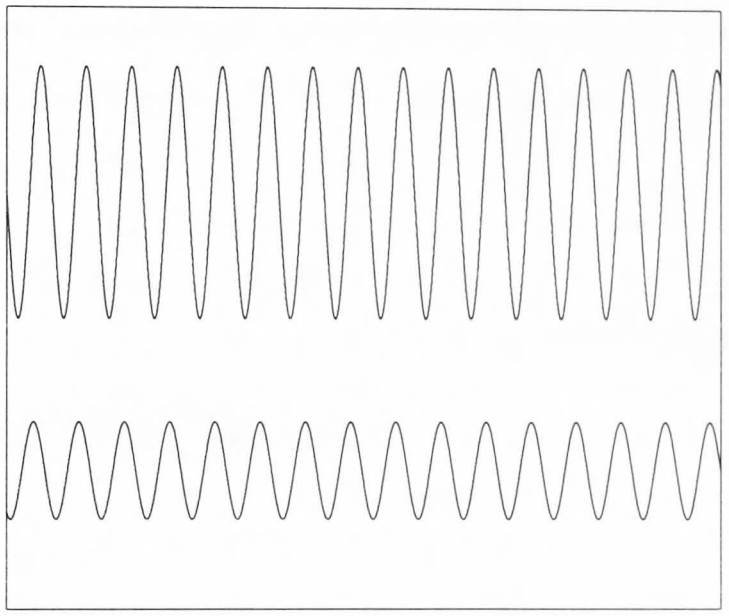

Graph (c)

Top trace- PZ Transducer

(11.8 Volts pk-to-pk)

Bottom trace- Fibre optic sensor

(3.2 Volts pk-to-pk)

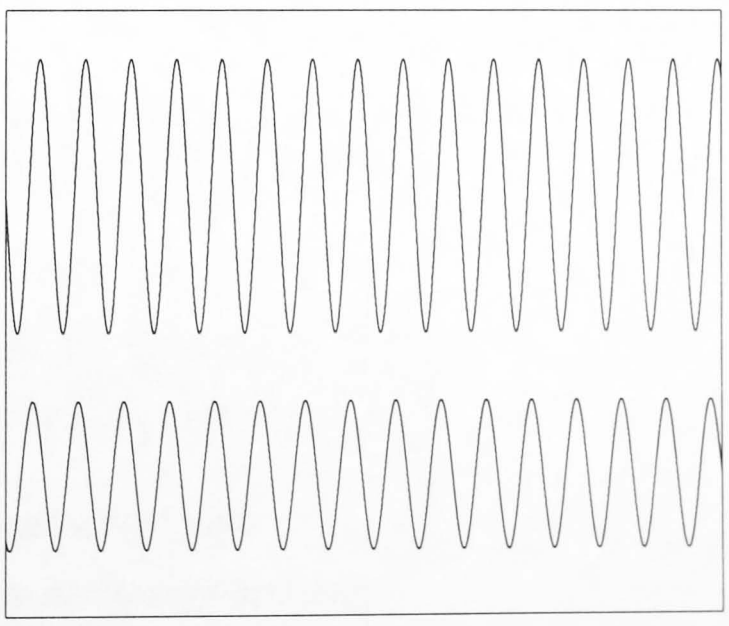

Figure 6.10a-c Graphical evidence that the fibre optic sensor output varies due to the inconsistencies in the bond between the sensor and the composite surface.

Once it was evident that the fibre optic sensor could pick up surface acoustic emissions it was necessary to embed the sensing length of the optical fibre within a composite material. The composites used in the test were fabricated from carbon/epoxy. This specimen was a 16-ply sample with a lay-up sequence of $(0, 90_2, 0_2, 90, 0, 90)_S$. The optical fibre sensor was embedded between the fourth and fifth ply. A dummy fibre was embedded between the 12th and 13th ply to maintain material symmetry. The first set of characterisation experiments for the embedded fibre optic sensor involved the active acoustic excitation of the composite specimen using a separate PZ transducer, driven sinusoidally at approximately 160 kHz. This source and the broadband PZ detector were placed approximately 50 mm apart. The responses of the optical sensor and the PZ transducer are shown in Figure 6.11a. The interferometric sensor results compare favourably with its electrical counterpart (Figure 6.11b).

a.

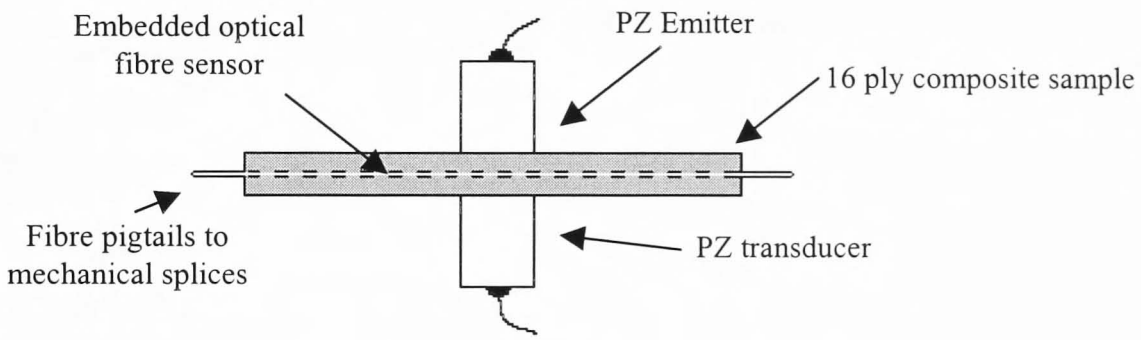

b.

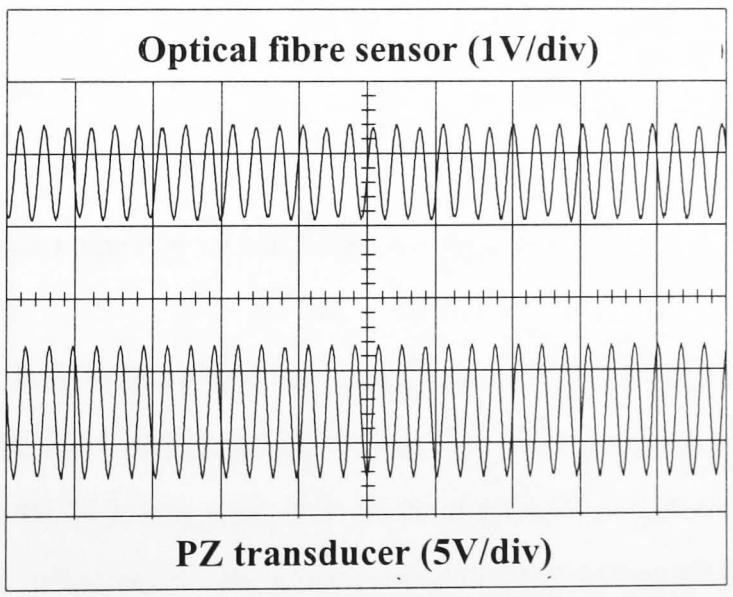

Note: 20μsec per division for both traces

Figure 6.11 (a) The characterisation of the embedded sensor system to active acoustic excitation and (b) the comparison between optically and electrically sensed signals due to this sinusoidal acoustic disturbance.

The characterisation of the frequency response of the embedded fibre optic sensor over the bandwidth of interest, that is, over the frequency range of 100kHz-1MHz, was the next step. In this experiment a wide-band piezoelectric transducer (PZT) was bonded to the composite surface using silicon matching gel. It is important that the transducer does not move at any time during the experiment as the acoustic signal transmitted into the material is affected. The acoustic pressure waves change the optical fibre dimensions thus modulating the phase and ultimately the electrical output. The response of the optical fibre sensor to wide-band excitation was compared to a piezoelectric transducer subjected to the same excitation (figure 6.12).

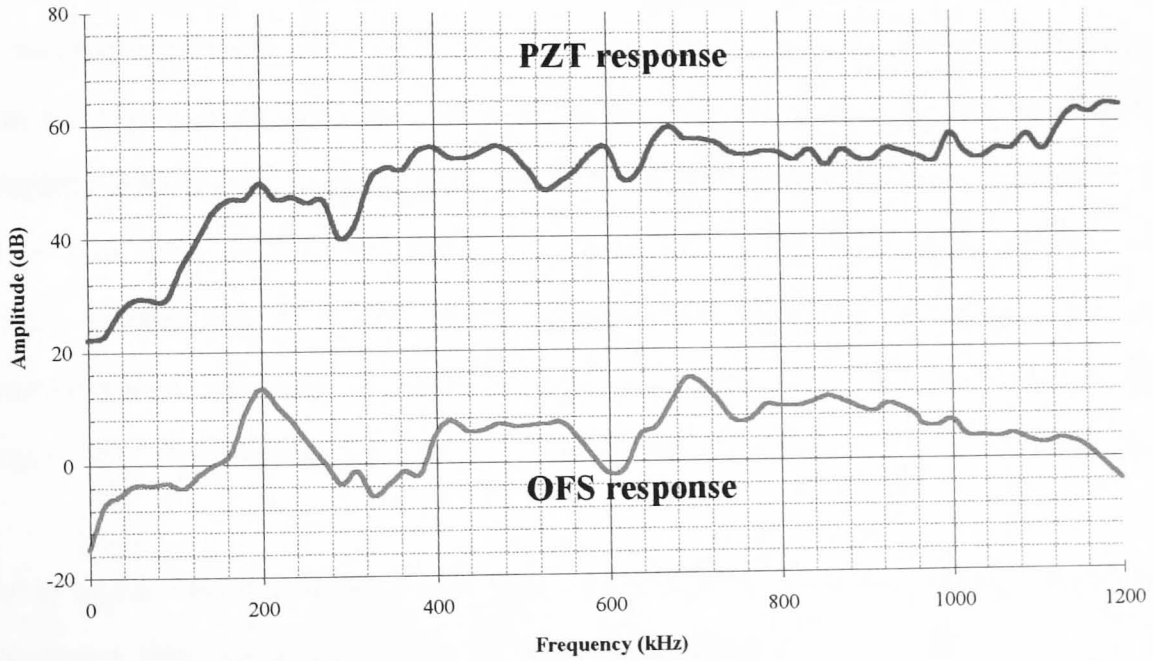

Figure 6.12 Sensor response to wideband excitation

From figure 6.12 it is evident that the response of the fibre optic sensor is of similar shape to that of the PZ transducer. However, the fibre optic sensor overall response is approximately 30-40dB lower than that of its electrical counterpart. This reduction in sensitivity will be reflected in the amplitude distribution graphs in composite testing later.

6.4.2 Simulated Acoustic Emission

The most common method of simulating acoustic emission signals in a material involves the fracture of graphite pencil lead (Nielson source) while the lead is in contact with the surface of the material. The variation in lead diameters and types, orientation of the pencil, and applied force produce differing results. Therefore, there was a need to standardise this technique. Researchers have developed a jig to hold the lead at a particular angle. The pencil-break tests are performed using a Teflon jig which maintained a constant angle between the pencil lead and the material surface (figure 6.13).

This pencil-break technique is used to evaluate the response of the piezoelectric transducer and the fibre optic system prior to collecting damage-induced acoustic emission data from materials. A mechanical pencil (Pentel) with 0.5mm diameter 2H graphite lead is held with its tip in contact with the graphite/epoxy composite specimen at 30 mm from the PZ transducer. The pencil is then pivoted until fracture occurs. The results yielded a reproducible high frequency acoustic pulse, which took the form of an exponentially decaying sinusoidal oscillation (figure 6.14). Subsequent tests must ensure that the threshold of the AET5500 is set above the noise level of this signal.

Once again, the response of the fibre optic sensor was compared to a PZ transducer subjected the same excitation. The results yielded a reproducible high frequency acoustic pulse, which took the form of an exponentially decaying sinusoidal oscillation.

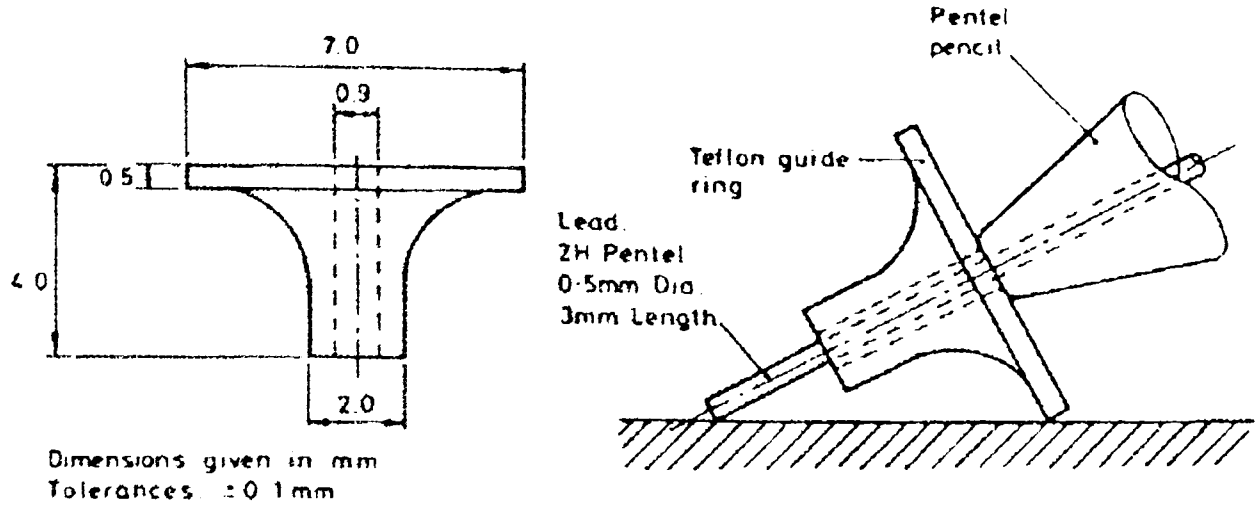

Figure 6.13 Testing the response of the PZ transducer and the fibre optic sensor to a single frequency excitation for threshold calibrations.

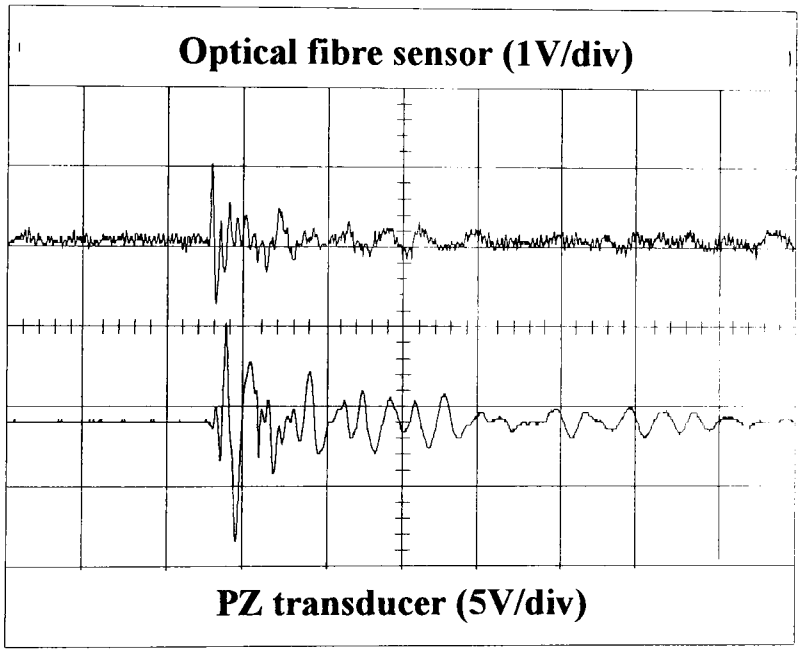

Note: 20μsec per division for both traces

Figure 6.14 A comparison between optically and electrically sensed AE activity caused by a pencil break on a composite sample.

6.5 AE from a composite specimen under tension.

From the characterisation tests it is evident that the embedded fibre optic Mach-Zehnder interferometric AE sensor could detect surface disturbances. Therefore, it was necessary to examine the possibility of using this sensor to monitor progressive damage occurring under load in CFRP specimens through the detection of the associated AE. Through the use of an AE data acquisition and processing, the characteristics of the associated AE signals could be evaluated. This data can then be used to determine information on material/structure strength and integrity. Alternatively, the AE data could be correlated back to the source of emission, that is, the specific damage mechanism.

The most important of the two is the monitoring of the degree of damage. It is necessary to determine the point where the accumulated damage has become severe enough for the safety and reliability of the sample to be compromised. In composite materials, critical damage is caused by delamination, that is, the internal debonding between two plies. Therefore, the sensor's potential for non-destructive evaluation purpose will be validated if it can respond to delamination damage.

Many authors have presented the case for using the AE counts versus load curve as a useful tool for evaluating the health of a composite material. The most obvious characteristic of the AE curve is that the slope changes abruptly at one point. The main significance of the 'knee' in the curve is that it correlates the point in the load history to the onset of irreversible damage in the sample. Therefore, the emphasis of the test was originally placed on monitoring the number of signals generated as the damage progressed through the sample, rather than the signal's AE parameters.

6.5.1 Event count vs. damage

The composite sample with the embedded optical fibre was placed in the grips of the tensile testing machine (Instron 1195) and loaded (with a crosshead speed of 1mm/min) to failure. The resulting AE signals due to the internal damage were

detected by the fibre optic sensor and processed by the AET5500 to produce the characteristics of the signal. As with the previous tests, the AE from the composite sample in tension was also monitored using a PZ transducer coupled to the composite surface with Silicone gel. The experimental set-up is shown in figure 6.13. The 'interferometric AE detection system' block consists of the Mach-Zehnder interferometer, the active homodyne unit, and the Kemo high pass filter (100kHz cut-off). The 'AE data acquisition system' block is the AET5500, which provides post-amplification of 30dB for the PZ transducer signal. The 'pre-amplification and filter unit' block is an Acoustic Emission Corporation self-contained unit which has a gain of 40dB and pass-band filter of 100kHz-1MHz. The full experimental procedure and signal processing details are explained in Appendix A.

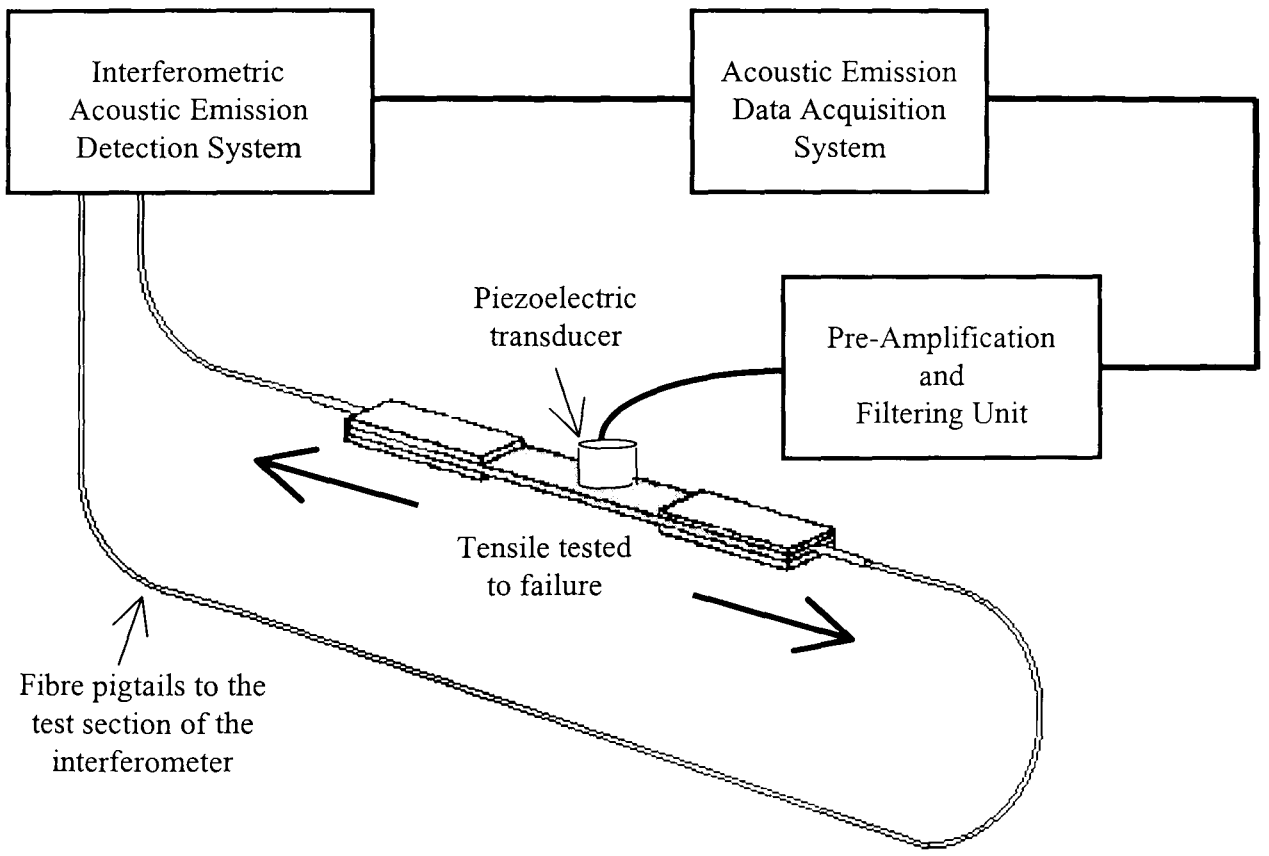

Figure 6.15 Schematic diagram of the experimental set-up for fibre optic and piezoelectric sensing of acoustic emission in composite materials

On the application of the load, the AE signals began to be detected, on average, at about 40% of the failure load. The rate of the AE signals increased until the failure load was reached. This indicated that internal damage initiated slowly then accelerated rapidly towards the end of the test. As the amount of damage in the composite increased, there was a point where the rate of AE activity significantly increased. To evaluate this, the event count and the cumulative event count were plotted as a function of damage. A typical combined event and cumulative count plot for both the fibre optic sensor and piezoelectric transducer are shown in figure 6.17. From these plots the cumulative AE patterns are similar to the exponentially increasing trend found by other authors (Fuwa et al, 1975, and Roy and El-Ghorba, 1988). The slow rate of change of the slope is indicated on the PZ graph. The asterix indicates the point where the rate of change of the slope starts to significantly increase. The point is termed the 'knee point'.

In this test, twelve samples were loaded in tension to failure and the resulting AE generated from the samples was detected using the fibre optic sensor and the piezoelectric transducer. As expected, the number of events detected by both sensors varied from test to test, as do the failure loads. To provide a means of comparison between the fibre optic sensor and the piezoelectric transducer for all twelve samples, it was necessary to calculate an 'average' plot for both sensors. Due to the differing failure loads of each sample, it would not be feasible to add together the number of events at a particular load. Therefore it was necessary to 'weight' each plot so that it appeared that each sample failed at the same load. By examining the fibre optic sensor cumulative event count graphs in Appendix B.1 it is apparent that test sample 11 fails at the highest load value whilst test sample 2 fails at the lowest load value. The difference between the two failure load values (D) would be the 'weighting' value needed to added to the sample 2 load data to superimpose the point of failure of sample 2 onto that of sample 11. This would simply appear as a plot shift along the x-axis. This 'weighting' value would obviously be different from sample to sample. This procedure is schematically shown in figure 6.16, where sample 2 could be associated with sample X and sample 11 associated with sample Y. The resultant 'average' plots for the fibre optic sensor and piezoelectric transducer are shown in figure 6.18.

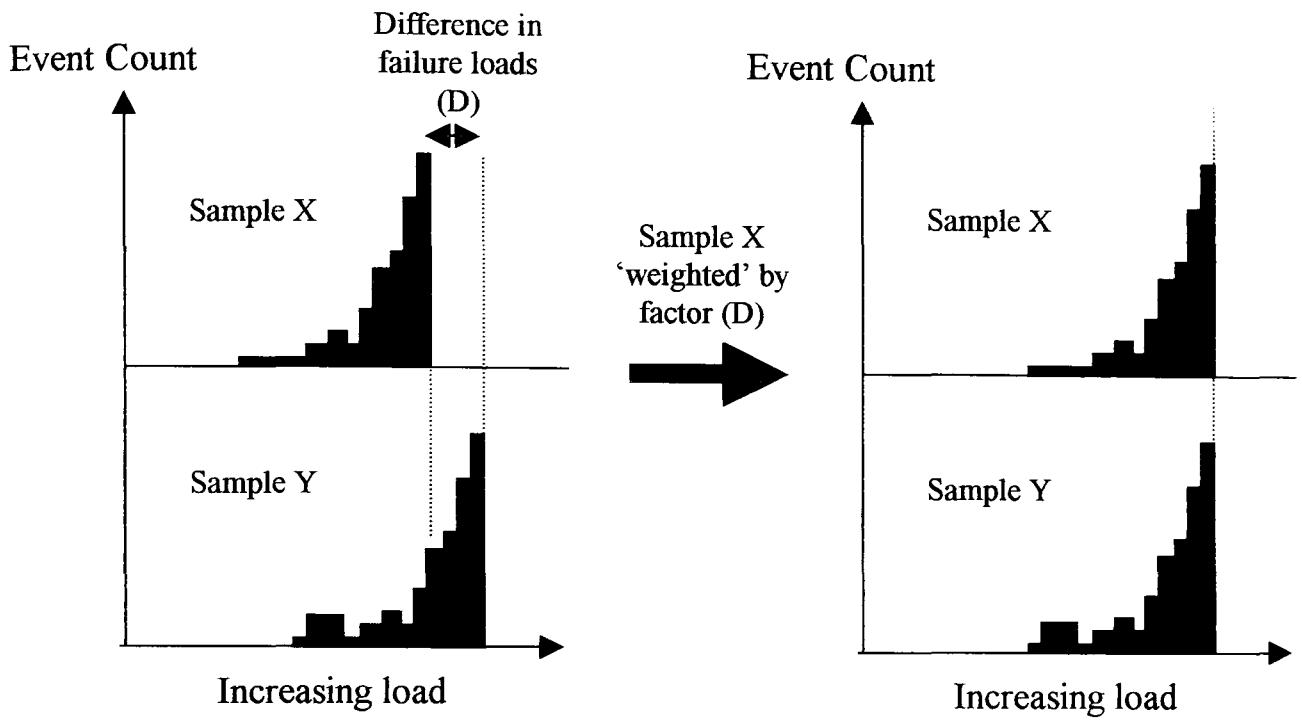

Figure 6.16 The idea of 'weighting' samples for the purpose of producing average plots to help make comparisons between the two sensors.

(a) Fibre Optic Sensor

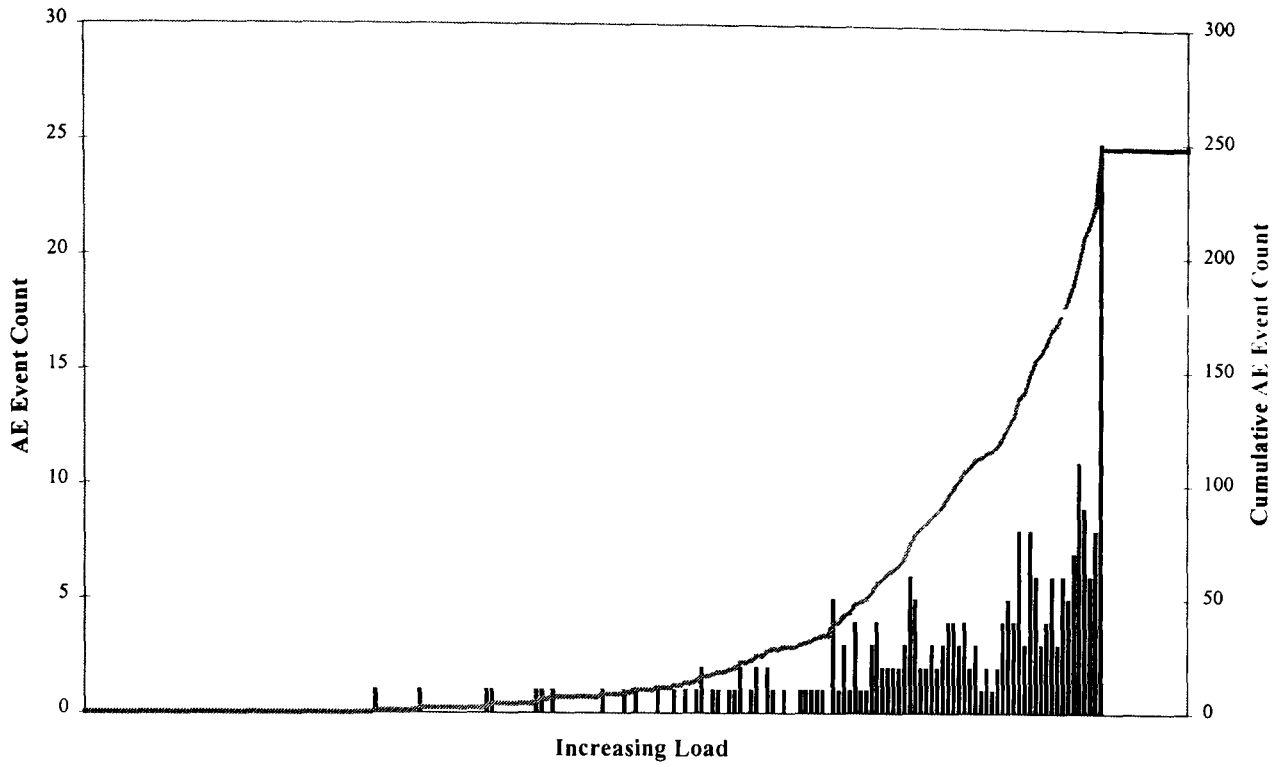

(b) Piezoelectric Transducer

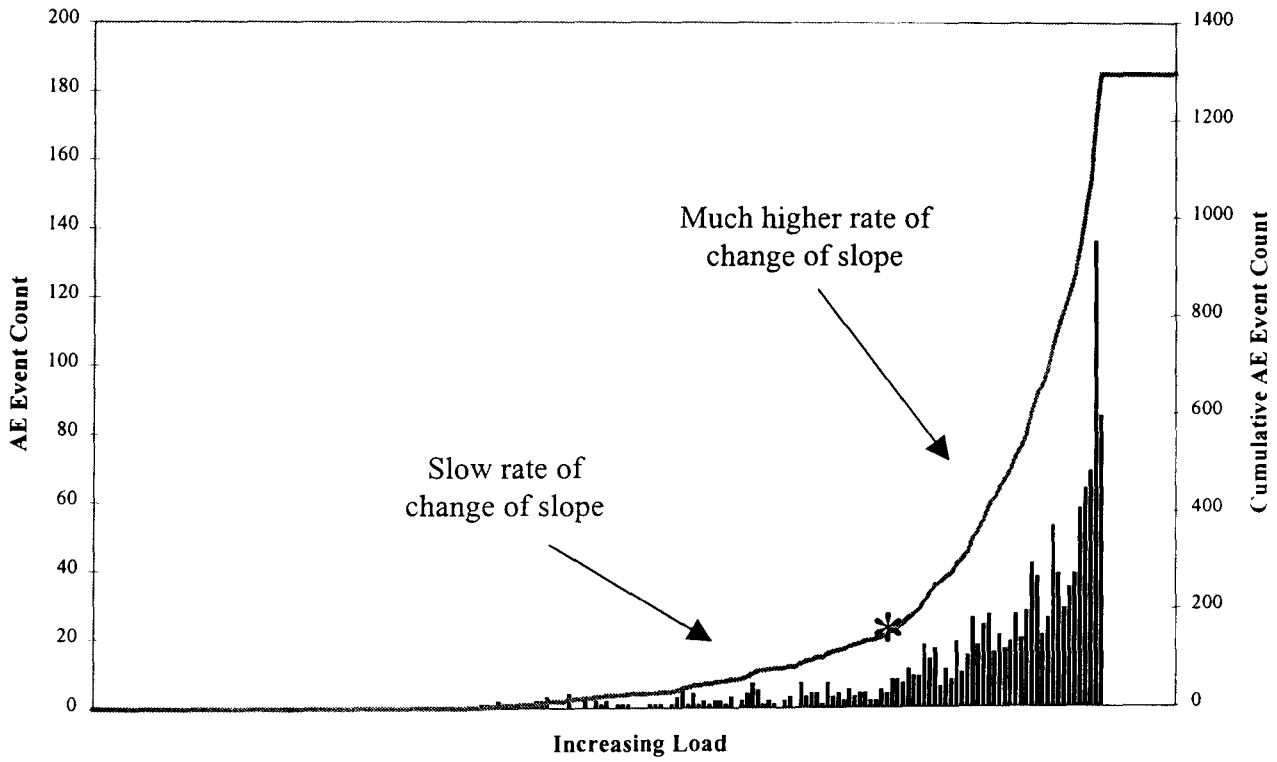

Figure 6.17 A typical example of the acoustic emission from a specimen loaded in tension to failure :- (top) Optical fibre sensor (bottom) Piezoelectric transducer

(a) Fibre Optic Sensor

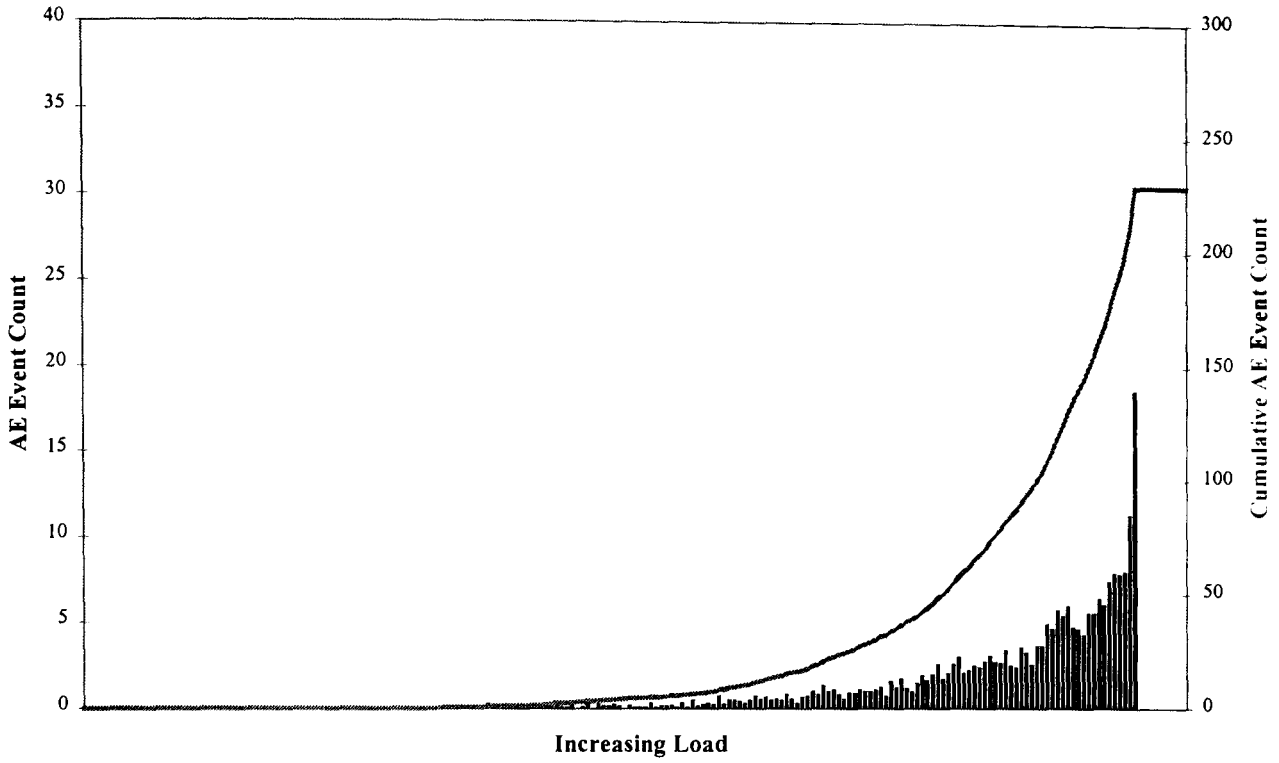

(b) Piezoelectric Transducer

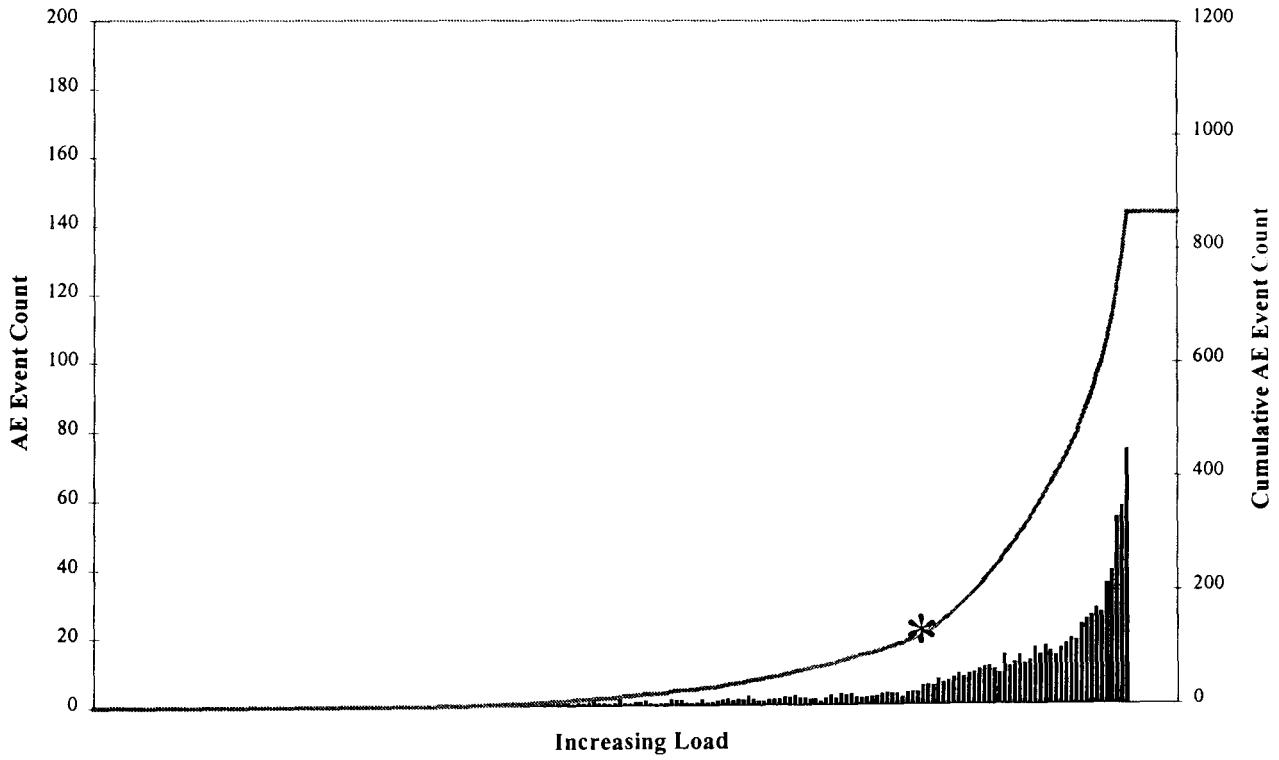

Figure 6.18 Average plot of the acoustic emission from a specimen loaded in tension to failure :- (top) Optical fibre sensor (bottom) Piezoelectric transducer

A similarity was noted between the curves representing the cumulative AE counts versus increasing load for both sensors. The tensile loading of the composite samples produced AE 'events v time' graphs which were consistent from test to test (refer to appendix B). That is, the shapes f the graphs were consistent, although there were some differences in terms of count and failure load. A comparison of the cumulative count plots for the fibre optic sensor and the piezoelectric transducer show that the embedded fibre optic sensor detected less events than its electrical counterpart. Through comparison of the average cumulative plots it is apparent that the shape of the curves for both sensors are almost identical (Figure 6.19). The averaged curves show a smoother increase in the cumulative counts. The knee point in the PZ graph is far more evident than that of the FOS curve. Once again the asterix highlights the knee point in the PZ cumulative count curve.

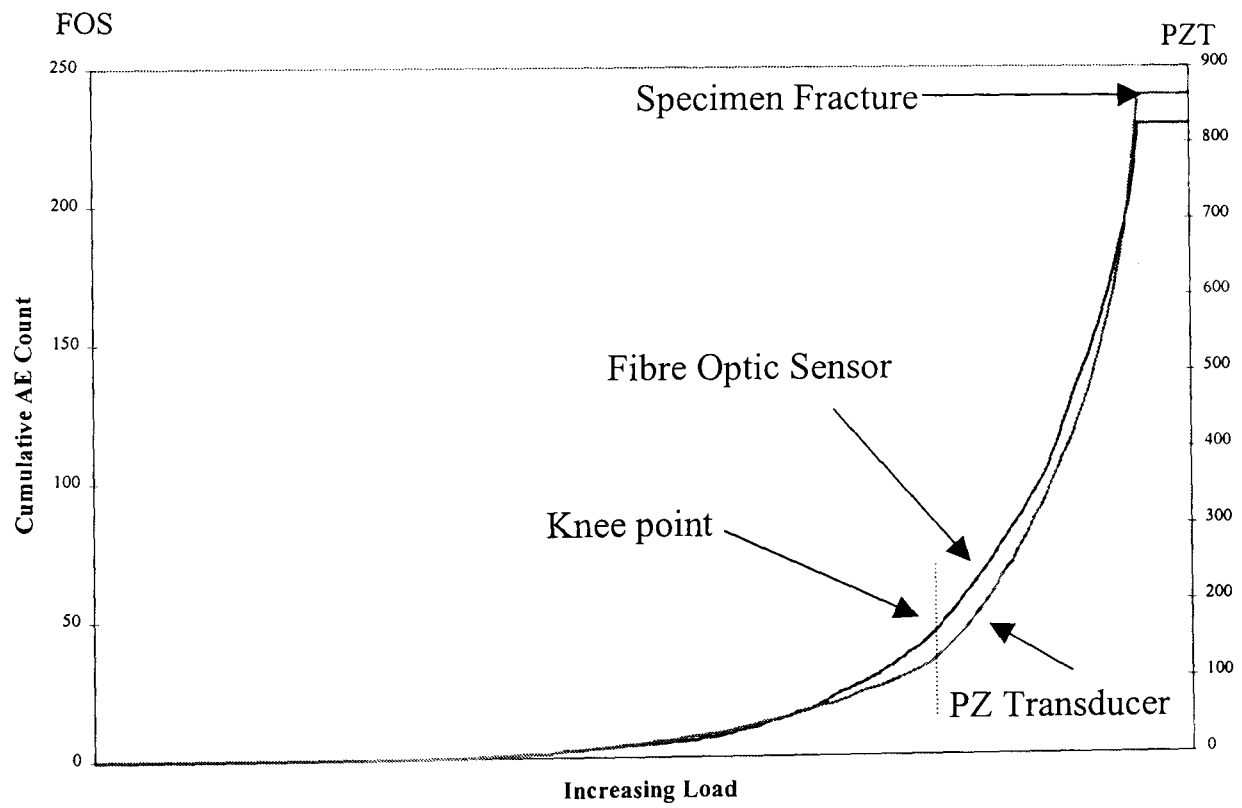

Figure 6.19 A comparison between the average optically and electrically sensed cumulative AE count plots.

In most of the cumulative plots for both sensors (Appendix B) it can be seen that the fibre optic sensor fails just before specimen failure. In figure 6.20 this case is

highlighted. A great deal of the AE signals emanate from the sample just before failure, which the fibre optic sensor fails to detect.

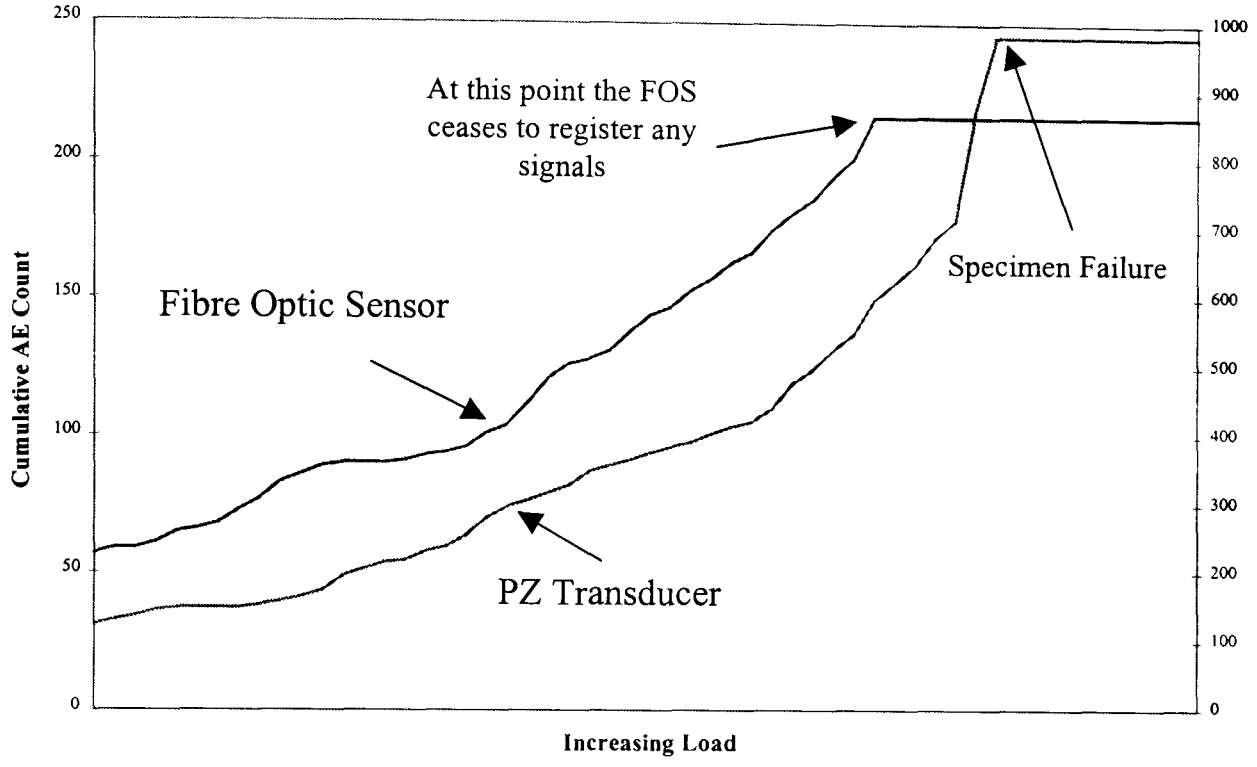

Figure 6.18 A comparison between a typical optically and electrically sensed cumulative AE count plots showing .

The most obvious characteristic of the optical fibre sensed cumulative AE curve is that the slope exhibited the knee point reported by Roy and El-Ghorba (1988). These authors claimed that the dramatic change in the slope of cumulative count curve coincided with the appearance of a delamination zone, which was evidenced by a sudden drop in the recorded load level. This is the point where the permanent damage is done to the sample, however, the mechanisms associated with this damage could not be ascertained from these types of graphs. Once it was established that the sensor could detect the AE emanating from the sample, the original AE signal parameters (that is, the time domain parameters) were analysed.

6.5.2 Time Domain Analysis Of The Detected Acoustic Emission Signals

In addition to capturing the AE signals emitted from a composite sample as it is loaded to failure, the data acquisition system (AET5500) also provides the parameters of the signal. This system needs to be programmed before the test starts if the relevant data is to be displayed. The program used in the AET5500 is displayed in full in Appendix A. The previous analysis of the cumulative event count graphs gives the point of crack initiation and propagation in the composite. This is important when attempting to determine the point when the overall health of the composite structure has been compromised. However, it is possible to use the actual parameters of the AE signal to distinguish between different failure modes. Two parameters of the original AE signal were measured using the fibre optic sensor and analysed for possible associations with types of damage in CFRP. Amplitude distributions have been analysed in an attempt to identify the damage mechanisms involved. The reference level for the amplitude levels is 0dB at 1μV at the sensor output.

Amplitude Distribution Analysis

(i) Fibre Optic Sensor

The data captured using the AET5500 was converted from binary form to ASCII and analysed using the Excel spreadsheet software. The amplitude data was then graphically analysed using distribution plots. A typical example of amplitude distribution graph using the AE detected by the fibre optic sensor from the cross-ply composites is shown in figure 6.21. In this plot there appear to be three modes of amplitude present: 24dB, 27dB, and 32dB. In the cross-ply specimens used it is expected that matrix cracking, fibre/matrix debonding, fibre fracture and delamination all occur. Therefore, it is assumed that each damage mechanism contributes to a certain amplitude range. At first glance, this cannot be seen from figure 6.21. It is possible that there is an overlapping of distributions; in statistical terms this scenario is termed finite mixture distributions. Since twelve samples were tested and the

resultant amplitude distributions determined (Appendix B), it would be advantageous if an 'average' distribution was calculated and displayed for the sake of analysis purposes. The 'average distribution graphs were achieved by combining the data from all the cross-ply tests and then dividing this total by the number of samples used, in this case, twelve. This 'average' amplitude distribution is illustrated in figure 6.22.

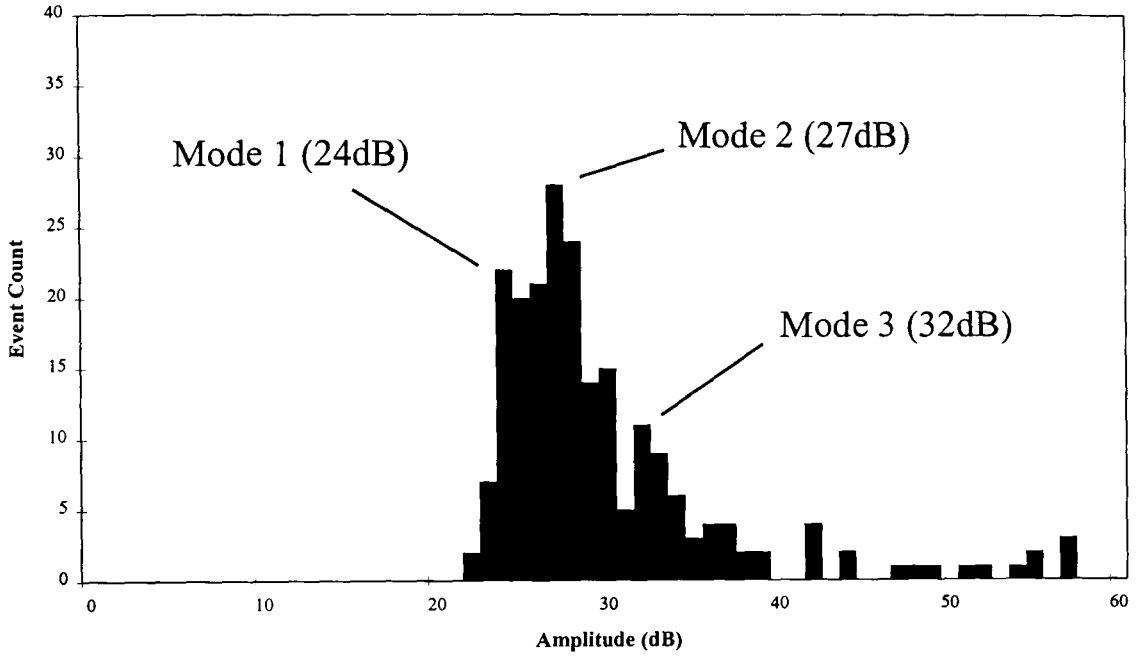

Figure 6.21 A typical example of the amplitude distribution of the AE signals detected using the fibre optic sensor from the cross-ply composites.

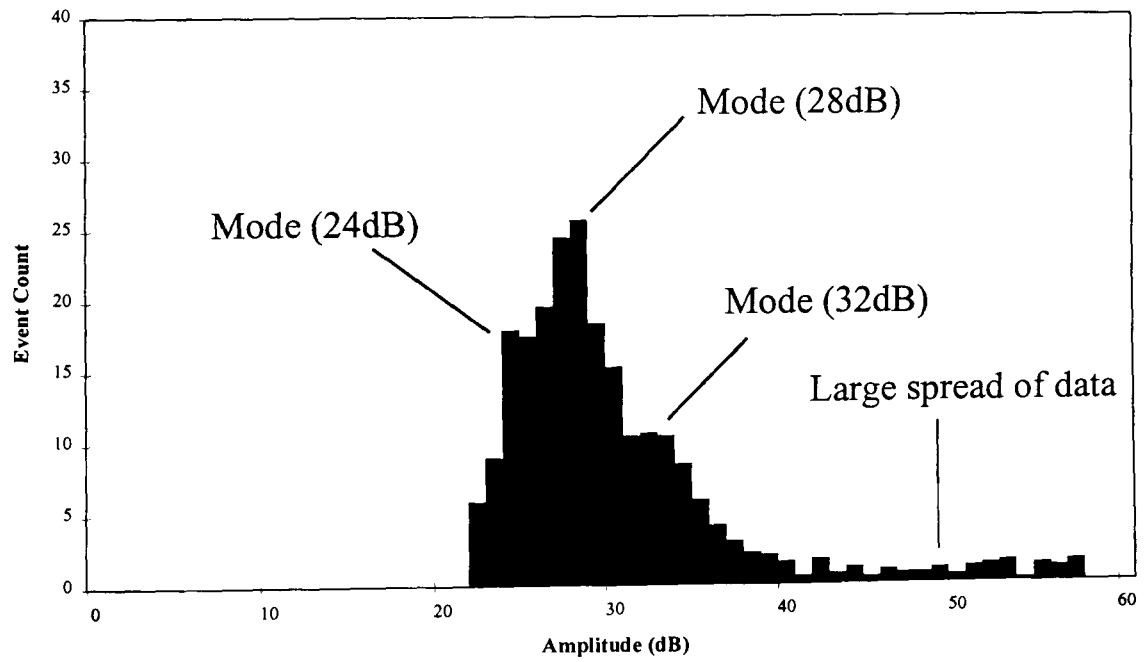

Figure 6.22 An 'average' amplitude distribution of the AE signals detected using the fibre optic sensor from the cross-ply composites.

From the 'average' graph there appear to be three modes of amplitude present. Also, there is a large spread of data above 40dB. The value of amplitude of an AE signal is considered to correspond to the value of elastic energy released by the formation of a crack. Generally, the AE signals of lower amplitude are considered to be emitted from cracks which release a small elastic energy, and those of higher amplitude from cracks which release higher elastic energy. Research studies (Berthelot et Rhazi, 1990, and Berthelot, 1988) have indicated that matrix cracking is associated with low amplitude signals, and carbon fibre fracture with higher signal amplitudes. It could be hypothesised that this large spread of data >40dB is due to fibre fracture. However, it is difficult to determine the damage mechanisms from the large distribution of amplitudes from 22-40dB. It is visibly apparent, however, that there may be at least two mixed distributions in this range.

From the fibre optic sensors 'average' cumulative count graph (figure 6.18) it is apparent that the appearance of AE occurs in the tests at approximately 40% of the failure load. The rate of AE increased in the load range higher than 70% and rapidly towards failure. To help determine the damage mechanisms involved in these types of samples, it was necessary to investigate the amplitude distributions in specific load ranges. The load ranges used were 0-60%, 60-80%, 80-90%, and 90% to failure load. In most of the specimens the embedded optical fibre sensor fractures before the composite sample fails. This is indicated by the time delay between the sensor and specimen failure in figure 6.20. Therefore, many AE signals occurring in some of the samples could not be detected before specimen failure.

A typical example of these four load range plots is shown in figure 6.23a-d. In this example, the first load range (0-60% of the sensor failure load), the results obtained using the fibre optic sensor showed that few signals were detected. In this small distribution of data there is a mode of amplitude of 26dB and a range of 23-27dB (figure 6.23a). The amplitude distribution of the next load range (60-80% of the sensor failure load) there were far more signals detected (42 compared to 9 for the previous range). In this distribution there were modes of amplitude at 25dB and 26dB but the distribution broadened to 36dB (figure 6.23b).

The 80-90% load range (figure 6.23c) there was a slight increase in the number of events detected. The distribution occurring in this load range exhibits the same range of amplitudes as found in the previous load range, however, there were more higher amplitude signals detected.

In the final load range (90% to sensor failure load) the distribution exhibits three distinct amplitude modes which could be linked to damage mechanisms: 24dB, 27dB, and 32dB. These values could be the modes of three distributions which overlap to produce a finite mixture distribution. However, this is difficult to prove. In this load range, however, there has been a definite broadening of the distribution, especially between 30-40dB. In addition to this there are many higher amplitude signals (>40dB).

To summarise, it is visibly apparent that there were few signals detected in the 0-60% load range. However, as the load increased there was a marked increase in the distribution range. In the 90% to sensor failure load range, there is a significant broadening of the distribution in the 30-40dB range with many higher amplitude signals being detected. From the cumulative graphs it was apparent that the appearance of the knee point in the plots occurred above 70% of the failure load. It is assumed that this point is due to the onset of delamination. In the 60-80% plot there is a definite broadening of the distribution above 30dB. Therefore, it is hypothesised that the broadening of the distributions in figures 6.23c-d is due to the growth of delamination. This type of damage leads to mass matrix cracking and carbon fibre failure toward specimen failure. In the 90% to sensor failure range, it could be hypothesised that the increase in data in the 22-29dB range could be due to matrix cracking and the higher amplitude signals (>50dB) due to carbon fibre fracture.

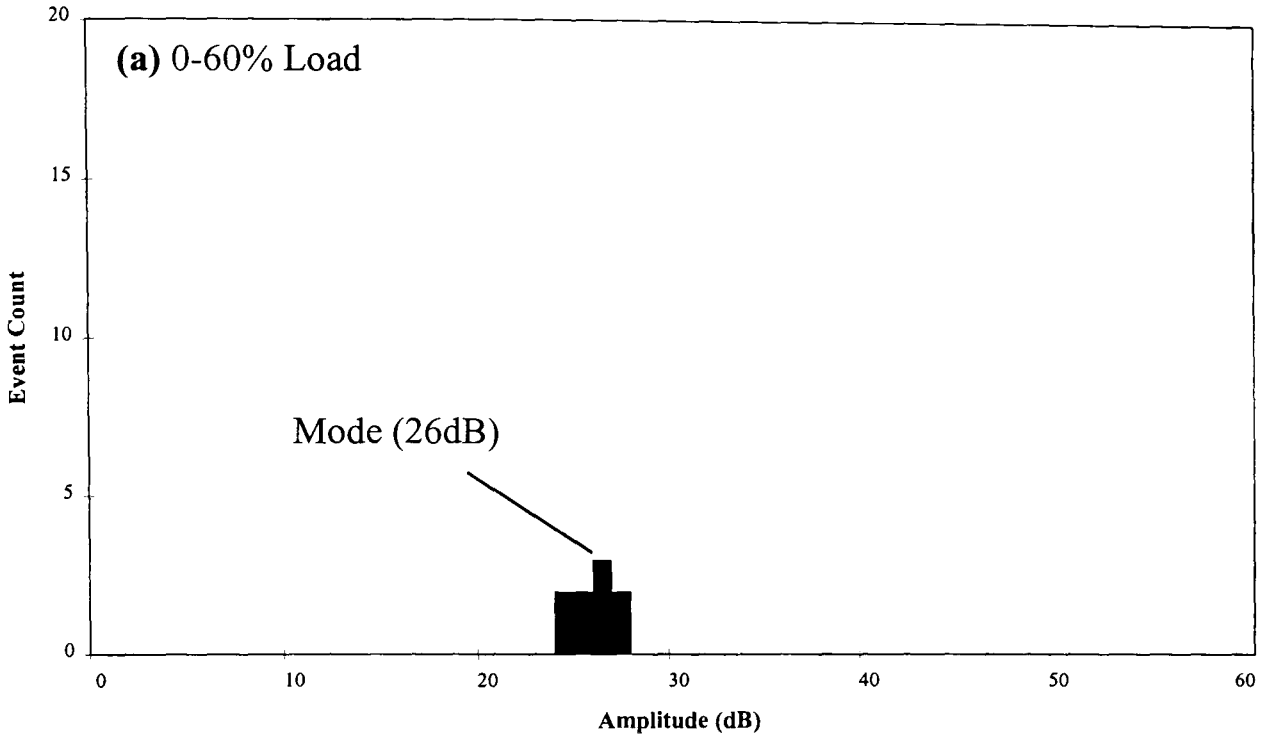

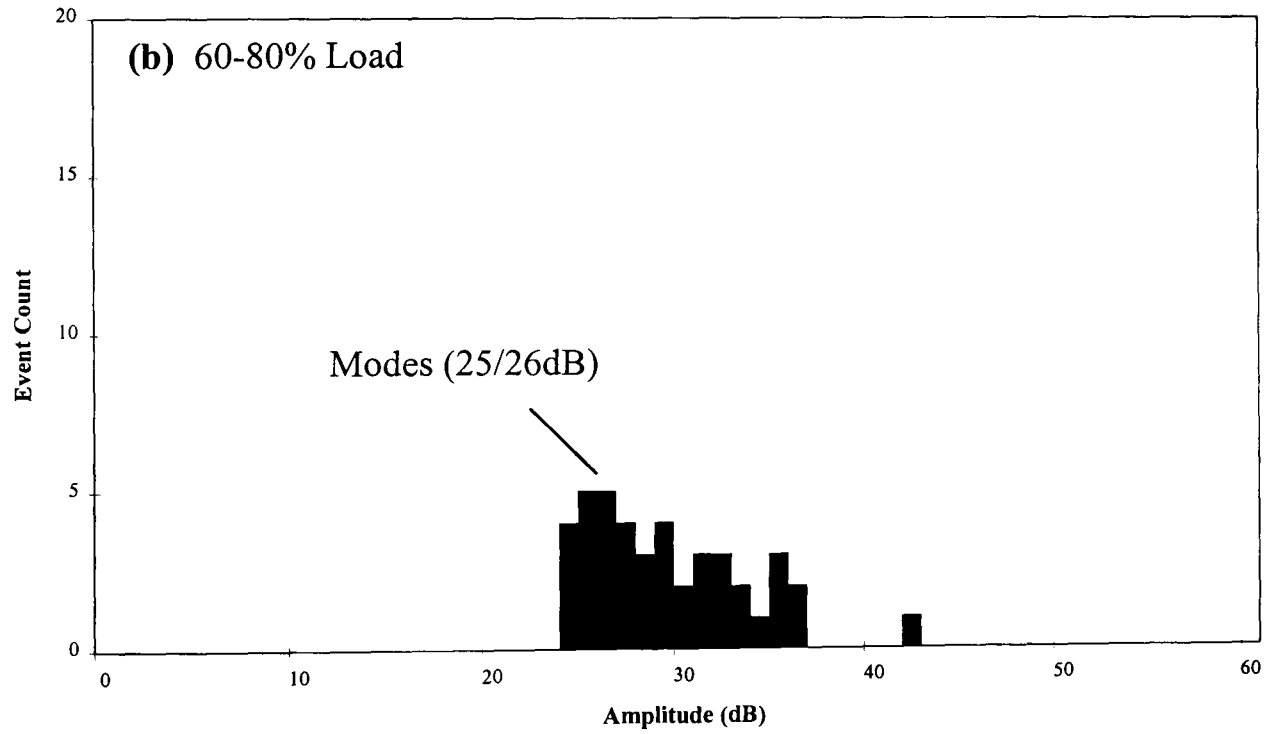

Figure 6.23a-b A typical example of the amplitude distribution analysis of the AE signals detected by the fibre optic sensor for various load ranges (0-60% and 60-80% of the sensor failure load).

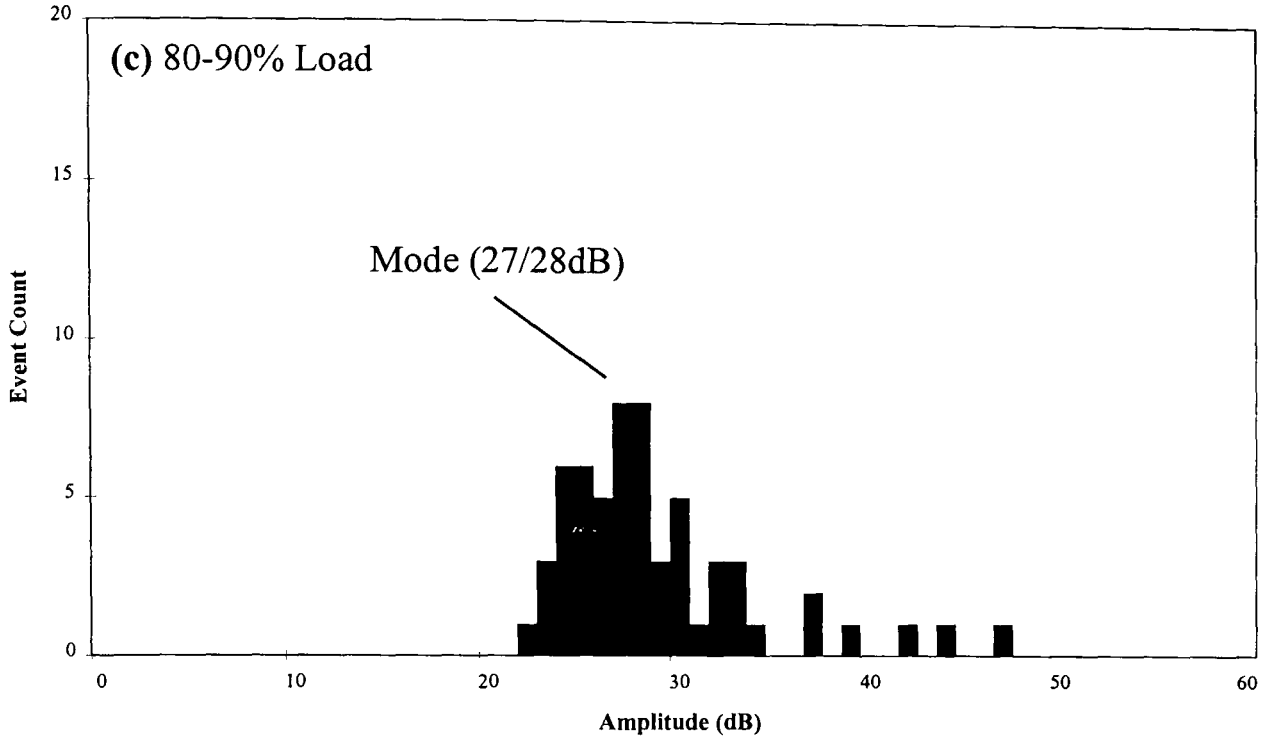

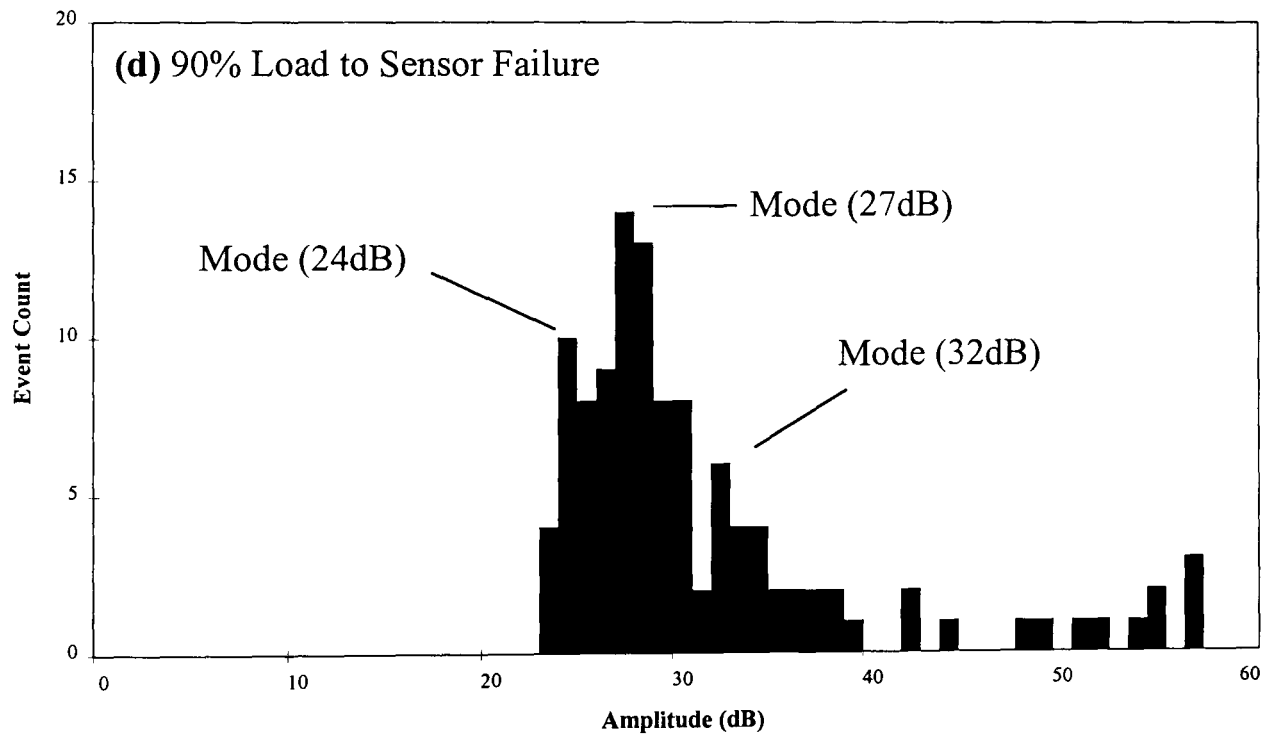

Figure 6.23c-d A typical example of the amplitude distribution analysis of the AE signals detected by the fibre optic sensor for various load ranges (80-90% and 90% to sensor failure load).

(ii) Piezoelectric Transducer

The AE emanating from the cross-ply composites was also detected by the piezoelectric transducer, captured using the AET5500, and converted from binary form to ASCII and analysed using the Excel spreadsheet software. A typical example of amplitude distribution graph using the AE detected by the piezoelectric transducer from the cross-ply composites is shown in figure 6.24. The AE data analysed is from the same sample used to produce the optical fibre sensor results. In this plot the distribution appears to be multi-modal, however, one distinct mode at 53dB can be seen. As in the fibre optic sensor distribution graphs, there is the possibility of an overlapping of distributions. By 'averaging' the amplitude data obtained for all twelve samples, the resulting plot (figure 6.25) can be analysed better than the typical example given in figure 6.24. The amplitude distribution graphs for all twelve samples are given in Appendix B.

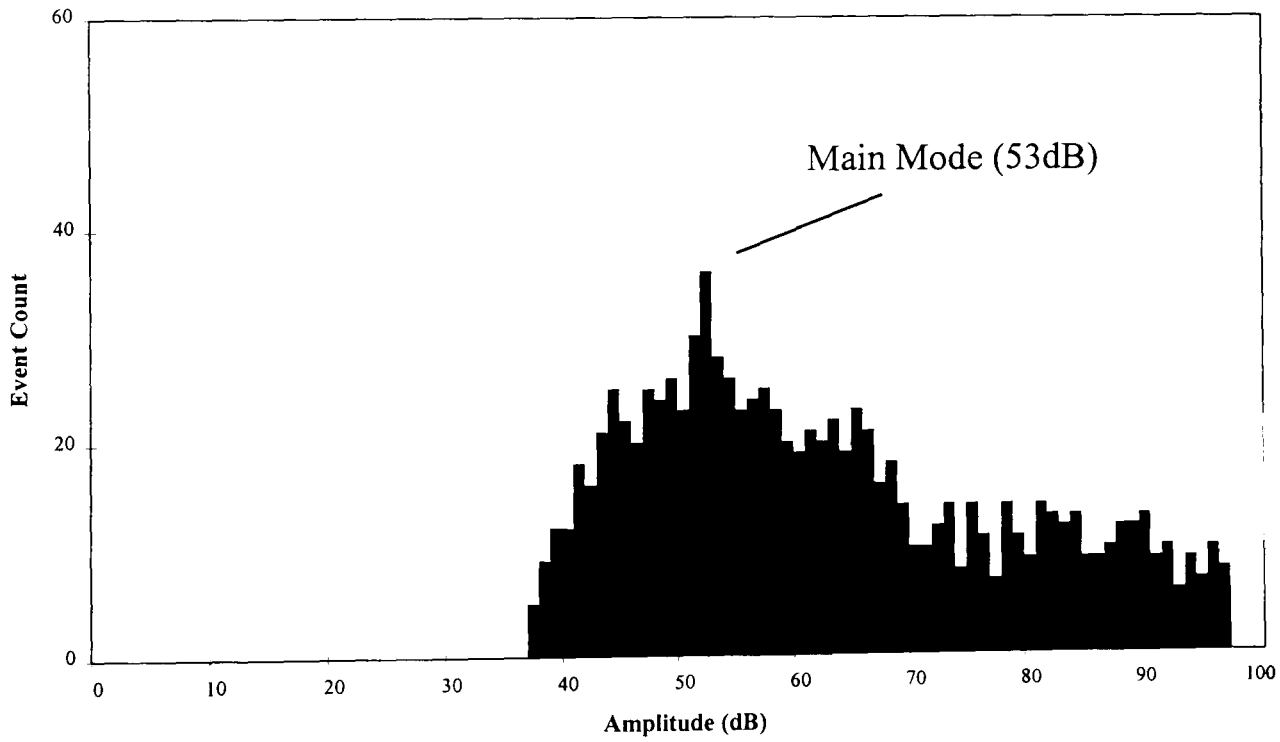

Figure 6.24 A typical example of the amplitude distribution of the AE signals detected using the piezoelectric transducer from the cross-ply composites.

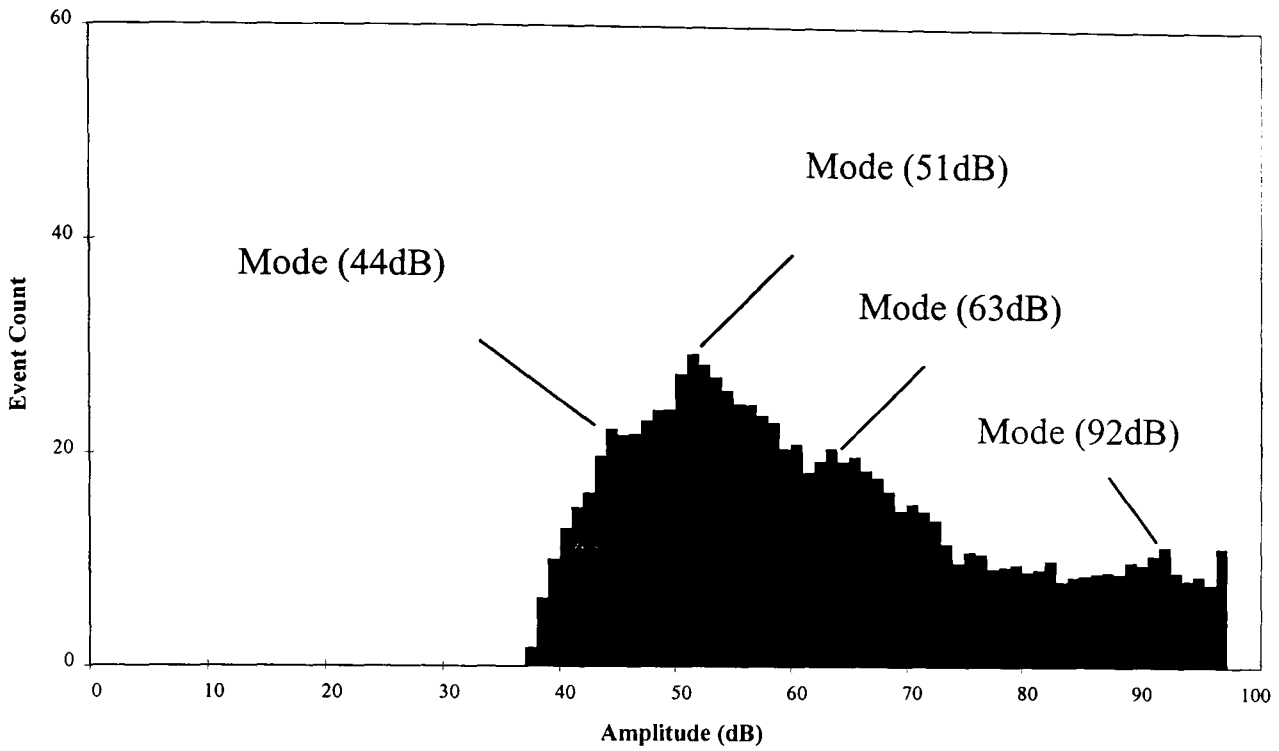

Figure 6.25 An 'average' amplitude distribution of the AE signals detected using the piezoelectric transducer from the cross-ply composites.

In the 'average' graph (figure 6.25), it is assumed that four distributions overlap and therefore indicate the presence of the four damage mechanisms which occur in these particular type of samples. In the graph, four possible modes have been presented: 44dB, 51dB, 63dB, and 92dB. It is difficult to prove this assumption to be correct as the formal techniques used to determine the mixture of distributions are complicated.

To help determine the damage mechanisms involved in these types of samples, it was necessary to investigate the amplitude distributions in specific load ranges. As with the analysis of the fibre optic detected data, the load ranges used were 0-60%, 60-80%, 80-90%, and 90% to failure load. A typical example of these four load range plots are shown in figure 6.26a-d. The AE data analysed is from the same sample used to produce the optical fibre sensor results.

In this example, the first load range (0-60% of the specimen failure load), the results obtained using the piezoelectric transducer showed a distinct mode of amplitude (44/45dB) and had a continuous distribution range of 37-49dB (figure 6.26a). There is also a small distribution of data above 50dB. In the amplitude distribution of the next

load range (60-80% of the specimen failure load) it is evident that there is a definite broadening of the continuous distribution (37-68dB). This distribution is multi-modal (figure 6.26b).

The 80-90% load range (figure 6.26c) showed an increase in the events detected, with almost double the events detected in the 60-80% range. The distribution is once again multi-modal, however, one mode is visible at 51dB. Also, there is a slight broadening of the continuous distribution (38dB-71dB), but more important, is the appearance of high amplitude signals above 80dB.

In the final load range (90% to specimen failure load) the multi-modal distribution extends continuously from 38-97dB (figure 6.26d). In this load range there is nearly three times the data than that detected in the 80-90% range. The most significant feature of this graph is the vast amount of data in the high amplitude region (>80dB).

To summarise, it is visibly apparent that all of the distributions are multi-modal. The most significant feature is the broadening of the distribution from graph to graph. In the 60-80% load range the distribution occurs in the 38-71dB (compared to 37-49dB in the 0-60% load range). From the piezoelectric sensors' cumulative graphs it was apparent that the appearance of the knee point in the plots occurred above 70% of the failure load. This point has been assumed to be due to the onset of delamination. Therefore, it could be hypothesised that the broadening of the distribution in the 60-80% load range (figure 6.26b) is due to the onset of delamination. In the 80-90% load range there is increase in data in the detected amplitude range (38-71dB) which may indicate the progression of delamination through the sample. In the 90% to specimen failure, there is a significant broadening of the distribution (38-97dB) which may be caused by mass carbon fibre fracture.

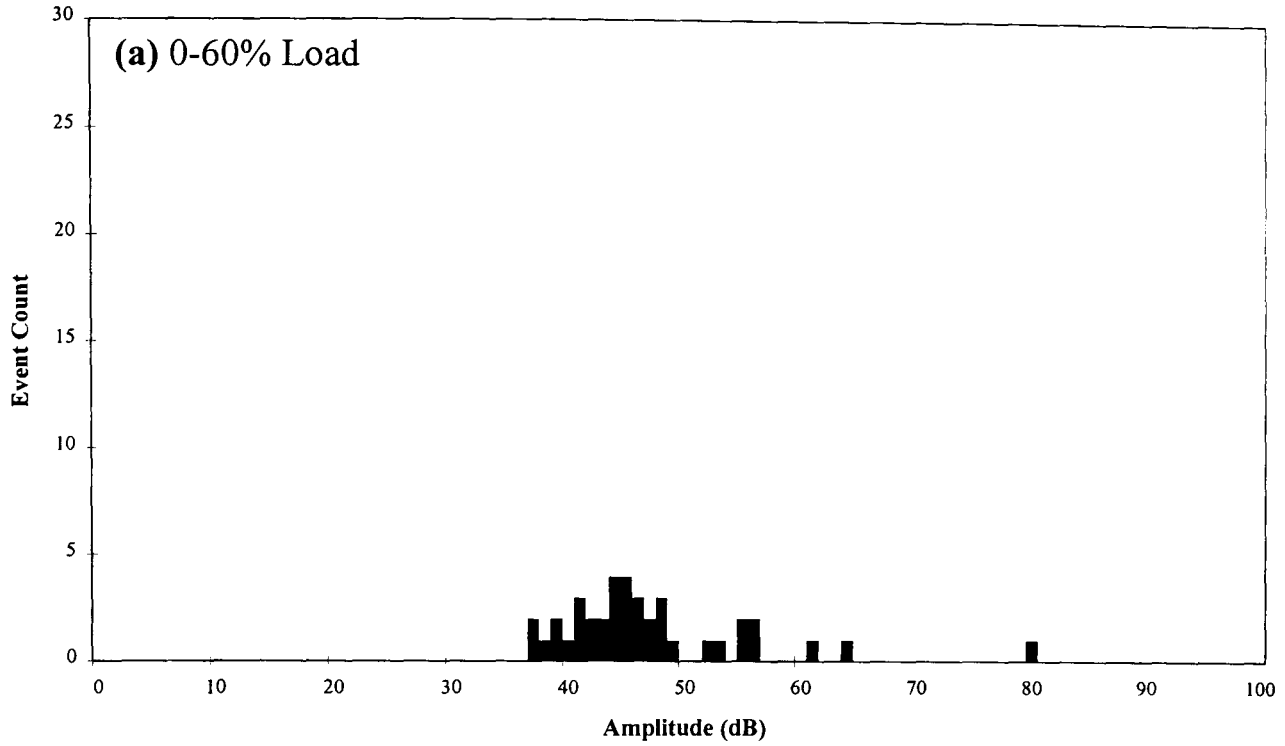

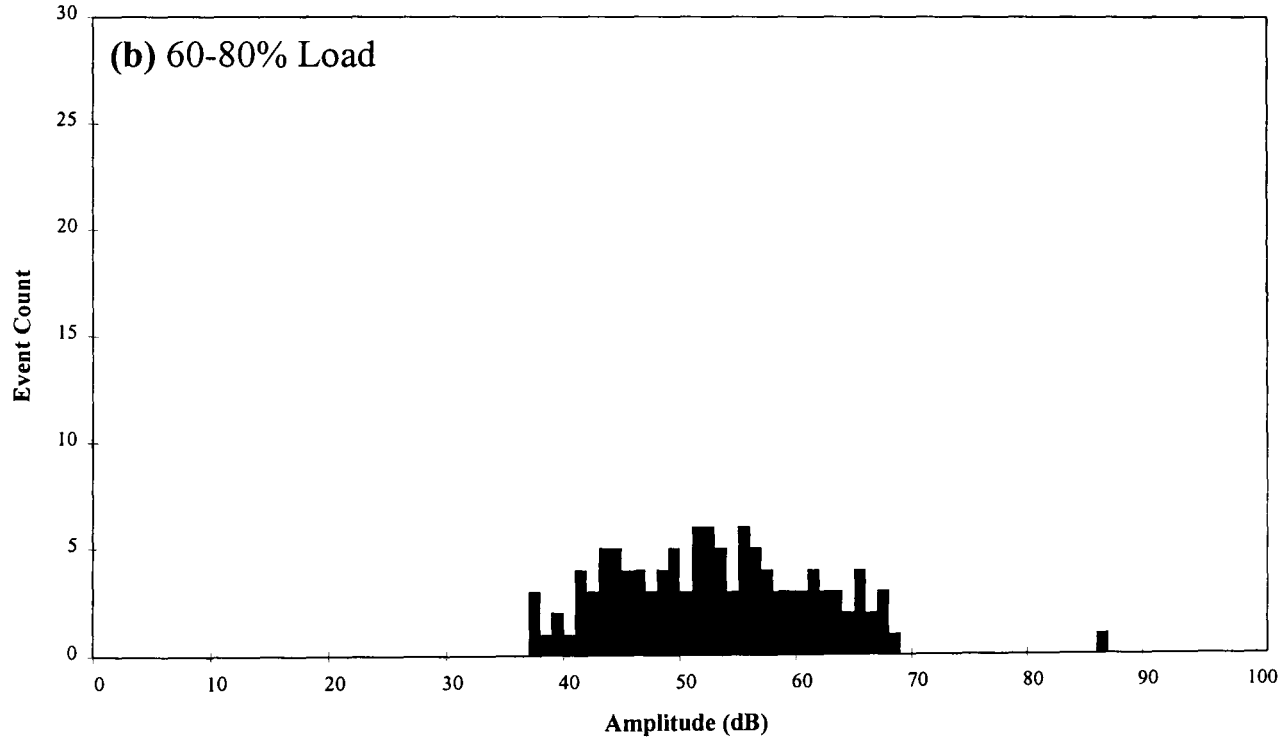

Figure 6.26a-b A typical example of the amplitude distribution analysis of the AE signals detected by the piezoelectric transducer for various load ranges (0-60% and 60-80% of the specimen failure load).

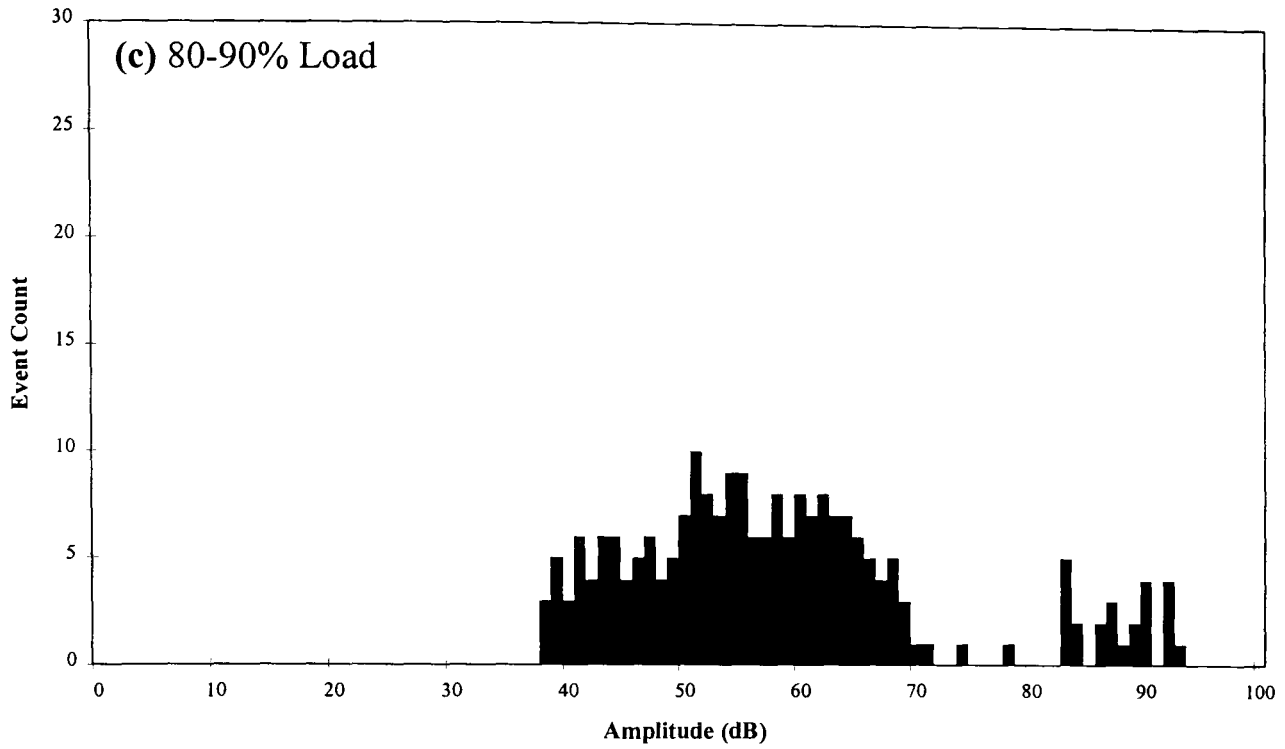

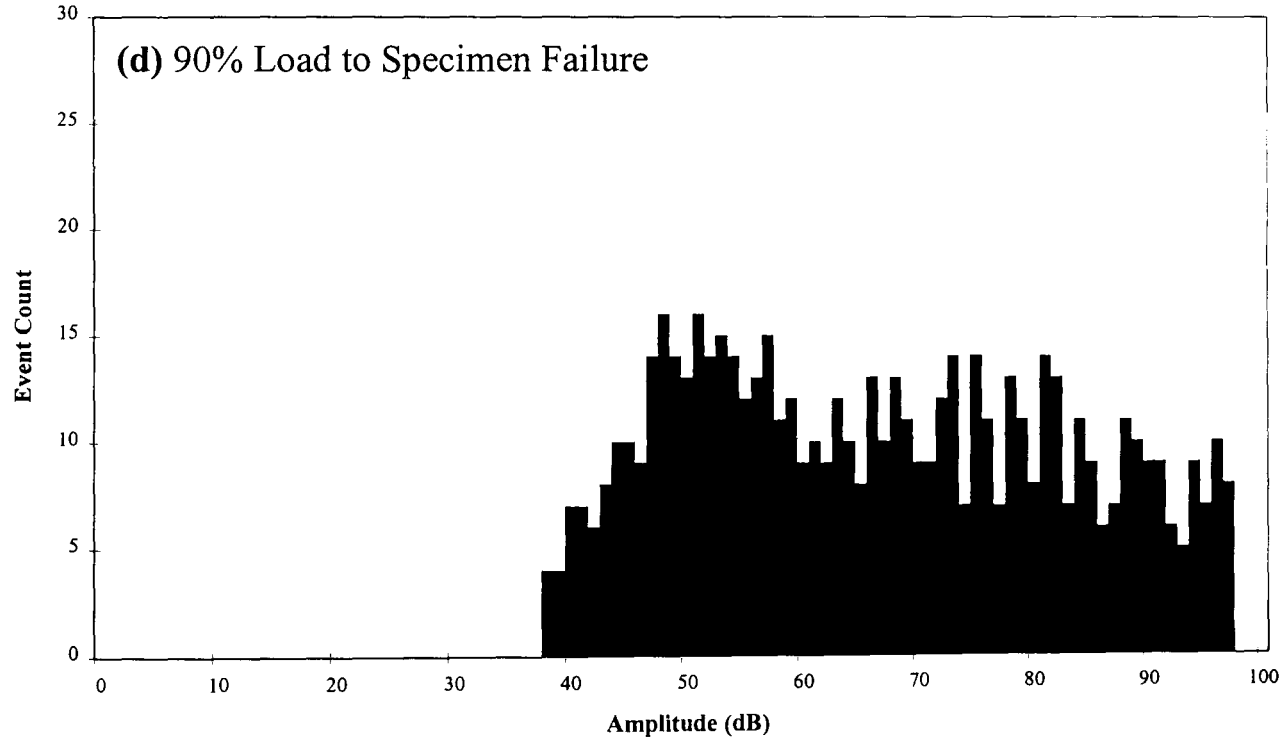

Figure 6.26c-d A typical example of the amplitude distribution analysis of the AE signals detected by the piezoelectric transducer for various load ranges (80-90% and 90% load to specimen failure).

Event Duration Analysis

The second parameter of the original acoustic signal which is of interest is the event duration. This parameter was plotted against increasing load/damage in a scatter graph. This plot is quantified by comparing two distinct 'zones'. Figure 6.27 shows the event duration in zone (a) for a sequence of signals prior to the 'knee' in the cumulative event count graph. Zone (b) shows the event duration of the signals in the part of the cumulative event count graph where the rate of AE activity dramatically increased.

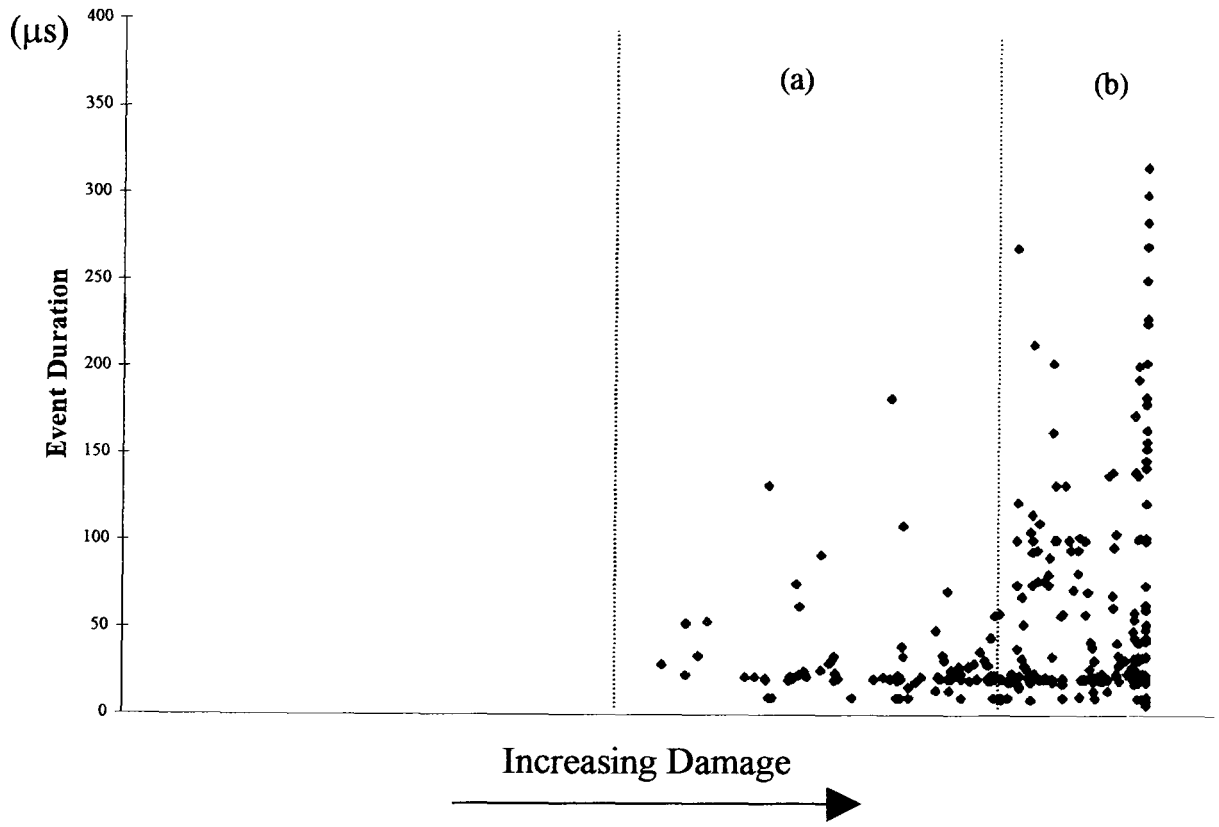

Figure 6.27 AE signal event duration vs. increasing load/damage.

In zone (a) the majority of signals have durations of less than 50μs. There are some signals in the 50-100 μs band with only three signals having durations of more than 100μs. In zone (b) there are still a vast amount of signals having durations less than 50μs, however, there is a substantial increase in the medium duration signals (between 50-150μs). Just before failure there are numerous higher duration signals (>150μs). Although an in depth analysis has not been made, this parameter could be used to filter

out the exceptional long duration signals caused by the overlapping of damage mechanisms.

6.6 Summary

In these experiments it has been shown that AE activity can be observed using an embedded optical fibre and that the results obtained compared favourably with those obtained from the standard PZ transducer under the same conditions. A Mach-Zehnder all-fibre interferometric fibre optic sensor has been applied to monitoring the AE resulting from progressive damage that occurs during loading of a CFRP composite. In general, fibre reinforced composites fail in a complex manner by a combination of fibre fracture, matrix cracking, interface failure and fibre pull-out. Each of these mechanisms contribute to the total acoustic emission. Since the appearance of delamination in a material seriously compromises the overall health of the structure, the detection of these zones using the embedded all-fibre Mach-Zehnder interferometric AE sensor demonstrates the feasibility of using such a sensor for non-destructive evaluation purposes and hence satisfies the first aim of this thesis. However, from the time domain analysis of the AE signals detected by the fibre optic sensor it was difficult to correlate these signals to specific damage mechanisms. These difficulties could be caused by the fact that each event may not be captured separately. There may be sufficient overlapping of events to hinder the use of amplitude and event duration analysis. Also, it has been shown that the fibre optic sensor fails to detect AE close to specimen failure. The data which was lost could shed more light on the damage mechanisms involved in the fracture process.

CHAPTER 7

EXPERIMENTS USING THE PIEZOELECTRIC TRANSDUCER

7. Experiments Using The Piezoelectric Transducer

7.1 Introduction

In the previous chapter, it was evident that the fibre optic acoustic emission sensor could determine the point where the damage in the material would compromise the overall safety and reliability of the sample. However, analysis of two of the time domain parameters of the acoustic emission signal provided no conclusive evidence of a correlation between these parameters and the type of damage present in the sample. Previous testing using the embedded fibre optic sensor was aimed at determining the damage mechanisms from a complex $[0, 90, 90, 0, 0, 90, 0, 90]_s$ cross-ply composite under tensile loading.

A series of tests was devised to isolate each damage mechanism so that the correlation of the acoustic emission signal parameters to damage would be more conclusive. In addition to time domain analysis of the detected signals, the frequency content of the signals was monitored. However, at the time of this experimentation the fibre optic sensor was experiencing sensitivity problems. The tests were resumed with only the piezoelectric transducer used to detect the acoustic emission emanating from the composite sample under tensile load. The intention of these tests was to gain conclusive evidence of a correlation between damage mechanism and the signal parameters, so that it could be used to aid the analysis of the data detected using the fibre optic sensor.

To achieve this, the carbon/epoxy material in the form of unidirectional pre-preg composite was loaded under different conditions to determine the time domain properties and frequency content of the acoustic emission signals. The specimens were specially designed to fail under well defined modes, such as matrix cracking, debonding between fibre and matrix, fibre pull-out, fibre failure, and delamination.

7.2 The Application Of Different Loading Conditions To Correlate Frequency And Time-Domain Content Of The AE Signal With Different Damage Mechanisms.

The tests undertaken involved the application of different loading conditions to the material to correlate the expected time domain properties and frequency bands with the failure mechanism. The mechanical testing of the samples were once again performed on an Instron 1195 tensile testing machine (with a cross-head speed of 0.5mm/min). The acoustic signals were detected using a wide-band transducer, and then pre-amplified (40dB) and filtered (100kHz-1MHz) using an AET Corporation Model 160 pre-amp and filter unit. The resulting signal was then fed via a shielded cable to the back panel of the acoustic emission data evaluation system (AET5500). Next the signal was fed from the output BNC on the front panel of the AET5500 into a burst spectrum analyser (Hewlett Packard HP 89410A), where the maximum frequency component was recorded. A schematic of the experimental set-up is shown in figure 7.1. The necessary experimental and signal processing details are found in Appendix A.

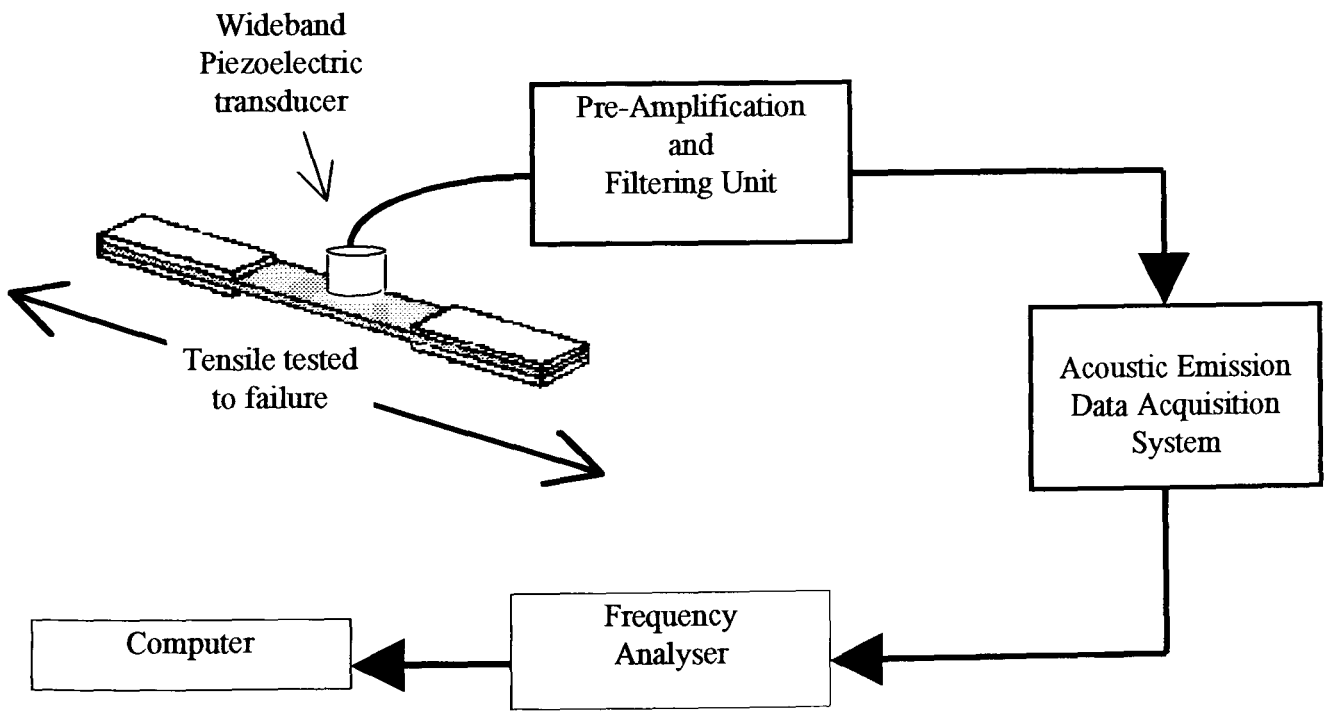

Figure 7.1 Experimental set-up for time and frequency domain analysis

7.2.1 Test Specimens And Their Expected Failure Mechanisms

The CFRP specimens used in these tests were designed to fail due to certain damage mechanisms. A systematic method of sample design was devised so that the first sample to be tested only exhibited one type of failure mechanism. Therefore, pure resin samples were manufactured to obtain the time domain parameters and frequency spectra of the acoustic emission signals due to matrix cracking. A schematic of this type of specimen and its expected damage mechanisms is shown in figure 7.2.

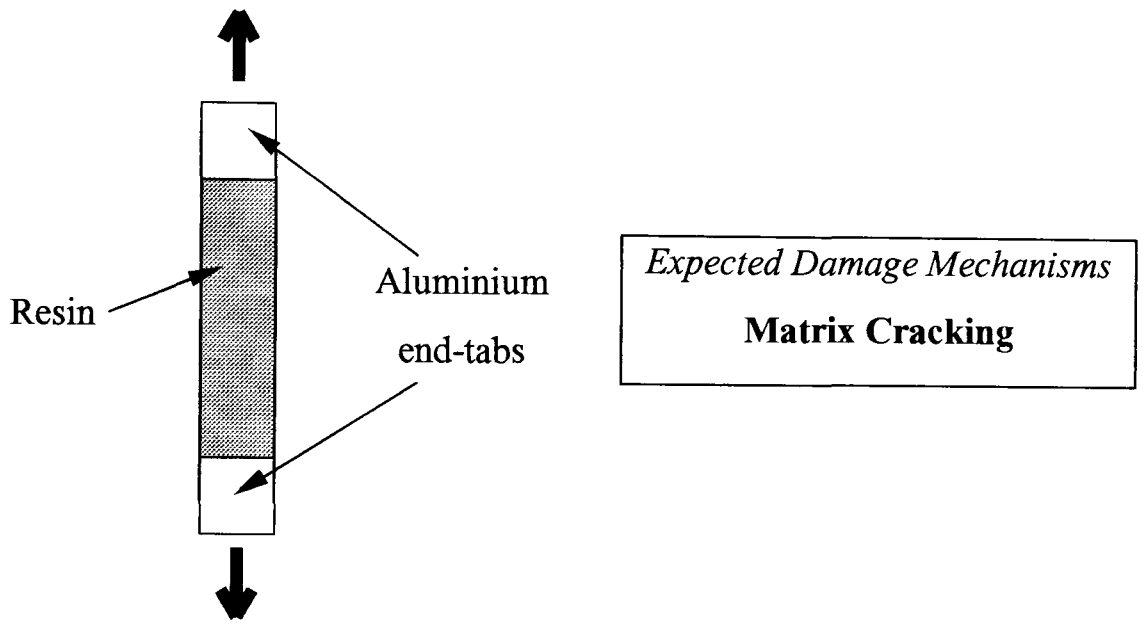

Figure 7.2 Schematic of the pure resin samples used for the piezoelectric tests.

The next type of sample must exhibit this type of damage mechanism so that a comparison can be made. To that end, a unidirectional sample was loaded 90 degrees to the reinforcing carbon fibres. In these samples the matrix bears the load and no fibre fracture should be obtained. In these samples, however, there would be some debonding of the fibre/matrix interface.

The third type of sample manufactured for these tests involved loading at an angle to the reinforcing fibres so that the matrix cracking and fibre/matrix debonding mechanisms are dominant. By loading the sample at 10 degrees to the reinforcing fibres, composite failure due to these two mechanisms occurs along with some minor cases of fibre pull-out.

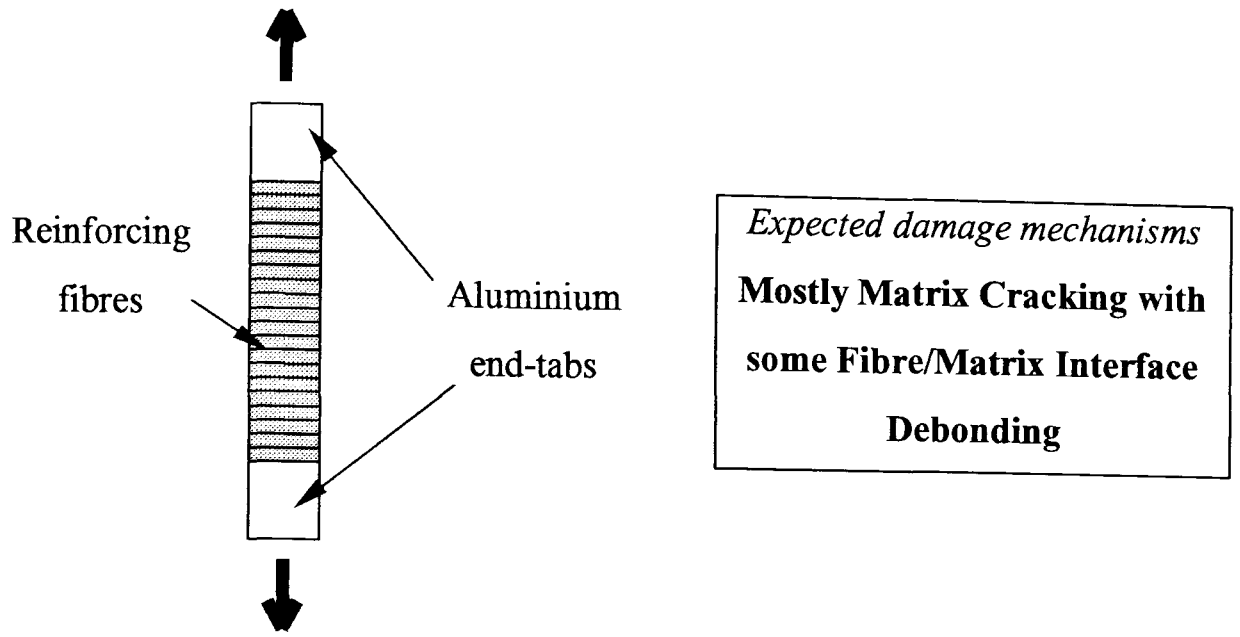

Figure 7.3 Schematic of the 90° samples used for the piezoelectric tests.

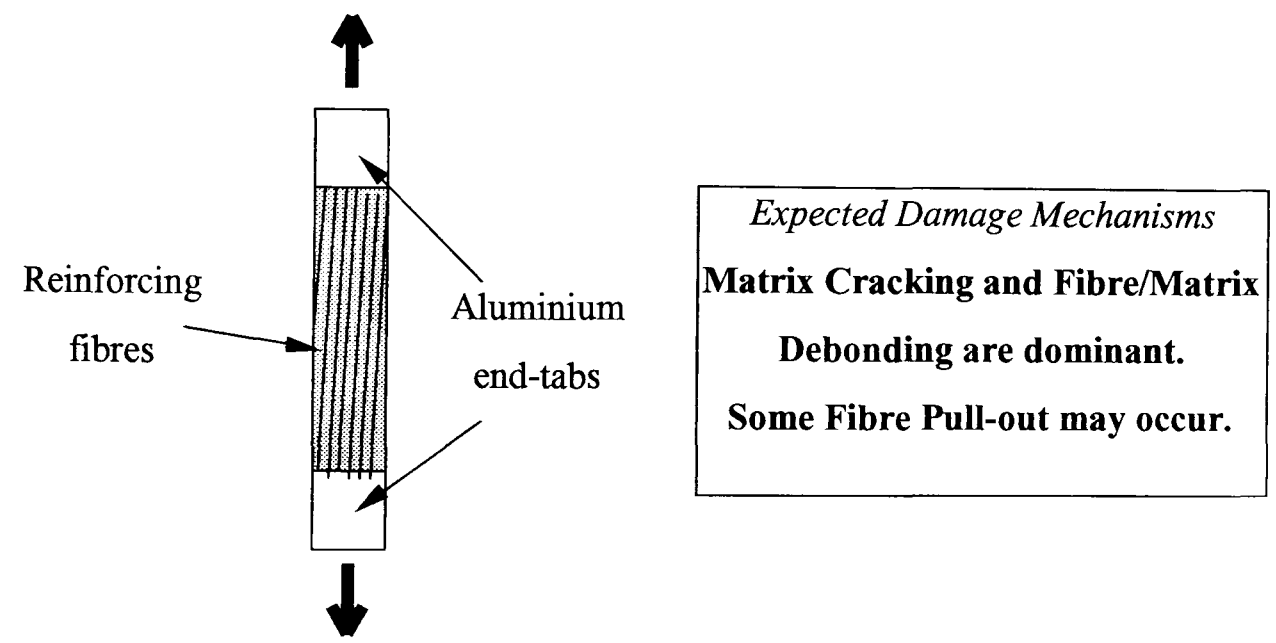

Figure 7.4 Schematic of the 10° samples used for the piezoelectric tests.

To check the acoustic emission signal characteristics for fibre fracture some uncured pre-preg samples were loaded in tension. The resulting information would help confirm the results obtain in the previous test as matrix cracking occurs.

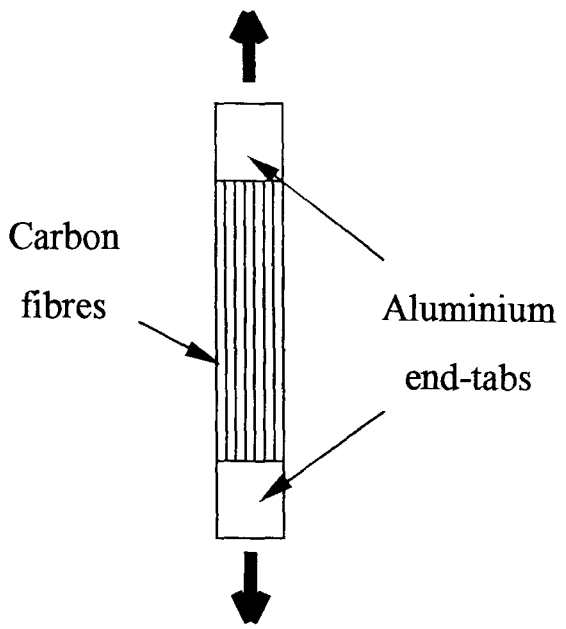

Expected Damage Mechanisms

Fibre Fracture is dominant. However, some cracking of the matrix surrounding the carbon fibre occurs.

Figure 7.5 Schematic of the uncured samples used for the piezoelectric tests.

The final type of sample manufactured introduces delamination. Since delamination only occurs between plies of differing material fibre orientation, an artificial damage initiator must be introduced into the unidirectional samples. The insertion of a small disc of Teflon sheeting between plies of a unidirectional composite specimen during manufacture can provide specimens which, on the application of load, primarily give acoustic emission due to delamination and some due to matrix and fibre failure.

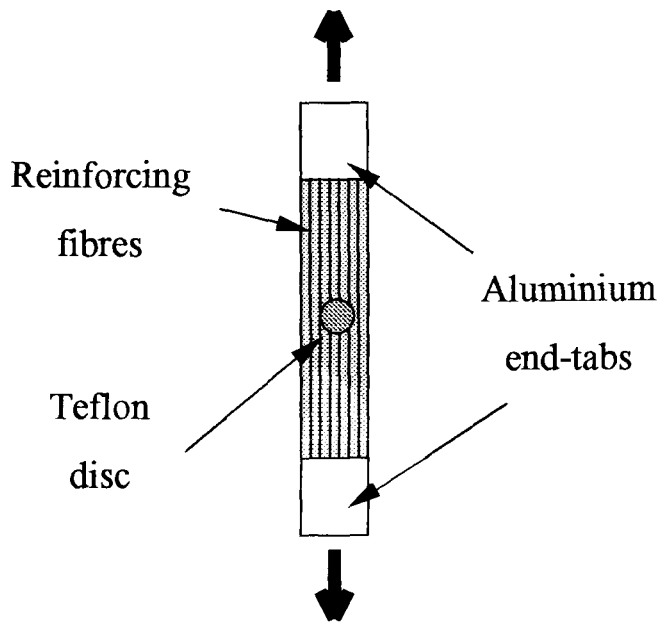

Expected Damage Mechanisms

Primarily Delamination although some Matrix Cracking and Fibre Fracture occurs.

Figure 7.6 Schematic of the Teflon-loaded samples used for the piezoelectric tests.

The previous schematics (figures 7.2 to 7.6) will be used in the results graphs for easy reference. A summary of the tests and the expected failure mechanisms are shown in table 7.1.

Mechanical Test	Damage Mechanism
Unreinforced epoxy bars- Tensile	Matrix fracture
90° Tensile	Mainly matrix cracking
10° Tensile	Almost no fibre breakage
Uncured pre-preg- Tensile	Carbon fibre fracture
Teflon insertion	Mainly delamination

Table 7.1 Summary of the mechanical tests and expected mechanisms

7.3 Amplitude Distribution Analysis

In an attempt to correlate the detected acoustic emission signals with its corresponding damage mechanism the amplitude distribution of the signals was monitored. Since the specimens have been designed to fail under distinct damage mechanisms, it was possible to isolate each amplitude distribution for each mode of failure. The reference level for the amplitude levels is 0dB at 1μV at the sensor output.

7.3.1 Tensile Loading Of Pure Resin Samples

The tensile testing towards failure of these specimens gives detectable acoustic emission signals which can be directly related to cracking of the matrix. The results of detectable amplitudes from pure resin samples take the form of a distribution shown in figure 7.7. This type of distribution is typical of the results obtained for each specimen. From this plot it is evident that one population curve exists in 38-54dB range with a distinct mode of 44dB.

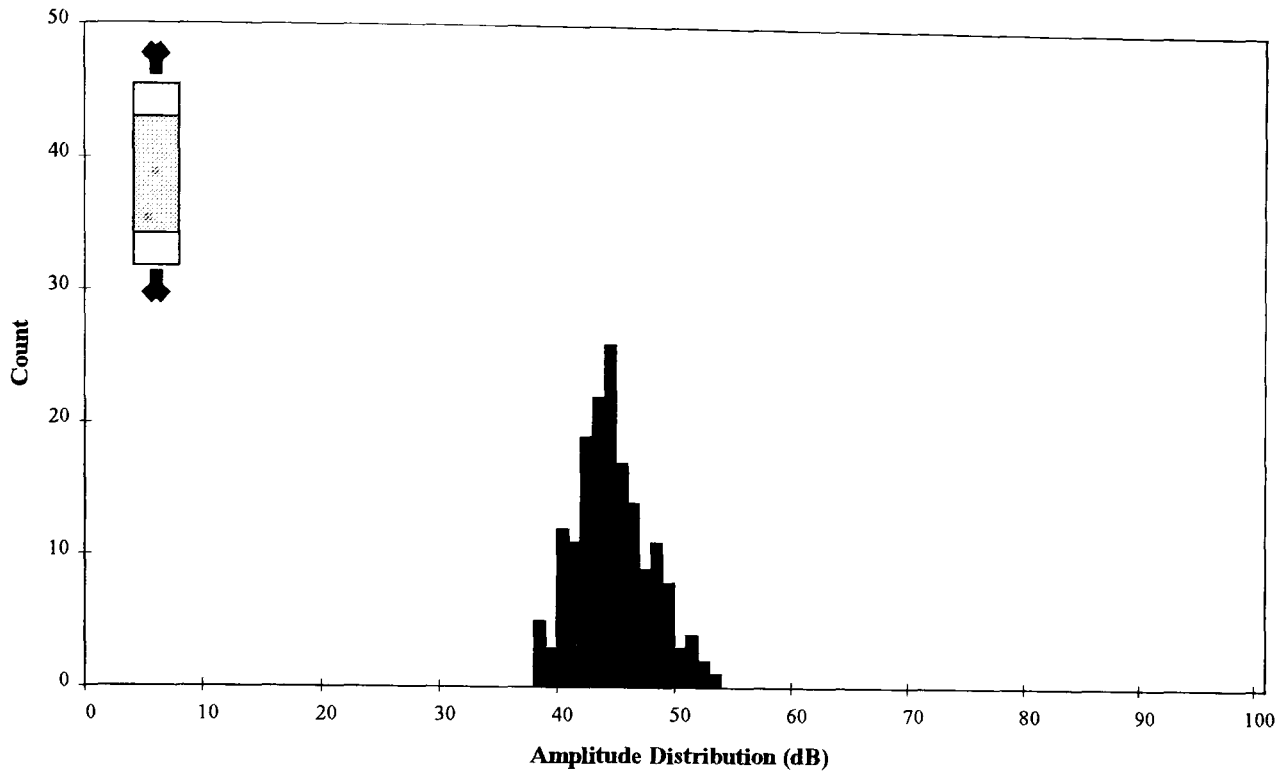

Figure 7.7 Amplitude distribution analysis of the AE signals from a typical pure resin samples using the piezoelectric transducer

In these tests twelve pure resin samples were loaded in tension to failure. The distributions obtained for these samples are illustrated in Appendix C. In order to perform the appropriate analysis of these distributions, it was necessary to obtain an 'average' distribution. This was achieved by simply combining the data for all the tests and then dividing the total by the number of samples used, in this case, twelve. The 'average' distribution calculated for the pure resin samples is shown in figure 7.8.

From figure 7.8 it was possible to obtain several statistical parameters from this normally distributed data. The spreadsheet package ***Excel*** was used to obtain the statistical parameters, such as mode, median, mean, standard deviation and skewness. A summary of the parameters is shown in table 7.2. The mean and standard deviation obtained from this distribution can be used to calculate an 'expected' or 'estimated' normal distribution, which can then be used for comparison purposes. The graph illustrated in figure 7.9 shows two probability distributions: the blue curve is the probability distribution calculated from the 'average' test data, whereas the red curve shows the 'expected' or 'estimated' distribution.

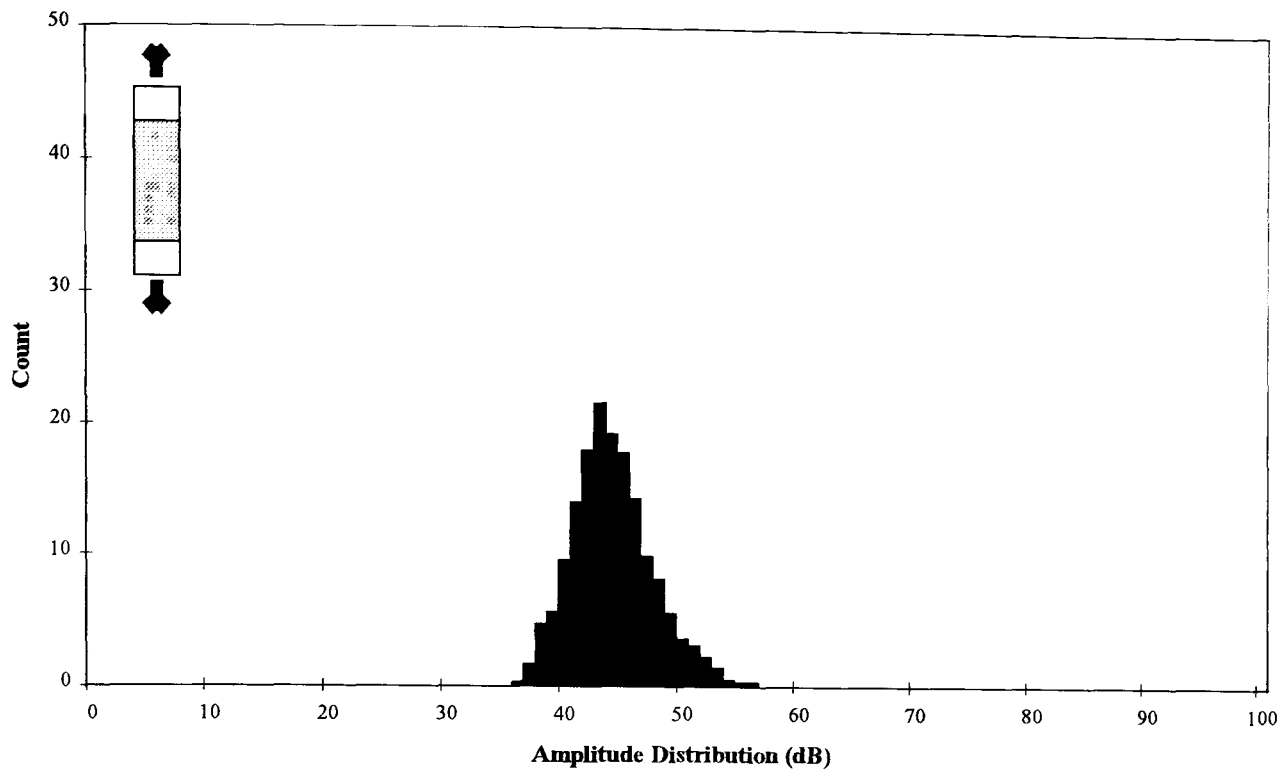

Figure 7.8 Average amplitude distribution of the AE signals from pure resin samples using the piezoelectric transducer

Statistical Parameters	
Mode	43
Median	45
Mean	44.086
Standard Deviation	3.423
Pearsons Coefficient (skewness)	-0.801
Distribution Range	37-56dB

Table 7.2 Statistical analysis of the 'average' amplitude distribution for pure resin samples.

From figure 7.9 it is evident, through a comparison of the actual and estimated distributions, that the test data is normally distributed.

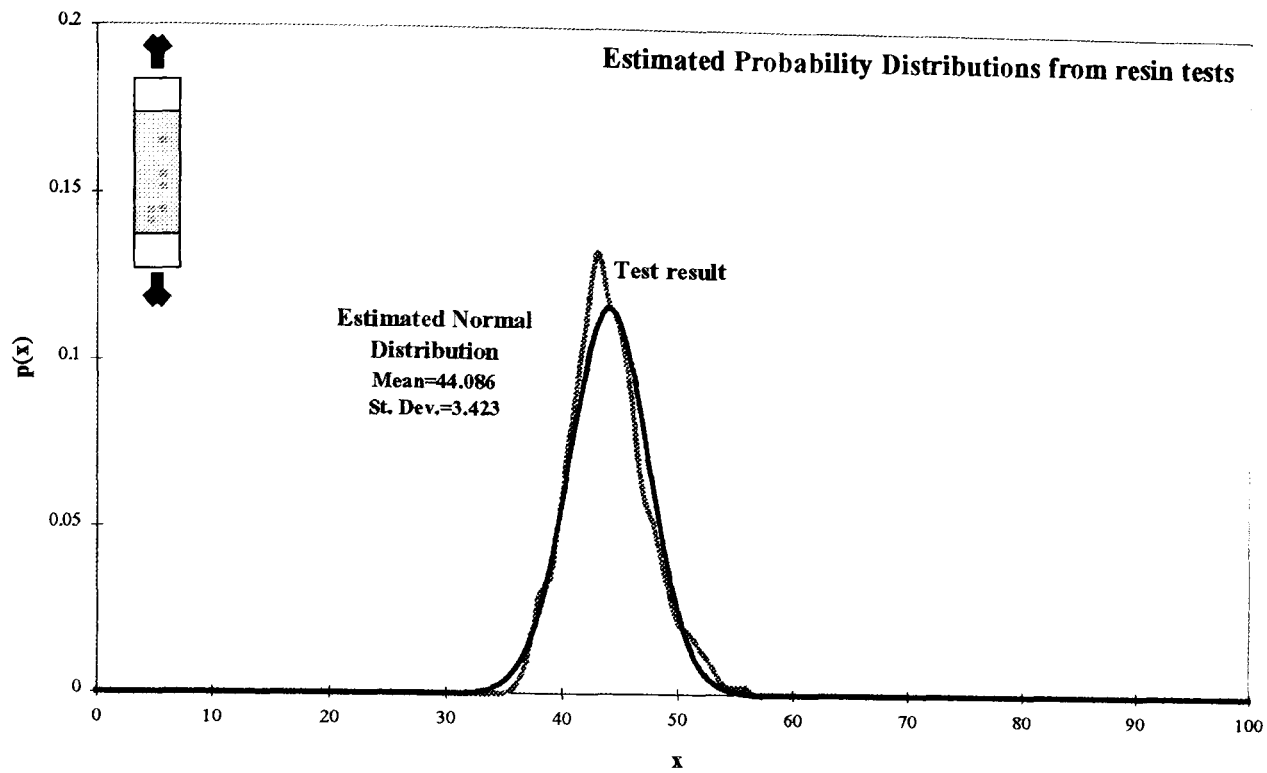

Figure 7.9 Actual and estimated probability distribution analysis of the AE signals from pure resin samples using the piezoelectric transducer

7.3.2. Tensile Loading Of 90° Specimens

Amplitude distribution analysis has been done on the acoustic emission data obtained from the tensile loading orthogonal to the reinforcing carbon fibres. A typical amplitude distribution graph from this type of specimen is shown figure 7.10. From the plot it appears that there is mixture of two normal distributions. In all twelve samples tested to failure, the resulting plots exhibited this trait (refer to Appendix C for these plots). In this plot it appears that the distribution is multi-modal. However, two modes particularly stand out. An indication of these modes displayed on the graph. The modes in question have amplitudes of 46dB and 62dB respectively. As with the previous section, an 'average' distribution was determined, which helps to highlight the bi-modality of the distribution. From this plot (figure 7.11) it is apparent that two distributions occur in these types of samples. There is also a small distribution of data in the higher range. This data may be due to many damage mechanism occurring virtually at the same time, thus giving a large signal amplitude.

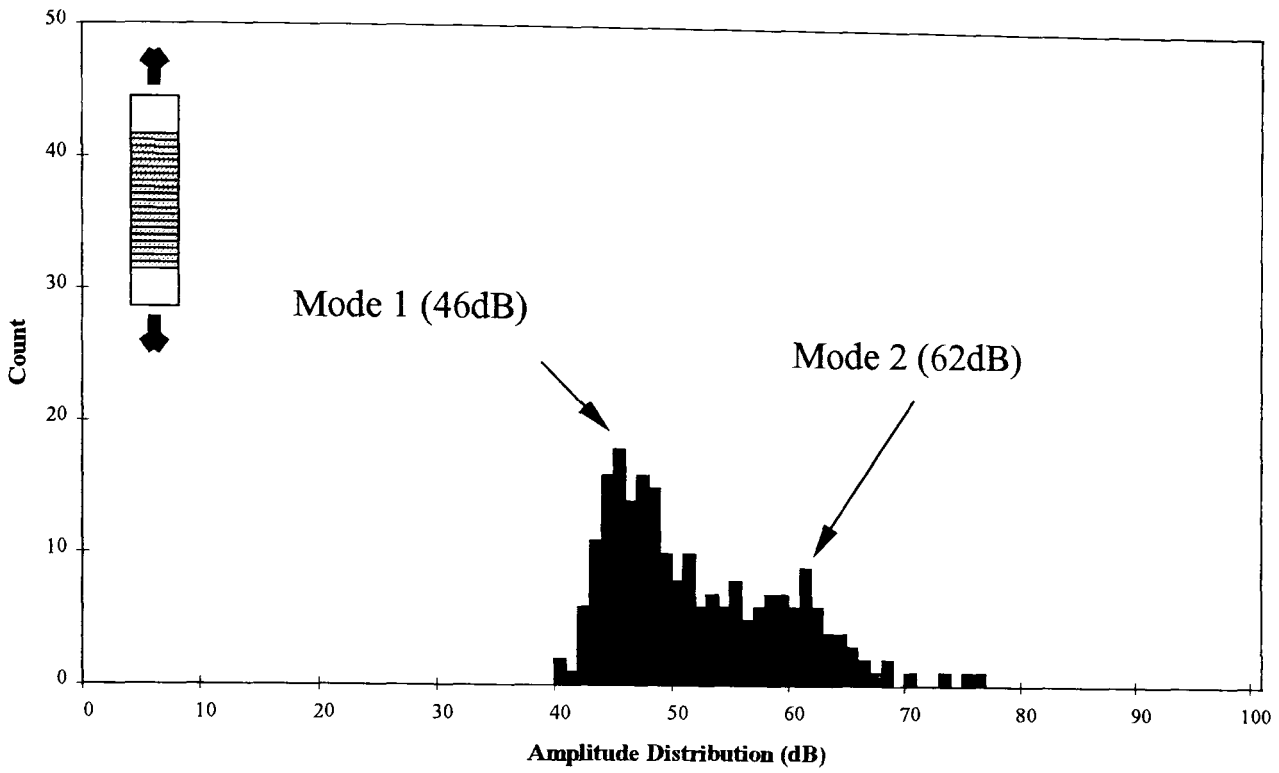

Figure 7.10 A typical plot of the amplitude distribution of the AE signals from the tensile loading to failure of 90° loaded CFRP specimen.

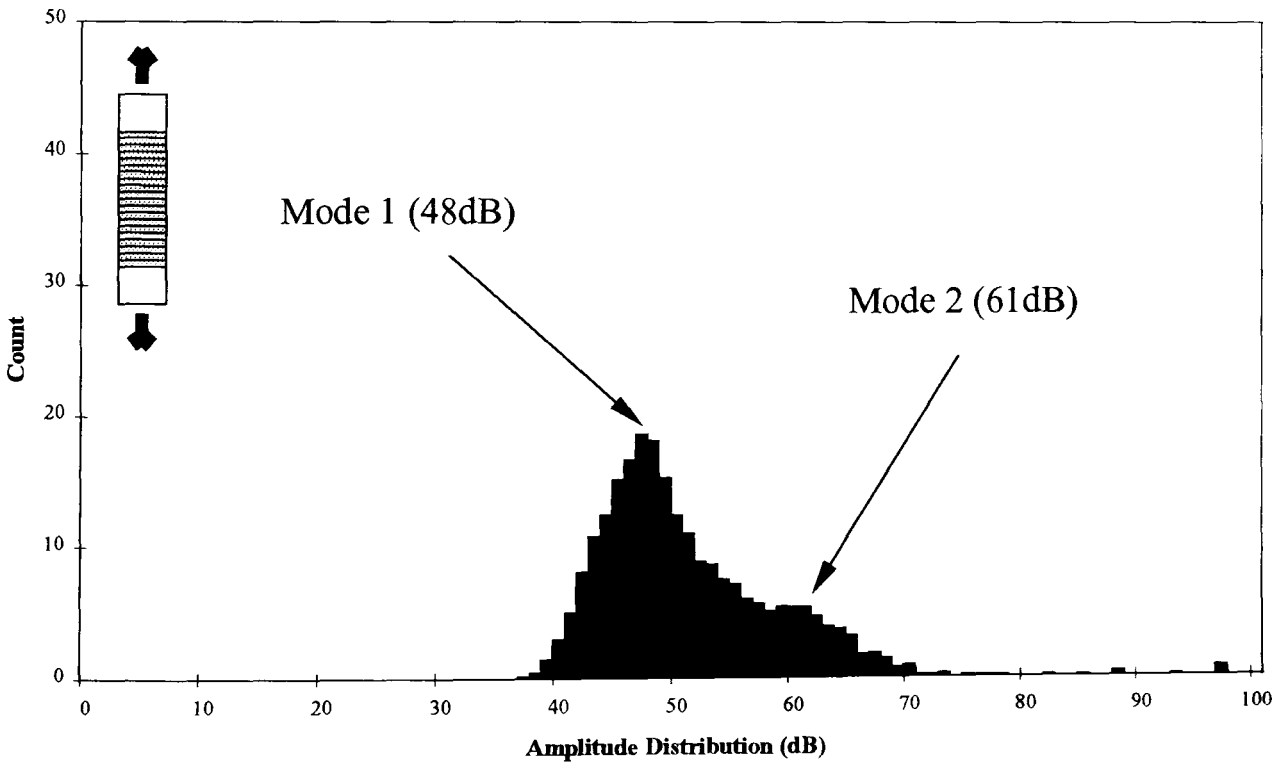

Figure 7.11 Average amplitude distribution of the AE signals from 90° loaded samples using the piezoelectric transducer

However, if it was assumed that only one distribution is present, then the statistical parameters can easily be obtained. These are displayed in table 7.3. If these parameters are used to determine the expected distribution, it is visibly apparent that there is a poor relationship between the actual and expected distributions (figure 7.12).

Statistical Parameters	
Mode	48
Median	49
Mean	51.008
Standard Deviation	6.872
Pearsons Coefficient (skewness)	-0.877
Distribution Range	38-71dB

Table 7.3 Statistical analysis of the 'average' amplitude distribution for 90° loaded samples.

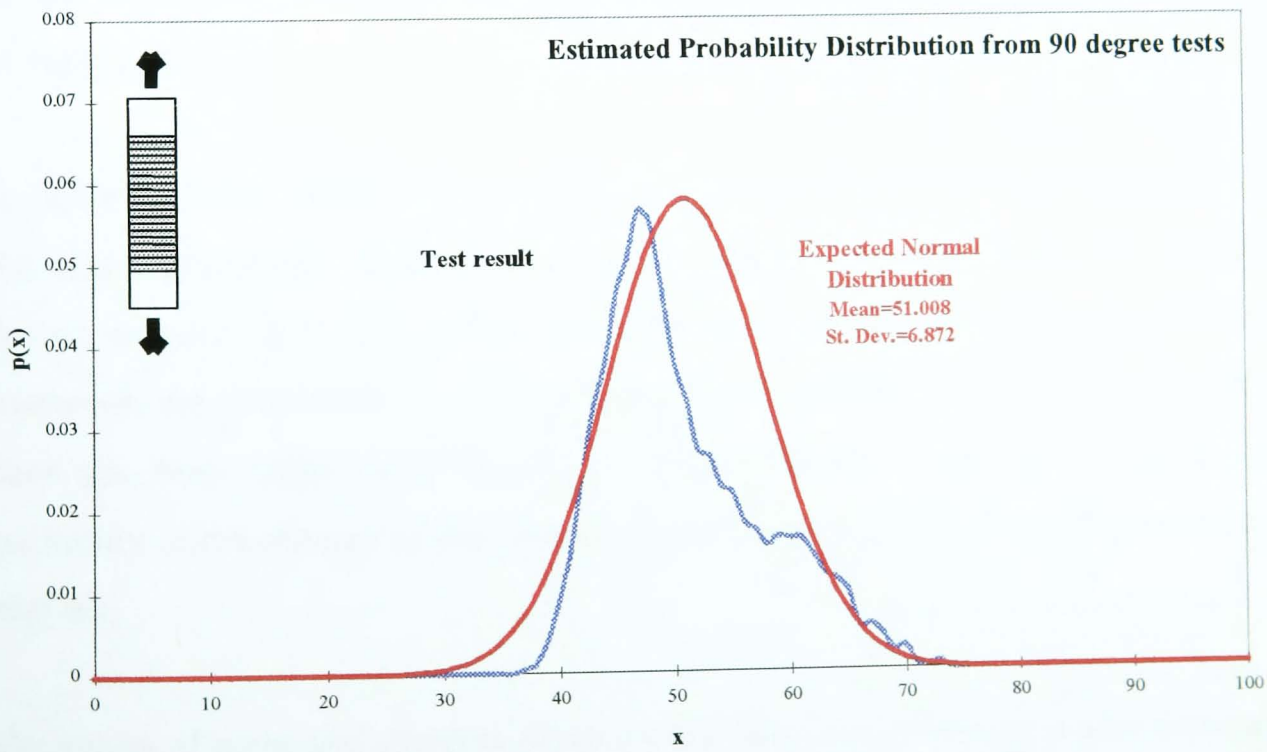

Figure 7.12 Actual and estimated probability distribution analysis of the AE signals from 90° loaded samples using the piezoelectric transducer. Estimated plot is based on the assumption that there is no mixture of distributions in the actual data.

In figure 7.12 it may appear that there is a mixing of distributions due to the number of damage mechanisms involved in the failure of the 90° specimens. In these types of specimens it is assumed that two damage mechanisms are involved: matrix cracking and some fibre/matrix debonding. Many methods have been devised and used for estimating the parameters of mixture distributions, ranging from Pearson's method of moments, through formal maximum likelihood approaches, to informal graphical approaches.

However, formal methods for estimating the mixing proportions and the component parameters are based on the assumption that the number of components (that is, the number of damage mechanisms occurring in a test) are known. In the 90° samples it is assumed that two mechanisms are present. Since the tests were of a preliminary nature and the visual inspection provided no detailed information on the damage mechanisms involved, the data detected did not merit detailed (formal) mixture distribution analysis. Therefore, the mixture distribution analysis was based on informal graphical techniques, that is, the study of the sample histogram. It must be stated that uni-modality of a distribution does not imply it is not a mixture. Moreover, sample distributions from single components can easily be multi-modal and thus seem to imply a mixture.

In figure 7.13 two estimated probability distributions have been superimposed onto the actual probability distribution graph. In these plots, the mean and standard deviations have been estimated to form the two normal probability distributions. Moreover, the proportions of data occurring within distribution 1 and distribution 2 have also been estimated (75% and 25% respectively). These plots indicate the possibility of the mixture of two distributions without the need for rigorous mixture analysis.

The values of mean and standard deviation for these two estimated distributions are not essentially important. However, the values chosen clearly indicate the possibility of the mixture of two distributions. As stated earlier, it is possible that one component (or damage mechanism) could be responsible for multi-modal distributions.

7.3.3. Tensile Loading Of 10° Specimens

Amplitude distribution analysis has been done on the acoustic emission data obtained from the tensile loading at an angle of 10° to the reinforcing carbon fibres. In these type of samples fibre pull-out is introduced in addition to the matrix cracking and fibre/matrix interfacial debonding. A typical amplitude distribution graph from this type of specimens is shown figure 7.14. This plot has two distinct population distributions: the largest distribution being between 41dB and 77dB, with the smaller distribution being above 80dB.

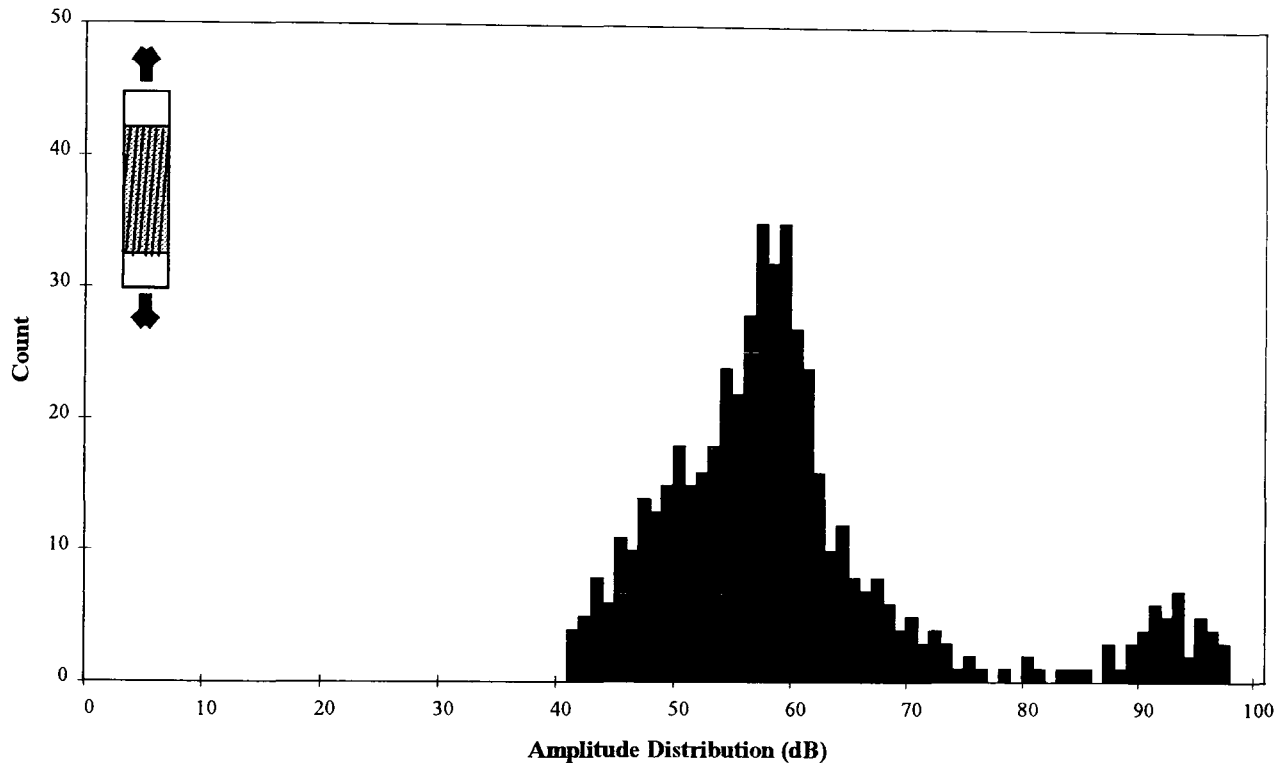

Figure 7.14 A typical amplitude distribution of the AE signals from the tensile loading to failure of 10° loaded CFRP specimen.

The 'average' distribution highlights these two distributions better (figure 7.15). In this plot, the largest distribution (between 41-79dB) has a mode amplitude of 57dB and appears to be skewed to the right. In the second distribution (80-97dB) the plot appears to be normally distributed except for the abrupt right hand edge. This is due to the fact that the AET5500 upper detectable amplitude threshold is 97dB, and therefore no signals above this value are registered. For statistical analysis purposes, values above 97dB have been estimated. This will be the case for subsequent graphs where the AET5500 threshold problem comes into effect.

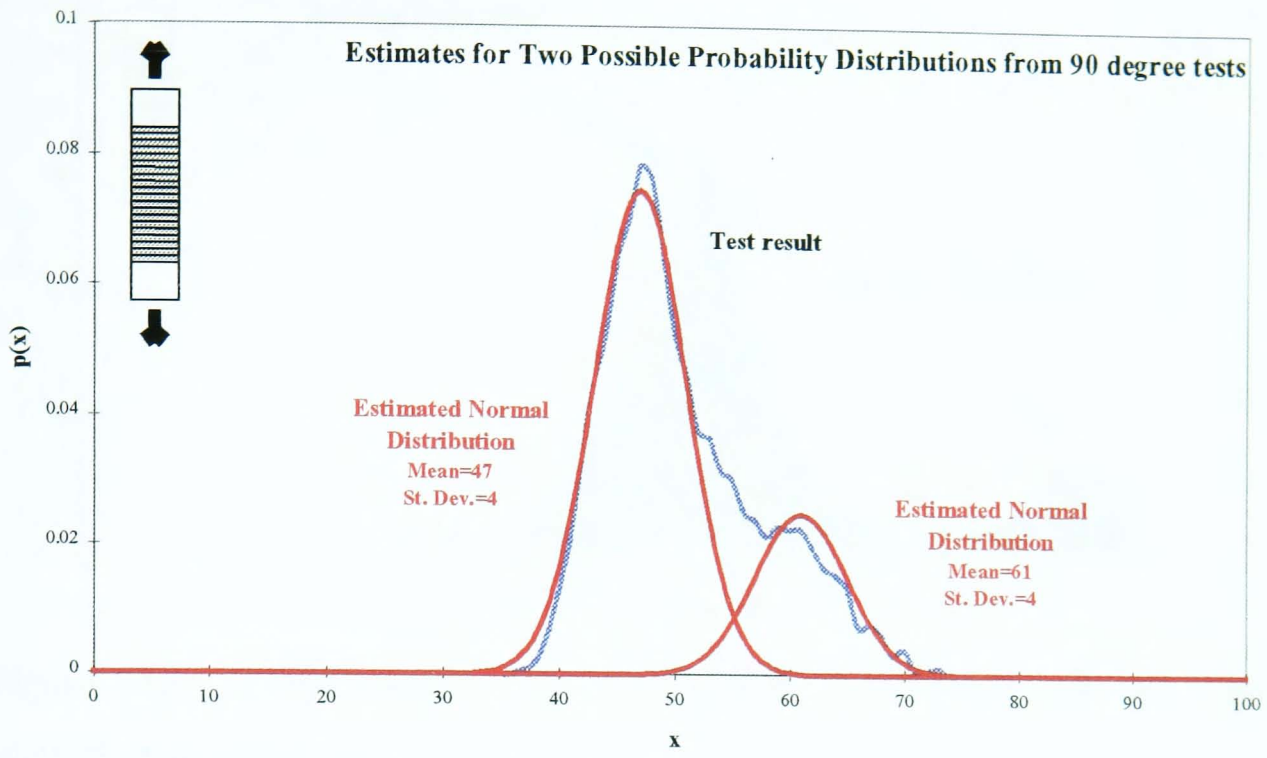

Figure 7.13 Actual and estimated probability distribution analysis of the AE signals from 90° loaded samples using the piezoelectric transducer. Estimated plot is based on the assumption that is two possible distributions are present.

If it is assumed that these types of specimen exhibit mainly matrix cracking with some matrix/fibre interface debonding then a comparison could be made with the previous tests described in section 7.3.1. By comparing figure 7.13 to the previous plots for pure resin specimens it is evident that matrix cracking exhibits the lower amplitude distribution. By visually analysing the 'average' distribution graphs for pure resin and 90° samples (figures 7.8 and 7.11 respectively) it can be seen that that latter has a definite broadening of the population curve. Through informal (graphical) mixture analysis, it has been hypothesised that two distributions are present. A comparison between figures 7.9 and 7.13 show comparable modes of amplitudes for matrix cracking. The second estimated population curve at this stage in the analysis is assumed to be due to the debonding of the fibre/matrix interface.

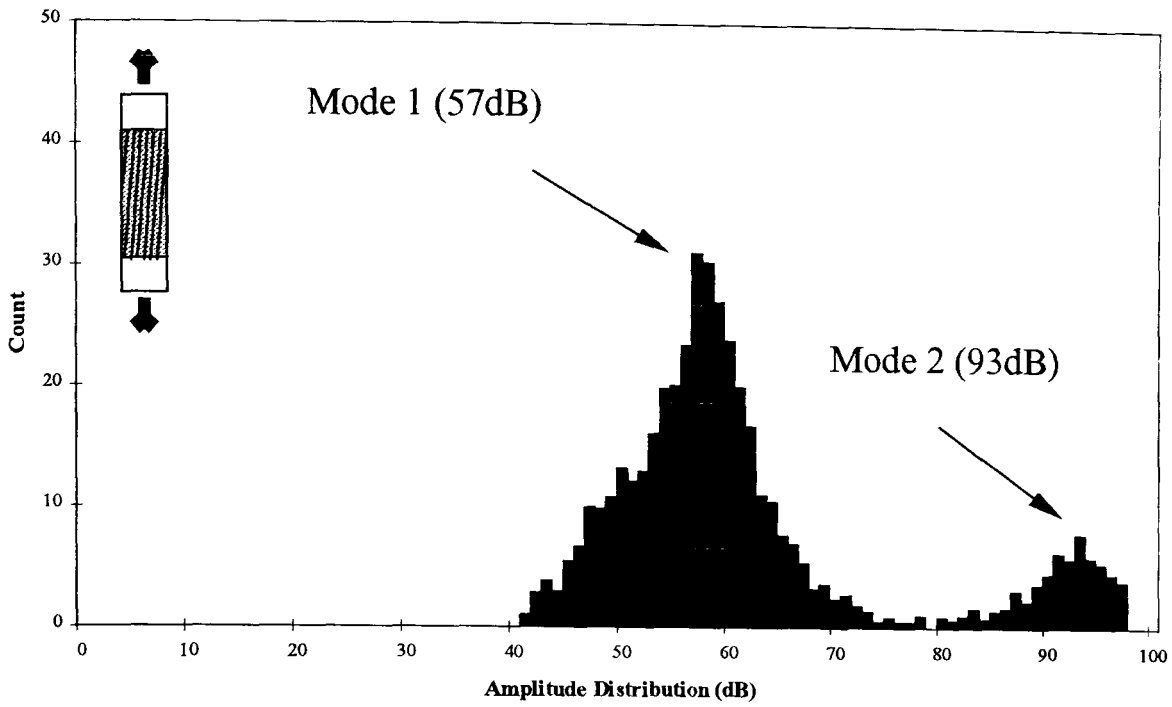

Figure 7.15 Average amplitude distribution of the AE signals from 10° loaded samples using the piezoelectric transducer

As with the previous 'average' distribution plots, statistical analysis using *Excel* was performed (Table 7.4). Using the values of mean and standard deviation for both distributions, it was possible to calculate the expected distributions (figure 7.16). Once again it was necessary to estimate the proportions of data in each distribution. It is difficult to determine whether or not there is any mixing of distributions in the first (largest) distribution. A comparison with the 90° samples show that these samples typically exhibit modes of 48dB and 61dB, whereas the 10° samples exhibits a mode of 57dB. A shift in the mode of the distribution may indicate that fibre/matrix debonding is the dominant damage mechanism. However, in these type of samples fibre-pull-out may occur. In figure 7.16, it appears that the second distribution could be attributed to fibre pull-out. However, the quality of the 10° samples dictates the types of damage occurring in the samples. The quality of the specimens is dependant upon the angle of the reinforcing fibres. Therefore, it is almost certain that in most, if not all, samples carbon fibre breakage occurs. By examining the graphs for all of the 10° samples it can be seen that there is very little consistency in the second distribution. This may be due to the inconsistency of the angle of the reinforcing fibres. The following set of tests confirm that this second distribution is due to carbon fibre breakage.

Statistical Parameters	
Distribution 1	
Mode	57
Median	57
Mean	56.603
Standard Deviation	6.173
Pearsons Coefficient (skewness)	-0.193
Distribution Range	41-79dB
Distribution 2	
Mode	93
Median	92
Mean	91.805
Standard Deviation	4.351
Pearsons Coefficient (skewness)	-0.134
Distribution Range	>80dB

Table 7.4 Statistical analysis of the 'average' amplitude distribution for 10° samples.

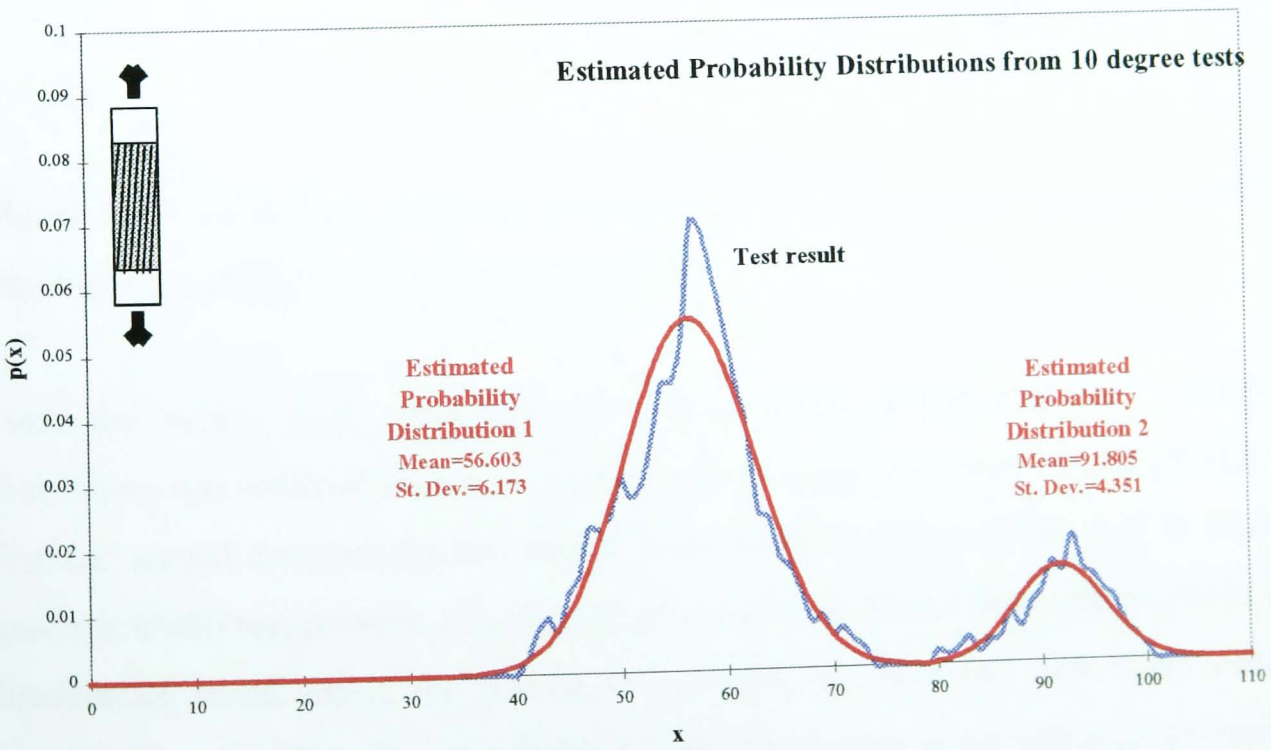

Figure 7.16 Actual and estimated probability distribution analysis of the AE signals from 10° loaded samples using the piezoelectric transducer.

7.3.4 Tensile Loading Of Uncured Carbon/Epoxy Pre-Preg Samples

Amplitude distribution analysis was done on the acoustic emission data obtained from the tensile loading of uncured carbon/epoxy samples. A typical amplitude distribution graph from this type of specimen is shown figure 7.17. From the plot it can be seen that there are two distinct population curves: 40-52dB and 72-97dB. On this plot the modes of these distributions are indicated (49dB and 89dB respectively).

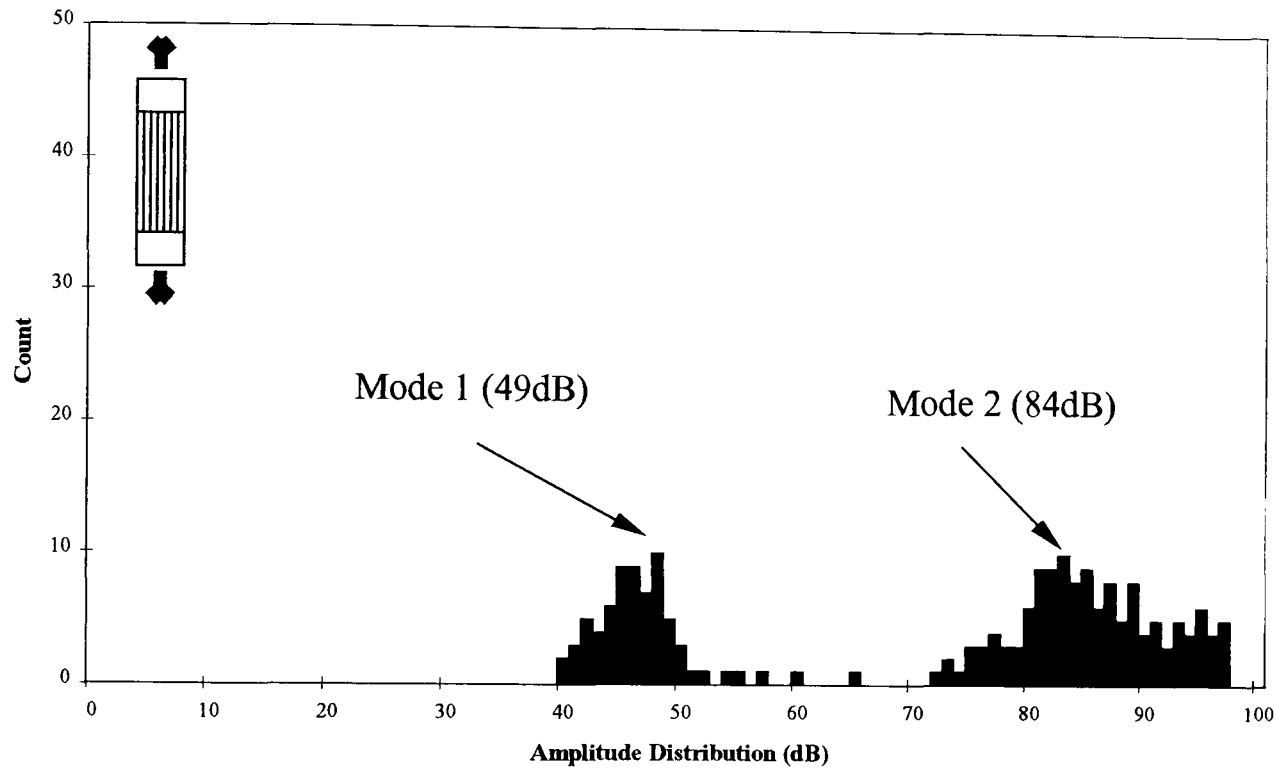

Figure 7.17 A typical amplitude distribution of the AE signals from the tensile loading of an uncured carbon/epoxy specimen

From the twelve tests undertaken with these types of samples, an 'average' distribution was obtained (figure 7.18). For analysis purposes it was assumed that the first and second distributions had ranges of 40-58dB (mode at 47dB) and 70-97dB (mode at 85dB) respectively. Although there is a distribution of data between the two distributions stated above, the process of averaging revealed that their count value was less than one. Therefore, this data has been disregarded in the statistical analysis. It must also be stated that due to the AET5500 amplitude threshold, values above 97dB have been estimated so that the proper statistical analysis of the data can be

performed. It was assumed that the AE data relating to the particular damage mechanism was normally distributed, and therefore symmetrical. The estimation of data greater than 97dB was performed to maintain approximate distribution symmetry. In Table 7.5, the resulting statistical analysis of the 'average' distribution graph is shown. From this data it was possible to plot the expected normal distributions from the means and standard deviations of the two actual distributions. These expected distributions were superimposed onto the 'average' distribution line graph (figure 7.19).

To attribute each damage mechanism to a particular population distribution it is necessary to look at the processes involved in the loading to failure of uncured carbon/epoxy samples. In uncured pre-preg, the carbon fibres have a resin cladding, and therefore, some amplitudes due to matrix cracking can occur. By referring to figure 7.18 it can ascertained that the population curve in the range 40-58dB appears to be due to the cracking of this resin cladding. As the energy emitted due to a fibre fracture is considerably greater than that from matrix cracking, it can be assumed that the high amplitude signals (>70dB) are due to fibre fracture.

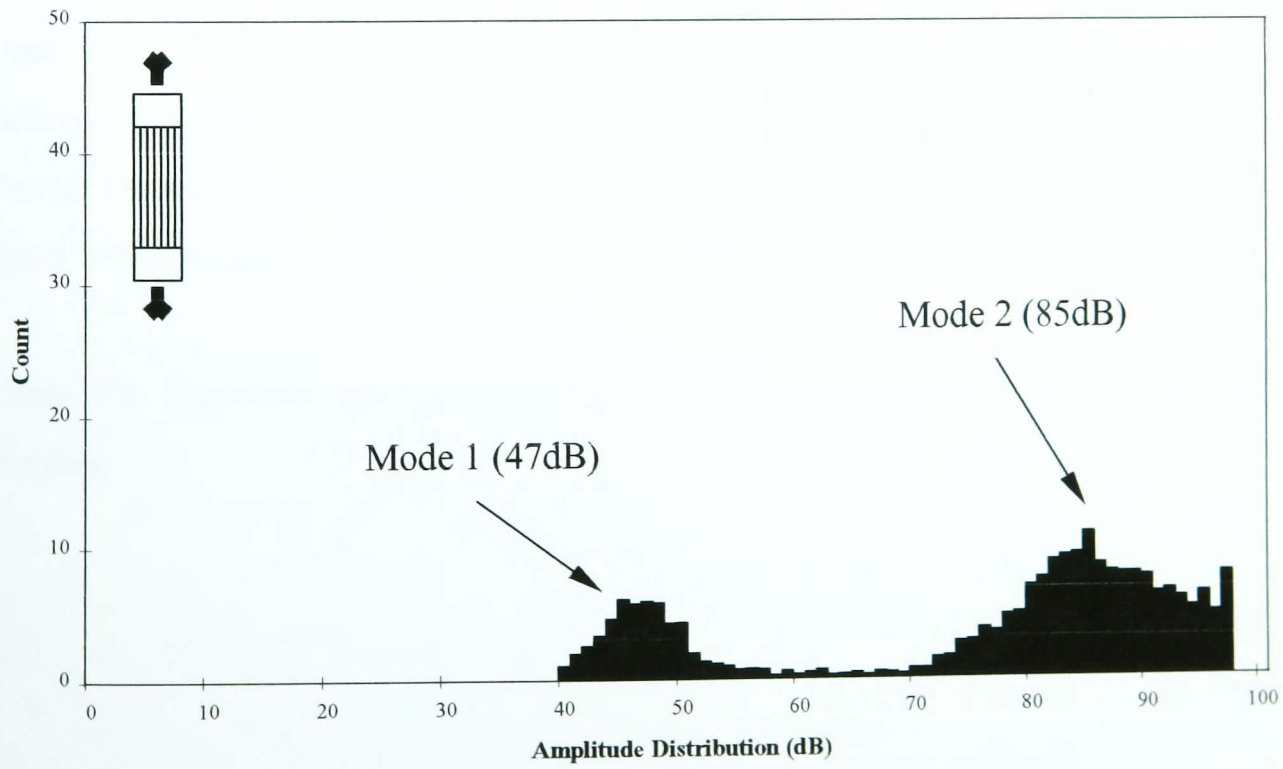

Figure 7.18 Average amplitude distribution of the AE signals from the tensile loading of an uncured carbon/epoxy specimen

Statistical Parameters	
Distribution 1	
Mode	47
Median	49
Mean	47.547
Standard Deviation	4.485
Pearsons Coefficient (skewness)	0.877
Distribution Range	40-58dB
Distribution 2	
Mode	85
Median	87
Mean	86.972
Standard Deviation	7.206
Pearsons Coefficient (skewness)	-0.012
Distribution Range	>70dB

Table 7.5 Statistical analysis of the 'average' amplitude distribution for uncured samples.

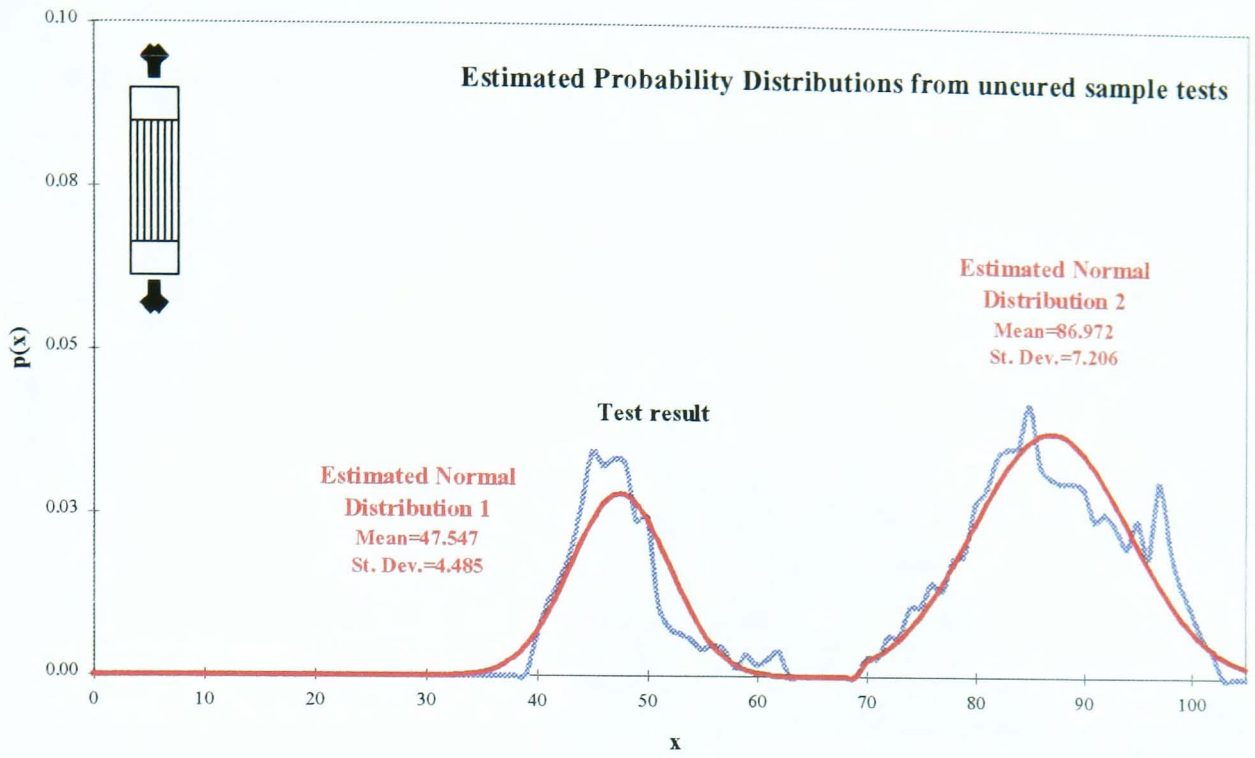

Figure 7.19 Actual and estimated probability distribution analysis of the AE signals from uncured samples using the piezoelectric transducer.

7.3.5 Tensile Loading Of Specimens Containing Embedded Teflon Discs

Amplitude distribution analysis was done on the acoustic emission data obtained from the tensile loading to failure of Teflon loaded specimens. These type of specimens delaminate at the onset of loading as the Teflon prevents a proper bond between the two plies. Near failure, the strength of the specimen deteriorates, which leads to mass fibre fracture and specimen failure. A typical amplitude distribution graph from these type of specimens is shown in figure 7.20.

This plot shows that the distribution between 40dB and 81dB is multi-modal. It is also apparent that there is a small distribution of data in the high amplitude range. The 'average' distribution plot in figure 7.21 gives a better indication whether or not there is a mixture of distributions in the data.

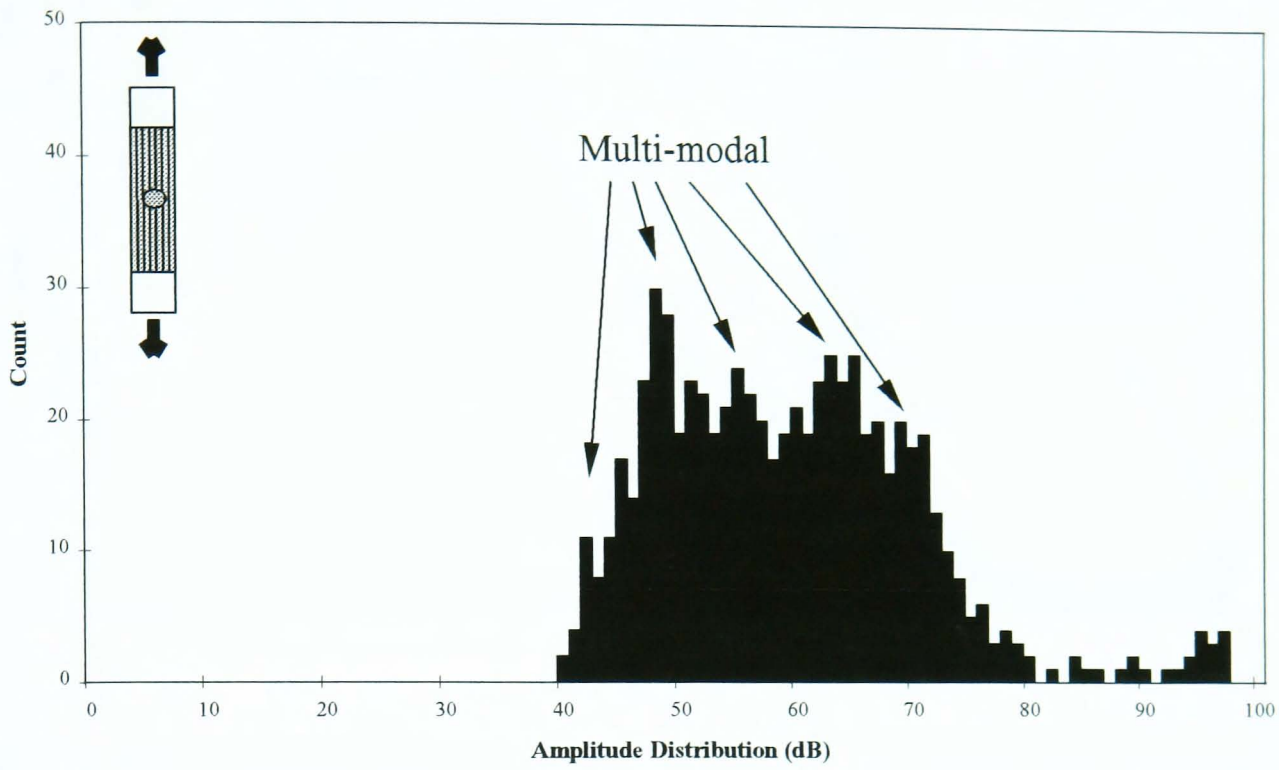

Figure 7.20 A typical amplitude distribution of the AE signals from the tensile loading of Teflon loaded samples

From the figure 7.21 there appears to be at least three population curves. Assuming that there is a mixture of distributions, the only possible parameter which can be identified is the modes of the distributions. These are indicated on figure 7.21 and have the following values: 50dB, 63dB, and 97dB.

For the purposes of statistical analysis, it was assumed that there were only two distributions present: 40-81dB and >84dB. As with the previous types of specimen, values greater than 97dB had to be estimated. The resulting analysis is presented in Table 7.6. The values of mean and standard deviation have been used to determine the expected normal distributions. Two separate graphs have been produced to show whether it is likely that just two distributions are present (figure 7.22).

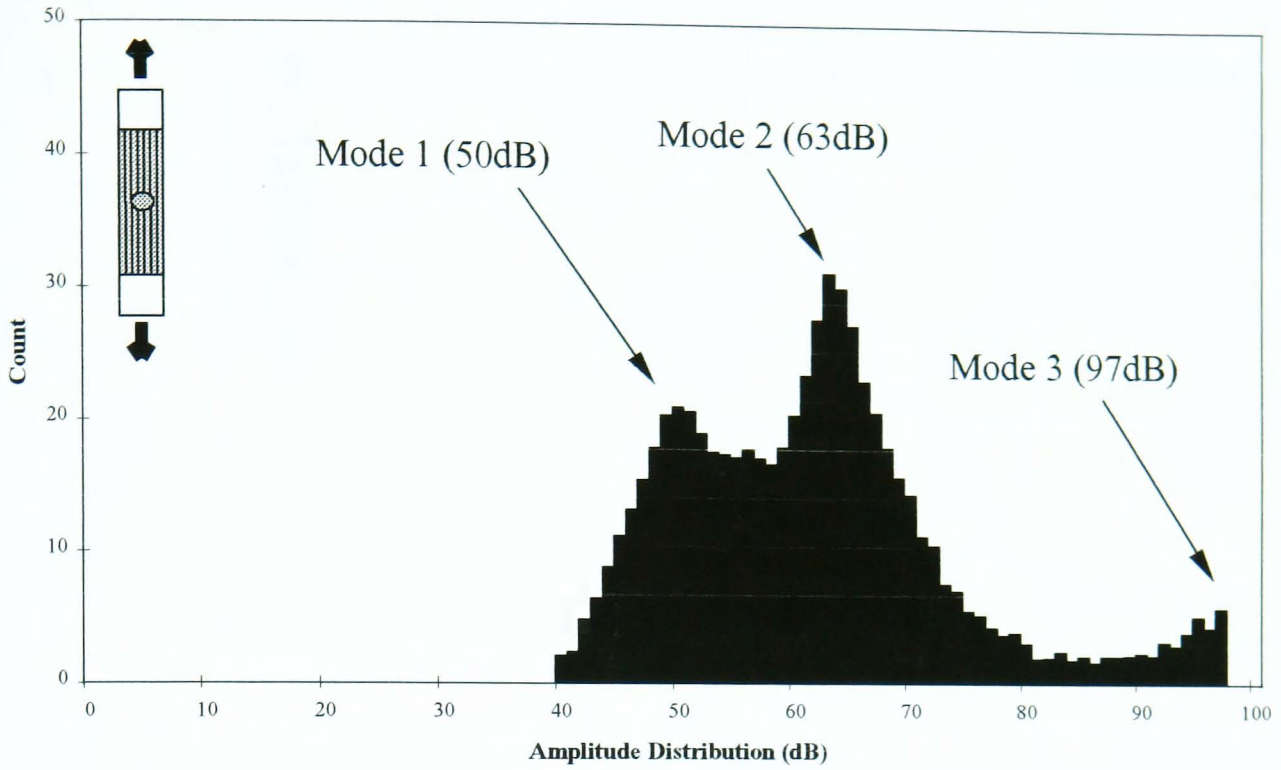

Figure 7.21 Average amplitude distribution of the AE signals from the tensile loading of Teflon loaded samples

Statistical Parameters

Distribution 1	
Mode	63
Median	61
Mean	56.603
Standard Deviation	9.375
Pearsons Coefficient (skewness)	-0.420
Distribution Range	40-81dB
Distribution 2	
Mode	97
Median	95
Mean	94.411
Standard Deviation	4.628
Pearsons Coefficient (skewness)	-0.382
Distribution Range	>84dB

Table 7.6 Statistical analysis of the 'average' amplitude distribution for Teflon loaded samples.

(a)

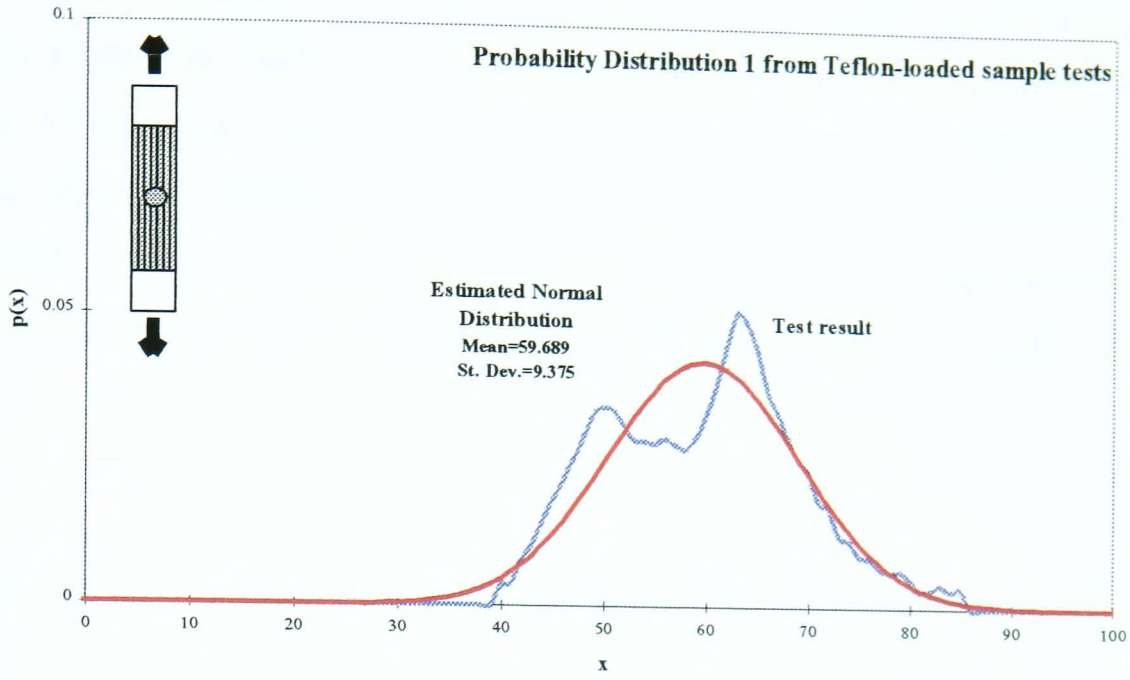

(b)

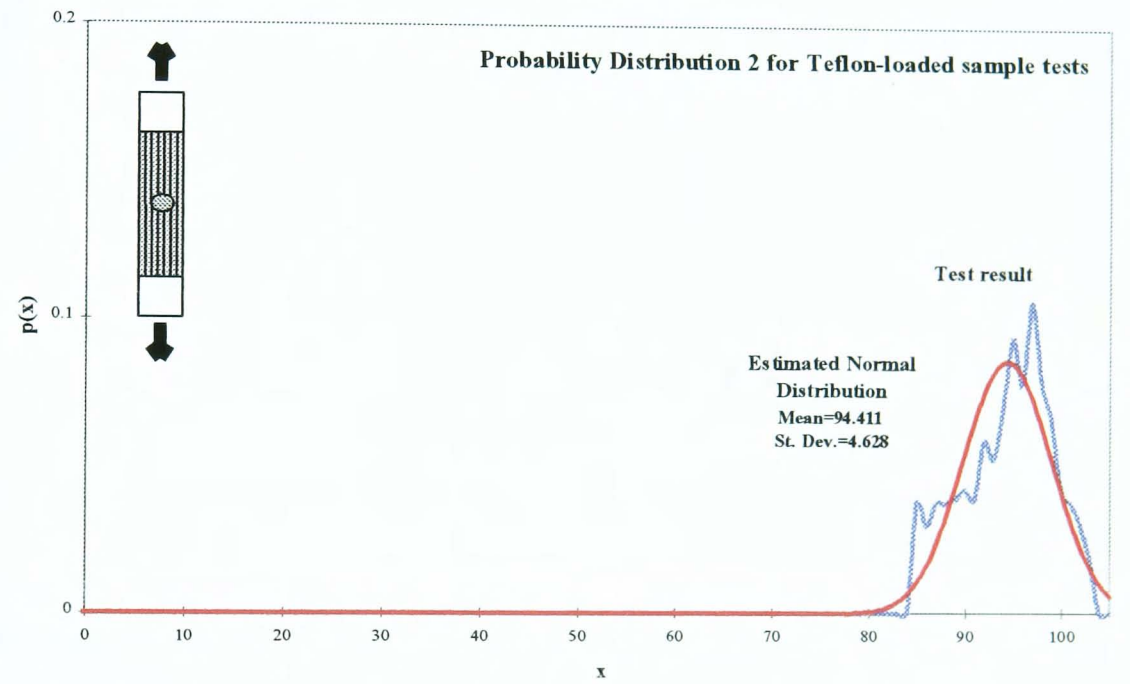

Figure 7.22 Actual and estimated probability distribution analysis of the AE signals from Teflon loaded samples using the piezoelectric transducer Plot (a) is the distribution between 41dB, and plot (b) is the distribution >84dB.

From plot (a) in the above graph it is visibly apparent that there is a poor relationship between the actual and expected distributions. Therefore, if it assumed that there is a mixture of distributions in plot (a) of figure 7.22, then two means and standard deviations, as well as mixture proportions, have to be estimated in order to obtain the new estimated mixture distributions.

From the 'average' data the following proportions were obtained for the three distributions (shown in figure 7.23): 36.7%, 55%,and 8.3%. For the estimated distribution 1, the mean and standard deviation was 50 and 4.5 respectively. However, the mean and standard deviation of the estimated distribution 2 were 64 and 4.5 respectively. It was unnecessary to estimate the mean and standard deviation of the third distribution as the values obtained through the statistical analysis (table 7.6) were used.

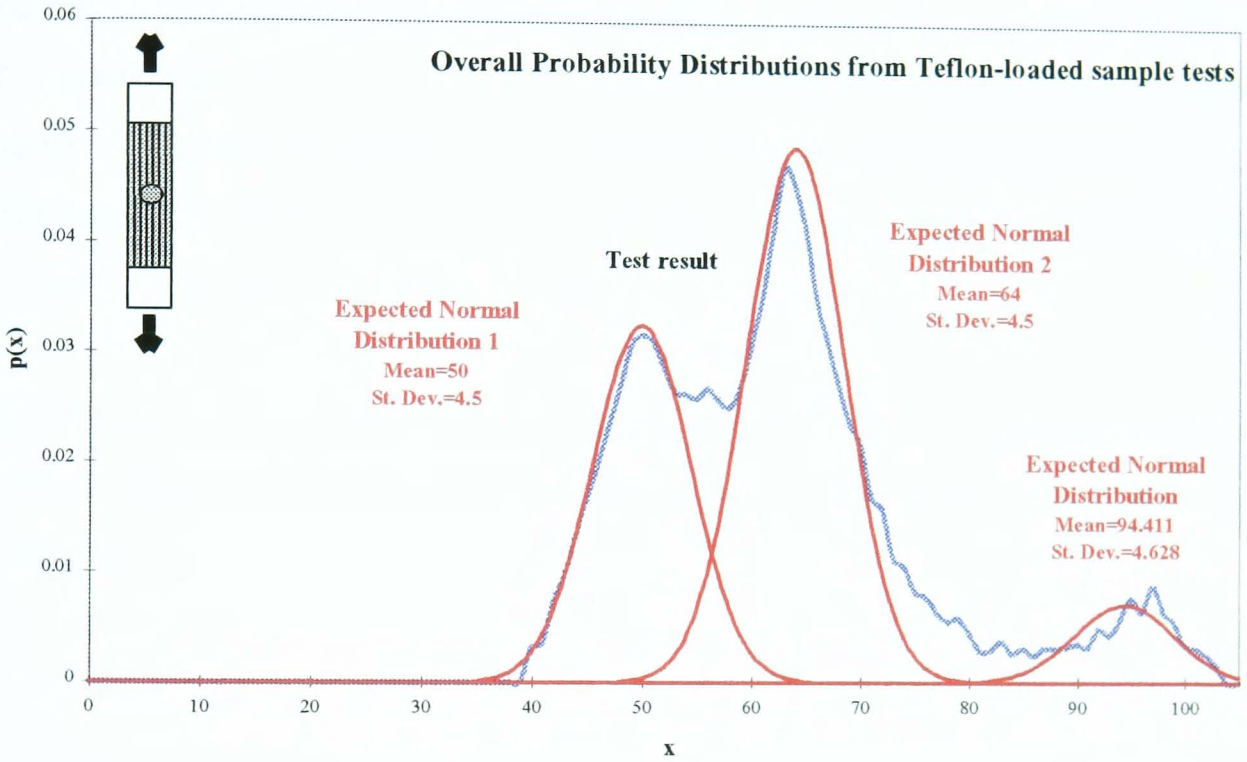

Figure 7.23 Actual and estimated probability distribution analysis of the AE signals from Teflon loaded samples using the piezoelectric transducer.

The estimated population plots, shown in figure 7.23, indicate the possibility of a mixture of distributions. However, as stated earlier, it is possible that one component (or damage mechanism) can be responsible for multi-modal distributions. On the assumption that two damage mechanisms are responsible for the distribution between 40-81dB, and another responsible for the small distribution above 84dB, a tentative correlation can be made.

The expected failure mechanisms from these type of specimens are delamination, matrix cracking and fibre failure. From the previous plots on different types of

samples, it has been ascertained that matrix cracking has values in the low amplitude range less than 55dB, whereas figure 7.6 indicates that fibre fractures have amplitudes in excess of 75dB. From this it can be assumed that amplitudes due to delamination occur in this middle population curve.

7.3.6 An Overview Of The Amplitude Distribution Results For All Samples

From the five types of tests undertaken, several graphs have been produced which exhibit a series of amplitude population distributions that can be correlated to specific damage mechanisms. In Table 7.7 the type of sample is documented, along with the obtained statistical parameters and its hypothesised damage mechanisms. Also, some comments have been added to aid the explanation why a specific distribution has been chosen for a particular damage mechanism.

In addition to the analysis of the original parameters of the AE signal, a correlation between frequency spectra of the detected signal and the damage mechanisms was attempted.

Sample Type	Statistical Parameters (dB) Mode	Mean	St.Dev.	Range	Damage Mechanism
Resin	43	44.086	3.423	37-56	Matrix Cracking
90°	48	51.008	6.872	38-71	Matrix Cracking
Comments:	*Informal graphical analysis has been made to highlight the possibility of two mixing distributions. This indicates that the broadening of the distribution is due to some fibre/matrix (F/M) debonding.*				
10°	57	56.603	6.173	41-79	Inconclusive
	93	91.805	4.351	>80	Fibre Fracture
Comments:	*In the first distribution it is not visibly apparent that a mixture of distributions occurs. It is therefore too difficult to determine the amplitude distributions for each mechanism. Subsequent tests reveal that the 2nd distribution is due to fibre fracture.*				
Uncured	47	47.547	4.485	40-58	Matrix Cracking
	85	86.972	7.206	>70dB	Fibre Fracture
Teflon Loaded	63	56.603	9.375	40-81	Inconclusive
	97	94.411	4.628	>84	Fibre Fracture
Comments:	*Informal graphical analysis has been made to highlight the possibility of two mixing distributions. However, it is too difficult to determine the exact distribution ranges for delamination and matrix cracking.*				

Table 7.7 An overview of the amplitude distribution results for all types of samples

7.4 Frequency Distribution Analysis

In the amplitude distribution analysis section it was apparent that the range of amplitudes for delamination was approximately similar to those detected for fibre/matrix debonding. In order to differentiate between these two mechanisms in particular, frequency analysis of the signals detected from all the types of samples under tension was undertaken. Although it was apparent from the amplitude distribution analysis section that the matrix cracking could be differentiated from the fibre fracture, it could be advantageous if the frequency spectra for each mechanism could be determined.

To evaluate the damage mechanisms the frequency distribution was plotted for each specimen type. Like the analysis of the amplitude distribution, it was necessary to calculate an 'average' distribution using all of the results from each particular test. From this 'average' chart it was possible to perform some statistical analysis. The parameters calculated are then used to obtain an 'expected' distribution for that particular test. This 'expected' distribution could then be used to determine damage mechanisms in other types of samples by simply superimposing it over another tests 'average' distribution.

7.4.1 Pure Resin Samples

When the pure resin samples are loaded in tension to failure the acoustic emission events generated can only be due to matrix cracking. In figure 7.24 a typical frequency distribution of the events detected is shown. In this graph, the events in the frequency range approximately between 80 and 150kHz are taken to be matrix cracking.

The 'average' distribution (figure 7.25) calculated for this particular test also exhibits a frequency range between 80-150kHz, with a mode of frequency at 115kHz. The data in this type of sample appears to be normally distributed. The calculation of

Pearson's coefficient reveals that this is the case. The statistical parameters calculated from the 'average' distribution are shown in Table 7.8.

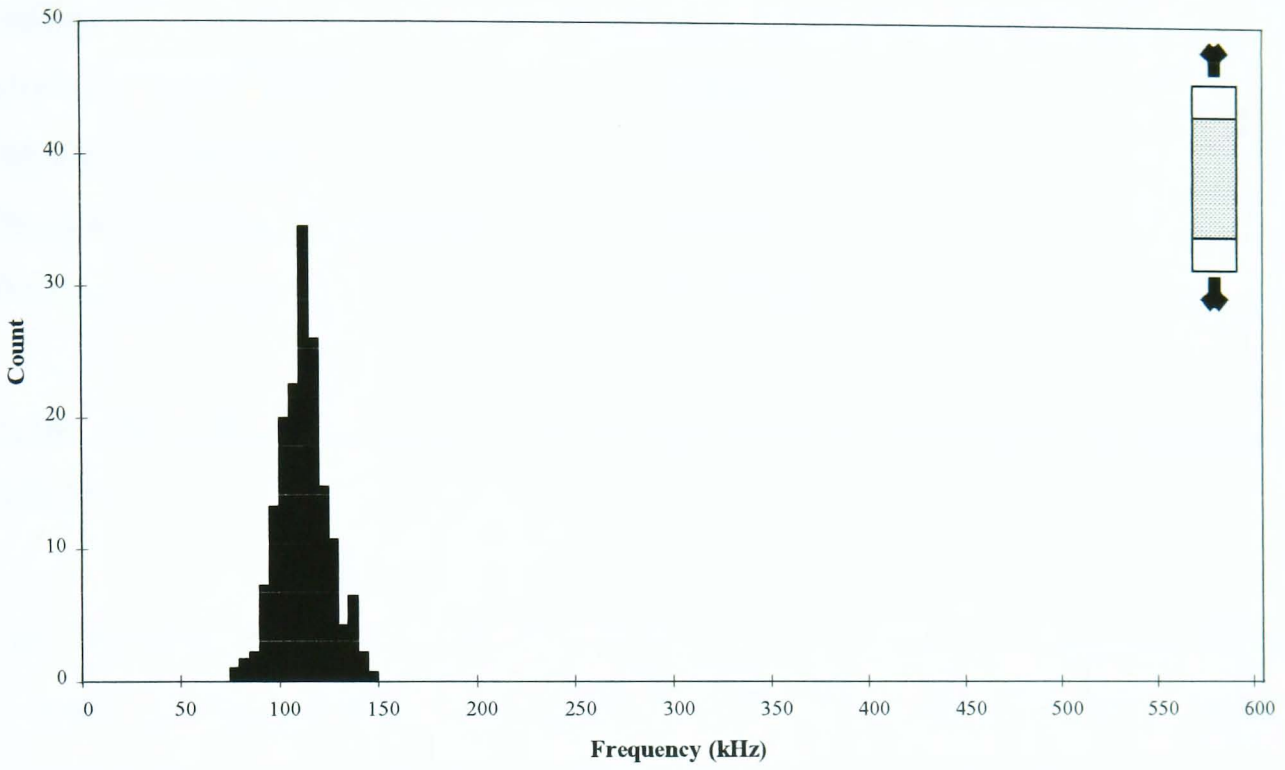

Figure 7.24 Frequency distribution analysis of the AE signals from a typical pure resin samples using the piezoelectric transducer

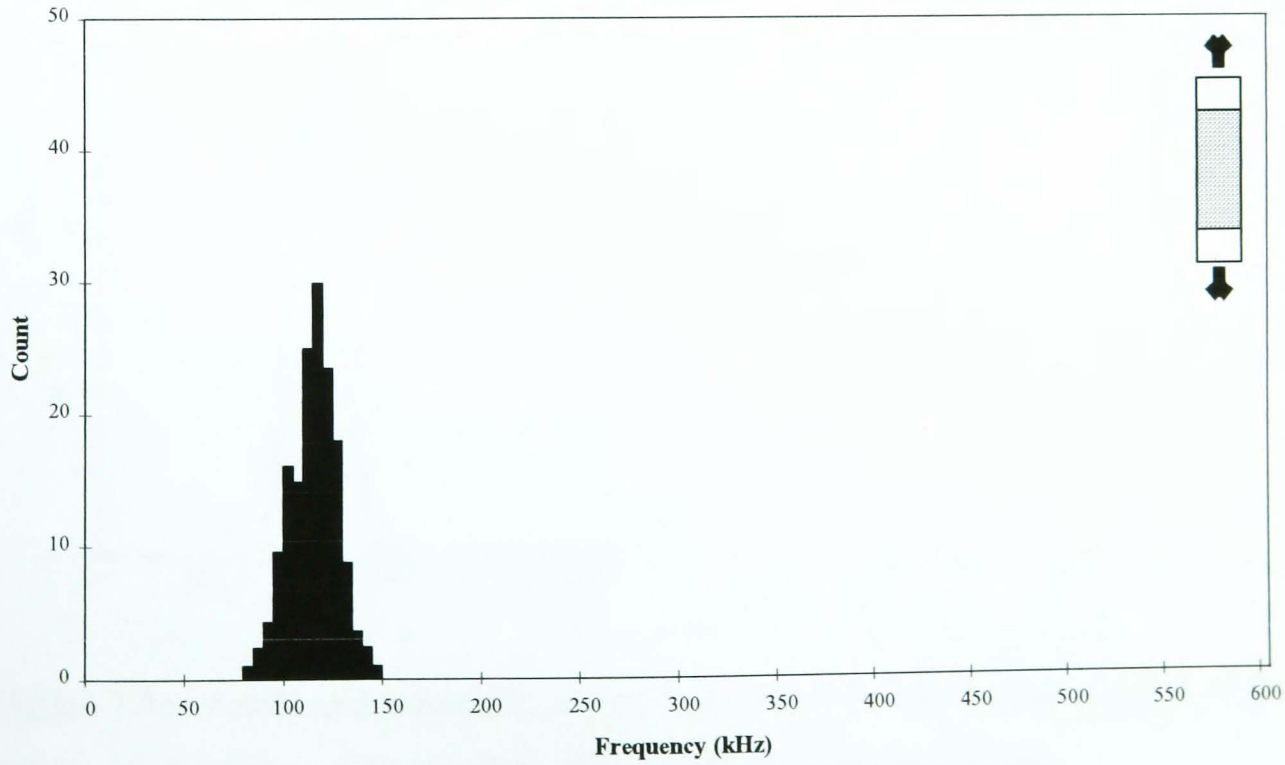

Figure 7.25 Average frequency distribution of the AE signals from pure resin samples using the piezoelectric transducer

Statistical Parameters	
Mode	115
Median	115
Mean	113.030
Standard Deviation	11.854
Pearsons Coefficient (skewness)	-0.498
Distribution Range	80-150kHz

Table 7.8 Statistical analysis of the 'average' frequency distribution for pure resin samples.

The 'expected' distribution plotted with the aid of the statistical analysis of the 'average' distribution is shown in figure 7.26. From this graph the overlay of the 'expected' plot could be used to determine matrix cracking in other samples.

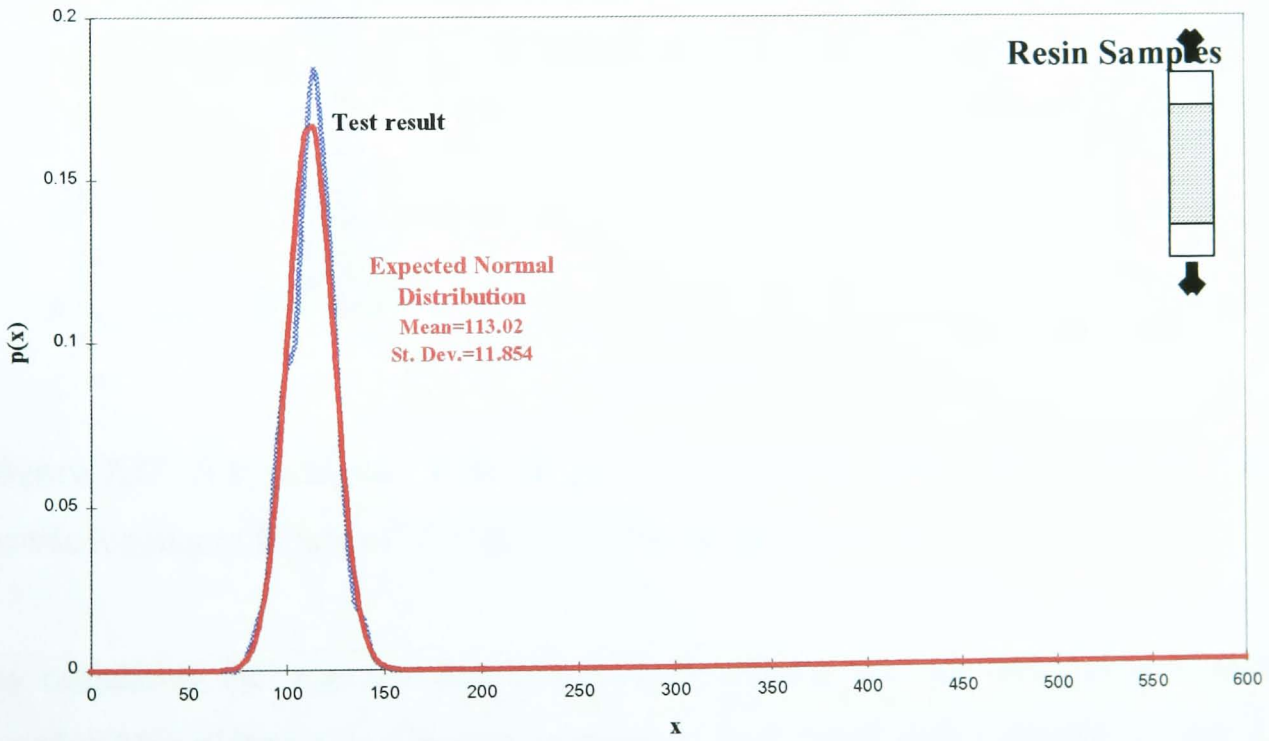

Figure 7.26 Actual and estimated frequency probability distribution analysis of the AE signals from pure resin samples using the piezoelectric transducer

7.4.2 Tensile Loading Of 90° Specimens

In these samples, loading to failure produces AE events primarily due to matrix cracking. However, it is possible that fibre/matrix debonding will occur. In figure 7.27 a typical example of the frequency distribution for these types of samples reveals a slight broadening of the population plot compared to that found through the resin tests.

In this plot the distribution range is found to be 80-195kHz with a mode frequency of 120kHz.

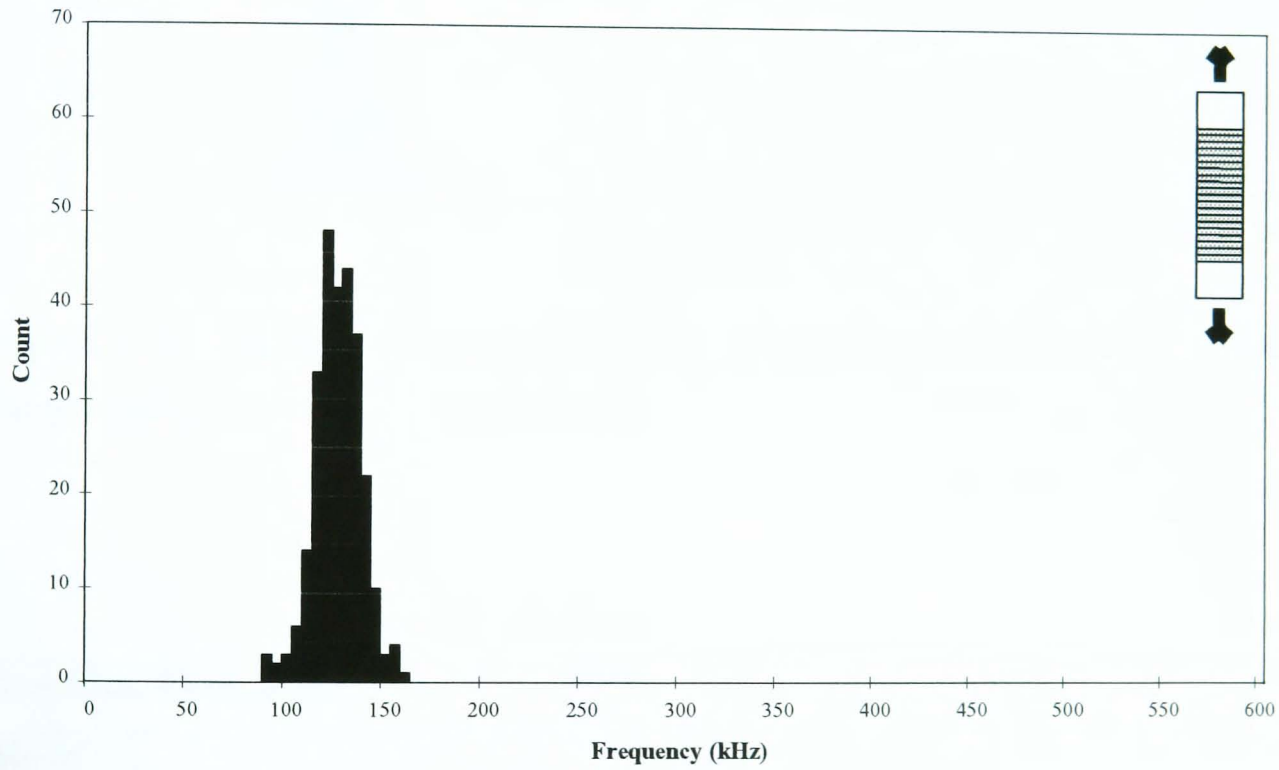

Figure 7.27 A typical plot of the frequency distribution of the AE signals from the tensile loading to failure of 90° loaded CFRP specimen.

By calculating the 'average' distribution, it is apparent that the distribution is even broader. This plot reveals a frequency range of 80-195kHz with a frequency mode of 130kHz. The broadening of the left hand side of the distribution plot results in a shift in the mean frequency compared to that found in the resin tests. The statistical analysis of this 'average' distribution for 90° tests is illustrated in Table 7.9. By comparing the statistical parameters found for resin and 90° tests it can be seen that

they both have comparable means (~113kHz and ~126kHz respectively) and standard deviations (~12kHz and ~14kHz respectively).

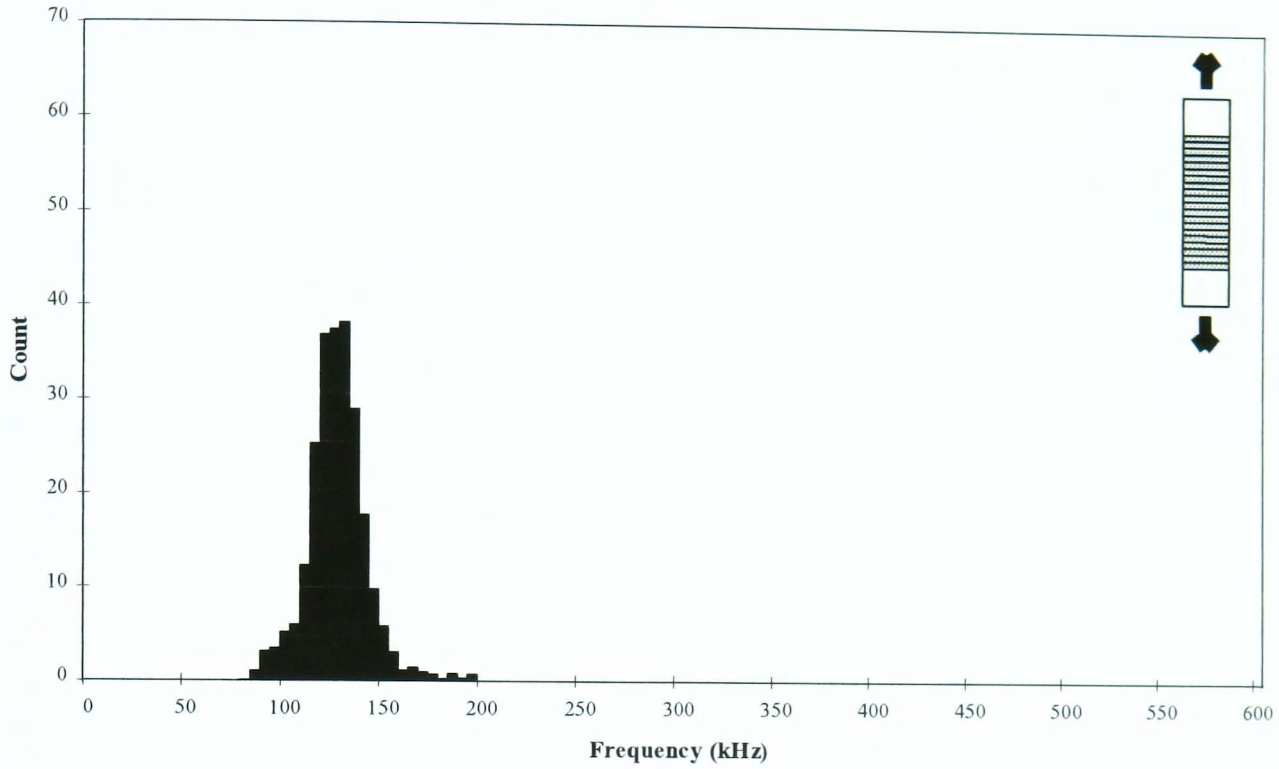

Figure 7.28 Average frequency distribution of the AE signals from 90° loaded samples using the piezoelectric transducer

Statistical Parameters	
Mode	130
Median	125
Mean	125.872
Standard Deviation	13.780
Pearsons Coefficient (skewness)	0.190
Distribution Range	80-195kHz

Table 7.9 Statistical analysis of the 'average' frequency distribution for 90° loaded samples.

By superimposing the 'expected' distribution onto the 'average' plot (figure 7.29), it can be seen that there is a slight shift in the results compared to those found in the resin tests. However, this slight shift may be due to the nature of the sample, that is, the effects of reinforcing fibres on the acoustic signal.

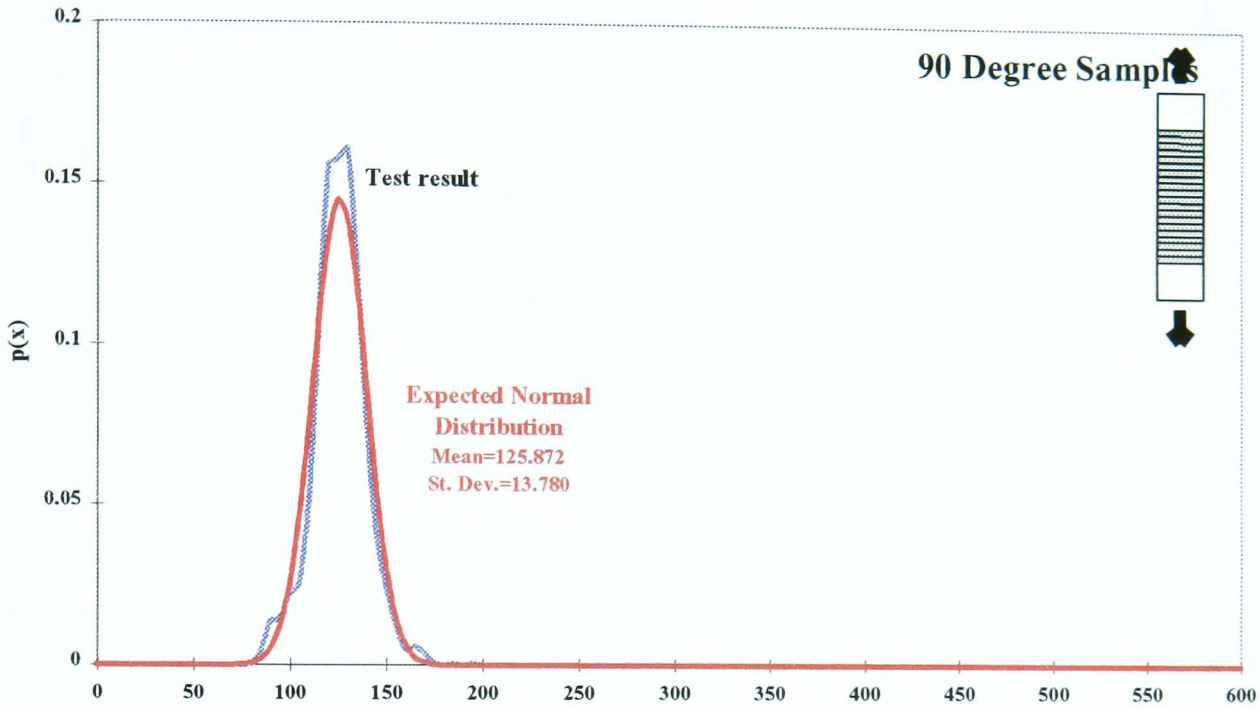

Figure 7.29 Actual and estimated frequency probability distribution analysis of the AE signals from 90° loaded samples using the piezoelectric transducer.

7.4.3 Tensile Loading Of 10° Specimens

The results obtained from the loading 10° to the reinforcing carbon fibres help confirm those found in sections 7.4.1 and 7.4.2. These samples generally fail due to a combination of matrix cracking and fibre/matrix debonding with almost no fibre fracture. However, fibre pull-out may exist. From the typical example of frequency distribution from 10° tensile tests (figure 7.30), it is apparent that there are two distinct heavily populated distributions: 80-130kHz and 165-290kHz. There are also small distributions of data centred around 350kHz and 525kHz. The broader distribution, with the distinct frequency mode at 215kHz, appears to have a mixture of two distributions. This is highlighted by the 'average' distribution in figure 7.31.

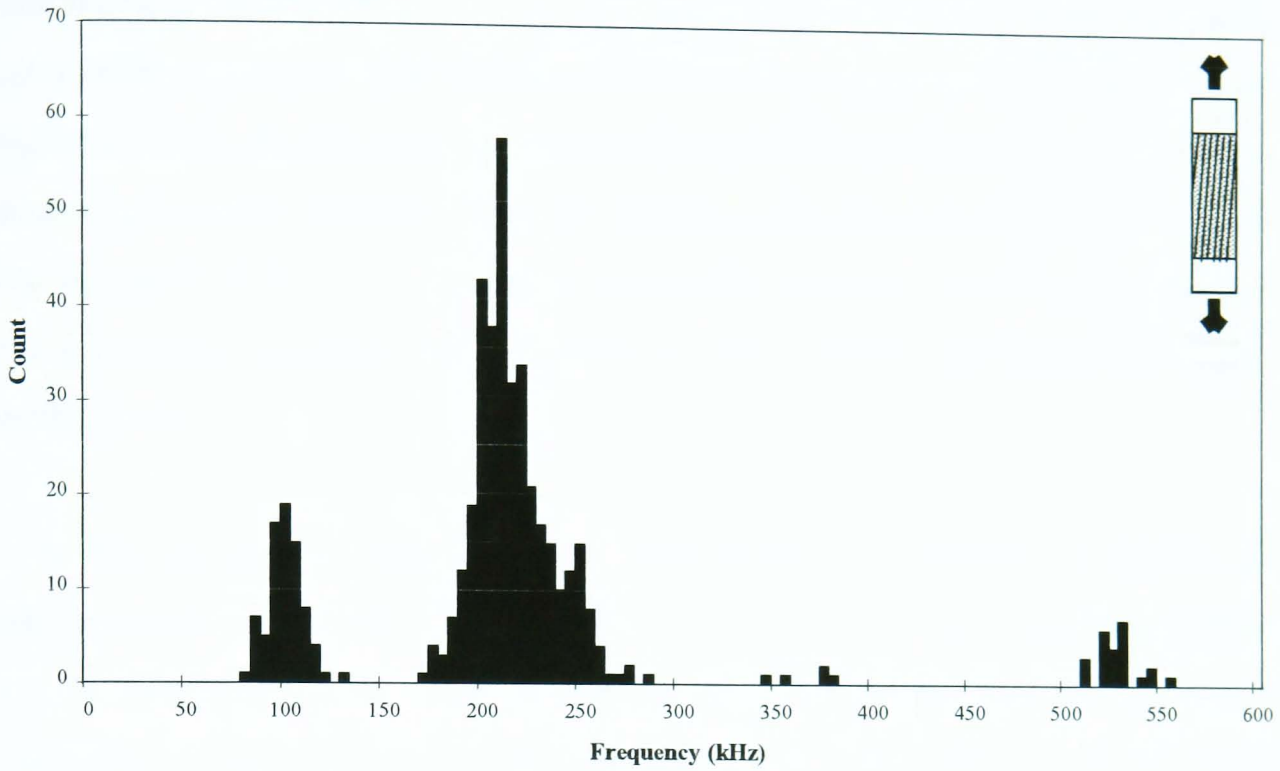

Figure 7.30 A typical frequency distribution of the AE signals from the tensile loading to failure of 10° loaded CFRP specimen.

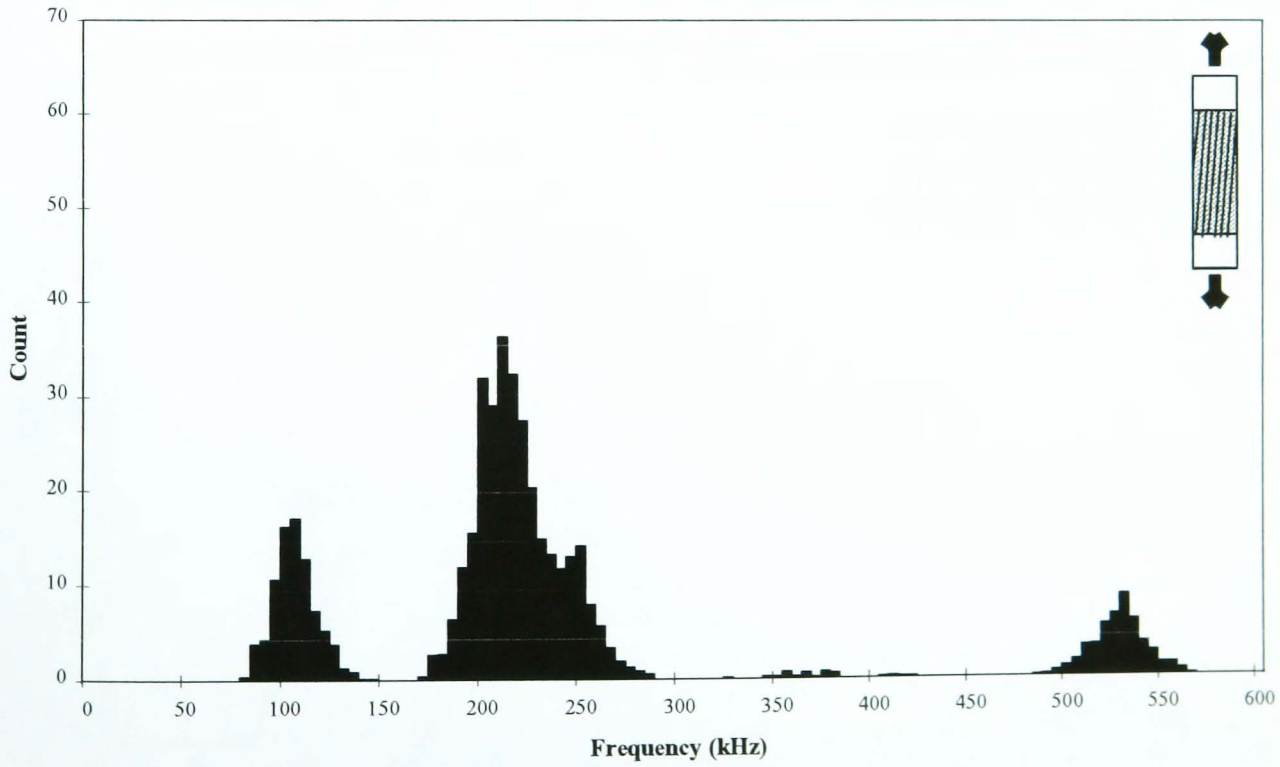

Figure 7.31 Average frequency distribution of the AE signals from 10° loaded samples using the piezoelectric transducer

In this 'average' graph, the distribution seen in the previous sections, that is from 80-145kHz, is found. This distribution is clearly related to matrix cracking. The broader distribution (170-285kHz) appears to be bi-modal. There is a main mode at 210kHz and another at 250kHz. It is possible that there is a mixture of distributions in this frequency range. As stated earlier, all mixture distribution analysis attempted in this chapter is based on informal graphical techniques. These types of techniques show visually that a mixture of distributions is feasible. However, all subsequent analysis and statements regarding the resolution of two mixture distributions is purely hypothetical.

From this 'average' distribution graph, there is also a population of data in the frequency range 490-570kHz. At this stage, however, it can only be stated for certain that the distribution in the range 80-145kHz can be attributed to a certain damage mechanism. Subsequent tests could help correlate the other distributions to certain damage mechanisms. Statistical analysis has been performed on the 'average' distribution and is tabulated in Table 7.10. This analysis has been used to plot the 'estimated' graph shown in figure 7.32.

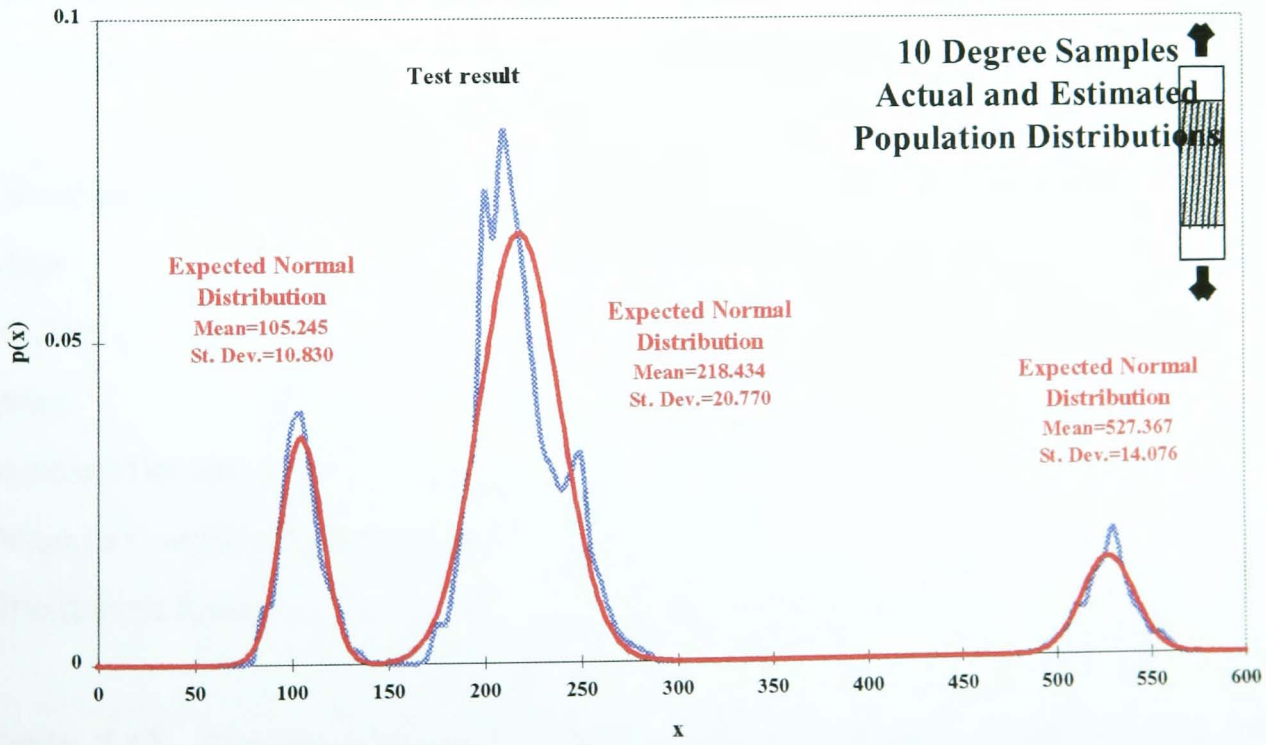

Figure 7.32 Actual and estimated frequency probability distribution analysis of the AE signals from 10° loaded samples using the piezoelectric transducer.

Statistical Parameters

Distribution 1	
Mode	105
Median	105
Mean	105.245
Standard Deviation	10.830
Pearsons Coefficient (skewness)	0.071
Distribution Range	80-145kHz
Distribution 2	
Mode	210
Median	215
Mean	218.434
Standard Deviation	20.770
Pearsons Coefficient (skewness)	0.496
Distribution Range	170-285kHz
Distribution 3	
Mode	530
Median	530
Mean	527.367
Standard Deviation	14.076
Pearsons Coefficient (skewness)	-0.561
Distribution Range	485-565kHz

Table 7.10 Statistical analysis of the 'average' frequency distribution for 10° samples.

From figure 7.32 it is visually apparent that there may be a mixing of distributions in the 170-285kHz population. To enhance this visually, two sets of mean and standard deviations have been estimated to produce an indication of this mixing. It was also necessary to estimate the proportions of the distributions. The resulting plot (figure 7.33) illustrates how it may be possible for two damage mechanisms to be responsible for the 170-285kHz distribution.

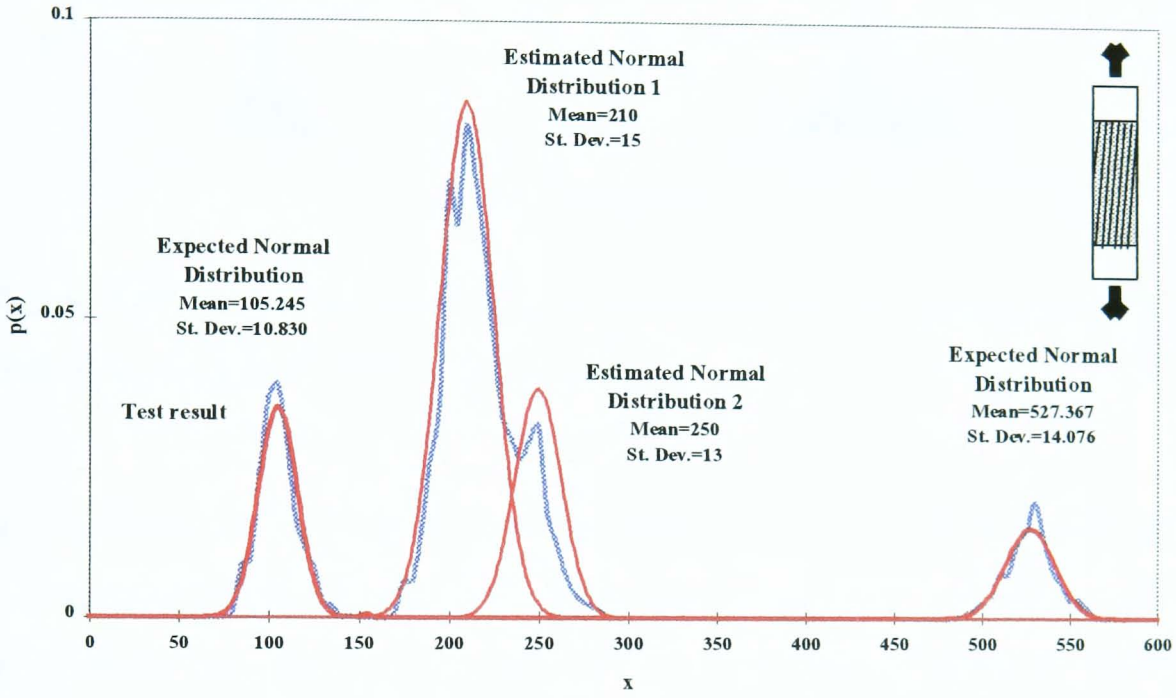

Figure 7.33 Actual and estimated frequency probability distribution analysis of the AE signals from 10° loaded samples using the piezoelectric transducer. This is based on the assumption that there is a mixture of distributions.

7.4.4 Tensile Loading Of Uncured Carbon/Epoxy Pre-Preg Samples

In uncured pre-pregs the carbon fibres have a resin coating. When the sample is loaded the matrix on the surface of the fibre cracks and therefore signals due to matrix cracking will be evident. This in turn could evolve into failure of the adhesion between the fibre and the matrix coating. Therefore, the tensile testing of these samples could exhibit three possible modes of failure. This is evident from a typical distribution plot shown in figure 7.34. There are two heavily populated distributions situated in the frequency ranges 80-135kHz and 370-510kHz. There is also a small discontinuous distribution of data in the range 170-240kHz.

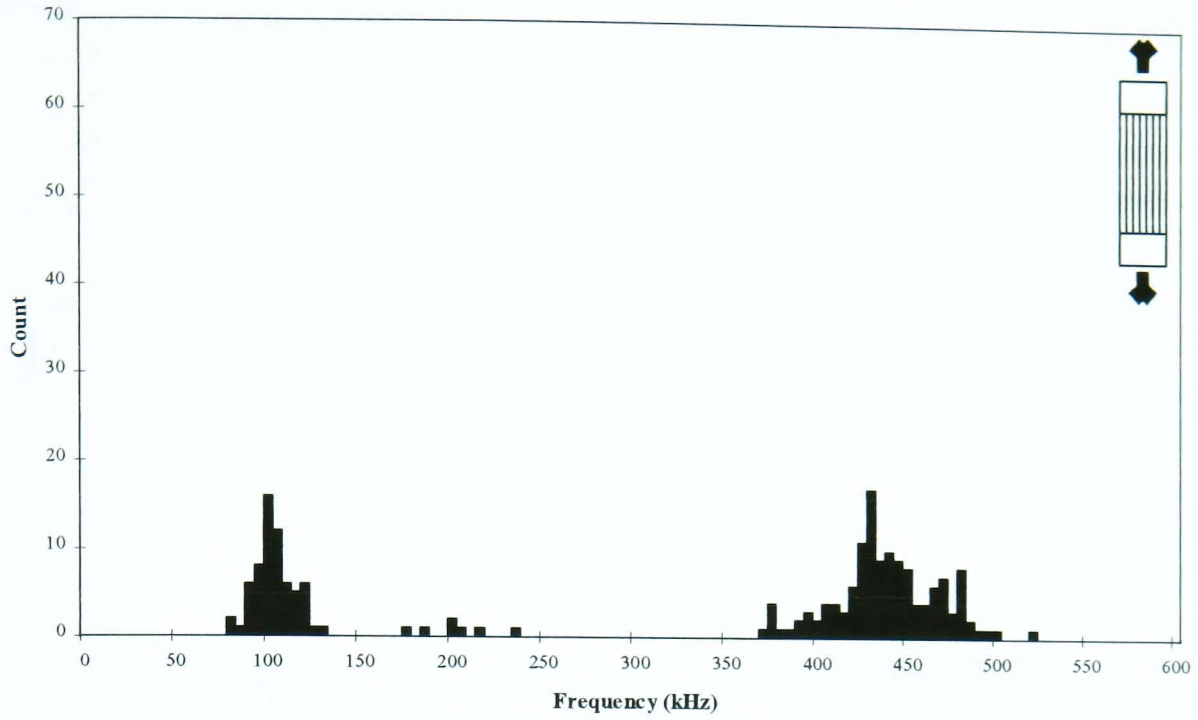

Figure 7.34 A typical frequency distribution of the AE signals from the tensile loading of an uncured carbon/epoxy specimen

By examining the 'average' distribution (figure 7.35), it is evident that three distinct continuous population distributions occur. As with all the previous tests, a distribution occurs in the frequency range below 150kHz with a modal frequency of 100kHz. This data population is once again associated with matrix cracking. The largest population distribution occurs in the high frequency range (355-550kHz), which has a frequency mode of 430kHz. Due to the nature of these samples, the most frequent damage mechanism occurring in the tensile testing to failure of these specimens would be carbon fibre fracture. Therefore, the high frequency distribution will be due to carbon fibre fracture.

By process of elimination, the small population distribution found in the range 175-240kHz must be due to the fibre/matrix debonding. This distribution has a modal frequency of 210kHz. The statistical analysis parameters calculated using this 'average' distribution plot can be found in Table 7.11. These parameters have been used to produce an 'expected' distribution plot for the uncured specimens (figure 7.36).

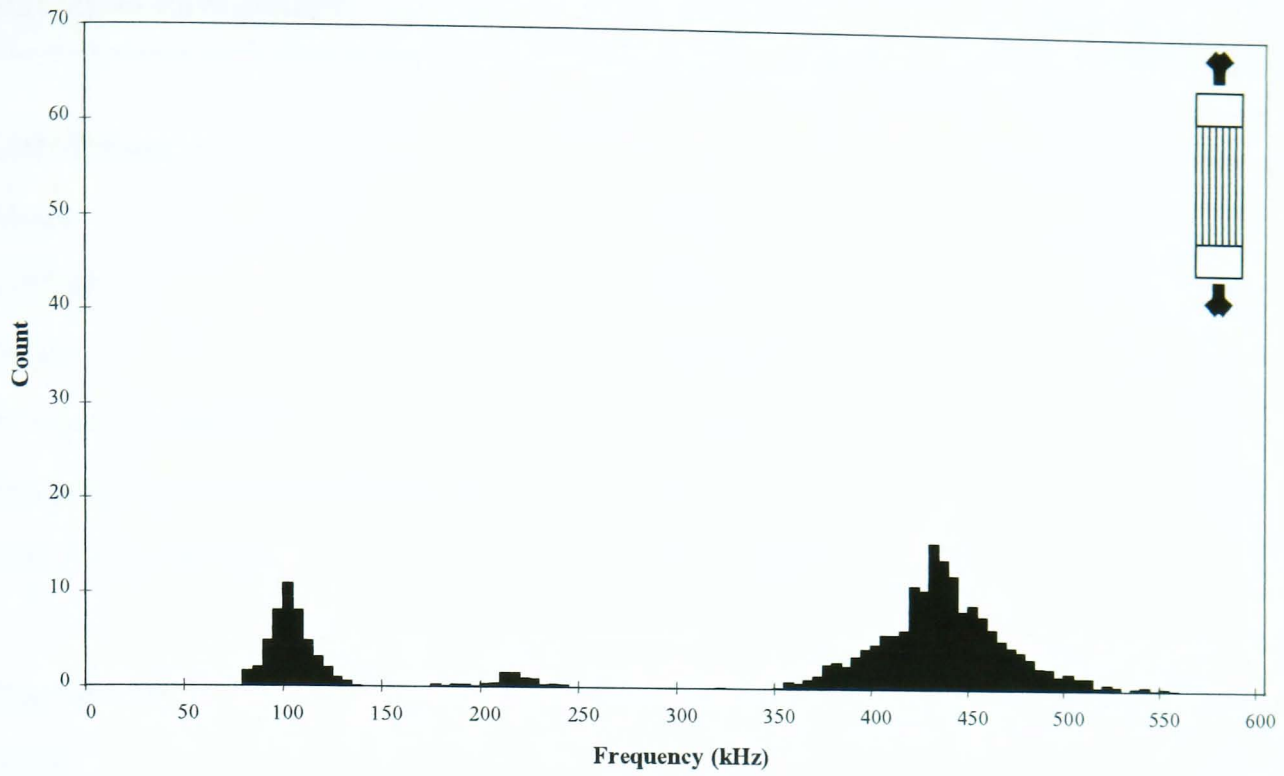

Figure 7.35 Average frequency distribution of the AE signals from the tensile loading of an uncured carbon/epoxy specimen

By plotting the 'expected' population distribution, it is possible to superimpose these results onto other graphs to aid the correlation of distributions to particular damage mechanisms. This plot would be particularly helpful in the analysis of the 10° tensile test graphs. Although the population of data in the intermediate frequency range (175-240kHz) is small, this distribution has the same modal frequency and comparable mean as the distribution found in the 10° samples. The high frequency distribution range found in the 10° samples can also be associated with the 355-550kHz range detected from the uncured samples. Although the 'expected' distribution plots do not completely superimpose, it can be assumed that both distributions are due to carbon fibre fracture. It was stated in section 7.3.3 that the consistency of the angle of reinforcing fibre dictated the quality of the specimen. Therefore, in these samples it is certain that carbon fibre fracture occurs. Also, the shift in distribution in the high frequency range between the 10° and uncured samples could be due the difference in material characteristics. The effects of cured and uncured matrix on the acoustic emission signal could result in this frequency distribution shift.

Statistical Parameters

Distribution 1	
Mode	100
Median	100
Mean	101.418
Standard Deviation	10.311
Pearsons Coefficient (skewness)	0.071
Distribution Range	80-135kHz
Distribution 2	
Mode	210
Median	215
Mean	213.333
Standard Deviation	13.326
Pearsons Coefficient (skewness)	-0.375
Distribution Range	175-240kHz
Distribution 3	
Mode	430
Median	435
Mean	435.565
Standard Deviation	32.061
Pearsons Coefficient (skewness)	0.053
Distribution Range	355-550kHz

Table 7.11 Statistical analysis of the 'average' frequency distribution for uncured samples.

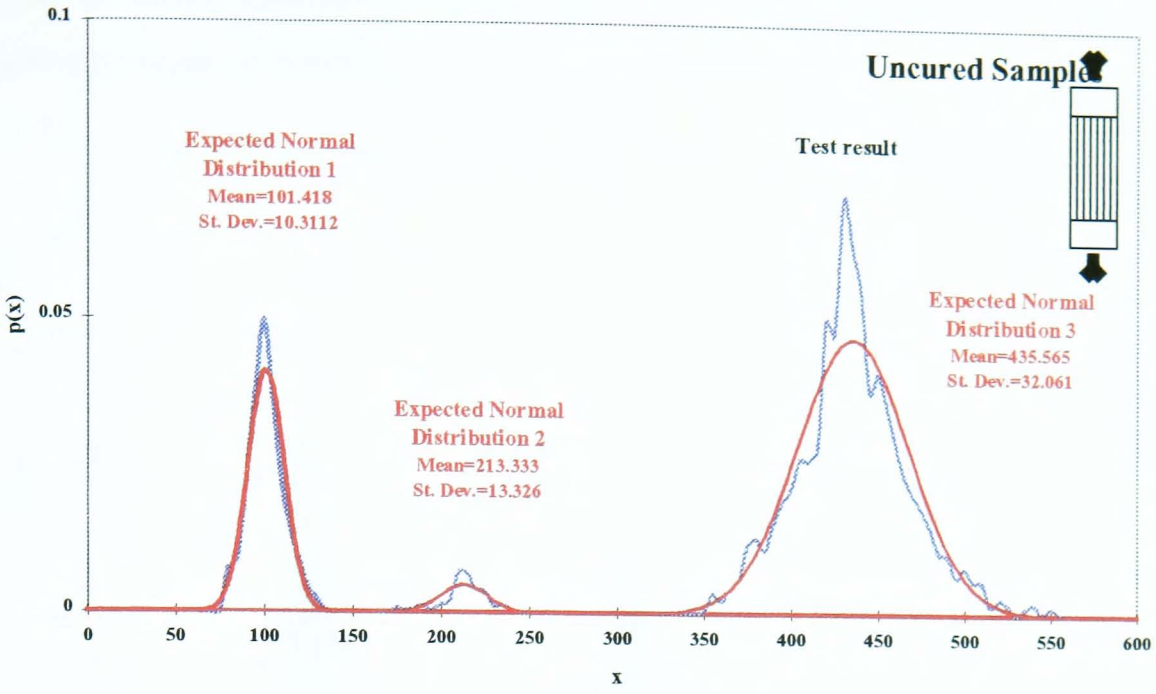

Figure 7.36 Actual and estimated frequency probability distribution analysis of the AE signals from uncured samples using the piezoelectric transducer.

7.4.5 Specimens Containing Embedded Teflon Discs

In these type of specimens, tensile loading results in the separation of the plies where the Teflon is inserted. In these specimens it is expected that delamination will be introduced as a damage mechanism but matrix cracking and carbon fibre fracture will also occur. A typical example of the frequency distributions found with Teflon loaded samples is shown in figure 7.37. It is evident that three distributions occur in these samples. The 'average' distribution plot (figure 7.38) exhibits these three distributions more clearly: 80-165kHz, 210-325kHz, and 430-505kHz. There is also a very small distribution situated in the range 370-410kHz. However, this distribution has been ignored as the process of averaging produced values less than unity. These three main distributions have modal frequencies of 110kHz, 275kHz, and 465kHz. Statistical analysis of this distribution has been calculated (Table 7.12) and has been used to produce an 'expected' distribution (figure 7.39)

From the previous sections, the first and third distribution have already been identified as matrix cracking and carbon fibre fracture respectively. Therefore, the

phenomenon of delamination must exhibit frequencies in the 210-325kHz in these particular types of samples.

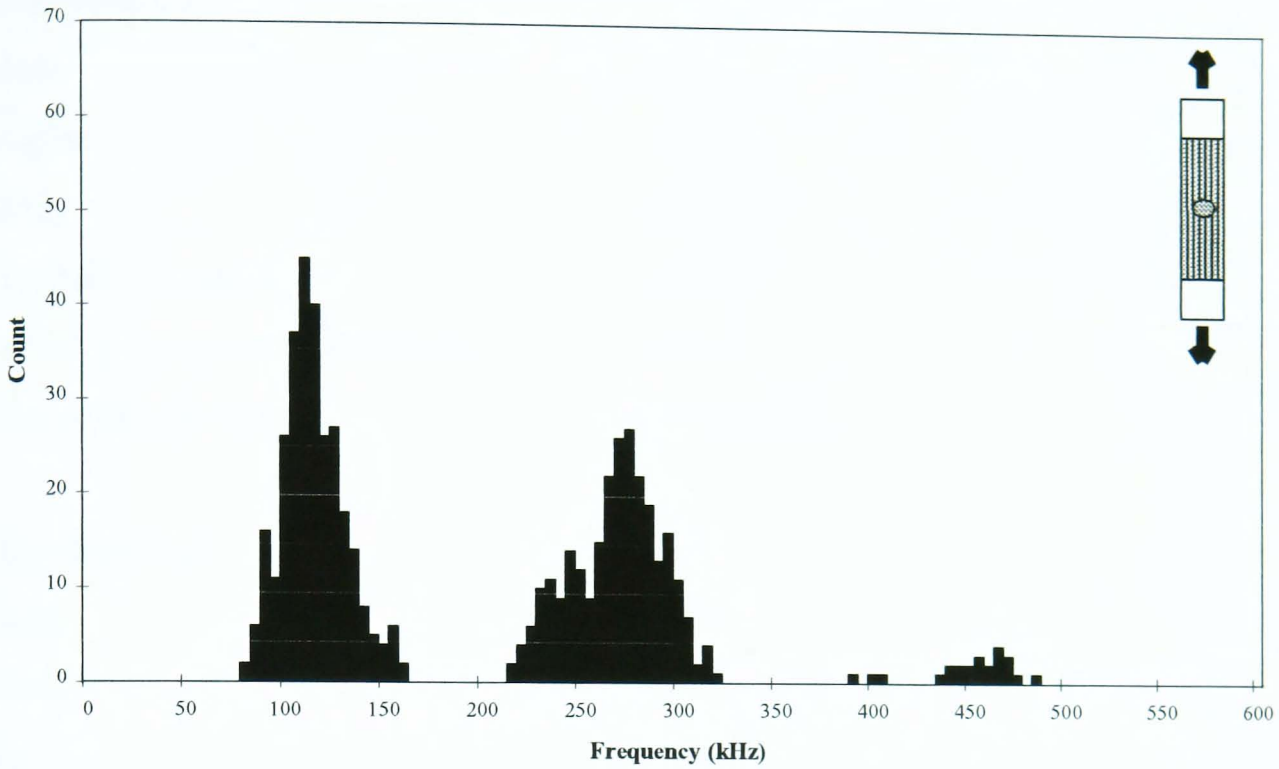

Figure 7.37 A typical frequency distribution of the AE signals from the tensile loading of Teflon loaded samples.

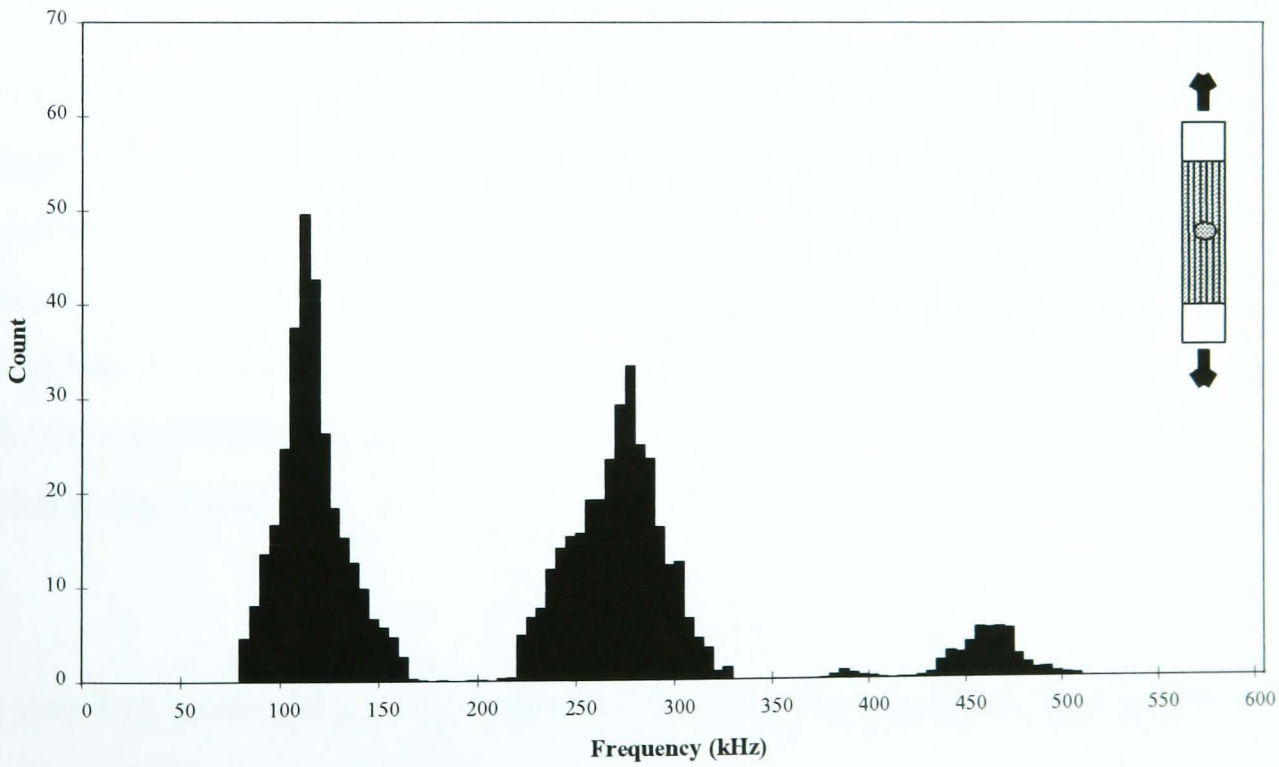

Figure 7.38 Average frequency distribution of the AE signals from the tensile loading of Teflon loaded samples

Statistical Parameters

Distribution 1	
Mode	110
Median	110
Mean	113.943
Standard Deviation	16.503
Pearsons Coefficient (skewness)	0.717
Distribution Range	80-160kHz
Distribution 2	
Mode	275
Median	270
Mean	268.142
Standard Deviation	22.214
Pearsons Coefficient (skewness)	-0.252
Distribution Range	210-325kHz
Distribution 3	
Mode	465
Median	460
Mean	460.629
Standard Deviation	15.083
Pearsons Coefficient (skewness)	0.125
Distribution Range	430-505kHz

Table 7.12 Statistical analysis of the 'average' frequency distribution for Teflon loaded samples.

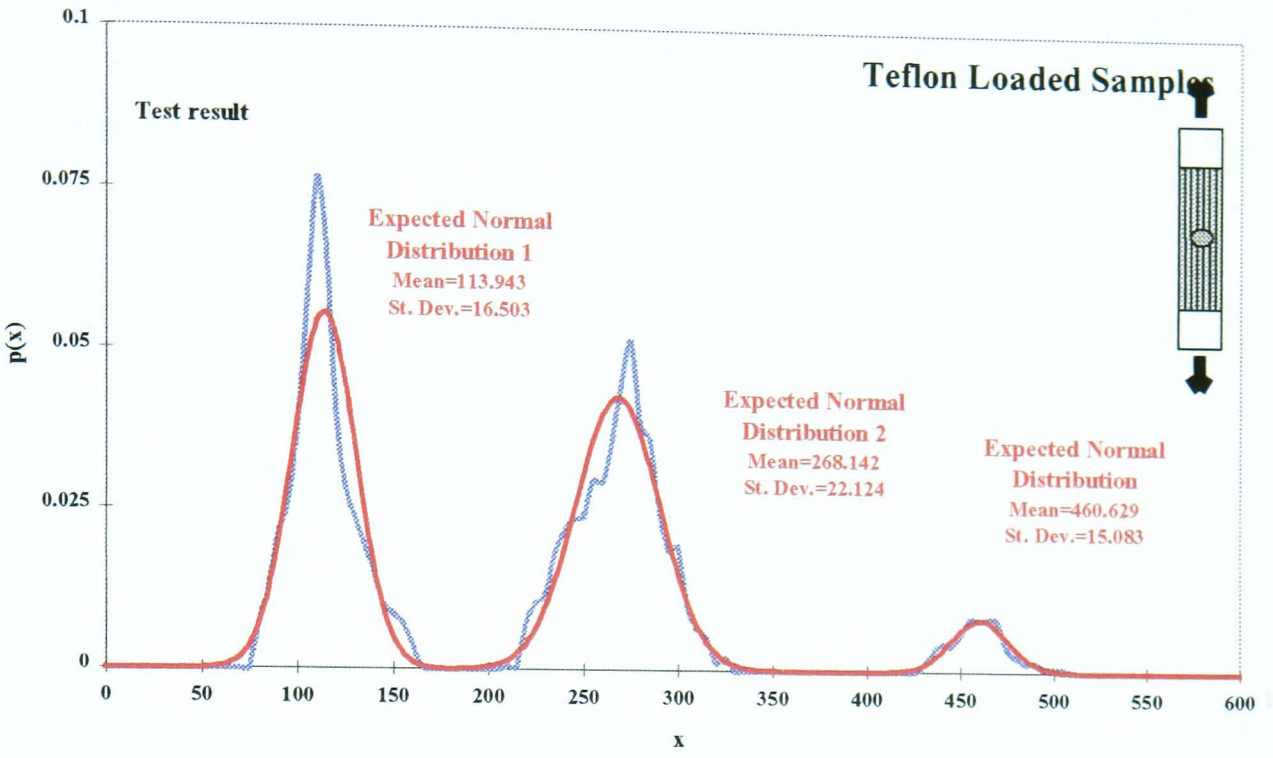

Figure 7.39 Actual and estimated frequency probability distribution analysis of the AE signals from Teflon loaded samples using the piezoelectric transducer.

7.4.6 An Overview Of The Frequency Distribution Results For All Samples

From the five types of tests undertaken, several graphs have been produced which exhibit a series of population distributions that can be correlated to specific damage mechanisms. In Table 7.13 the type of sample is documented, along with the statistical parameters obtained and the hypothesised damage mechanisms. Also, some comments have been added to aid the explanation why a specific distribution has been chosen for a particular damage mechanism.

Sample Type	Statistical Parameters (kHz) Mode	Mean	St.Dev.	Range	Damage Mechanism
Resin	115	113.030	11.854	80-150	Matrix Cracking
90°	130	125.872	13.780	80-195	Matrix Cracking
Comments:	*It is possible that the broadening of the distribution is due to a little fibre/matrix (F/M) debonding.*				
10°	105	105.245	10.830	80-145	Matrix Cracking
	210	218.434	20.770	170-285	F/M Debonding
	530	527.367	14.076	485-565	Fibre Fracture
Comments:	*In the mid-range distribution it appears visually that there may be a mixture of distributions Informal graphical techniques illustrate that this may be the case. If so, this distribution could be due to F/M Debonding and Fibre Pullout.*				
Uncured	100	101.418	10.311	80-135	Matrix Cracking
	210	213.333	13.326	175-240	F/M Debonding
	430	435.565	32.061	355-550	Fibre Fracture
Teflon Loaded	110	113.943	16.503	80-160	Matrix Cracking
	275	268.142	22.124	210-325	Delamination
	465	460.629	15.083	430-505	Fibre Fracture

Table 7.13 An overview of the frequency distribution results for all types of samples

7.5 Summary

A series of tests were devised to isolate each damage mechanism so that the correlation of the acoustic emission parameters to damage in the composite could be made. Amplitude distribution and frequency analysis was undertaken in an attempt to provide an 'acoustic signature' for each mechanism. The results obtained for each specimen type indicated that a correlation for some of the damage mechanisms could be made. It must be stated, however, that in some of these graphs it appears that there is a mixture of distributions. In these cases an informal graphical technique was used to highlight the possibility of distribution mixtures. From the tests undertaken, matrix cracking exhibits amplitudes less than 60dB and has frequencies in the 80-150kHz range. Conversely, the energy released during carbon fibre fracture is much higher with amplitudes in excess of 75dB. It also has frequencies in excess of 350kHz. It has been hypothesised that the debonding of the fibre/matrix interface has amplitudes and frequencies in the ranges 55-75dB and 180-240kHz respectively. However, this is difficult to confirm as it appears visually that there may be a mixture of distributions in this range for the 10° samples. The damage mechanism of greatest importance is delamination. From the amplitude distribution analysis it was difficult to make a concrete statement, however, it was apparent from the frequency distribution analysis that delamination exhibited frequencies in the range 210-325kHz. Once again it was difficult to confirm these values for delamination as only one type of sample (Teflon-loaded samples) was used in the delamination studies. Confirmation of the 'acoustic signatures' for each damage mechanism will only be achieved with a comprehensive study of these types of samples and specimens with different lay-ups.

CHAPTER 8

DISCUSSION AND RECOMMENDATIONS FOR FUTURE WORK

8. Discussion And Recommendations For Future Work

The following sections will attempt to establish the significance of the results presented in chapter 6 and 7. The object of the experimentation in chapter 6 was to evaluate the all-fibre Mach-Zehnder interferometric acoustic emission sensor as a potential diagnostic tool for damage in composite materials. This was attempted in two ways: (1) demonstrate the feasibility of using this embedded fibre optic sensor through the evaluation of its characteristics and (2) the interpretation of the collected AE information from damaged CFRP composites. In addition to the data evaluation some of the problems and possible solutions associated with the fibre optic acoustic emission sensor will be discussed. The tests performed using the piezoelectric transducer (chapter 7) attempted to provide an 'acoustic signature' for each damage mechanism via its time domain and frequency characteristics.

8.1 Fibre Optic Acoustic Emission Detection System Characteristics

To establish the feasibility of such a sensor, the fibre optic sensor was subjected to continuous and transient acoustic excitations (section 6.4). Initial tests involved a surface mounted sensor exposed to single frequency sinusoidal excitations. The fibre optic AE sensors' response varied from test to test. This was due to the inconsistency in the bond between the optical fibre and the composite surface. Once it was evident that the surface-mounted fibre optic sensor could pick up surface AE it was necessary to embed the sensing length of the optical fibre within a composite material. The embedded sensor was once again subjected to the single frequency sinusoidal excitation. The response of the AE sensor improved and became consistent from test to test. In these tests the sensitivity of the fibre optic AE sensor was approximately seven times less sensitive than the PZ transducer. The characterisation of the frequency response of the embedded optical fibre sensor over the bandwidth of interest, that is, over the frequency range of 100kHz - 1MHz, was made. These tests indicated that the sensor had a flat spectral response over the frequency range of 400-580kHz.

To investigate the feasibility of using the fibre optic sensor to detect transient acoustic disturbances, the response of the embedded AE sensor to pencil break tests. Once again, the response of the fibre optic sensor was compared to the PZ transducer subjected to the same excitation. The results yielded a reproducible high frequency acoustic pulse, which took the form of an exponentially decaying sinusoidal oscillation. As well as the sensitivity of the fibre optic sensor being less than its electrical counterpart, it was evident that the noise content of the signal was also greater.

From the results it is evident that the noise present in the fibre optic acoustic emission detection system limits its sensitivity to the measurand of interest. In the detection system, two primary contributions to the background noise have been identified: laser instability and unmatched optical path lengths. The contributions of laser stability and unmatched optical path lengths to the overall noise of the system result in two distinct problems. Firstly, the most obvious problem associated with system noise is that it limits the detection of low amplitude signals. The analysis of detected signals in the frequency is also impaired by system noise. Since the noise is not uniform at all frequencies, the spurious contributions will obscure the spectral features of any given signal.

There are a few ways of improving the overall performance of the sensor. The reflection of light from the launching lens back into the laser cavity causes instability and leads to phase noise at the output of the interferometer. Attempts have been made to reduce this laser instability by simply tilting the laser source so that the reflected light can be seen on the laser casing. However, the improvement in the sensitivity of the system could be improved by a frequency stabilised laser and an optical isolator. To reduce feedback into the laser cavity the optical isolator would be placed between the laser and the launching optics. The isolator uses a Faraday rotator in conjunction with two polarisers to allow light to pass in only one direction.

The second and most difficult technique for minimising the phase present in the interferometric system was to ensure that the optical path lengths of the reference and sensing arms were as close as possible. At first, the path lengths could be matched to within a few millimetres. However, the inclusion of the composite test section affected the sensitivity of the detection system. The test section consisted of an embedded length of optical fibre and pigtails which was connected to the sensing arm using mechanical splices. The length of optical fibre in this test section obviously had to be a set length, and therefore deviations in this length introduced additional phase noise. To combat this, fibre collimators were inserted in the sensing arm so that the optical path length difference could be maintained at a set value, and therefore maintain the sensitivity of the detection system from test to test.

Despite the affects of noise, the information gained from the simulated AE tests showed that the embedded fibre optic AE sensor was sensitive to surface disturbances. With the confidence established in the fibre optic system through this process of characterisation, it seemed reasonable to proceed with actual damage induced acoustic emission experiments.

8.2 Relating Fibre Optic Sensed AE Signals To Damage In CFRP Composites

There were two categories of interpretation which have been investigated: (1) the correlation of the AE data to the source of emission, that is, the specific damage mechanism, (2) determination of the point where the accumulated damage has become severe enough that the overall structural integrity of the component under consideration has been compromised in terms of safety and reliability. If the fibre optic acoustic emission sensor is to be used as a potential diagnostic tool for the non-destructive evaluation of composite materials, the latter must be satisfied.

The composite sample with the embedded optical fibre was loaded in tension to failure, and the resulting AE emanating from the internal damage was monitored. The signal characteristics were initially disregarded, but the number of events recorded

were examined as a function of increasing load. In these tests the appearance of AE signals occurred at approximately 40% of the failure load. The rate of AE signals detected rose slightly until the specimen reached approximately 70% of the failure load. At this point the rate of AE increased significantly until failure. In chapter 6, two forms of this type of graph were presented: a typical example and an 'average' plot of the cumulative event count. A similarity was noted between the typical plots representing the cumulative AE counts versus increasing load for both sensors, with each exhibiting a 'knee' in the curve. The 'weighted' comparison of the 'average' plots showed that the shapes of the curves due to the fibre optic sensor and piezoelectric transducer were almost identical. Since visual confirmation of this delamination sustained in the composite samples could not be made it was difficult to determine the damage mechanisms involved. In all tests the embedded optical fibre sensor fractured before the composite specimen. This is shown by the fact the piezoelectric transducer continues to detect AE signals until failure although the fibre optic sensor ceases to observe any damage.

The dummy fibre embedded in the composite samples could have been used to provide real-time evidence of the onset of a delamination zone in the sample. The dummy fibre was placed in the specimen to maintain overall material symmetry. The fibre could have been treated such that fracture of the optical fibre would occur in response to significant material damage. Therefore, the fibre could be treated to coincide with the appearance of the 'knee' in the cumulative event count graph. A system for confirming damage in composite materials through optical fibre fracture has been demonstrated by many authors (Hofer, 1987, and Hale et al, 1980). Laser light is launched into the optical fibre, so that fracture of the embedded fibre is detected by a loss of transmitted light intensity.

The same principle could be used to verify the fracture of the optical fibre sensor before the specimen fracture. However, the dummy optical fibre would not be treated in any way. Therefore, the loss of transmitted light due to the fracture of the dummy fibre could indicate the sensor failure. A schematic of this possible technique is shown in figure 8.1.

Although the confirmation of the onset of delamination has not been made, previous research has indicated that the knee of the cumulative event count coincides with this type of damage. As the appearance of delamination in a material seriously compromises the overall health of the structure, the detection of these zones using the embedded all-fibre Mach-Zehnder interferometric AE sensor demonstrates the feasibility of using such a sensor for non-destructive evaluation purposes.

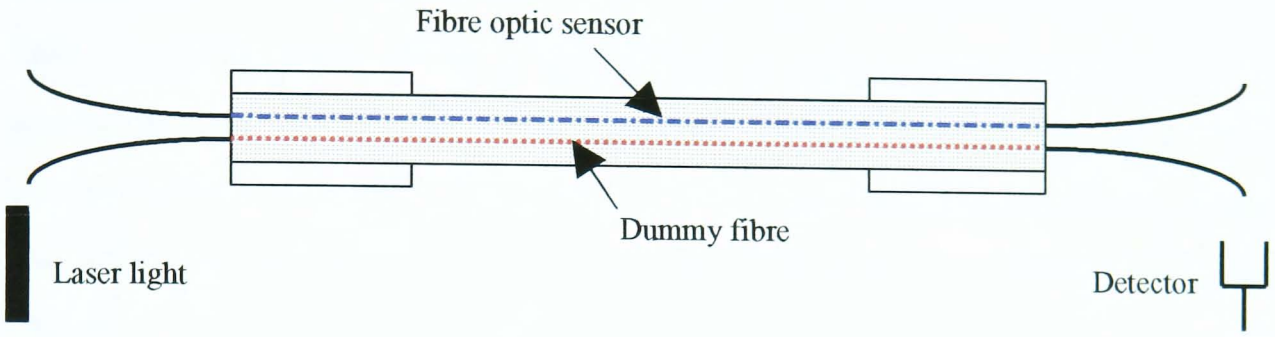

Figure 8.1 Schematic of the possible use of the dummy fibre for the confirmation of damage.

Once the feasibility of the sensor was established the latter category of data interpretation, that is, the correlation of the AE data to the specific damage mechanism was investigated. In these tests a total of twelve samples were loaded in tension to failure, and the resulting AE was detected using the fibre optic sensor and the piezoelectric transducer. In the time domain, the amplitude of the acoustic emission signals were measured and analysed for possible associations with type of damage in the CFRP composites. The resulting data detected using both sensors is documented in Appendix B. Amplitude distributions have been analysed in an attempt to identify the damage mechanisms involved. In the typical example given in figure 6.21, three modes of amplitude have been given (24dB, 27dB, and 32dB) which indicate the possibility of a mixture of distributions. To aid the analysis of the data detected, it was necessary to determine an 'average' distribution for both sensors. Through the 'average' distribution analysis it is apparent that three modes of amplitude were also present.However, the hypothesis made regarding the overlapping

of distributions cannot substantiated as the determination of distribution mixtures is complex. From the 'average' graph, there was a continuous distribution ranging from 22dB to 57dB. However, the vast majority of data appears to be resident in the range approximately 22-40dB. The small distribution above 40dB, at this point, appears to be due to a specific damage mechanism.

The AE emanating from the twelve samples were also detected using the piezoelectric transducer. A typical example of the amplitudes detected is shown in figure 6.22. The distribution of data indicated a main mode of 53dB in a multi-modal distribution. The most interesting detail of this graph was the numerous events detected in the high amplitude range (>70dB). By averaging the data detected (figure 6.23) it appeared that four modes of amplitude could be seen: 44dB, 51dB, 63dB, and 92dB. Once again, it was difficult to ascertain whether four damage mechanisms were responsible for these values.

In the fibre optic sensor tests, the amplitude distributions of the AE signals were monitored in specific load ranges in an attempt to differentiate between the sequence of damage mechanisms. As stated earlier, it is important to note that the fibre optic sensor failed in most of the specimens before the specimen failed. Therefore, the load ranges used were 0-60%, 60-80%, 80-90%, and 90% to sensor failure load. In the first chart (0-60% of the specimen failure load) there were few signals detected. However, as the load increased there was a marked increases in the signals detected. In the 60-80% sensor failure load range there was a definite broadening of the distribution above 30dB. At the next load range, there was an increase in data in the same amplitude range (22-36dB) although there was an appearance of some higher amplitude signals. In the final load range, more signals in the higher amplitude range (>40dB) were detected.

The analysis of data detected by the piezoelectric transducer in the four load ranges (figure 6.24a-d) were more revealing than those plotted for the fibre optic sensor. These plots can aid the evaluation of the data detected using the fibre optic sensor.

It was visibly apparent that there was a broadening of the distribution in the 60-80% load range (38-71dB). This graph indicates that this distribution broadening could be due to a specific damage mechanism. As stated earlier, the cumulative event graphs displays a marked increase in the number of events detected around 70% of the composite failure load. The analysis of the data detected in this load range using the fibre optic sensor also revealed a broadening of the amplitude distribution. This may have been expected as few signals were detected in the 0-60% load range. However, the piezoelectrically sensed data exhibits a comprehensive broadening of the amplitude distribution. The 'knee point' in the cumulative event curve has been hypothesised by other authors to be due to the onset of delamination.

Compared to the previous load range, the next load range (80-90% of the specimen failure load) showed an increase in the data detected within the same amplitude range (that is, 38-71dB). However, there were many signals detected in the high amplitude region (>70dB). In the final load range, there was a significant broadening of the distribution (38-97dB). The most important aspect of this graph was the vast amount of data in the high amplitude region. In the fibre optic sensor analysis of the data, it was found that there was a distribution of high amplitude signals.

The value of amplitude of an AE signal is considered to correspond to the value of elastic energy released by the formation of a crack. Generally, the AE signal of lower amplitudes are considered to be emitted from a crack which released a small elastic energy, and the AE signal of higher amplitudes emitted from a crack which released a larger elastic energy. Research studies have indicated that matrix cracking is associated with low amplitude signals, and carbon fibre fracture with higher signal amplitudes (Berthelot and Rhazi, 1990). It can be hypothesised that the matrix cracking occurred at the onset of damage. It has been assumed that in the 60-80% load range that the onset of delamination occurs, which leads to the broadening of the amplitude data detected. Through the mathematical relationship by Berthelot (1988), it can be assumed that the broadening of the population curve at the latter stages of loading (80-90% of the failure load) is due to a combination of matrix cracking and carbon fibre fracture, as well as delamination. The higher amplitude signals, obtained

just before the sensor failure, were almost certainly due to carbon fibre fractures and partial delamination.

From the fibre optic sensor plots alone it was difficult to make a concrete statement about the correlation of the AE signal to the type of damage occurring in the sample. However, with the aid of the piezoelectrically sensed data it is possible to determine the sequence of events occurring in the composite sample as it is loaded to failure. Even through the analysis of the piezoelectrically sensed signals, it is difficult to determine the actual range of amplitudes which are due to a specific damage mechanism.

There are several difficulties with an analysis of acoustic emission signals on the basis of peak amplitude. It is now well known that the failure of composite materials is an accumulation of basic damage mechanisms such as fibre breakages, matrix cracking, interfacial fibre/matrix debonding and delamination. However, the failure of a composite specimen results from a combination of these basic mechanisms. Therefore an event must not be necessarily associated with a basic rupture mechanism, but more often results from a cascading of basic mechanisms. For example, fibre rupture involves a redistribution of stresses in adjacent fibres and can cause multiple fibre fractures. Also, a break in a reinforcing can involve processes of interlaminar failure or matrix cracking parallel to the fibres in neighbouring crossed layers. Since signals rarely occur singly it is difficult to determine that the number of events that the fibre optic sensor's response represents. Without the confidence in the identification of individual events, it becomes difficult to assess the acoustic emission parameters. The analysis of the event duration can be clouded by the overlapping of damage mechanisms. In this scatter plot it could be seen that there was an increase in event duration of the signals which coincided with the 'knee' in cumulative event count graph. At the knee point the rate of AE activity significantly increased and as stated earlier coincides with the onset of delamination. Berthelot and Rhazi (1990) state that delamination and longitudinal cracking of the matrix are characterised by long duration signals. However, they also state that abnormally long durations can be mistaken for this type of damage although it is actually due to friction of the fracture

surfaces. It cannot be hypothesised to relate the increase in event duration to the progression of delamination as it is possible that the event duration could be due to multiple damage mechanisms. The massive rise in event duration at failure confirms this statement.

Another factor which influences the nature of the acoustic emission signal is the microstructure of the composite material, that is, the material nature, dimensions, and arrangement of the reinforcing fibres. The source wave undergoes significant change as it interacts with the material. Also, the failure mechanisms involved during a mechanical test depend on the strain rate and the rigidity of the specimen in the mechanical grips.

In tests using the embedded fibre optic sensor there were several factors which hinder the comparison of the signal amplitudes between different samples. The sensitivity of the embedded sensor is a function of several variables: bonding between the embedded optical fibres and the composite laminate and the quality of the coupling of the optical fibres in the mechanical splice. The amplitude of signals generated within the sample will depend not only on the magnitude of the event, but also on the proximity of the source to the optical fibre sensor. Therefore, comparisons between results obtained in various tests is often difficult.

8.3 Time And Frequency Domain Analysis Of AE From Specially Designed Samples

The work undertaken using the fibre optic sensor yielded results in which the information obtained explained little about the damage mechanisms involved in the fracture process of these cross-ply composites. In an attempt to isolate the damage mechanisms occurring in a composite under mechanical testing a series of samples were designed. These specimens were designed with the fibre optic sensor in mind, that is, the information obtained from these specimens could help determine the damage mechanisms involved in the cross-ply composites detailed in Chapter 6.

However, before testing commenced the fibre optic acoustic emission detection system developed a fault which seriously reduced the sensitivity of the sensor. Despite this, the results obtained from the systematic tests using the piezoelectric transducer only could still shed light on the results obtained in Chapter 6.

Since amplitude analysis of the AE emanating from the cross-ply composites yielded limited success, it was necessary to combine this type of time domain analysis with spectral analysis. Therefore, the object of the tests were to monitor the time domain parameters and frequency spectra of the signals detected with the piezoelectric transducer only.

The analysis of the data was made by plotting the amplitude and frequency distributions. In Chapter 7 a typical example of these distributions are given for each type of sample. However, for the purpose of statistical analysis it was necessary to calculate an 'average' distribution for each sample. However, in some of the distribution plots it was apparent that there was a mixing of distributions due to the number of damage mechanisms involved. The preliminary nature of the tests and the lack of visual inspection resulted in an informal analysis of the mixture distributions. To highlight the possibility of mixture distributions, 'estimated' distributions have been superimposed onto the 'average' distribution graphs. These 'estimated distributions' are calculated by estimating the standard deviation and mean, as well as the proportion of data. The discussion of the results obtained for the various samples is as follows:-

(a) Resin samples

The first sample to be monitored in this series of experimentation was a pure resin sample. When the pure resin samples are loaded in tension to failure the acoustic emission events generated can only be due to matrix cracking. Subsequent analysis of the 'average' amplitude distribution revealed a mode of amplitude at 43dB and a range 37-56dB.

As with the amplitude distribution analysis, the results obtained using the spectrum analyser were conclusive. The 'average' frequency distribution (figure 7.25) exhibited a frequency range between 80-150kHz, with a mode of frequency at 115kHz. The data in this type of sample appears to be normally distributed. The calculation of Pearson's coefficient reveals that this is the case. Therefore, in the resin tests it was possible to determine the amplitude and frequency characteristics due to matrix cracking.

(b) 90° samples

The next tests to be undertaken intended to confirm the results obtained above. The samples were manufactured in such a way that the load was applied 90° to the reinforcing fibres. In these samples, loading to failure produces AE events primarily due to matrix cracking. However, it was possible that fibre/matrix debonding would also occur. Amplitude distribution analysis of the 'average' data obtained from the tensile loading orthogonal to the reinforcing carbon fibres reveals that the distribution is bi-modal (48dB and 62dB) and has a range 38-71dB. The broadening of the distribution could be due to the presence of fibre/matrix debonding. The statistical parameters calculated from the data produced an 'estimated' distribution, which when superimposed onto the 'average' graph revealed a poor relationship between the two distributions. Through the informal (graphical) mixture analysis, it has been hypothesised that two distributions are present. The superimposed 'estimated' distributions reveal the possibility of mixtures (figure 7.13). From this plot, the second estimated population curve at this stage in the analysis could be due to the fibre/matrix debonding.

The analysis of the frequency spectra showed that the 'average' frequency distribution was broader than that detected from the resin tests (frequency range of 80-195kHz with a frequency mode of 130kHz). It has been hypothesised that the reinforcing fibres in the composite material affect the propagation of the AE signal, which could account for the slight shift in the frequency distribution (compared to that found in the resin tests). It was expected that fibre/matrix debonding would occur in these samples. From figure 7.29 it is not visibly apparent that this mechanism occurs. However, the

analysis of the amplitude distribution through informal mixture analysis implies that this mechanism may occur.

(iii) 10° samples

Amplitude distribution analysis has been done on the acoustic emission data obtained from the tensile loading at an angle of 10° to the reinforcing carbon fibres. In these type of samples fibre pull-out is introduced in addition to the matrix cracking and fibre/matrix interfacial debonding. The 'average' amplitude distribution (figure 7.15) revealed a large distribution (between 41-79dB) with a mode amplitude of 57dB. In the second distribution (80-97dB) the values greater than 97dB were estimated for statistical analysis purposes.

It is difficult to determine whether or not there is any mixing of distributions in the first (largest) distribution. Compared to the results obtained from the 90° samples (modes at 48dB and 61dB), the mode of amplitude for the 10° samples was 57dB. A shift in the mode of the largest distribution may indicate that fibre/matrix debonding was the dominant damage mechanism with matrix cracking also occurring. However, in these type of samples fibre-pull-out may occur.

The frequency distribution analysis of the AE data from a typical sample in the 10° tensile tests revealed two heavily populated distributions of data (80-130kHz and 165-290kHz). There was also some data distributed above 350kHz. To highlight the possibility of mixture distributions an 'average' distribution graph was calculated. This graph (figure 7.31) shows the distribution which was clearly related to matrix cracking (80-145kHz). From this 'average' graph it was also evident that the distribution in the range 170-285kHz appeared to be a mixture of two distributions. By superimposing two estimated normal distributions over this range it is apparent that a mixture of distributions is a definite possibility. Therefore, the frequency range 170-285kHz could be due to two separate damage mechanisms. In figure 7.31, there was also a distribution of data in the range 490-570kHz. From these tests only matrix

cracking could be correlated to the AE data detected, however, subsequent tests would help reveal the damage mechanisms involved in the 10° tensile tests.

(iv) Uncured samples

To investigate the time and frequency domain parameters of signals due to carbon fibre fracture some uncured pre-preg samples were loaded in tension to failure. In uncured pre-preg the carbon fibres have a resin cladding, and therefore, some amplitudes due to matrix cracking and fibre/matrix interfacial failure can occur. Therefore, the tensile testing of these samples could exhibit three possible modes of failure. From the 'average' amplitude distribution plot it could be seen that there are two distinct population curves (40-58dB and 70-97dB). These distributions have modes of 47dB and 85dB respectively. In the 'average' plot there was a small distribution of data between 60 and 70dB which was disregarded, as the process of averaging revealed an event count less than unity.

Since it has been ascertained that the low amplitude signals are due to matrix cracking then the lower amplitude distribution appears to be due to the cracking of this resin cladding. Therefore, it can be assumed that the high amplitude signals (>70dB) are due to fibre fracture.

The analysis of the frequency data through the 'average' distribution graph (figure 7.35) reveals three distinct distributions (80-135kHz, 170-240kHz, and 355-550kHz). The first distribution exhibits properties which have already been associated with matrix cracking, that is, frequencies below 150kHz and a modal frequency of 100kHz. In these type of samples the predominant damage mechanism is carbon fibre fracture. This mode of failure can be associated with the high frequency range (355-550kHz). By process of elimination the mid-frequency range (175-240kHz) can be associated with the debonding of the fibre/matrix interface. This test reveals that the high frequency results found in the 10° tensile tests are due to fibre fracture and not fibre pull-out.

(v) Teflon-loaded samples

In these type of samples a Teflon disc was placed in the mid-planes during lay-up. On curing the Teflon prevents a proper bond between the adjacent plies. Therefore, at the onset of loading the sample immediately delaminates. As the load approaches failure the strength of the specimen severely deteriorates resulting in mass fibre fracture and sample failure. The AE data obtained from these tests was again analysed through amplitude and frequency distributions.

From the 'average' amplitude distribution graph (figure 7.21) there appeared to be at least three population curves. Initially, it was assumed that were only two distributions present: 40-81dB and >84dB. As with the previous types of specimen, values greater than 97dB had to be estimated. The values of mean and standard deviation have been used determine the two 'expected' normal distributions. However, when superimposed onto the actual plot, it was evident that there was a poor relationship between the plots (figure 7.22). Therefore, it was assumed that there was a mixture of distributions in the range 40-81dB. The only possible parameter which can be identified are the modes of the distributions (50dB, 63dB, and 97dB).

Through estimated statistics and data proportions an estimated population plot indicated the possibility of mixture distributions. From the assumption that two damage mechanisms were responsible for the distribution between 40-81dB, and another mechanism was responsible for the small distribution above 84dB, a tentative correlation was made.

The expected failure mechanisms from these type of specimens are delamination, matrix cracking and fibre failure. From the previous discussions on the different types of samples, it has been ascertained that matrix cracking has values in the low amplitude range less than 55dB, whereas fibre fractures have amplitudes in excess of 75dB. From this it can be assumed that amplitudes due to delamination occur in this middle population curve (estimated to be in the range 50-80dB). However, like all of the above analysis, it is possible that multiple mechanisms contributed to the signal

amplitude. Therefore, the actual amplitude range for delamination cannot be stated for certain as no other samples exhibited delamination. However, the sharp distribution curve centred at 63dB could be observed. Future work should involve double cantilever beam tests to give more samples which exhibit delamination under load.

Frequency distribution analysis of these type of samples was achieved using the 'average' plot (figure 7.38). From this graph it is evident that three prominent distributions occur: 80-165kHz, 210-325kHz, and 430-505kHz. A very small distribution (370-410kHz) has been ignored as averaging produced values less than unity. From the previous sections, the first and third distribution have already been identified as matrix cracking and carbon fibre fracture respectively. Therefore, the phenomenon of delamination must exhibit frequencies in the 210-325kHz in these particular types of samples.

From the amplitude and frequency analysis of the acoustic emission emanating from these five specimen types it was possible to make some statements regarding the damage mechanism acoustic signatures. It was possible to identify the amplitude and frequency characteristics of two modes of failure. Low amplitude and frequency components could be attributed to matrix cracking while high amplitude and frequency components could be associated with fibre fracture. It has been suggested that the intermediate amplitude and frequency distributions could be associated to other possible damage mechanisms, such as delamination, fibre/matrix debonding, and pull-out.

In the 90° samples informal graphical analysis has been made to highlight the possibility of two mixing distributions in the amplitude analysis. It was hypothesised that the broadening of the both the amplitude and frequency distributions was due to some fibre/matrix debonding. However, specific ranges could not be stated for certain for this mechanism.

In the tests designed to highlight debonding of the fibre/matrix interface (10° samples) it was difficult to make a concrete statement regarding its amplitude and frequency

components. From the 41-79dB amplitude distribution it is difficult to determine specific ranges of data due to matrix cracking, fibre/matrix debonding and fibre pull-out, whereas subsequent tests reveal the distribution >80dB to be due to fibre fracture. In the frequency domain, the mid-range distribution visually appears to be a mixture of distributions Informal graphical techniques illustrate that this may be the case. If so, this distribution could be due to fibre/matrix debonding and fibre pullout.

In Teflon-loaded samples, the predominant failure mode is delamination. In the frequency distribution graphs it was possible to determine the frequency range for delamination through the process of elimination as the approximate ranges for matrix cracking and fibre fracture had been determined. In the amplitude distribution analysis, informal graphical analysis had been made to highlight the possibility of two mixing distributions. However, it was too difficult to determine the exact distribution ranges for delamination and matrix cracking.

A graphical summary is illustrated in figures 8.2 and 8.3.

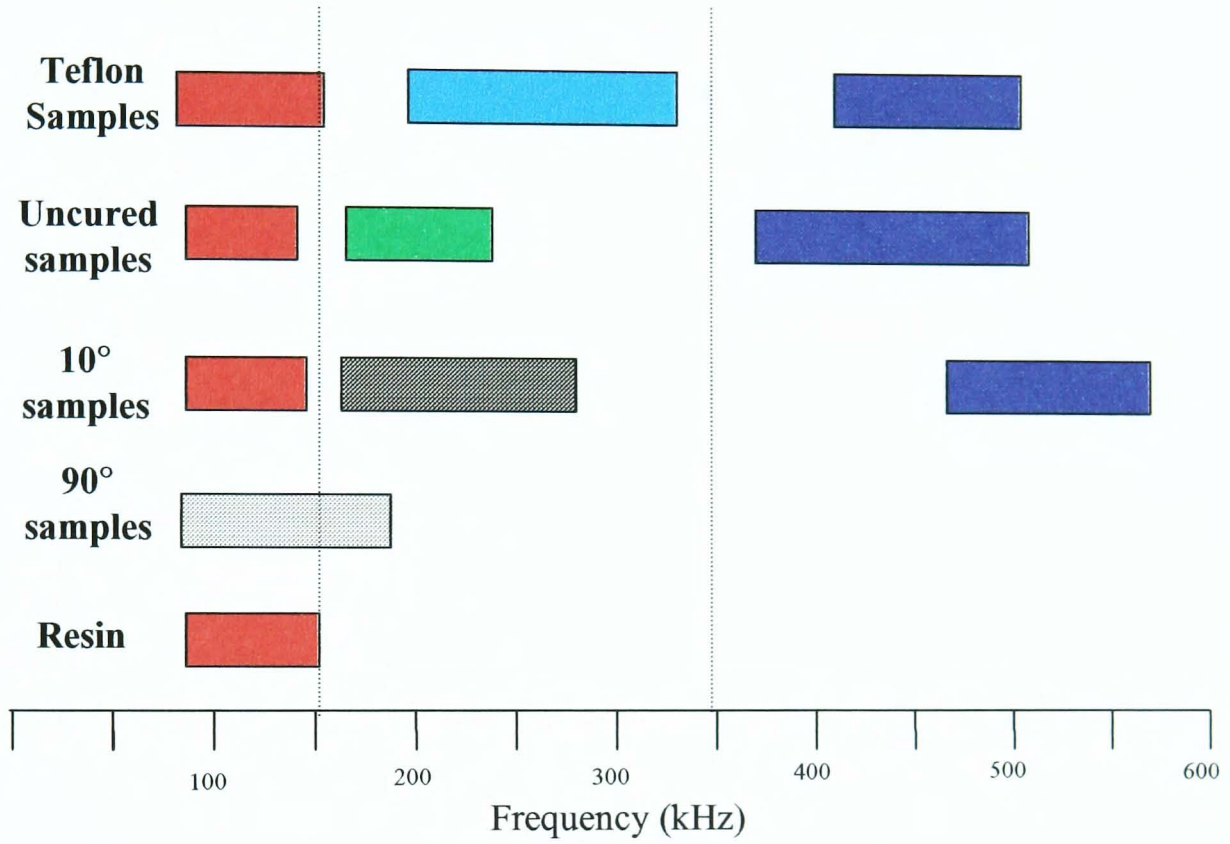

Colour Code:

- Matrix cracking
- Fibre/matrix debonding
- Fibre Fracture
- Delamination
- Matrix cracking and fibre/matrix debonding (possible mixture of distributions)
- Fibre/matrix debonding and fibre pull-out (possible mixture of distributions)

Figure 8.3 Summary of the frequency ranges and the corresponding damage mechanisms found through the testing of five different types of sample.

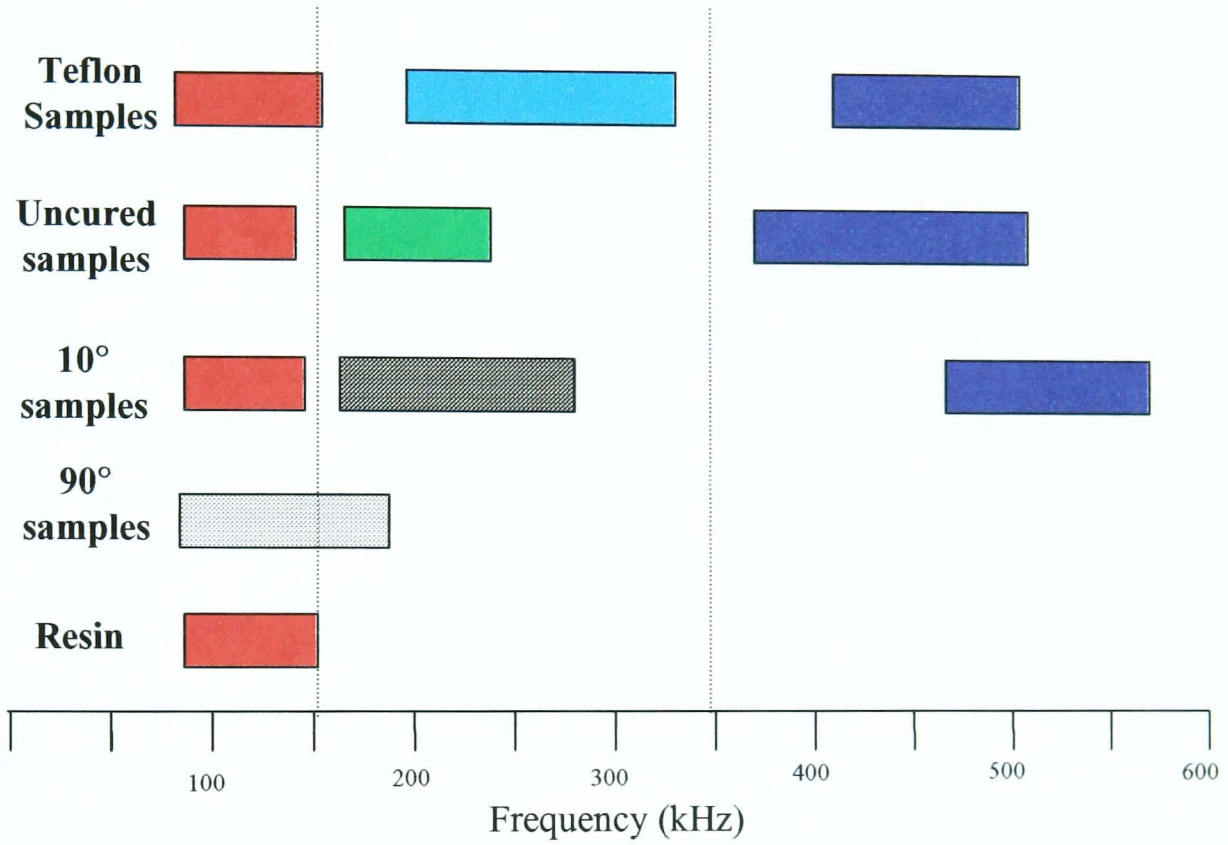

Colour Code:

- Matrix cracking
- Fibre/matrix debonding
- Fibre Fracture
- Delamination
- Matrix cracking and fibre/matrix debonding (possible mixture of distributions)
- Fibre/matrix debonding and fibre pull-out (possible mixture of distributions)

Figure 8.3 Summary of the frequency ranges and the corresponding damage mechanisms found through the testing of five different types of sample.

Table 8.1 summarises the amplitude and frequency distributions obtained through this particular series of tests.

Damage Mechanism	**Amplitude**	**Frequency**
Matrix cracking	< 55dB	80-165kHz
Fibre fracture	> 80dB	> 350kHz
Fibre/Matrix debonding	Inconclusive	175-240kHz
Fibre pull-out	Inconclusive	Inconclusive
Delamination	Inconclusive	210-325kHz

Table 8.1 Summary of the preliminary analysis of the time and frequency domain parameters of AE signals from specially designed samples.

During the processes of damage, the duration of events induced by fibre rupture and transverse cracking of the matrix are of similar range for usual portions of fibres. However, established results (Berthelot, 1988) suggest that energy released during fibre fracture is much higher and the highest amplitude signals are associated with mechanisms controlled by fibre rupture. The author suggests that the energy released during transverse cracking is low (by the order of 30 times lower) and produces much lower amplitude signals. Longitudinal cracking and delamination of the matrix involve energies for a given crack area comparable to the transverse cracking of the matrix, and therefore lead to similar amplitudes.

The interpretation given to the experimentally observed frequency ranges is based on the assumed relationship between spectral content of the AE signals detected and damage within the material. However, if the frequency domain information from the piezoelectric detected AE signals is to be used to indicate damage in CFRP composites then the characterisation of the spectral properties of acoustic waves

travelling through carbon/epoxy materials must be taken into consideration in future work. The analysis of this kind is beyond the scope of this document.

From the work undertaken in Chapter 7 it is evident that there is a need for formal techniques to determine the mixture of distributions in both the amplitude and frequency data. Once this was achieved it would be possible to compare the results obtained using the piezoelectric transducer in chapters 6 and 7. It was possible to determine the approximate amplitude ranges for matrix cracking and fibre fracture in Chapter 7. However, it appears that there was a mixture of distributions in the piezoelectrically sensed data from the cross-ply composites in chapter 6. Despite this, through the analysis of data of the AE at different load stages it was possible to determine matrix cracking and fibre fracture. From the data analysed in Chapter 7, it was evident that low amplitude signals (<55dB) were due to matrix cracking, mid amplitude signals (55-80dB) were due to fibre/matrix debonding, fibre-pull-out, and delamination, whereas high amplitude signals (>80dB) were caused by fracture. A comparison of amplitude values cannot be made with those obtained using the fibre optic sensor. At the onset of damage, it is evident that the low amplitude values obtained optically are due to matrix cracking, whereas the small amount of high amplitude data obtained close to failure was due to fibre fracture. It has been shown earlier that the fibre optic sensor fails before the composite fails. It is necessary to treat the fibre so that the sensor remains intact until failure, thus ensuring the detection of the mass fibre fracture just before structural failure. This is just one improvement which is needed to make the fibre optic sensor a viable option for industrial applications. The following section highlights the further work needed to improve the sensor.

8.4 Future Work

If the Mach-Zehnder interferometric acoustic emission sensor is to be used an integral part of a 'Smart Structures' package then future development is needed. In assessing the suitability of any fibre optic sensor for use with smart structures many authors have listed a number of requirements (Measures et al, 1991) namely:

- the required selectivity of the chosen technique;
- robustness of the fibre-optic interconnect at the surface/edge of the host structure;
- the effect of embedded fibre-optics on the composite's structural integrity;
- the need to provide localised measurement;
- amenable to multiplexing to form sensing networks within structures;
- the need to determine the measurand directly and provide an absolute value;
- the need to give a reproducible, ideally, linear response;
- the need to avoid down lead sensitivity;
- the need for compatible signal processing technology.

A Mach-Zehnder interferometric sensor, like other interferometric sensors, cannot satisfy all the requirements. However, the major disadvantage of this type of sensor is that it is a two-fibre configuration, which implies larger physical size and greater noise sensitivity. The sensor is also difficult to localise, since the standard configuration is to have one 'arm' in the sensed field and the other isolated from the field. The sensor described in this document is actively compensated to prevent significant noise problems. In Mach-Zehnder interferometers, the non identical path lengths of the 'arms' results in additional phase noise. The developed AE sensor has incorporated fibre collimators which can adjust the optical path length of one of the arms in the interferometer. Although the fibre optic acoustic emission has been developed to eradicate some of the problems associated with Mach-Zehnder interferometric sensors, certain requirements of the criterion stated above have to be investigated.

8.4.1 Multiplexing

It is necessary to arrange a number of sensors in arrays to provide complete monitoring of a structure. To manipulate the signals from the sensors individually in a centrally localised processor, it is important to organise the array elements so that they can be individually addressed. For economical reasons it is strongly desired to send the signals along one single fibre that is running along the entire array. For the majority of applications one fibre has sufficient capacity to required the amount of information. To resolve and separate the individual signals, multiplexing is used. A large amount of approaches to this problem have been proposed (Turner et al, 1990). The conceptually simplest technique is time division multiplexing. The most straight forward version of this techniques the ladder structure. In figure 8.4 a number of Mach-Zehnder interferometers are coupled to the same main fibre and separated with optical delay coils. The optical input is pulsed with pulse lengths smaller than the optical delay (T) between two successive sensors. The pulse repetition rate is high compared to the frequencies of interest. The optical detector senses a series of pulses for each input pulse, each pulse representing the output from one interferometric sensor (S_i). Each sensor can then be selected in the time domain by a time division multiplexor. An array of sensors in the composite material will be able to determine the location of the flaw.

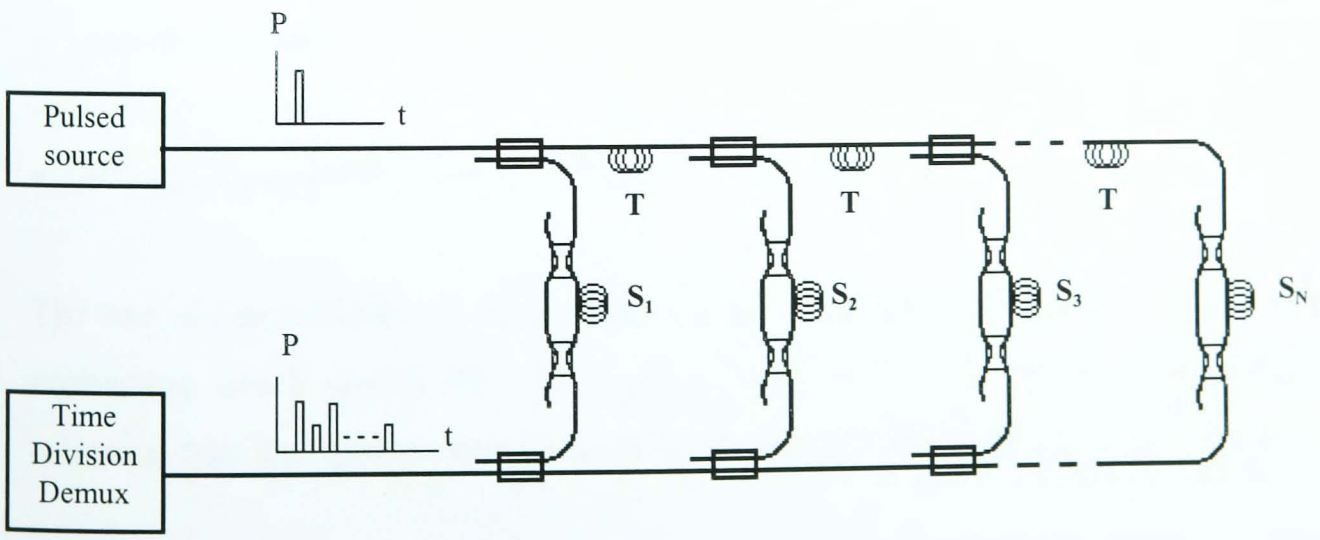

Figure 8.4 Basic configuration of time multiplexed sensors

8.4.2 Connectors

The present fibre optic acoustic emission sensor uses mechanical splices to connect the embedded fibre to the sensing arm of the interferometer. However, repeated matings have resulted in damage to the fibres in the sensing arm. Also, misalignments of the butt-coupled fibres results in a severe loss in signal. During tests, the mechanical splice had to be opened and re-closed many times until the alignment was achieved. This results in the degradation of the butted surface of both fibres. Therefore, suitable connectors must be used. Fibre optic connectors for the use in smart structures require the following features:

- low insertion loss that remains constant after repeated matings;
- minimal back reflections;
- minimal external contamination problems. Designs should minimise dirt, moisture, and chemical ingress;
- effective environmental sealing;
- easy inspection and cleaning of fibre end surfaces;
- end face protection;
- straight forward termination and repair features

The use of mechanical splices for test section connections are unsuitable, therefore connectors which satisfy the above criteria are needed if the fibre optic acoustic emission detection system is to used in an industrial environment.

A recent publication by Green and Shafir (1999) highlights methods for the termination and connection of optical fibres embedded into composite materials

intended for structural airframe applications. The development work was divided into three stages: studies on bare fibres, use of edge connectors, and incorporating surface mounted connectors. The developed work enabled the connection via standard optical fibre communications hardware to monitoring instrumentation, and interconnection to other composite parts. The authors connection system was designed to withstand the rigours of the composite material manufacturing process, the aircraft assembly line and routine service.

8.4.3 Fabrication Techniques

The specimens used in all the tests were personally hand-laid and cured using specially designed moulds. The exit fibres protruded from the end edges of the specimen and were protected from damage with thin PTFE tubing. However, in certain structures access to the exit fibres could only be made from the composite surface. Therefore, techniques for bringing optical fibres out of the laminates must be investigated. One possible solution is schematically illustrated in figure 8.5.

The problem with this possible technique is bringing the fibre out of the composite surface. The plies directly on top would have to be slit at the lay-up stage to create a gap for the fibre to exit. This would damage some of the carbon fibres. If the gap is large there would be a discontinuity in the carbon fibres. On curing the reinforcing fibres would not fully fill the gap and resin-areas would be present. Therefore, the introduction of the sensor into the composite would degrade the mechanical performance of the material. The requirements for smart structures state that the mechanical performance of the material must not be compromised by embedded optical fibres. However, if the slit is made sufficiently small the mechanical properties of the material may not be affected. At the surface of the composite the exit fibre could be protected from resin bleeding by using PTFE tubing. Optical fibre bushing could then be used to protect the fibre from external damage. The connection to the composite test could be made at the top of the bushing.

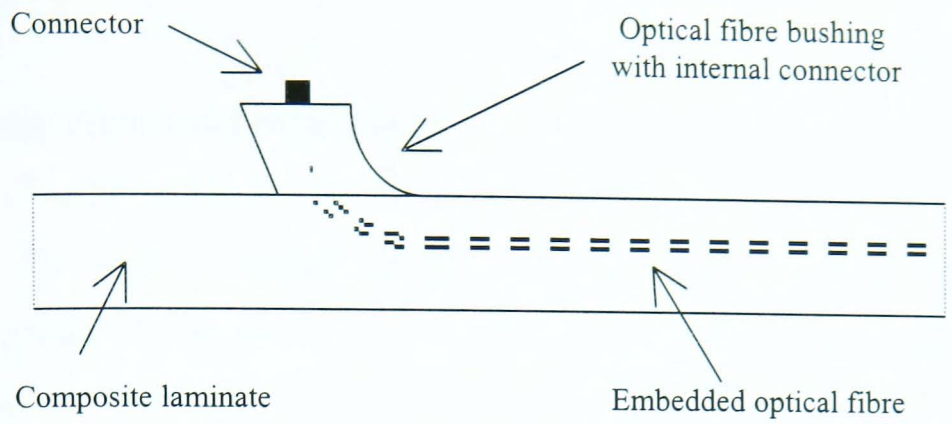

Figure 8.5 Possible technique for bring the optical fibre out of the composite surface

The above technique must be used in any industrial situation. However, the fabrication procedure described in Chapter 6 is sufficient for laboratory investigations. These type of samples have embedded optical fibres which traverse the length of the specimen. Therefore, damage occurring anywhere in the sample can be sensed by the optical fibre. Modifications in the single specimen moulds could result in the fabrication of samples, where the fibre traverses the width of the specimen. In this type of sample, there would be no need for a dummy fibre. This is due to the fact that the embedded optical fibre needs to be parallel to the reinforcing carbon fibres to ensure minimum change in the overall material characteristics. Figure 8.6 illustrates this new type of laboratory specimen. The lay-up sequence would now be $[0,90,90,0,0,90,0,90,(FOS)]_S$. These specimens could then be used for laboratory damage localisation investigations.

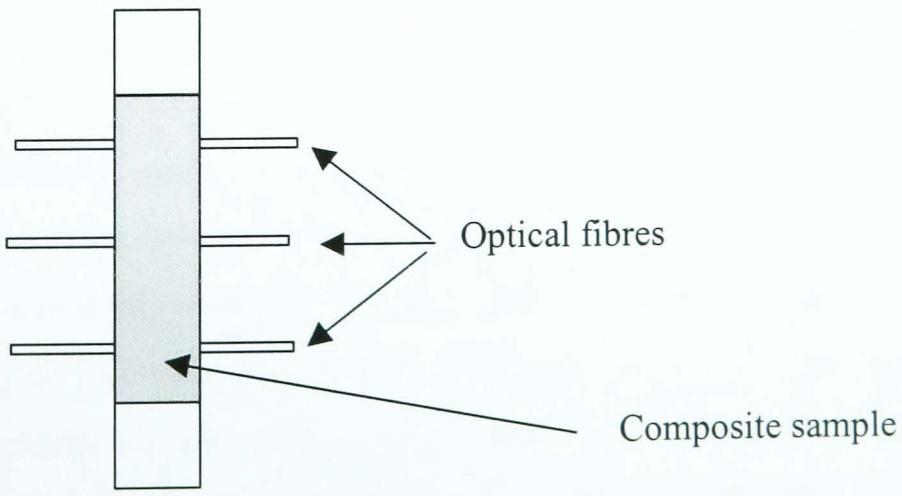

Figure 8.6 Alternate laboratory specimen lay-up for damage localisation investigations

8.4.4 Analysis Techniques

In the work presented in this document the AE signals generated by damage mechanisms were detected by the optical fibre sensor and analysed in the time domain. However, it has been shown that analysis of the amplitude of the AE signal is difficult due to many factors. Over the last decade many researchers have monitored the frequency content of the signal and the subsequent analysis has been more fruitful. In the work presented a series of specimens have been designed, and along with systematic testing, specific damage mechanisms can be isolated. The frequency analysis of the AE emanating through the specimen is therefore easier. From the results, it is evident that low amplitude and frequency components could be attributed to matrix cracking while high amplitude and frequency components could be associated with fibre fracture. However, other possible damage mechanisms, such as delamination, fibre/matrix debonding, and fibre pull-out exhibit intermediate amplitudes and frequencies. From the tests, it was difficult to differentiate between the three in terms of amplitude components since it appears that their respective amplitude distributions overlap. This intermediate amplitude band ranges from 55-75dB. However, it was possible to determine the frequency range of delamination from the Teflon-loaded sample tests. Despite this, it appears that the frequencies due fibre/matrix debonding and fibre pull-out overlap into this frequency range. If samples were tested that exhibited these three mechanisms, it would be difficult to differentiate between them in terms of frequencies.

A possible method of obtaining a correlation between frequency components and the damage mechanisms could be accomplished by introducing specific frequency acceptance 'windows'. Since the intermediate frequency range (~170-320kHz) includes frequency components for delamination, fibre/matrix debonding, and fibre pull-out, acceptance windows could be set up to determine certain characteristics of the AE signals within each zone. Alternatively, the level of damage sustained by a composite could be ascertained by setting up zones in the low, intermediate, and high frequency ranges and then comparing the characteristics obtained for each zone.

This technique was used by Lui et al (1990) to monitor the progression of damage and the mechanisms associated with it. The authors examined the frequency components of the acoustic emission signals obtained from square Kevlar specimens under transverse loading using FFT analysis. The authors quantified the distribution of energy in the frequency domain by comparing the measured areas of defined frequency 'zones' (figure 8.7). Three broad frequency ranges of (1) below 300kHz, (2) between 300kHz and 600kHz, and (3) above 600kHz. were defined, and the area under the spectrum for each range compared.

The authors noticed a trend whereby the signal energy shifted from higher to lower frequencies as the amount of damage in a composite specimen progressed. This is apparent from figure 8.8. The signal energy concentrated below 300kHz (Area A1) increased whereas the signal energy in the 300-600kHz zone (Area A2) decreased as the damage progressed through the sample. With the aid of an image-enhanced backlighting system, the authors were able to visually identify the amount of damage in the translucent Kevlar samples.

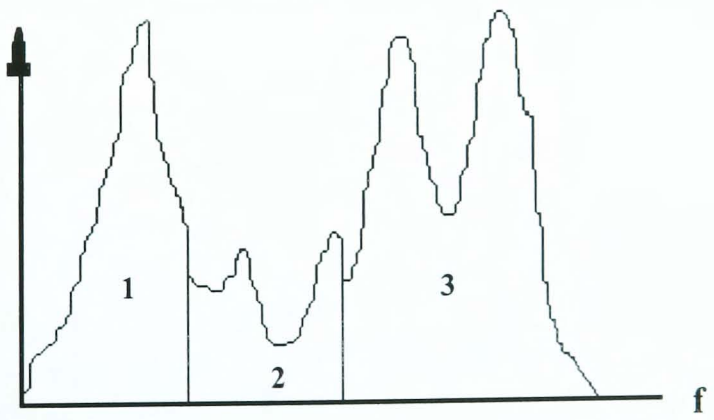

Figure 8.7 Divisions of the frequency spectrum

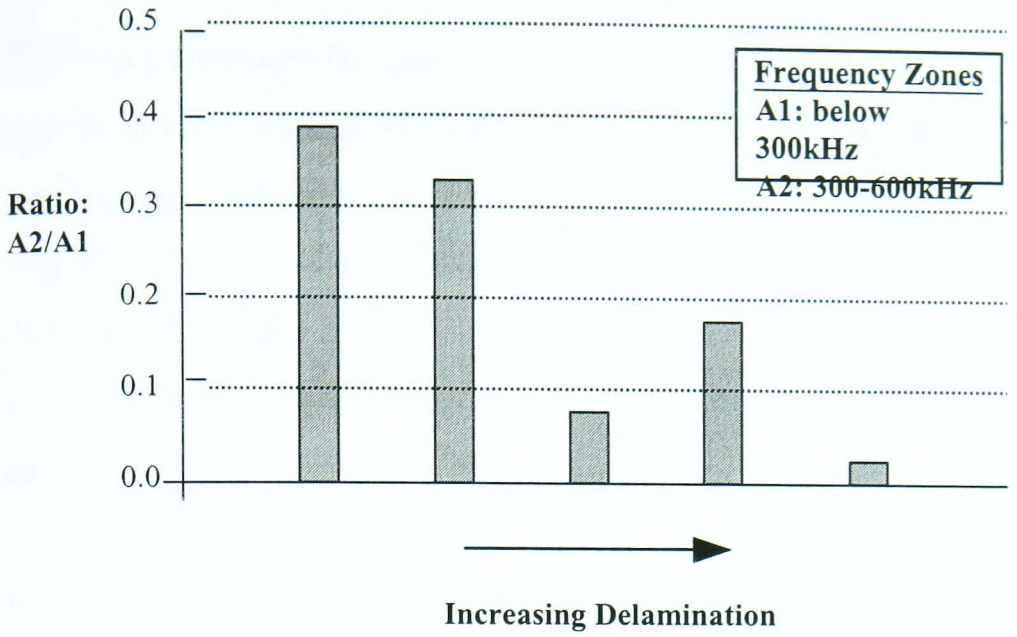

Figure 8.8 Percent concentration of one zone against the other to help determine the spectral shifts of the acoustic emission signal with the increase in damage.

To associate the frequency content of the signals to the possible damage mechanisms, the acoustic events were analysed in the same manner outlined above. In figure 8.9, the upper left points of the plot occurred at low loads and damage, whereas the lower right points occurred at high levels of load and damage. Since, matrix cracking occurs well below 300kHz, the points at the extreme lower right can be attributed to this mechanism, whereas the points in the upper left can be associated with fibre fracture. The points in the middle of the plot can be associated with delamination.

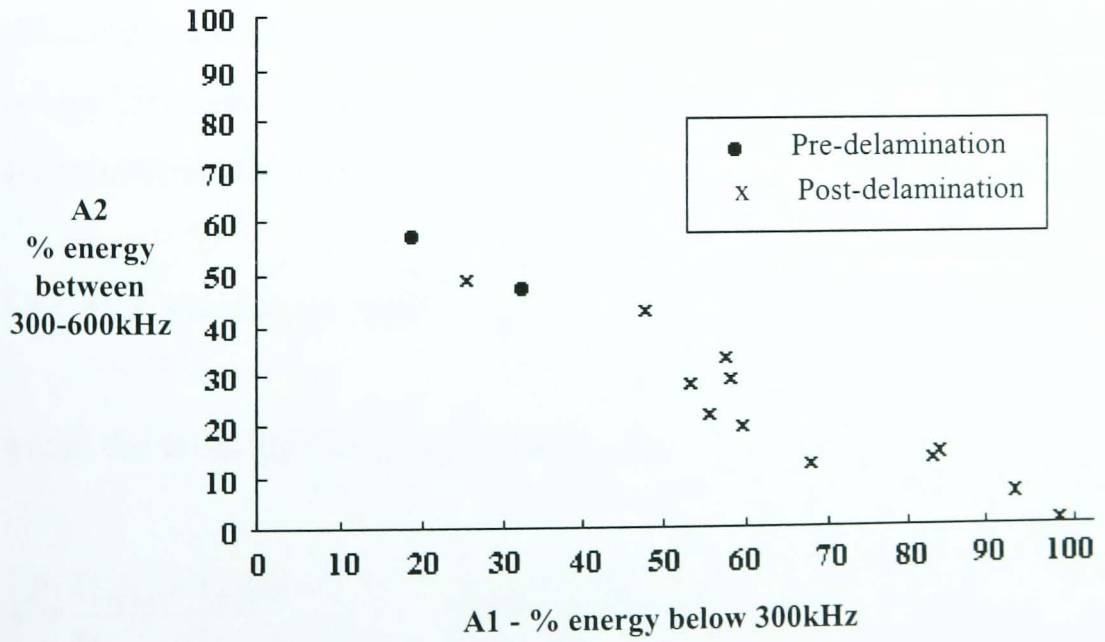

Figure 8.9 Acoustic emission signal characterisation: a frequency analysis.

This work presented by Lui et al (1990) shows that a comparison of acoustic emission signals in each can help determine the level of damage and the its associated damage mechanisms. However, the use of neural networks would be required if this technique was to be used to locate and assess the extent of damage in a structure. Since a comparison of three frequency zones (low, intermediate, and high) could be made, the ratios obtained from each comparison could be used by an adaptive learning system to provide an advance warning of potential failure

It has also been highlighted in chapters 6 and 7 that in certain graphs there appears to be a mixing of distributions. The analysis of these distributions was done using informal graphical techniques. However, formal techniques must be used in future work to determine whether or not finite mixing distributions are present. There are very little technical papers published, however, books by Everitt and Hand (1981) and Tetterington, Smith and Makov (1985) highlight the theory behind this complex statistical process.

8.4.5 General System Improvements

In section 8.1 some techniques have been proposed to reduce the phase noise in the detection system, however more modifications could be made to increase the sensitivity of the system. It has been shown that the overall sensitivity of the detection system depends on the visibility or fringe contrast (V). From chapter 4 this is expressed mathematically by the formula:

$$I = I_0 [1 \pm V\cos(\phi_{sig} - \phi_{ref})]$$

where the visibility can be calculated using

$$V = \frac{(I_{max} - I_{min})}{(I_{max} + I_{min})} \qquad \text{where } 0 < V < 1$$

The measurement of the visibility can only be made when the feedback circuit of the active homodyne detection system is disabled. The visibility itself depends on three factors;

1. The coherence length of the source is not large enough in comparison with the optical path imbalance between the interferometer arms;

2. The components of signal and reference beams reaching a specific detector are unequal in intensity;

3. The states of polarisation of the signal and reference beams are unequal.

As mentioned earlier, fibre collimators can be used to adjust the optical path length in the 'signal' arm. It is theoretically possible to adjust the optical path imbalance close to zero. In the detection system, a HeNe laser was used to provide coherent radiation. This has a coherence length of approximately 200mm. The actual optical path difference was less than 3mm, and therefore this laser was adequate. However, the HeNe laser is rather bulky and the need for a smaller source may be required if the system is to be used for an industrial application. A low coherence LED source could be used, which is a great deal smaller than the HeNe laser. This type of source has a coherence length of approximately 20μm. Therefore, if the LED source is used it is imperative that the optical path difference is zero. This may not be obtained by adjusting the fibre collimators manually. A possible solution, which could be applied to the present detection system, is to use a motor system to mechanically move one of the fibre collimators until maximum visibility is achieved. This solution could be based on the concept used to track the phase in the reference arm (active homodyne detection system). Therefore, the visibility would be continually measured and a feedback system could be used to control the movement of the fibre collimator. As one of the fibre collimators is mechanically moved, the visibility would be tracked from zero towards and through the maximum. Once the maximum visibility is ascertained the feedback system would move the fibre collimator to the point where

the optical path difference was zero. Realistically, a maximum value of one would be difficult to achieve due to the other factors.

The states of polarisation of the signal and reference beams are altered using the polarisation controllers. However, the polarisation controllers could be mechanically adjusted to achieve maximum visibility using the same technique described above.

The visibility could also be maximised by using better quality fibre couplers. Present couplers used in the fibre optic AE detection system had a 53:47 split. However, if 50:50 couplers were used then the components of the signal and reference beams reaching the detectors would theoretically be equal in intensity. However, the losses in the signal and reference arms are different. Although both arms have two fusion splices, the losses due to each fusion splice are non-identical. Also, the signal arm has mechanical splices used for the composite test section. As stated earlier, improved connectors are need to replace the mechanical splices, however, all connectors exhibit insertion losses. In addition to the losses in the signal arm, the fibre collimators exhibit losses which depend on the distance between the lenses.

These are some of the improvements which could be made to the fibre optic acoustic emission detection system to help increase the sensitivity. However, these type of improvements would significantly increase the cost of the system.

8.5 Summary

A series of experiments were undertaken to evaluate the embedded fibre optic acoustic emission sensor as a potential diagnostic tool for the evaluation of damage in composites. It was shown that the fibre optic sensor was capable of detecting AE emanating from a sample under load. Basic analysis of this data, through cumulative event count graphs, showed that the fibre optic sensor could detect the point where the rate of AE significantly increased. The 'knee' in these plots has been associated with the onset of delamination. Therefore, the fibre optic sensor was capable of

determining the point where the accumulated damage has compromised the structural integrity of the sample. The determination of the damage mechanisms through their associated AE was less fruitful. Amplitude distribution analysis revealed a broadening of the curve as the sample was loaded towards failure. However, no concrete associations could be made between the amplitude distributions and the damage mechanisms. Event duration analysis revealed that after the 'knee' point in the cumulative event count graphs the durations of some of the signals increased. Delamination can usually be identified by its long event duration, however, it cannot be claimed that all of these signals are due to delamination since it is possible that overlapping of events occur. In addition to the cross-ply samples, a series of specimens were designed to isolate specific damage mechanisms. However, the fibre optic sensor experienced sensitivity problems which resulted in the tests being monitored only by the piezoelectric transducer. Time and frequency domain analysis of the resulting AE signals showed it was possible to associate matrix cracking and fibre fracture to specific amplitude and frequency ranges. A tentative relationship has been made between these signal parameters and delamination, debonding of the fibre/matrix interface, and fibre pull-out. However, there seems to be an overlapping of the amplitude and frequency distributions for each mechanism which makes identification difficult.

The fibre optic AE detection system must be modified to increase the sensitivity of the sensor. To be accepted as a potential NDE tool for monitoring structural integrity, the sensitivity of the fibre optic sensor must be comparable to the piezoelectric transducer. Several components and techniques have been proposed which could significantly increase the sensitivity of the embedded sensor. In addition to this, improved analysis of the signals must be achieved. There is no standard technique used for the analysis of AE signals. A possible analysis technique has been given which could be used in conjunction with neural networks to form an adaptive learning system. This system could give advance warning of potential structural failure.

CHAPTER 9

THESIS OVERVIEW AND CONCLUSIONS

9. Thesis Overview and Conclusions

The use of composite materials, such as carbon fibre reinforced plastics, to form part or all of major structural components has become more common. These materials have many advantages which have been exploited by the aerospace, automobile, marine, and retail sectors. The non-destructive evaluation (NDE) of composite materials uses methods of flaw detection and characterisation after fabrication and in-service, to monitor flaw growth under loading and environmental variations. Flaws can be inadvertently introduced in composite laminates during processing and fabrication. Also, sources of stress concentration and damage growth, such as holes of various sizes and shapes, are often necessary for design functions. Defects are also induced or enlarged in-service with age, loading and environmental conditions. Failure to detect a problem associated with one of these factors can lead to premature failure of the structure at some later date when in service.

A variety of NDE methods are used for the evaluation of the structural integrity of composite materials. These include ultrasonic, radiographic, thermographic, and optical techniques. However, all of these techniques require inspection by an external source and are all implemented either as a check that the composite has been fabricated correctly or as an assessment of damage that has already taken place. The phenomena of acoustic emission (AE) lends itself well to the NDE of composite materials. AE is the phenomenon of transient elastic wave generation due to the rapid release of strain energy caused by a structural alteration in a material. Therefore, damage events in a composite material generate elastic waves which propagate outwards from the source site. Also, this technique has the added advantage that examination is non-directional. This means that larger volumes of material can be monitored with fewer sensors and only limited access to the material under inspection is needed.

The successful application of AE as an NDE technique requires both the detection of the acoustic energy associated with a damage event, and the interpretation of the detected AE signal in terms of damage type, size, and location. The collection of AE

data itself is relatively easy, however, the difficulty lies in the interpretation of the signal information. This is particularly true when considering materials as complex as composites. Composites by definition are inhomogeneous and anisotropic materials, and therefore considerably alter the nature of the wave originally emitted from the source as it propagates to the detector. The overall result is that the source characteristics are difficult to retrieve. Surface mounted piezoelectric (PZ) transducers are the most widely used technology for AE detection, and are capable of detecting the high frequency, low amplitude surface waves associated with AE. The difficulty in monitoring in-depth defects in composite materials has led to the concept of incorporating internally embedded optical fibre to measure AE and provide the possibility of giving early warning of potential structural failure.

Fibre optic sensors have many advantages over conventional sensors, such as immunity from the effects of electromagnetic interference, geometric versatility, high electrical isolation, composite compatible, and they are practically incapable of initiating fires or explosions. If fibre optic sensors are incorporated into the composite structure then they provide the basis of an embedded sensor capable of detecting damage related AE within the composite structure at all stages of its life from manufacture through to service. Fibre optic sensors are analogous to the nervous system in that they can sense damage in its host. Further stages of development could lead to structures capable of active response whereby the embedded 'nervous system' activates 'muscles' controlled with appropriate software through a neural network 'brain' to produce a smart/intelligent structure. In short, the 'smart structure' would be able to detect-analyse-decide-act. The interest in smart structure technology has grown over the last ten years, however, the damage detection of composite structures with embedded fibre optic sensors is one of the primary tasks in the development of smart materials and structures.

In a fibre optic sensor, the optical signal is changed by an external stimulus. The optical beam within the fibre is characterised by a number of variables such as intensity, wavelength, state of polarisation, and phase. The phase modulation of the light can be measured by interferometry. In all-fibre interferometric sensors, the basic

mechanisms exploited is the measurand induced change in optical path length and/or the refractive index properties of the fibre. When an acoustic emission signal emanates from a source of damage, it impinges on the optical fibre. This acoustic pressure modulates the phase of the light in the fibre. Much research has been done over the past ten years using fibre optic sensors for the detection of AE in composite materials. However, the most frequently used interferometric configurations were Fabry-Perot and Michelson. Like all other interferometric configurations, the Michelson and Fabry-Perot set-ups have their demerits (table 4.2). The 'mirror' splices at the ends of the Fabry-Perot cavity are of reduced physical strength relative to normal fibre splices. Lee et al. (1989) have reported a breakage strength about 50% of that for non-mirrored splices. This strength drop would affect the physical robustness of the sensor. Also, the manufacture of the sensor itself is not easy as the mirrored splices usually involves sputtering with titanium oxide (TiO_2). The Michelson interferometer has a pair of "lead in" arms (i.e., sensing and reference fibres) which can be adhered to each other for very close matching of the sensor leads. This arrangement can still result in significant sensor noise due to non-common path length in the leads. Also, some of the system noise is generated as a result of reflected light from the mirrors propagating back into the laser cavity.

The Mach-Zehnder interferometer itself has its disadvantages in that the sensor is difficult to localise, and the lengths of the sensing and reference fibres must be identical or the system will have additional phase noise. The problem of localisation still exists, however, a method of matching the sensing and reference arms has been used to minimise this excess phase noise. The standard Mach-Zehnder configuration has been modified to include an embedded test section, where the connections to the main 'sensing' arm are made just outside the composite specimen. The overall length of the test section needed to be kept the same from test to test to maintain overall sensitivity. However, this was difficult to implement which resulted in varying additional phase noise. To combat this, a fibre collimator rig was built to adjust the sensing path length to maintain the sensitivity from test to test. Using the set-up it is possible to adjust the optical path difference to approximately zero. The sensitivity of the detection system also relies on states of polarisation (SOP) of the sensing and

reference beams. By using polarisation controllers it was possible to ensure that the SOP of the two beams were equal. The Mach-Zehnder interferometer is a two-fibre configuration which implies that the reference arm must be isolated from any external perturbations. This is difficult to achieve, however, the phase of the light in the reference arm can be maintained at its maximum sensitivity point (quadrature point) by active compensation. The phase in the reference arm was continually tracked by an 'active homodyne' detection system and maintained at quadrature. A length of the reference arm was wrapped around a piezoelectric drum. A feedback signal from the phase tracking unit modulates the piezoelectric drum, which in turn stretches the fibre and induces a phase change in the reference arm. Once the modifications were made to the basic Mach-Zehnder configuration, several tests were performed using the interferometric acoustic emission detection system to establish its feasibility as a potential NDE tool.

At this point, it is useful to state the aims of this research. The primary aim of the preceding document was to demonstrate the feasibility of using an embedded fibre optic Mach-Zehnder interferometer to monitor the damage which had occurred under load in carbon fibre reinforced plastic (CFRP) composites through the detection of the associated AE. To establish the feasibility of such a sensor, the fibre optic sensor was subjected to continuous and transient acoustic excitations. It was possible to characterise the response of the system to these known disturbances and therefore demonstrates the feasibility of using this fibre optic sensor for the evaluation of composites.

The secondary aim was the interpretation of the collected AE information from both sensors. There were two categories of interpretation which were investigated: (1) to correlate the AE data to the source of emission, that is, the specific damage mechanism, and (2) determine the point where the accumulated damage has become severe enough that the overall structural integrity of the component under consideration has been compromised in terms of safety and reliability.

To establish whether the latter could be satisfied the composite sample with the embedded optical fibre was loaded in tension to failure, and the resulting AE emanating from the internal damage was monitored. The signal characteristics were disregarded, but the number of events recorded were examined as a function of increasing load. A similarity was noted between the curves for fibre optic sensor and those reported by other authors. The change in the slope of the cumulative count curve coincided with the appearance of a delamination zone, as evidenced by a sudden drop in the recorded load level. Since the appearance of delamination in a material seriously compromises the overall health of the structure, the detection of these zones using the embedded all-fibre Mach-Zehnder interferometric AE sensor demonstrates the feasibility of using such a sensor for non-destructive evaluation purposes and hence satisfies statement (2) of the second aim of this thesis.

In an attempt to differentiate between delamination and other types of damage mechanisms (fibre fracture, epoxy damage) signal analysis was performed on two parameters of the acoustic emission signal detected by the fibre optic sensor; amplitude distribution and event duration. A concrete relationship between particular damage mechanisms could not be found using amplitude distribution analysis. The analysis of amplitudes in specific load ranges did indicate that more than one mechanism was present. The broadening of the population curve in the latter stages of loading (80-90% of the failure load) confirms this. The analysis of the event durations revealed that the onset of the knee in the cumulative event count graph coincided with higher event durations. However, it was impossible to make a comparison between this parameter and specific flaws since a detected event could be the result of multiple events occurring at the same time.

Specially designed samples were manufactured to isolate specific damage mechanisms. Fibre optic sensor sensitivity problems resulted in the testing and analysis using the piezoelectric transducer. Rudimentary signal analysis was performed on two selected parameters: peak amplitude in the time domain and the frequency spectra. This study on the discrete components of the composite material, that is, pure epoxy, carbon fibres, and basic unidirectional specimens has revealed

repetitive amplitude and frequency distributions. A tentative correlation was made between the some of the damage mechanisms and their corresponding frequency spectra and amplitude distribution. It was possible to identify the amplitude and frequency characteristics of two modes of failure. Amplitude distribution analysis of the AE signals from the samples revealed that matrix cracking had amplitudes less than 55dB, whereas carbon fibre fractures exhibited amplitudes in excess of 80dB. In the frequency domain, matrix cracking could be associated with low frequency components of the AE (80-165kHz). Conversely, fibre fracture could be correlated with high frequency components of the signals obtained (>350kHz). A concrete relationship between the other mechanisms, i.e. fibre/matrix debonding and fibre pull-out, could not be made from the amplitude distributions present in the intermediate range 55-80dB. In Teflon-loaded samples, the predominant failure mode is delamination. In the frequency distribution graphs it was possible to determine the frequency range for delamination (210-325kHz) through the process of elimination as the approximate ranges for matrix cracking and fibre fracture had been determined. In the amplitude distribution analysis, it was too difficult to determine the exact distribution ranges for delamination and matrix cracking. There were no other specially designed samples whose predominant failure mode was delamination, an therefore these values could not be confirmed.

On the basis of this preliminary work, and especially considering the promise of frequency domain analysis, the author recommends that these tests be carried out using the fibre optic sensor. However, this type of analysis must be done on a larger amount of data than currently being detected using the fibre optic sensor.

If this sensor is to used to carry out a comprehensive study of acoustic emission in composite materials, then the sensitivity has to be increased to that obtained with piezoelectric transducers. There are several factors that influence the sensitivity of the fibre optic sensor, namely, the bonding between the glass fibre and the composite matrix and the optical connectors in the system. The latter must be investigated to find improved methods of connecting the embedded sensor to the composite test section. Current connections were made using mechanical splices. However, alignment

problems, contamination, and constant butting and re-butting of the fibres caused the sensitivity of the sensor to drop over time.

However, if this sensor is to be incorporated into a 'smart structure' package the sensitivity must significantly increase. Once this is achieved, the system can be further improved by including a second damage detection system. This system would be based on typical crack detection techniques. The dummy fibre in all the composite samples could be treated to fail at a specific point in the load history. The fracture of the dummy fibre could indicate the onset of delamination and therefore trigger the collection of signals using the fibre optic sensor. Other areas of interest that could be investigated are: multiplexing, advanced fabrication techniques, and improved signal analysis.

Of the three other areas of interest, signal analysis techniques is the most important. This is no standardised method of analysing signals emanating from a material. Pattern recognition and frequency analysis are just two of the techniques currently being implemented for acoustic emission monitoring. However, if the concept of 'smart structures' is to be realised then standard analysis, packaged with neural networks, is a must. The analysis technique presented by Lui et al (1990) illustrated that it was possible to obtain a correlation between frequency components and the damage mechanisms by introducing specific frequency acceptance 'windows'. These acceptance windows could be set up to determine certain characteristics of the AE signals within each 'zone'. Alternatively, the level of damage sustained by a composite component could be ascertained by setting up zones in the low, intermediate, and high frequency ranges and then comparing the characteristics obtained for each zone.

In industry there may be no need to determine the types of damage mechanisms occurring in a composite structure whilst it is in-service. However, it may be beneficial if the detection of delamination was highlighted by the fibre optic sensor. The most important aspect of any sensor should be that it must be able to give advance warning of impending structural failure. It has been shown that it is feasible

to use the fibre optic sensor for this purpose. However, it has been stated earlier that it is difficult to localise the sensor. Therefore, it is paramount that the sensor is embedded close to where damage is expected. In an industrial situation it would be necessary to embed a fibre length smaller than that used for laboratory specimens. Therefore, further work should involve the investigations into novel fabrication and connecterisation techniques. For this reason, the industrial uses of the fibre optic acoustic emission sensor based on the Mach-Zehnder interferometer for structural monitoring seem limited. However, if localisation of the fibre optic sensor could be made, the sensor could be applied in the aerospace and gas sectors.

Over recent years many parts of aeroplanes have been fabricated from glass and carbon fibre reinforced plastic composites. Some of the composite components used in the Boeing 737-700 and the Learjet 45 are given in Table 9.1 (Hatchard, 1995). These parts are not only fixed but are mechanically moved for flying control.

These composite parts are riveted to the other metal components of the aeroplane. These drilled holes in the composite structures act as stress concentrators. In flight, some composite structures undergo extreme environmental changes, which through time must damage the composite parts, especially near the riveted edges. Therefore, it could be possible to embed fibre optic sensors, at fixed separations, near these riveted edges. As well as extreme environmental temperatures, in-flight service can also degrade the structural integrity of the mechanically moved composite parts. These parts are especially susceptible to impact damage. Although impact damage would be random, an array of embedded fibre optic sensors could detect the position and severity of the damage. The advantages of using fibre optic acoustic emission sensors in aerospace structures over conventional sensors are many. For example, the fibre optic sensors can operate normally under extreme environmental conditions and can operate in hazardous areas without initiating explosions. Most importantly, the evaluation of the composite structures can be made in-flight.

Structural	
Boeing 737-700	*Learjet 45*
Dorsel fin (tail)	Nosecone
Trailing edge panel (tail)	Tailcone
Tailcone	
Fixed wing leading edge	
Wing secondary structure	
Wing/Fuselage flaps fairing	
Portable water storage tanks	
Flying Controls	
(Boeing 737-700 only)	
Aileron panel (wing)	
Flight spoiler panel (used as air brakes)	
One piece rudder panel	

Table 9.1 Fibre reinforced plastic composite parts contained in the Boeing 737-700 and Learjet 45 commercial aeroplanes.

These fibre optic acoustic emission sensors could also be used in the gas industry. Many gas pressure vessels are constructed from fibre reinforced plastic composites. In large vessels it is impossible to mould and cure a single composite structure. Like aerospace structures, the overall structure is made up of composite panels riveted together. As mentioned before, the drilled holes in these types of structures act as stress concentrators. The continual fatiguing of the structure would result in damage around these riveted areas. Fibre optic sensors could be embedded close to these points to determine the location and severity of the damage. The data detected by the fibre optic sensors could be analysed real time without the structure being taken out of service.

These are two industrial areas where the fibre optic Mach-Zehnder interferometric acoustic emission could be applied. However, it would be necessary to make future

improvements. Rapid advances in the research of the extrinsic Fabry-Perot interferometric sensor has resulted in the manufacture and marketing of such a sensor for AE monitoring. Although easy to manufacture, the disadvantages of being a 'two-fibre' configuration may discourage the use of Mach-Zehnder interferometric sensors in a 'smart structures' package. Despite this, the work presented in this thesis has indicated that the fibre optic sensor can detect significant damage in carbon fibre reinforced plastic composite specimens. For a damage detection device, the capabilities of the fibre optic sensor is adequate. However, improved sensitivity, combined with the advantages of an embedded, as opposed to surface mounted, sensor can give the fibre optic sensor a place among the accepted tools for non-destructive evaluation.

The primary aim of this Ph.D thesis was to demonstrate the feasibility of using an embedded fibre optic Mach-Zehnder interferometer to monitor the damage which had occurred under load in carbon fibre reinforced plastic (CFRP) composites through the detection of the associated AE. Through continuous and transient disturbance experiments, it was possible to characterise the response of the system to these known disturbances. The feasibility of using this fibre optic sensor for the evaluation of composites has been demonstrated, and therefore, the first primary aim has been satisfied. The secondary aim was the interpretation of the collected AE information from both sensors. There were two categories of interpretation which were investigated: (1) to correlate the AE data to the source of emission, that is, the specific damage mechanism, and (2) determine the point where the accumulated damage has become severe enough that the overall structural integrity of the component under consideration has been compromised in terms of safety and reliability. The association between AE signals and their corresponding damage mechanisms could not be established using the fibre optic sensor. However, the determination of the severity of damage could be established. The detection of the knee in the cumulative event count graphs indicates that the fibre optic sensor can detect the onset and propagation of delamination in a sample. For the purposes of non-destructive evaluation, and given the sensitivity of the fibre optic sensor, the latter suggests itself as a better method.

APPENDIX A

EXPERIMENTAL PROCEDURES AND SIGNAL PROCESSING DETAILS

Appendix A: Experimental Procedures And Signal Processing Details

This appendix lists all the experimental procedures and signal processing details for the tests undertaken. The purpose of this appendix is to provide a simple step by step guide to setting up the system and equipment, and also as a quick reference of the values chosen for specific equipment.

In Chapter 5 a detailed explanation of the Mach-Zehnder interferometric system is given. However, this system needed to incorporate an active homodyne unit to ensure that the phase of the reference arm was maintained at quadrature, and therefore maintain optimum sensitivity. A step by step guide to the connections between these two systems is given, as is the experimental procedure needed to ensure the correct characterisation of the fibre-optic AE detection system (section A.1).

Once the characterisation tests revealed that the detection system was capable of detecting AE, the optical fibre sensor was embedded in a composite material, which was subsequently loaded in tension to failure (chapter 6). The AE emanating from the composite material was detected by the fibre optic sensor and a piezoelectric transducer and these signals were inputted to a data acquisition and analysis unit (AET5500). This unit needed to be programmed to acquire and analyse these signals. The binary data from the AET5500 was converted to ASCII format using the BAWIN software so that the post-analysis of the data could be done using Excel. All the experimental techniques and procedures and the relevant signal processing details used in the production of the results in Chapter 6 are given in section A.2.

In chapter 7, specialised composite specimens were loaded in tension to failure and the resulting AE was detected using the piezoelectric transducer. The signals obtained were analysed in the time domain and frequency domain using the AET5500 and the Hewlett Packard HP89410A Spectrum Analyser respectively. The signal processing details relating to the production of the results documented in chapter 7 are given in section A.3.

A.1 Experimental Procedures And Signal Processing Details Involved In The Characterisation Of The Fibre-Optic Detection System.

Before tests are done on the detection system one must ensure that the complete detection system is connected correctly. The following figure shows the steps involved in the detection system set-up that ensures that the demodulator transforms the output from the interferometer into an electrical signal proportional to the differential optical phase signal.

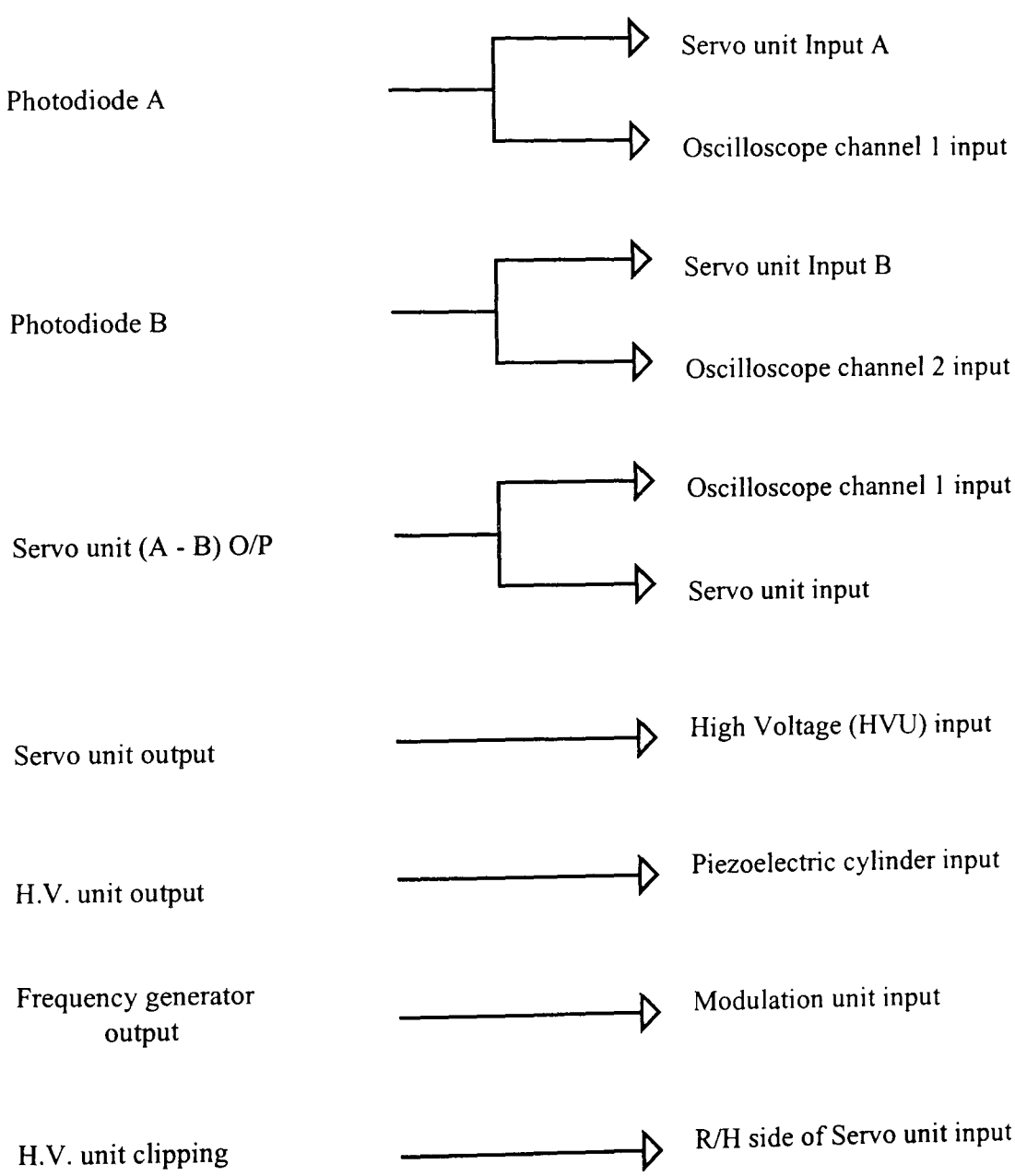

Figure A.1 Connections between the interferometric system and homodyne unit.

The High Voltage Unit (HVU) of the homodyne unit must be on the 100-150V setting and the knob adjusted to give 124 Volts and 0.029 amps.

A.1.1 Obtaining the anti-phase signals

When using the Active homodyne unit to obtain the anti-phase signals the following procedure must be undertaken:-

(a) The Servo Unit 'Servo Type' is switched to position 0 (i.e. the servo is out of lock).

(b) The differential amplifier output (A-B) was monitored on oscilloscope channel 1 (set on AC instead of DC V/div.)

(c) The Frequency Generator is switched on at 500Hz with 5V amplitude.

(d) The Servo Unit Modulation is set to approximately level 1 to produce two signals in anti-phase (figure A.3). Too little or too much modulation causes a loss of the required signals. The fringe output is monitored on the scope as the PZ phase shifter is modulated by a ramp waveform (figure A.2).

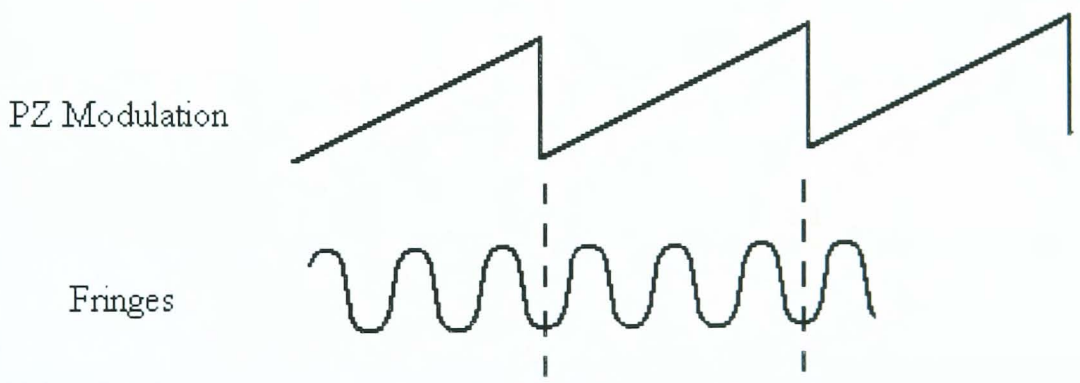

Figure A.2 PZ modulation and fringe output

(e) Adjust the Polarisation Controller (i.e. reels 1, 2 and 3) to give maximum fringe visibility.

It is important to check the optical alignment and optimise the launching optics and polarisation controllers to give good fringes before any attempt to test out the embedded sensor.

The expected outputs from the interferometer are two anti-phase signals like those illustrated in figure A.3.

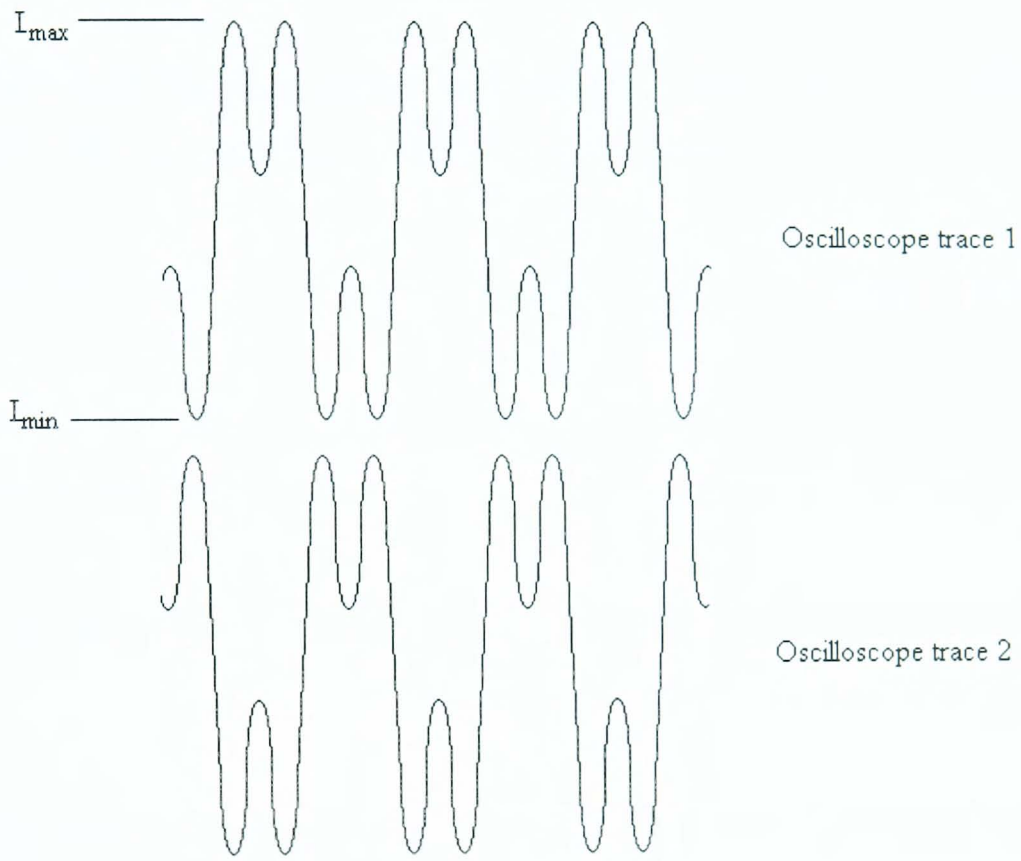

Figure A.3 The anti-phase output signals from the Mach-Zehnder interferometer.

The fringes (see figure A.2) were measured and the visibility (or fringe contrast) could be calculated :

Fringe maximum $I_{max.}$=3V

Fringe minimum I_{min}=0.04V

$$\text{Visibilty} = \frac{I_{max} - I_{min}}{I_{max} + I_{min}} = \frac{3 - 0.04}{3 + 0.04} = 0.973 = 97.3\%$$

A.1.2 Detecting Acoustic Emission signals.

In order to characterise the fibre-optic system to known disturbances the following procedure was implemented:-

(a) Initially, the Frequency Generator is switched off thus removing any form of modulation, or alternatively, switch off the Servo Unit Modulation.

(b) The Servo unit A-B output (with gain A-B set at X100 or even this could be set at X10 or X1) is connected to an Oscilloscope channel.

(c) The Servo Unit 'Servo Type' is switched to position 1 (instead of position 0)

(d) The result should be that the Mach-Zehnder Interferometer signal is maintained at Quadrature ($\pi/2$).

(e) The Servo offset coarse should be off and the Offset fine should be midway i.e. zero.

(f) The A-B output is fed into a Kemo high pass filter (3dB point: 100kHz) and the output from the filter is monitored using a digital oscilloscope.

A.1.4 Signal Processing Details

In figure A.4 the block diagram shows the set-up used for the detection of AE emanating from a composite loaded in tension to failure. This set-up was also used for the characterisation tests. The following bullet-points indicate the relevant processing details for this type of test.

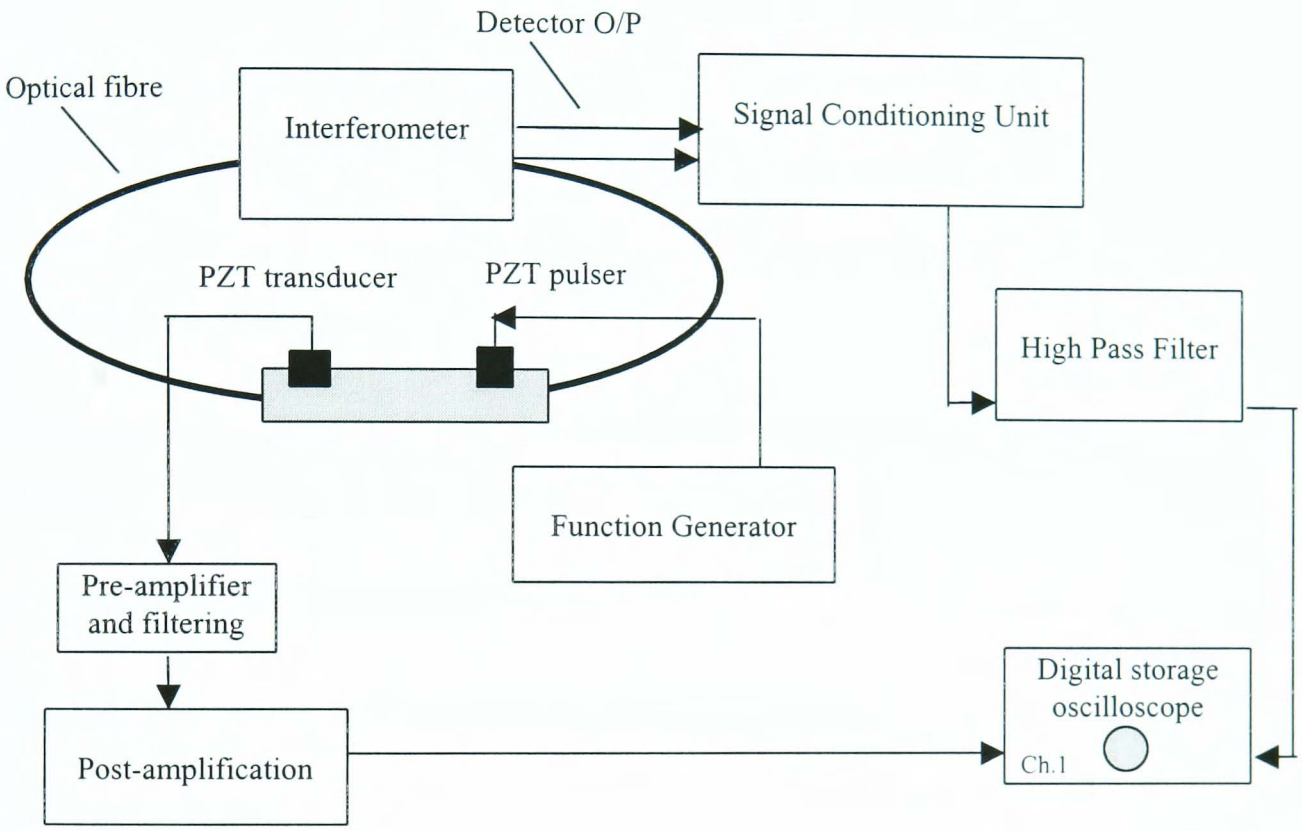

Figure A.4 The detection of AE using the optical fibre sensor and the piezoelectric transducer.

- Interferometer

Mach Zehnder optical fibre interferometer

- Signal Conditioning

Custom built signal conditioning unit by Mirage instruments which includes :-
(i) Differential amplifier (Gain A=X5, Gain B=X5, Gain A-B=X100)
(ii) Servo unit (Modulation value approximately 1)
(iii) Reset circuitry
(iv) High voltage (HV) supply (124V)

- **Filtering**

Kemo Dual variable filter :- Range of cut-off frequency 1Hz to 100kHz
Gain range - 1, 3, or 10.
Settings: 100kHz highpass filter with unity gain

- **Digital Storage oscilloscope**

LeCroy 9410 Dual 150MHz Oscillator.
Settings: timebase 0.5ms, Volts/div 50mV

- **Function Generators**

A Krohnhite oscillator and a Thandar 2MHz function generator.
Settings: Sinusoidal- 500Hz and 5V

- **Pre-amplifier and filtering**

Pre-amplification of 40dB and 100kHz-1MHz filter unit

- **Post amplification**

Gain Setting 12 (30dB) through the AET5500 front-end

A.2 Experimental Procedures And Signal Processing Details Involved In The Detection of AE From Composite Materials Under Tension.

In figure A.4, the post-amplification unit is the data acquisition and analysis unit, the AET5500. In the composite tests this unit is used to analyse the signals detected by the optical fibre sensor and the piezoelectric transducer. However, the AET5500 unit must be fully programmed to ensure that (i) its acquisition boards are ready to store the incoming signals from two of its channels and (ii) to instruct it to analyse the signals and provide the relevant information. The following steps ensured that all the necessary information was detected and analysed.

{Note :- <sp> is short for <space>. If help is needed press Shift / (?).}

Sensor 1: OFS

Sensor 2: PZT

(i) Setting up the parameters.

- It is possible to change the time intervals and no. of intervals presented on the graphs.

(ii) Setting up displays.

• [Ctrl + S] U S 1 <sp>	{Set Up displays for Sensor 1}
• E S T <sp>	{Plot EventS against Time}
• [Ctrl + L] D S 1 <sp>	{List Displays for Sensor 1}
• [Ctrl + S] U S 2 <sp>	{Set Up displays for Sensor 1}
• E S T <sp>	{Plot EventS against Time}
• [Ctrl + L] D S 2 <sp>	{List Displays for Sensor 1}

(iii) Setting up the Threshold level.

- [Ctrl + S] T S 1 <sp>0.5V fixed<sp> {Set Threshold for Sensor 1= 0.5V}
- [Ctrl + S] T S 2 <sp>1V fixed<sp> {Set Threshold for Sensor 1= 1V}

(iv) Setting up the system to begin testing and record data.

- [Ctrl + B] R S 1 <sp> {Begin Run for Sensor 1}
- [Ctrl + B] R S 2 <sp> {Begin Run for Sensor 2}
- [Ctrl + Q] D *filename* <sp> {Queue Data recording for *Filename*}
- [Ctrl + B] E *filename* <sp> Y S 1 {Begin Event recording to *Filename*....Yes for Sensor 1}
- Recording reject ratio =1 <sp>
- [Ctrl + B] E *filename* <sp> Y S 2 {Begin Event recording to *Filename*....Yes for Sensor 2}
- Recording reject ratio =1 <sp>

(v) Outputting the events to screen to view real-time data.

- [Ctrl +O] E S 1 <sp> {Output Events for Sensor 1}
- [Ctrl +O] E S 2 <sp> {Output Events for Sensor 2}

(vi) ***** Start tensile loading the composite sample. *********

(vii) Ending the test run and data recording.

- [Ctrl + E] R S 1 <sp> {End Run for Sensor 1}
- [Ctrl + E] R S 2 <sp> {End Run for Sensor 2}

- [Ctrl + E] D <sp> {**E**nd **D**ata recording}
- [Ctrl + B] P <sp> {**B**egin **P**layback}
- Queue + P *filename* <sp> {Queue **P**ost-processing for *filename*}

(viii) Displaying graphs.

- [Ctrl + D] E S T S 1 <sp> {**D**isplay **E**vent**S** v **T**ime for **S**ensor **1**}
- [Ctrl + D] T E S T S 1 <sp> {**D**isplay **T**otal **E**vent**S** v **T**ime for **S**ensor **1**}
- [Ctrl + D] Shift 8 <sp> {Autoscales current graph}
- [Ctrl + A} E S <sp> {Changes sc**A**le for **E**vent**S** axis}

(ix) Ending the playback of recorded data.

- [Ctrl + E] P <sp> {**E**nd **P**layback}

The step by step guide to setting up the AET5500 does not include any details regarding the post-amplification. The adjustment of gain could only be made by manually adjusting the gain switch on the front-end of the unit. The values of gain used in these tests are the same as those mentioned in section A.1.4.

From this guide it can be seen that it is possible to display graphs on the AET5500 screen. However, it is necessary to set-up all the graphs before testing has begun, and it was not possible to import these charts into word processing packages. Therefore, the binary data from the AET5500 had to be converted to ASCII so that the data could be analysed with the aid of a spreadsheet package. The conversion of binary data to ASCII would done using the BAWIN software package.

BAWIN is a Microsoft Windows application that converts AET5500 **binary** files to **ASCII** files. The ASCII files created by BAWIN can be imported into spreadsheet, data analysis, and graphing programs for statistical analyses and display of the data. The ASCII files generated by BAWIN, in this particular case, are in the **event data for sensors** format. This type of file is in column format which can be imported into spreadsheet, data analysis, and graphing programs.

To set up the software to convert the binary data from the tests undertaken into ASCII files is done in the following steps :-

(i) Selecting **Binary** from the **File** menu allows one to choose the AET5500 binary data file for translation. The binary data files have the extension xxx.D01

(ii) Selecting **ASCII** from the **File** menu allows one to specify the name of a file in which to store the ASCII data generated from the translation of the data in the binary source file. There is a choice of four formats in which to express the **Time** variable in the ASCII file. The format chosen for these particular tests was the **seconds** choice. The ASCII data files have the extension xxx.TXT

(iii) Select **Event** from the **Data** menu. There are two types of Event data that can be stored in AET5500 binary files : **Sensor** and **Test**. The appropriate item type can be selected from the **Item** menu

(iv) In these particular tests a single sensor is used, therefore sensor event data will be produced. In this case, **Sensor** was selected from the **Item** menu.

(v) To select the specific item number (or in this case the sensor number) to be data processed, the **Number** menu must be highlighted. Since the tests involved two sensors, the number **1** is chosen for the optical fibre sensor and the number **2** for the piezoelectric transducer.

(vi) Selecting **AE parameters** from the **Filters** menu allows definition of filters based on classic acoustic emission characteristics, analogue parameter voltages, and sensor RMS. If the data fail to pass through any one activated filter, the binary data will not be translated to ASCII data. But since the default values are selected no filtering of the binary data will take place, therefore, every event will be translated. Selecting the AE filters menu brings up the following table:-

Parameter	Minimum	Maximum	Enable
Ringdown Counts	0	4095	Yes/No
Event Duration	0	65520	Yes/No
Peak Amplitude	0	117	Yes/No
Energy	0	165	Yes/No
Rise Time	0	65520	Yes/No
Slope	0	65520	Yes/No
Analogue Parameter 1	0	10240	Yes/No
Analogue Parameter 1	0	10240	Yes/No
Analogue Parameter 1	0	10240	Yes/No
Sensor RMS	0	10240	Yes/No

OK	**Cancel**	**Default Values**

(vii) After defining the set-up for conversion of binary to ASCII data, the conversion process is started by selecting **Begin** from the **Translate** menu. The software indicates when the conversion is completed.

Now the data was in ASCII form and could now be analysed and displayed with the aid of **Excel** (spreadsheet software package).

A.3 Experimental Procedures And Signal Processing Details Involved In The Detection of AE From Specially Designed Composite Samples Under Tension.

In these tests specially designed composite samples were loaded in tension to failure and the resulting AE was detected using the piezoelectric transducer. The object of the tests was to monitor the signals in the time domain and the frequency domain. The time domain characteristics were determined using the AET5500. Previous sections indicate the experimental procedures and signal processing details involve in this type of equipment. However, it is necessary to provide the steps taken to set-up the Hewlett Packard Spectrum Analyser has been set up to determine in real time the maximum frequency component in a signal burst and then storing this value in the computer memory.

The frequencies of the acoustic emission generated by damage mechanisms generally occur in the 50-600kHz range. Therefore, the wideband range would have to be set to 550kHz and the central frequency set to 325kHz. This results in the determination of frequencies in the range 50-600kHz.

The procedure to set-up the frequency analyser is as follows:-

(i) Connect the AE output to channel 2.

(ii) Set-up the trigger

- Select the **Trigger** button
- Then chose 'Trigger type' and 'channel 2'

(iii) Selecting the wideband and centre frequencies

- Select **Frequency** button

- Then chose 'Wideband' and insert *550kHz*
- Then chose 'Centre Frequency' and insert *325kHz*

(iv) Selecting mode of input

- Select the **Input** button
- Choose 'Channel 2'
- Then choose '50 ohms standard'

(v) Selecting time duration

- Select **Time** button
- Choose 'Maximum default'

(vi) Type of sweep

- Select **Sweep** button
- Choose 'Continuous'

(vii) Signal Averaging

- Select **Average** button
- Ensure that 'No' is selected

(viii) Marking the maximum frequency

- Select **Marker Function** button
- Choose 'Peak track on'

(ix) Choosing scale

- Select **Autoscale** button

(x) Stating what has to be measured

- Select **Measurement Data** button
- Choose 'Spectrum'
- Then Choose 'Channel 2'

(xi) Determining mode of instrument

- Select Instrument Mode button
- Choose 'Vector'

(xii) Choosing filter type

- Select **Res BW Window** button
- Choose 'Hanning'

(xiii) Now the equipment is set-up (note: Ensure that the **Pause/Single** button is off before starting the test).

Once the AE signals are detected by the piezoelectric transducer the Spectrum Analyser monitors the peak frequency value and stores it to memory. The data obtained from the test is saved as a text file which can be imported into **Excel** for analysis and graphical display.

The sections included in this appendix give all the necessary experimental procedures and signal processing details needed to detect, analyse and display the results given in Chapters 6 and 7.

APPENDIX B

ANALYSIS OF THE RESULTS FROM THE FIBRE OPTIC SENSOR TESTS

B. Analysis Of The Results From The Fibre Optic Sensor Tests

In Chapter 6 cross-ply CFRP specimens were loaded in tension to failure. The resulting AE was monitored using the fibre optic sensor and the piezoelectric transducer. The detected AE data was analysed using event and cumulative count graphs. A total of twelve samples were tested and the results obtained are as follows:-

B.1 Cumulative Event Count- Fibre Optic Sensor Results

FOS Test 1

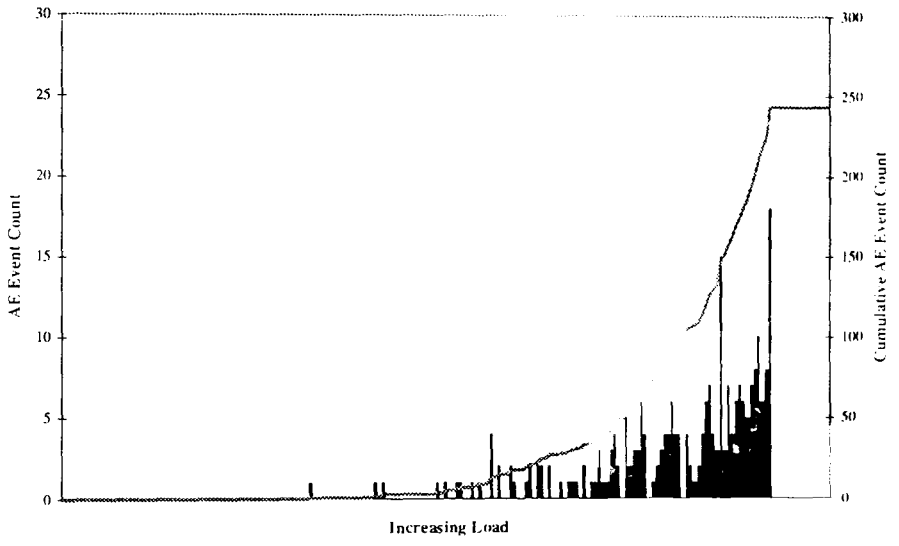

FOS Test 2

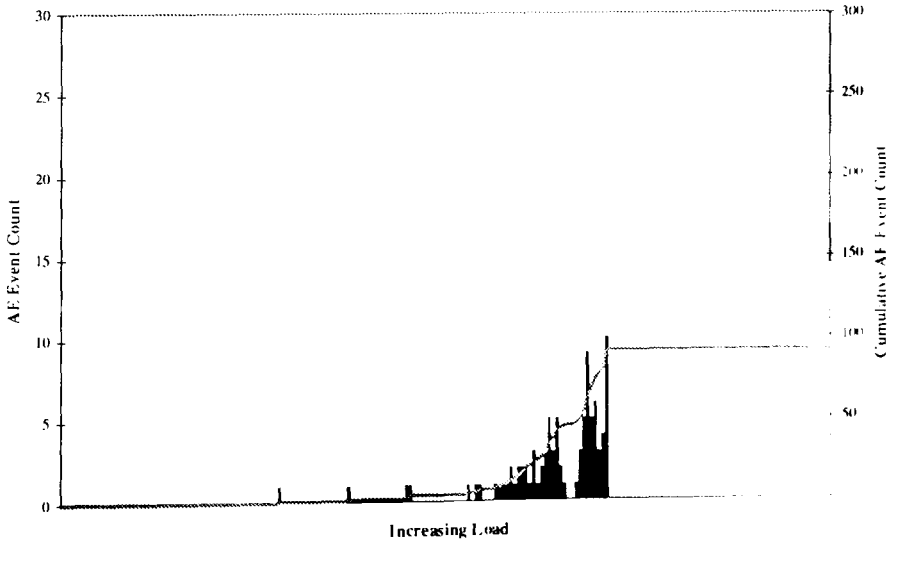

FOS Test 3

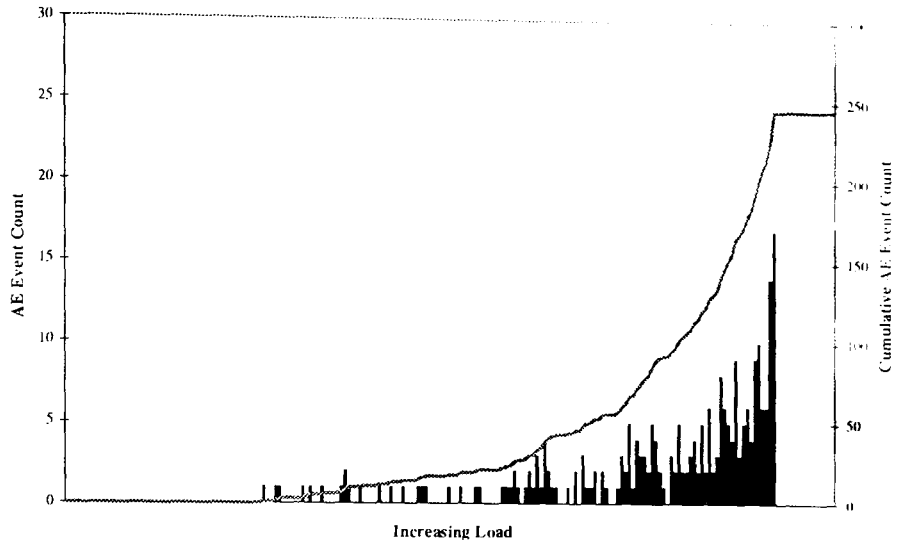

FOS Test 4

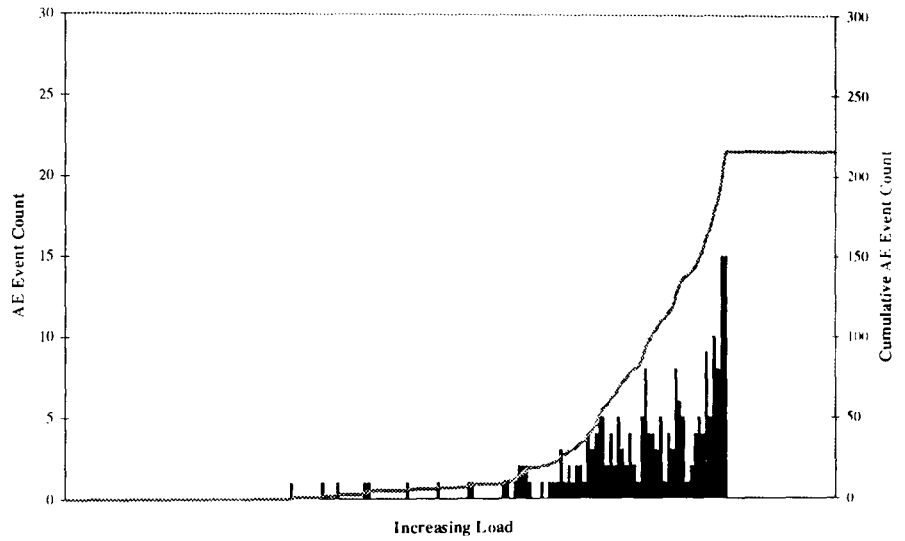

FOS Test 5

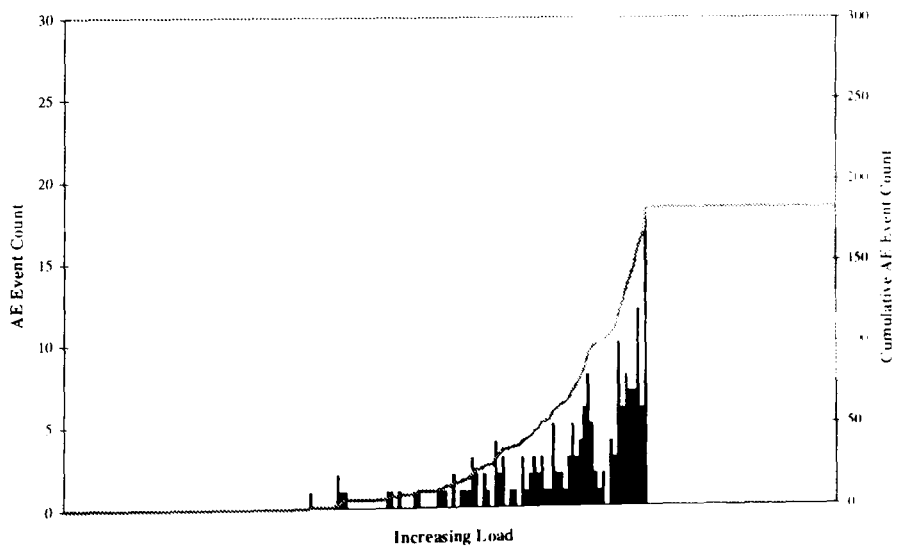

FOS Test 6

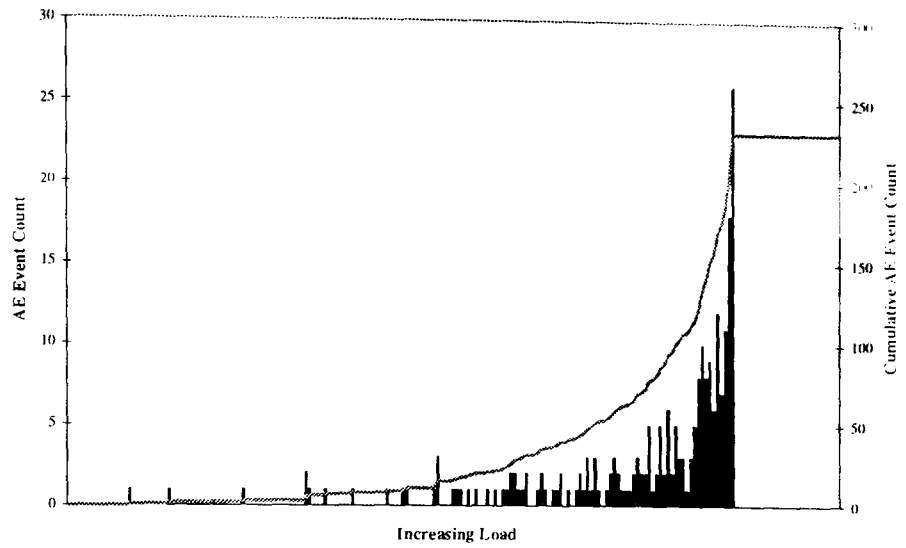

FOS Test 7

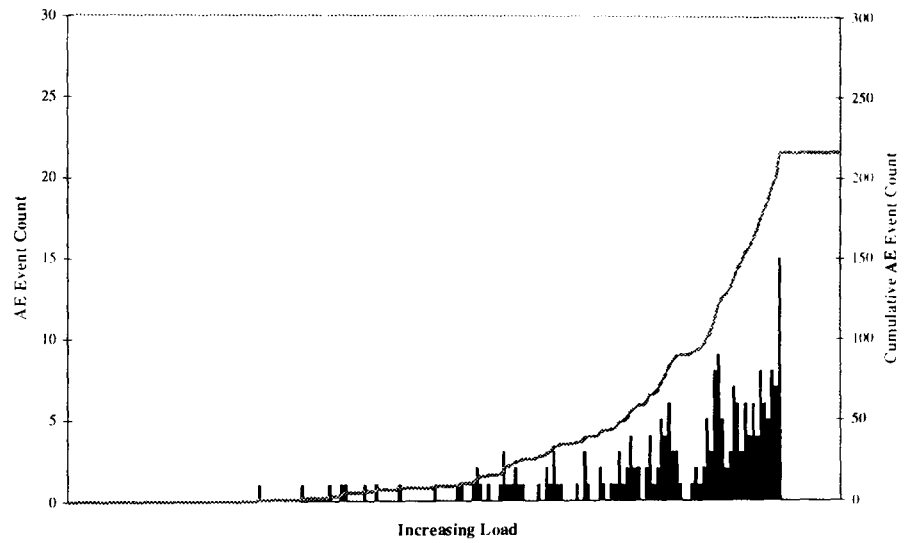

FOS Test 8

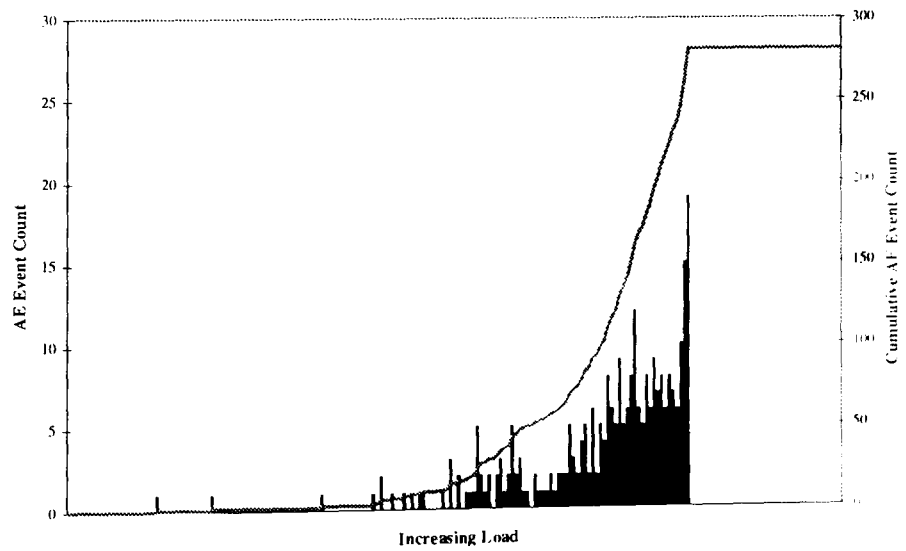

FOS Test 9

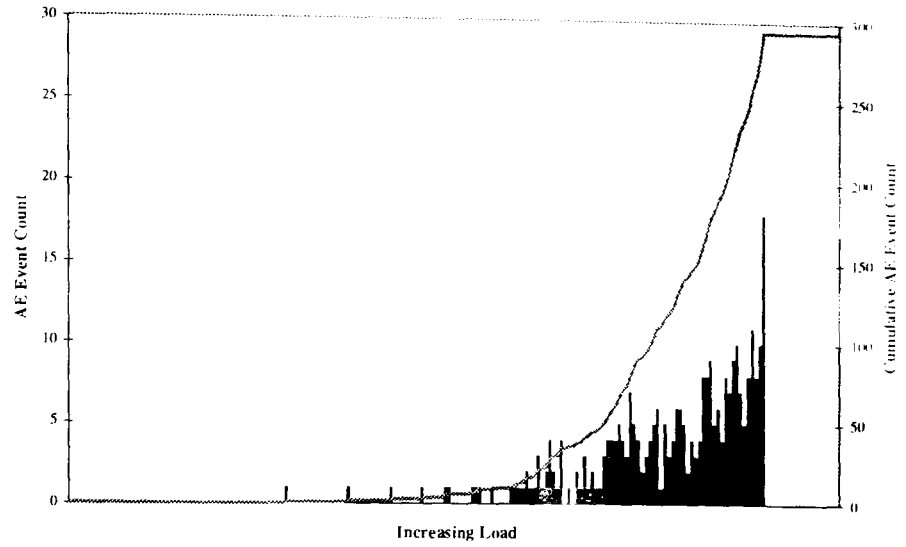

FOS Test 10

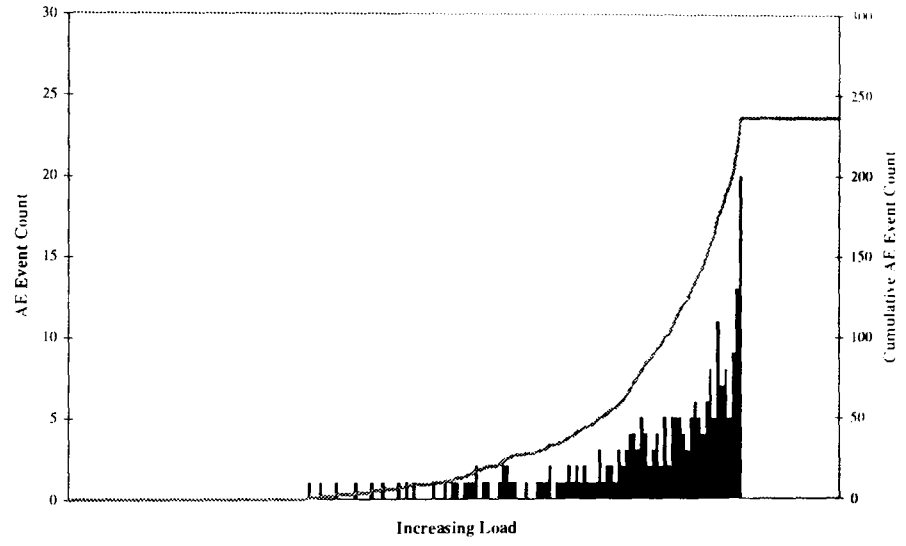

FOS Test 11

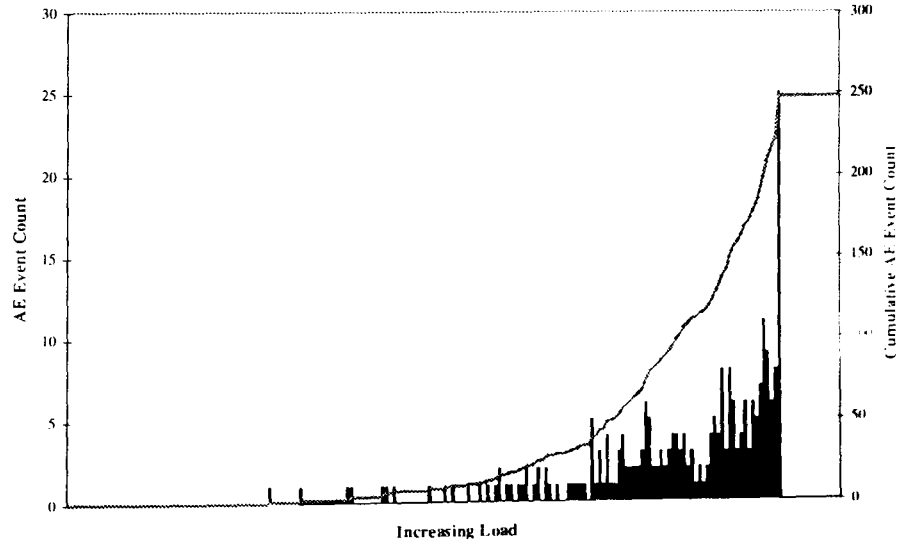

FOS Test 12

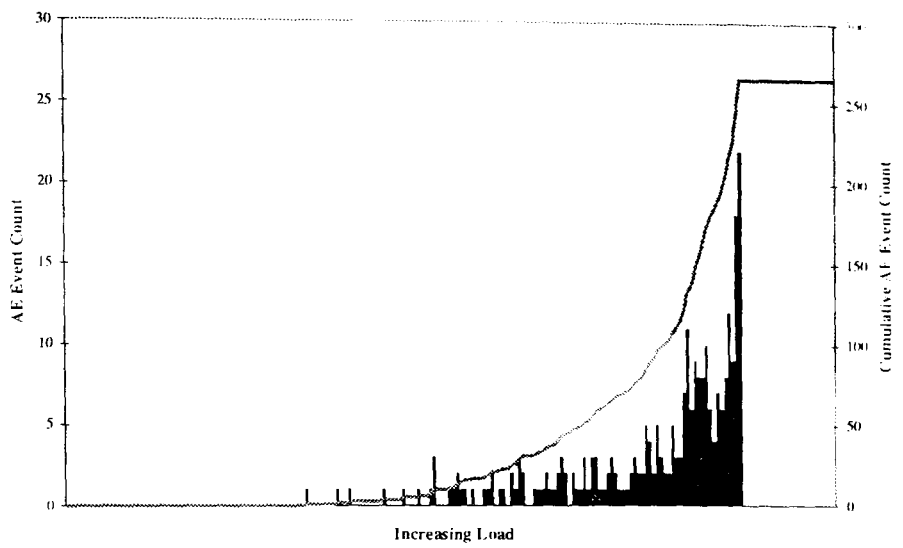
AE Event Count
Cumulative AE Event Count
Increasing Load
0
5
10
15
20
25
30
50
100
150
200
250

B.2 Cumulative Event Count- Piezoelectric Transducer Results

PZT Test 1

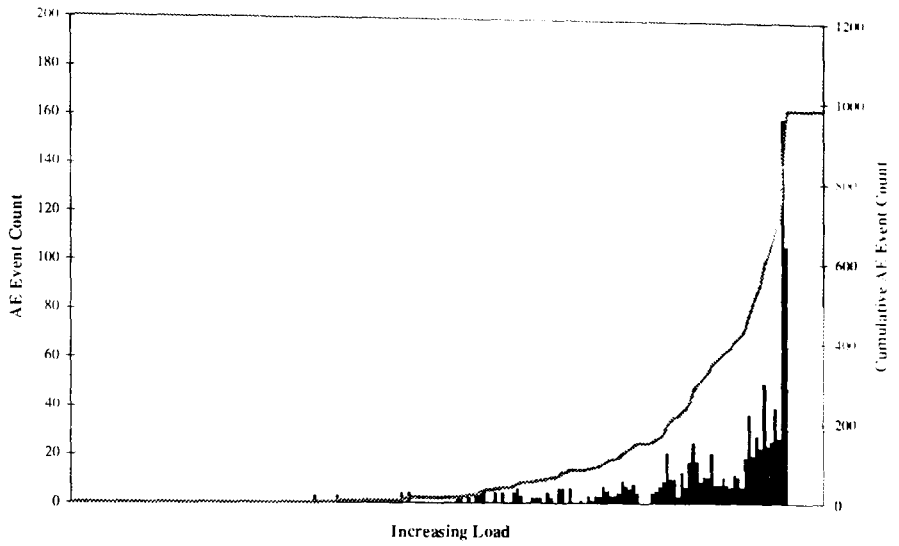

PZT Test 2

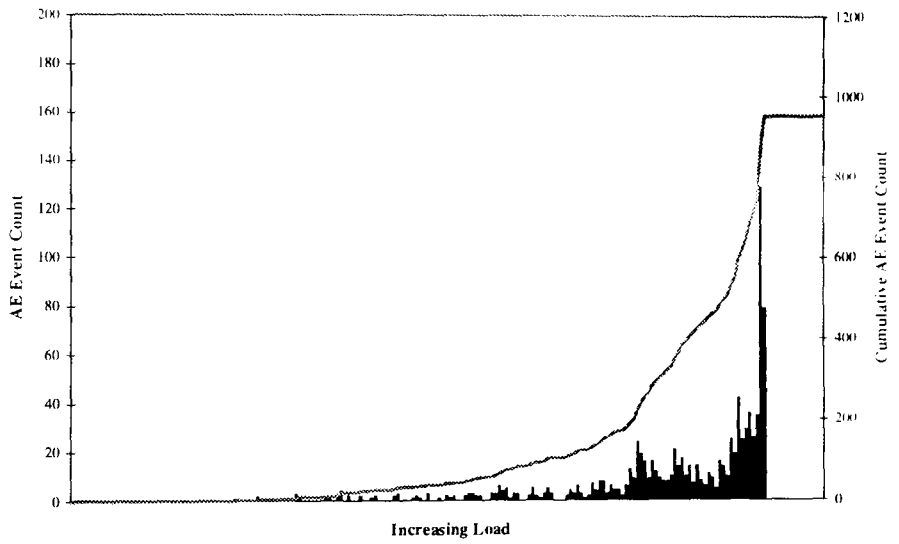

PZT Test 3

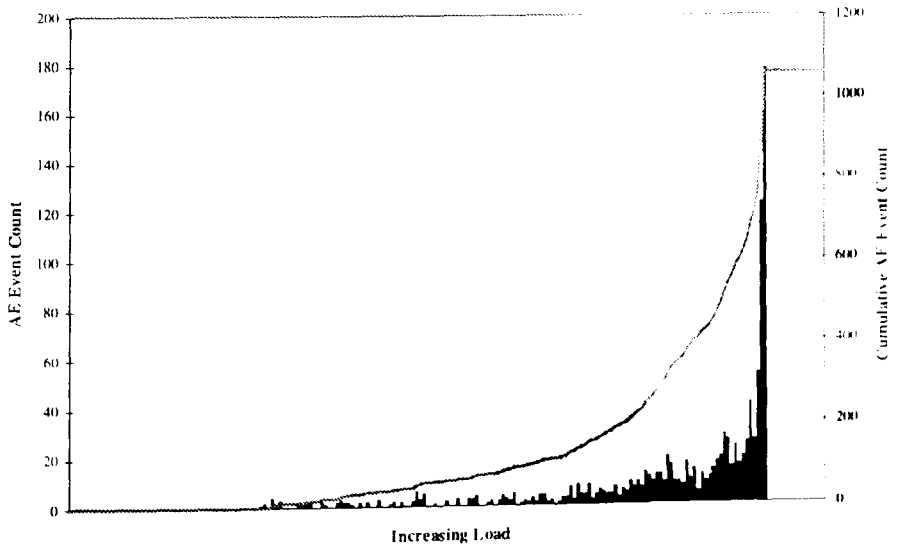

PZT Test 4

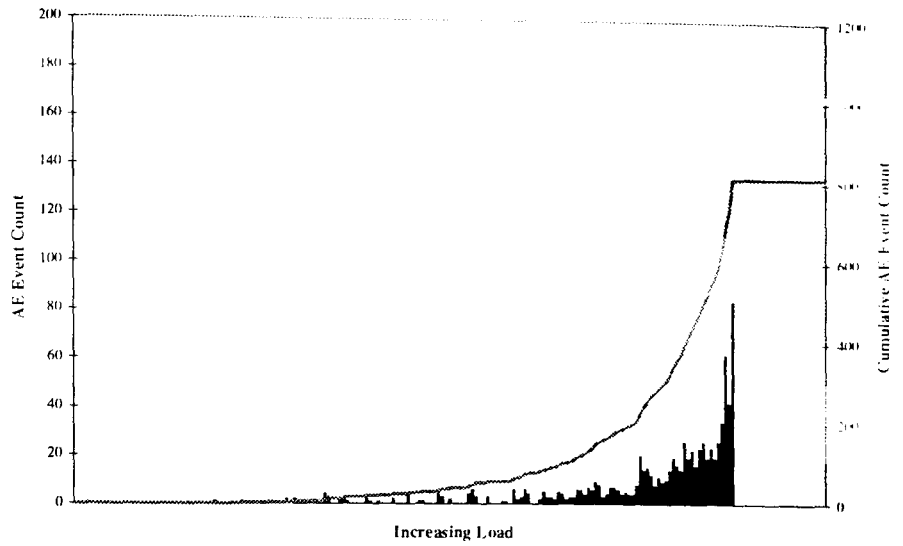

PZT Test 5

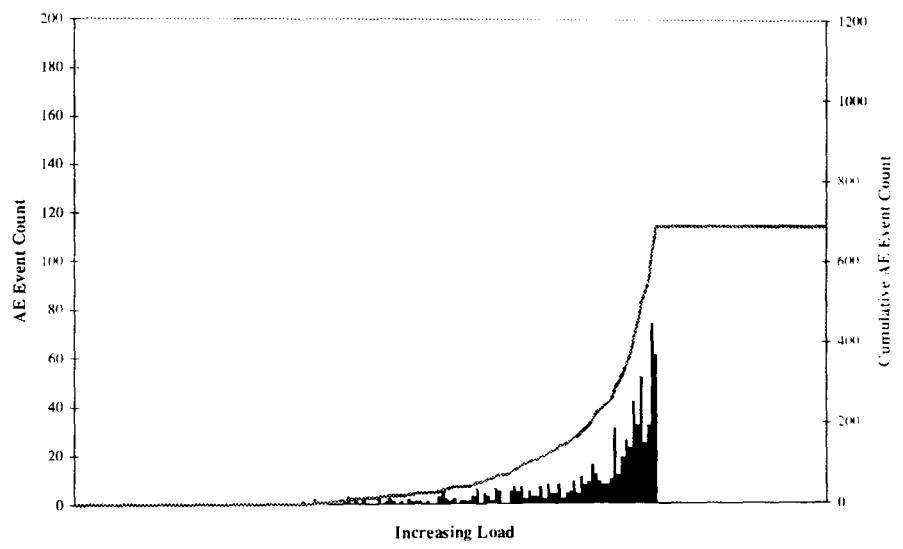

PZT Test 6

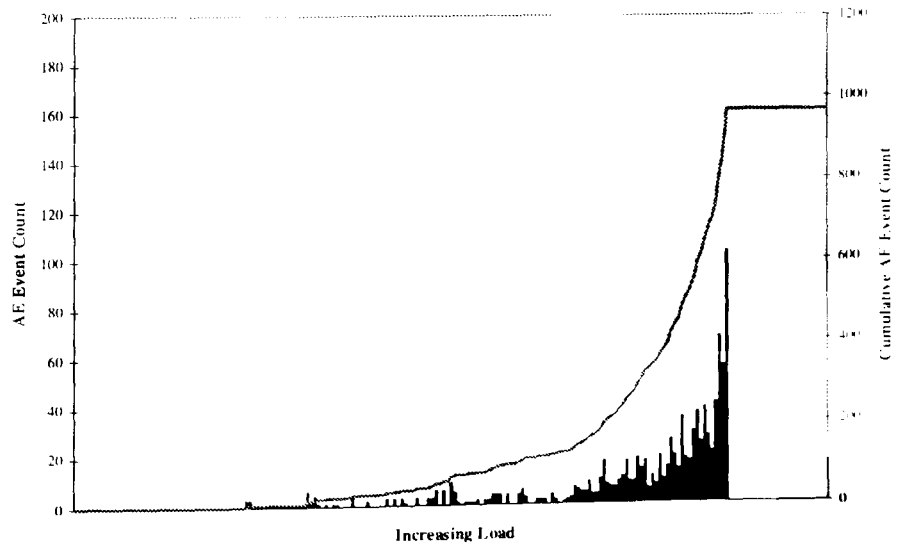

PZT Test 7

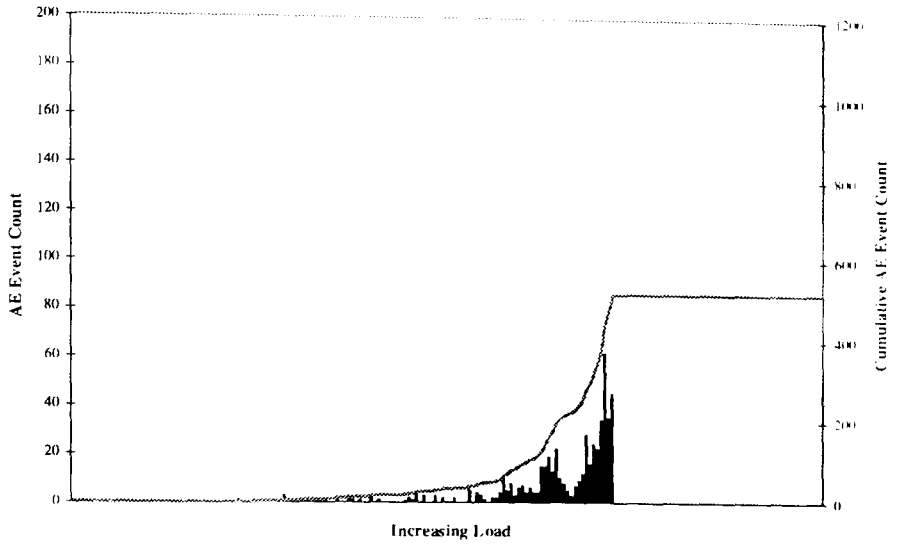

PZT Test 8

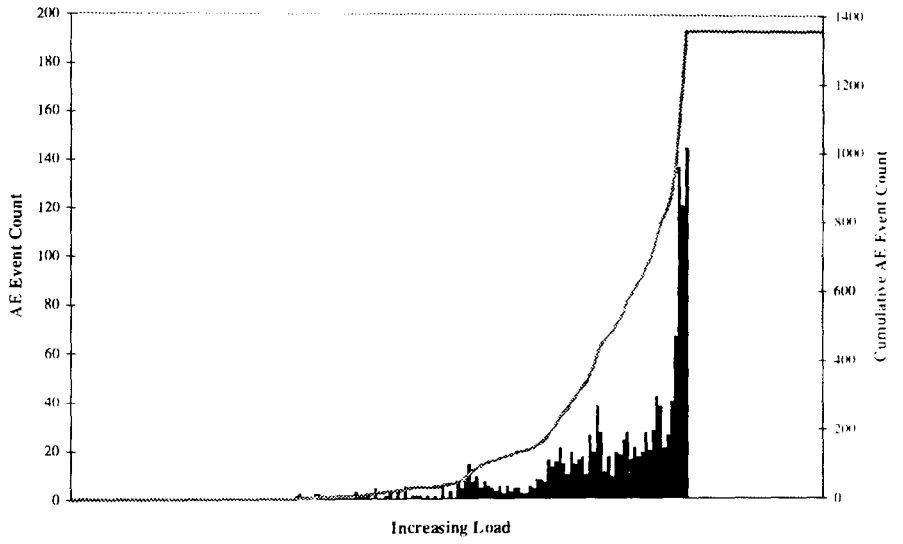

PZT Test 9

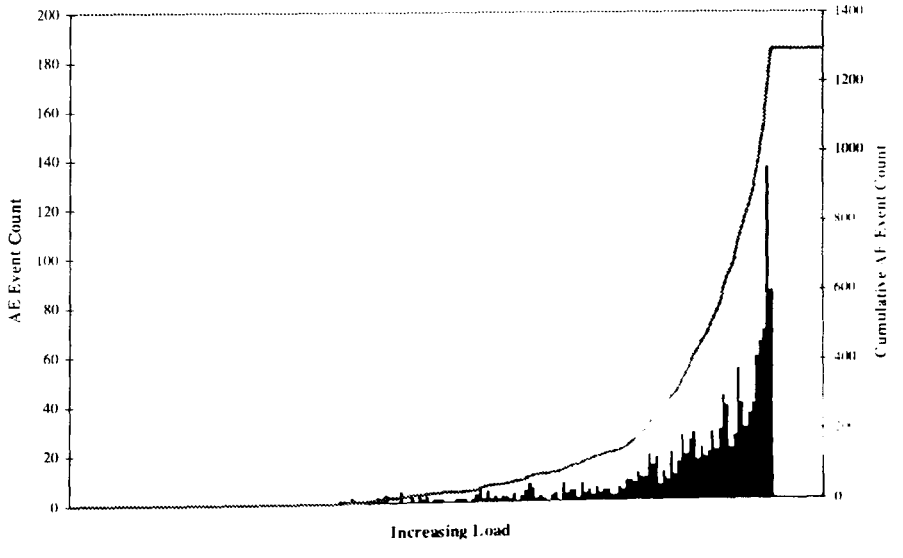

PZT Test 10

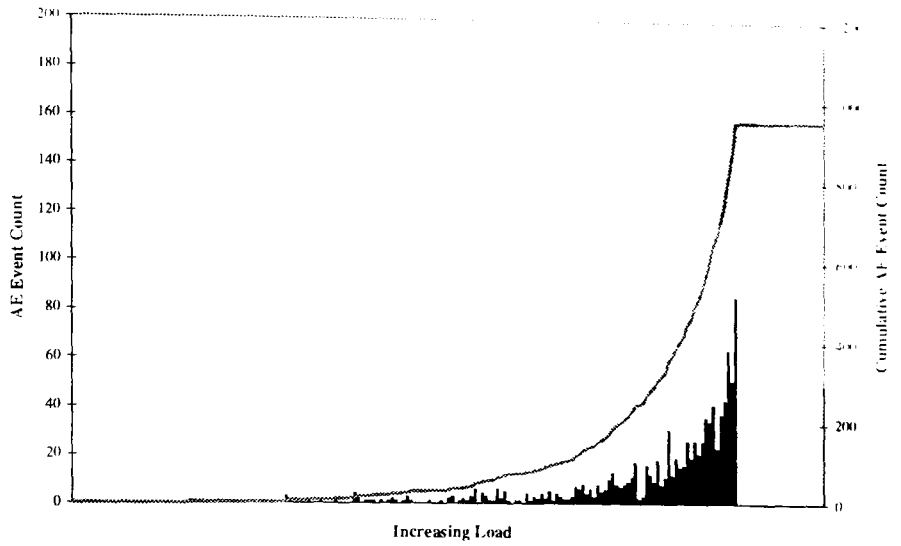

PZT Test 11

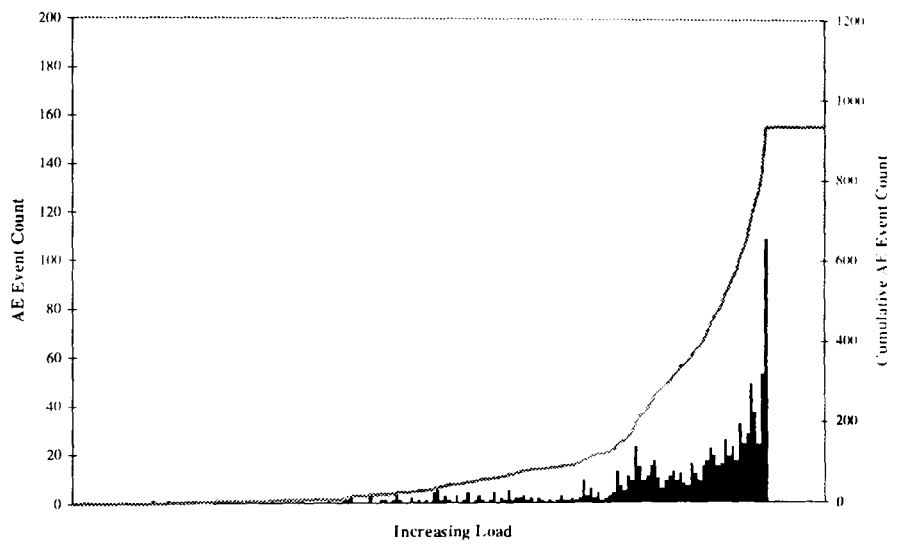

PZT Test 12

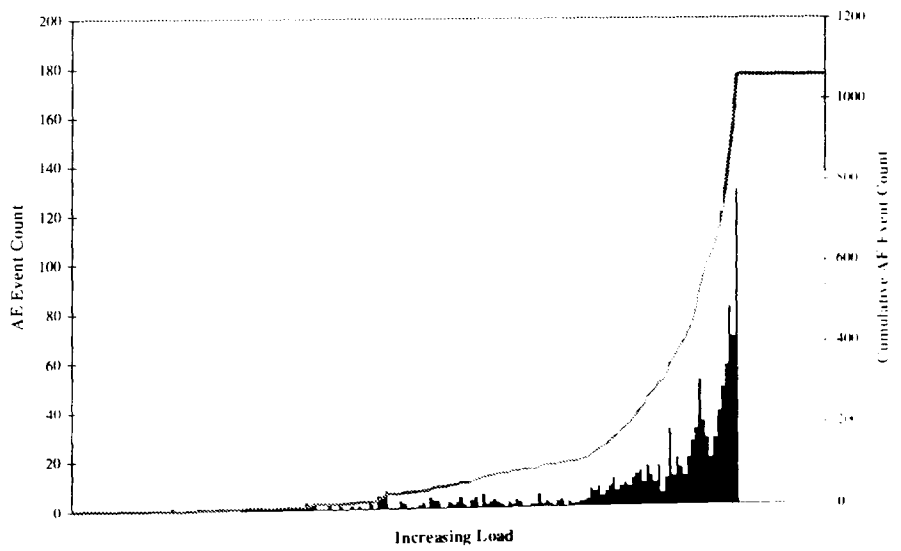

APPENDIX C

AMPLITUDE AND FREQUENCY ANALYSIS OF THE RESULTS FROM THE PIEZOELECTRIC TESTS

C.1 Amplitude Distribution Analysis

The CFRP specimens used in these tests were designed to fail due to certain damage mechanisms. These test specimens were as follows:-

Mechanical Test	No. of Specimens	Test Number
Unreinforced Epoxy bars (tensile)	12	Tests 1A-1M
90° (tensile)	12	Tests 2A-2M
10° (tensile)	8	Tests 3A-3M
Uncured pre-preg bars (tensile)	12	Tests 4A-4M
Teflon insertion (tensile)	12	Tests 5A-5M

The resulting amplitudes of the AE signals obtained from these specimens were plotted in a distribution form. For easy reference, a small illustration of the type of composite tested is placed in the left hand side of each graph. Theses illustrations are as follows:

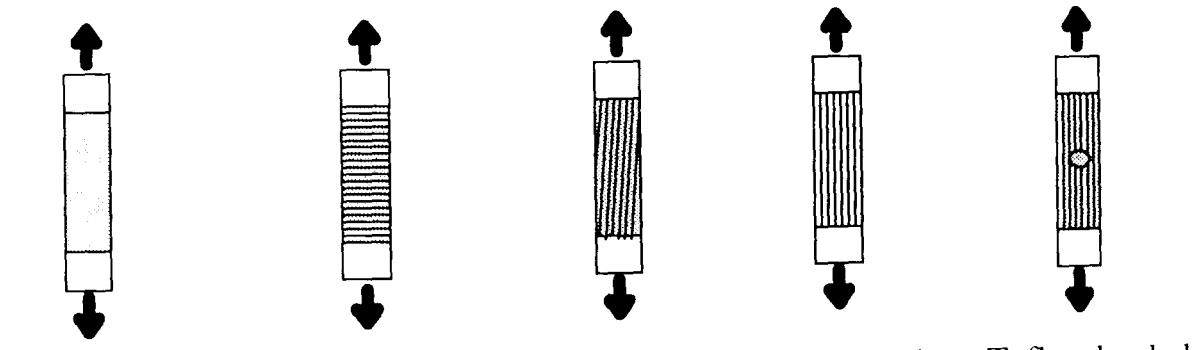

The results from each test were as follows:-

C.1.1 Tensile Loading of Pure Resin Samples

Test 1A

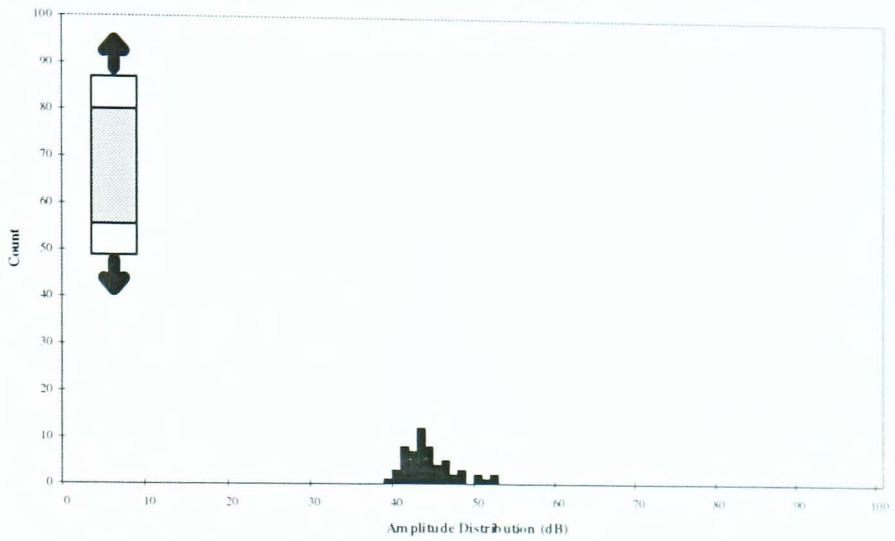

Test 1B

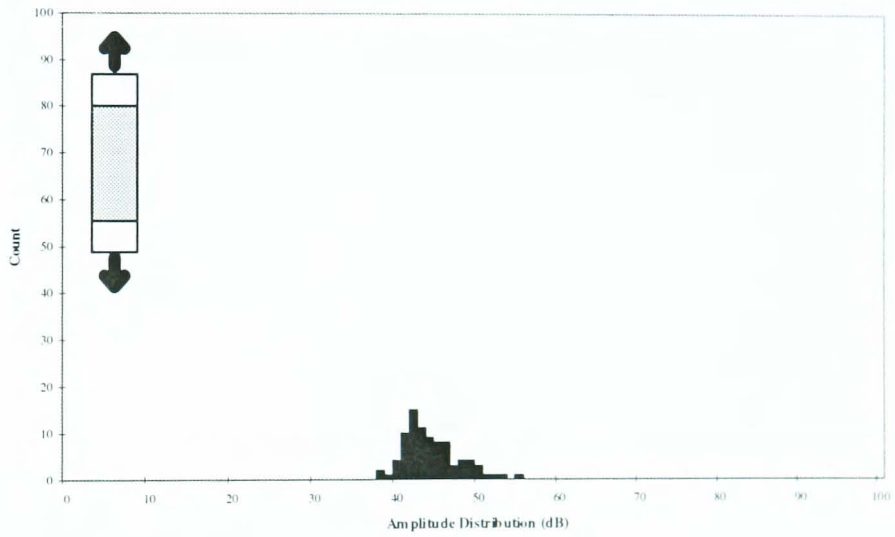

Test 1C

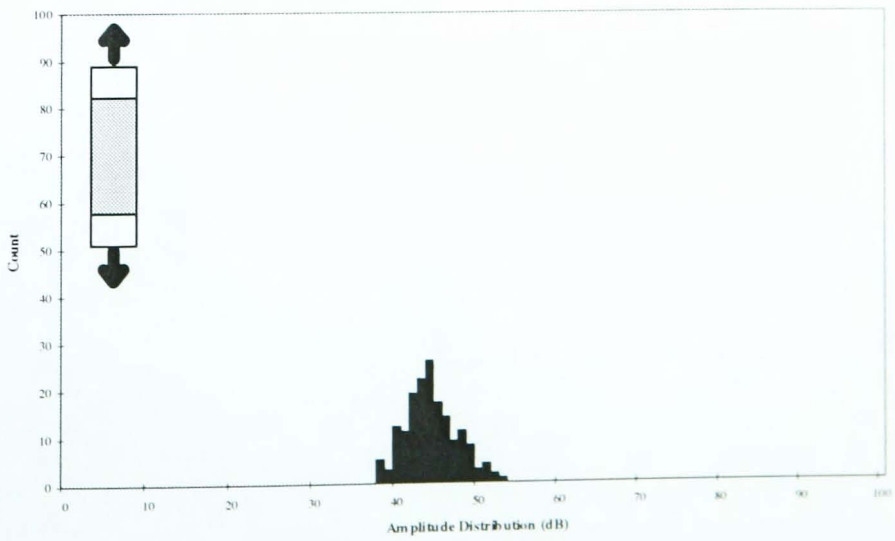

Test 1D

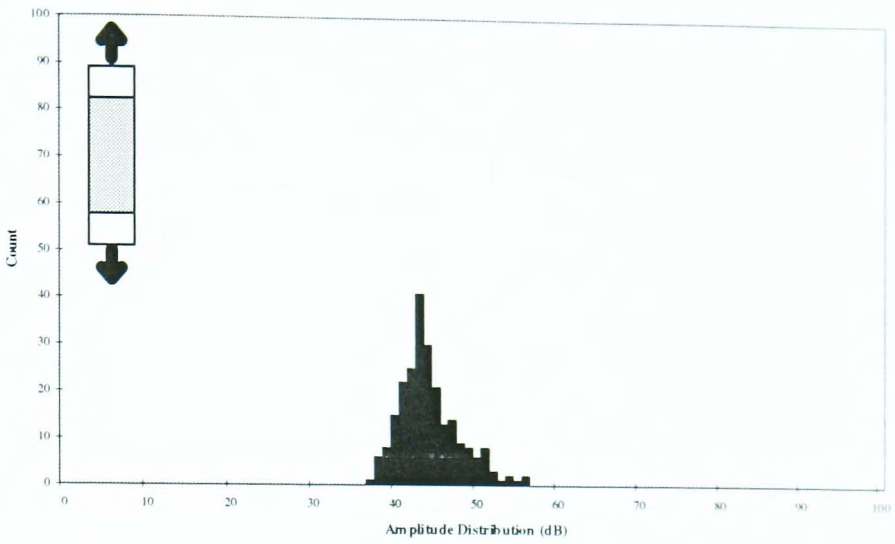

Test 1E

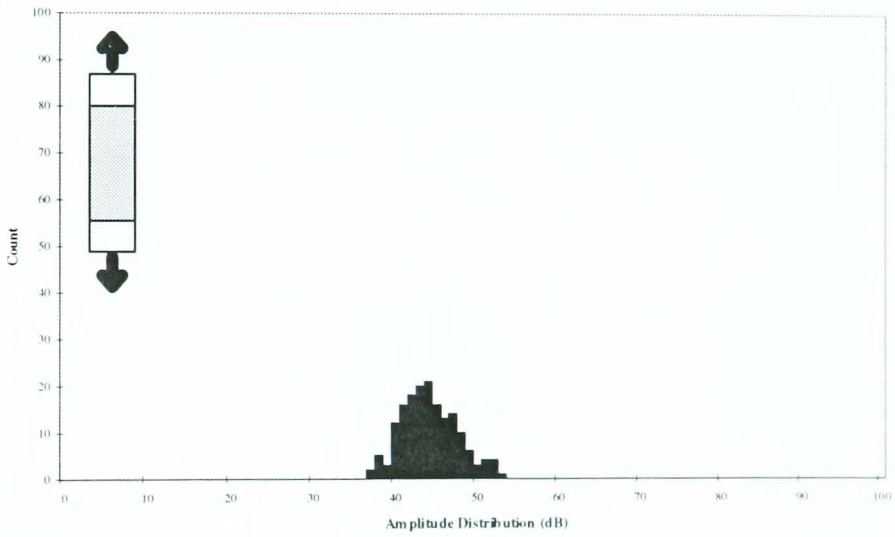

Test 1F

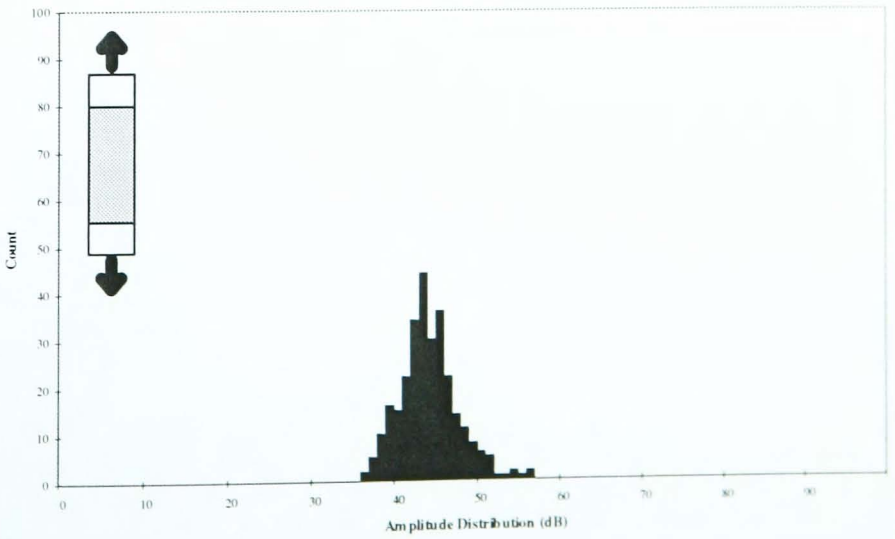

Test 1G

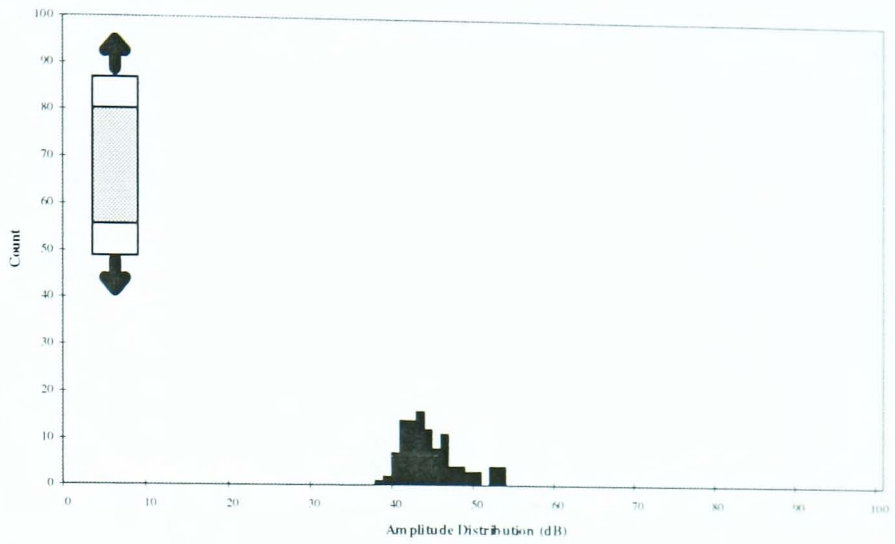

Test 1H

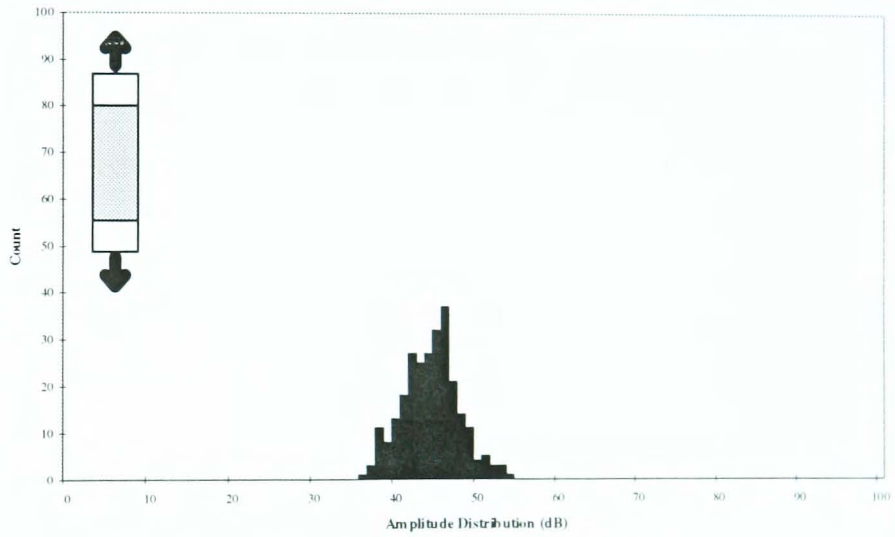

Test 1J

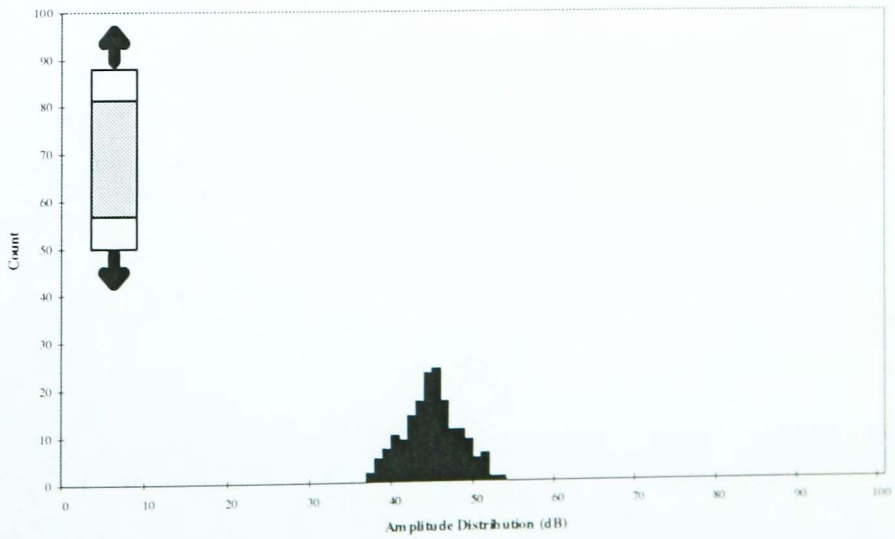

Test 1K

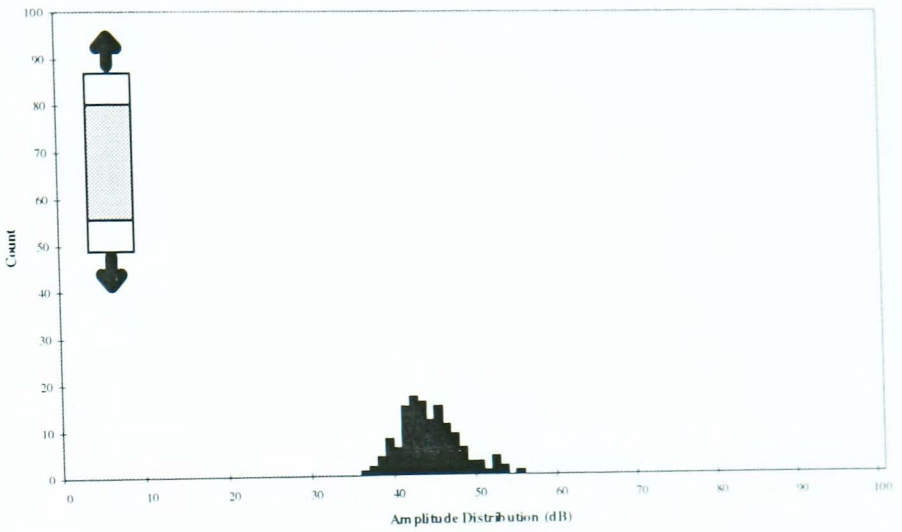

Test 1L

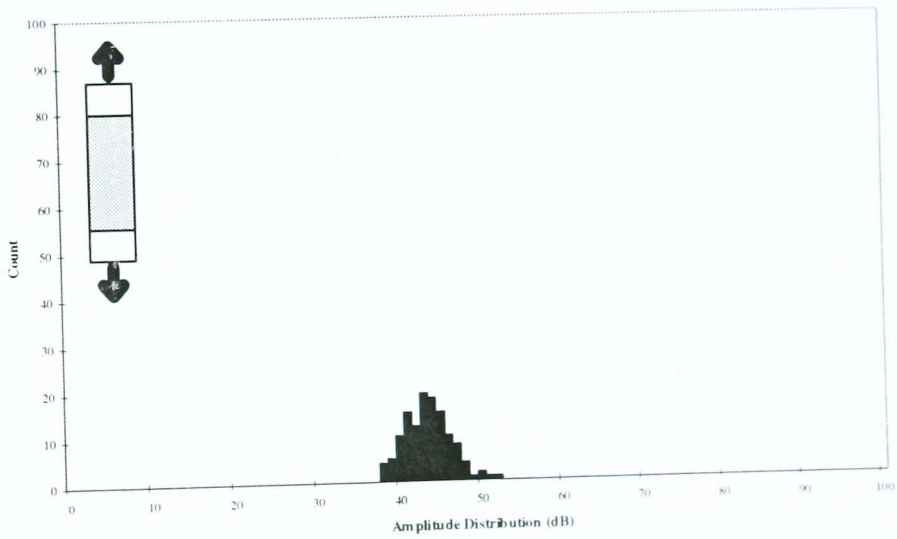

Test 1M

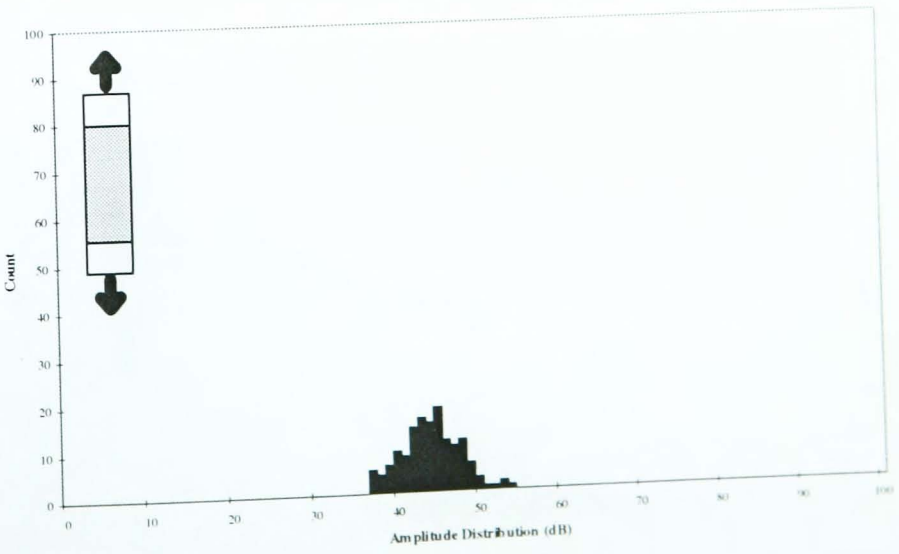

C.1.2 Tensile Loading of 90° Samples

Test 2A

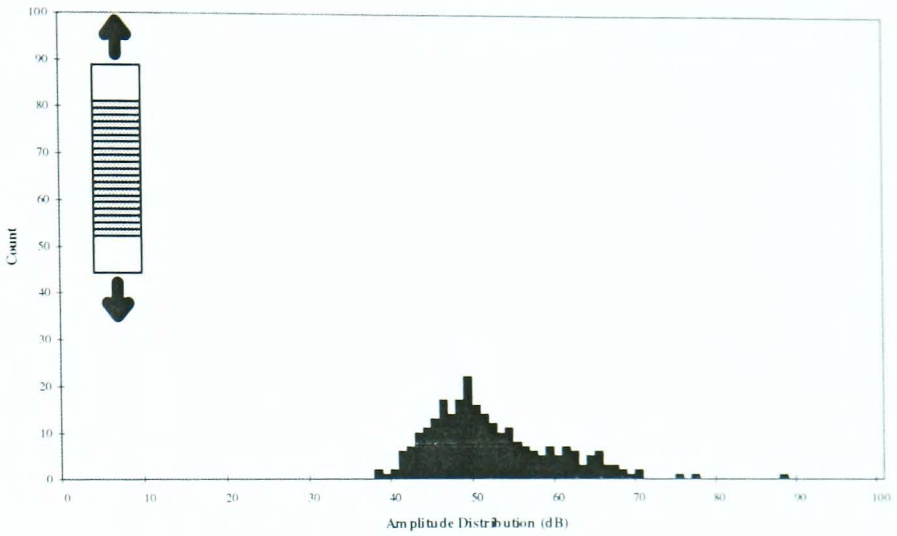

Test 2B

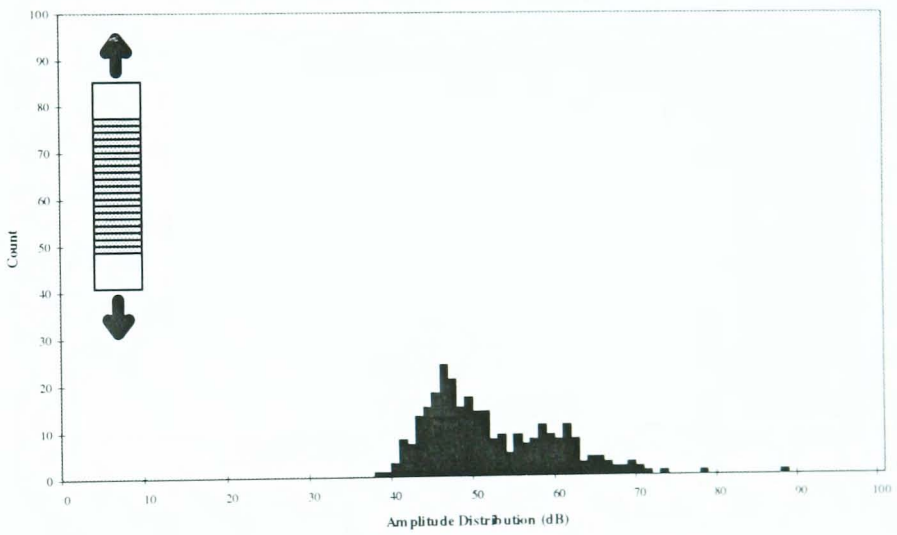

Test 2C

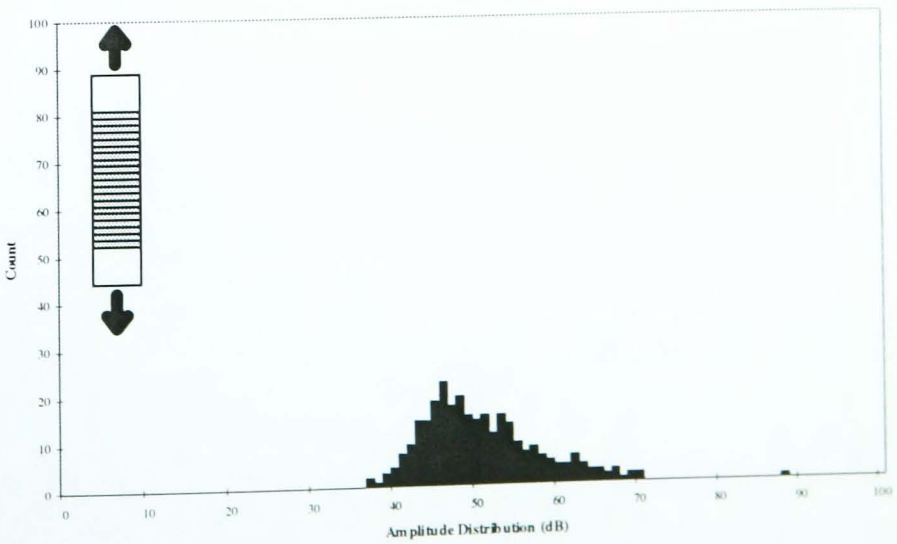

Test 2D

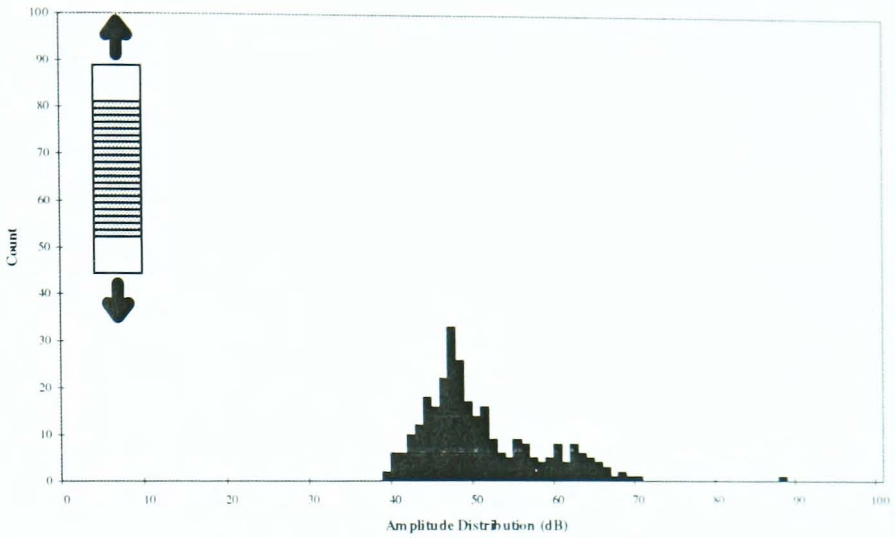

Test 2E

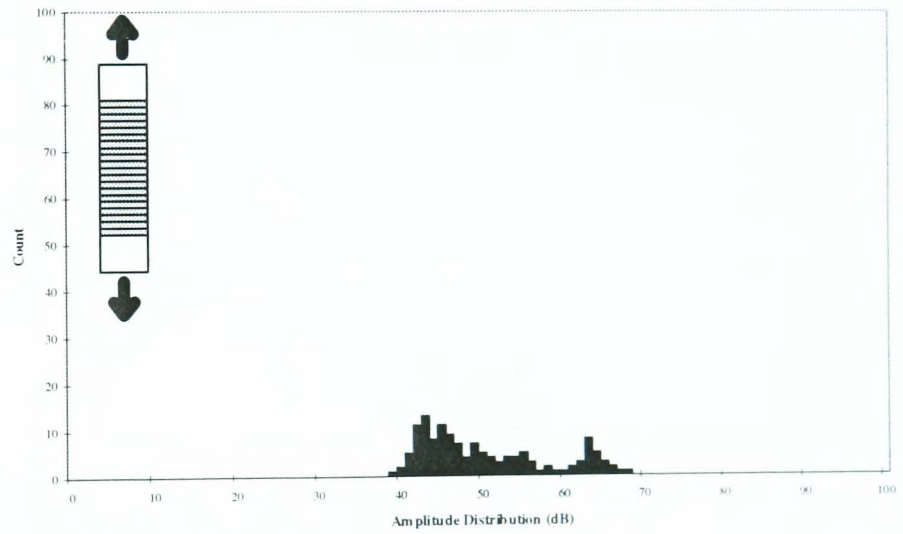

Test 2F

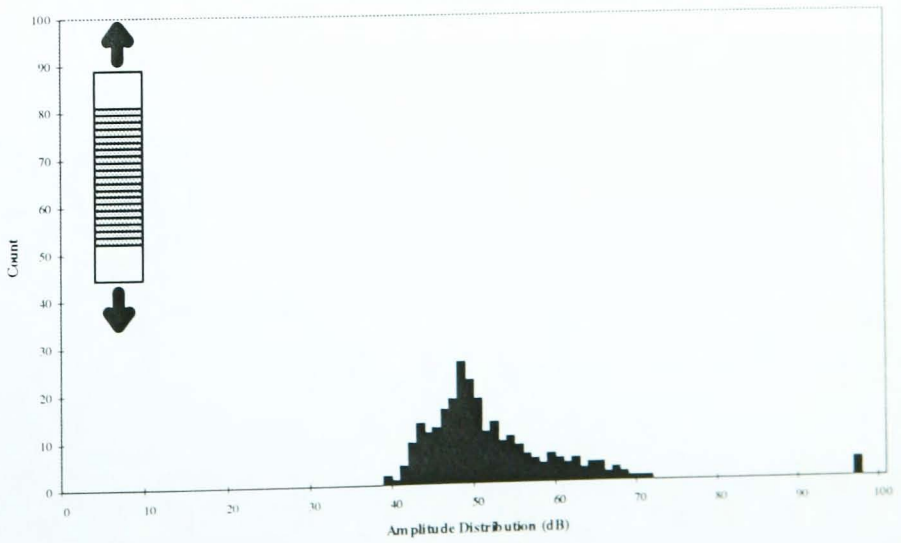

Test 2G

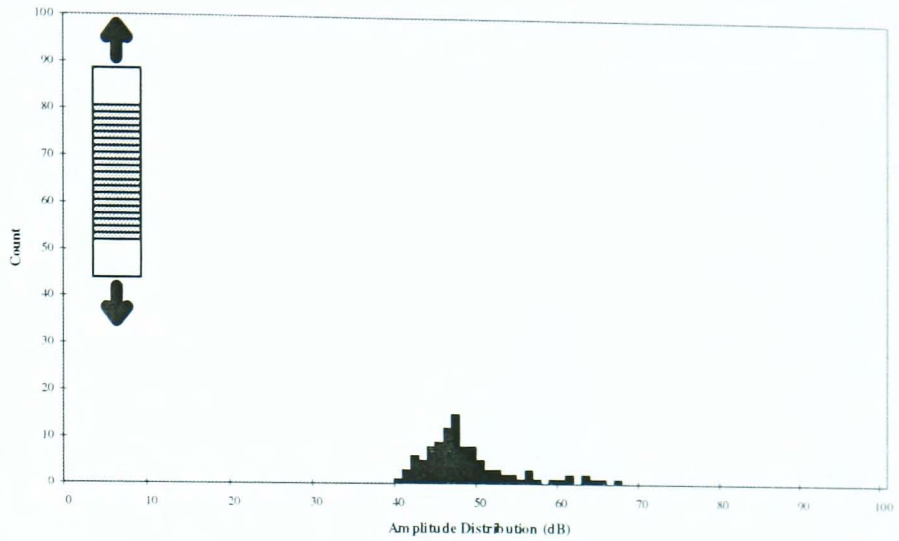

Test 2H

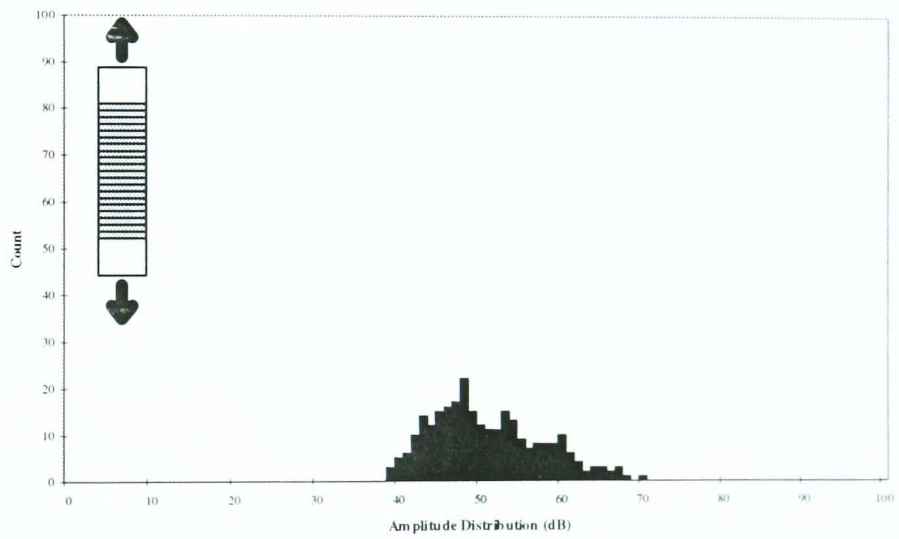

Test 2J

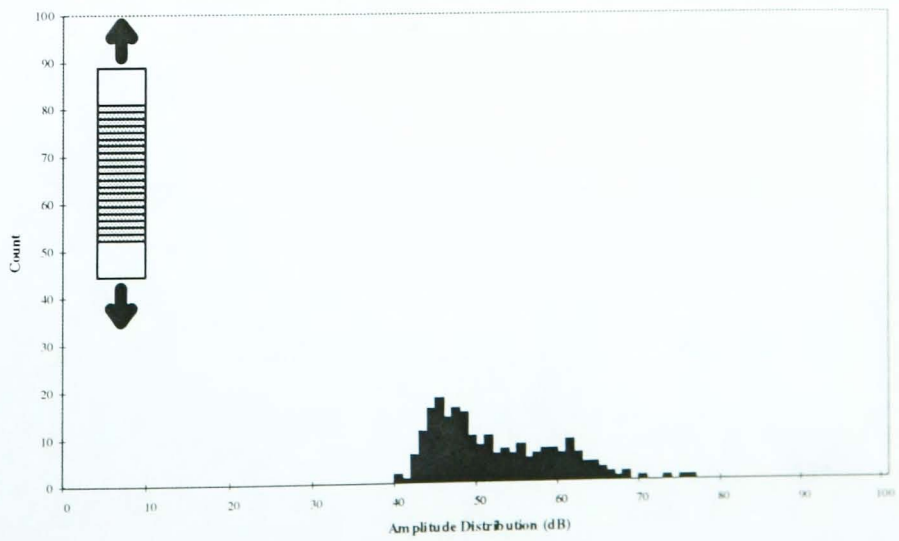

C.1.3 Tensile Loading of 10° Samples

Test 3A

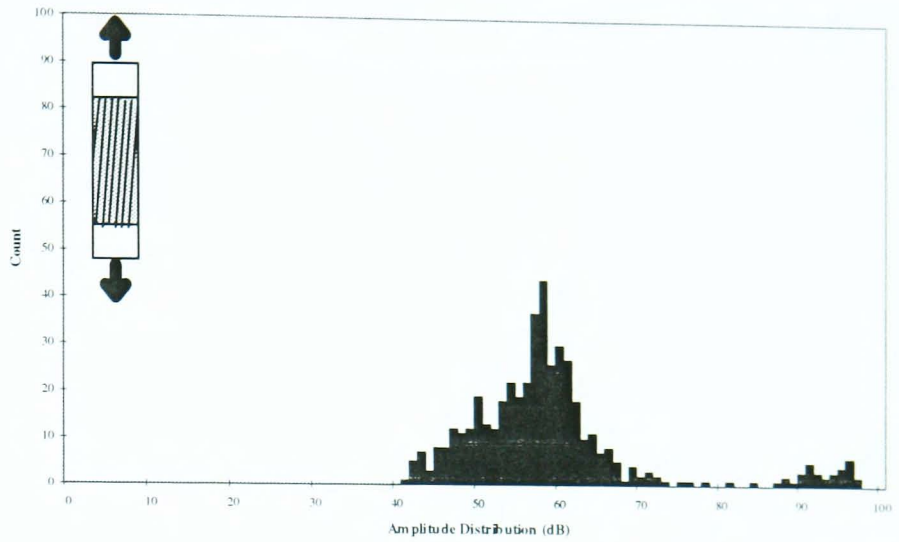

Test 3B

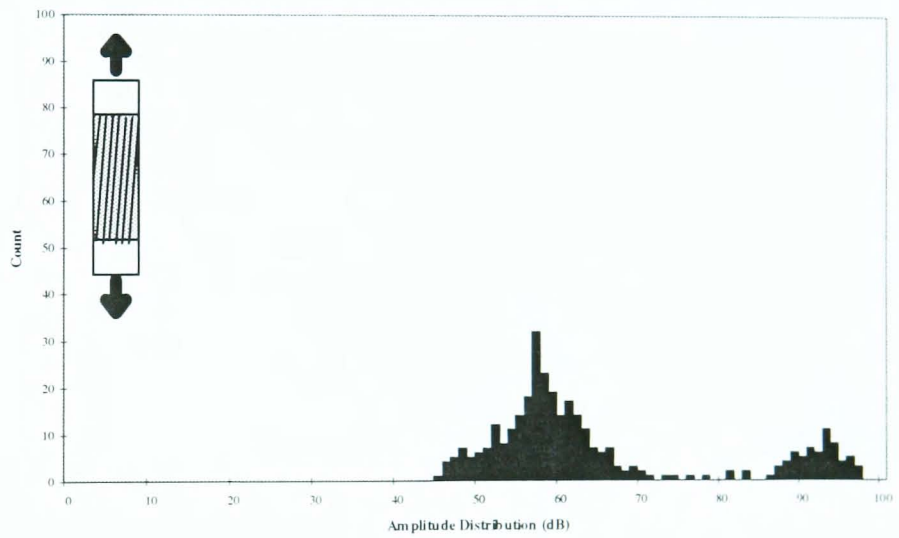

Test 3C

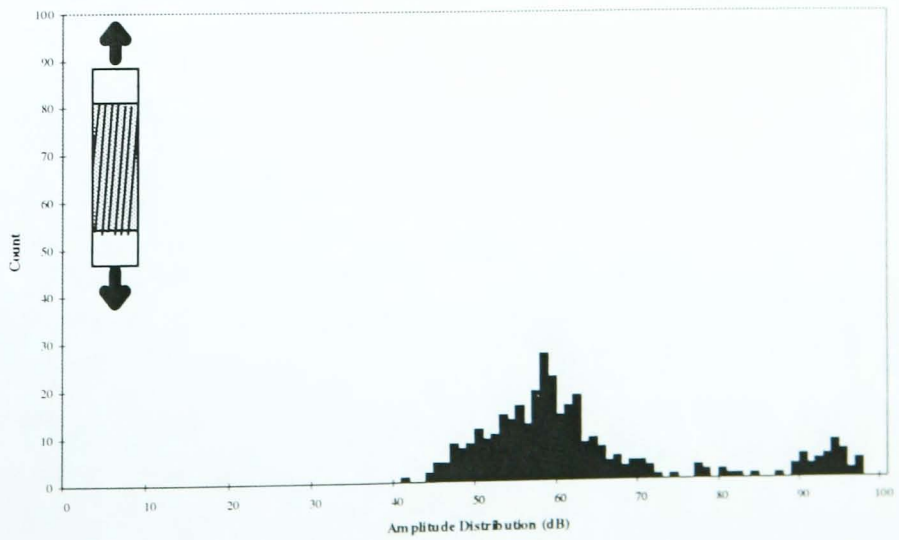

Test 3D

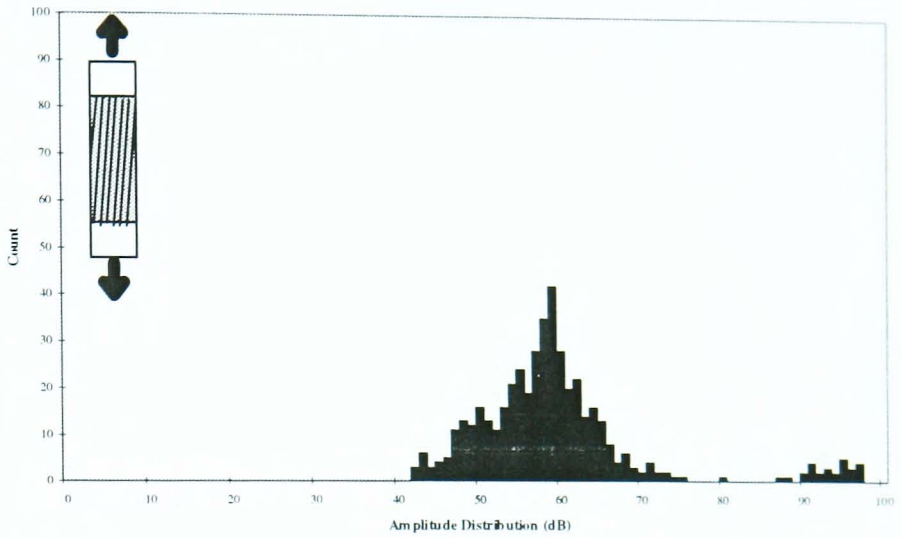

Test 3E

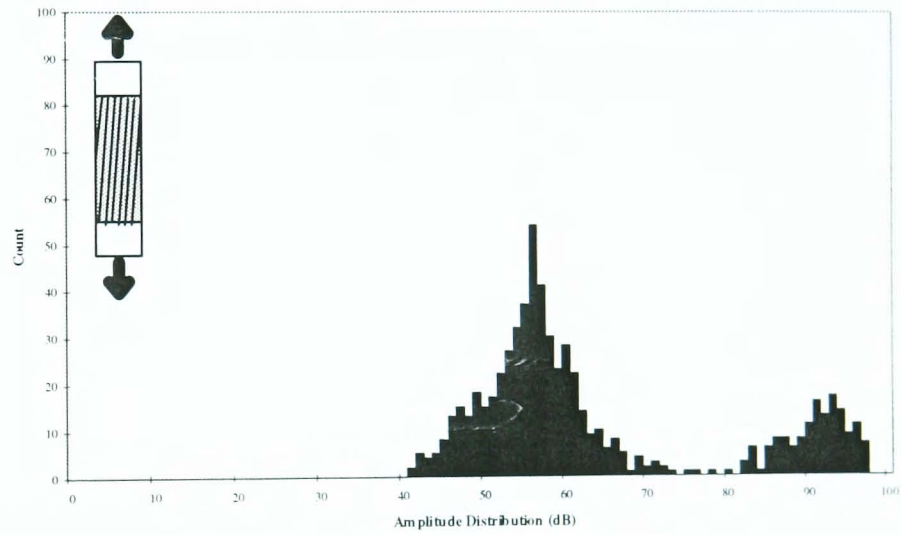

Test 3F

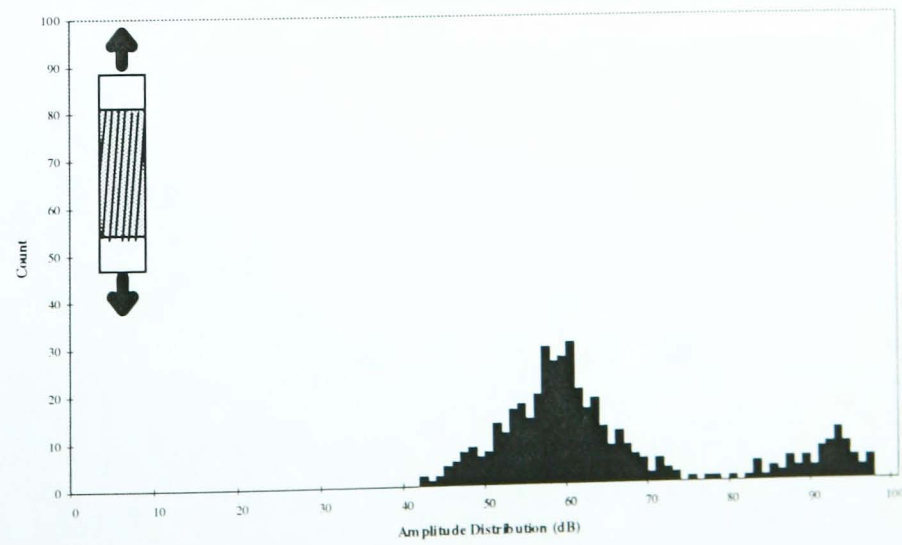

Test 3G

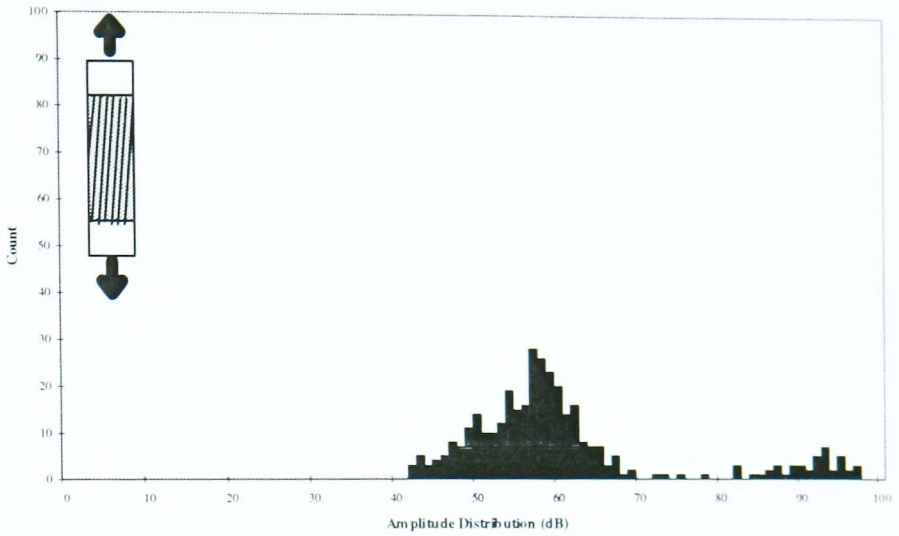

Test 3H

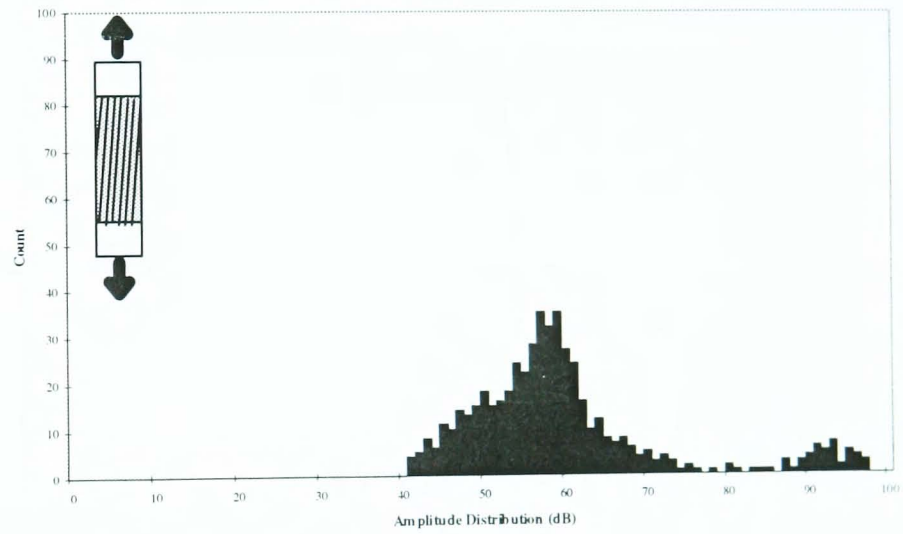

C.1.4 Tensile Loading of Uncured Carbon/Epoxy Pre-Preg Samples

Test 4A

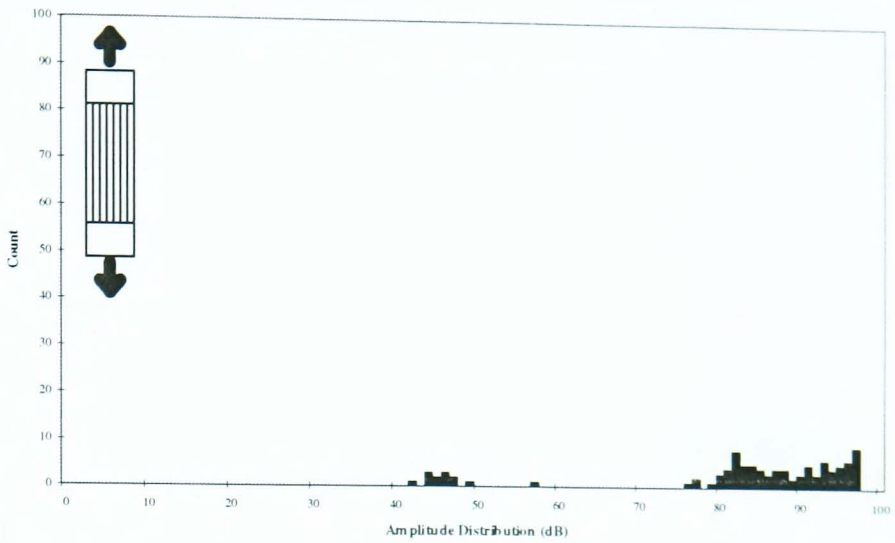

Test 4B

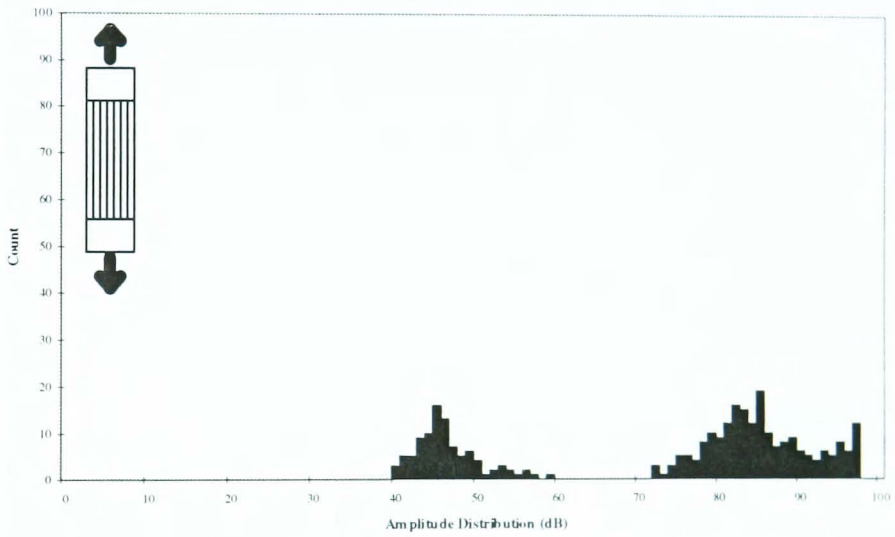

Test 4C

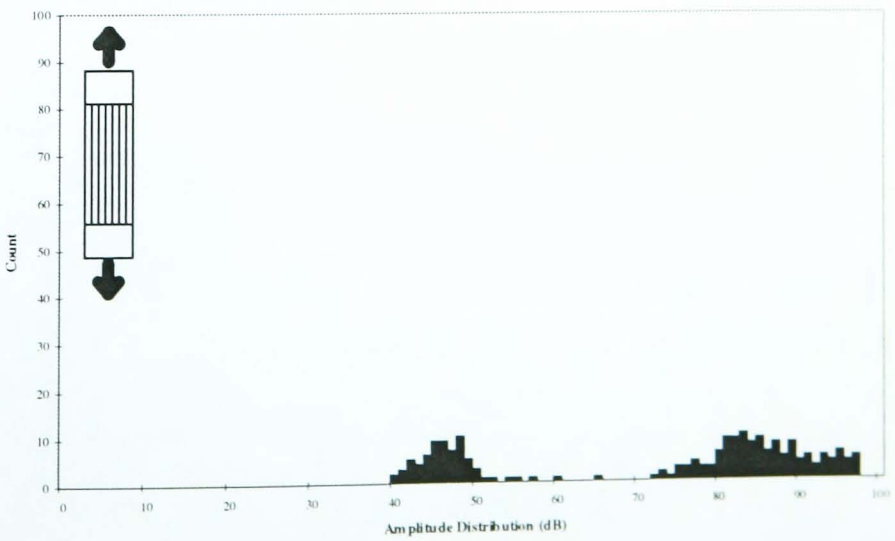

Test 4D

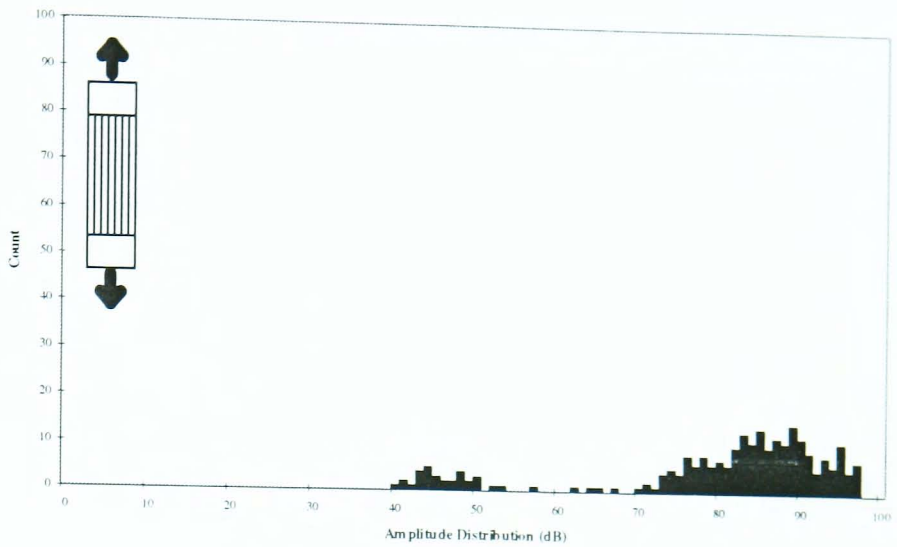

Test 4E

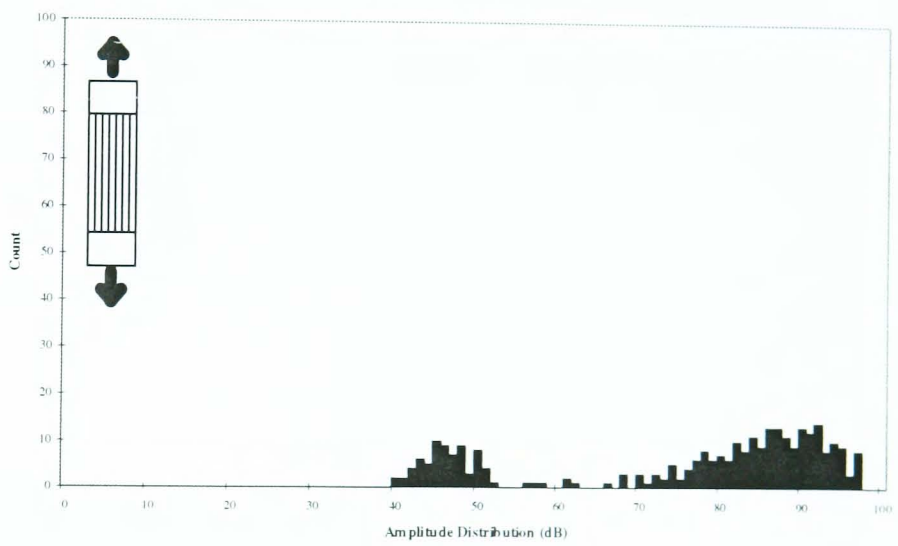

Test 4F

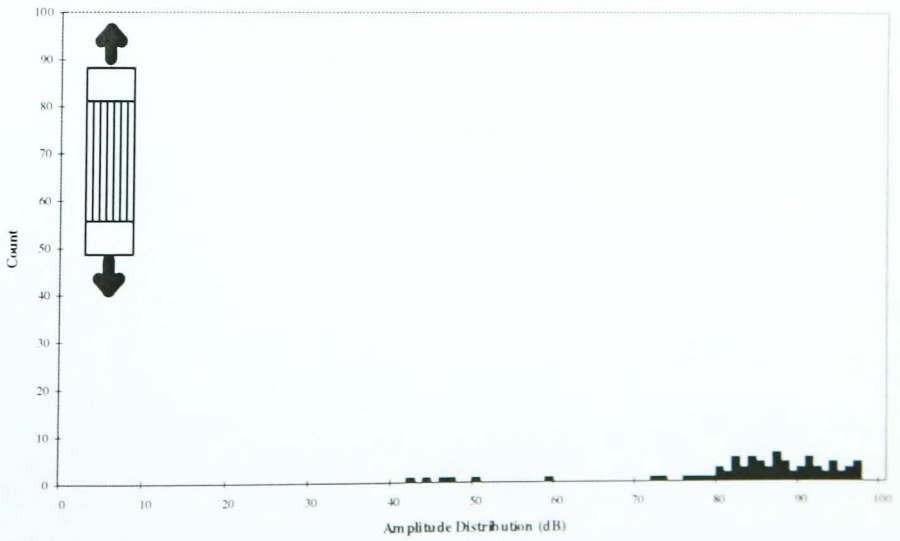

Test 4G

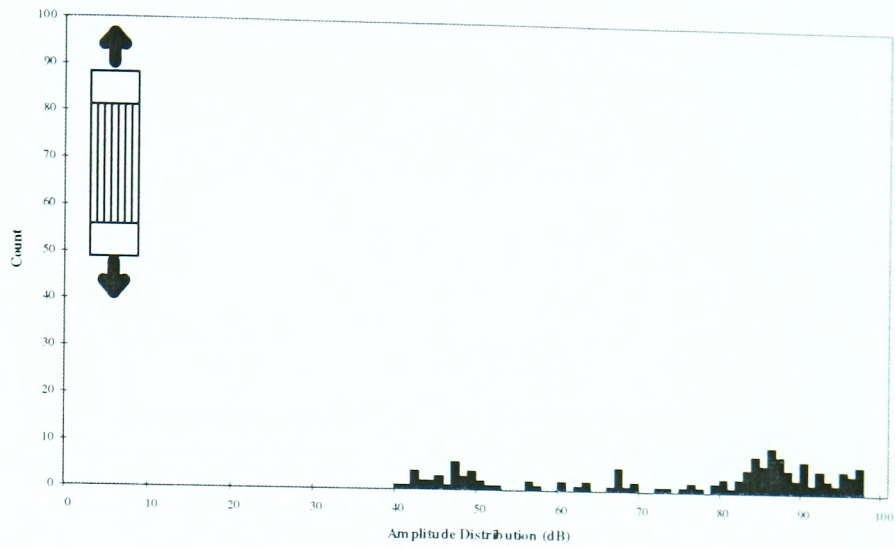

Test 4H

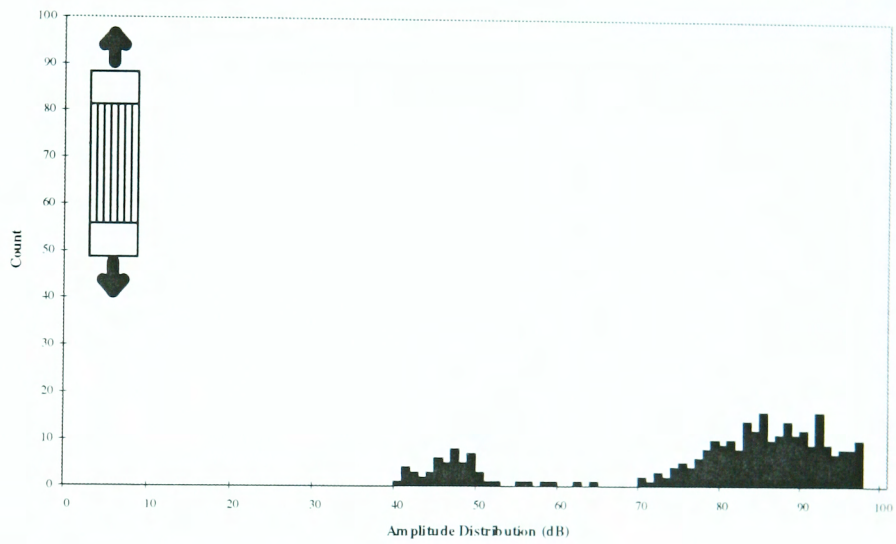

Test 4J

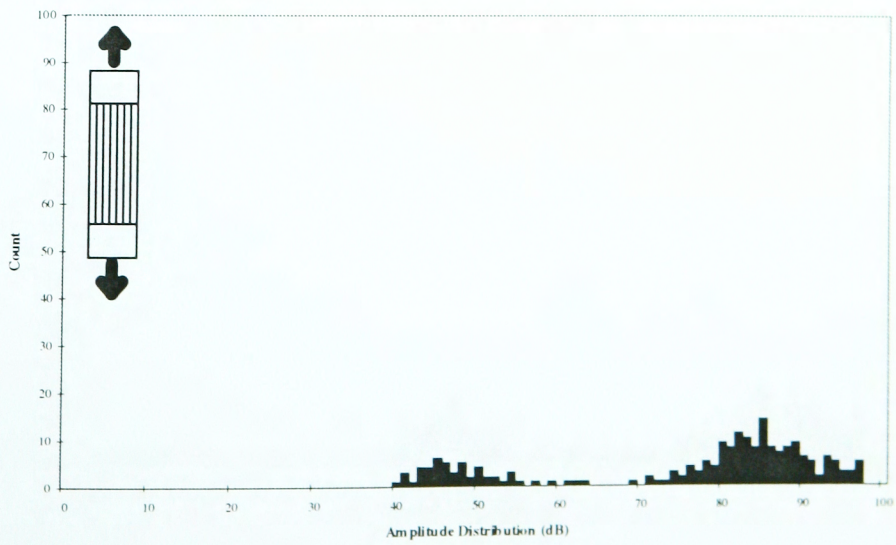

Test 4K

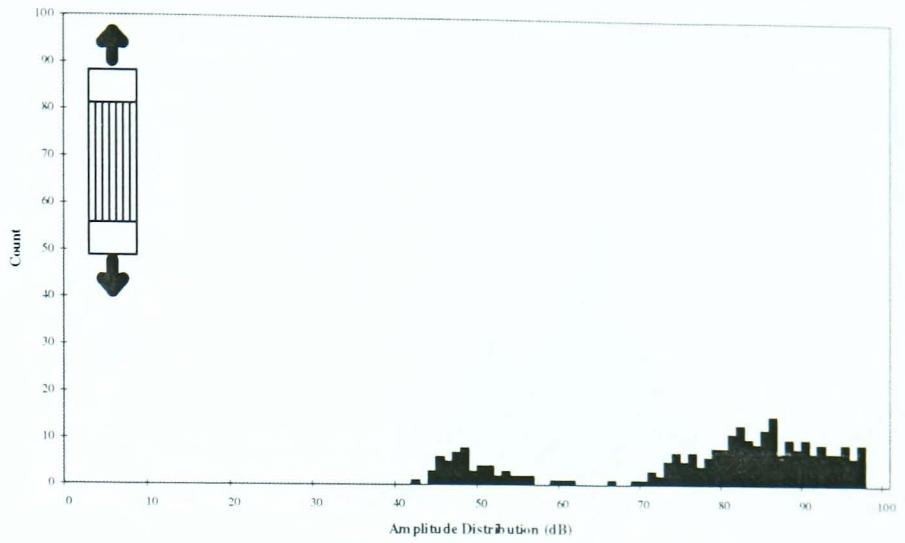

Test 4L

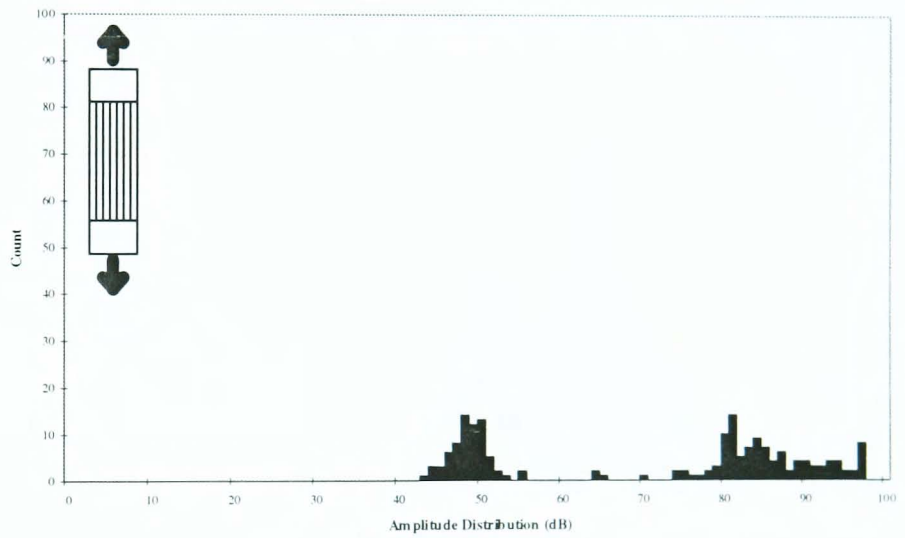

Test 4M

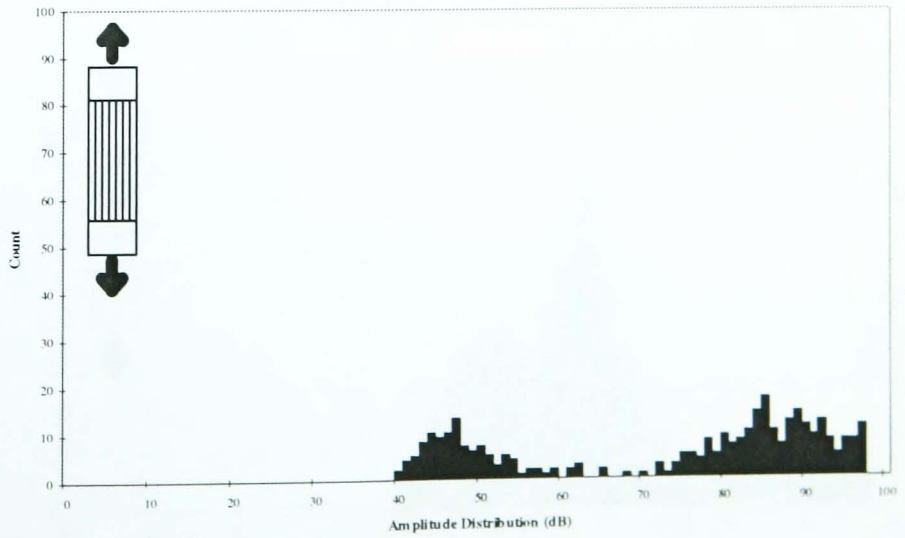

C.1.5 Tensile Loading of Teflon-Loaded Samples

Test 5A

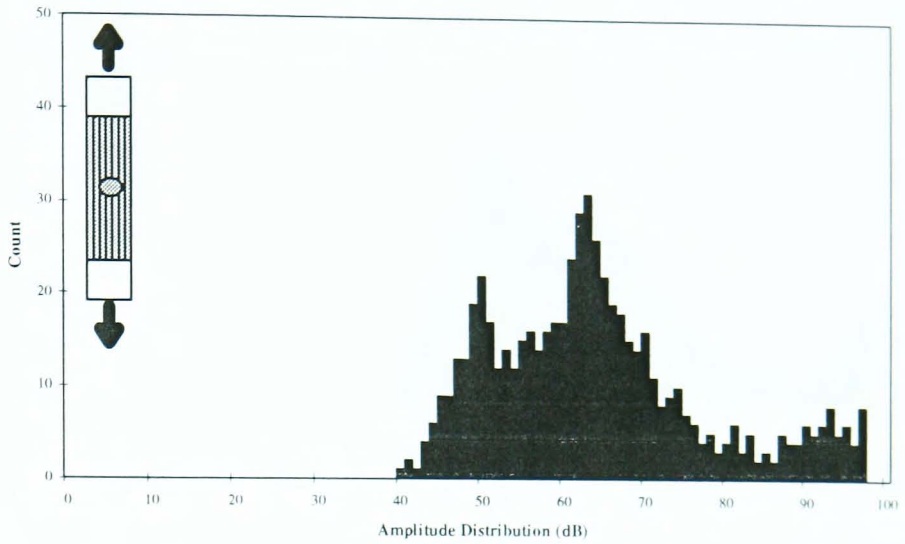

Test 5B

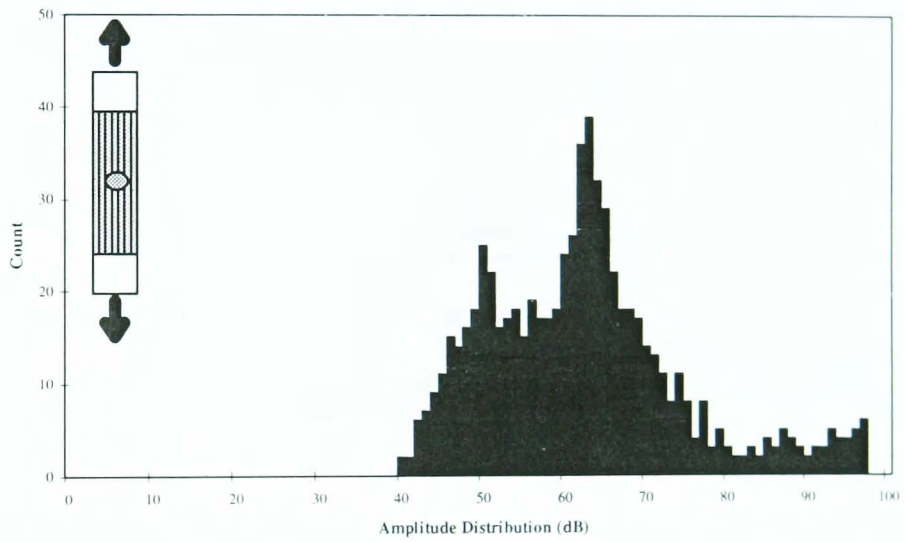

Test 5C

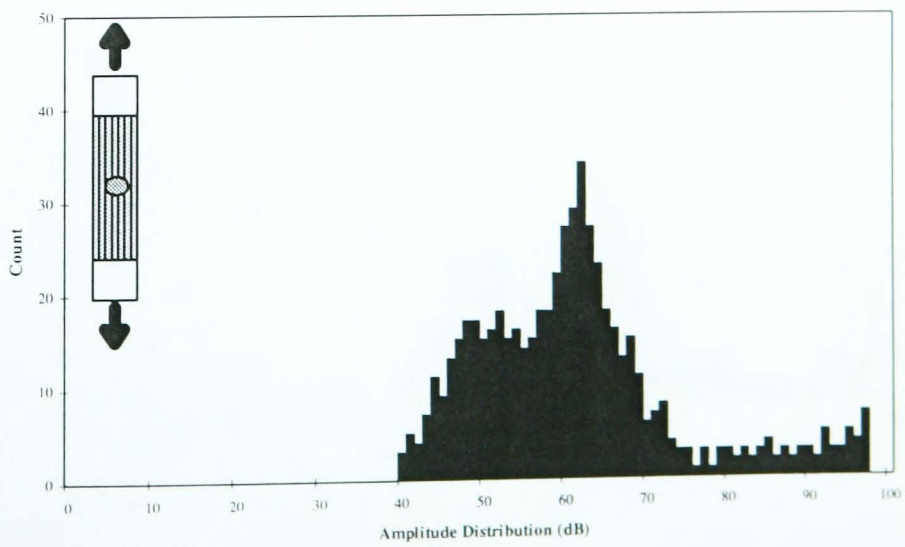

Test 5D

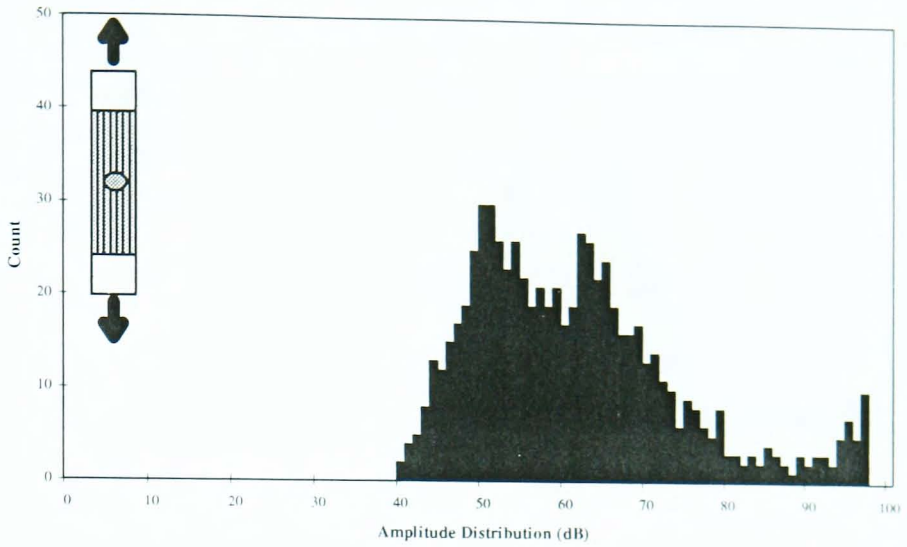

Test 5E

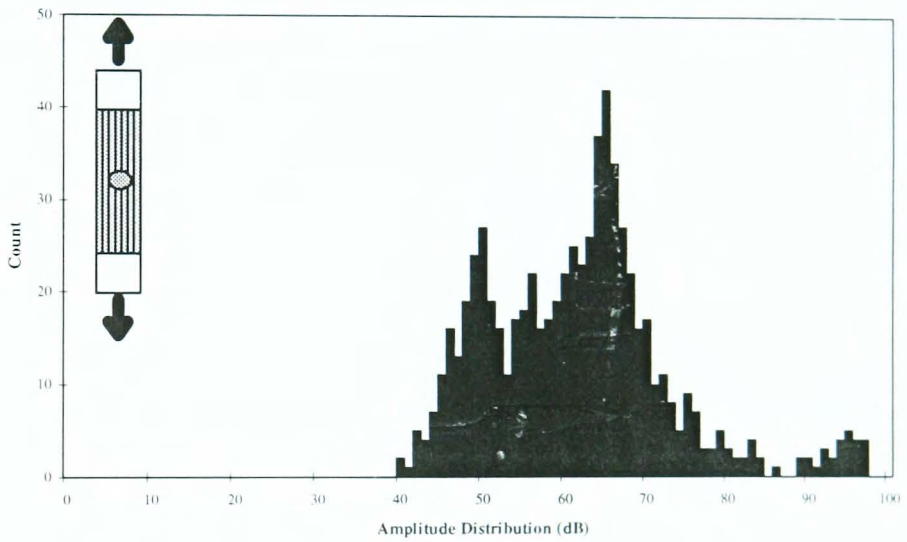

Test 5F

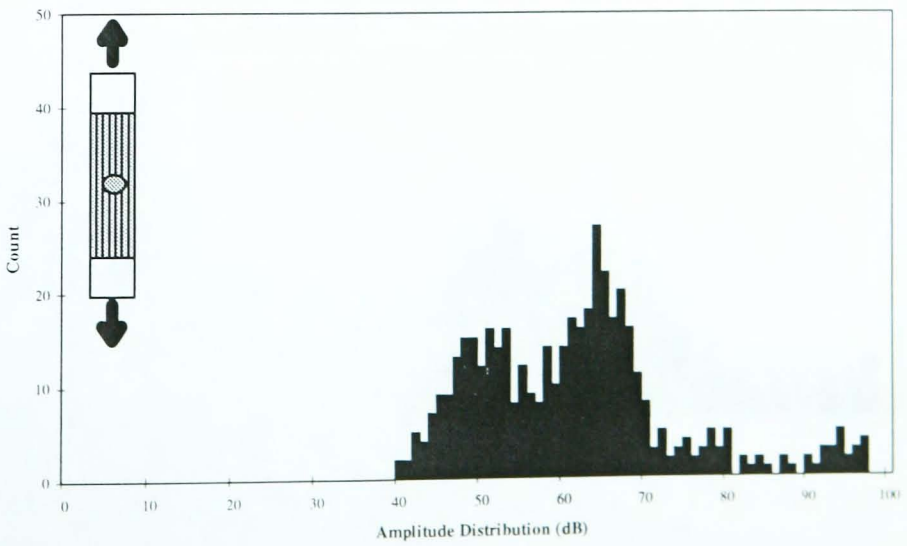

Test 5G

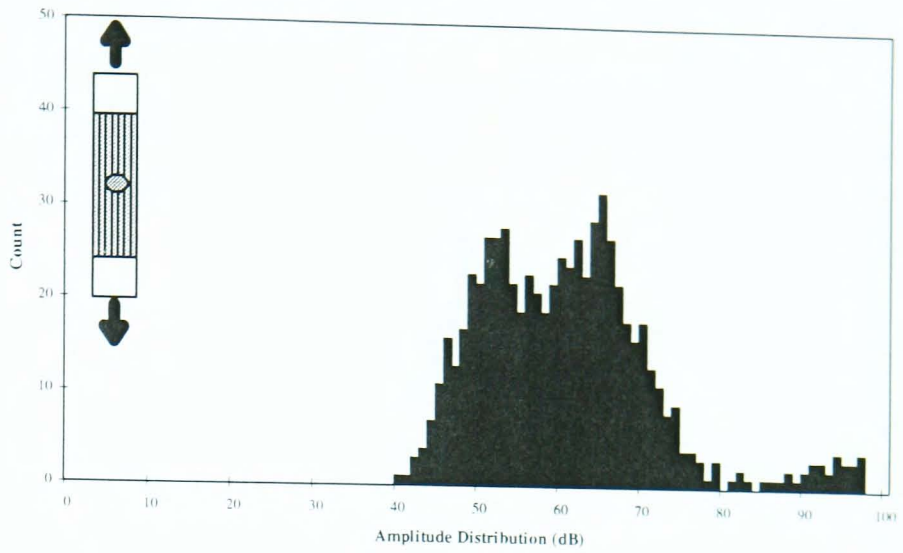

Test 5H

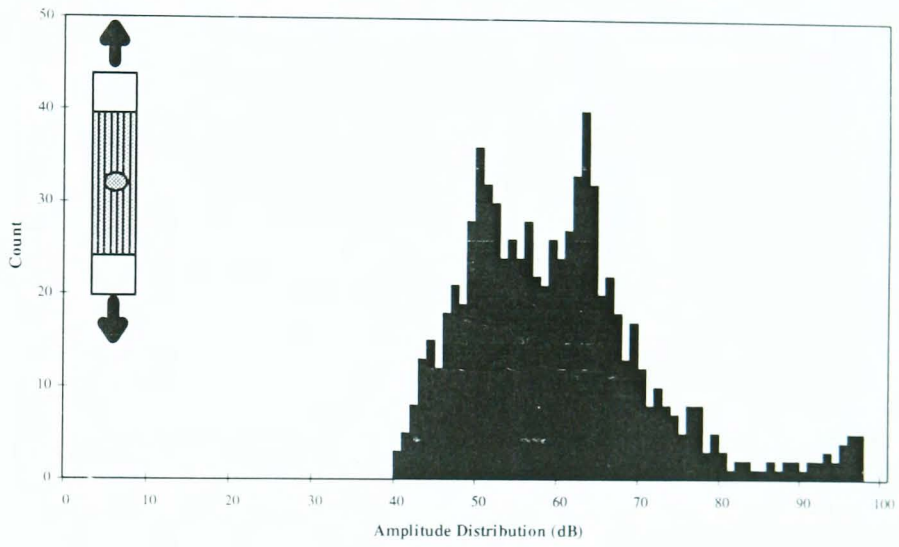

Test 5J

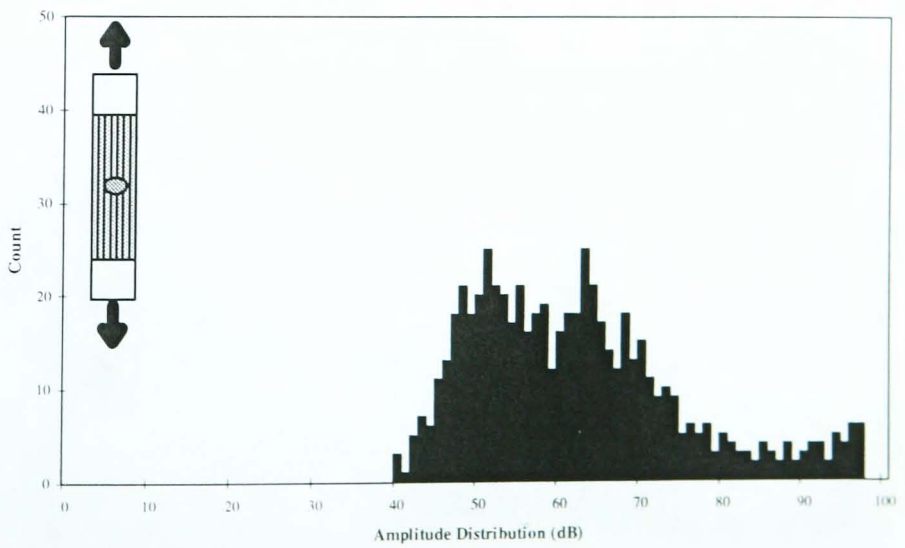

Test 5K

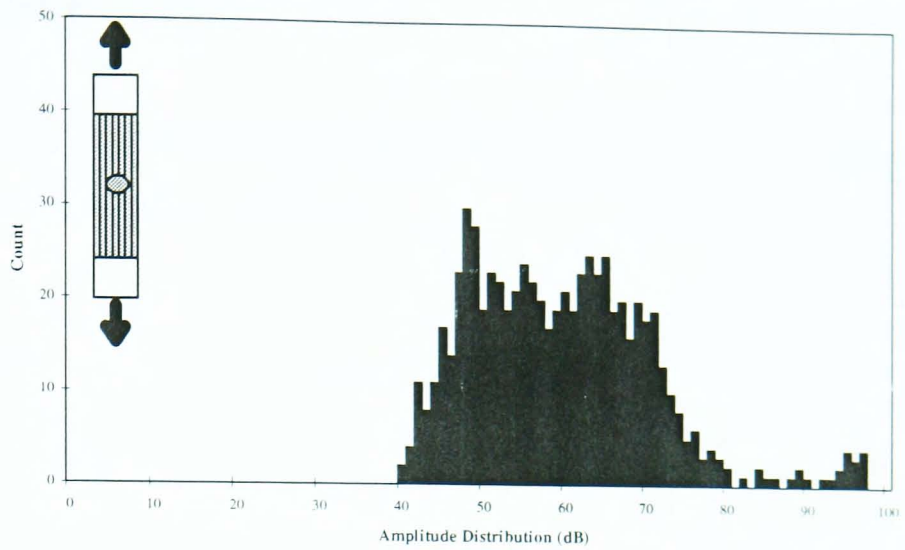

Test 5L

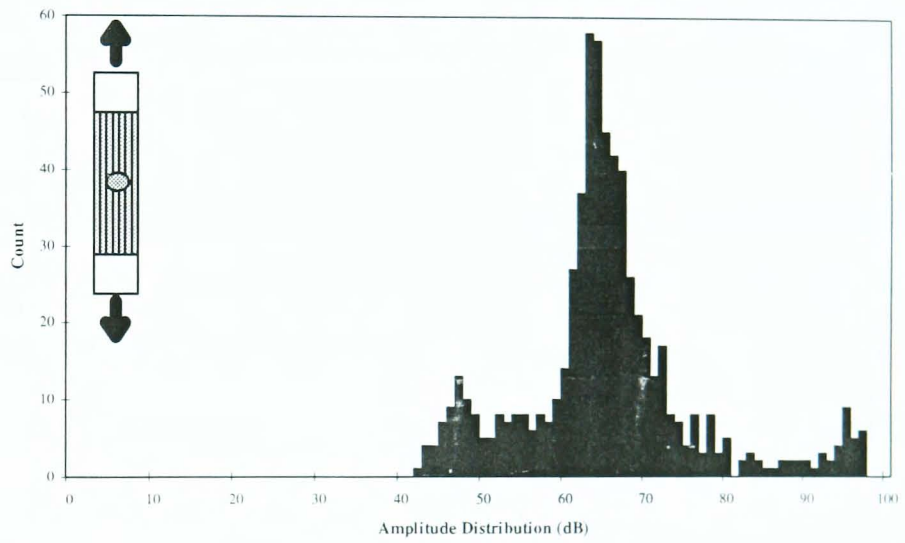

Test 5M

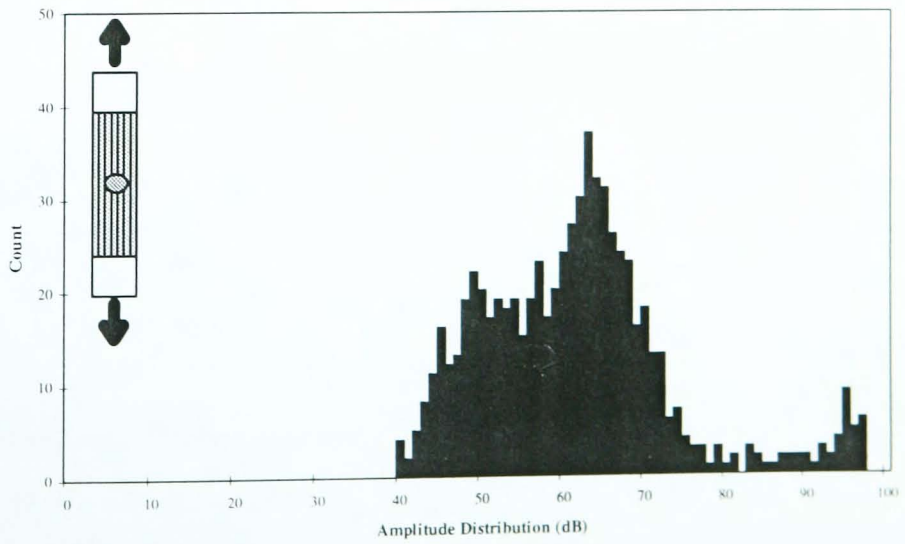

C.2 Amplitude Distribution Analysis

The CFRP specimens used in these tests were designed to fail due to certain damage mechanisms. These test specimens were as follows:-

Mechanical Test	No. of Specimens	Test Number
Unreinforced Epoxy bars (tensile)	12	Tests 1A-1M
90° (tensile)	12	Tests 2A-2M
10° (tensile)	8	Tests 3A-3M
Uncured pre-preg bars (tensile)	12	Tests 4A-4M
Teflon insertion (tensile)	12	Tests 5A-5M

The resulting maximum frequency of the AE obtained from these specimens were plotted in a distribution form. For easy reference, a small illustration of the type of composite tested is placed in the right hand side of each graph.

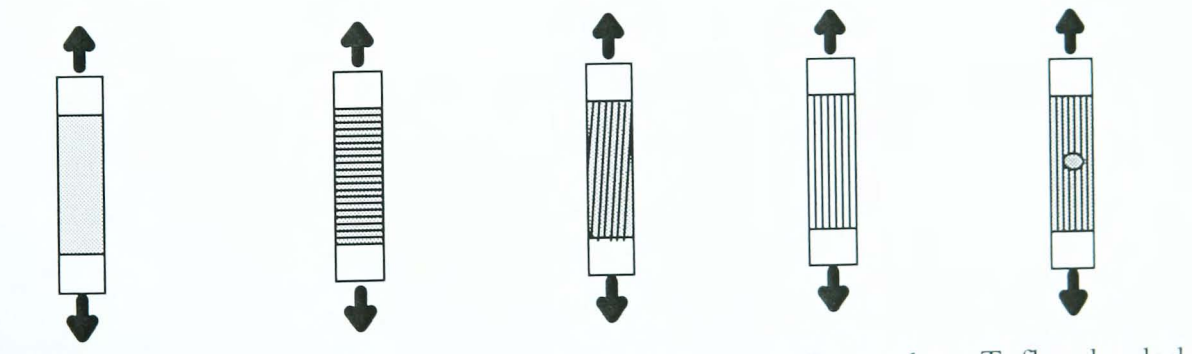

The results from each test were as follows:-

C.2.1 Tensile Loading of Pure Resin Samples

Test 1A

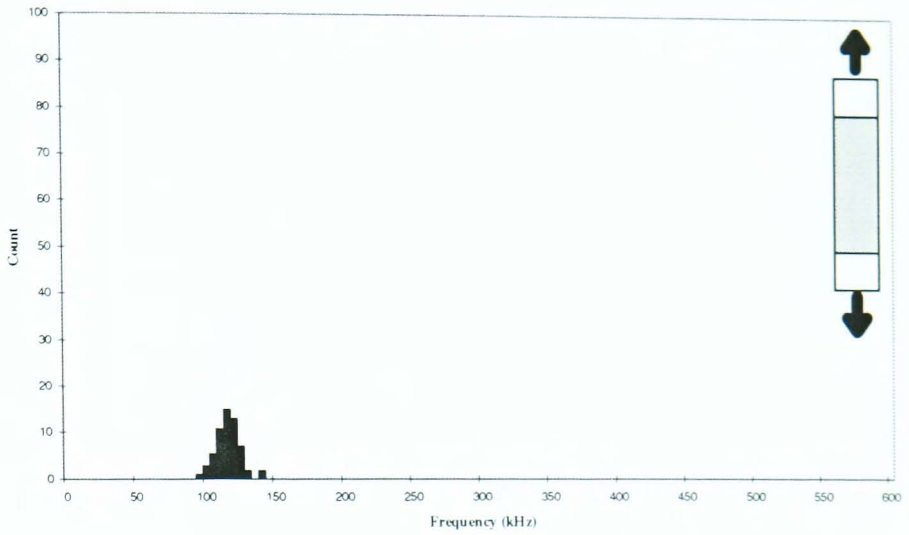

Test 1B

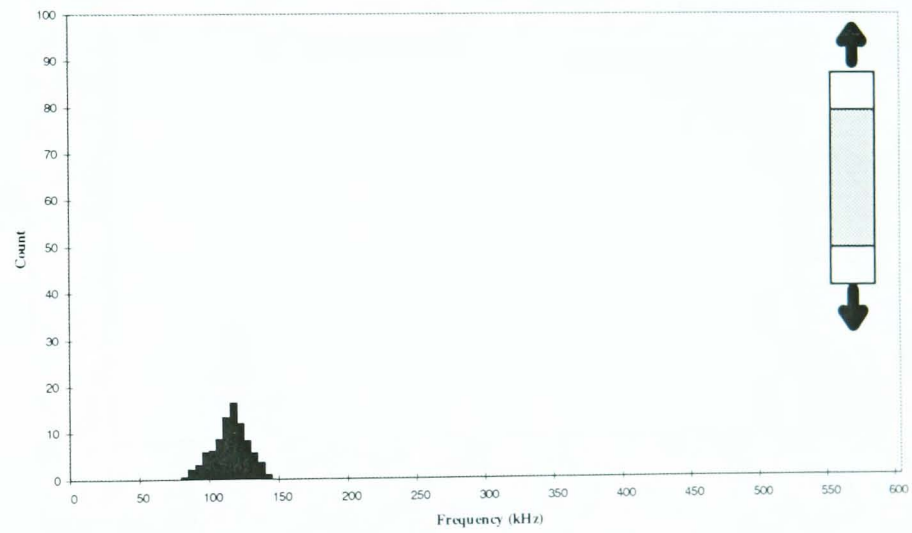

Test 1C

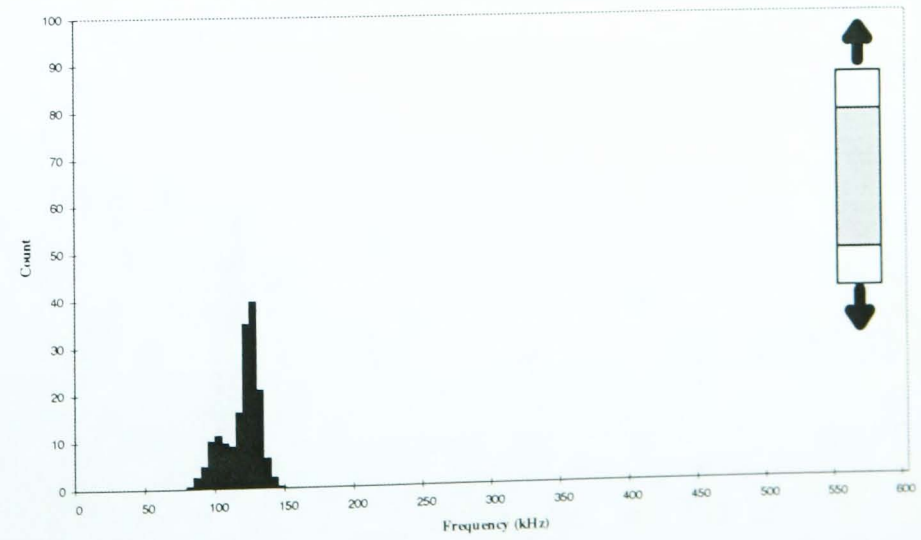

Test 1D

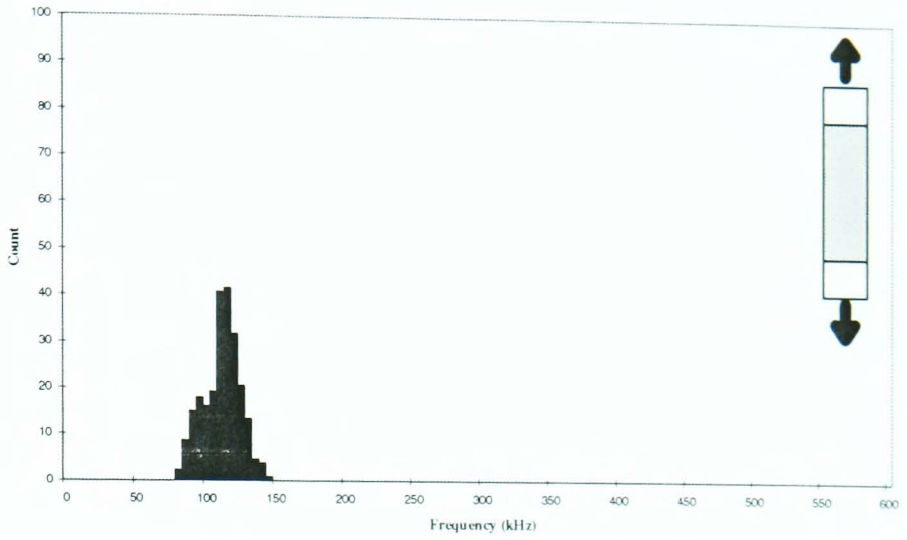

Test 1E

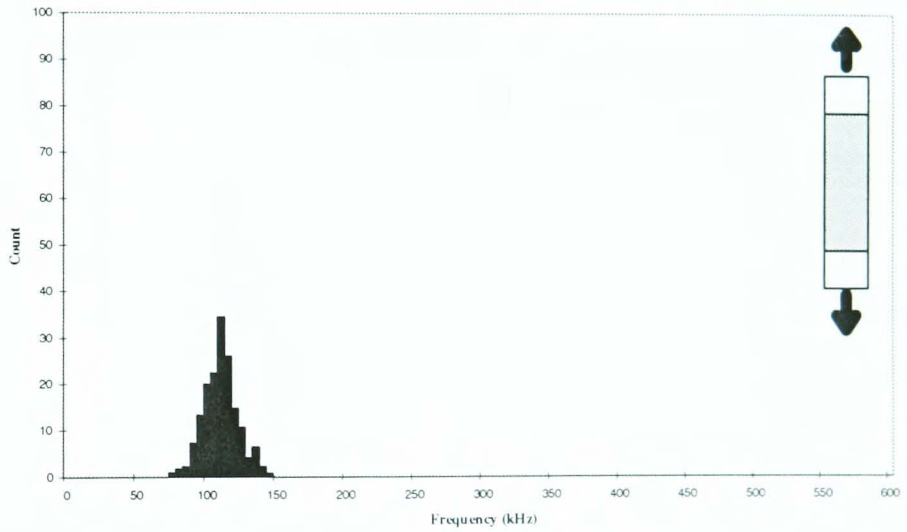

Test 1F

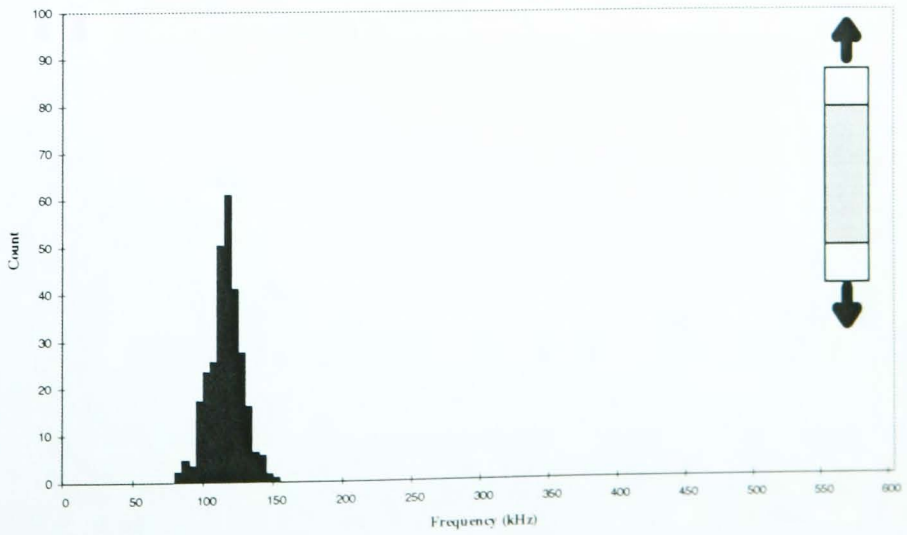

Test 1G

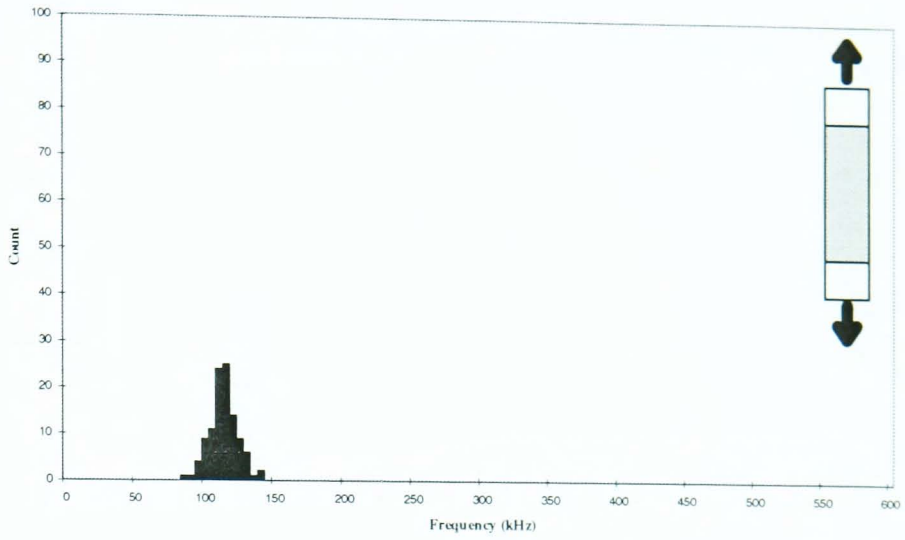

Test 1H

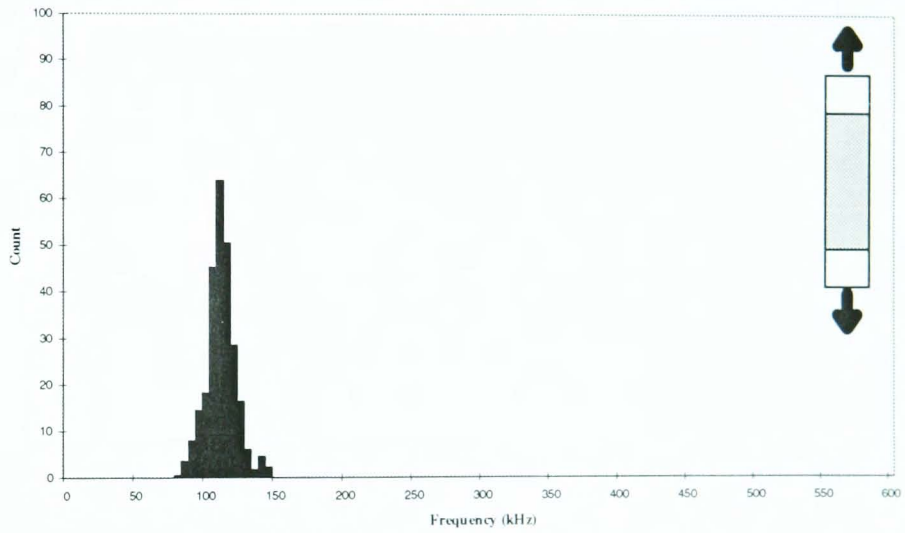

Test 1J

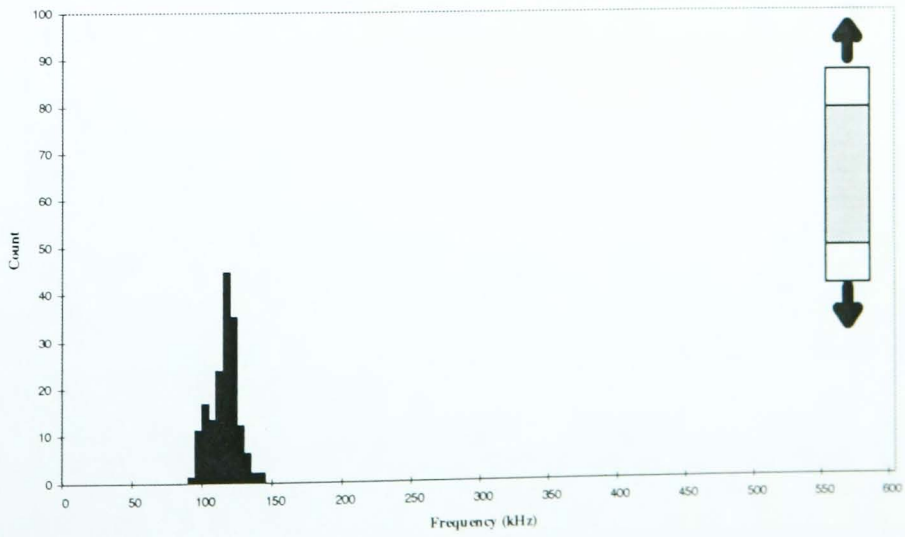

Test 1K

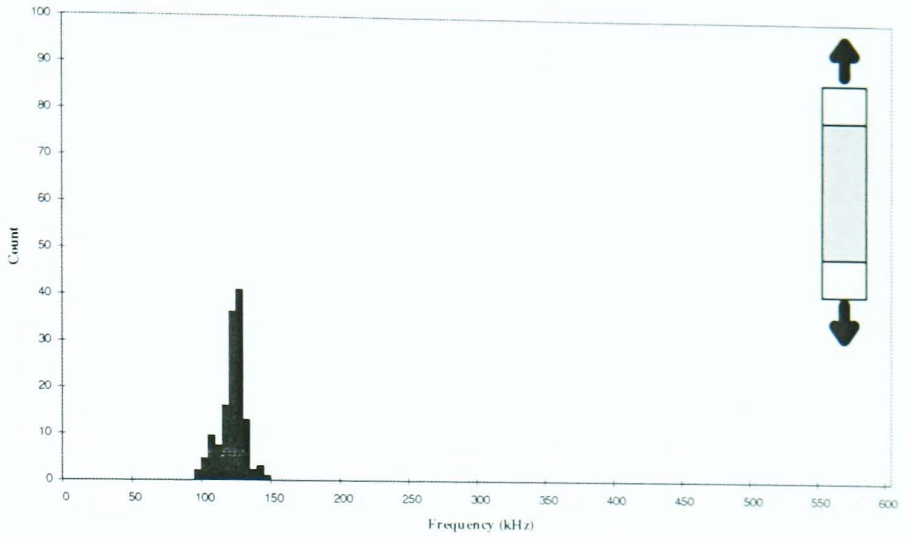

Test 1L

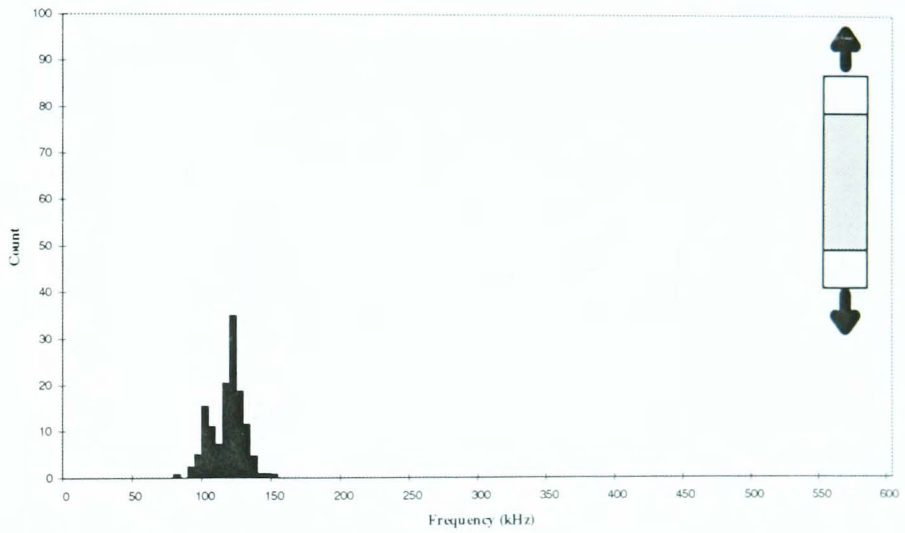

Test 1M

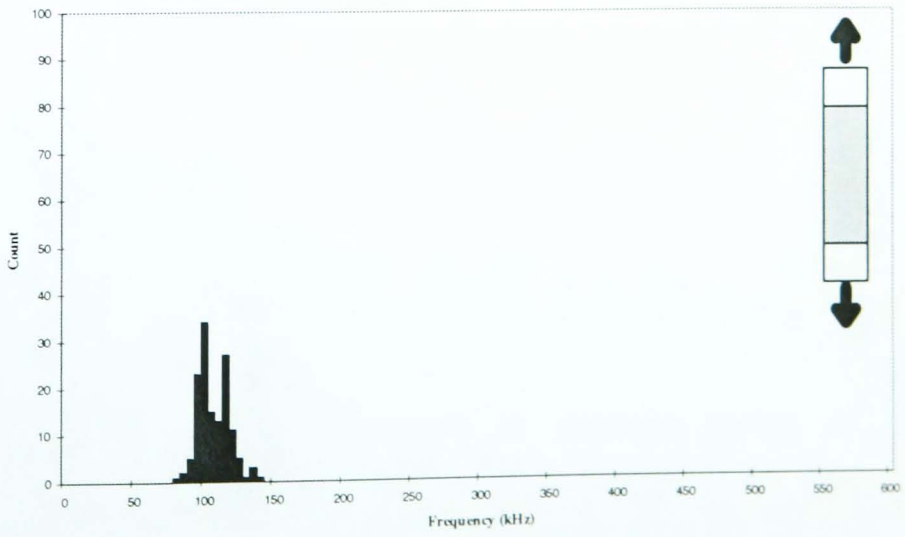

C.2.2 Tensile Loading of 90° Samples

Test 2A

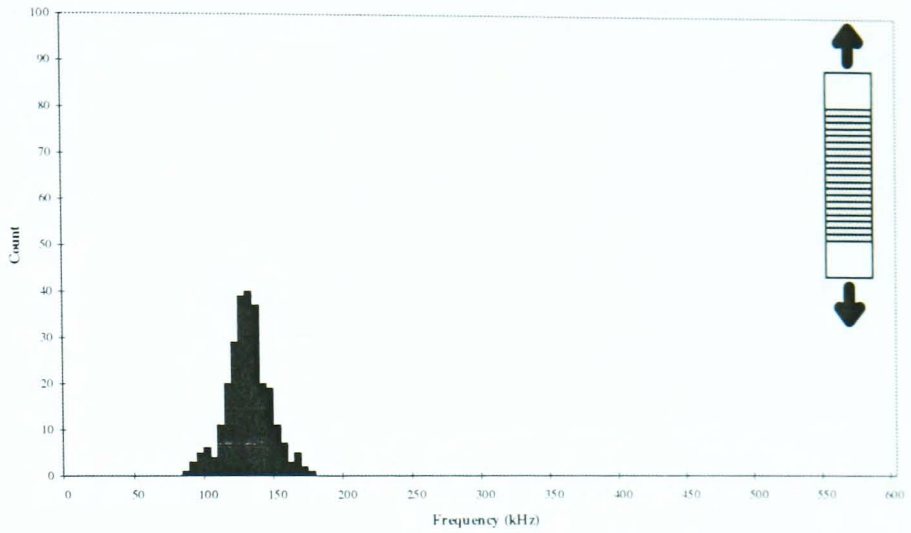

Test 2B

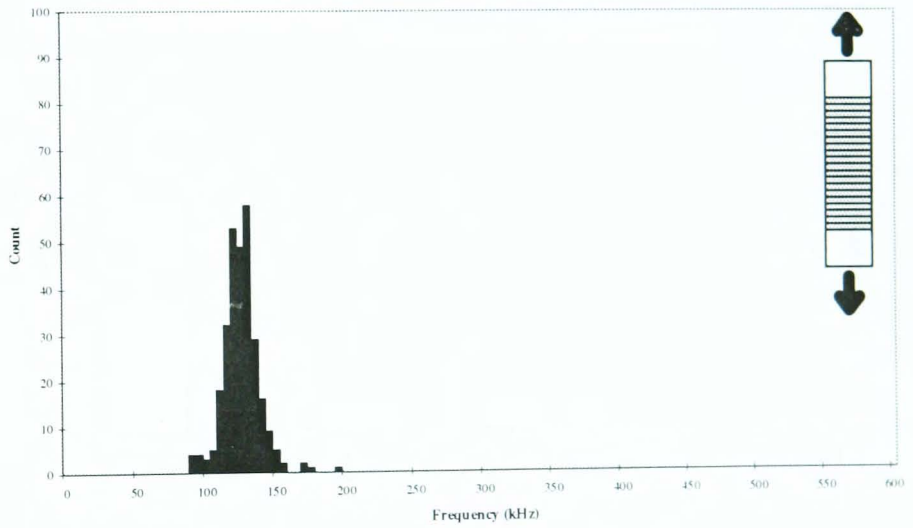

Test 2C

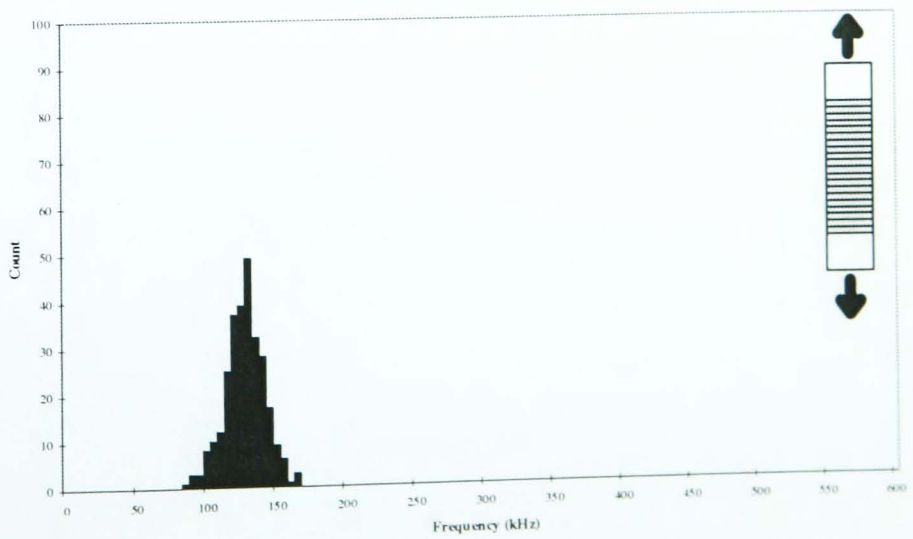

Test 2D

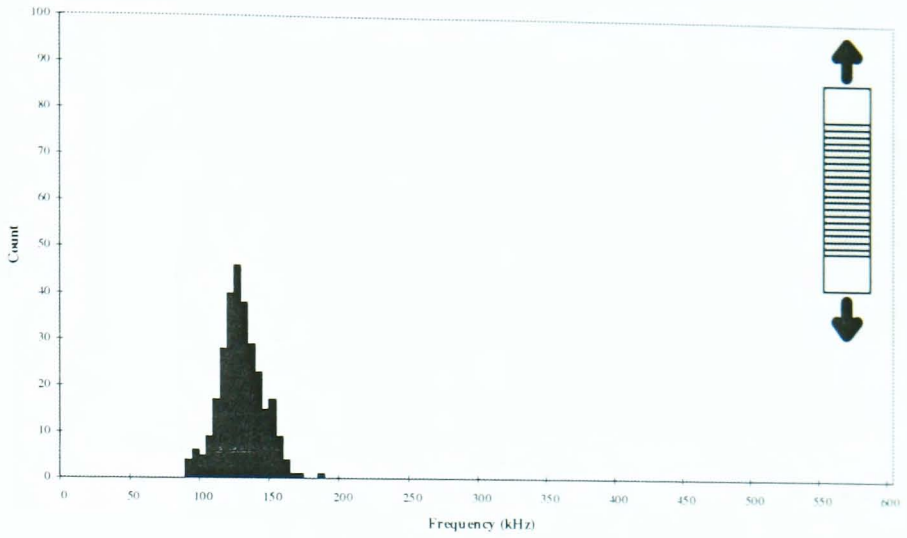

Test 2E

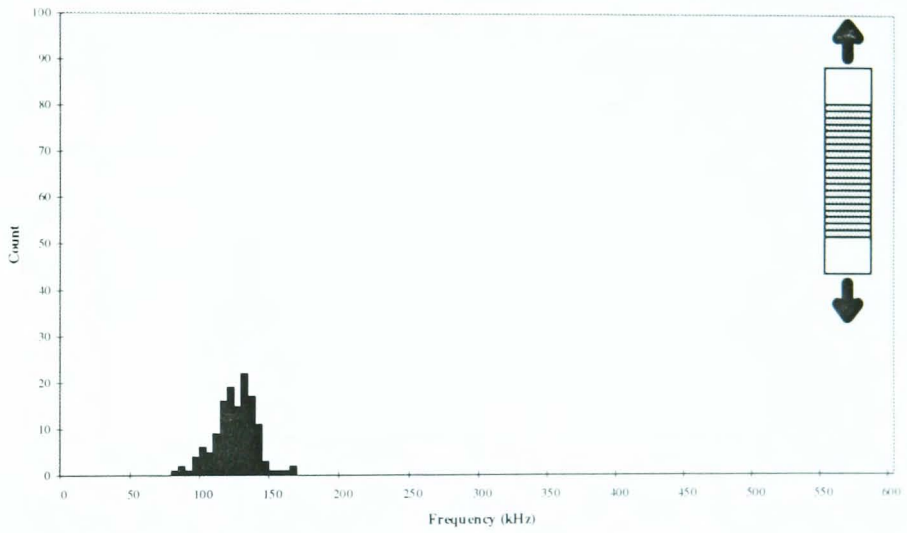

Test 2F

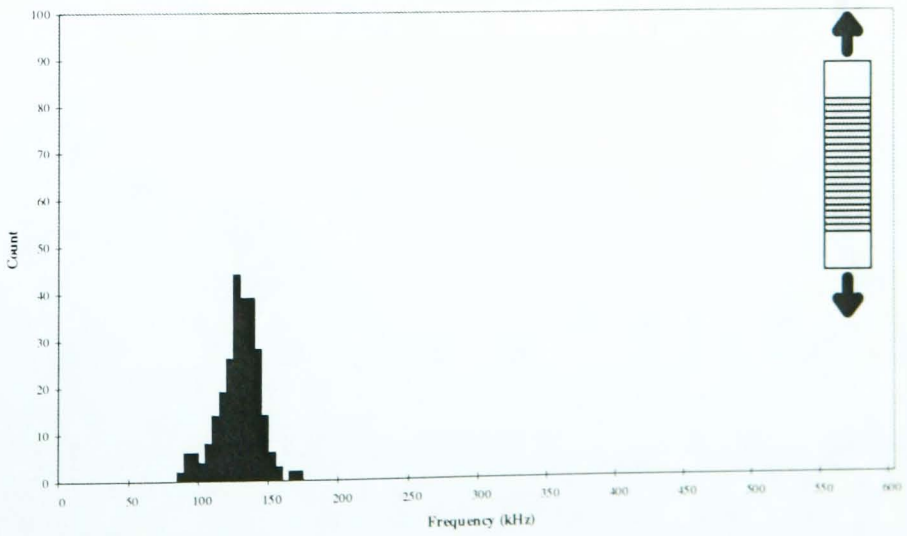

Test 2K

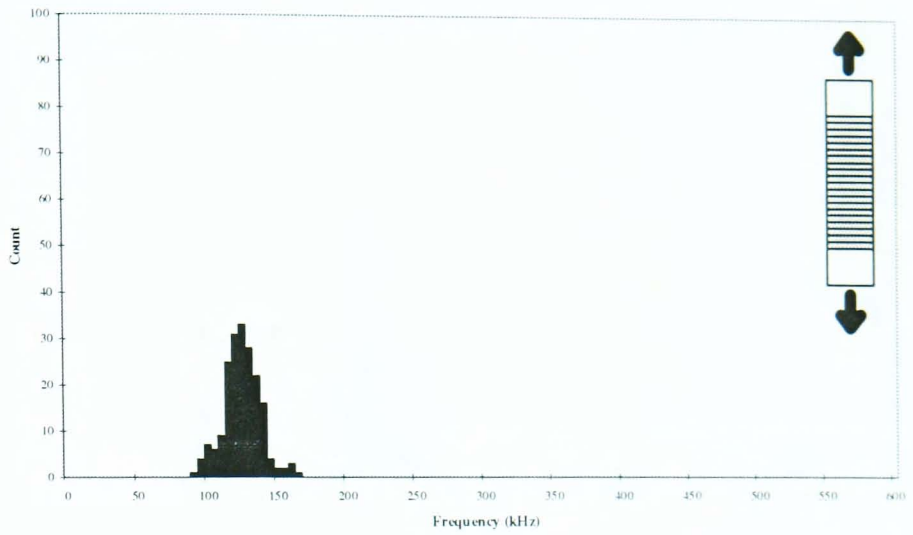

Test 2L

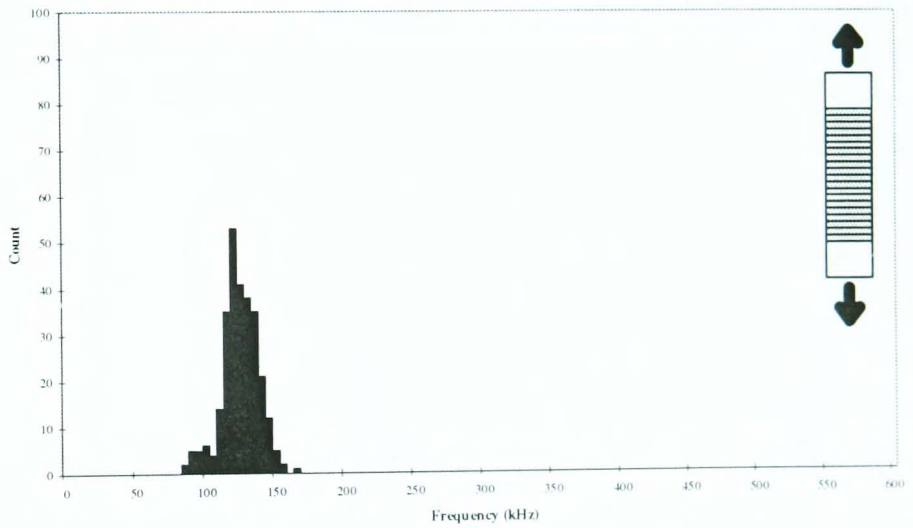

Test 2M

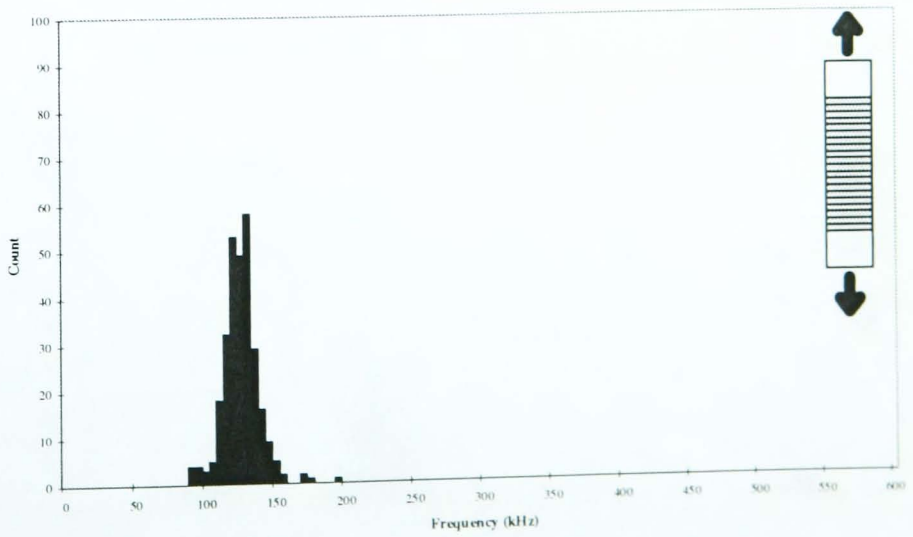

C.2.3 Tensile Loading of 10° Samples

Test 3A

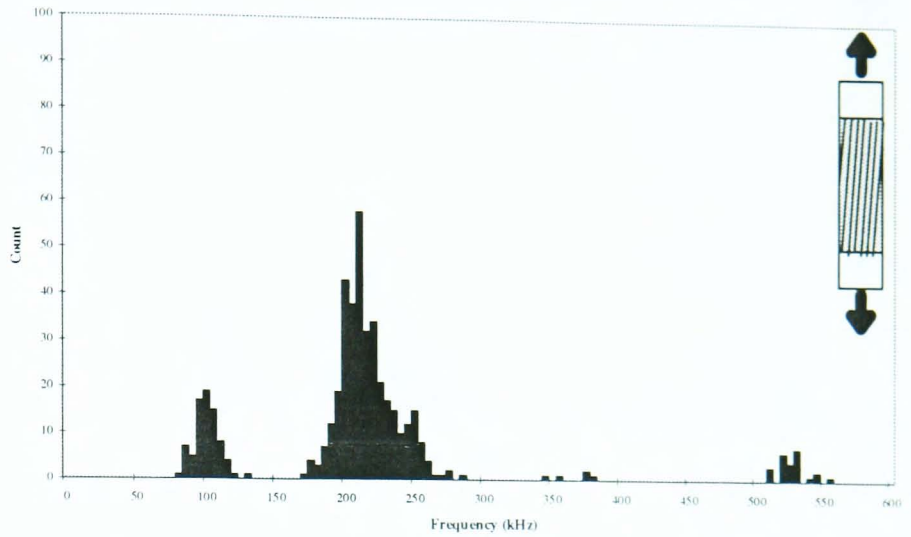

Test 3B

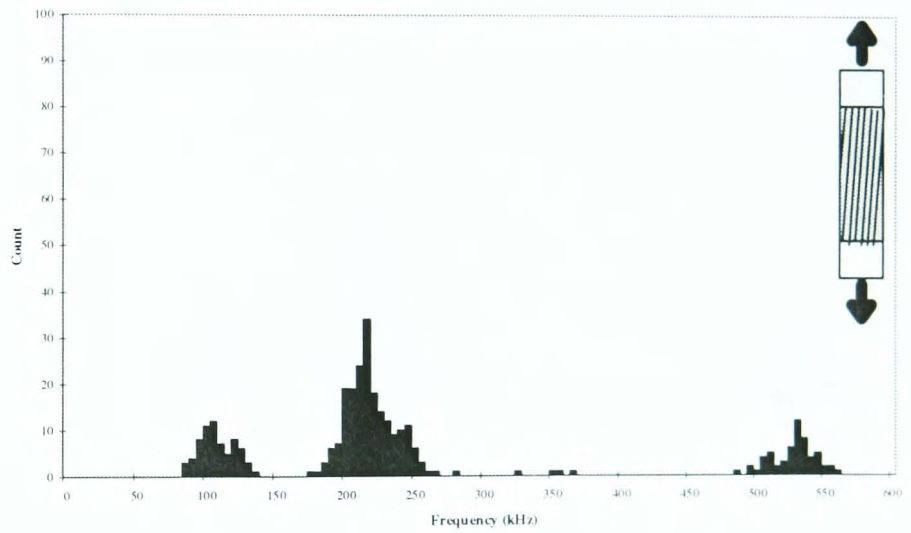

Test 3C

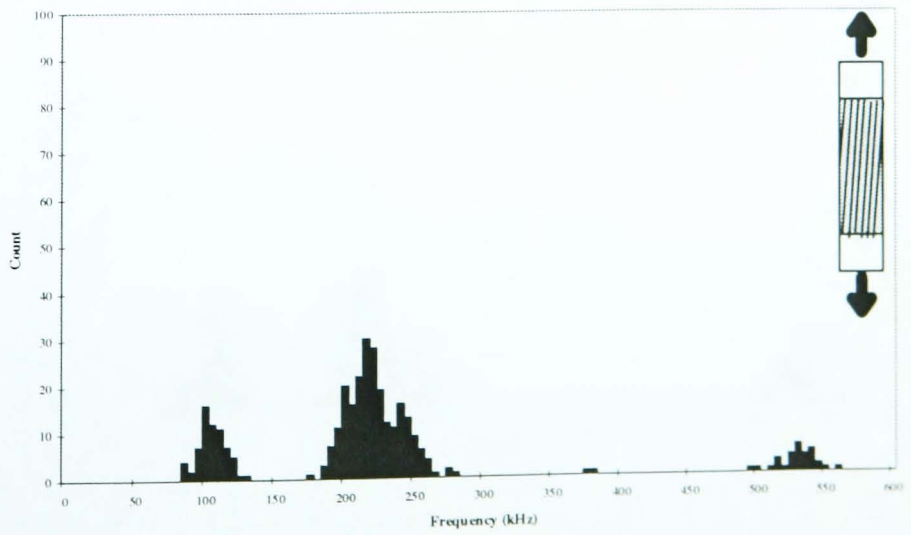

Test 3D

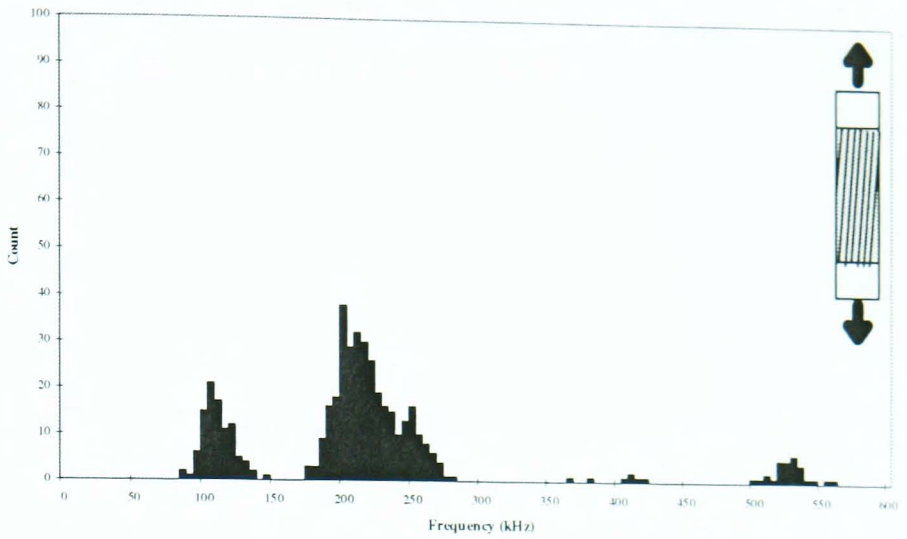

Test 3E

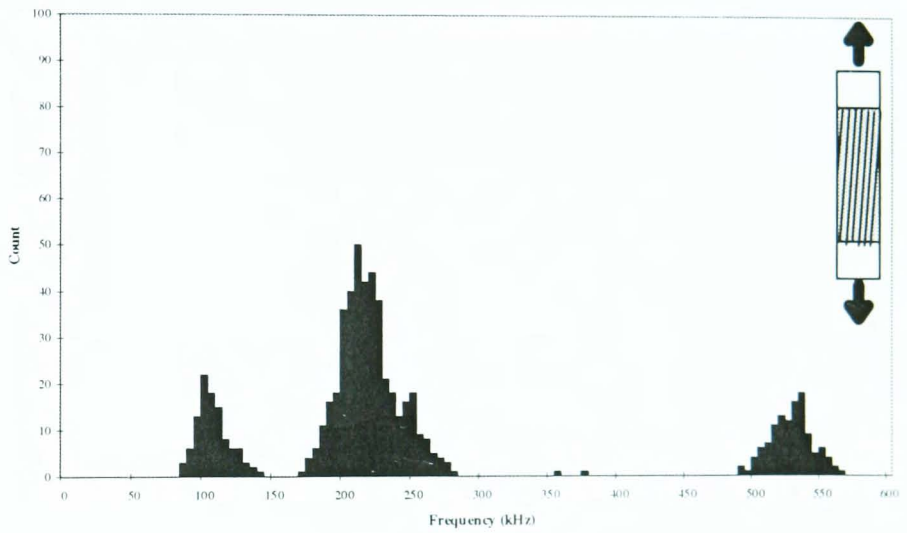

Test 3F

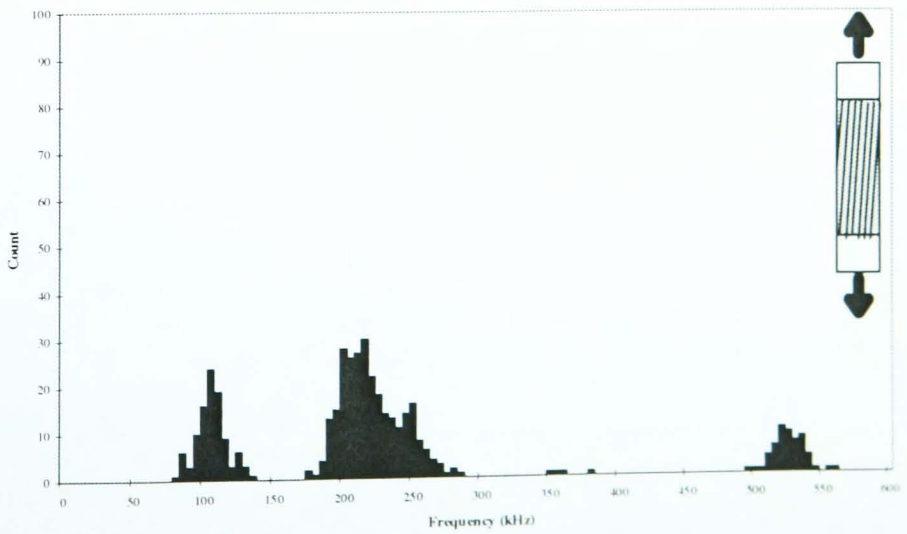

Test 3G

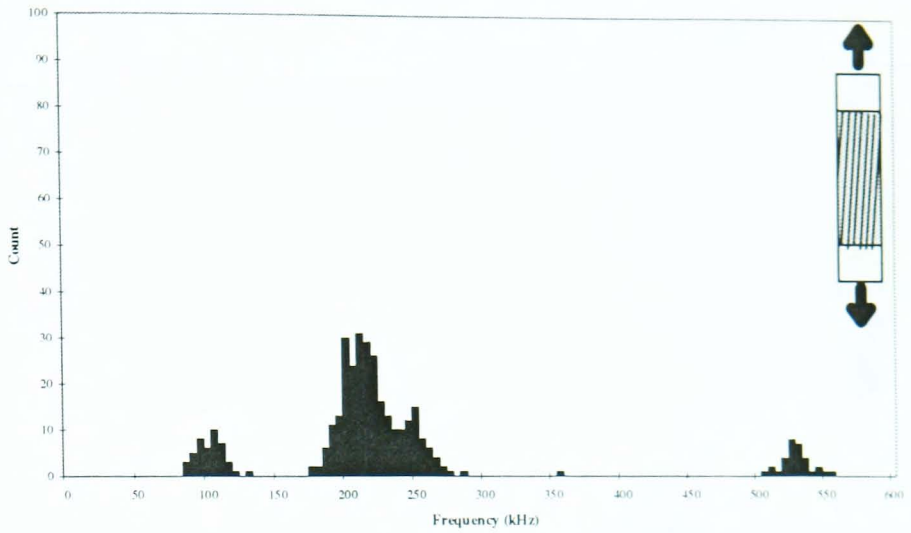

Test 3H

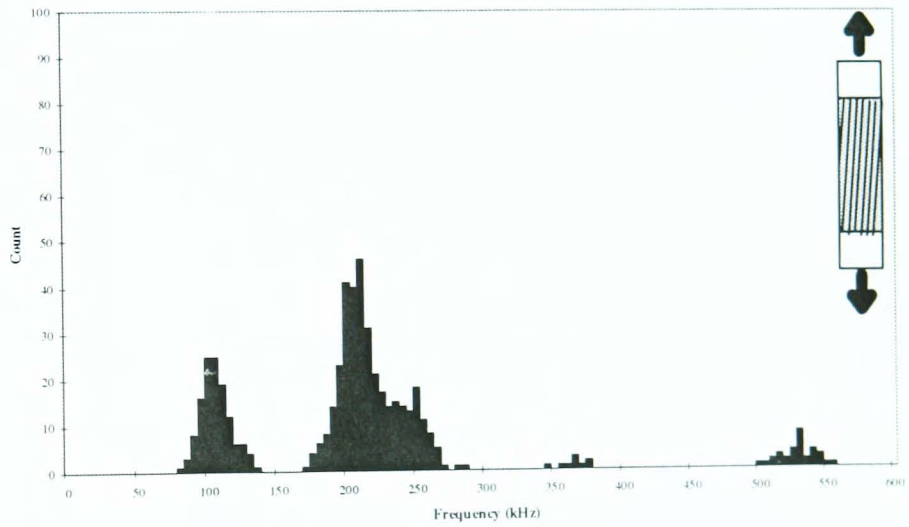

C.2.4 Tensile Loading of Uncured Carbon/Epoxy Pre-Preg Samples

Test 4A

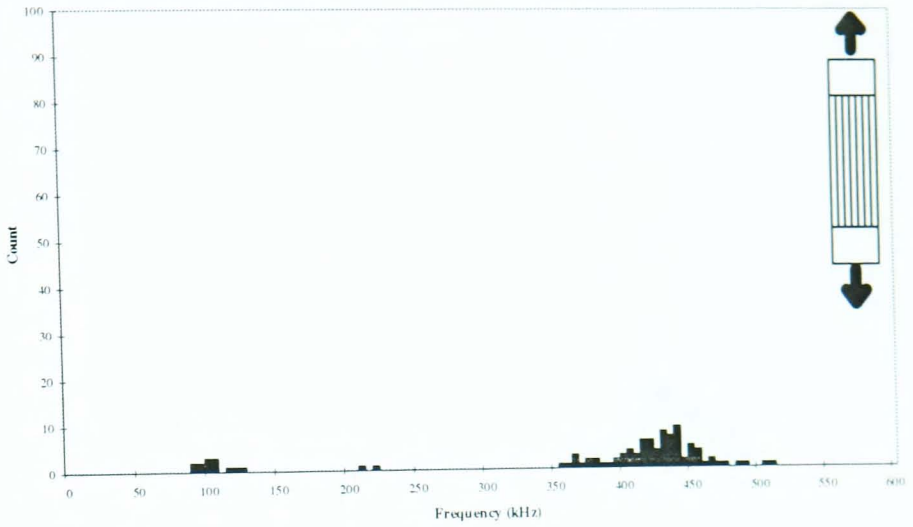

Test 4B

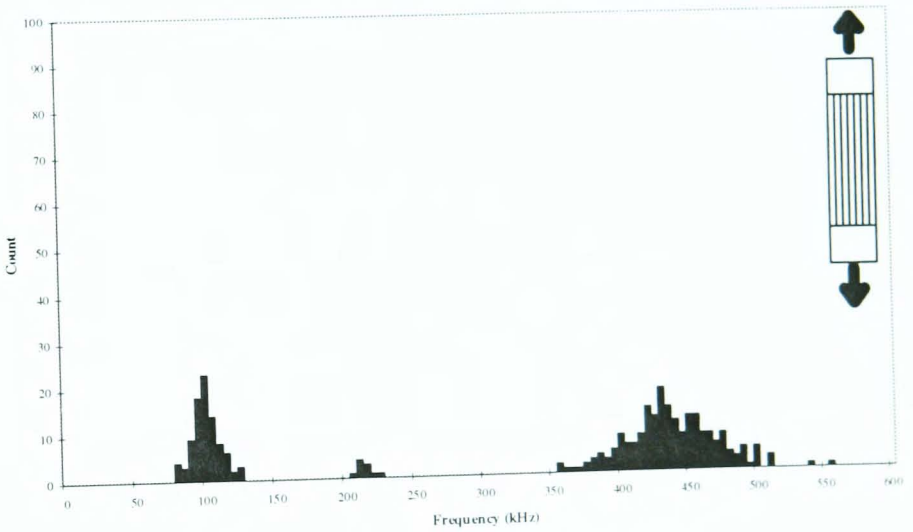

Test 4C

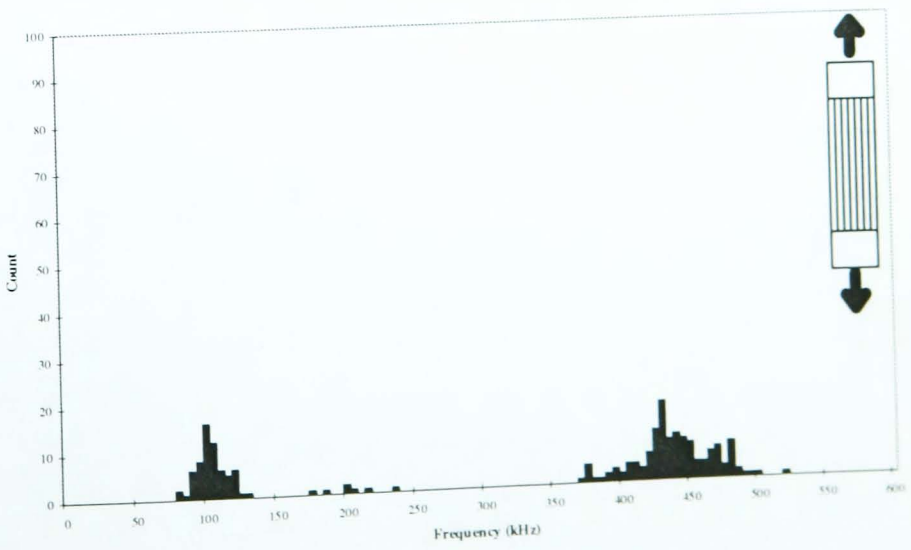

Test 4D

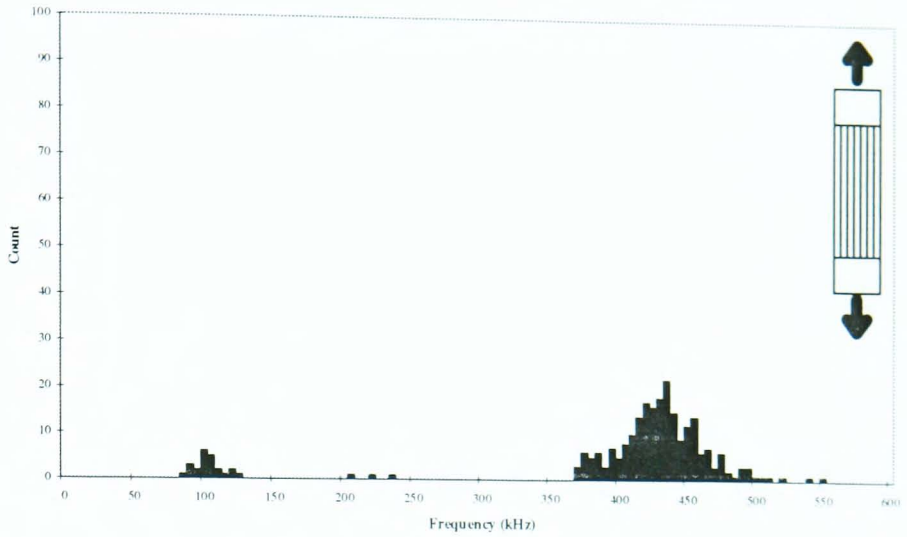

Test 4E

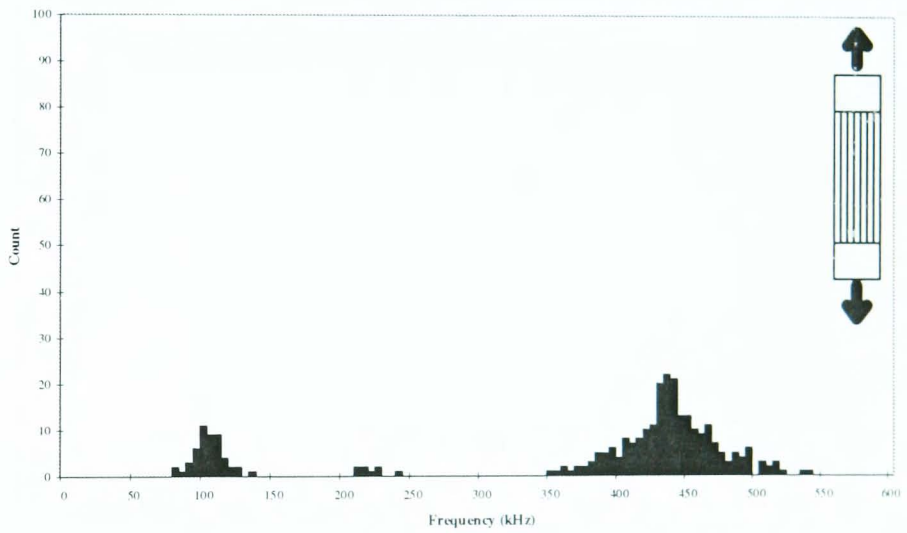

Test 4F

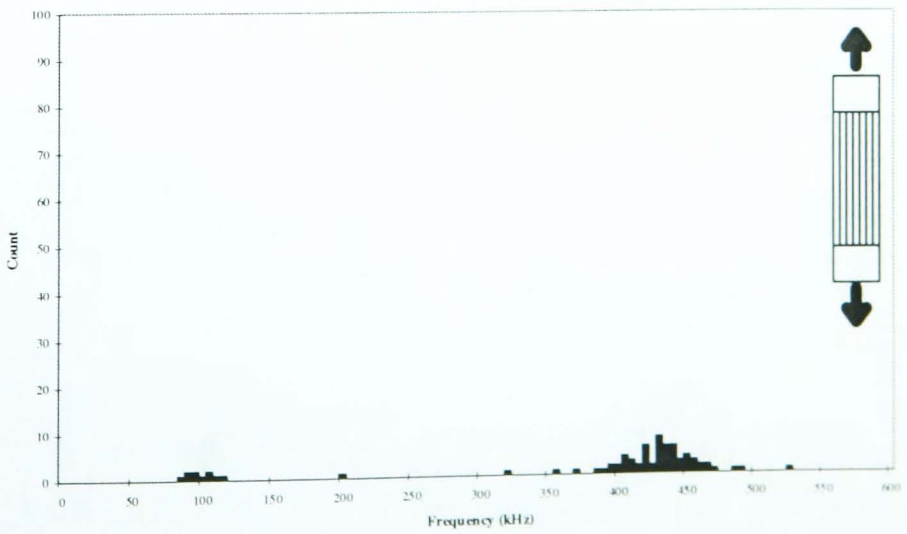

Test 4G

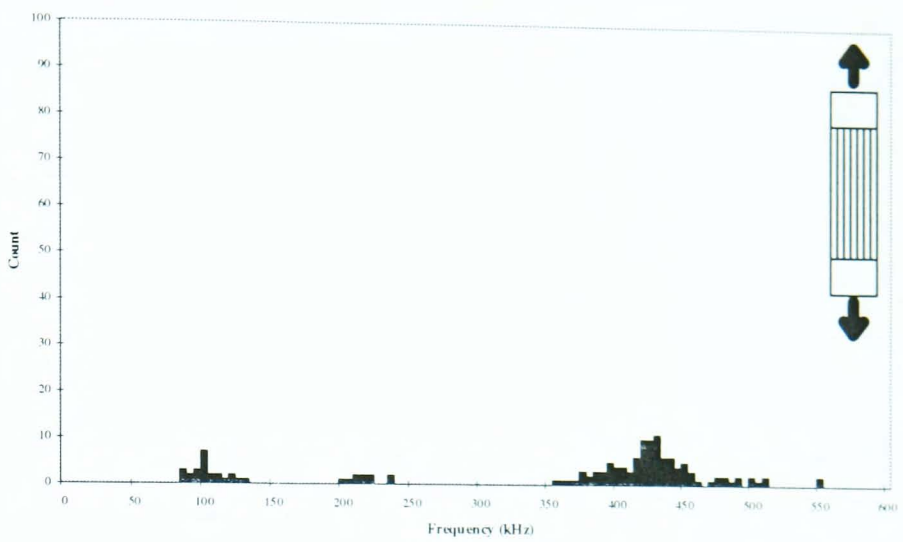

Test 4H

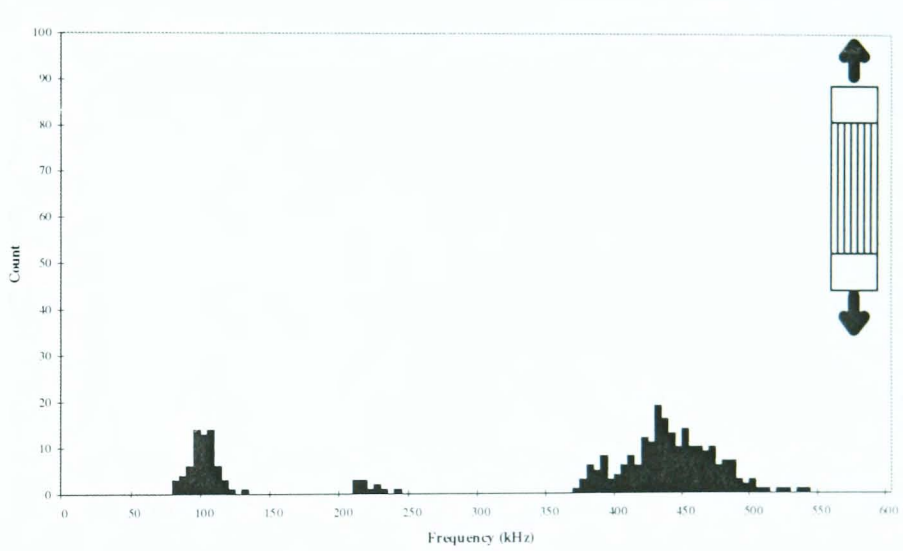

Test 4J

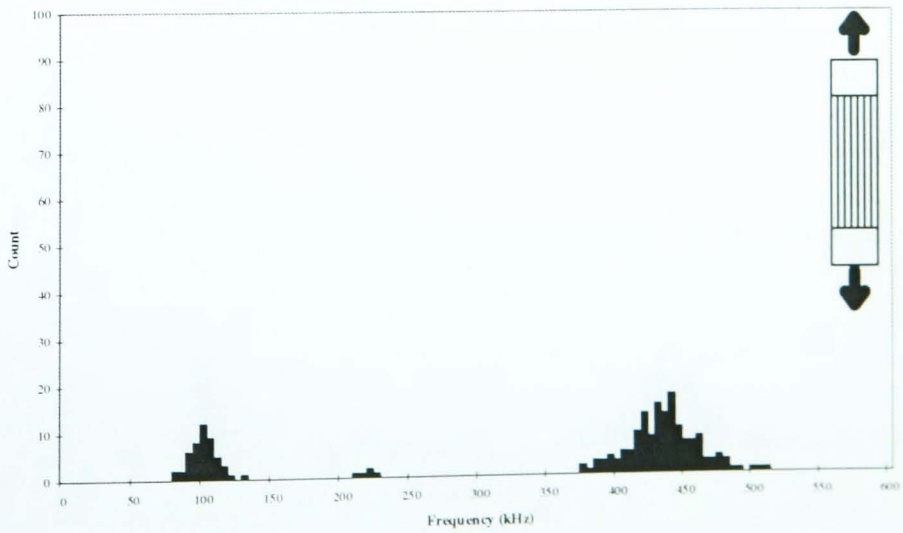

Test 4K

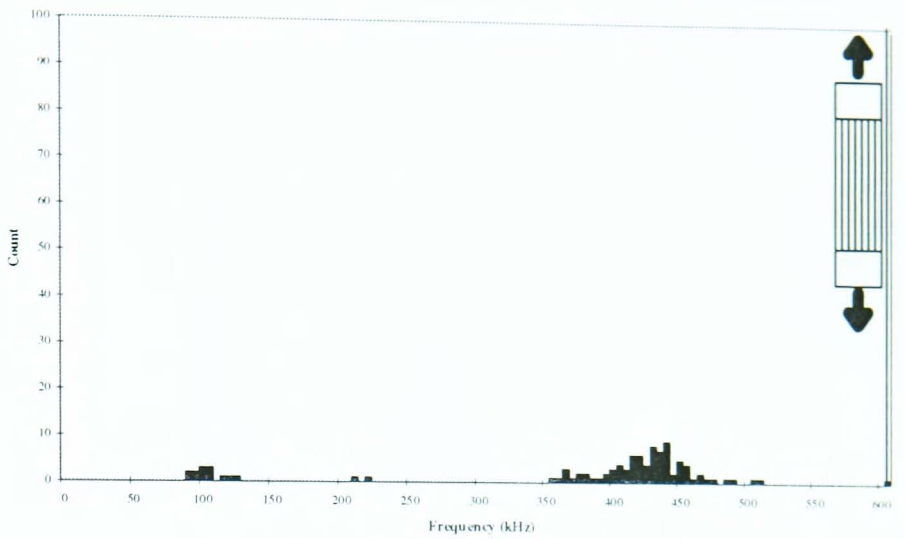

Test 4L

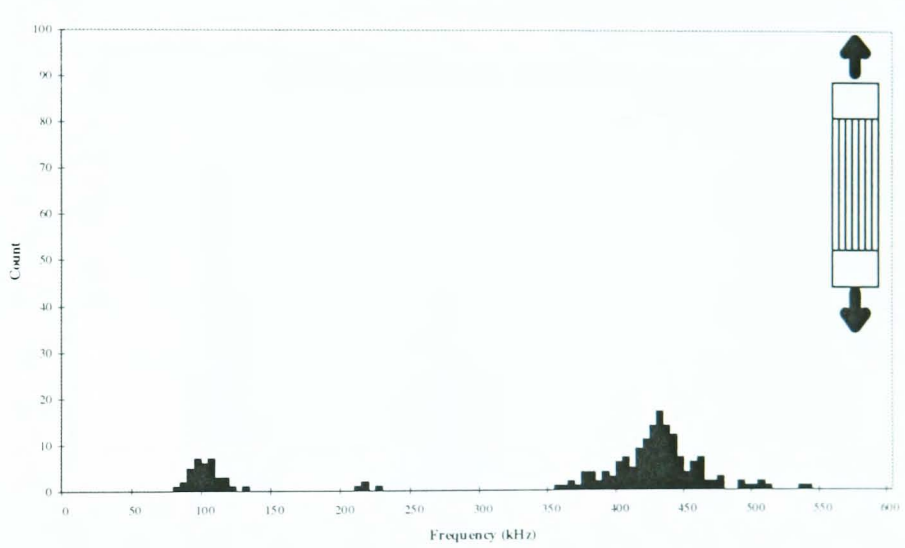

Test 4M

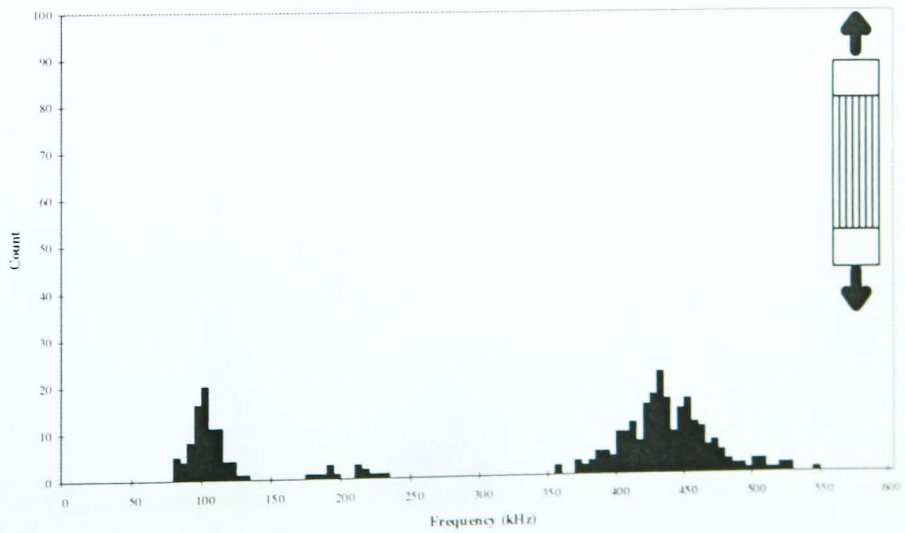

C.2.5 Tensile Loading of Specimens Containing Embedded Teflon Discs

Test 5A

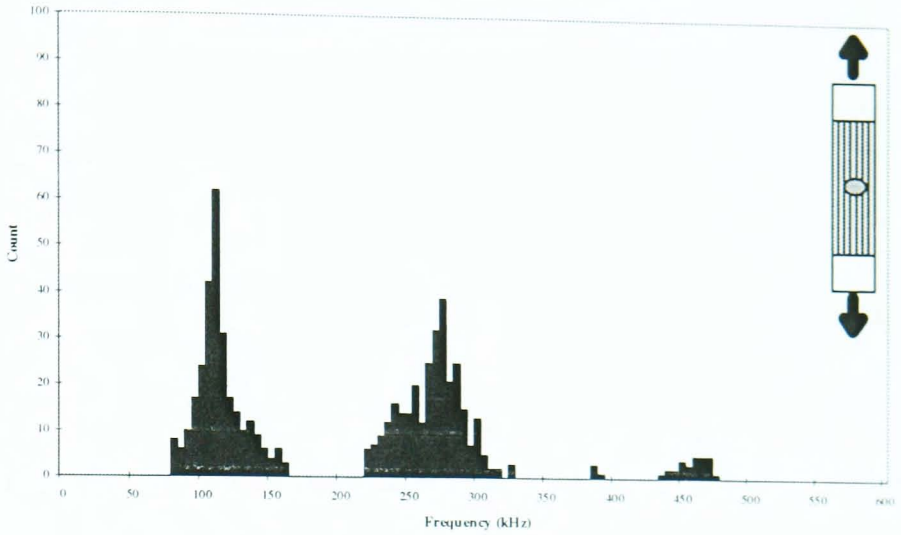

Test 5B

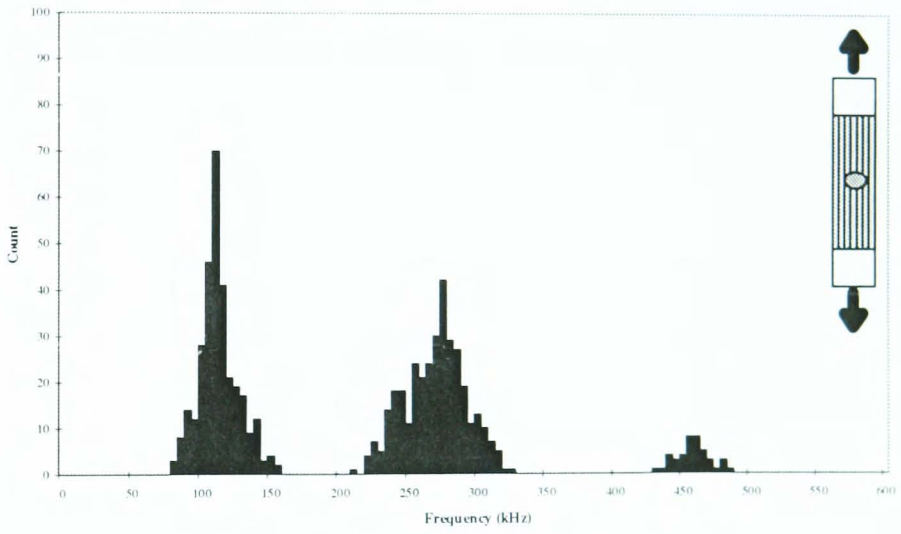

Test 5C

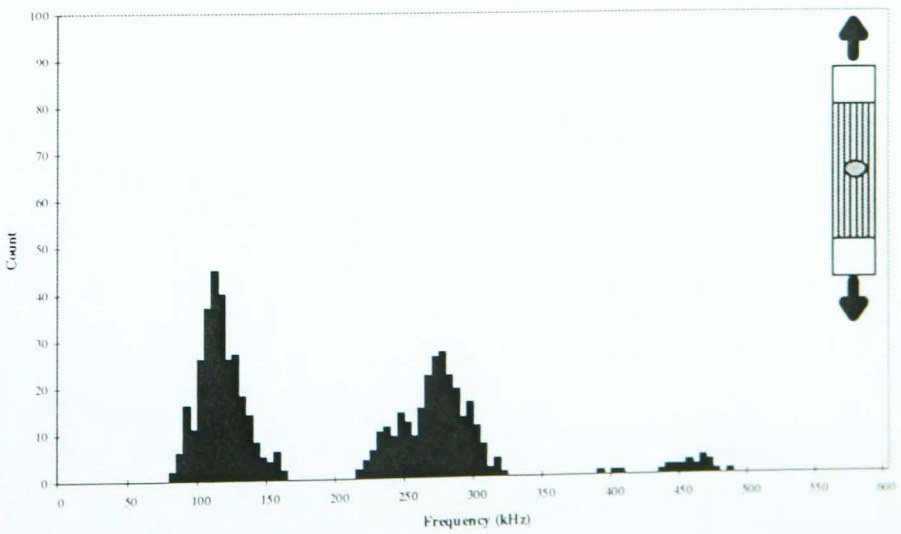

Test 5G

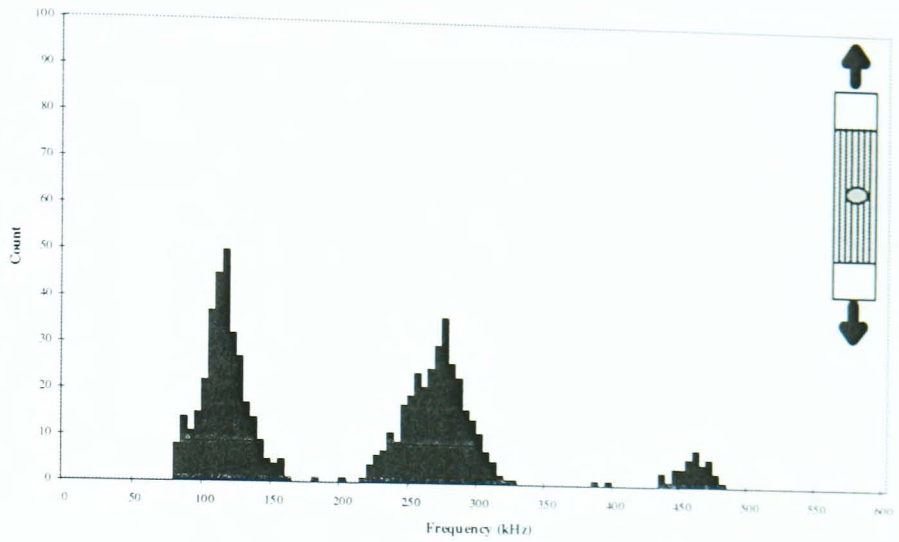

Test 5H

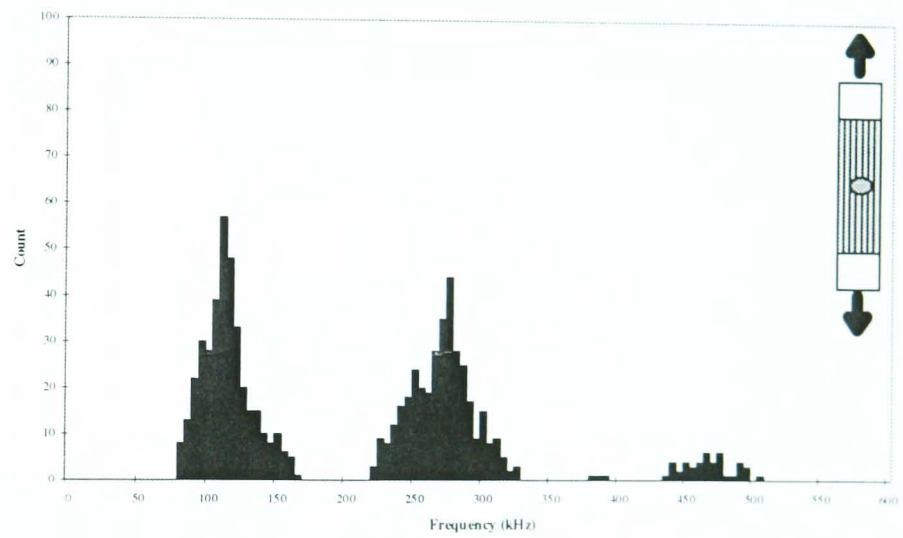

Test 5J

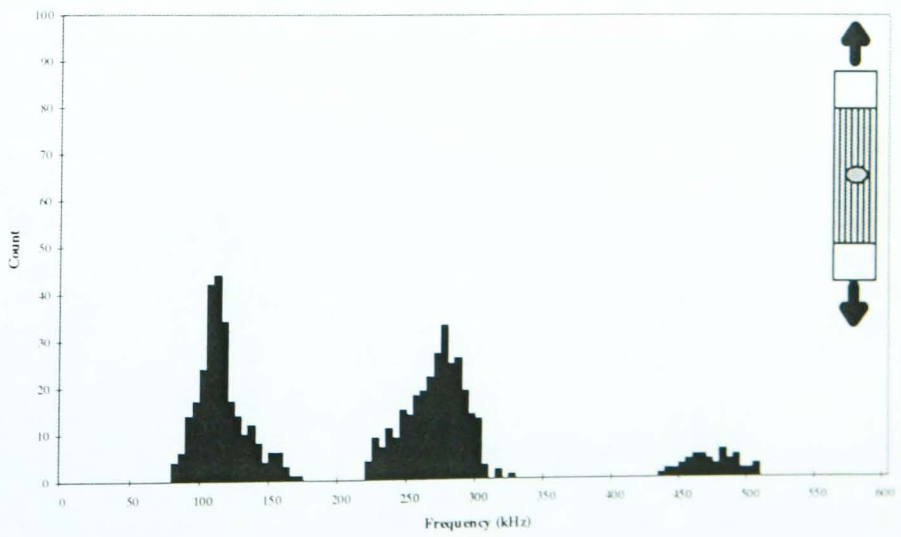

Test 5K

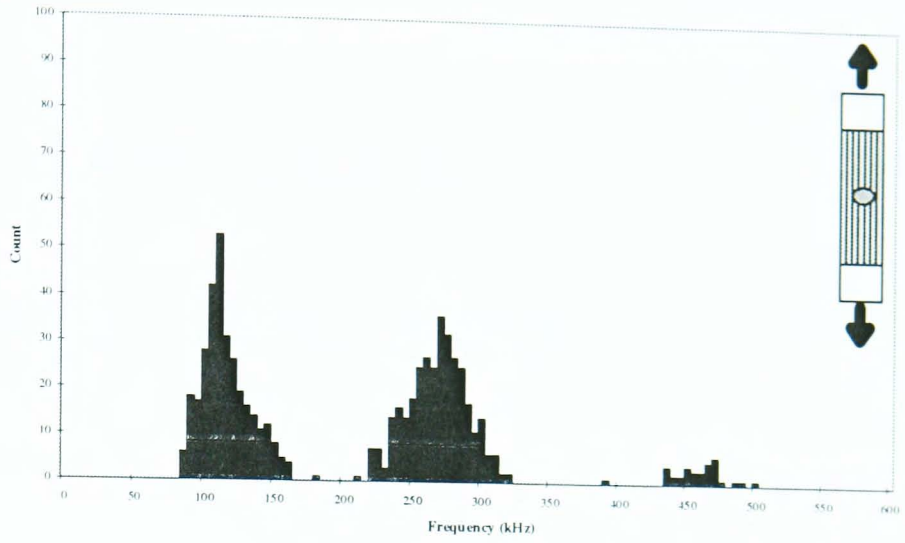

Test 5L

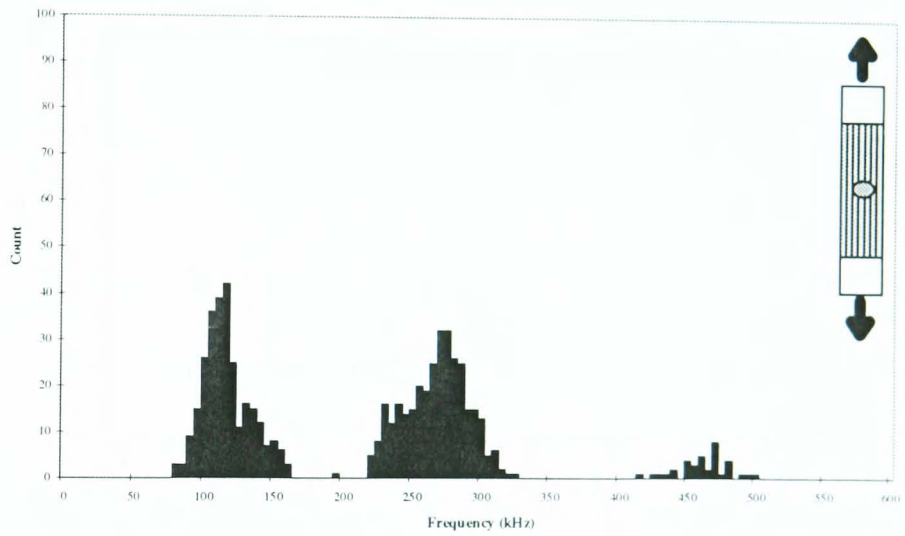

Test 5M

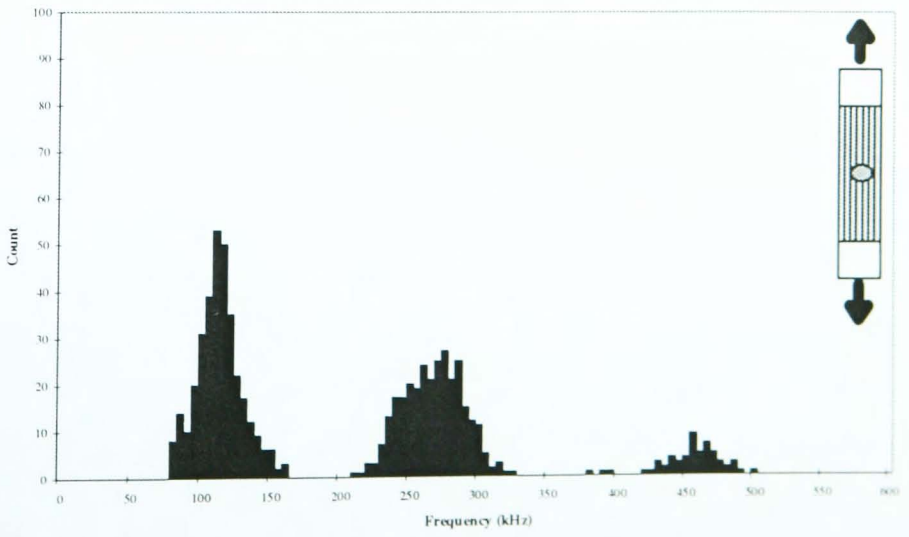

APPENDIX D

PAPERS PUBLISHED

Optical fibre sensing of acoustic emission in fibre reinforced composites

P W R Baillie, K F Hale[1], G F Fernando[2] and B E Jones

The Brunel Centre for Manufacturing Metrology and [2]The Department of Materials Technology, Brunel University, Uxbridge, Middlesex, UB8 3PH, UK
[1]To whom correspondence should be addressed.

Abstract: Over the last decade there has been a rapid growth in the use of advanced composite materials offering enormous potential for use in a wide number of engineering applications. Therefore, information about the integrity of the composite component during its service life is an ongoing concern. In many industrial applications the composite component being assessed is usually taken out of service and tested under conditions alien to the material. The development of a real-time, in-situ damage detection system would ensure that material inspection could be conducted on site under normal service conditions without withdrawing the component from service. This paper describes the development of an acoustic emission (AE) detection system, where the monitoring of AE activity emitted from within a carbon/epoxy composite material is achieved using an all-fibre Mach-Zehnder interferometric sensor. This single mode optical fibre sensor has been embedded in the material to give an in-situ capability.

1. Introduction

In recent years there has been an increasing use of advanced composite materials for a variety of applications, for example, aircraft structures, sports equipment and automotive components. These materials offer high specific strength and stiffness properties, excellent fatigue and corrosion resistance and can be used to manufacture complex component shapes. However, the structural integrity of the composite material may deteriorate under service conditions due to manufacturing defects such as voids, impact damage, fatigue loading, and environmental effects such as ingression of moisture.

Once initiated, damage propagation can develop and is not readily evident from visual inspection or other non-destructive techniques such as x-ray, ultrasonics, and edge replication. Therefore, the development of a built-in damage detection system based on optical fibres embedded within the composite structure at the time of manufacture represents a very attractive proposition for the non-destructive evaluation (NDE) of composite structures. This clearly has both safety and economic advantages and therefore could lead to a greater confidence in the use of advanced composite materials, possibly even permit current design criteria to be reviewed.

The onset of micro-damage in composites is accompanied by a sudden release of energy within the material. Some of this energy is dissipated in the form of elastic waves, known as Acoustic Emission (AE). Numerous mechanisms have been proposed and confirmed as sources of AE, for example, fracture of fibres and matrix, fibre/matrix debonding, initiation and propagation of intra-laminar and inter-laminar cracks, and debonding between lamina (delamination).

Therefore, the goal of the AE measuring system is to detect the acoustic event and provide suitable signal processing to characterise it and determine its significance. The most critical component of any AE measurement system is the transducer. The conventional NDE technique for monitoring material degradation through AE is based on the piezoelectric effect. Piezoelectric (PZ) transducers are sensitive over the frequency range of interest (100kHz-2MHz), easy to use, relatively cheap and are an established technology. However, these type of transducers are contacted externally to the material and are not suitable for monitoring AE in-situ within the material. This paper reports the use of an all optical fibre Mach-Zehnder interferometric sensor to monitor AE. The optical fibre sensor (OFS) is

embedded into the composite at the time of manufacture. Any AE activity due to internal composite damage will modulate the dimensions and refractive index of this embedded optical fibre, and result in the modulation of the phase in the sensing arm of the interferometer.

2. Optical fibre sensing of AE in composite materials

In 1950 Kaiser showed that the micro-damage present in many materials can be evaluated by the detection of internally generated acoustic stress waves, or AE. Since then AE has received growing attention due to the relative ease of detection and in-situ and real-time mode of operation. It is possible to obtain information about the defect (type, geometry, and possibly location) through the detection of acoustic events using the conventional PZ transducer[1]. However, there are many advantages of using optical fibres over their electrical counterparts, such as immunity from electromagnetic interference, high electrical isolation and corrosion and fatigue resistance[2]. An optical sensor is a device in which an optical signal can be modulated by an external stimulus, such as temperature, pressure, and strain. There has been some published work in the open literature covering embedded optical fibre sensors for measuring AE[5-8], and sufficient work has been done to show that such a sensing system is feasible.

In 1989 a breakthrough in the development of a localised embedded AE detection system for composite damage monitoring based on fibre optic Michelson interferometry was reported by Liu et al [3,4]. At this time, little had been done to develop a fibre optic sensor for AE detection that could sense damage in real time. Their research included the development and testing of a system employing an active homodyne detection scheme (used to maintain linearity and maximum sensitivity). The system provided single-ended sensing with real-time monitoring capabilities and a certain degree of localisation. The optical fibre AE sensors were embedded into Kevlar/epoxy composite specimens which were subject to tensile loading. The resulting AE signals were detected and found to have a broad-band response of 100kHz to 1MHz. This OFS detected acoustic signals associated with the formation of threshold regions of delaminations[5, 6].

The research work reported to date has shown that the high sensitivity of an interferometric OFS allows it to detect damage within a composite material. The all-fibre Mach-Zehnder interferometer reported here is being used to monitor AE emanating from damaged carbon fibre reinforced plastic (CFRP) specimen under tensile stress. The Mach-Zehnder interferometer has the advantage of not requiring mirrors at the end of the fibres

3. Experimental techniques

3.1. The fibre optic AE detection system

The design of the optical-fibre phase-modulated sensor was a two-stage process. The first stage involved the sensing element, where the mechanical interactions between the measurand and the optical fibre produces a phase shift in light transmitted. In the second stage the interferometer detects these phase shifts by modulating the output intensity. In the all-fibre Mach-Zehnder interferometer[7] (Figure 1) the light is coupled from a coherent source (for example, a polarised He-Ne laser or a laser diode) into a monomode optical fibre, and the optical signal is divided into two paths by means of a 2x2 directional coupler (DC1).

In the signal arm of the interferometer, polarisation controllers (PC1 and PC2) enable the recombining beams to be mutually coherent and have identical polarisation states. In the reference arm, several turns of fibre are wrapped around a PZ drum, which is driven by a high voltage feedback to produce a controllable phase shift. In the sensing arm, a length of single-mode optical fibre is embedded in the material under consideration. A section of the sensing arm, equal to the embedded and pigtail lengths of the test piece, has been cut out and replaced with a demountable composite test section.

The signal and reference beams are recombined at a second directional coupler (DC2), giving two optical outputs at the photodiode detectors (PD1 and PD2). The signal beam is phase modulated by the external stimulus (that is, the AE activity), whereas the phase of the reference beam remains constant. The reference is set at the quadrature point of the system by implementing an active homodyne feedback technique[8]. This technique locks out any environmental phase perturbations. After passing through a high-pass filter (100kHz cut-off frequency) the output signal becomes the optical

phase change induced by high frequency AE waves. The output from the fibre optic AE detection system has been monitored using an AE signal analyser (AET5500). This collects the output AE events which cross its preset threshold level and determines in real-time a series of AE parameters which will help distinguish the level of damage.

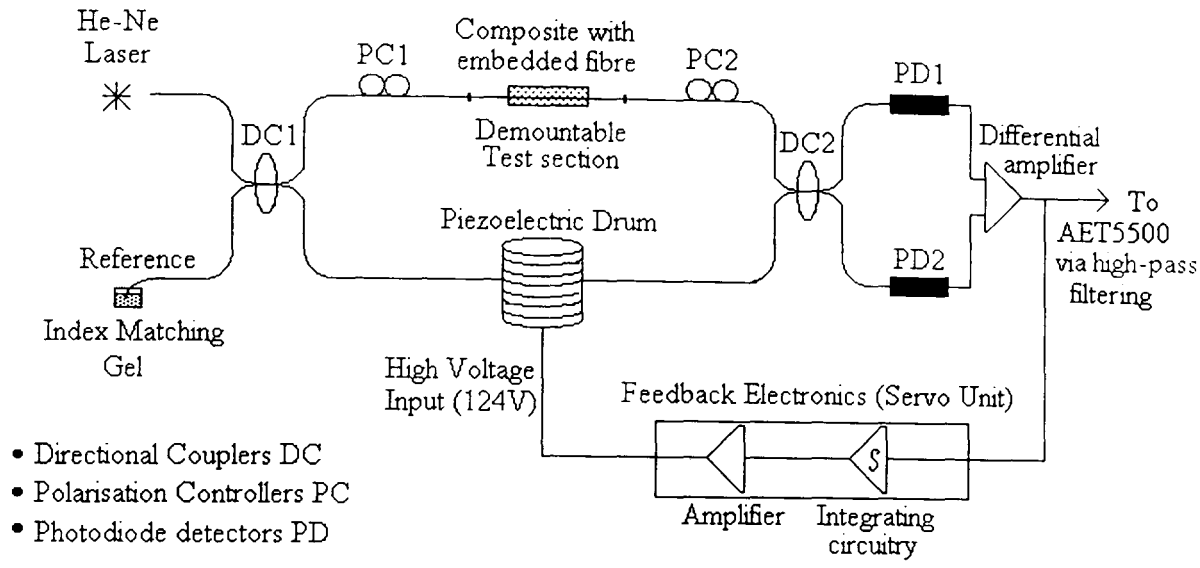

Figure 1. Schematic diagram of the all optical fibre Mach-Zehnder interferometric sensor.

3.2. Material and specimens

The tensile specimens were manufactured by hand laying 16 plies of pre-impregnated carbon fibre (Ciba Geigy T300/920) prepreg using a $[0, 90, 90, 0, 0, 90, 0, 90]_S$ sequence. The prepregs were cut into strips and placed in individual specimen moulds. The optical fibre's acrylate layer was stripped and the fibre was placed along the length of the composite specimen at the 8/9 ply interface. The samples were cured at 0.62MPa for 1 hour at 125°C. A schematic illustration of the test specimen is shown in Figure 2. In order to distinguish the AE activity of damaged and undamaged composite materials, samples were pre-damaged by drilling two 2mm holes either side of the optical fibre in the centre of the composite specimens.

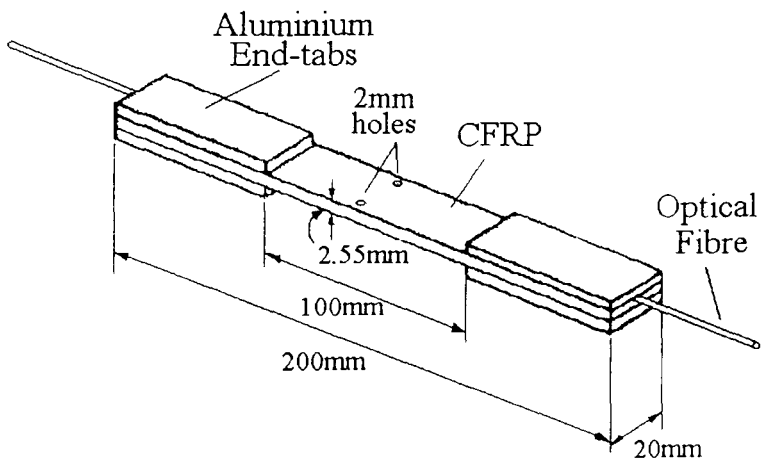

Figure 2. The dimensions of the CFRP tensile specimens. The optical fibre is protected from damage at the fibre/composite interface by embedded PTFE tubing.

4. Experimental results and discussion

It is essential to characterise the AE detection system before it can be used to progressive damage. Several tests have been carried out to characterise the system for known acoustic events. These tests were as follows: active acoustic excitation and simulated AE event detection. Once this was achieved the composite specimen was tensile tested using a Hounsfield tensometer. The AE activity was monitored using the embedded optical fibre sensor and the PZ transducer so that a comparison between the two sensors could be made.

4.1. Active acoustic excitation

The first set of characterisation experiments involved the acoustic excitation of the composite specimen using a separate PZ transducer, driven sinusoidally at approximately 160kHz. This source and the broadband PZ detector were placed approximately 50mm apart. The responses of the optical sensor and the PZ transducer are shown in Figure 3. The interferometric sensor results compare favourably with its electrical counterpart. The difference in the two signals was due to the fact that the OFS gain was limited by the processing unit.

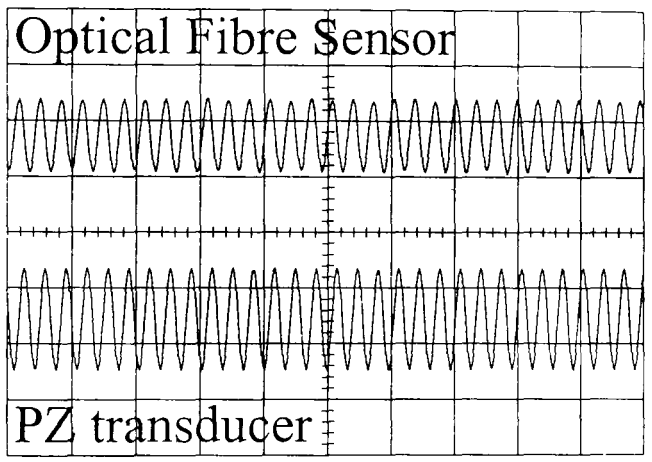

Figure 3. A comparison between optically and electrically sensed signals due to an applied AE signal at a frequency of 160kHz. The amplitude scale for the OFS and PZ transducer was 1V and 5V per division respectively whereas the time base for both traces was 20μs per division.

4.2. Simulated acoustic emission

The most common method of simulating broadband AE signals in a material involves the fracture of a 0.5mm 2H graphite pencil lead (Nielson source) while the lead is in contact with the surface of the material. The pencil-break tests were performed using a Teflon jig which maintained a constant angle between the pencil lead and the material surface. This pencil-break technique was used to evaluate the response of the fibre optic system prior to collecting damage-induced AE data from materials. Once again, the response of the optical fibre sensor was compared to a PZ transducer subjected the same excitation (Figure 4). The results yielded a reproducible high frequency AE signal, which took the form of an exponentially decaying sinusoidal oscillation.

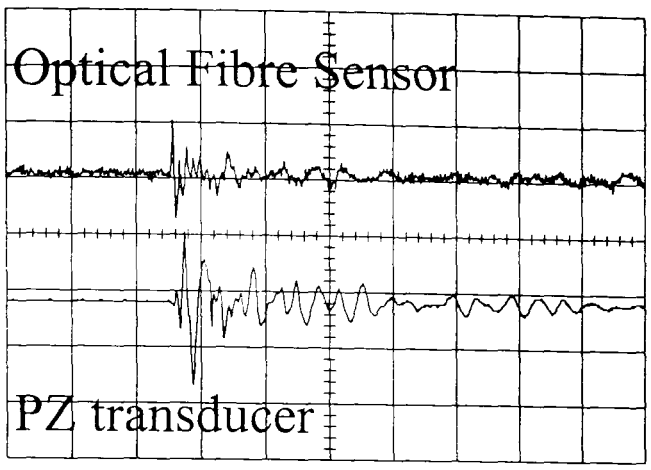

Figure 4. A comparison between optically and electrically sensed AE activity caused by a pencil break on a composite sample. The amplitude scale for the OFS and PZ transducer was 1V and 5V per division respectively whereas the time base for both traces was 20μs per division.

4.3. AE from a damaged composite

The pre-damaged composite sample with the embedded optical fibre was placed in the grips of the Hounsfield tensometer. The emphasis of the test was placed on counting the number of AE signals generated as damage progressed through the specimen. On the application of the load there was a small amount of AE activity, indicating the onset of micro-damage. As the amount of damage in the composite increased, there was a point where the rate of AE activity dramatically increased. In the cumulative AE event count graph this can be seen by the 'knee' in the curve (Figure 5). The dramatic increases in AE could be due to significant matrix cracks, delaminations, and ultimately, fibre fractures.

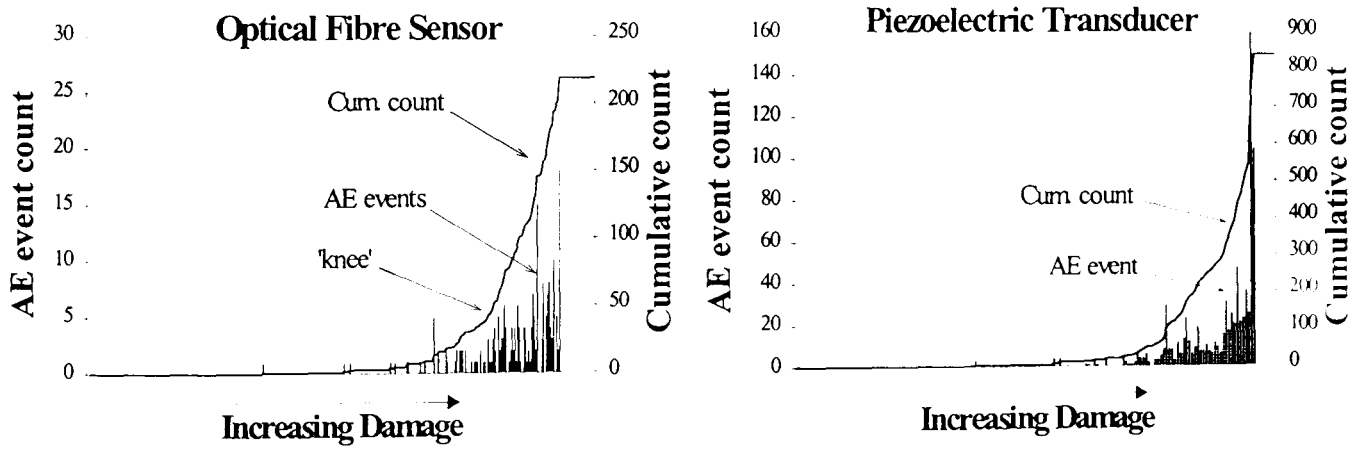

Figure 5. Acoustic Emission from a CFRP specimen loaded in tension to failure

The tensile loading of the composite samples produced AE 'events v time' graphs which was consistent from test to test. The cumulative AE event count graphs were also all similar to the exponentially increasing trend found using PZ transducers[9,10] by other authors for CFRP samples loaded in tension. The AE from the composite sample in tension was also monitored using a PZ transducer mounted on the composite surface. The combined event and cumulative count plots for both the OFS and PZ transducer are shown in figure 5. A comparison of the cumulative count plots for the OFS and the PZ transducer show that the embedded OFS was the less sensitive (Figure 6).

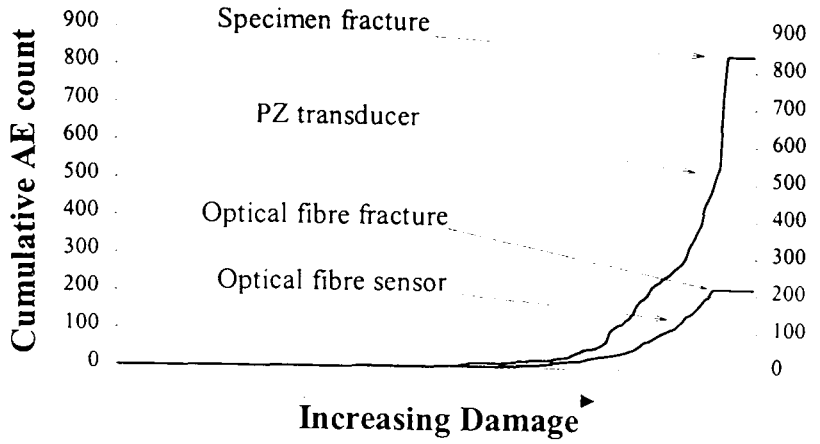

Figure 6. A comparison between optically and electrically sensed cumulative AE count plots.

The overall gain of the OFS was 10dB less than the electrical system and therefore fewer signals crossed the threshold voltage of the AET5500. The gain of the OFS was limited by the processing electronics. The number of events captured by the OFS was also limited by the fact that the embedded optical fibre fractures just before specimen failure. This was due to the high crosshead speed used for the tensile test.

5. Conclusions and future work

In these experiments it has been shown that AE activity can be observed using an embedded optical fibre and that the results compared favourably with those obtained from the standard PZ transducer under the same conditions. A Mach-Zehnder all-fibre interferometric OFS has been applied to monitoring the AE resulting from progressive damage that occurs during loading of a CFRP composite. The sensitivity of the interferometer is dependent on the optical path difference (OPD) between the two arms. The introduction of fibre collimators into the sensing arm would improve the OPD towards the ideal zero. As the gain of the OFS is governed by its processing unit, different AET5500 threshold levels will need to be investigated to ensure that the system is sensitive to smaller amplitude AE signals. Further characterisation of the AE signals generated by progressive composite damage will be performed to determine the most effective operation of the sensor. Frequency and time domain analysis of the AE will enable characterisation of the severity of the accumulated damage.

Acknowledgements

The authors gratefully acknowledge financial support from UK Engineering and Physical Sciences Research Council.

References

(1) Zimcik DG, Proulx D, Roy C, Mashouli A.
"Real time monitoring of carbon epoxy composites using acoustic emission "
NDE, SAMPE Quarterly, January, pp5-11, (1988)
(2) Jackson DA.
"Monomode optical fibre interferometers for precision measurement"
J.Phys.E: Sci.Instrum.,18 , pp981-1001, (1985)
(3) Liu K, Ferguson SM. and Measures RM.
"Damage detection in composites with embedded fiber optic interferometric sensors"
Fibre optic smart structures and skins II , pp205-210, (1989)
(4) Liu K, Ferguson SM, Measures RM.
"Fiber optic interferometric sensor for the detection of acoustic emission within composite materials"
Optics letters, 15 No.22, pp1255-1257, (1990)
(5) Measures RM, Valis T, Liu K, Hogg D, Ferguson SM, Tapanes E.

"Interferometric fiber optic sensors for use with composite materials"
Optical testing and metrology III, SPIE 1332, pp421-430, (1990)
(6) Liu K, Ferguson SM, McEwan K, Tapanes E, Measures RM.
"Acoustic emission detection for composite damage assessment using embedded ordinary single mode fiber optic interferometric sensors"
Fiber optic smart structures and skins III, SPIE 1370, pp316-323, (1990)
(7) Zheng SX, McBride R, Barton JS, Jones JDC, Hale KF, Jones BE.
"Intrinsic optical fibre sensor for monitoring acoustic emission"
Sensors and Actuators A, 31, pp110-114, (1992)
(8) Udd E.
"Fiber Optic Sensors- An introduction for engineers and scientists"
Ch.10, (John Wiley & Sons, Inc.), (1991)
(9) Fuwa M, Bunsell AR, and Harris B.
"Tensile failure mechanisms in carbon fibre reinforced plastics"
J.Material Science, 10, pp2062-2070, (1975)
(10)Miller RK. and McIntire P. (Editors)
"Nondestructive Testing Handbook: Volume 5- Acoustic Emission Testing (2nd Ed.)"
Sect.12, Part 3, (Amer. Soc. NDT), (1987)

A Study of the Acoustic Emission Behaviour from Carbon Fibre Reinforced Plastic Composites using an Optical Fibre Sensor

P.W.R. Baillie, K.F. Hale[1], B.E. Jones and G.F. Fernando[2]

The Brunel Centre for Manufacturing Metrology and [2]The Department of Materials Technology, Brunel University, Uxbridge, Middlesex, UB8 3PH, UK

[1]To whom correspondence should be addressed.

Abstract: In recent years there has been a rapid growth in the use of advanced composite offering enormous potential for use in a wide number of engineering applications, ranging from sports goods to advanced aircraft structures. Therefore, information about the integrity of the composite component during its service life is an ongoing concern. Many investigations on material evaluation have been studied, however, the failure mechanisms associated with on-going damage are difficult to clarify because composite materials have complex failure processes due to their anisotropic and non-homogeneous properties. To evaluate the state of health of the composite, a real-time, in-situ acoustic emission (AE) damage detection system has been developed, where the monitoring of AE activity emitted from within a carbon/epoxy composite material (CFRP) is achieved using an all-fibre Mach-Zehnder interferometric sensor. This paper describes the development of this detection system and its attempts to compare the fracture behaviour and AE characteristics generated during tensile tests using CFRP laminates.

1 Introduction

In recent years the use of composite materials, such as Kevlar and graphite reinforced epoxy laminates, to form structural components in a variety of engineering applications has increased rapidly and current trends indicate that this will continue. These materials offer high specific strength and stiffness properties, excellent fatigue and corrosion resistance and can be used to manufacture complex component shapes. However, the structural integrity of the composite material may actually deteriorate during fabrication. Damage may also be initiated at a low applied stress level loading under service conditions, where the component is subjected to impact or fatigue loading.

The onset of micro-damage in composites is accompanied by a sudden release of energy within the material. Some of this energy is dissipated in the form of elastic waves, known as Acoustic Emission (AE). Numerous failure mechanisms in composites have been proposed and confirmed as sources of AE, for example, fracture of fibres and matrix, fibre/matrix debonding, initiation and propagation of intra-laminar and inter-laminar cracks, and debonding between laminae (delamination).

The fracture analysis of fibre reinforced composites has received a great deal of attention in recent years with intensive experimental and theoretical studies being conducted on all types of composites. The focus of most failure analysis research

studies has been on laminated composites. This class of structural laminates is fabricated from a basic two-part composite system consisting of a polymeric matrix reinforced by continuous fibres. The laminate investigated in this report, a carbon fibre reinforced plastic (CFRP), is such a system whereby the laminate panel is fabricated by pressing a number of prepreg plies in the pre-determined ply stacking and fibre orientation order and then hardened into a layered structure.

Once initiated, damage propagation can develop and is not readily evident from visual inspection or other non-destructive techniques such as x-ray, ultrasonics, and thermography. Therefore, the development of a real time, in-situ damage detection system based on optical fibres embedded within the composite structure at the time of manufacture represents a very attractive proposition for the non-destructive evaluation (NDE) of composite structures. The goal of the AE measuring system is to detect the acoustic event and provide suitable signal processing to characterise it and determine its significance. The most critical component of any AE measurement system is the transducer. Piezoelectric (PZ) transducers are sensitive over the frequency range of interest (100 kHz-2 MHz), easy to use, relatively cheap and are an established technology. However, these type of transducers are contacted externally to the material and are not suitable for in-situ monitoring AE within the material.

This paper reports the development and use of an all optical fibre Mach-Zehnder interferometric sensor to monitor the AE behaviour within a CFRP composite under applied tension. The object of the tests undertaken was to determine the degree of delamination in the composite. Although other fracture mechanisms contribute to the degradation of the structural integrity of the specimen, the onset of delamination results in accelerated damage in the material.

2 Optical Fibre Sensing of Acoustic Emission in Composite Materials

In 1950 Kaiser showed that the micro-damage present in many materials can be evaluated by the detection of internally generated acoustic stress waves, or AE. Since then AE has received growing attention due to the relative ease of detection and in-situ and real-time mode of operation. It is possible to obtain information about the defect (type, geometry, and possibly location) through the detection of acoustic events using the conventional PZ transducer [1]. However, there are many advantages of using optical fibres over their electrical counterparts, such as immunity from electromagnetic interference, high electrical isolation and corrosion and fatigue resistance [2]. An optical fibre sensor (OFS) is a device in which an optical signal can be modulated by an external stimulus, such as temperature, pressure, and strain. There has been some published work in the open literature covering embedded optical fibre sensors for measuring AE [5-8], and sufficient work has been done to show that such a sensing system is feasible.

In 1989 a breakthrough in the development of a localised embedded AE detection system for composite damage monitoring based on fibre optic Michelson interferometry was reported by Liu et al [3,4]. At this time, little had been done to develop a fibre optic sensor for AE detection that could sense damage in real time.

The system provided single-ended sensing with real-time monitoring capabilities and a certain degree of localisation. The optical fibre AE sensors were embedded into Kevlar/epoxy composite specimens which were subject to tensile loading. The resulting AE signals were detected and found to have a broad-band response of 100 kHz to 1 MHz. This OFS detected acoustic signals associated with the formation of threshold regions of delaminations [5, 6]. The research work reported to date has shown that the high sensitivity of an interferometric OFS allows it to detect damage within a composite material. The Mach-Zehnder interferometer, however, has the added advantage over other interferometric methods of not requiring mirrors at the end of the fibres.

3 Experimental Techniques

3.1 The fibre optic AE detection system

The design of the optical-fibre phase-modulated sensor was a two-stage process. The first stage involved the sensing element, where the mechanical interactions between the measurand and the optical fibre produces a phase shift in the light transmitted. In the second stage the interferometer detects these phase shifts by modulating the output intensity. In the all-fibre Mach-Zehnder interferometer [7] (Figure 1) the light is coupled from a coherent source (for example, a polarised He-Ne laser or a laser diode) into a monomode optical fibre, and the optical signal is divided into two paths by means of a 2x2 directional coupler (DC1).

In the signal arm of the interferometer, polarisation controllers (PC1 and PC2) enable the recombining beams to be mutually coherent and have identical polarisation states. In the reference arm, several turns of fibre are wrapped around a PZ drum, which is driven by a high voltage feedback to produce a controllable phase shift. In the sensing arm, a length of single-mode optical fibre is embedded in the material under consideration. A section of the sensing arm, equal to the embedded and pigtail lengths of the test piece, has been cut out and replaced with a demountable composite test section.

The signal and reference beams are recombined at a second directional coupler (DC2), giving two optical outputs at the photodiode detectors (PD1 and PD2). Any AE activity due to internal composite damage will modulate the dimensions and refractive index of this embedded optical fibre, and result in the modulation of the phase in the sensing arm of the interferometer. The phase of the reference beam remains constant (set at the quadrature point of the system) by implementing an active homodyne feedback technique [8]. This technique locks out any environmental phase perturbations. After passing through a high-pass filter (100 kHz cut-off frequency) the output signal becomes the optical phase change induced by high frequency AE waves. The output from the fibre optic AE detection system has been monitored using an AE signal analyser (AET5500). This collects the output AE events which cross its pre-set threshold level and in real-time determines a series of AE parameters which will help distinguish the level of damage.

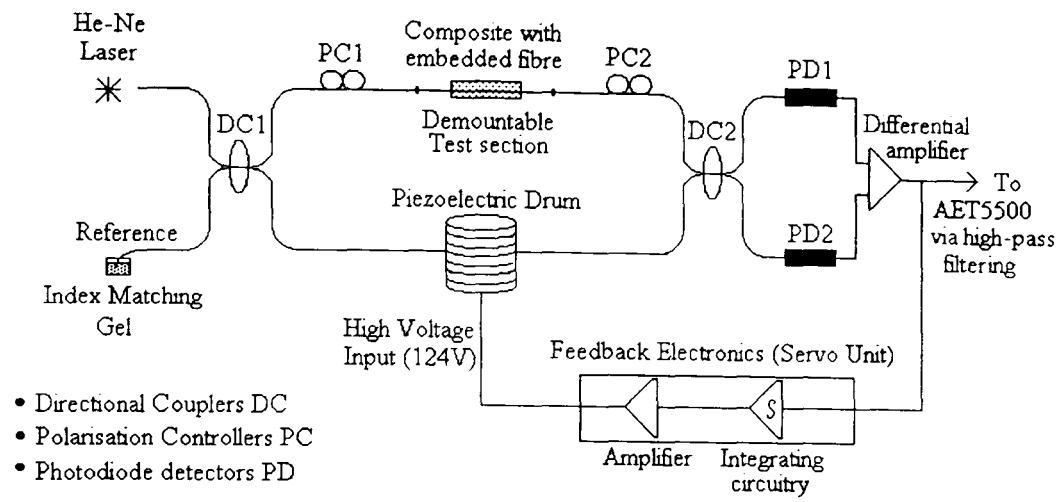

Figure 1 Schematic diagram of the all optical fibre Mach-Zehnder interferometric sensor.

3.2 Material and specimen preparation

The material system used for this study was T300/920 carbon fibre prepreg manufactured by Ciba Geigy. The fibre volume fraction of this material was approximately 0.60 and the average ply thickness is 0.16mm. The test specimens were manufactured by hand-laying 16 plies of the pre-preg material using a $[0, 90_2, 0_2, 90, 0, 90]_S$ sequence. The uncured panel was cut into 200mm X 20mm strips and placed in individual specimen moulds. The optical fibre sensor's acrylate outer layer was removed and the stripped fibre placed along the length of the composite specimen in the 4/5 ply interface. A dummy fibre was also placed in the 12/13 ply interface to maintain overall material symmetry. The samples were cured at 0.62MPa for 1 hour at 125°C. A schematic illustration of the test specimen is shown in Figure 2.

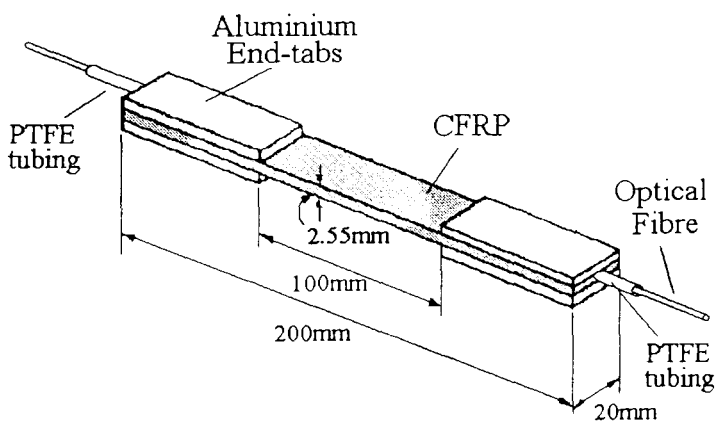

Figure 2 The dimensions of the CFRP tensile specimens.

3.3 Mechanical test facilities

The tensile tests on the CFRP samples were performed within the Department of Materials Technology at Brunel University. An Instron 1195 testing machine was used to load the specimen, and the resulting load was recorded via both a chart recorder and the analogue port of the AET5500 acoustic emission monitoring system. The specimen was loaded at a crosshead speed of 1 mm/min.

3.4 The acoustic emission data acquisition and processing

The AE signals were collected from the OFS and PZ resonant transducer 375 kHz (AET Corp. AC375L), preamplified (40 dB) and filtered (100 kHz-1 MHz and 250-500 kHz respectively). The AET5500 mainframe amplification was fixed at 30 dB and the threshold level of this system was set to 1V to ensure that only significant AE events were recorded. Once the signal has been processed, analysis of the AE signal could be made through events and peak amplitude.

4 Experimental Results and Discussions

4.1 Characterisation of the fibre optic acoustic emission detection system

It is essential to characterise the AE detection system before it can be used to monitor progressive damage. Several tests have been carried out to characterise the system for known acoustic events. These tests were as follows: *active acoustic excitation* and *simulated AE event detection*. The first set of characterisation experiments involved the active acoustic excitation of the composite specimen using a separate PZ transducer, driven sinusoidally at approximately 160 kHz. This source and the broadband PZ detector were placed approximately 50 mm apart. The responses of the optical sensor and the PZ transducer are shown in Figure 3(a). The interferometric sensor results compare favourably with its electrical counterpart.

The most common method of simulating broadband AE signals in a material involves the fracture of a 0.5mm 2H graphite pencil lead (Nielson source) while the lead is in contact with the surface of the material. The pencil-break tests were performed using a Teflon jig which maintained a constant angle between the pencil lead and the material surface. This pencil-break technique was used to evaluate the response of the fibre optic system prior to collecting damage-induced AE data from materials. Once again, the response of the optical fibre sensor was compared to a PZ transducer subjected to the same excitation (Figure 3b). The results yielded a reproducible high frequency AE signal, which took the form of an exponentially decaying sinusoidal oscillation.

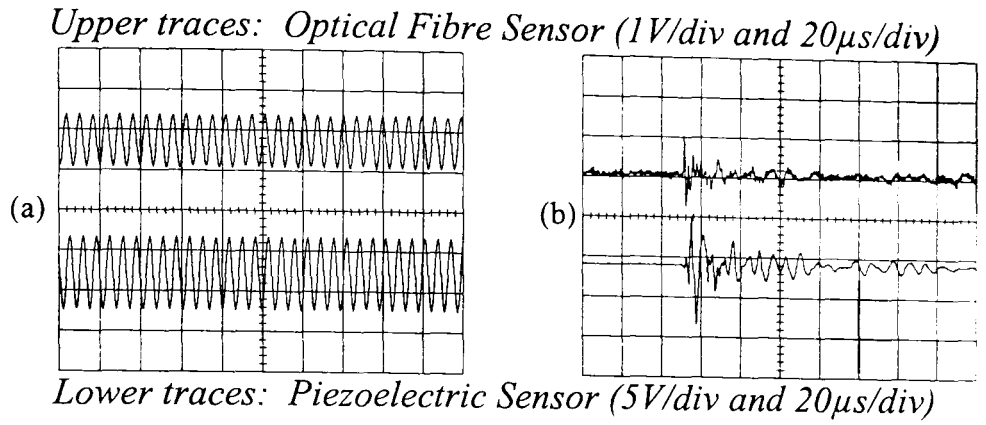

Figure 3 A comparison between optically and electrically sensed signals due to (a) an applied AE signal at a frequency of 160kHz and (b) a pencil break on the composite surface.

4.2 AE from a composite specimen under tension.

The composite sample with the embedded optical fibre was placed in the grips of the tensile testing machine (Instron 1195). The emphasis of the test was placed on monitoring the AE signal parameters generated as damage progressed through the specimen. On the application of the load, the AE signals began to occur at a load of about 50% of the failure load. They then significantly increased until the failure load is reached. This indicated that internal damage initiated slowly then accelerated rapidly towards the end of the maximum load. As the amount of damage in the composite increased, there was a point where the rate of AE activity dramatically increased. In the cumulative AE event count graph this can be seen by the 'knee' in the curve (Figure 4a). In previous studies this knee in the curve indicated the onset of delamination [9]. The cumulative AE event count graphs were also all similar to the exponentially increasing trend found using PZ transducers by other authors for CFRP samples loaded in tension [10,11]. The AE from the composite sample in tension was also monitored using a PZ transducer mounted on the composite surface. The combined event and cumulative count plots for both the OFS and PZ transducer are shown in figure 4b.

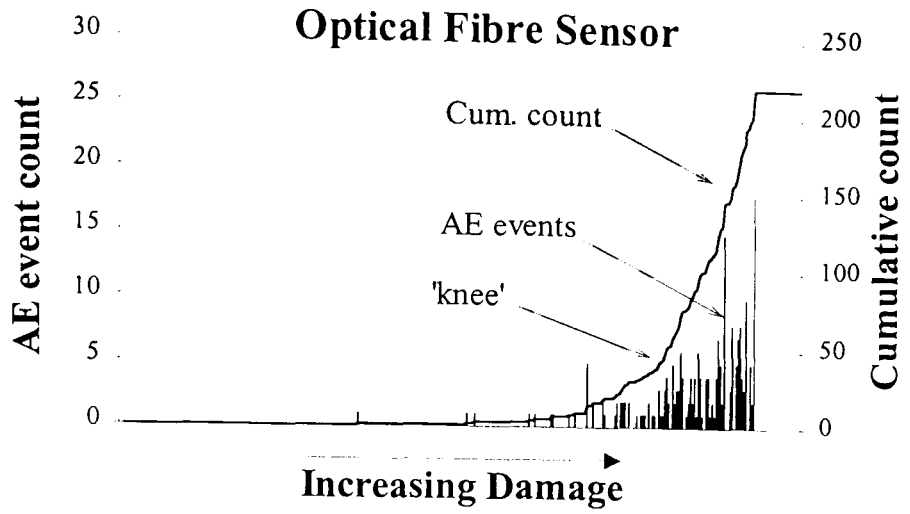

(a)

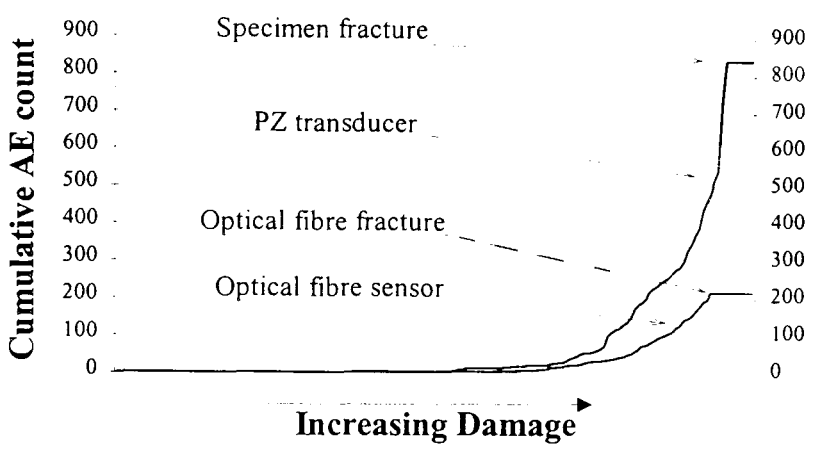

(b)

Figure 4 Acoustic emission from a CFRP specimen load in tension to failure:- (a) Event count and cumulative event count graph, and (b) and comparison between the OFS and the PZ transducer in terms of cumulative event count. This graph also shows that the OFS fractured before the specimen failed.

The load ranges used were 0-60%, 60-80%, 80-90%, and 90% to failure load. The embedded optical fibre sensor fractures at around 98% of the failure load. This is indicated by the time delay between the sensor and specimen failure in figure 4(b). Therefore, many AE signals which occur just before the specimen failure could not be detected.

The results obtained using the OFS showed that a population curve with a mean amplitude of 28dB could be observed during the 0-60% range. As the load increased towards the final loading stage the population curve became more broad with the amplitude ranging from 23-57dB (figure 5).

Generally, the AE signal of lower amplitudes are considered to be emitted from a crack which released a small elastic energy, and the AE signal of higher amplitudes emitted from a crack which released a larger elastic energy. Research studies [12, 13]

have indicated that matrix cracking is associated with low amplitude signals, and carbon fibre fracture with higher signal amplitudes. It has also been shown [14] that the initiation and slow growth of delamination have amplitudes in the range 50-70 dB. Rapid advances of delaminations, which consists of many fibre breakages and a large matrix crack, have amplitudes in excess of 70 dB. It is difficult to make a comparison between these stated values and the experimental results, as the response of the OFS is lower than the PZ transducer response.

It can be hypothesised that the matrix cracking occurred at the onset of damage. Through the mathematical relationship by Berthelot [12], it can be assumed that the broadening of the population curve at the latter stages of loading (80-90% of the failure load) is due to a combination of matrix cracking and carbon fibre fracture. The higher amplitude signals, obtained just before the sensor failure, were almost certainly due to matrix cracking, carbon fibre fractures and partial delamination. However, the development of damage in the specimen could not be accurately correlated with the AE signals obtained. It is necessary to combine the time domain analysis with edge replication techniques [15] to help discriminate between each mode of failure and estimate the relevance of the AE output.

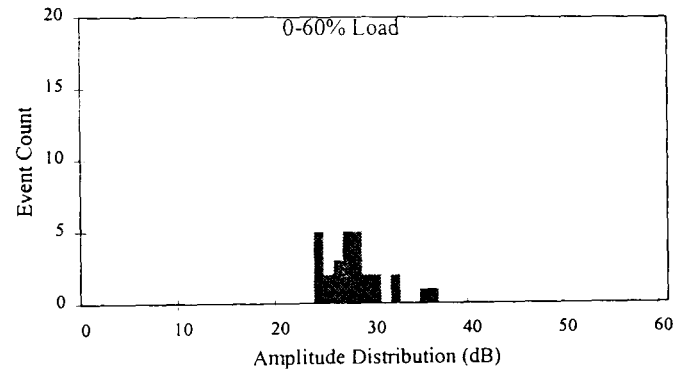

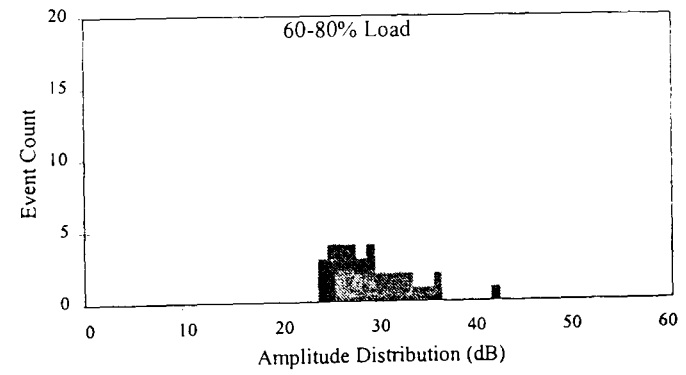

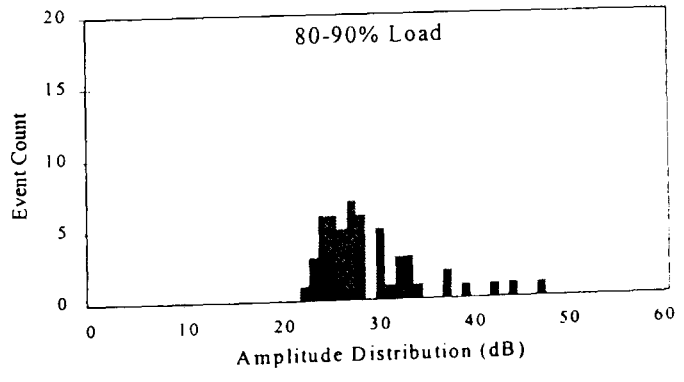

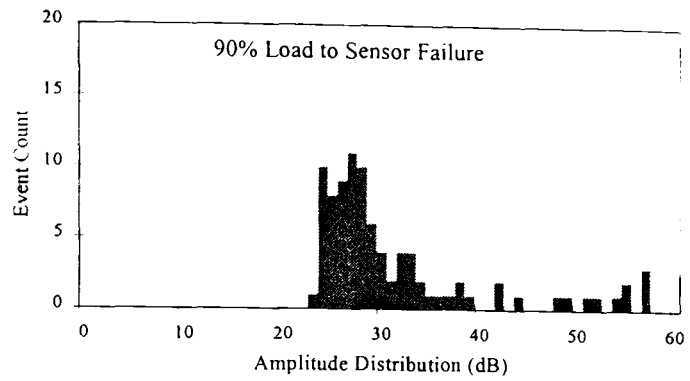

Figure 5 Amplitude distribution analysis of the AE signals detected by the optical fibre sensor for various load ranges up to specimen failure

5 Conclusions and Future Work

In these experiments it has been shown that AE activity can be observed using an embedded optical fibre and that the results compared favourably with those obtained from the standard PZ transducer under the same conditions. A Mach-Zehnder all-fibre interferometric OFS has been applied to monitoring the AE resulting from progressive damage that occurs during loading of a CFRP composite. In general, fibre reinforced composites fail in a complex manner by a combination of fibre fracture, matrix cracking, interface failure and fibre pull-out and each of these mechanisms contribute to the total acoustic emission. From the time domain results obtained, it was difficult to distinguish between each individual damage mechanism. To discriminate between each mode of failure it is necessary to combine the time-domain analysis with optical observations made using edge replication. Replicas of the polished composite edge can be taken at pre-set load intervals to provide a permanent record of the damage occurring in the sample. This technique, coupled with frequency and time domain analysis of the AE, will enable further characterisation of the AE signals generated by progressive composite damage and help determine the most effective operation of the sensor. Future material testing will incorporate composite samples which have predominant modes of failure. Artificial delamination initiators, such as Teflon inclusions or holes drilled in the composite laminate, will provide an early indication of the growth of delamination.

Acknowledgements

The authors gratefully acknowledge financial support from UK Engineering and Physical Sciences Research Council.

References

[1] Zimcik D.G., Proulx D., Roy C., Mashouli A., *Real Time Monitoring of Carbon Epoxy Composites using Acoustic Emission,* NDE, SAMPE Quarterly, January, pp5-11, (1988)

[2] Jackson D.A., *Monomode Optical Fibre Interferometers for Precision Measurement,* J.Phys.E: Sci.Instrum., Vol. 18 , pp981-1001, (1985)

[3] Liu K., Ferguson S.M. and Measures R.M., *Damage Detection in Composites with Embedded Fiber Optic Interferometric Sensors,* Fibre optic smart structures and skins II, pp205-210, (1989)

[4] Liu K., Ferguson S.M., Measures R.M., *Fiber Optic Interferometric Sensor for the Detection of Acoustic Emission within Composite Materials*, Optics letters, Vol. 15 No.22, pp1255-1257, (1990)

[5] Measures R.M., Valis T., Liu K., Hogg D., Ferguson S.M., Tapanes E., *Interferometric Fiber Optic Sensors for use with Composite Materials,* Optical testing and metrology III, SPIE 1332, pp421-430, (1990)

[6] Liu K., Ferguson S.M., McEwan K., Tapanes E., Measures R.M., *Acoustic Emission Detection for Composite Damage Assessment using Embedded Ordinary Single Mode Fiber Optic Interferometric Sensors,* Fiber optic smart structures and skins III, SPIE 1370, pp316-323, (1990)

[7] Zheng S.X., McBride R., Barton J.S., Jones J.D.C., Hale K.F., Jones B.E., *Intrinsic Optical Fibre Sensor for Monitoring Acoustic Emission,* Sensors and Actuators A, 31, pp110-114, (1992)

[8] Udd E., *Fiber Optic Sensors- An Introduction for Engineers and Scientists,* Ch.10, (John Wiley & Sons, Inc.), (1991)

[9] Roy C., Mashouli A., and Piasta Z., *Classification of Acoustic Emission Sources in CFRP Assisted by Pattern Recognition Analysis*, Canadian Aeronautics and Space J.,Vol. 34, No. 4, pp224-232

[10] Fuwa M., Bunsell A.R., and Harris B., *Tensile Failure Mechanisms in Carbon Fibre Reinforced Plastic,* J.Material Science, 10, pp2062-2070, (1975)

[11] Miller R.K. and McIntire P. (Editors), *Nondestructive Testing Handbook: Volume 5- Acoustic Emission Testing (2nd Ed.),* Sect.12, Part 3, (Amer. Soc. NDT), (1987)

[12] Berthelot J.M., *Relation between Amplitudes and Rupture Mechanisms in Composite Materials*, Proc. 2nd Int. Symp. on Acoustic Emission from Reinforced Plastics, Montreal, Canada, July 1986, pp126-133

[13] Berthelot J.M. and Rhazi J., *Acoustic Emission in Carbon Fibre Composites*, Composite Science and Technology, Vol. 37, pp411-428, (1990)

[14] Ono K., *Acoustic Emission Behaviour of Flawed Unidirectional Carbon Fiber-Epoxy Composites*, J. Reinforced Plastics and Composites, Vol. 7, pp90-105, (1988)

[15] Steiner K.V., Eduljee R.F., Huang X., and Gillespie J.W., *Ultrasonic NDE Techniques for the Evaluation of Matrix Cracking in Composite Laminates*, Composite Science and Technology, Vol. 53, pp193-198, (1995)

REFERENCES

Chapter 1

Cantwell W.J., and Morton J. (1992), *The Significance Of Damage And Their Detection In Composite Materials: A Review*, J. Strain. Anal., Vol. 27, no. 1, pp. 29-42.

Cole P.T. (1988), *The Capabilities And Limitations Of NDT: Part 7- Acoustic Emission*, Brit. Inst. of NDT.

Fuhr P.L. (1993), *Simultaneous Single-Fiber Active Vibration Sensing And Impact Detection For Large Space Structures*, Smart Sensing, Processing and Instrumentation, SPIE 1918, pp. 145-153.

Hamstad M.A., and Sendeckyj G.P. (1993), *Acoustic Emission Technology For Smart Structures*, J. Acoustic Emission, Vol. 11, no. 1, pp. 33-41.

Harris, B. (1986), *Engineering Composite Materials*, Inst. Materials, London UK.

Measures R.M. (1989), *Smart Structures With Nerves Of Glass*, Prog. Aerospace Sci., Vol. 26, pp. 289-351.

Measures R.M. (1991), *Fiber Optic Considerations And Developments For Smart Structures*, Fiber Optic Smart Structures and Skins III, SPIE 1588, pp. 282-299.

Melle S.M. (1994), *Todays Sensors For Tomorrows Structures*, Photonics Spectra, pp. 88-94.

Scruby C.B. (1987), *An Introduction To Acoustic Emission*, J. Phys.E: Sci. Instrum., Vol. 20, pp. 946-953.

Chapter 2

Halmshaw R. (1991), *Non-Destructive Testing*, 2nd ed., Edward Arnold, London UK.

Liu D., Lillycrop L.S., Malvern L.E., and Sun C.T. (1987), *Evaluation Of Delamination: An Edge Replication Study*, Experimental Techniques, Vol. 11, No. 5

Summerscales J. (1987) (editor), *Non-Destructive Testing Of Fibre Reinforced Plastics Composites*, Vol. 1, Elsevier Applied Science Ltd, Barking UK.

Summerscales J. (1990) (editor), *Non-Destructive Testing Of Fibre Reinforced Plastics Composites*, Vol. 2, Elsevier Applied Science Ltd, Barking UK.

Chapter 3

The ASME Boiler and Pressure Vessel Code (1983) , Section V (Non-Destructive Testing), The American Society of Mechanical Engineers, 1983

CARP/C. Howard Adams (1982), *Recommended Practice for Acoustic Emission Testing of Fiberglass Reinforced Plastic Tanks/Vessels*, 37th Annual Conf., Reinforced Plastics/Composites Institute, The Society of the Plastics Industry, Jan. 11-15th, 1982.

Awerbuch J., Gorman M.R., and Madhukar M. (1983), *Monitoring Acoustic Emission During Quasi-static Loading/Unloading Cycles of Filament-Wound Graphite Epoxy Laminate Coupons*, 1st Int. Symp. Acoustic Emission from Reinforced Composites, SPI, New York, pp. 1-19.

Baillie P.W.R, Fernando G.F., Hale K.F., and Jones B.E. (1995), *Optical Fibre Sensing of Acoustic Emission in Fibre Reinforced Composites*, Sensors and their Applications VII, Dublin

Barre S. and Benzeggagh M.L. (1994), *On the use of Acoustic Emisson to investigate damage mechanisms in glass-fibre-reinforced polypropolene, Composites. Science and Technology*, Vol. 52, pp. 369-376

Berthelot J.M. and Rhazi J. (1990), *Acoustic emission in carbon fibre composites,* Composites Science and Technology, Vol. 37, pp. 411-428

Ceysson O., Salvia M. and Vincent L. (1996), *Damage mechanisms characterisation of carbon fibre/epoxy composite laminates by both electrical resistance measurements and acoustic emission analysis,* Scripta Materialia, Vol. 34, No. 8, pp. 1273-1280

Degroot P.J., Wijnen P. and Jansen R.B.F. (1995), *Real time frequency determination of Acoustic Emission for different fracture mechanisms in carbon/epoxy composites,* Composites Science and Technology, Vol. 55, pp. 405-412

Hamstad M.A. and Moore R.L. (1986), *Acoustic emisson from single and multiple Kevlar 49 Filament breaks,* Journal of Composite Materials, Vol. 20, pp. 46-66

Hamstad M.A. (1992), *An Examination of Acoustic Emission Evaluation Criteriafor Advanced Type Fiber/Polymer Composites*, Proc. 4th Int Symp, on Acoustic Emission from Composite Materials, Am. Soc. NDT, Columbus, Ohio, pp. 436-449

Hamstad M.S., and Downs K.S. (1995), *On characterisation and Location of Acoustic Emission Sources in Real Size Composite Structures- A Waveform Study*, Journal of Acoustic Emission, Vol. 13, Nos. 1/2, (1995)

Kawamoto K. and Ono K. (1986), *Pattern recognition analysis of Acoustic Emission Signals from carbon fibre/epoxy composites,* International Conference in AE from composites 1986 Paris, pp. 230-239

Kawamoto K. and Ono K.(1989), *Pattern Recognition Analysis of Acoustic Emission from Carbon/Epoxy Composites*, Proc. 3rd Int. Symp. on Acoustic Emission from Comosite Material, Am. Soc. NDT, Columbus, Ohio, pp. 230-239

Krietsch T., and Bohse J. (1998), *Selection of acoustic emissions and classification of damage mechanisms in fiber composite materials*, J. of Acoustic Emission, Vol. 16, pp S233-242

Liu D. (1988), *Impact-Induced Delamination- A View Of Bending Stiffness Mismatching*, J. Composite Materials, Vol. 22, pp. 674-692.

Miller R.K. and McIntyre P. (editors), (1987) , NonDestructive Testing Handbook, Volume 7- Acoustic Emission Testing, 2nd. ed., American Society For Nondestructive Testing, Columbus ,Ohio.

Mittleman A. and Roman I. (1991), Monitoring *the tensile deformation in real unidirectional Kevlar/epoxy composites,* NDT & E International, Vol. 24, no. 2, pp.85-89.

Ono K. (1988), *Acoustic emission behaviour of flawed unidirectional carbon fibre/epoxy composites,* Journal Reinforced plastics and composites, Vol. 1, pp. 90-105

Pappas Y.Z., Markopoulos Y.P., and Kostopoulos V. (1998), *Failure mechanisms analysis of 2D carbon/carbon using acoustic emission monitoring*, NDT&E International, Vol. 31, No. 3, pp 157-163

Wevers M. (1997), *Listening to the sound of materials: acoustic emission for the analysis of material behaviour*, NDT&E International, Vol. 30, No. 2, pp 99-106

Zimcik D.G., Proulx D., Roy C. and Maslouhi A. (1988), *Real-time monitoring of carbon-epoxy composites using acoustic emisson NDE.* SAMPE Quarterly, Vol. 19, No. 2, pp. 5-11

Chapter 4

Bennett KD. and Claus RO. (1986), *Internal Monitoring Of Acoustic Emission In Graphite Epoxy Composites Using Imbedded Optical Fiber Sensors*, Conf.Proc., Rev.Progress in quantitative NDE, San Diego.

Blagojevic B., Tsaw W., McEwen K., and Measures R.M. (1990), *The Influence Of Embedded Fibres On The Interlamina Fracture Toughness Of Composite Materials*, Review of Progress in Quantitative NDE, Vol 9, pp. 1213-1218

Carolan T.A., Reuben R.L.,Barton J.S., and Jones J.D.C. (1997a), *Fiber optic Sagnac interferometer for non-contact structural monitoring in power plant applications*, Applied Optics, Vol. 36, No. 1, pp 380-385

Carolan T.A., Kidd S.R., Hand D.P., Wilcox S.J., Wilkinson P., Barton J.S., Jones J.D.C., and Reuben R.L. (1997b), *Acoustic emission monitoring of tool wear during the face milling of steels and aluminium alloys using a fibre optic sensor, Part1: Energy analysis*, Proc. Inst. Mech. Engrs, Vol 211 Part B, pp 299-309

Carolan T.A., Kidd S.R., Hand D.P., Wilcox S.J., Wilkinson P., Barton J.S., Jones J.D.C., and Reuben R.L. (1997c), *Acoustic emission monitoring of tool wear during the face milling of steels and aluminium alloys using a fibre optic sensor. Part1: Frequency analysis*, Proc. Inst. Mech. Engrs, Vol 211 Part B, pp 311-319

Phillippidis T.P., Nikolaidis V.N, and Anastassopoulos A.A. (1998), *Damage characterisation of carbon/carbon laminates using neural network techniques on AE signals*, NDT&E International, Vol. 31, No. 5, pp 329-340

Qi G., Barhorst A., Hashemi J., and Kamala G. (1997), *Discrete wavelet decomposition of acoustic emission signals from carbon fiber reinforced composites*, Comp. Sci. Tech., Vol. 57, pp389-403

Raj B. and Jha B.B. (1994), *Fundamentals of Acoustic Emission*, British Journal of NDT, Vol. 36, No. 1, pp. 16-23.

Rotem A. (1984), *Fracture Mode Identification of Composite Materials by Acoustic Emission Analysis*, Composites Technical Review, Vol. 6, No. 4, pp 145-168

Sato N., Kurauchi T. and Kamigaito O. (1986), *Fracture mechanism of unidirectional carbon-fibre reinforced epoxy-resin composites,* Journal Materials Science, Vol. 21, pp. 1005-1010

Takahashi K., and Choi N.S. (1998), *Characterisation of fracture process in short fibre reinforced plastics by acoustic emission*, J. of Acoustic Emission, Vol. 16, pp S224-232

Tang, W.I. Lee and G.S. Springer (1987), *Effects of cure pressure on resin flow, voids, and mechanical performance* , J.Composite material, 1987, Vo.21, pp. 412-440.

Thompson, H.C. Kim, and F.L.Matthews (1973), *The effect of processing on the microstructure of CFRP*, Composites, Vol. 4, pp. 86-87

Valis et al (1991), *Passive-Quadrature demodulated localised Michelson fiber-optic strain sensor*, J.Lightwave.Tech.. Vol.9, No. 4., April 1991

Cielo P. and Lapierre J. (1986), *Fibre Optic Ultrasound Sensing For The Evaluation Of Materials*, Applied Optics, Vol. 21, No. 4, pp. 572-576

Claus RO. and Cantrell JH. (1980), *Detection Of Ultrasonic Waves In Solids By An Optical Fiber Interferometer*, IEEE Ultrasonics Symp., pp. 719-721,

Dasgupta A., Wan Y., Sirkis J.S., and Singh H.(1990), *Micromechanical investigation of an optical fibre embedded in a laminated composite,* Fibre Optic Smart Structures and Skins III, SPIE 1370, pp119-128

Glossop N.D., Dubois S., Tsaw W., Leblanc M., Lymer J., Measures R.M, and Tennyson R.C. (1990), *Optical Fibre Damage Detection For An Aircraft Composite Leading Edge*, Composites., vol. 21, pp. 71-80

Greene J.A., Tran T.A., Bhatia V., Gunther M.F., Wang A., Murphy K.A., and Claus R.O. (1995), *Optical fiber sensing technique for impact detection and location in composites and metal specimens*, Smart Mater. Struct., Vol 4., No. 2, pp 93-99

Gunther M.F., Wang A., Fogg B.R., Starr S.E., Murphy K.A., and Claus R.O. (1993), *Fiber optic impact detection and location system embedded in a composite material*, Fiber Optic Smart Structures and Skins V, SPIE 1798, pp 262-269

Hale K.F., Hockenhull B.S, and Christodoulou G. (1980), *The Application Of Optical Fibres As Witness Devices For The Detection Of Plastic Strain And Cracking*, Strain, Vol. 16, No. 4, pp. 2234

Jackson D.A. (1985), *Monomode Optical Fibre Interferometers For Precision Measurement*, J. Phys E: Instrun.Sci, Vol.18, pp. 981-1001

Jensen D.W, Pascual J., and August J.A. (1992), *Tensile Strength And Stiffness Reduction In Graphite/Bismalemide Lamininates With Embedded Fibre Optic Sensors*, Active Materials and Adaptive Structures, pp. 115-120

Kurmer J.P., Kingsley S.A., Laudo J.S., and Krak S.J. (1993), *Applicability of a novel distributed fiber optic acoustic sensor for leak detection.* Distributed and Multiplexed Fiber Optic Sensors II, SPIE 1797, pp 63-71

Liu K, Ferguson SM. and Measures RM. (1989), *Damage Detection In Composites With Embedded Fiber Optic Interferometric Sensors*, Fibre optic smart structures and skins II (1989), pp. 205-215

Liu K, Ferguson SM, and Measures RM. (1990a), *Fiber-Optic Interferometric Sensor For The Detection Of Acoustic Emission Within Composite Materials*, Optics Letters, vol.15, no.22.

Lui K, Ferguson SM, McEwan K, Tapanes E, and Measures RM. (1990b), *Acoustic Emission Detection For Composite Damage Assessment Using Embedded Ordinary Single Mode Fiber Optic Interferometric Sensors*, Fiber optic smart structures and skins III, SPIE Vol. 1370, pp. 316-323

McBride R., Barton J.S., Jones J.D.C., and Borthwick W.K.D. (1990), *Fibre Optic Interferometry For Acoustic Emission Sensing In Machine Tool Wear Monitoring*, Electro-optics and Laser international conference

McBride R, Carolan T, Barton JS, Borthwick WKD, and Jones JDC. (1992), *Detection Of Acoustic Emission In Cutting Processes By Fibre Optic Interferometry*, 5th Conf. on Optical Fibre Sensors , Monterey CA.

McBride R., Carolan T.A., Barton J.S., Wilcox S., Borthwick W.K.D., and Jones J.D.C. (1993), *Detection of acoustic emission in cutting processes by fibre optic interferometry, Measurement science and technology* , Vol. 4 , pp. 1122-1128

Measures RM, Valis T, Liu K, Hogg D, Ferguson S, and Tapanes E. (1990), *Interferometric Fiber Optic Sensors For Use With Composite Material*, Optical testing and metrology III: Recent advances in industrial optical inspection, SPIE Vol.1332 , pp. 421-430

Measures R.M, and Liu K. (1990), *Fiber Optics Sensors Focus On Smart Systems*, Circuits and Devices, July, pp. 37-46

Measures R.M. (1992), *Advances Toward Fiber Optic Based Smart Structures*, Optical Engineering, Vol. 31, No. 1, pp. 34-47

Measures R.M., Glossop N.D.W., Lymer J., LeBlanc M., West J., Dubois S., Tsaw W., and Tennyson R.C. (1989), *Structurally Integrated Fiber Optic Damage Assessment System For Composite Materials*, Applied Optics, Vol. 28, pp. 2626-2633

Measures R.M., Liu K., and Melle S. (1992), *Fibre Optic Sensing System Critical Issues And Developments For Smart Structures*, Active Materials and Adaptive Structures - Session 18, pp. 301-307

Murphy K.A., Gunther M.F., Wang A., Claus R.O., Greene J., and Tran T. (1994), *Detection of acoustic emission location using optical fibre sensors*, Smart. Struct. Materials: Smart Sensing, Processing and Instrumentation, SPIE 2191, pp 282-290

Palmer C.H., and Green R.E. (1977), *Optical Detection Of Acoustic Emission Waves*, Applied Optics, Vol. 16, pp. 2333-2334

Robertson P.A. and Luddon B.F. (1997), *A fiber optic distributed sensor system for condition monitoring of synthetic ropes*, IEE Coll. Opt. Tech. Smart. Struct. and Struct. Monit., p12/1-6

Schoess J.N., and Zook D (1993), *Conformal acoustic waveguide sensor development*, Smart. Struct. Materials: Smart Sensing, Processing and Instrumentation 1993, SPIE 1918, pp 90-96

Schoess, J.N., Zook, J.D., and Burns D.W. (1994), *Resonant integrated micromachined (RIMS) acoustic sensor development*, Smart. Struct. Materials: Smart Sensing, Processing and Instrumentation 1994, SPIE 2191, pp 276-281

Tapanes E. *(1991),* *Real Time Structural Integrity Monitoring Using A Passive Quadrature Demodulated, Localised Michelson Optical Fibre Interferometer Capable Of Simultaneous Strain And Acoustic Emission Sensing* ', Fiber optic smart structures and skins IV (1991) SPIE Vol.1588

Valis T, Tapanes E, Liu K, and Measures RM. (1991), *Passive Quadrature Demodulated Localised Michelson Fiber Optic Strain Sensor Embedded In Composite Materials*, J.Lightwave Tech. Vol.9, No.4 ,pp. 535-543

Valis T., Tapanes E., and Measures RM. (1989), *Localised Fiber Optic Strain Sensors Embedded In Composite Materials*, Fibre optic smart structures and skins III(1989), pp. 1150-1153

Wade JC., Zerwekh PS., and Claus RO. (1981), *Detection Of Acoustic Emission In Composites By Optical Fibre Interferometry*, Proc.IEEE Ultrasonics Symp., pp. 849-853

Zheng S.X, McBride R., Hale K.F, Jones B.E, Barton J.S, and Jones J.D.C (1991a), *Optical Fibre Interferometry For Monitoring Tool Wear*, Int.Conf. on Optical fibre sensors, China, SPIE 1572, pp359-365

Zheng S.X, Hale K.F, and Jones B.E (1991b), *Polarimetric Monomode Optical Fibre Sensor For Monitoring Tool Wear*, Int. Conf. on Optical Fibre Sensors, China, SPIE Vol. 1572, pp. 268-272

Zheng S.X., Mcbride R., Barton J.S., Jones J.D.C., Hale K.F, And Jones B.E (1992), *Intrinsic Optical Fibre Sensor For Monitoring Acoustic Emission*, Sensors and Actuators A , Vol. 31, pp. 110-114

Chapter 5

Johnson M. (1979), *In-line fibre-optical polarisation transformer*, Applied Optics, Vol. 18, No. 9, pp. 1288-1289

Lefevre H.C. (1980), *Single mode fibre fractional wave devices and polarisation controllers*, Electronic letters, Vol. 16, No.20, pp. 778-780

Matsumato T. and Kano H. (1986), *Endlessly rotational fractional wave devices for single mode fibre optics*, Electronic Letters, Vol. 22, No. 2, pp. 78-79

Okoshi T. (1985), *Polarisation-state control schemes for heterodyne or homodyne optical fibre communications*, J. Lightwave Tech., Vol.3, No. 6, pp. 1232-1237

Ulrich R. (1979), *Polarisation stabilisation on single mode* fibre, Applied Physic Letters, Vol. 35, No. 11, pp. 840-842

Zheng S.X., Mcbride R., Barton J.S., Jones J.D.C., Hale K.F, And Jones B.E (1992), *Intrinsic Optical Fibre Sensor For Monitoring Acoustic Emission*, Sensors and Actuators A , Vol. 31, pp. 110-114

Chapter 6

Ciba Geigy (1991), *Ciba Geigy Composites Ltd Carbon/epoxy 920 Data sheet*

Fuwa M., Bunsell A.R., and Harris B., (1975), *Tensile Failure Mechanisms in Carbon Fibre Reinforced Plastics Composites*, J. Materials Science, 10, pp. 2062-2070

Roy,C. and M. El-Ghorba (1988), *Monitoring Progression Of Mode II Delamination During Fatigue Loading Through Acoustic Emission In Laminated Glass Fiber Composite*, Polymer Composites, Vol. 9, No. 5, pp.345-351

Chapter 8

Berthelot J.M. (1988), *Relationship between Amplitudes and Rupture Mechanisms in Composite Materials*, J. Reinforced Plastics and Composites, Vol 7, pp284-299

Green A.K., and Shafir E. (1999), *Termination and connection methods for optical fibres embedded in aerospace composite components*, Smart Mater. Struct., Vol 8., pp269-273

Berthelot J.M., and Rhazi J. (1990), Acoustic Emission in Carbon Fibre Composites, Composites Science and Technology, Vol. 37, pp 411-428, (1990)

Everitt B.S. and Hand D.J. (1981), *Finite Mixture Distributions*, Published by Chapman and Hall.

Hale KF., Hockenhull B.S., Christodoulou G. (1980), *The application of optical fibres as witness devices for the detection of plastic strain and cracking*, Strain, Vol. 16, No. 4.

Hofer B. (1987), *Fibre Optic Damage Detection In Composite Structures*, Composites, Vol. 18, No. 4, pp. 309-316

Liu K., Ferguson S.M., McEwan K., Tapanes E., and Measures R.M. (1990), *Acoustic Emission Detection For Composite Damage Assessment Using Embedded Ordinary Single-Mode Fiber-Optic Interferometric Sensors*, Fiber Optic Smart Structures and Skins III, SPIE Vol. 1370, pp.316-323.

Measures R.M. (1991), Fiber Optic Sensor Considerations and Developments for Smart Structures, *Fiber Optic Smart Structures and Skins IV*, SPIE Vol. 1588, pp 282-298

Roy,C. and M. El-Ghorba (1988), *Monitoring Progression Of Mode II Delamination During Fatigue Loading Through Acoustic Emission In Laminated Glass Fiber Composite*, Polymer Composites, Vol. 9, No. 5, pp.345-351

Titterington D.M., Smith A.F.M, and Makov U.E. (1985), *Statistical Analysis of Finite Mixture Distributions*, published by Wiley

Turner R.D., Valis T., Hogg W.D., and Measures R.M. (1990), Fiber Optic Sensors for Smart Structures, J. Intelligent Materials Systems and Structures, Vol. 1, pp 26-49

Chapter 9

Hatchard D. (1995), *The Flight Collection*, Reed Business Publishing

Lee C.H., Taylor H.F., Markus A.M., and Udd E. (1989), *Optical-Fiber Fabry-Perot Embedded Sensor*, Optics Letters, Vol. 14, pp. 1225-1227.

Lui K., Ferguson S.M., McEwan K., Tapanes E., and Measures R.M. (1990), *Acoustic Emission Detection For Composite Damage Assessment Using Embedded Ordinary Single-Mode Fiber-Optic Interferometric Sensors*, Fiber Optic Smart Structures and Skins III, SPIE Vol. 1370, pp. 316-323